SAND76-5586
Unlimited Release

UC-60

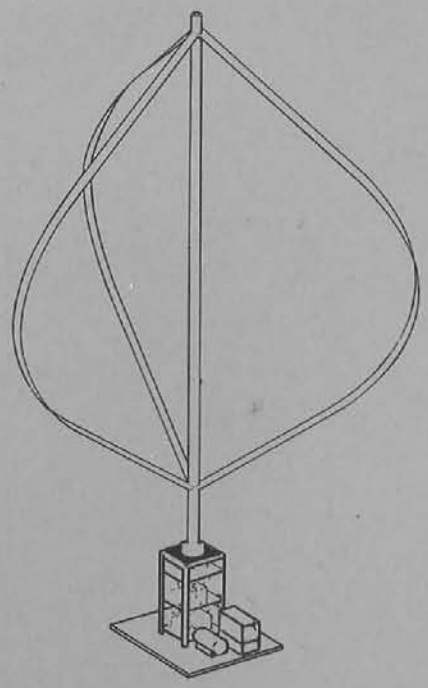

vertical-axis wind turbine technology workshop

May 17-20, 1976

Sponsored by ERDA
and hosted by

Sandia Laboratories
Albuquerque, New Mexico 87115

When printing a copy of any digitized SAND Report, you are required to update the markings to current standards.

Issued by Sandia Laboratories, operated for the United States Energy Research & Development Administration by Sandia Corporation.

NOTICE

This report was prepared as an account of work sponsored by the United States Government. Neither the United States nor the United States Energy Research & Development Administration, nor any of their employees, nor any of their contractors, subcontractors, or their employees, makes any warranty, express or implied, or assumes any legal liability or responsibility for the accuracy, completeness or usefulness of any information, apparatus, product or process disclosed, or represents that its use would not infringe privately owned rights.

Printed in the United States of America

Available from
National Technical Information Service
U. S. Department of Commerce
5285 Port Royal Road
Springfield, Virginia 22161
Price: Printed Copy $13.75; Microfiche $2.25

SAND76-5586
Unlimited Release
Printed July 1976

Distribution
Category UC-60

PROCEEDINGS OF THE VERTICAL-AXIS WIND TURBINE TECHNOLOGY WORKSHOP

Albuquerque, New Mexico, May 18-20, 1976

Sponsored by the

Energy Research and Development Administration
Division of Solar Energy
Wind Energy Conversion Branch
Louis Divone, Branch Chief

Hosted by

Sandia Laboratories
Advanced Energy Projects Division, 5715
Richard H. Braasch, Supervisor

Proceedings Assembled by

Lyle Wetherholt, Workshop Coordinator

ACKNOWLEDGMENT

The workshop coordinator acknowledges the support of Louis Divone, Chief of the Wind Energy Conversion Branch, ERDA; also that of Richard Braasch, Sandia Laboratories, who helped outline the workshop procedures. Thanks are due to W. Lyle Donaldson, Senior Vice President, Southwest Research Institute, for a banquet address which combined wisdom with wit. Joan Gillon and Marylee Adams, Sandia Laboratories, carried the greatest burdens: handling speaker invitations, registrations, typing innumerable letters, lists, and other necessary documents to make it all fit together. Projectionists Hugh Taylor, George Skinner, and Howard Hayden made the visual aids flow effortlessly and in tune with the presentations in spite of some not apparent difficulties. The Albuquerque Inn and Convention Center provided excellent facilities and many amenities that made all participants feel welcome. To the many other employees of Sandia Laboratories who assisted with arrangements, attended to participants' travel needs, etc., special thanks; without them it would not have been possible.

CONTENTS

		Page
	Foreword	9
	Conference Makeup	9
	Introduction	11
	Agenda	13
	List of Attendees	17
I.	PROGRAM OVERVIEWS	
	Federal Wind Energy Program L. V. Divone, ERDA	I-1
	Large Experimental Wind Turbines - Where We Are Now R. L. Thomas, Lewis Research Center	I-9
	Vertical-Axis Wind Turbine Program R. H. Braasch, Sandia Laboratories	I-33
	Electric Power Research Institute Program Piet Bos, EPRI	I-55
	Canadian Wind Energy Program R. J. Templin and P. South, NRC of Canada	I-57
II.	ERDA's DARRIEUS VERTICAL-AXIS WIND TURBINE PROGRAM	
	(System Engineering)	
	System Design - 17-Meter Research Turbine E. G. Kadlec, Sandia	II-1
	System Engineering - Performance Considerations W. N. Sullivan, Sandia	II-10
	Economic Considerations J. F. Banas, Sandia	II-19
	(Aerodynamics - Analysis and Testing)	
	Aerodynamics of the Darrieus Turbine J. H. Strickland, Texas Tech University	II-29
	Selected Wind Turbine Test Results B. F. Blackwell, Sandia	II-59

CONTENTS (Cont)

	Page
Aerodynamics of Four Symmetrical Airfoil Sections R. E. Sheldahl, Sandia	II-73
5-m Turbine Field Testing W. N. Sullivan, Sandia	II-107
Performance Prediction for the 17-m Turbine J. F. Banas, Sandia	II-118
(Structural Design)	
Structural Overview R. C. Reuter, Jr., Sandia	II-126
Structural Loads for the 17-m Darrieus Turbine W. N. Sullivan, Sandia	II-130
Blade Structural Analysis L. I. Weingarten and D. W. Lobitz, Sandia	II-137
Tower Analysis R. C. Reuter, Jr., Sandia	II-151
System Structural Response J. H. Biffle, Sandia	II-168
Effects of System Imbalance R. Rodeman, Sandia	II-180
Aeroelastic Analysis of the Troposkien-Type Wind Turbine N. D. Ham, Massachusetts Institute of Technology	II-185
Blade Design and Fabrication of 17-m VAWT J. J. Barzda, Kaman Aerospace Corp.	II-205
Low-Cost Blade Design Considerations L. V. Feltz, Sandia	II-222
(Electrical Subsystem, Control and Data Acquisition)	
Electrical Power System A. F. Veneruso, Sandia	II-241
Automatic Control and Data Acquisition A. F. Veneruso, Sandia	II-263
Anemometry Data and Processing J. W. Reed, Sandia	II-270
BANQUET ADDRESS--Wind Power, Fact or Fantasy W. L. Donaldson, Southwest Research Institute	II-291

CONTENTS (Cont)

		Page
III.	PROMINENT VERTICAL-AXIS WIND TURBINE PROGRAMS	
	Aerodynamics of the Darrieus Rotor R. E. Wilson, Oregon State University	III-1
	Darrieus Structural Studies R. W. Thresher and E. E. Meyer, Oregon State	III-10
	Commercial Vertical-Axis Wind Turbines L. H. J. Maile, Dominion Aluminum Fabricating, Ltd.	III-28
	Feasibility Investigation of the Giromill R. V. Brulle, McDonnell Aircraft Company	III-39
	Innovative Wind Machines - Theoretical Performance J. B. Fanucci and R. E. Walters, West Virginia University	III-61
IV.	REPORTS OF THE WORKING GROUPS	
	Chairman: R. E. Wilson Oregon State University	IV-1
	Chairman's Closing Statement L. V. Divone, ERDA	IV-13

PROCEEDINGS OF THE VERTICAL-AXIS WIND TURBINE TECHNOLOGY WORKSHOP

Foreword

These proceedings are published with only one main objective - to assemble and present to the workshop participants in the most timely possible manner the papers as presented while the activities of the workshop are fresh in everyone's mind. For this reason papers are printed as received without editorial correction or retyping. The figures do not follow a rigid form of notation or identification; however, in most cases they are easily identifiable and correlate with the paper to which they belong. We sincerely hope that our original publication goal of conference closing plus three weeks is viewed by the recipients as an important enough goal to tolerate a rather loose publication format and even an occasional error. We regret that we were unable to meet this goal (some papers simply were not received in time). But had we done much editing or retyping of errors, the tardiness would have been compounded. Papers are presented in the order in which they were presented. Page and figure numbers are for each paper rather than for the proceedings as a whole.

Conference Makeup

The Vertical-Axis Wind Turbine Technology Workshop was attended by 145 persons from 34 states and 5 countries. Various disciplines, universities, and company and organizational affiliations were represented. A brief synopsis follows:

Total participation	145
Countries represented	5
U.S. states represented	34
Universities represented	27
Large companies	16

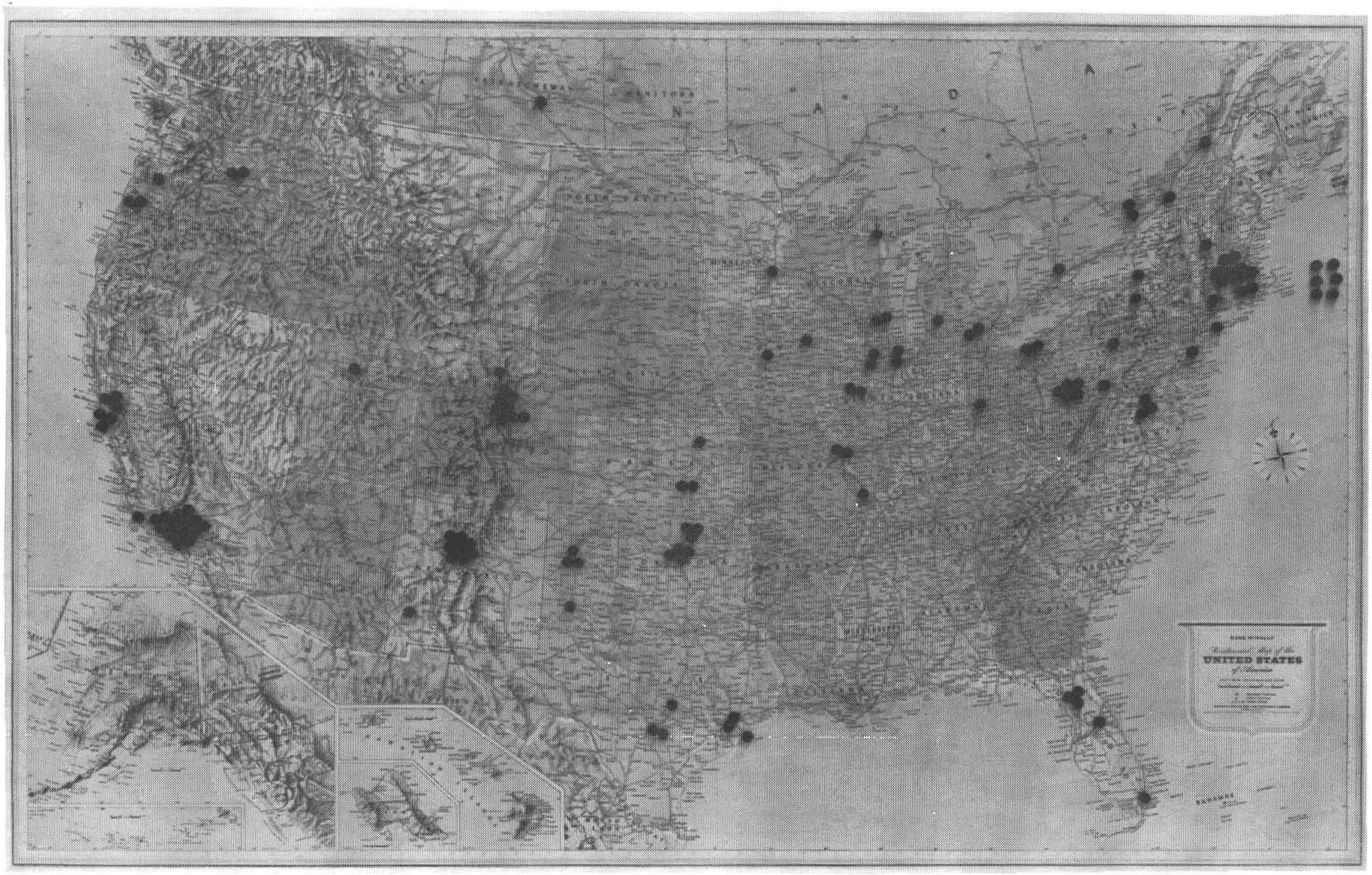

Map Indicating Attendees' Origins

Small companies	29
Government agencies	6
Government laboratories	6
ERDA-supported project organizations	8
Research institutes	3
Utilities	2
International organizations	1
Other organizations and individuals	7

Introduction

During the year since the Second Workshop on Wind Energy Conversion Systems the state of the art has progressed from one of emerging concepts to demonstrated prototype and test hardware. Both large and small systems have continued to capture the imaginations of scientists, engineers, and laymen alike. Vertical-axis wind turbines in particular have received considerably more technological attention and are now being worked on in terms of the near problems of actual application and use. Persons with a broad range of backgrounds were invited to this workshop to generate ideas for both technological innovation and application planning. The attendees represented universities, manufacturing firms, research institutes, government agencies, and concerned individuals. Since the workshop announcements and agenda stressed technical detail, the overall attendance was somewhat limited but this assured a very high percentage of attendance at each session throughout three very long days.

In general the workshop was divided into four sessions covering wind energy overviews, the Darrieus program, other vertical-axis programs, and reports of the working groups. These sessions were chaired by four different persons who handled both the proceedings and the question-and-answer periods. Arrangements for each day's session were made at a speaker's breakfast. The first day also included a tour of Sandia Laboratories on Kirtland Air Force Base to view the 15-foot Darrieus test system and the Solar Total Energy System Test Facility. There was an evening display and

general discussion of about two dozen hardware items from audio/visual aids to electromechanical interactive displays.

The second day was highlighted by a banquet dinner and a thought-provoking adress by W. Lyle Donaldson of Southwest Research Institute. Dinner was followed by breakaway meetings in four general areas; Systems Engineering and Analysis, Aerodynamics, Structural Design, and Electrical Systems. The Chairmen of these groups reported their results in the final session of the Workshop on the third day. In addition the third day included valuable data on prominent vertical-axis wind turbine systems other than Darrieus.

Enthusiasm for wind energy conversion permeated the workshop and most participants left with a sense of urgency. Hopefully future workshops will be able to concentrate on results of on-line systems.

Lyle Wetherholt
Workshop Coordinator

AGENDA

Vertical-Axis Wind Turbine Workshop
May 18, 19 & 20

Monday Evening, May 17, 1976

5-9 P.M. Registration

5-7:30 P.M. Early Bird Social Hour

Tuesday, May 18, 1976

7:30-5 P.M. Registration

9:00 A.M. Welcoming Address - A. Narath, Vice President, Research, Sandia Laboratories

Session I: Program Overviews

Louis Divone, Chief, Wind Energy Conversion Branch, ERDA, Chairman

9:10 Federal Wind Energy Program, Louis Divone, ERDA

9:40 Horizontal-Axis Wind Turbine Program, Ronald Thomas, NASA

10:25 Coffee Break

10:35 Vertical-Axis Wind Turbine Program, Richard Braasch, Sandia

11:20 Electric Power Research Institute Program, Piet Bos, EPRI

11:50 Lunch

1:15 Canadian Wind Energy Program, R. J. Templin, NRC

2:15 Session Question and Answer Period

Session II: ERDA's Darrieus Vertical-Axis Wind Turbine Program

Richard Braasch, Sandia Laboratories, Chairman

IIA: System Engineering

2:30 System Design 17-meter Research Turbine, Emil Kadlec, Sandia

2:55 Performance Considerations, William Sullivan, Sandia

3:20 Economic Considerations, James Banas, Sandia

3:45 Session Question and Answer Period

4:00 Bus Tour of Wind Turbine Test Facility and Solar Total Energy Test Facility--Sandia Laboratories, Area I

8:00 Evening Display and Open Discussion

Wednesday, May 19, 1976

IIB: Aerodynamics - Analysis and Testing

8:00 Aerodynamic Performance Model, James H. Strickland, Texas Tech University

8:25 Wind Tunnel Turbine Tests, Ben Blackwell, Sandia

8:50 Wind Tunnel Blade Section Tests, Robert Sheldahl, Sandia

9:10 5-meter Turbine Field Testing, William Sullivan, Sandia

9:30 Performance Prediction - 17-meter Turbine, James Banas, Sandia

9:50 Session Question and Answer Period

10:00 Coffee Break

AGENDA (Cont)

IIC: Structural Design

10:20 Structural Overview, Robert Reuter, Sandia

10:40 Structural Loads, William Sullivan, Sandia

11:00 Blade Structural Analysis, Larry Weingarten, Sandia

11:20 Tower Analysis, Robert Reuter, Sandia

11:40 System Response Code, Johnny Biffle, Sandia

11:55 The Effects of System Imbalance, Ronald Rodeman, Sandia

12:10 Lunch

1:30 Aeroelasticity, Norman Ham, MIT

1:55 Blade Design and Fabrication - 17-meter, Justin Barzda, Kaman Aerospace

2:15 Blade Manufacturing Studies, Louis Feltz, Sandia

2:35 Session Question and Answer Period

2:55 Coffee Break

IID: Electrical Subsystem, Control and Data Acquisition

3:05 Electrical Power System, Anthony Veneruso, Sandia

3:25 Automatic Control and Data Acquisition, Anthony Veneruso, Sandia

3:45 Anemometry Data Processing, Jack Reed, Sandia

4:10 Session Question and Answer Period

6:00 Workshop Dinner

Guest Speaker: W. Lyle Donaldson, Senior Vice President, Southwest Research Institute

8:00 Working Group Meetings

System Engineering and Analysis, Chairman, Emil Kadlec, Sandia
Aerodynamics, Chairman, Ben Blackwell, Sandia
Structural Design, Chairman, Robert Reuter, Sandia
Electrical Systems, Chairman, Anthony Veneruso, Sandia

Thursday, May 20, 1976

Session III: Prominent Vertical-Axis Wind Turbine Programs

Emil Kadlec, Sandia, Chairman

8:30 Vertical-Axis Wind Turbine Aerodynamics, R. E. Wilson, Oregon State University

9:00 Vertical-Axis Wind Turbine Structures, R. W. Thresher, Oregon State University

9:30 NRC Blade Fabrication, Lynn Maile, Dominion Aluminum Fabricating, Ltd.

10:00 Coffee Break

10:15 Giromill, Robert Brulle, McDonnell Douglas Corp.

11:00 Innovative Vertical-Axis Wind Machines, Richard Walters, West Virginia University

11:45 Session Question and Answer Period

12:15 Lunch

AGENDA (Cont)

Session IV: Reports of the Working Groups

Robert E. Wilson, Oregon State University, Chairman

1:30	System Engineering and Analysis, Emil Kadlec, Sandia
1:45	Aerodynamics, Ben Blackwell, Sandia
2:00	Structural Design, Robert Reuter, Sandia
2:15	Electrical Systems, Anthony Veneruso, Sandia
2:30	Closing Statement, L. V. Divone
2:45	Adjournment of the Workshop

ATTENDEES

Ai, Daniel K.
Senior Scientific Assoc.
Alcoa Tech. Center
(Aluminium Composites of America)
Alcoa Center, PA 15069

Aimone, Anthony F.
c/o Ceasar Aimone
200 Fifth Street
Iron Mountain, MI 49801

Andrews, Carl
Altruistic Communities
Project Engineer
110 E. Anaheim
Long Beach, CA 90813

Banas, James - 5742
Sandia Laboratories
Albuquerque, NM 87115

Barieau, Dr. Robert
Research Professor
West Texas State Univ.
Box 248, W.T. Station
Canyon, TX 79016

Barzda, Justin
Chief of Systems Research
Kaman Aerospace Corporation
Old Windsor Road
Bloomfield, CT 06002

Bea, Karl J.
Enerjair, Ltd.
(American Ultramar, Ltd.)
128 Dewitt Street
Syracuse, NY 13203

Beckman, Ralph
REDE Research Institute
P.O. 212
Providence, RI 02901

Benjamin, John
Assoc. Director
Pollution Control Research Institute
3875 Jackson Station #19
Riverside, CA 92503

Bergey, Mike
University of Oklahoma
Rt #1 Box 151B
Norman, OK 73069

Biffle, Johnnie - 1281
Sandia Laboratories
Albuquerque, NM 87115

Bill, Donald F.
Org. CDI
1080 N. River Drive
Miami, FL 33136

Blackwell, Ben - 1333
Sandia Laboratories
Albuquerque, NM 87115

Bolt, Jan B.D.H.
Fokker-VFW
P.O. Box 7600
Schiphol-cost, The Netherlands
020/731044

Boland, Joseph F.
Rockwell International
Rocky Flats Plant
Box 474
Golden, CO 80401

Bos, Piet
Program Manager, Solar Energy
Electric Power Research Institute
3412 Hillview Avenue
Palo Alto, CA 94303

Braasch, R. H. - 5715
Sandia Laboratories
Albuquerque, NM 87115

Braz, John
TCHUBA
98 Camp Street
Providence, RI 82906

Breed, Robert A.
Wood World
579 Calle Dia
Carpinteria, CA 93013

Brulle, Robert V.
Giromill Project Manager
McDonnell Aircraft Co.
P.O. Box 516, Dept. 241, Bldg. 32
St. Louis, MO 63166

Carlin, Palmer
Colorado University
Professor Electrical Engineering
2209-4th Street
Boulder, CO 80302

Carlis, Bill
Southwest Energy Options
109 W. California Street
Silver City, NM 88061

Ceiderburg, John W.
Ceiderburg Engineering
Box 259
Aptos, CA 95003

Charron, R.
The American Committee for Cape Verde
14 Beacon Street
Boston, MA 02108

Clark, John M.
Institute of Arctic Apline Research
University of Colorado
Boulder, CO 80309

Cole, Alan L.
Northern Illinois University
Dept. of Geography
DeKalb, IL 60115

Craik, Darrel W.
Teledyne Aero-Cal
523 E. Mission Road
San Marcos, CA 92069

Cromack, Duane E.
Dept. of Mechanical Engineering
University of Massachusetts
Amherst, MA 01002

Davenport, Steven R.
Oklahoma State University
900 N. Portland
Oklahoma City, OK 73107

Davitian, Harry
Brookhaven National Laboratory
Bldg. 475
Upton, NY 11973

Dennis, Tom L.
Brunswick Corporation
504 Sweetwater Blvd.
Longwood, FL 32750

Dhande, Sanjay G.
Mechanical Engineering Dept.
University of Florida
Gainesville, FL 32677

Divone, Louis V.
Chief, Wind Energy Conversion Branch
Division of Solar Energy
Energy Research and Development Admin.
Washington, DC 20545

Dodge, Robert J.
Automatic Power, Inc.
213 Hutcheson Street
Houston, TX 77003

Donaldson, W. Lyle
Senior Vice President
Southwest Research Institute
P.O. Drawer 28510
San Antonio, TX 78284

Dorn, Dave W.
Lawrence Livermore Laboratory
P.O. Box 808
Livermore, CA 94550

Dougan, David
Hamilton Standard
Area Representative
Box 58096
Houston, TX 77058

Drake, William E.
Enertech Corporation
P.O. Box 420
Norwich, VT 05055

Drees, Herman M.
Pinson Energy Corporation
76 Ashford Street
Allston, MA 02134

Dunitz, Margie
University of Michigan
1620 Cambridge Rd.
Ann Arbor, MI 48104

Espeset, Nick
Foundation for Rural Technology
903 Pine Street
Boulder, CO 80302

Fanucci, Jerome B.
Professor and Chairman
Dept. of Aerospace
West Virginia University
Morgantown, WV 26506

Fekete, G. I.
Asst. Assoc. Professor
McGill Univ.
Montreal, Canada

Feltz, Louis - 1324
Sandia Laboratories
Albuquerque, NM 87115

Francis, Serre
Rohn Manufacturing Co.
P.O. 23428
San Jose, CA 95153

Frenchman, R. M.
The American Committee for Cape Verde
14 Beacon Street
Boston, MA 02108

Fuller, Gerald
University of Regina
Faculty of Engineering
Regina, Canada

Gillies, Alan
University of Oklahoma
209 Cedar Lane
Moore, OK

Gilmore, Earl H.
WTSU-AC-SIGMA
Rt 1 Box 430
Amarillo, TX 79106

Gordon, Robert
Structural Composites Industries, Inc.
6344 North Irwindale Ave.
Azusa, CA 91702

Gross, William A.
Dean, College of Engineering
University of New Mexico
107 Farris Engr. Center
Albuquerque, NM 87131

Grover, Robert D.
10213 Norman Avenue, NE
Albuquerque, NM 87112

Groves, Donald J., Jr.
Public Service Co.
P.O. Box 2267
Albuquerque, NM 87103

Hadlock, R. K.
Battelle Pacific Northwest Laboratory
P.O. Box 999
Richland, WA 99352

Ham, Norman D.
Massachusetts Institute of Technology
77 Massachusetts Avenue
Cambridge, MA 02139

Heckman, Ken
Teledyne Aero-Cal
528 E. Mission Rd.
San Marcos, CA 92069

Hill, John M.
Assoc. Prof. of Civil Engineering
University of Wyoming
Laramie, WY 82071

Hill, P. Ward
Hercules, Inc.
P.O. Box 210
Cumberland, MD 21502

Holme, Olof A. M.
SAAB-SCANIA AB Aerospace Div.
Linkoping, Sweden S-58188

Hughes, W. L.
Oklahoma State University
202 Engineering South
Stillwater, OK 74074

Johnson, Steven A.
Wind Energy Association
4594 Creek View Drive
Salt Lake City, UT 84107

Jones, Brian H.
Compositer Engineering Corp.
6960-5 Aragon Circle
Buena Park, CA 90620

Jones, Robert
R&M Ranch, Inc.
570 N. Lillian Way
Los Angeles, CA 90004

Jayadev, T. S.
College of Applied Science
University of Wisconsin
Milwaukee, WI 53201

Kadlec, Emil - 5715
Sandia Laboratories
Albuquerque, NM 87115

Krug, Edwin H.
Director, Military Planning
Lear Siegler, Inc.
4141 Eastern Avenue SE
Grand Rapids, MI 49508

Langerman, Lowell
Rt 2
Fayette, IA 52142

Larsen, Harold C.
Air Force Institute of Technology
AFIT/END, WPAFB
Dayton, OH 45433

Lechner, T. Michael
Bovay Engineers, Inc.
P.O. Box 30068
Albuquerque, NM 87110

Lefever, Dan
Sonnewald Service
Rt #1, Box 457
Spring Grove, PA 17362

Lefever, Evan
Route 2, Box 203
Berkeley Springs, WV 25411

Lefever, Tim
Sonnewald Service
Route #1, Box 457
Spring Grove, PA 17362

Lissaman, Peter
Aerovironment
Las Vista
Pasadena, CA 91107

Ljungstroem, Olle
N.E. National Swedish Board for Energy
Source Development
STU, FACK S-(0072)
Stockholm 43, Sweden

Lopez, Gilbert
Bureau of Indian Affairs
P.O. Box 1248
Albuquerque, NM 87103

Maile, L. H. J.
Engineering Manager
Dominion Aluminum Fanricating, Ltd.
3570 Hawkestone Road
Mississauga, Ontario, Canada
L5C 2V8

Malver, Fred
Honeywell, Inc.
2600 Ridgeway Pkwy
Minneapolis, MN 55413

Matakovich, George J.
Store, Matakovich & Wolfberg
715 E. Mission Drive
San Gabriel, CA 91776

McCarthy, John S.
McDonnell Douglas Corp.
345 Gray Avenue
St. Louis, MO 63119

McClure, Paul
Asst. Professor of Aerospace Engr.
University of Texas
Taylor Hall 227
Austin, TX 78712

Merriam, Marshal
Lawrence Berkeley Laboratory
University of California
Dept. of Materials Science
Hearst Mining
Berkeley, CA 94720

Metcalf, Philip
Unarco-Rohn
P.O. Box 2000
Peoria, IL 61601

Meyer, Hans
Windworks
Box 329, Route 3
Mukwonago, WI 53149

McConnell, Robert
Institute of Research of Hydro-Quebec
1800 Montec Ste Julie
Varrenes, Quebec, Canada JOL 2 PO

Michlin, Steven B.
University of Michigan
1620 Cambridge Rd.
Ann Arbor, MI 48104

Miller, Larry
Oklahoma State University Technical Institute
900 N. Portland
Oklahoma City, OK 73107

Mims, Forrest M., Jr.
UTSA
234 Five Oaks Drive
San Antonio, TX 78209

Mitcham, Tina
Pollution Control Research Institute
3875 Jackson Station #19
Riverside, CA 92503

Mortimer, A. J.
Box 72
Oldwick, NJ 08858

Nassar, Esam
Illinois Institute of Technology
3110 S. State Street
Chicago, IL 60616

Nelson, Vaughn
West Texas State University
Dept. of Physics
Box 248, W. T. Station
Canyon, TX 79016

Packard, Lyle E.
Packard Marine
505 N. Lake Shore Drive
Chicago, IL 60611

Palmer, Darwin G.
701 Wagon Trail, SE
Albuquerque, NM 87123

Park, Jack
Helion
Box 4301
Sylmar, CA 91342

Pedersen, Bjarne Maribo
Technical University Denmark
Danish Academy of Technical Sciences
Dept. of Fluid Mech.
Bygn 404 DTH, 2800 Lyngby
Denmark

Penrod, Robert
P.O. Box 1047
Cape Girardeau, MO 63701

Piepers, G. G.
Reactor Centrum Nederland
Westerduinweg 3 Petten
(N. H.) The Netherlands

Ramakumar, Dr. R.
Assoc. Prof., Electric Engineering
Oklahoma State University
202 Engineering South
Stillwater, OK 74074

Ramos, A. D.
The American Committee for Cape Verde
14 Beacon Street
Boston, MA 02108

Ramsdell, J. V.
Bettelle Pacific Northwest Laboratory
Research Scientist
P.O. Box 999
Richland, WA 99352

Reed, Jack - 5443
Sandia Laboratories
Albuquerque, NM 87115

Reuter, Robert - 5715
Sandia Laboratories
Albuquerque, NM 87115

Rodeman, Ronald - 1281
Sandia Laboratories
Albuquerque, NM 87115

Rollins, Charles
Box 737
El Cerrito, CA

Root, David H.
U. S. Geological Survey
Mail Stop 922
Reston, VA 22092

Sandor, G. N.
M. E. Dept.
University of Florida
Gainesville, FL 32677

Sayler, John P.
American Energy Alternatives, Inc.
P.O. Box 905
Boulder, CO 80302

Scully, Dan
Total Environment Action
Box 47
Harrisville, NH 03450

Seath, Donald D.
University of Texas at Arlington
Aerospace Engr. Dept.
UTA Box 19428
Arlington, TX 76019

Seaverson, Louis A.
Rockwell International
P.O. Box 464
Golden, CO 80401

Sheehan, John L.
Chief Engineer
Sheehan Consultants
5320 Ken Caryl Rd.
Littleton, CO 80123

Shepardson, William P.
Pinson Energy Corp.
76 Ashford Street
Allston, MA 02134

Sholes, John E.
NASA-Lewis Research Center
21000 Brook Park Rd.
Cleveland, OH 44135

Skoglund, Victor J.
University of New Mexico
ME 101
Albuquerque, NM 87131

Smith, Brent
ISTARA Research
P.O. Box 735
Boulder, CO 80302

Synder, Melvin H.
Wichita State University
Wichita, KS 67208

Soderholm, L. H.
USDA-ARS
Room 213 Ag. Engr.
Iowa State University
Ames, IO 50011

South, Peter
National Research Council of Canada
Research Office
Bldg. M-2, Montreal Rd.
Ottawa, Ontario (Canada) KLA OR6

Stein, Bill
Natural Power
Francestown Turnpike
New Boston, NH 03070

Takanashi, Akihiro
University of Florida
Dept. of Mechanical Engineering
Gainesville, FL 32611

Teague, Don
Energy Research and Development Admin.
Washington, DC 20545

Thomann, Gary C.
Wichita State University
Wichita, KS 67208

Thomas, Robert
Wind Harvest Co.
750 Mission
Camarillo, CA 93010

Todd, Clement
U.S. Bureau of Reclamation
Denver FC Bldg. 67 Room 620
Denver, CO 80225

Sheldahl, Robert - 1333
Sandia Laboratories
Albuquerque, NM 87115

Strickland, James H.
Mechanical Engineering Department
Texas Tech University
Lubbock, TX 79409

Sullivan, William N. - 1284
Sandia Laboratories
Albuquerque, NM 87115

Templin, R. J.
Head, Low Speed Aerodynamics Lab
National Research Council (Canada)
Montreal Road
Ottawa, Canada K1H 6R6

Thomas, Ronald L.
Head, Windpower Office
NASA-Lewis Research Center
21000 Brookpark Road
Cleveland, OH 44135

Thresher, Robert W.
Associate Professor
Mechanical Engineering Department
Oregon State University
Corvallis, OR 97331

Veneruso, Anthony - 5715
Sandia Laboratories
Albuquerque, NM 87115

Walters, Richard E.
Associate Professor of Aerospace Engineering
West Virginia University
Morgantown, WV 26506

Weingarten, Larry - 1284
Sandia Laboratories
Albuquerque, NM 87115

Wilson, Robert E.
Professor, Mechanical Engineering Dept.
Oregon State University
Corvallis, OR 97331

Tsao, Peter
Northern Illinois University
Physics Dept.
DeKalb, IL 60115

Turnquist, Ralph O.
Kansas State University
1100 Pioneer Lane
Manhattan, KS 66502

Van Dalen, Gerritt
FDO-Engineering Consultants
P.O. Box 194
Hengelo, Netherlands

Warchol, Edward J.
Bonneville Power Administration
P.O. Box 3621
Portland, OR 97208

Weeks, Stanley A.
Agricultural Engineering Department
Cornell University
312 Agr. Engr. Dept.
Ithaca, NY 14853

Werner, Charles
Unarco-Rohn
Sales and Engr. Department
P.O. Box 2000
Peoria, IL 61601

Wood, Rhande Paul
1180 Alvarado, SE #208
Albuquerque, NM 87108

Worstell, Mark
University of Oklahoma
1319 S. Jenkins - Apt. B
Norman, OK 83069

Zweig, Pete R.
Associate Director
Pollution Control Research Institute
3875 Jackson Station #19
Riverside, CA 92503

Louis V. Divone
Chief, Wind Energy Conversion Branch
Energy Research and Development Administration

I'm not going to speak very long this morning since I know you all are waiting to hear the large number of technical presentations that will be made over the next three days. I would like to welcome you here to Albuquerque today and discuss a number of points to set the stage for this workshop.

At the wind energy workshop in June in Washington, we stated that it was the intention of the program to hold a number of small workshops. The purpose of these small workshops would be to disseminate the results of research in our program to other researchers and to industry and to provide a forum for discussion of ideas, results and problems. I must say, however, looking at the size of the audience here today, that small is obviously relative. I am delighted, however, at the number of people who came here to Albuquerque to discuss this specialized subject in wind energy. So let me welcome you to the first of our specialized workshops, our workshop on vertical-axis wind energy systems.

Secondly, I would like to place these systems and their problems and our goals in context with the overall program.

Most of you are familiar with the structure of our program and have seen these first viewgraphs before, but let me use them to start our discussion of the problem of wind energy systems. The elements listed under Item 1 are basically the research and development and analytical study efforts in the program. Items 2-5 are the major systems development activities. Most of the early work on large systems is devoted to the "conventional" horizontal axis propeller-type system. This is primarily because these are the only systems that we have sufficient information on to proceed with on a large scale and at a rapid pace.

But they are not the only systems that can work. In fact, as you well know, essentially anything can work; any asymmetrical device or device

which can produce an asymmetrical force can be placed on a bearing, stuck in the wind and made to work. The question is, which of these many alternatives stands the highest possibility of achieving a significant advance in the performance-per-unit cost of wind energy systems? So, while the bulk of our large system effort is devoted to the conventional configuration element, it is the advanced and innovative systems element we use to probe, investigate, compare, and where appropriate, develop alternative approaches. Of these many alternatives, the vertical axis system is considered to have the highest potential and least risk at our present stage of understanding and represents the prime thrust in our advanced system element and that is why we are here today.

Before proceeding let me mention a number of developments which have occurred since the wind energy workshop in June. The 100-kilowatt Model 0 wind system is up and running at the NASA Lewis Research Center Test Station at Plumbrook, Ohio. Its operation is confirming the basic performance predictions of the design. As you are well aware, the major technological problem in large wind turbines is the amelioration of structural dynamics and vibration conditions. The Model 0 has encountered some resonance problems induced by higher than predicted aerodynamic blockage from the tower. Changes are now underway to reduce the tower blockage and to change the natural frequency of several components, particularly the yaw drive system, so as to remove resonance point.

The megawatt scale preliminary designs have been completed and a design point has been selected at 1.5 megawatts rated power and approximately a 200-foot diameter. We are now in the process of selecting a contractor to design and build this system. Ron Thomas of NASA will describe this program in more detail later today.

Separately we are in the process of selecting approximately 12 sites from utility company proposals around the United States and after selection, erecting meteorological towers on those sites. We will then select four final sites for the actual installation of our plan

for initial systems. These systems represent two more powerful versions of the Model 0, which are termed Model OA's. The second two machines will be the 200-foot diameter megawatt systems described earlier. The purpose of the Model OA test will be to identify, as early as possible, user interface problems and requirements. The purpose of the second test will be technical and economic, an operational test of the very large machines.

One of the major recommendations that evolved at the June workshop was the recommendation to increase our thrust on the development of small systems, the 5-50 kilowatt systems useful for small homes and farms. It is my pleasure to announce today that the Rocky Flats Plant of Rockwell International, an ERDA laboratory near Denver, Colorado, has been selected to coordinate and direct that effort for ERDA. They will have a similar role to that of the NASA Lewis Research Center in progressively pursuing the development of small systems. I might add that we do anticipate that the majority of the actual research and system developments will be performed at universities and industries under contract, as we are presently doing, and that Rocky Flats' role will be that of a test center coordinator and planner for that element of the program. They will interface with the Department of Agriculture in the actual operational testing of the systems.

Now, let me talk for a moment about the deterrents to wind energy systems. Again, many of you have seen the next two viewgraphs. I'm going to take a very difficult tack here this morning because all of us are enthusiasts for wind energy. Therefore, I want to talk of the deterrents and problems with wind energy systems, particularly in view of the goals which vertical axis systems must achieve in order to become commercial and economically viable successes. As you are well aware, cost, both capital cost and more importantly energy cost, are the key deterrents to wind energy systems. The question we must answer is, what are the costs, which designs promise lowest costs, and how do we go about minimizing those costs? We are now beginning to get

realistic and believable cost estimates for conventional machines. The more important economic estimates, that is, the actual economic value of wind systems in a real utility operation including all the time and transient effects, are still at a very preliminary state. We do have three sets of numbers now from GE, Lockheed and Boeing, and these are sufficiently similar to begin to give us some confidence in these estimates. But we have to remember that these are still paper estimates.

I've flipped a four-sided coin here and I'm showing the Lockheed cost estimate curves, however, the curves from the other contractors are quite similar. You'll note that the costs do not appear bad at both the small and large sizes but that it is the intermediate size which has the most difficult cost differential problem.

Now this is one of two cost goals which vertical-axis systems must shoot for. First, they must do better than these predicted curves. To do just equal is not sufficient because there is never enough incentive to proceed with a major development or for industry to risk its capital to merely equal a product which is further ahead in terms of its potential production. Rather it must do sufficiently better to encourage the production of such systems. Secondly, the vertical axis systems must do even better than that. Because the current economics of wind systems are such that the existing machines are not economically competitive at today's state of the art and today's fuel prices, we must improve the performance of these systems in order to achieve a sufficiently large market to where commercialization might occur. I have one last viewgraph that I would like to show you. Unfortunately, it is not too clear. I mentioned earlier that almost anything will work and that before we get carried away with our great new inventions let me show you this slide from the cover of a recent booklet. The fuzzy device on the left is in fact a vertical axis windmill. It was built in 1825 to power a sawmill. It nailed the planks, turned the columns, and in fact made broom

handles at $2.50 per hundred, which says something about the moving target for cost goals. The system was 50 feet in diameter and 72 feet to the top of the center pole. It had 18 cloth-covered sails which articulated and pivoted via weights so that it filled going down wind and feathered going up wind. I receive a number of proposals each month which propose to invent similar systems. This particular machine worked until 1867 when it was damaged in a storm. So I guess that our 30-year amelioration estimate seems reasonable.

Not much over a year ago Sandia provided me with a model of a Darrieus, partly so that we would have a display model for exhibits and meetings back in Washington and partly so that those of us in Washington could pretend that we knew how it worked. Now I would like to join you in the audience for a few days to find out how it really does work. More importantly, I want to view with you the developments in this field over the past year and to listen to your observations, comments and suggestions as we proceed with the investigations and development of this most intriguing class of wind energy machines.

Thank you very much.

WIND ENERGY PROGRAM

MAJOR PROGRAM ELEMENTS

PROGRAM DEVELOPMENT AND TECHNOLOGY

- MISSION/REGION ANALYSIS
- WIND CHARACTERISTICS
- COMPONENT/SUBSYSTEM SR&T
- ADVANCED RESEARCH/CONCEPTS
- ENERGY STORAGE
- ENVIRONMENTAL, LEGAL, AESTHETICS, ETC.

FARM SYSTEMS (UP TO 100 KW)

100-KW SCALE (50 KW TO 250 KW)

MW SCALE (0.5 MW TO 3.0 MW)

MULTI-UNIT SYSTEMS (10 MW TO 100 MW)

Figure 1

DETERRENTS TO WIND ENERGY USE

- CAPITAL COST PER RATED KW
- COST PER KW-HR
  - CAPITAL COST
  - COST OF MONEY
  - SITE WIND CHARACTERISTICS
  - APPLICATION
  - COMPETITION IN LOCATION
- COST PREDICTABILITY
  - UNCERTAIN SYSTEM COSTS
  - SITE WIND PREDICTABILITY

Figure 2

WIND ENERGY SYSTEMS - OTHER DETERRENTS

- NONTRADITIONAL SYSTEM CHARACTER
- AESTHETICS AND PUBLIC ACCEPTANCE
- DISPERSED SYSTEM - LAND USE
- PROOF OF ENVIRONMENTAL IMPACT
- WIND RIGHTS
- INSTITUTIONAL ISSUES

Figure 3

WIND ENERGY MISSION ANALYSIS

WECS RATING VS ENERGY COST

LARGE WECS – 1975 DOLLARS

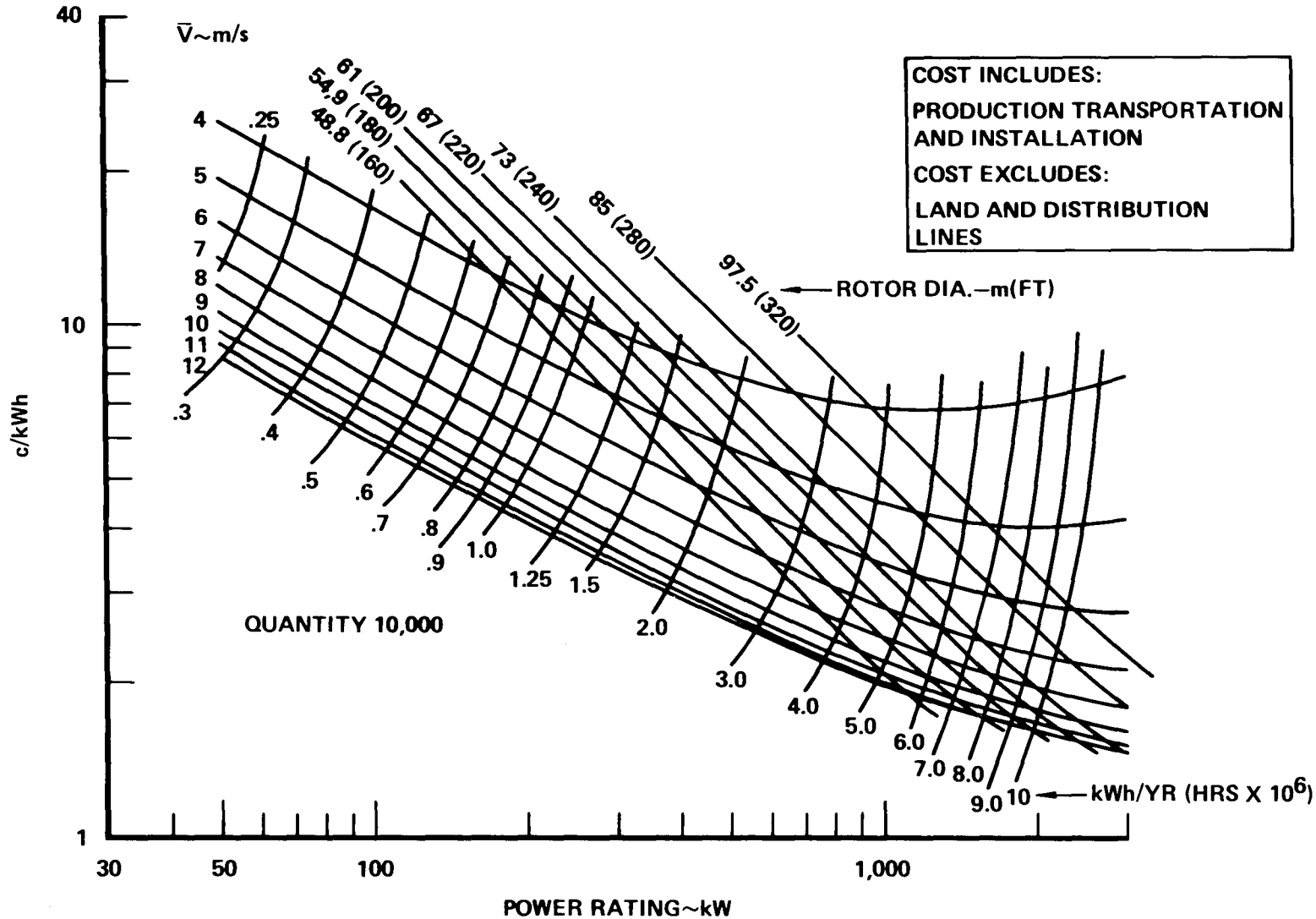

Figure 4.

Figure 5

Large Experimental Wind Turbines - Where We Are Now

Ronald L. Thomas

Lewis Research Center
National Aeronautics and Space Administration
Cleveland, Ohio 44135

Summary

Several large wind turbine projects have been initiated by NASA-Lewis as part of the ERDA wind energy program. The projects consist of progressively large wind turbines ranging from 100 kW with a rotor diameter of 125 feet to 1500 kW with rotor diameters of 200 to 300 feet. Also included is supporting research and technology for large wind turbines and for lowering the costs and increasing the reliability of the major wind turbine components. The results and status of the above projects are briefly discussed in this report. In addition, a brief summary and status of the plans for selecting the utility sites for the experimental wind turbines is also discussed.

Introduction

Wind energy systems have been used for centuries as a source of energy for many applications. These applications have included sailing ships for transportation and windmills for providing mechanical energy. The windmill applications have included the pumping of water, the sawing of wood, the grinding of grain, and more recently the generation of electricity.

The recent national concern over the future availability of energy sources has resulted in the federal government's initiating a program to investigate alternative energy sources. The recently formed Energy Research and Development Administration (ERDA) has been assigned the responsibility for the management of there programs. Among the many alternatives under consideration is the utilization of wind energy. A recently published summary report of the Federal Wind Energy Program (Ref. 1) describes the scope of the federal wind energy program. This federal wind energy program includes several projects for the development of large horizontal-axis propeller-type wind turbines for generating electricity. Under the overall program management of ERDA, the NASA-Lewis Research Center (LeRC) will provide project management for the large horizontal-axis wind turbines projects and the associated supporting research and technology. This report briefly describes the status and results of these several wind energy projects and the plans under way for selecting the utility sites for these first large experimental wind turbines.

Large Experimental Wind Turbines

The large wind turbine phase of the federal wind energy program has several projects, these include:

(1) The 125-foot-diameter rotor 100-kW wind turbine which has been designated Mod-0; this wind turbine became operational on September 4, 1976.

(2) Two 125-diameter-rotor wind turbines of 125 and 200 kW each.

These wind turbines are similar to the Mod-0 and have been designated Mod-0A. These two wind turbines are to become operational in selected utility sites in January and June of 1976.

(3) One or two nominal 200-feet-diameter rotor wind turbines of 1500 kW each. These wind turbines have been designated Mod-1 and are to become operational in selected utility sites in December, 1977, and June, 1978.

(4) A nominal 300-foot-diameter rotor wind turbine with an output of 1000 to 2000 kW. This wind turbine has been designated Mod-2 and is being designed to deliver 1000 kW or more at lower wind speeds than the above wind turbines. This Mod-2 wind turbine is to be operational by the end of 1979.

The planned schedule for these several projects is shown in Fig. 1.

100 kW Mod-0 Experimental Wind Turbine

The 100 kW experimental wind turbine project has been described in several earlier reports (Refs. 2 to 5). The objective of this project is to provide engineering data, as early as possible, for use as a base for the entire wind energy program and to serve as a test bed for improved components and subsystems. To meet this objective a 100 kW wind turbine was designed using current technology and catalog items where possible. Information in previously designed large two-bladed wind turbines was obtained from Hutter (Refs. 6 to 8) and Putnam (Ref. 9). The design, fabrication, and assembly of the 100 kW Mod-0 wind turbine was completed in approximately 18 months with initial operation beginning on September 4, 1976.

Description. The 100 kW wind turbine (Fig. 2) has a two-bladed 125-foot-diameter rotor driving a 100 kW synchronous alternator through a step-up gear box. The rotor is located downwind of the tower and rotates at a constant speed of 40 rpm. The alternator operates at 1800 rpm and delivers 60 Hz three-phase power. Details of the drive train assembly and yaw system are shown in Fig. 3. The wind turbine rotor starts rotating at a wind speed of 5 mph and reaches 40 rpm and begins to deliver power at 9.5 mph. Fig. 4 shows the variation of power output of the wind turbine as a function of wind velocity.

Assembly. The 100 kW wind turbine drive train was assembled at LeRC and tested prior to final assembly at the site. The drive train assembly was tested for 50 hours to make certain all components and subsystems worked satisfactorily (Fig. 5). The drive train assembly was then mounted in the yaw drive system and the rotor hub and blades attached (Fig. 6). In this condition all systems were checked except for rotation of the blades. The blades were then removed and the system was transported to the site for final checkout and assembly.

Final site assembly. The wind turbine was assembled on a test stand near the base of the tower (Fig. 7(a)). After all systems were checked out, the wind turbine was lifted on the morning of September 4, 1976, and assembled and placed on the tower by a crane (Figs. 7(b) and (c)). This operation took approximately 4 hours and went very smoothly.

Test results. Checkout of the wind turbine systems and preliminary operation, performance, and engineering data were obtained over the next several months. Fig. 8 is a plot of predicted blade angle at 40 rpm versus wind speed to obtain 0 kW or 100 kW. Shown in the figure are several test points at 0 kW and 100 kW for different wind speeds; these test points agree fairly well with the predicted values. On December 18, 1976, the wind turbine was operated for the first time at the design conditions of 40 rpm and 100 kW. When electric power is generated by the wind turbine, the wind turbine is connected to a variable resistance load bank. To date, the wind turbine is performing as expected except for larger than expected bending movements at the blade

roots. During testing at wind speeds of 27 mph these bending moments are nearly twice as high as expected. Fig. 9 shows the predicted and actual blade bending moment during one revolution of the blade. Zero degrees is with the blade straight down behind the tower. The expected bending moment was calculated from the MOSTAB helicopter rotor loads computer code modified for wind turbines (Ref. 10). Assuming the tower retarded the wind by 24 percent, the MOSTAB code predicted a cyclic bending moment that varied from -60 000 ft-lb to about 4 000 ft-lb. The actual test data, however, showed the bending moment varying from -120 000 ft-lb to 7 000 ft-lb. The MOSTAB code nearly predicts this larger bending moment if it is assumed the tower retards the wind by 93 percent behind the tower. Analysis and tests are underway to fully understand this problem and to determine ways to reduce the blade bending moments.

Test plans. In addition to understanding the larger than expected blade bending moments planned wind turbine tests include the following:

(1) Full mapping of all operational conditions including failure modes to determine blade, tower and mechanical loads, and wind turbine performance.

(2) Automatic startup and shutdown including synchronization to the local utility network.

(3) Measurement of effects of rotor in downstream winds to determine how close together wind turbines can be spaced.

(4) Monitoring of local television receivers to determine if the wind turbine blades have any effect on reception.

(5) Measurement of tower deflections and rotor noise.

(6) Connecting the wind turbine to a small (100 to 200 kW) diesel electric generator to simulate operation of the wind turbine when connected to a small power system.

Also, the Mod-0 will be used as a test bed for evaluating components developed under the supporting research and technology project such as composite blades and teetered hubs. A teetered hub is a rotor hub that allows the rotor blades to move a few degrees in and out of the plane of rotation to reduce the blade root bending moments.

125 to 200 kW Mod-OA Experimental Wind Turbine Project

The objective of the Mod-OA project is to gain early experience with wind turbines operating in utility networks. In particular we plan to obtain actual utility interface requirements, operations information, and uncover any institutional problems for wind turbines operating in conjunction with a utility network.

To meet this objective, two wind turbines similar to the 100 kW Mod-0 wind turbine but of higher power output are in the process of being fabricated. Both wind turbines have been slightly re-designed to increase their power output from 100 kW at 18 mph to 200 kW at 23 mph. However, the first Mod-OA wind turbine will be initially rated at 125 kW since it utilizes a spare gearbox from the Mod-0 wind turbine to provide a faster schedule. We plan to later replace this 125 kW gearbox with a 200 kW gearbox. Both Mod-OA wind turbines will use 200 kW alternators. The rotor blades for the Mod-OA will be identical to the metal blades in use on the Mod-0 wind turbine.

The Mod-OA towers will be of the steel truss design similar to the Mod-0. The Mod-OA towers, however, are being designed to minimize blockage of the wind and to therefore reduce the effect of tower shadow in the blade bending moment. The Mod-OA towers will utilize a simple cable supported electric personnel lift for access to the top with a simple ladder for use in the event of an emergency in place of the Mod-0 tower staircase.

Although we've already ordered long-lead items, the actual assembly of the wind turbines will be under industrial contract as part of our effect to involve and utilize U. S. industry as fully and effectively as we can. The industrial contracter will final assemble both wind turbines at the selected utility sites and be responsible for checkout and initial operation. The first 125 kW Mod-OA wind turbine is scheduled for final site assembly in January, 1977, and the second for June, 1977.

1500 kW Mod-1 Experimental Wind Turbine Project

The objective of the Mod-1 wind energy project is to involve industry and users in the design and implementation of optimized wind turbines that are capable of supplying electrical power at costs competitive with conventional power sources. Also during the course of this effort, attention will be paid to evaluating the public reaction and/or acceptance of large wind turbines. To meet these objectives the following multi-phased project has been initiated:

(1) Design study contracts

(2) Evaluation of designs and competitive contract preparation

(3) Detail design, fabrication, assembly, and operation contracts

(4) Operation and reporting of performance of experimental wind turbines.

The objectives and plans for these phases of the Mod-1 wind energy project have been fully described in Ref. 1. This report concentrates on the results of the Mod-1 project.

Design study contracts. Two parallel 9 month study contracts were awarded in mid-November, 1974, for the selection and design of minimum energy cost wind turbines. These contracts, at a cost of approximately $500 000 each were awarded to the General Electric Company and the Kaman Aerospace Corporation. The contract scope was limited to the study of horizontal-axis, propeller type wind turbines that could produce electric power acceptable for utility grids. The effort encompassed four major tasks (Fig. 10) which included conceptual design; parametric analysis; preliminary design and definition of utility interface requirements.

The contractors evaluated a number of candidate configurations for wind turbines. Fig. 11 summarizes the various trade-off considerations. After initial cost studies, both contractors independently concluded that for minimum energy cost the wind turbine should have a variable-pitch constant-speed two-bladed rotor operating downwind of the tower; and the rotor should drive a synchronous or induction alternator through a conventional step-up gearbox (Fig. 12). The early results of these studies obtained by Kaman were summarized by Meier in a paper presented at the American Helicopter Society in May, 1975 (Ref. 11).

During the parametric and optimization task, capital and energy costs were determined for a range of wind turbines optimized for minimum energy cost (¢/kW hr). The wind turbines analyzed range from 50 kW to 3000 kW. NASA furnished wind velocity duration curves (Fig. 13) were used for all energy calculations in the design studies. It was assumed that the wind velocity is defined at an elevation of 30 feet.

The results of the parametric and optimization task for the two contracts are shown as solid lines in Fig. 14 for energy costs (¢/kW hr) as a function of median wind speed and rated wind turbine power. These curves represent a wind turbine optimized for lowest energy cost for that specific median wind speed. For comparison purposes, generation cost for power in the U. S. today generally falls in the 0.1 to 5¢/kW hr range. These curves indicate that wind turbines could be competitive today with some existing power generation systems.

Both studies show that at each medium wind speed the energy costs are higher at the lower power levers over the range studied. The GE study shows that energy costs continue to go down very slowly with increased power level for all medium wind speeds. The Kaman studies show, however, a bottoming effect to the curves with energy costs increasing as power levels go above approximately: (1) 700 kW at 12 mph, (2) 800 kW at 15 mph; and (3) 1500 kW at 18 mph. The fact that one curve has a minimum while the other continues to slowly decrease is primarily due to the difference in assumptions used for the rotor costs as the diameter goes up.

The energy costs for the parametric studies shown in Fig. 14 differs by up to a factor of two. These were early studies and are based on the conceptual design results. Later in the program as the preliminary design studies at 1500 kW and 500 kW were completed, the cost differences between the two studies come closer together with the Kaman energy costs decreasing and the GE costs increasing. The cost estimates resulting from the preliminary designs are shown as data points (+) for each of the designs in Fig. 14. These later energy costs were calculated using the estimated capital costs, energy capture and the yearly rate of charge for money, operation, maintenance, taxes, etc. The GE study uses a rate of approximately 0.16/year while Kaman used approximately 0.20/year. This difference also accounts for a major difference between the energy cost results of the earlier parametric studies shown by the solid lines in Fig. 14. To compare the energy costs from both studies, the 0.16/year rate was used to calculate energy costs for each wind turbine preliminary design and these energy costs are shown as data points (+) on Fig. 14. The following equation was used for calculating energy cost:

$$\frac{¢}{\text{kW-hr}} = \frac{(\text{Total capital cost}) \times (0.16/\text{yr})}{(\text{kW-hr})/\text{yr}}$$

Referring to Fig. 14 it can be seen that the energy cost estimates for the Kaman 500 kW and 1500 kW design are 5.5 ¢/kW-hr and 2.0 ¢/kW-hr, respectively, while the energy cost estimate for the GE 500 kW and 1500 kW designs are 4.2 ¢/kW-hr and 1.7 ¢/kW-hr, respectively.

In addition to minimum energy cost there is also the question of the wind turbine plant factor. Plant factor (PF) is defined as the ratio of the energy the wind turbine will deliver over a year for mean wind speed to the amount of energy it would generate in a year if it operated at rated power continuously.

$$PF = \frac{\text{Generated annual-kW hr}}{\text{Rated kW} \times 8760 \text{ hr}}$$

Plant factor gives an indication of how effectively a wind turbine is being utilized. High plant factor wind turbines generally have large rotors in comparison to their rated power output or alternator size and thereby operate more hours at rated output. However, wind turbines with high plant factors will not necessarily generate the lowest cost energy. High PF wind turbines generally capture more energy but are also more expensive to build because of the larger rotors.

The selection of a minimum energy cost wind turbine versus a wind turbine with a higher PF is definitely an issue that depends on how the wind turbine is to be used. If the application can use bulk energy whenever it is available, then the minimum energy cost design is preferred. If energy storage is needed, then the higher plant factor wind turbine probably will result in the best overall systems choice. This option is clearly dependent on the resultant user's application.

Before selecting the wind turbine sizes and the mean wind speeds for preliminary design, the following question was addressed: How sensitive to mean wind speed is an optimized design? That is, given an optimized design of, say, 1500 kW for an 18 mph site, what is the effect on energy costs of putting this design on sites with a mean wind speed of 15 mph or 21 mph. Studies were conducted by both contractors to answer this question. The results of these studies for a 500 kW wind

turbine, 12 mph mean wind speed site and a 1500 kW wind turbine, 18 mph mean wind speed site are plotted in Fig. 15.

Significantly, the results show that for less than 10 percent increase in energy costs the wind turbine designed for 500 kW at 12 mph can be used at sites with 9 to 15 mph and the 1500 kW design can be used at sites with 15 to 21 mph wind. Thus it appears that the two designs could be used for a relatively wide range of sites with only a small penalty in energy cost.

From the results of the parametric study and optimization tasks, two designs were selected for further definition during the preliminary design task; 500 kW at 12 mph and 1500 kW at 18 mph. The conceptual, and parametric analysis studies were performed to obtain the minimum energy cost wind turbine designs. However, in the final selection attention was paid to plant factor and the designs selected were slightly off optimum to take advantage of higher plant factors at increase in energy cost of only a few percent. The capital cost of these higher plant factor wind turbines is greater but because more energy is generated, the resulting energy costs are nearly those of the minimum energy-cost design.

Table I summarizes the results of the 500 kW and 1500 kW wind turbine designs for each of the contractors. Figs. 16 and 17 show the artist concepts for the GE and Kaman wind turbine designs.

In addition to determining the optimum wind turbine designs, a major task of the design studies was to determine the interface requirements for connecting wind turbines to typical utility grids. These interface requirements included items such as required electrical interface switchgear, automatic protection and controls and required operation and maintenance procedures. Fig. 18 summarizes the interface requirements. Fig. 17 identifies some of the operational and institutional issues considered. These studies show no interface or institutional problems that pose major barriers to the installation of wind turbines on utility grids.

This paper does not summarize all the results of the four design study tasks but has only discussed the major results. The two final contractor reports will contain all the information determined from the two parallel design studies.

Fabrication, assembly, and initial operation contact. A competitive request for proposals (RFP) is planned to be issued in the spring of 1976 for the detail design, fabrication, assembly, and initial operation of a 1500 kW wind turbine. The specifications for this wind turbine were determined from the design study contacts with some specifications left as optional. We plan to have this contractural effort under way during the summer of 1976 and to have the 1500 kW wind turbine assembled and ready for initial operation by December, 1977. A decision to build a second wind turbine will depend on proposed costs and funding available. The utility sites for these two wind turbines will be selected according to the plan described later in this paper.

1000 to 2000 kW Mod-2 Experimental Wind Turbine Project

The object of the Mod-2 project is to develop large wind turbines that can generate low-cost electricity when operating at sites that have median wind speeds near 12 mph. Preliminary designs of these wind turbines indicate that rotors of approximately 300 feet in diameter are required for optimized wind turbines at the 12 mph median wind sites. The present federal wind energy plan calls for the operation of the first of these large wind turbines to occur near the end of 1979. At the present time the plans and procurement packages for the design. fabrication, assembly, and initial operation of such a wind turbines are being prepared.

Supporting Research and Technology

In parallel with the large wind turbine projects, a supporting re-

search and technology project (SR&T) has been implemented. The objective of this project is to reduce the costs of wind turbine components and subsystems, simplify the overall designs, and to make the wind turbines more reliable.

Rotor Systems

Low-cost rotor blades. The major emphasis of the SR&T project is directed toward reducing the costs of the rotor systems. The Mod-0 and Mod-1 projects have clearly shown that the rotor systems offer the greatest potential for reducing costs. Several tasks have been initiated to explore low-cost technologies for manufacturing rotor blades, these include: (1) the design and fabrication of filament wound composite blades for the Mod-0 wind turbine; (2) the investigation of prestressed materials such as concrete and the use of variable density urethanes; (3) low-cost methods of fabricating all metal blades similar to the present Mod-0 blades.

Large rotor blades. Another major effort of the SR&T project is directed toward the fabrication of large blades, nominally 150 feet, for the future large Mod-2 wind turbines. A major task will be initiated in 1976 for the analysis, design, fabrication, and ground testing of a nominal 150 foot rotor blade.

Rotor hubs and blade pitch controls. The SR&T project also contains tasks for the investigation of low-cost, reliable hubs. These tasks include the analysis, design, fabrication, and testing of selected hubs in the Mod-0 wind turbine. One hub under consideration is a teetered hub that allows the two blades to move in an art-of-the-plane of rotation. Such a system is expected to reduce the blade bending moments and result in lower-cost and/or longer life blades. The advantages of a teetered hub have been reported by Spera (Ref. 10). A three-bladed hub is also under consideration as well as other hubs and methods of blade attachment for possible tests on the Mod-0 wind turbine. The purpose of the three-bladed tests would be to experimentally quantify the difference in loads between two-bladed and three-bladed wind turbines. Such test results may be important as the wind turbine program is directed toward progressively larger wind turbines to take advantage of the many available lower wind speed sites.

Towers

The Mod-0 100 kW wind turbine has a steel truss tower similar to many of the utility transmission towers. The Mod-1 design studies investigated steel shell and concrete towers in addition to the steel truss towers. The design studies showed that the steel shell and concrete towers could compete with the truss tower economically if they were produced in sufficient quantity and if favorable soil conditions existed. These alternate towers appear to most persons to be more esthetically pleasing than the truss towers and will be investigated as well as other designs that show promise in futher detail under the SR&T project.

Other Components

In addition to the rotor systems and the towers, other major wind turbine components and subsystems will also be investigated under the SR&T project. These include the gear boxes, the alternators, the electric control systems, and the yaw systems for orienting the rotor into the wind. As particular components and subsystems show promise for simpler and/or lower cost wind turbines, they will be tested in the field on the Mod-0 wind turbine. The Mod-0 wind turbine is designed to serve the wind energy program as a test bed for obtaining the necessary engineering and operation data for evaluation of promising components and subsystems.

Utility Site Selection

In parallel with the design and fabrication projects a plan has

been developed for selecting sites for the Mod-OA and Mod-1 wind turbines.

Background. To initiate the site selection action inquiries were sent in 1974 to many of the utility companies in the United States. These inquiries briefly described the wind energy program and asked the utility companies if they were interested in participating in the program. A meeting was held at the LeRC in December, 1974, with approximately 40 representatives of 30 utility companies. At this meeting the wind energy program was described and a proposed plan presented for site selection and the degree of involvement of the utilities. Since the December, 1974, meeting, additional utilities have expressed interest in possible participation. In December, 1975, ERDA sent a second invitation, this time to all the utilities listed in the Electrical World Directory. To date, a total of 63 utilities have indicated an interest in possible participation in the Mod-OA and Mod-1 wind turbine experiments. Fig. 20 shows the locations of these utilities.

Site selection plan. A plan has been developed for selecting utility sites for the first experimental wind turbines. This plan in the form of a Request for Proposals (RFP) will be mailed out in the spring of 1976, to all the utility companies that have indicated an interest in possible participation in the program. The utility companies will have 6 weeks in which to return proposals describing their proposed wind turbine sites. The sites will be evaluated by an ERDA/NASA team with the final selections made by ERDA. ERDA plans to select a minimum of 12 sites. These sites will be selected primarily to maximize the amount of information for the wind energy program and for the whole utility industry. In addition, the following site factors and variables are considerations for the 12 site selection:

Wind energy available at the site

Utilities utilization of variable wind power

Mode of power generation, the wind turbine will interface with, hydro, steam, diesel, etc.

Size of utility company and network

Cost of competitive power

Geographical location and environment

Project visibility to assess public reaction

Site meteorological data. The government plans to install towers and instrumentation in each of the 12 sites selected to measure the site wind data. The towers will be 165 feet tall and will have annemometers and wind direction sensors at two altitudes. The towers, instrumentation, and recording equipment will be installed and serviced by a government contractor. The utility companies will be expected to install the meteorological tower foundations and to check the towers and recording equipment on a regular basis. The data from the towers will be recorded automatically, but it is to be collected by the utilities regularly and mailed to the government contractor. The contractor will be responsible for all reduction of meteorological data and for preparing summary reports for each of the sites. It is expected that the meteorological tower will be similar to the tower now being used at the 100 kW wind turbine site at Plum Brook (Fig. 21).

Mod-OA and Mod-1 wind turbine sites. The sites for the Mod-OA and Mod-1 wind turbines will be selected from the above 12 sites. These sites will be selected based on the results of the wind data and the other considerations listed above. The sites will be selected as needed to allow time for site preparation prior to final assembly of the wind turbines at the sites. The planned schedule for the site situations is shown in Fig. 22. When a wind turbine site is selected, the plan calls for both the government and the utility to provide some

items. The government is to supply at no cost to the utilities the following major items:

(1) The wind turbine and its foundation

(2) All necessary controls, instrumentation, and recording equipment

(3) NASA and NASA contractor personnel for installation, checkout, maintenance, and general support during the 2 years of operation.

The utilities will be asked to provide the following at no cost to the government:

(1) The site on which the wind turbine is to be located

(2) Site preparation including an access road, control room, security fencing, and necessary electrical interface equipment

(3) Personnel to interface with NASA and the NASA contractor during site preparation, final assembly and checkout, and personnel for operation and routine maintenance of the wind turbine for up to 2 years.

Concluding Remarks

Several large wind turbine projects have been initiated by NASA-Lewis as part of the ERDA wind energy program. This paper has briefly discussed the results and status of these projects.

1. A 100 kW experimental wind turbine was assembled in September 4, 1975, at the NASA Plum Brook site Sandusky, Ohio. The wind turbine achieved rated power of 100 kW at 18 mph and 40 rpm in December 18, 1975. The wind turbine has been undergoing experimental testing to obtain engineering data over the full operation range. The wind turbine has been performing as expected except for some larger than expected blade bending moments. These blade bending moments appear to be the result of the wind retardation caused by tower blockage. Analysis and tests are underway to understand and reduce these bending moments. To date, the WT has been operated into a variable resistance load bank. Tests for operating the wind turbine connected to the local utility network are planned for early 1976. Additional tests are planned for determining wind velocity retardation through the tower, TV interference from rotor blades and tests to determine the effects of the rotor in the winds downstream of the rotor. This latter test is needed to determine how close together wind turbines can be placed without seriously reducing these power outputs.

2. Two wind turbines of similar design to the Mod-0 are under fabrication for operation in utility networks. The objective of these upgraded Mod-0 wind turbines (Mod-OA) is to obtain early operating experience with utilities. These two machines are scheduled for initial operation in January and June of 1977. The sites are to be selected in the summer and winter of 1976.

3. Preliminary design studies for the Mod-1 wind turbines have been completed. These studies concluded that a constant rpm two-bladed rotor located downwind of the tower with the drive train assembly and alternator located on the top of the tower provides the lowest cost wind turbine designs. The studies showed that an optimized 1500 kW wind turbine operating on a site with a median wind speed of 18 mph could generate electricity at 1.7 to 2.0 ¢/kW hr if these wind turbines were produced in quantities of 100 a year or greater. The studies also showed that a wind turbine optimized for an 18 mph site could be operated on a site with a median wind speed of 15 mph with an increase in energy cost of only 10 percent over that of a wind turbine optimized for the 15 mph site. A request for procurement has been advertized for the detail design, fabrication, assembly, and initial operation of one

or two nominal 200 foot diameter rotor 1500 kW wind turbines. These wind turbines are planned for installation in December, 1977, and June, 1978, on utility sites to be selected.

4. A program plan is presently being prepared for the design, fabrication, assembly, and installation of a nominal 300 foot diameter rotor Mod-2 1000 kW wind turbine. This wind turbine will be designed to produce low-cost electricity at the many lower wind speed sites available in the United States.

5. A supporting research and technology (SR&T) project has been initiated to develop the technology for large low-cost wind turbines. The major efforts of the SR&T project are directed toward the rotor system. The Mod-0 project and Mod-1 design studies showed that the rotor system is the highest cost subsystem of the wind turbine. Contracts for composite blades, and pre-stressed concrete, and urethane model blades have been initiated to investigate low-cost blade technology. Also, a task to design, fab, assemble, and test a large 150 foot blade (300 ft/rates) are underway. In addition, to rotor blades, tasks for reducing the costs of towers, drive train assemblies, and the major subsystems are underway.

6. Plans for selecting utility sites for large experimental wind turbines are well underway. An ERDA invitation for participation in the program was sent in December, 1975, to all the utilities in the U.S. listed in the Electrical World Directory. A request for proposals was sent by ERDA in March, 1976, soliciting proposed wind turbine sites from the 63 utilities that have expressed interest in participating in the program. Twelve or more candidate sites are to be selected in the early summer of 1976. These 12 sites will be supplied with government installed meteorological towers instrumentation and data recording equipment for determining the site wind data. The sites for the early experimental wind turbines will be selected from these sites.

References

1. "Federal Wind Energy Program," Energy Research and Development Administration Report ERDA-84, 1975.

2. R. Thomas, et al, "Plans and Status of the NASA-Lewis Research Center Wind Energy Project," NASA TM X-71701, 1975.

3. R. L. Puthoff and P. J. Sirocky, "Preliminary Design of a 100 kW Wind Turbine Generator," NASA TM X-71585, 1974.

4. R. L. Puthoff and P. J. Sirocky, "Status Report of 100 kW Experimental Wind Turbine Generator Project," NASA TM X-71758, 1975.

5. R. E. Donham, J. Schmidt, B. S. Linscott, "100 kW Hingeless Metal Wind Turbine Blade Design, Analysis and Fabrication," American Helicopter Society, Preprint No. S-998, 1975.

6. U. Hutter, "Operating Experience Obtained with a 100-kW Wind Power Plant," NASA TT-F-15, 068, 1973.

7. U. Hutter, "Influence of Wind Frequency on Rotational Speed Adjustments of Windmill Generators," NASA TT-F-15, 184, 1973.

8. U. Hutter, "The Development of Wind Power Installations for Electrical Power Generation in Germany," NASA TT-F-15, 050, 1973.

9. P. C. Putnam, "Power from the Wind," D. Van Nostrand Co., Inc., 1948.

10. G. A. Hoffman, "Basic Methodology for the Modular Stability Derivative Program (C-version)," Mechanics Research Inc. Report 4343-2, 1970.

11. R. C. Meier, "Concept Selection and Analysis of Large Wind Generator Systems," presented at the 31st Annual National Forum of the American Helicopter Society, Washington, D.C., May 1975.

12. D. A. Spera, "Structural Analysis of Wind Turbines Rotors for NSF-NASA MOD-O Wind Power Systems," NASA TM X-3198, 1975.

TABLE I. - RESULTS OF PRELIMINARY DESIGN TASK FOR 500 kW AND 1500 kW Mod-1 WIND TURBINES

	500 kW		1500 kW	
	GE	Kaman	GE	Kaman
Mean Wind Speed	12	12	18	18
Rated Power, kW	500	500	1500	1500
Rated Wind Speed, mph	16.3	20.5	22.5	25
Energy Capture, kW-hr/yr	1.88×10^6	1.3×10^6	6.6×10^6	5.7×10^6
Rotor Diameter, ft	183	150	190	180
Rotor Solidity, %	3	3	3	3
Rotor Speed, rpm	29	32.3	40	34.4
Energy Cost, ¢/kW Hr[a]	4.2	5.5	1.7	2.0
Capital Cost, $/kW	974	901	449	481
Wind Turbine Cost, $	486 000	450 670	674 000	720 800
Plant Factor	0.42	0.29	0.51	0.43

[a]Assumed 16 percent of capital costs per year for interest, operations, maintenance, taxes, etc.

OPERATION DATES

CY	75	76	77	78	79
100 kW MOD-0	▽				
125 kW MOD-0A			▽		
200 kW MOD-0A			▽		
1500 kW MOD-1			▽	▽	
1000 kW MOD-2					▽

Figure 1. - Schedule - large experimental wind turbines.

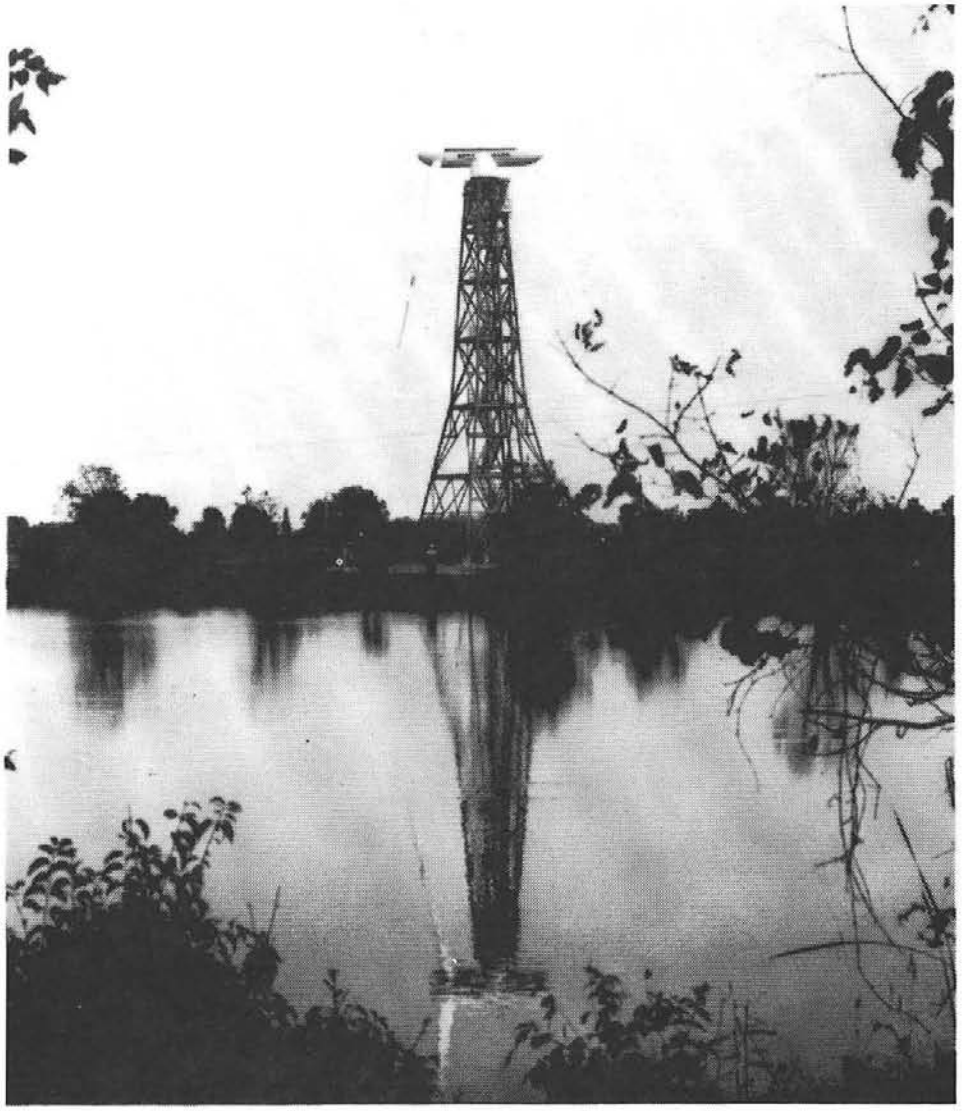

Figure 2. - ERDA/NASA 100 KW experimental wind turbine.

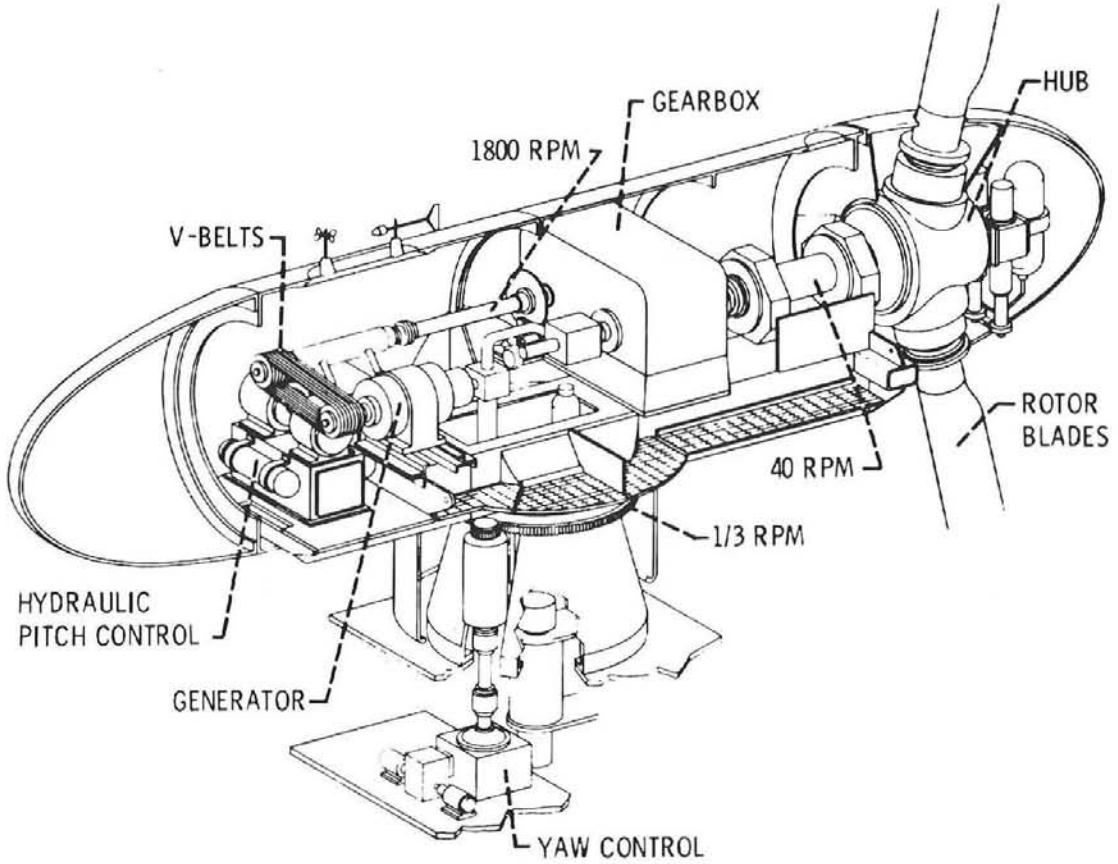

Figure 3. - 100 kW wind turbine drive train assembly and yaw system.

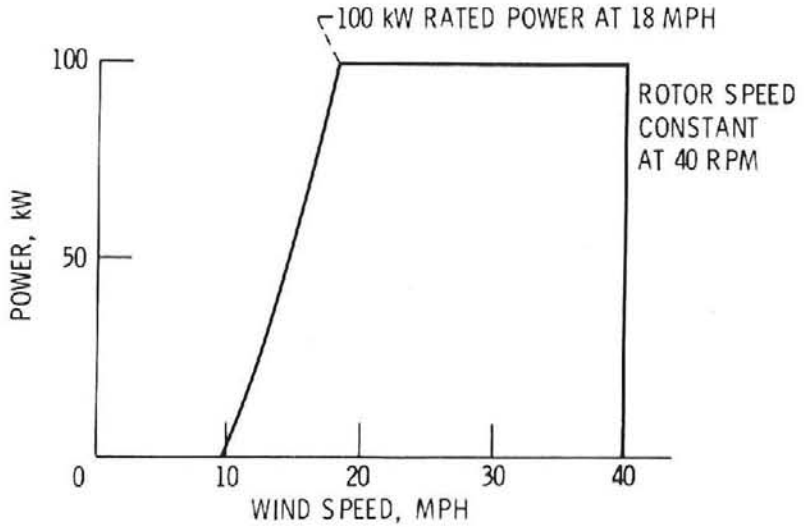

Figure 4. - Power out versus wind speed for the 100 kW wind turbine.

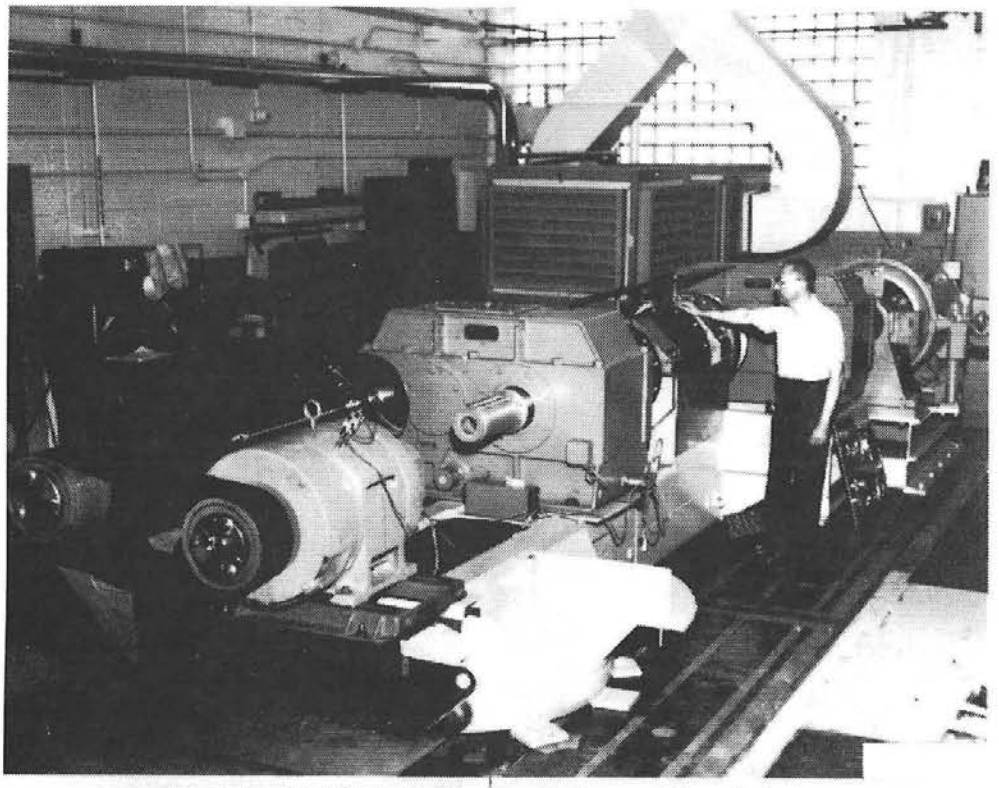

Figure 5. - 100 KW Wind turbine power train assembly under test.

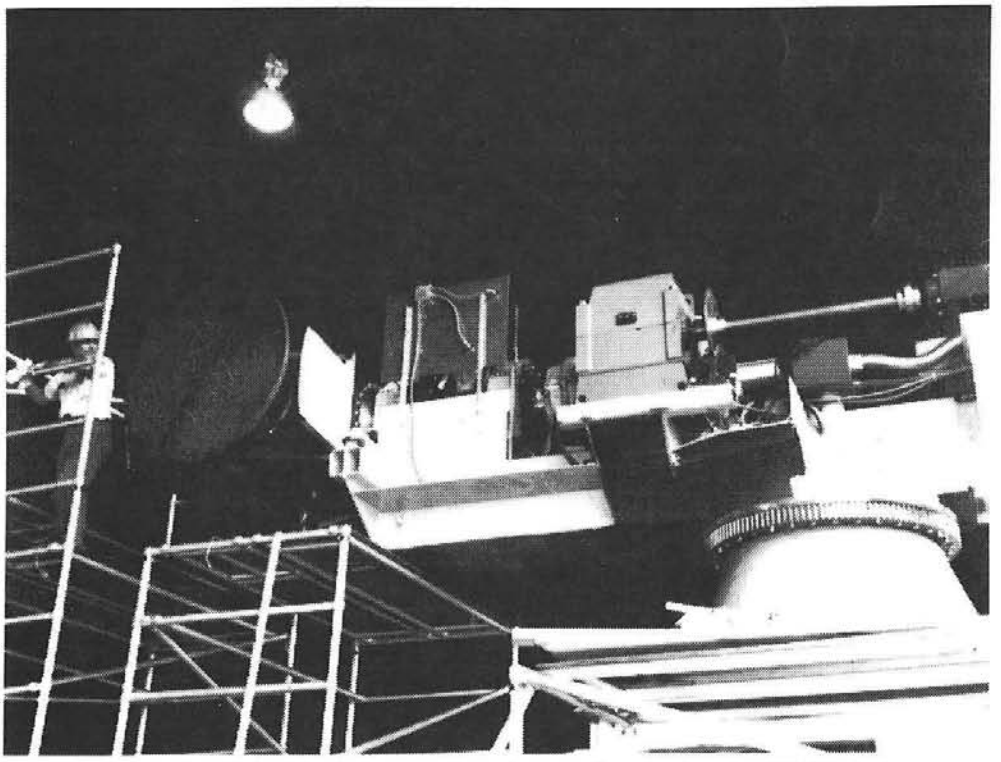

Figure 6. - Hub, drive train assembly and rpw system checkout for 100 KW wind turbine.

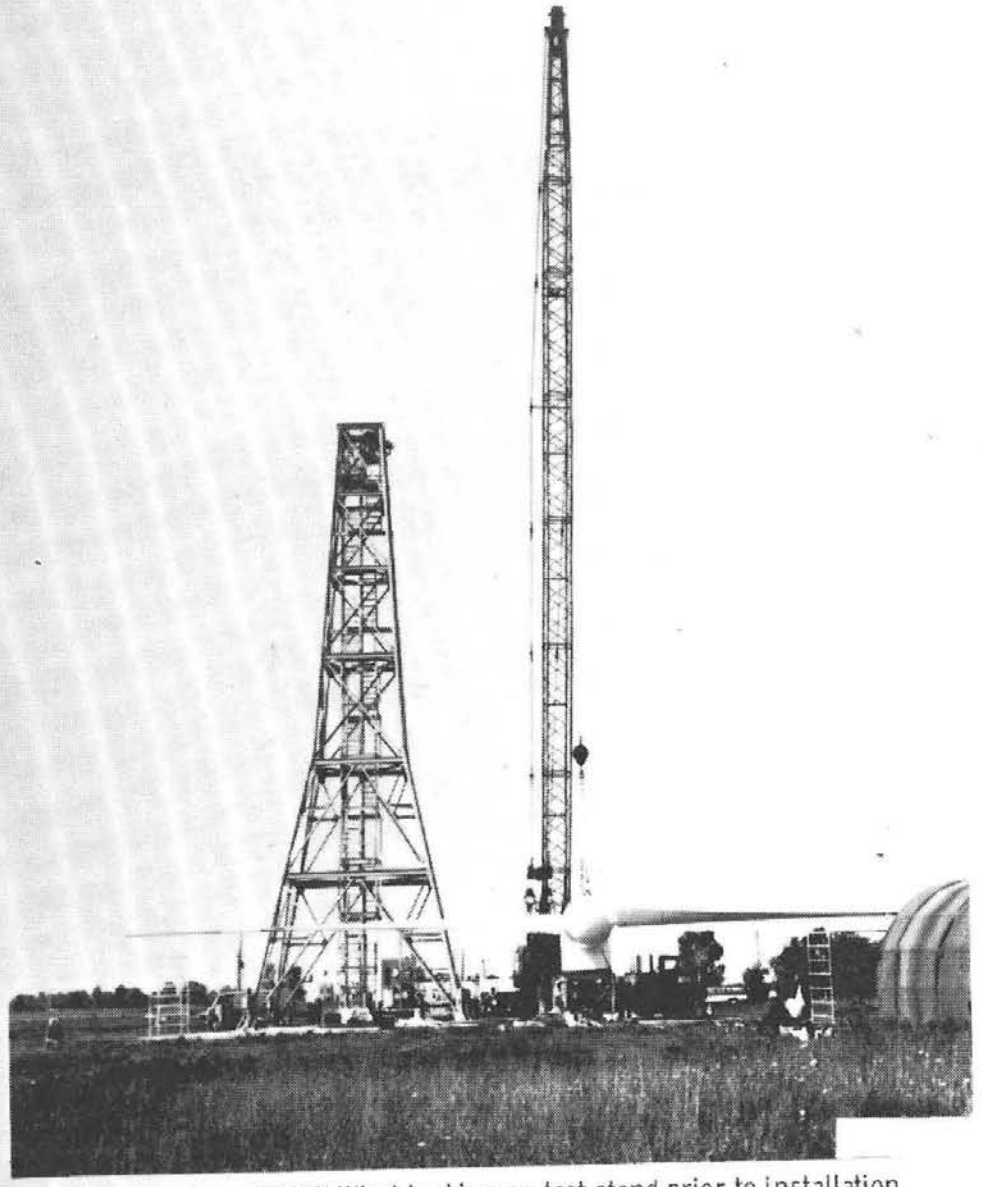

Figure 7(a). - 100 KW Wind turbine on test stand prior to installation.

Figure 7(b). - 100 KW Wind turbine being lifted to top of tower.

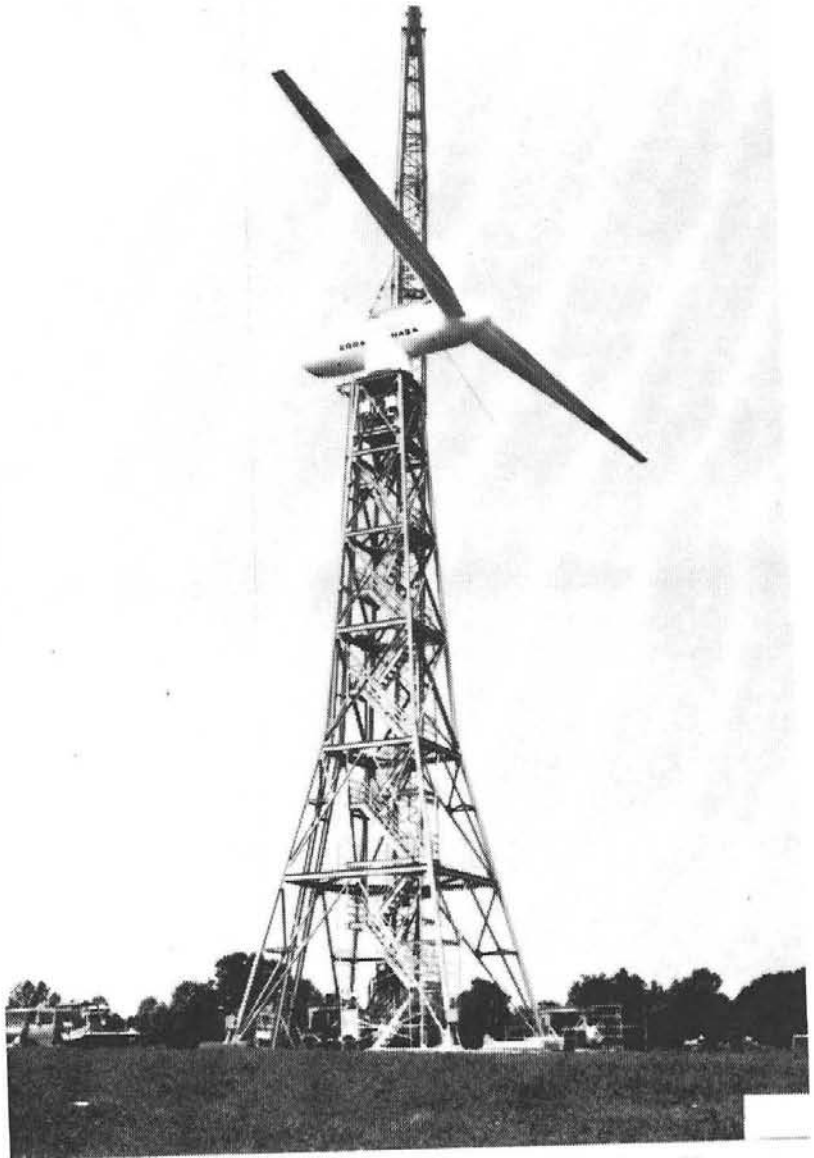

Figure 7(c). - 100 KW Wind turbine installed in top of tower.

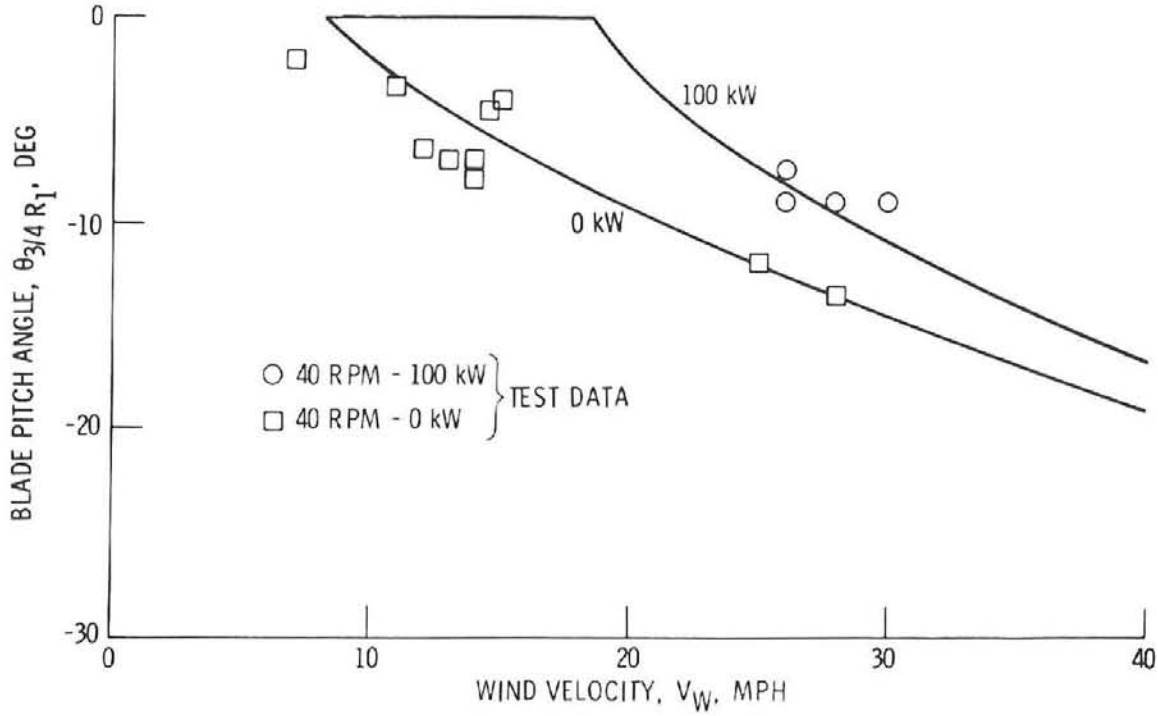

Figure 8. - Mod-0 blade pitch angle schedule.

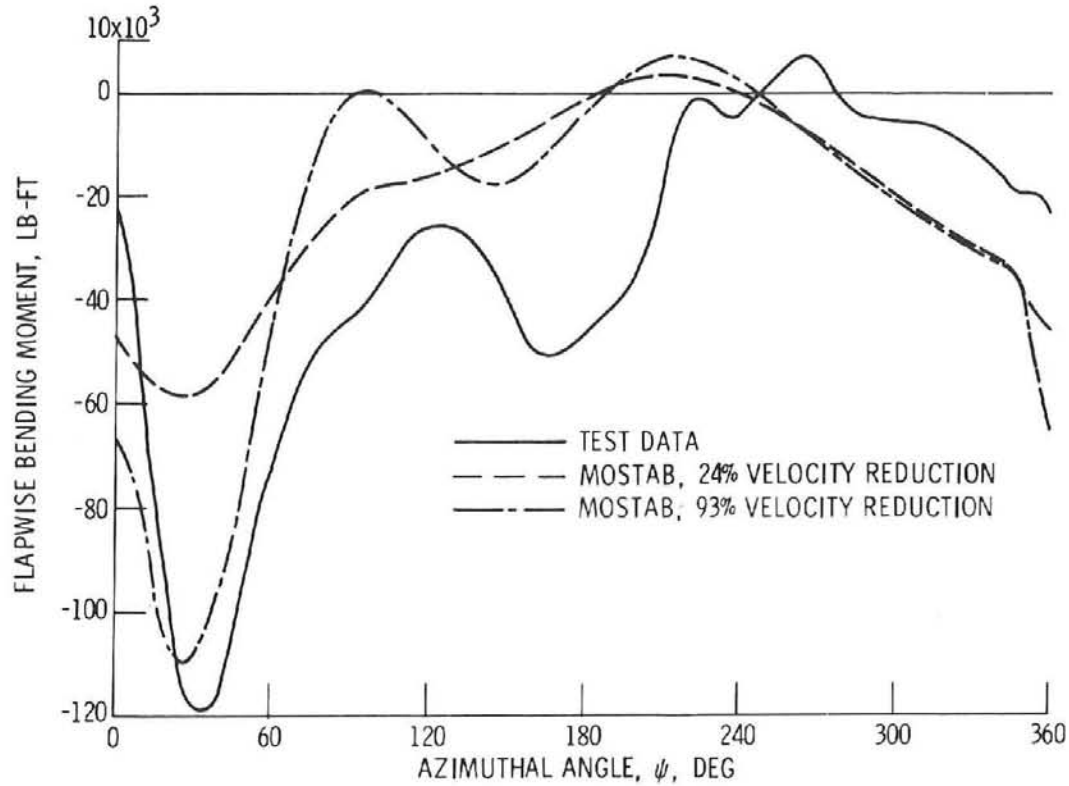

Figure 9. - Blade load comparison for MOSTAB predictions vs. test data. 40 rpm, 100 kW, $\theta_P = -8^0$, $V_{WIND} \cong 27$ mph.

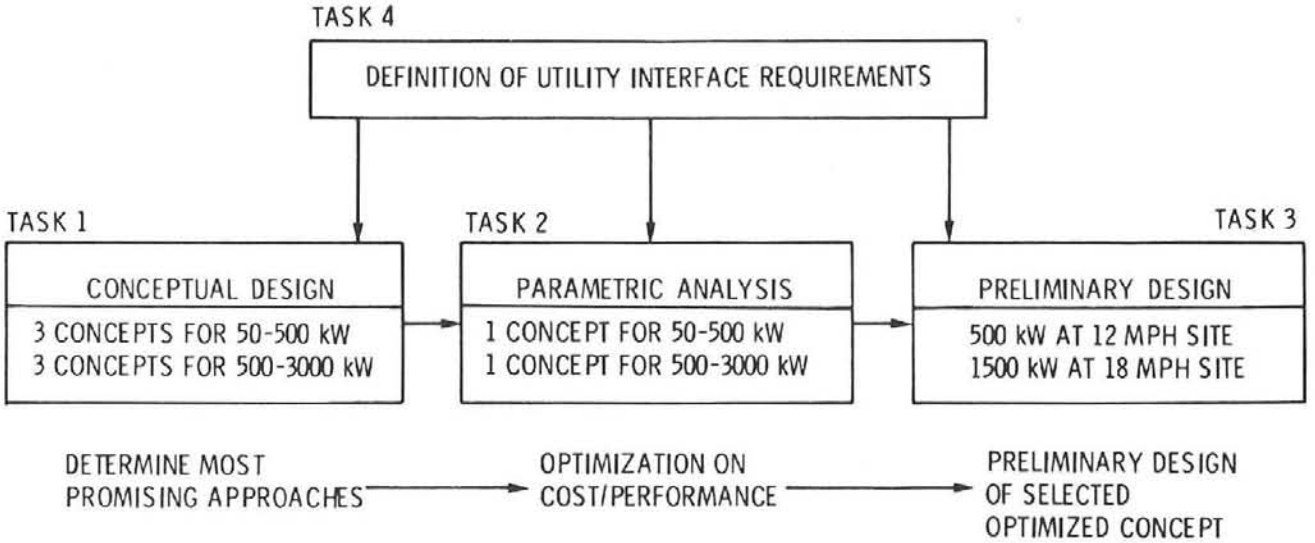

Figure 10. - Wind turbine design study tasks.

ROTOR

- CONSTANT OR VARIABLE SPEED
- DIAMETER
- NUMBER OF BLADES
- TWIST, TAPER, AIRFOIL
- FIXED PITCH, VARIABLE PITCH
- UPWIND OR DOWNWIND OF TOWER

TOWER

- OPTIMUM HEIGHT
- TYPE - TRUSS, GUYED POLE, SHELL, CONCRETE

MECHANICAL TRANSMISSION

- GEAR BOX (FIXED OR VARIABLE RATIO)
- CHAIN DRIVE, BELT AND PULLEYS

GENERATOR

- SYNCHRONOUS, INDUCTION, DC

Figure 11. - Mod-1 wind turbine tradeoff considerations.

ROTOR

TWO BLADED
CONSTANT RPM (PITCH CONTROL)
RIGID HUB
TWIST, TAPER (STILL OPTION)
DOWNWIND OF TOWER

TOWER

TRUSS, SHELL, CONCRETE

MECHANICAL TRANSMISSION

GEAR BOX (FIXED RATIO)

GENERATOR

SYNCHRONOUS (INDUCTION IS AN OPTION)

LOCATE MAJOR EQUIPMENT ON TOP OF TOWER

Figure 12. - Mod-1 wind turbine study results.

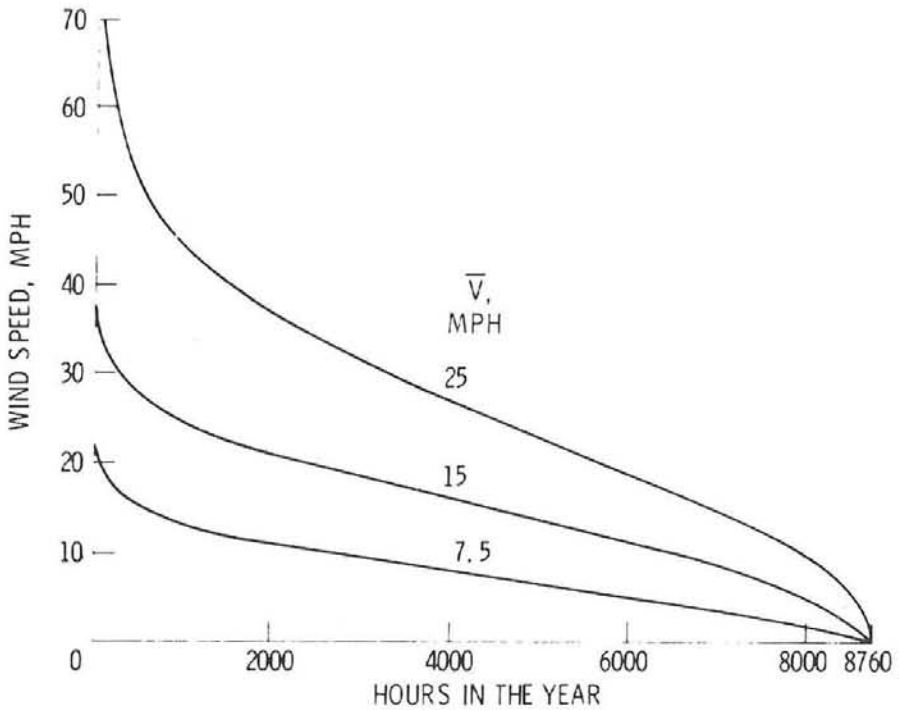

Figure 13. - NASA furnished wind velocity duration curves (30 ft elevation).

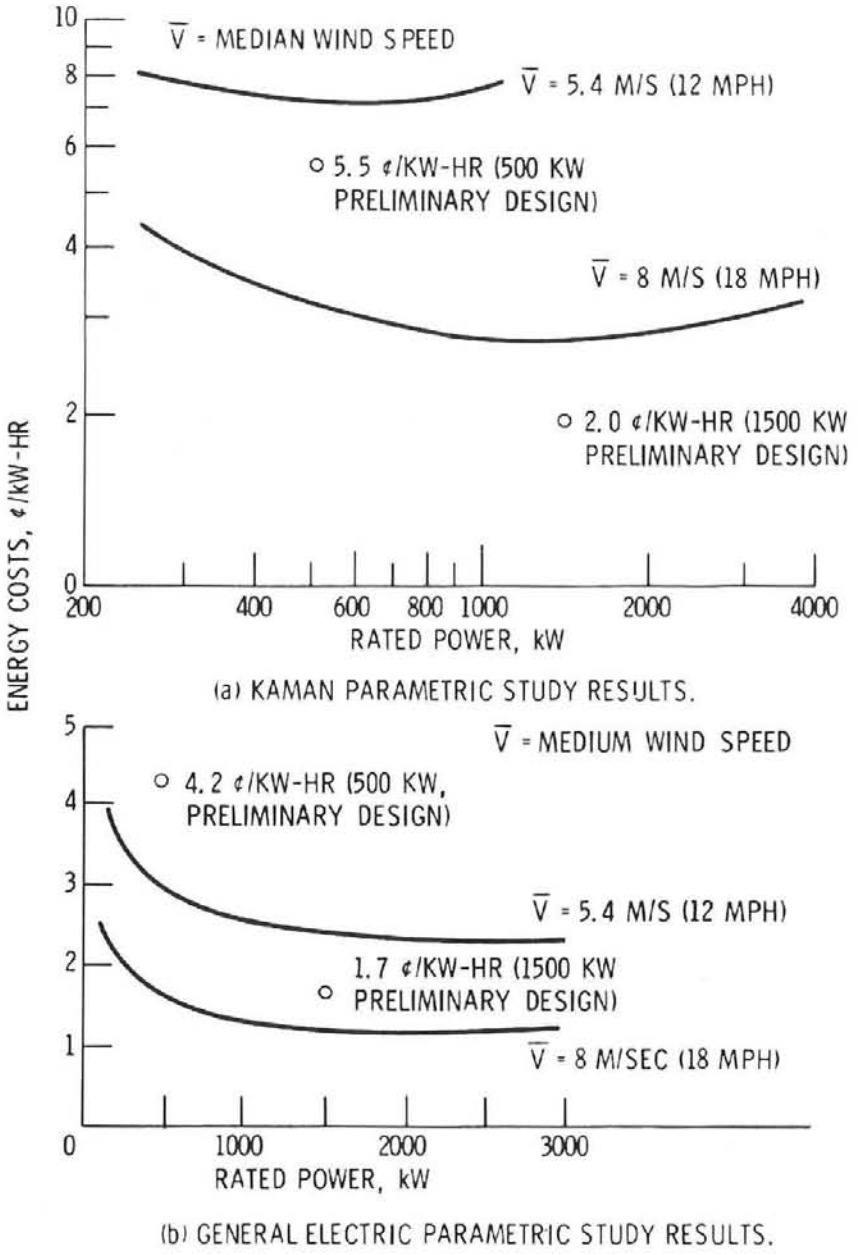

Figure 14. - Wind turbine energy costs as a function of median wind speed and rated power.

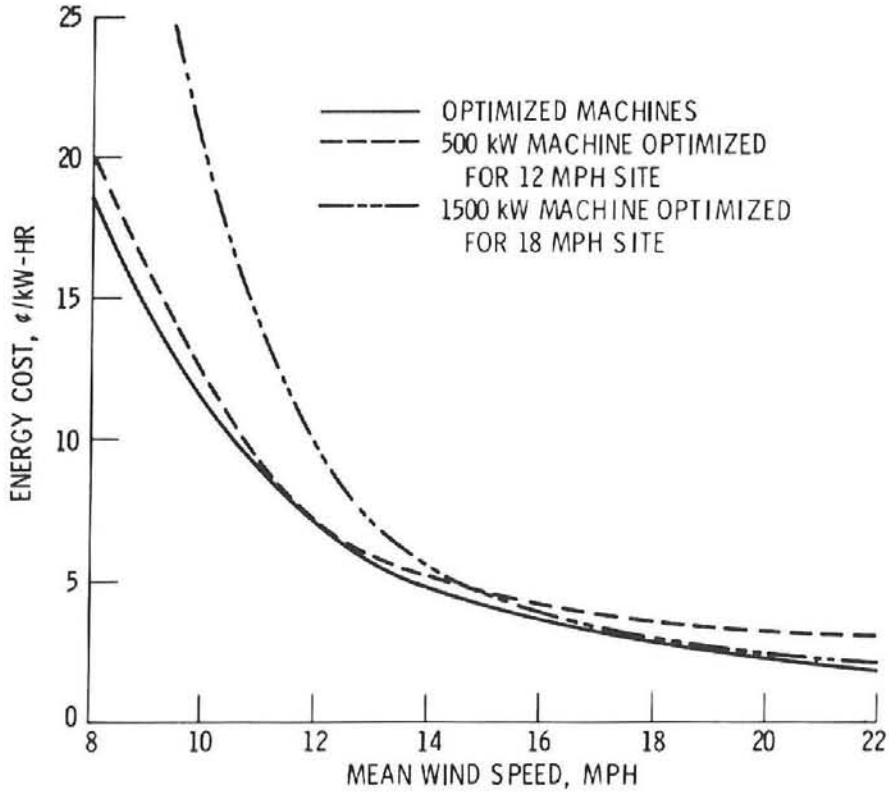

Figure 15. - Effect of siting-12 and 18 mph optimized machines located in various wind regimes.

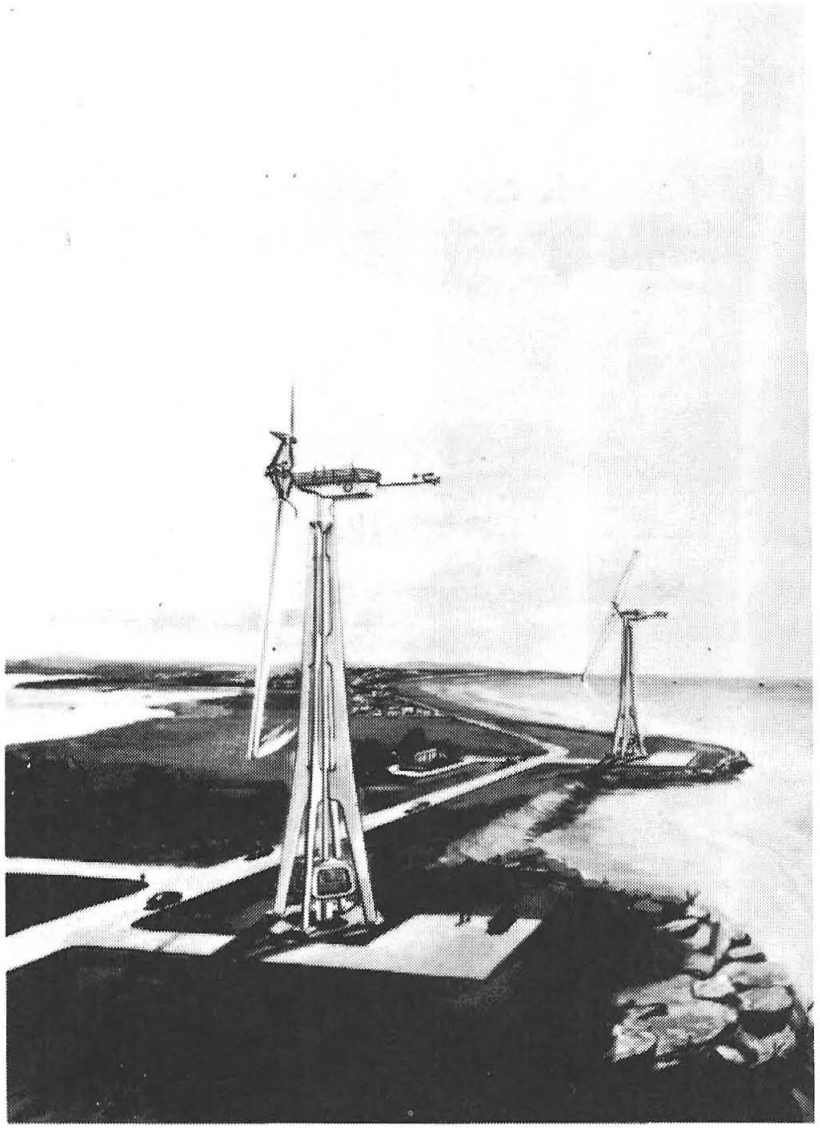

Figure 16. - GE 1500 KW wind turbine.

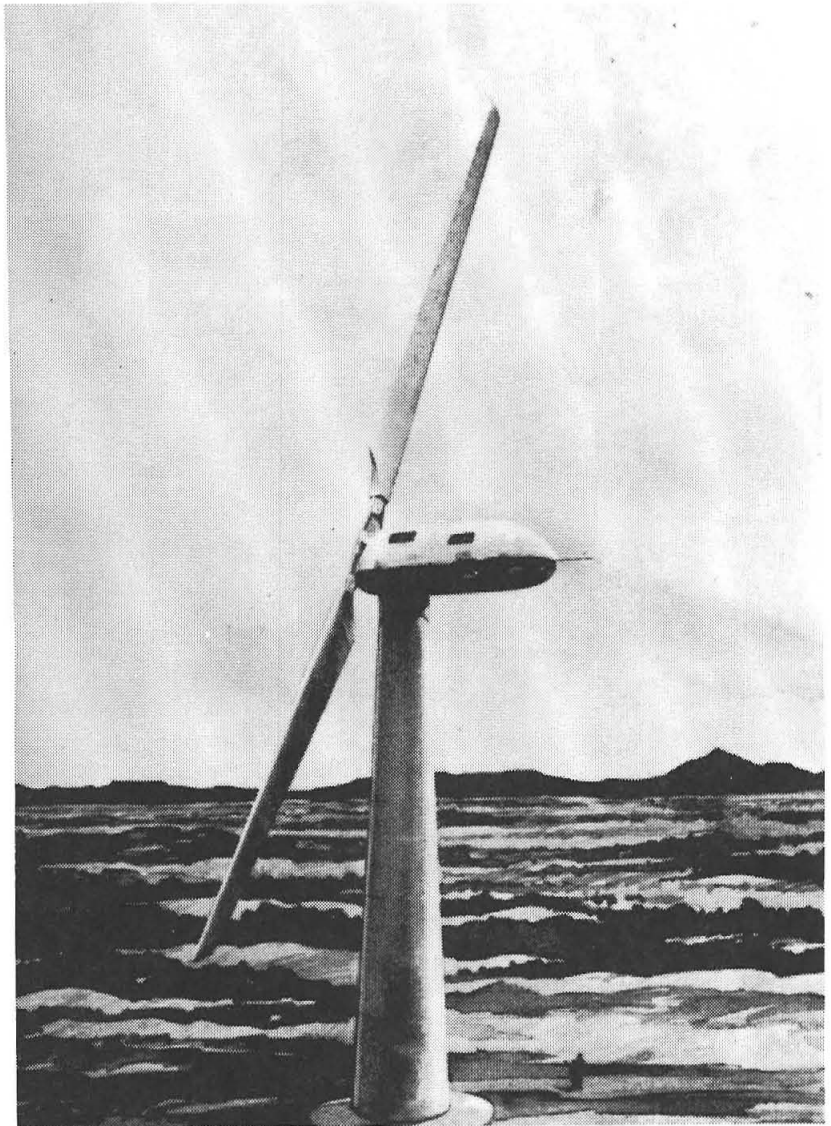

Figure 17. - Kaman 1500 KW wind turbine.

MANUAL DISCONNECTS MANDATORY
SINGLE BREAKER ON TRANSFORMER HIGH SIDE
UNIT CONNECTIONS TO DISTRIBUTION SYSTEM
LOCK OUT FOR INTERNAL FAULTS
RE-SYNC FOR EXTERNAL FAULTS - (STAND BY MODE)
1 MINUTE DELAY - LOCK OUT AFTER 3 CYCLES
SEPARATE STATION SERVICE TRANSFORMER
EMERGENCY POWER - BATTERY 48 V
PF CAPACITORS - HIGH SIDE, SEPARATE BREAKER
REGULATION & STABILITY REQUIREMENTS DEPEND ON SITE
LIGHTNING SUPPRESSION AT GENERATOR & TRANSFORMER
DISTRIBUTION VOLTAGES FROM 2400 TO 34 500 V

Figure 18. - Wind turbine interface requirements for connection to a utility grid.

MAINTENANCE AND SAFETY
ENVIRONMENTAL IMPACT
LICENSING
APPLICATIONS

Figure 19. - Wind turbine operational and institutional issues.

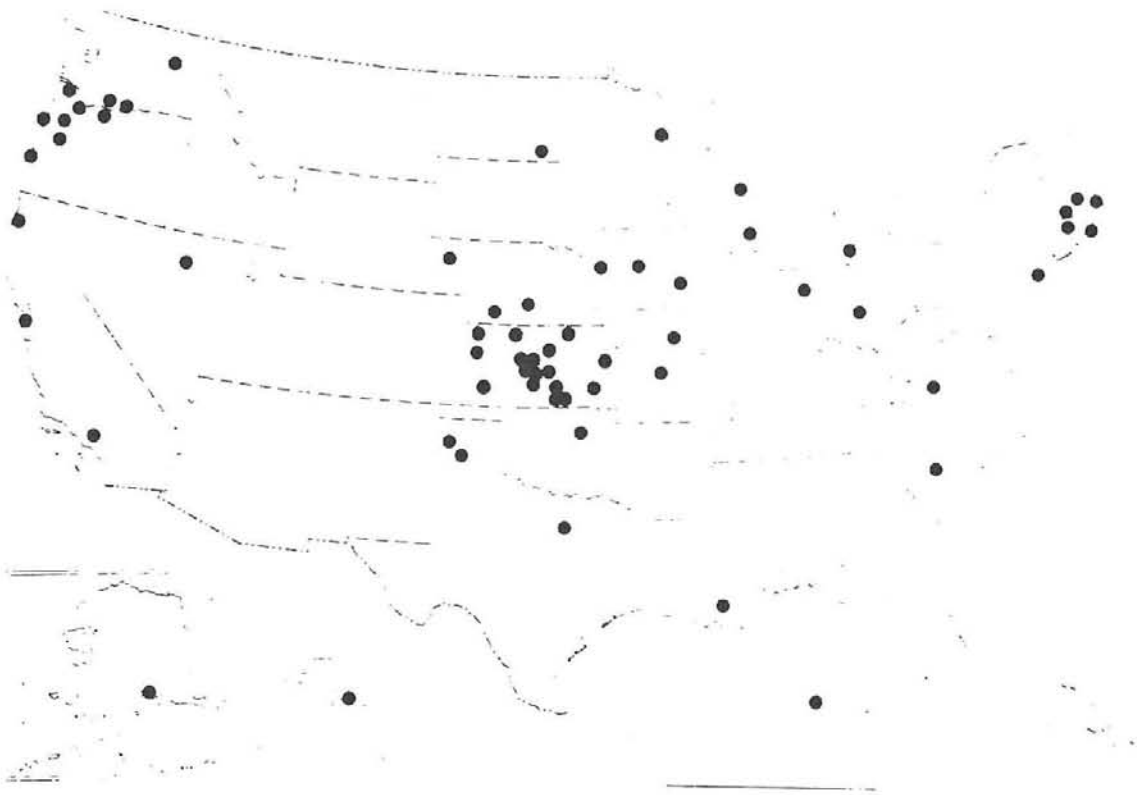

Figure 20. - Locations of utility companies that have expressed interest in the wind energy program.

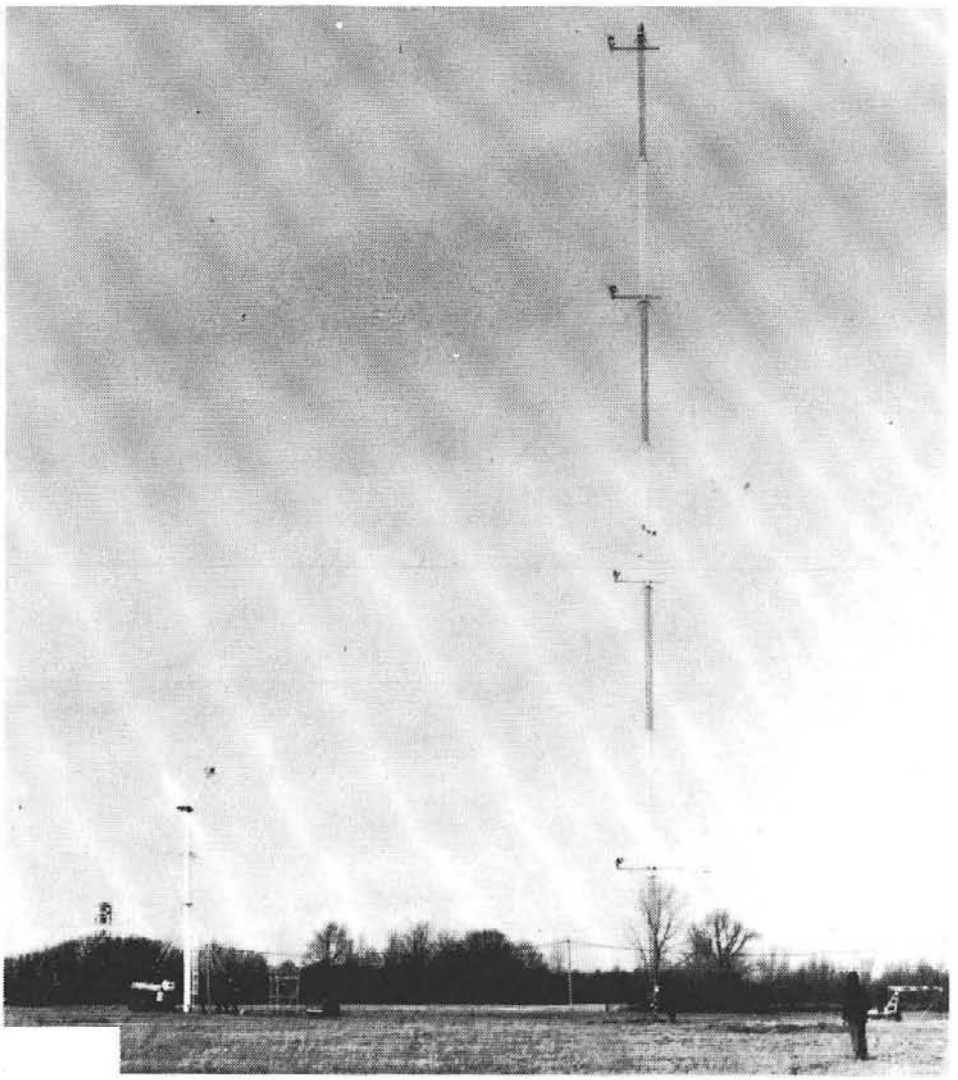

Figure 21. - 60M (200 H) meteorological tower at Plum Brook wind turbine site.

	76	77	78
SELECT SITES FOR MET. TOWERS	▽		
SELECT MOD-0A SITES	▽ ▽		
SELECT MOD-1 SITES		▽	▽

Figure 22. - Schedule for selecting mod-0A and mod-1 wind turbine sites.

VERTICAL-AXIS WIND TURBINE PROGRAM

R. H. Braasch
Sandia Laboratories

This presentation provides an overview of the Darrieus Vertical-Axis Wind Turbine (VAWT) Program being conducted at Sandia Laboratories for ERDA. The primary technical content of the program is contained in Section II - A, B, C and D of this workshop.

Figure 1 suggests that emphasis to date has been directed toward understanding the utilization of the Darrieus VAWT for utility grid applications. The significant major subsystems are shown in Figure 2. The wind turbine itself has generally been characterized by the power coefficient versus tip speed ratio curve. This curve, for several indicated wind turbines, is shown in Figure 3. For utility grid applications, interest is generally directed toward those machines which possess a large power coefficient at a high tip speed ratio. At first encounter, the curves of Figure 3 lead one to believe that the entire story has been presented. The importance of the specific shape of these curves will be broadly discussed in the presentations which follow. In addition, from Figure 2, the transmission torque rating and resulting cost required for a given rated power are significantly influenced by the operational tip speed ratios of the machine.

In utility grid applications, site selections and the optimum machine sizes are such that machines, in general, will be located remote from large population centers. This will allow use of high wind velocity sites and requires automatic operation of the installed machines due to the relative cost of on-site personnel compared to the rated power level of even the largest machines discussed to date (1-3 MW). Figure 4 is presented to suggest this situation and shows the basic appearance of a VAWT.

The VAWT is a lift-driven machine. The aerodynamic force acting on a rotating airfoil is shown in Figure 5. The wind velocity acting

on a blade section consists of two components, one component due to the velocity of the blade section as it rotates ($-R\omega$) and one component due to the wind velocity itself (V). The vector addition of these components produces the resultant wind velocity (W) at blade angular posisiton Θ. When this resultant wind velocity acts at angle of attack α relative to the airfoil chord line, lift (L) and drag (D) forces are produced. Resolving these lift and drag forces along the blade chord line determines the force driving the blade. The blade torque is produced by the sum of the blade section torques determined by the above force times the section radius (R). Normalized aerodynamic torque for 1-, 2- and 3-bladed rotors, operating at a tip speed ratio associated with the peak of the power coefficient curve, are shown in Figure 6. These torque variation plots change significantly with tip speed ratio and their spectral content represents sources for exciting structural dynamics.

Figure 7 lists the primary advantages of the VAWT. The first three advantages are self-explanatory while the fourth noted advantage remains to be proven, although subsequent papers indicate the reasons for this claim. The last advantage requires some discussion.

Figures 8 and 9 show typical power versus wind velocity response curves for conventional or horizontal-axis wind turbines (HAWT). Power limiting in Figure 9 is achieved by pitch control and is required to avoid exceeding the electrical generator rated power level for excessive periods of time. Returning to the power coefficient versus tip speed ratio characteristic for a typical HAWT in Figure 10, the effect of regulation or power limiting is to truncate the high wind velocity side of the curve into a cubic shaped curve to match the cubic power generation property of the machine. In effect, the power coefficient curve is so good that devices must be added to the machine to truncate its performance.

A typical power versus wind velocity characteristic for a VAWT operating at constant rotational speed is shown in Figure 11. High wind velocity cases are self-regulating due to the shape of the power

coefficient versus tip speed ratio curve. A typical comparison of power coefficient curves for VAWT and HAWT is shown in Figure 12, but this self-regulating property is not at all apparent from the figure. Figure 12, however, also indicates a disadvantage of the VAWT. That is, the machine operates at a lower tip speed ratio than the HAWT. This condition affects the required transmission torque rating and results in the VAWT possibly having higher transmission costs than the HAWT. More will be said about this later.

Figure 13 is a block diagram of an automatic windpower system. Figure 11 indicates that fixed rotational speed is required to obtain the noted characteristic. In Figure 13, fixed rotational speed is maintained by synchronizing a synchronous generator to the utility grid frequency and then coupling the generator to the wind turbine through a fixed speed changer. Selection of wind turbine rotational speeds and the electrical system required are discussed in subsequent papers. The major areas being emphasized in designing a system such as that outlined in Figure 13 are shown in Figure 14. Section II - A, B, C and D of this workshop will present material on each of these noted major areas. This presentation will highlight some selected topics.

From the system analysis activities, Figure 15 shows energy cost versus machine rated power based upon machines optimized by selecting the machine solidity that will give a maximum in power coefficient. Investigating the component costs of such machines, it was determined that for large machines the transmission was the most costly item. Figures 16 and 17 show power coefficient versus tip speed ratio for various solidities at two Reynolds numbers. An investigation of these figures shows significant improvements in peak performance with increased Reynolds number. Also, higher tip speed ratio machines are possible by lowering machine solidity at the cost of reduced power coefficient. Increasing the Reynolds number by going to large machines not only increases machine performance but increases the shape of the power coefficient curve for high wind velocities and

hence affects the power versus wind velocity plot contained in Figure 11. Figure 18 shows experimental wind tunnel test data which verifies the trends with solidity shown in Figures 16 and 17.

Transmission costs used in the machines associated with Figure 15 were obtained from studies conducted by contractors on HAWT designs for NASA. Figure 19 indicates the basic constraint that these transmissions cannot have large input/output shaft offsets. The VAWT, however, as shown in Figure 19, can employ transmissions with large input/output shaft offsets. A summary chart shown in Figure 20 indicates four different transmission and generator combinations and their comparative costs. It is anticipated that the use of a large diameter speed increaser will lower the transmission costs for the VAWT.

Figures 21 and 22 display the energy cost versus machine rated power for 12-mph and 18-mph average wind velocity sites, respectively. Included in these figures is the effect of reducing solidity to reduce, primarily, transmission costs and the anticipated effect of further reducing transmission costs by incorporating transmissions as suggested in Figures 19 and 20. Also shown on some curves in Figures 21 and 23 are diameters and rotor rotational rates for selected machines. If achievable, the energy costs shown in Figures 21 and 22 are competitive with other methods of electricity generation.

From the structural dynamics activities, Figure 23 shows a plot of predicted machine (17-meter diameter) natural frequencies versus turbine speed. Since this machine employs a three-bladed rotor, Figure 23 includes the anticipated 1/REV, 2/REV, 3/REV and 6/REV excitation frequencies. Curves labeled ω_{C1} and ω_{C2} are asymmetric system modes which will be discussed in the Structures section of the workshop. The curves labeled ω_{C1} and ω_{C2} are the first and second chord-wise or lead-lag modes of vibration. A computer-generated motion picture of these two chord-wise modes and the first blade flat-wise mode (not shown in Figure 23) when the turbine rotating speed may excite these modes was shown as part of the workshop presentation.

In summary, the VAWT appears to be a viable competitor to the HAWT. Future development plans are shown by the machine sizes indicated in Figure 24.

In conclusion, Figure 25 shows the VAWT test facility that was toured as part of the workshop.

Application of Wind Turbines For Generation of Electrical Power

Figure 1

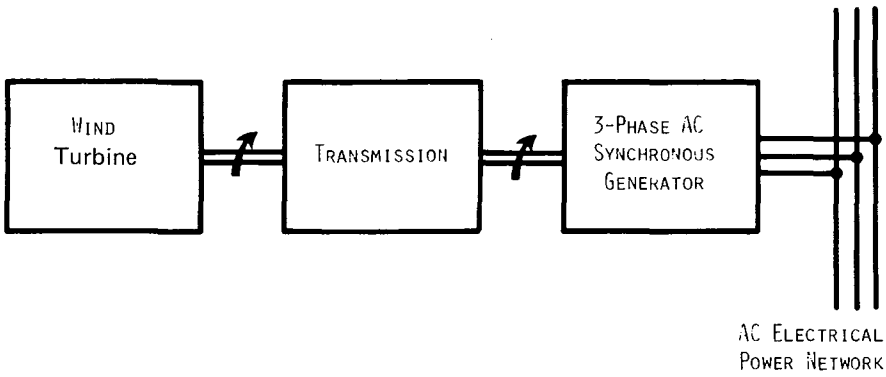

Figure 2. System Diagram

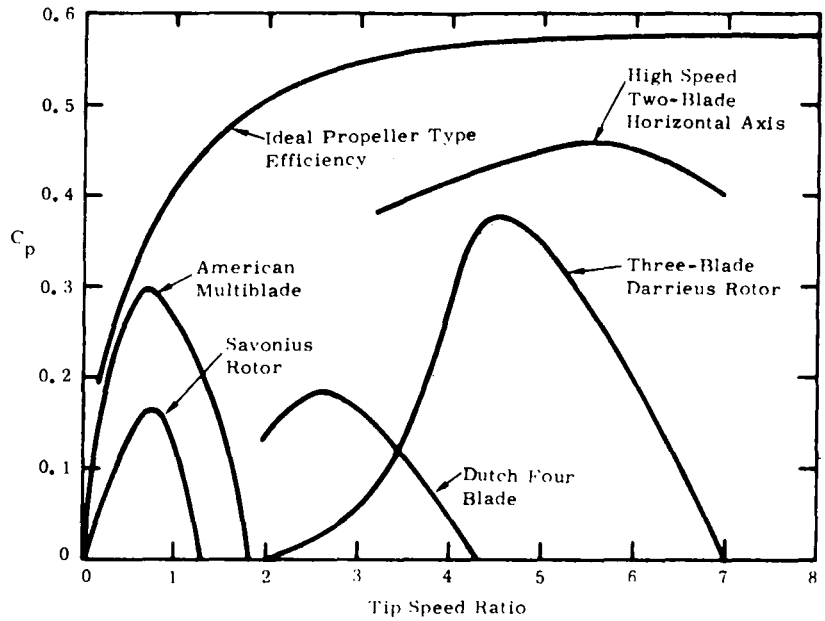

Figure 3. Efficiency Characteristics for a Selection of Wind Turbines

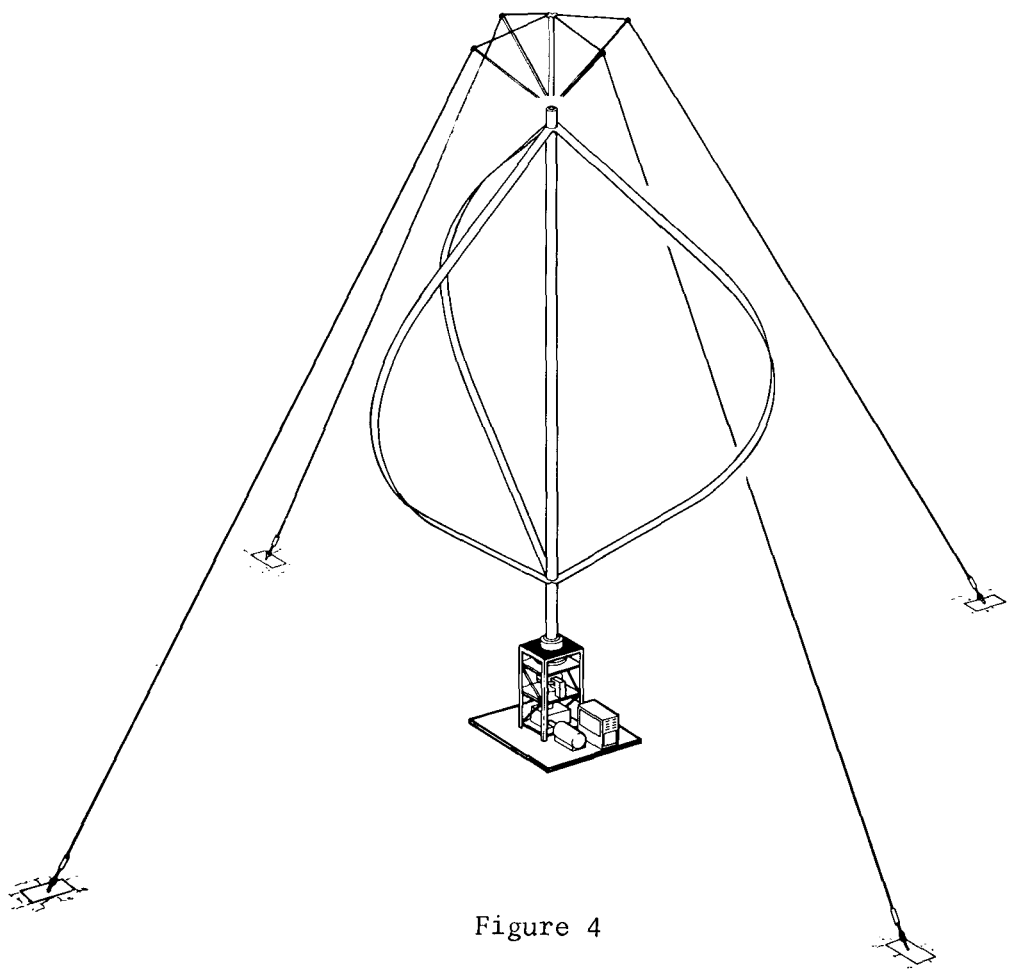

Figure 4

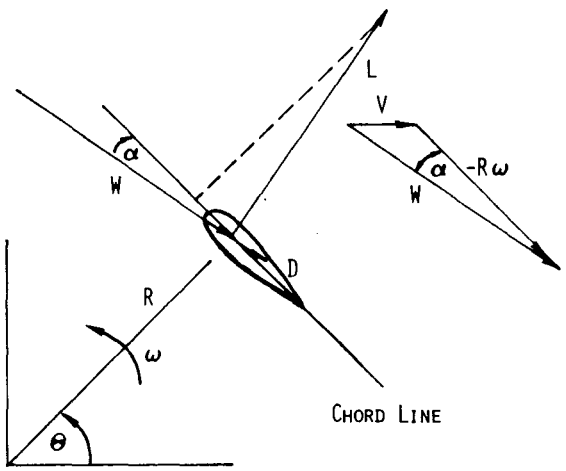

Figure 5. Aerodynamic Forces Acting on a Rotating Airfoil

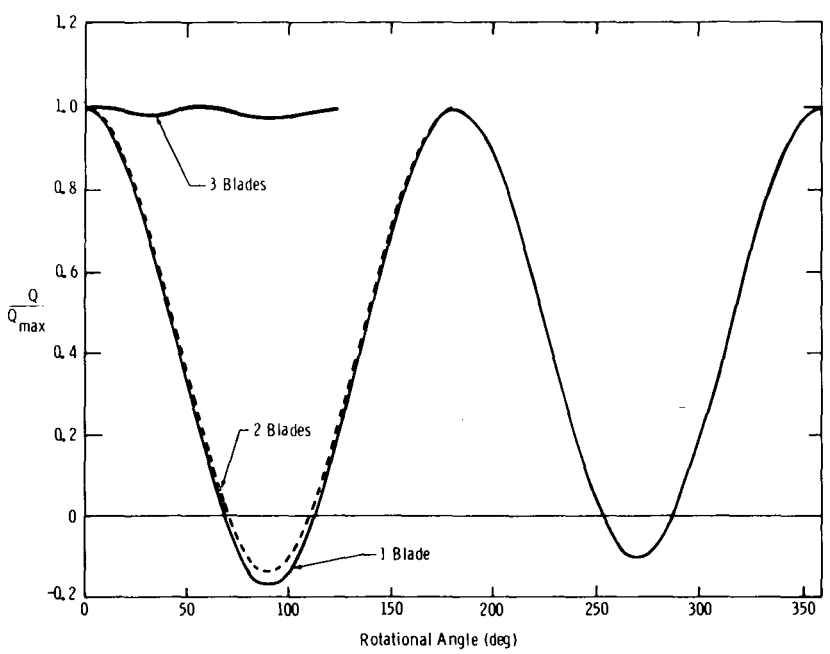

Figure 6. Variation of Torque with Rotational Angle for a Darrieus Wind Turbine with Various Numbers of Blades

ADVANTAGES OF DARRIEUS WIND TURBINE

- VERTICAL SYMMETRY ELIMINATES NEED FOR YAW CONTROL
- DELIVERS MECHANICAL POWER AT GROUND LEVEL
- SIMPLE SUPPORT TOWER CONSTRUCTION
- REDUCED BLADE FABRICATION COSTS
- REQUIRES NO PITCH CONTROL FOR SYNCHRONOUS APPLICATION

Figure 7

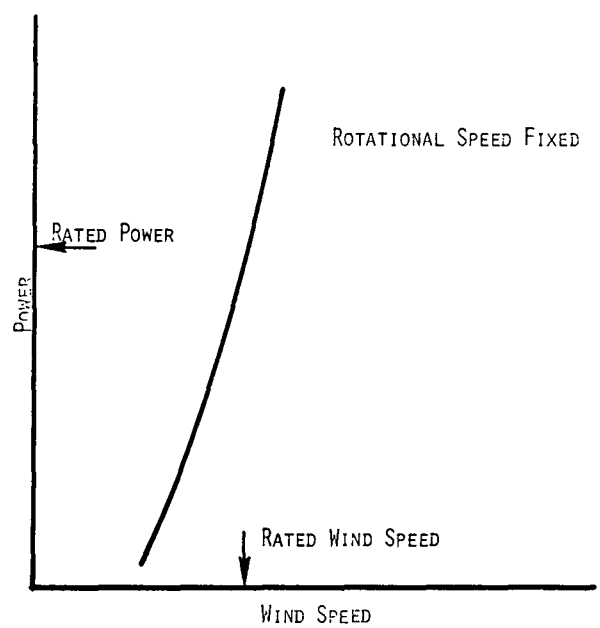

Figure 8. Conventional Propeller-Type Wind Turbine Characteristic

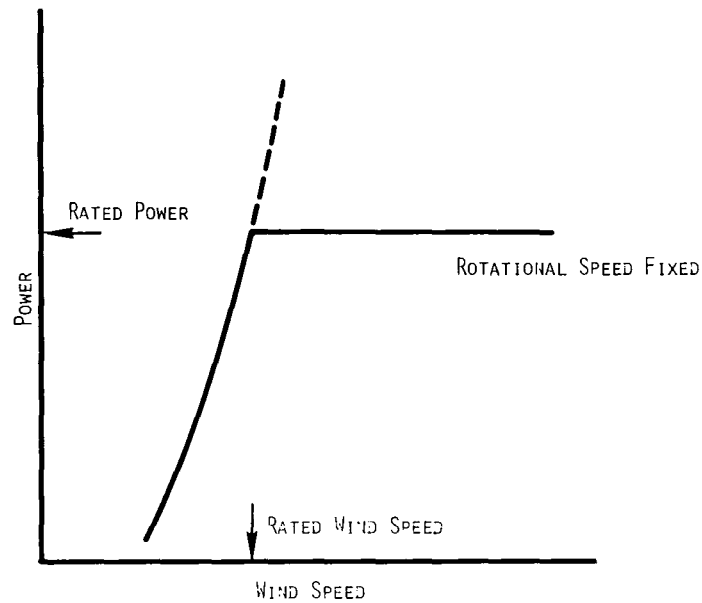

Figure 9. Power Regulation to Spoil Performance of Conventional Propeller-Type Wind Turbine

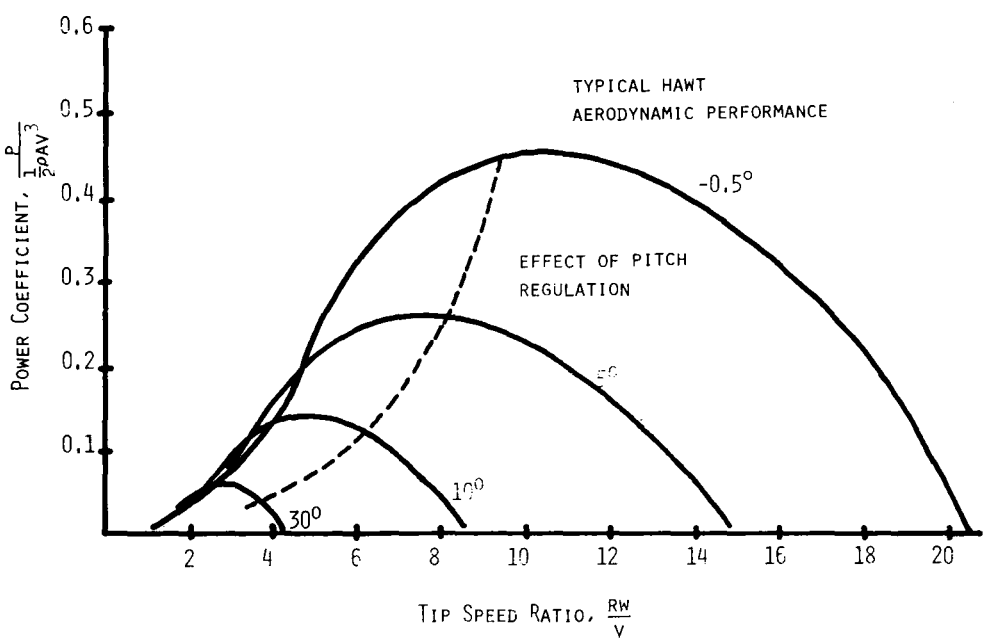

Figure 10

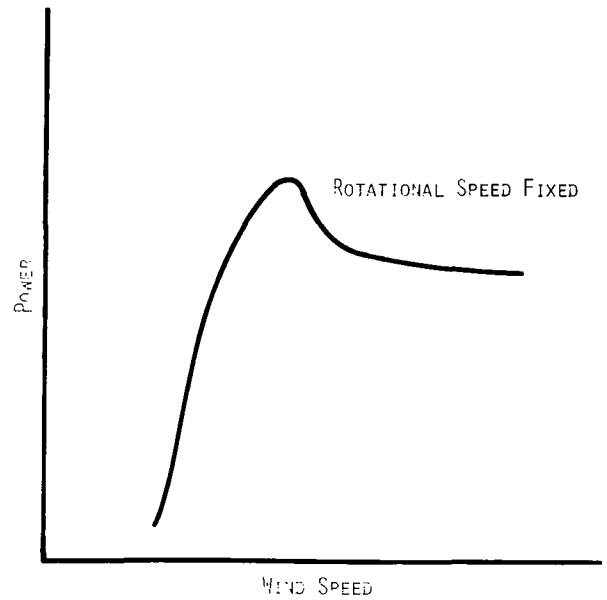

Figure 11. Theoretical Darrieus Wind Turbine Characteristic

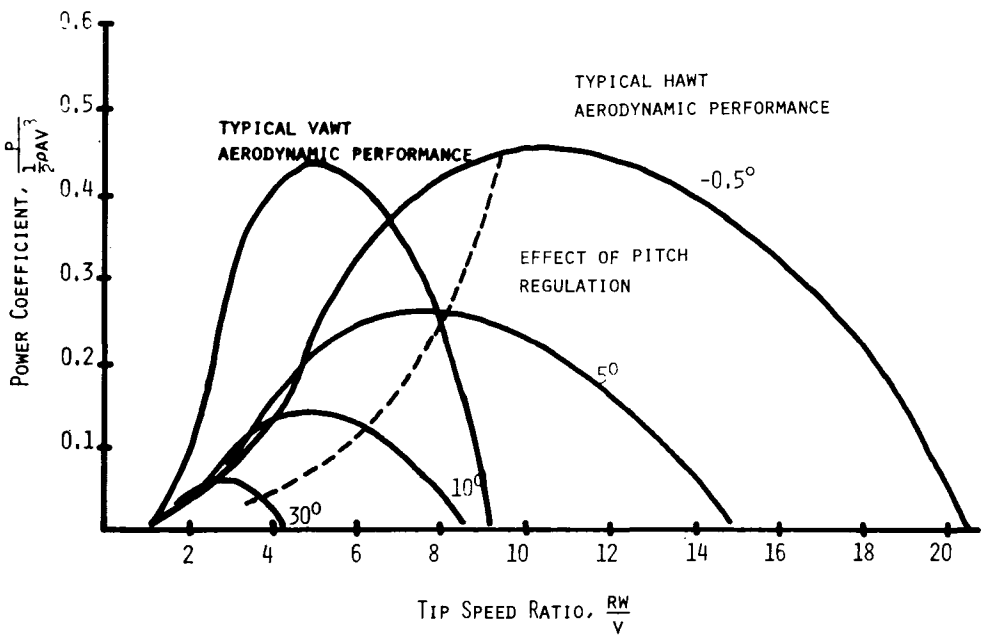

Figure 12

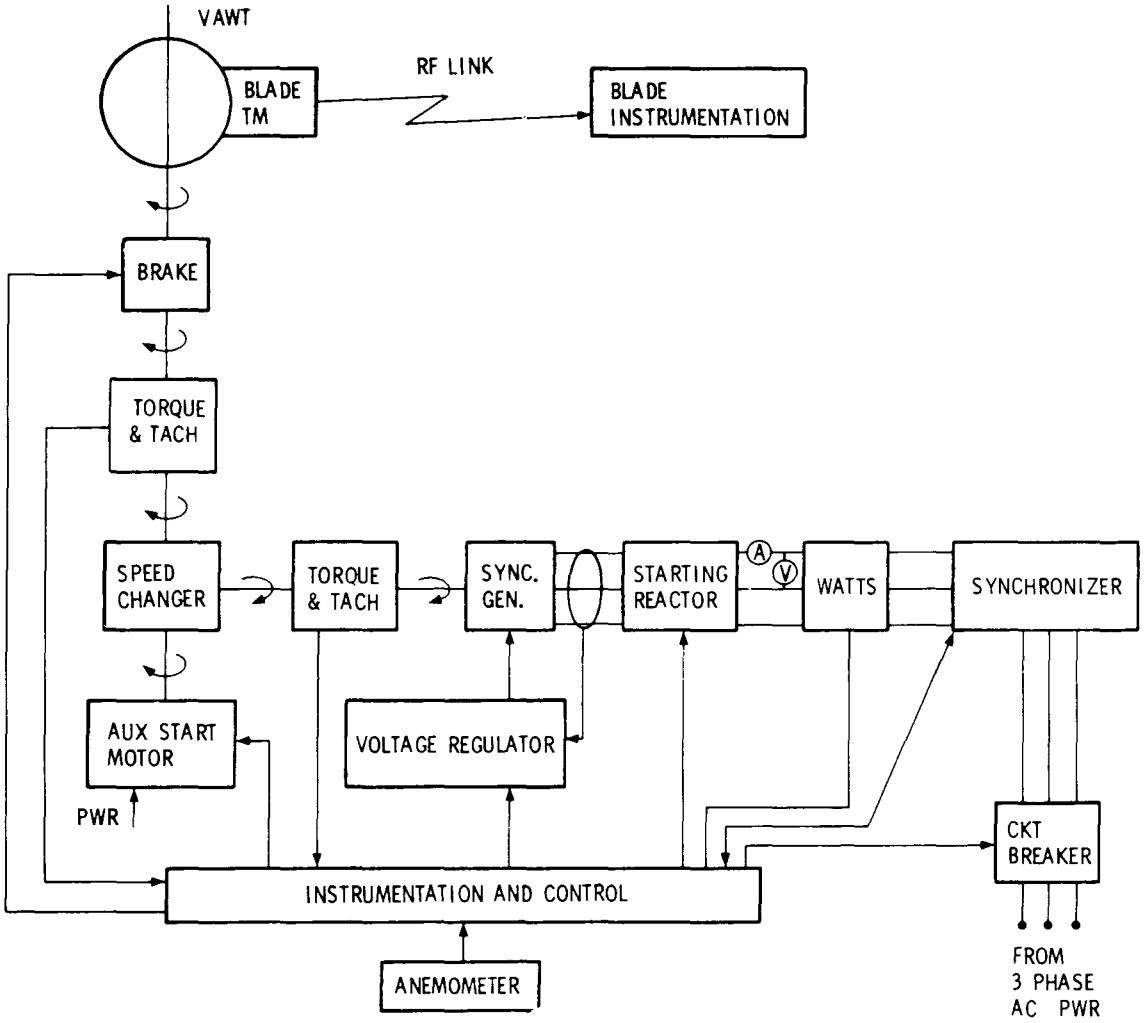

Figure 13. Synchronous Windpower System

MAJOR AREAS BEING EMPHASIZED

- SYSTEM ENGINEERING AND ANALYSIS
- AERODYNAMICS
- STRUCTURAL DESIGN
- ELECTRICAL SUBSYSTEMS

Figure 14

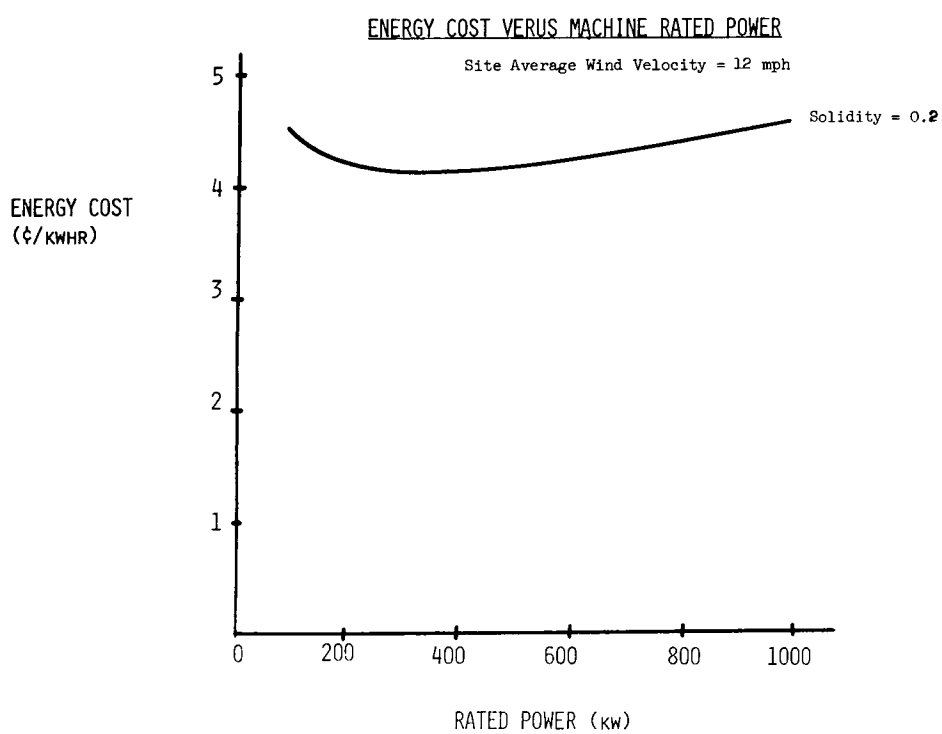

Figure 15

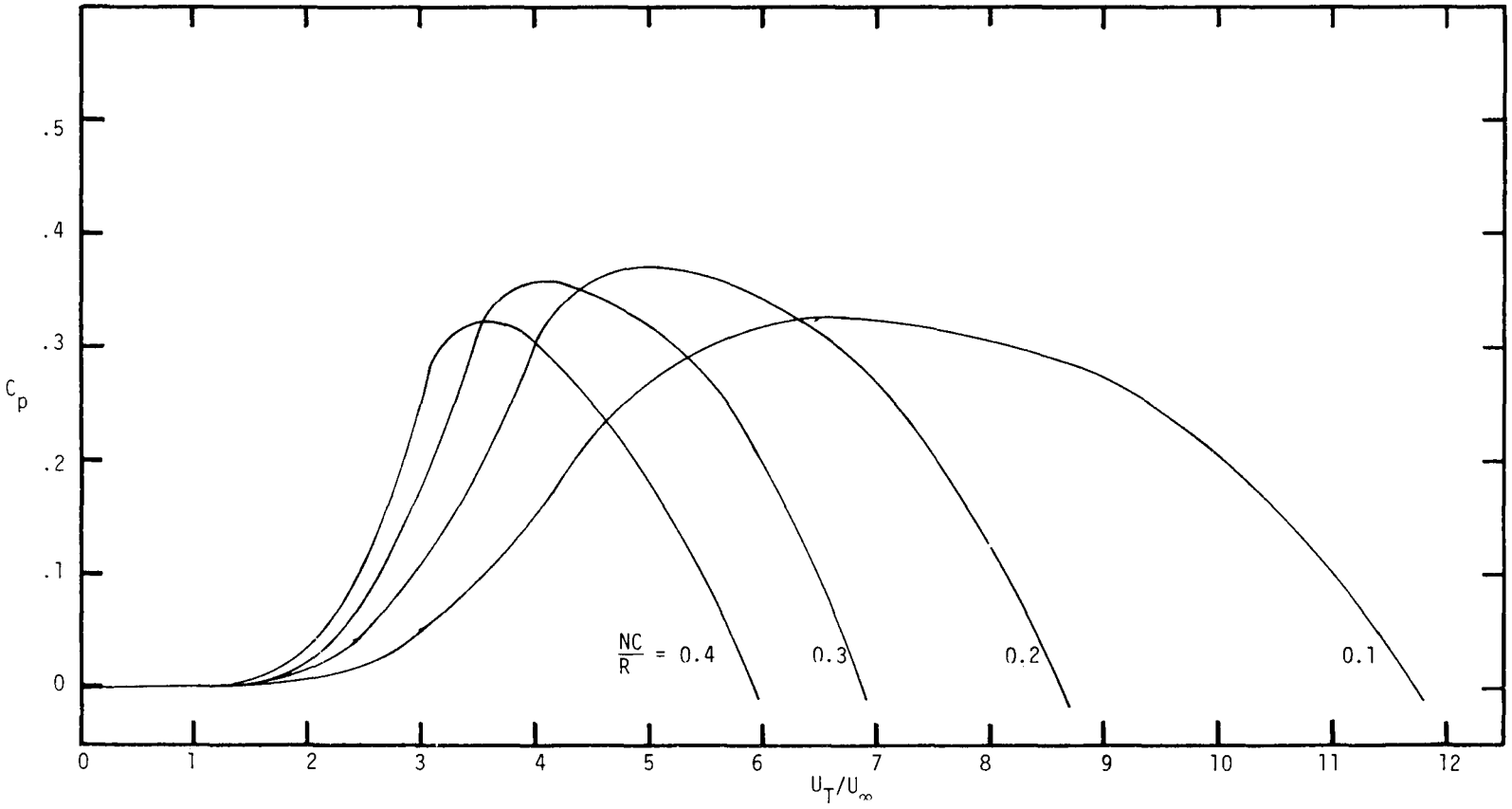

Figure 16. The Effect of Solidity on C_p (Re = 0.3 x 10^6)

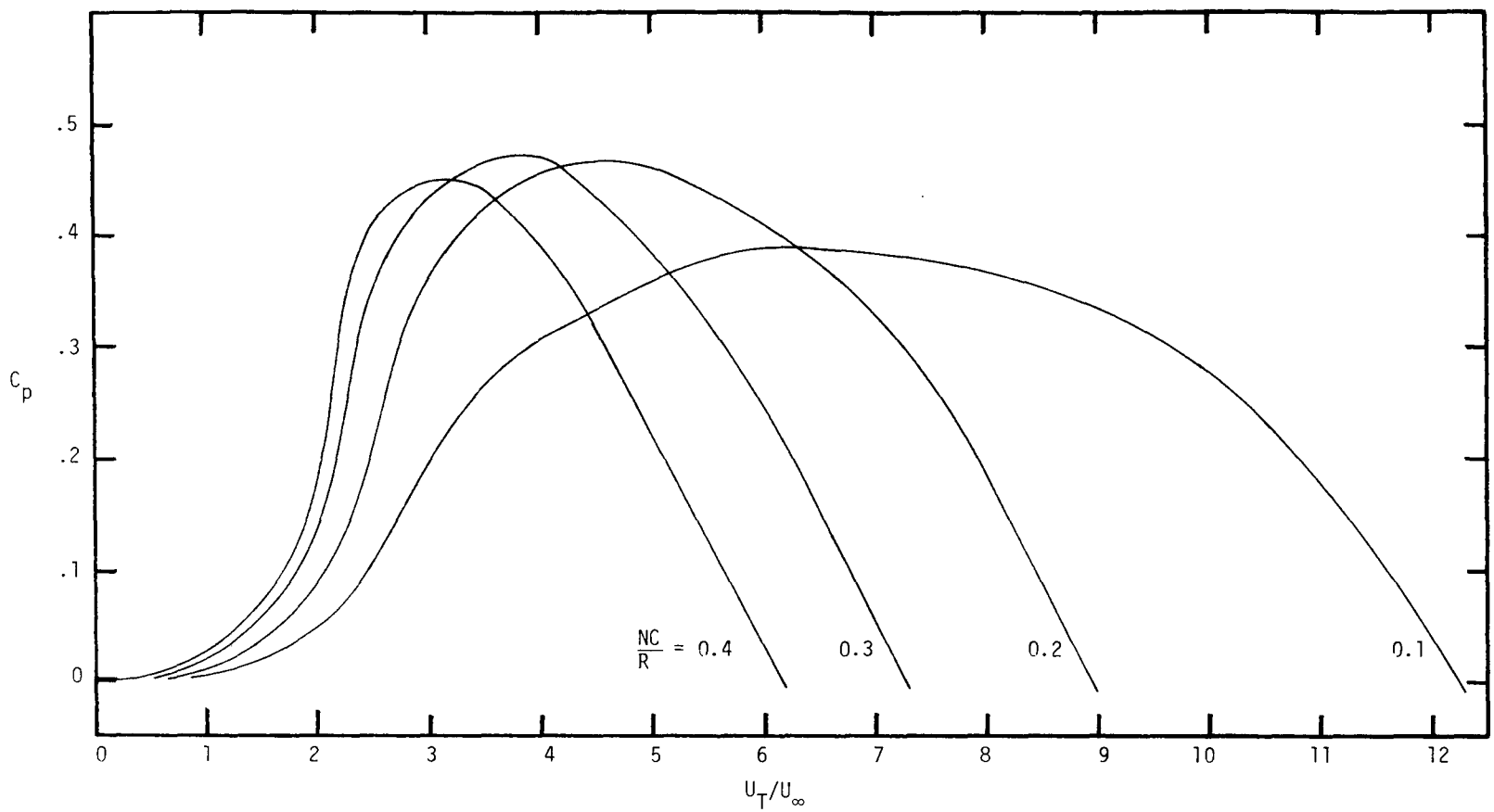

Figure 17. The Effect of Solidity on C_p (Re = 3.0 x 10^6)

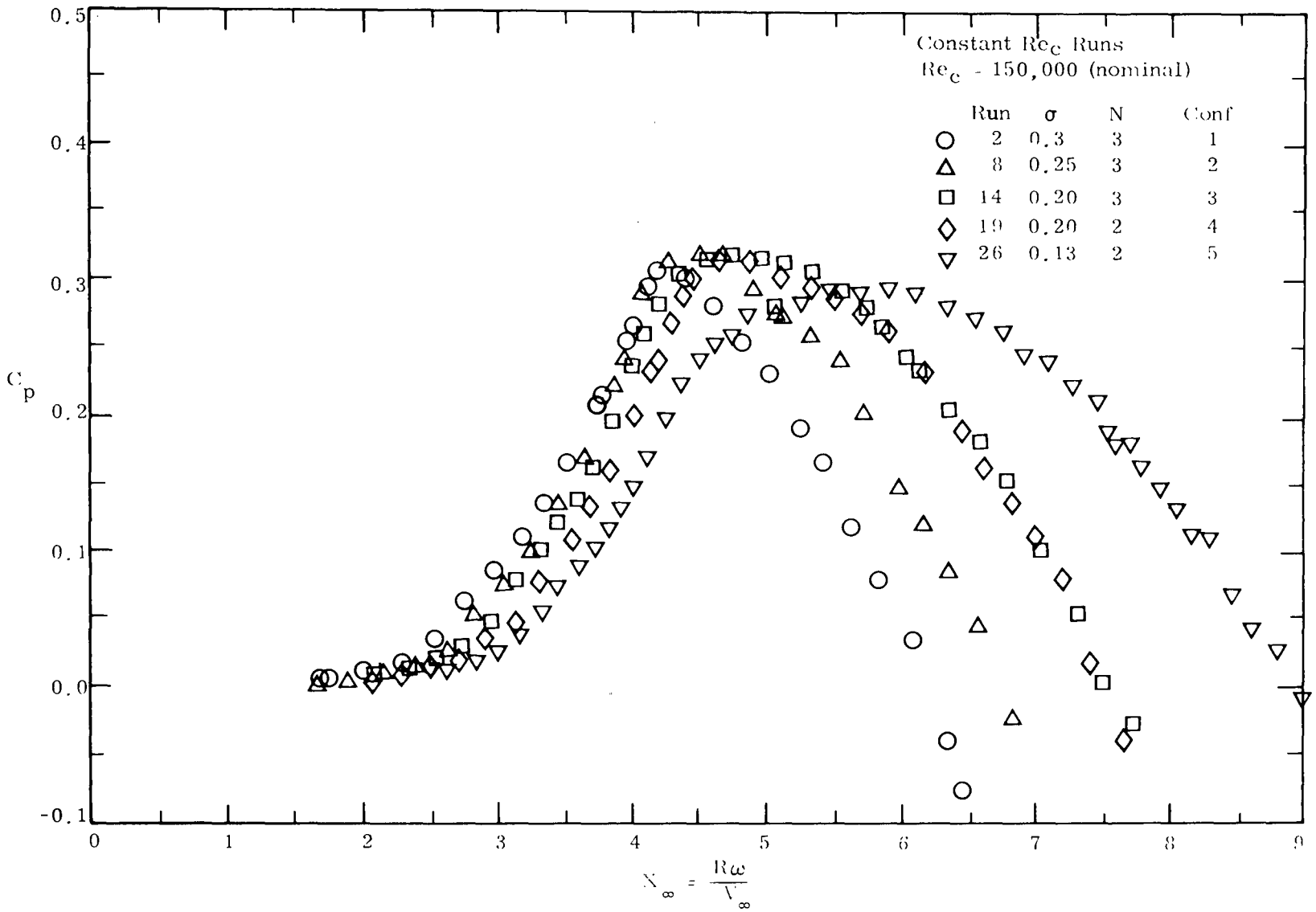

Figure 18. Effect of Solidity on Power Coefficient Data at Re_c = 150,000

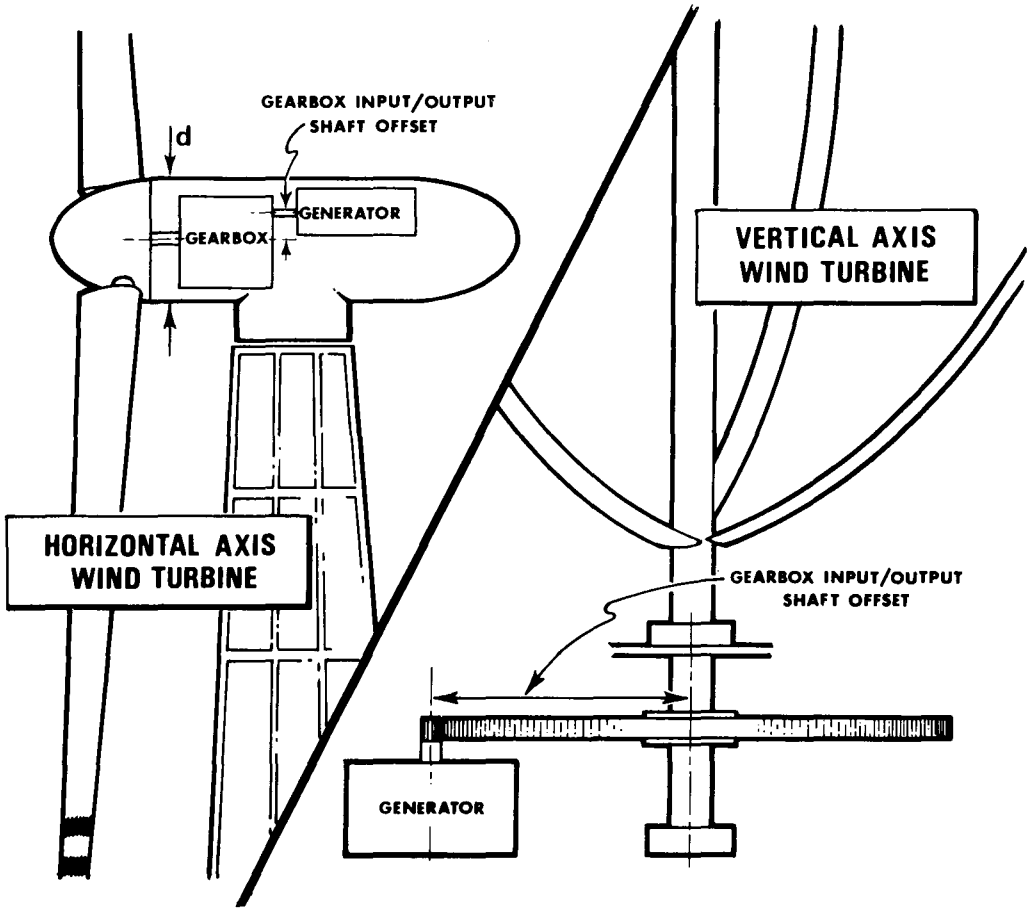
GEARBOX INPUT/OUTPUT
SHAFT OFFSET
d
GENERATOR
GEARBOX
VERTICAL AXIS
WIND TURBINE
HORIZONTAL AXIS
WIND TURBINE
GEARBOX INPUT/OUTPUT
SHAFT OFFSET
GENERATOR

Figure 19

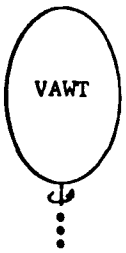

Power Conversion Tradeoff

	Speed Changer					Generator	
	Large Dia. Speed Incr.		Gearbox				
	Torque Rating	Gear Forces	Torque Rating	Gear Forces	Cost	Speed	Cost
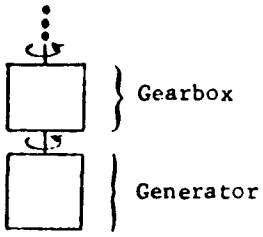	---	---	High	High	High	High	Low
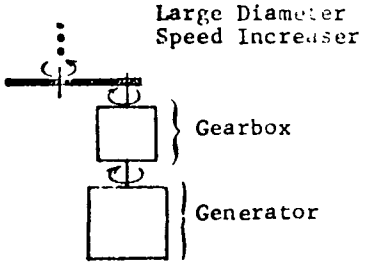	High	Med to Low	Med	Low	Med	High	Low
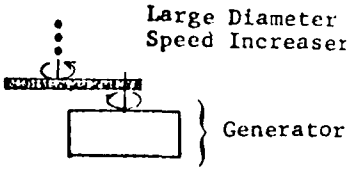	High	Med to Low	---	---	Med	Med	Med
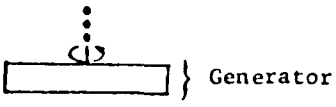	---	---	---	---	---	Low	High

Figure 20

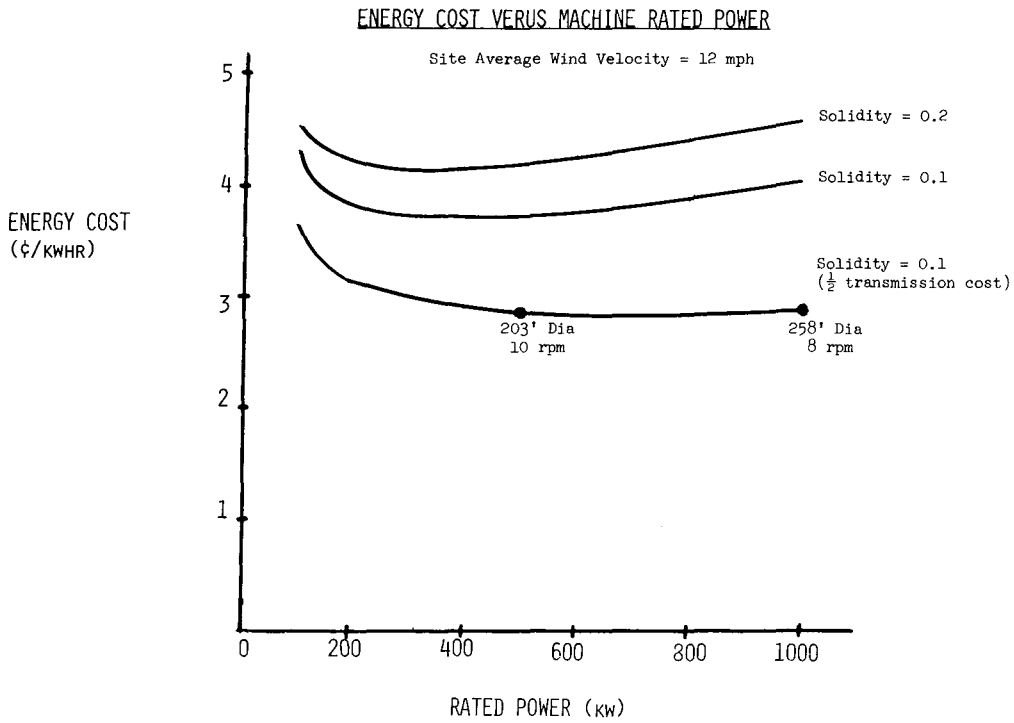

Figure 21

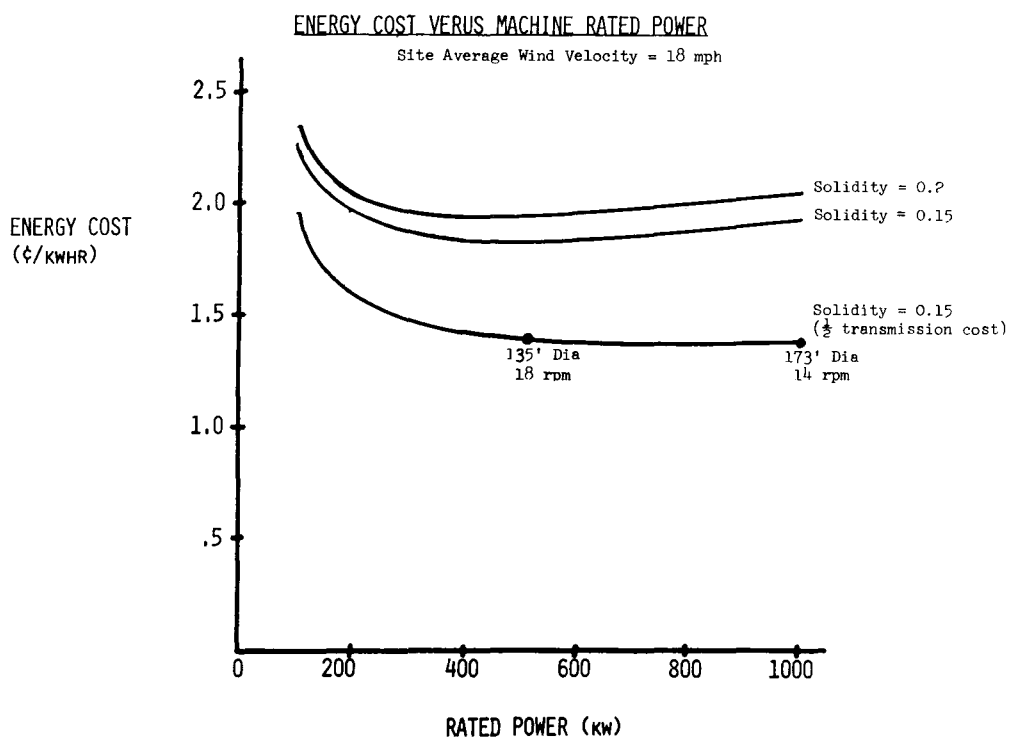

Figure 22

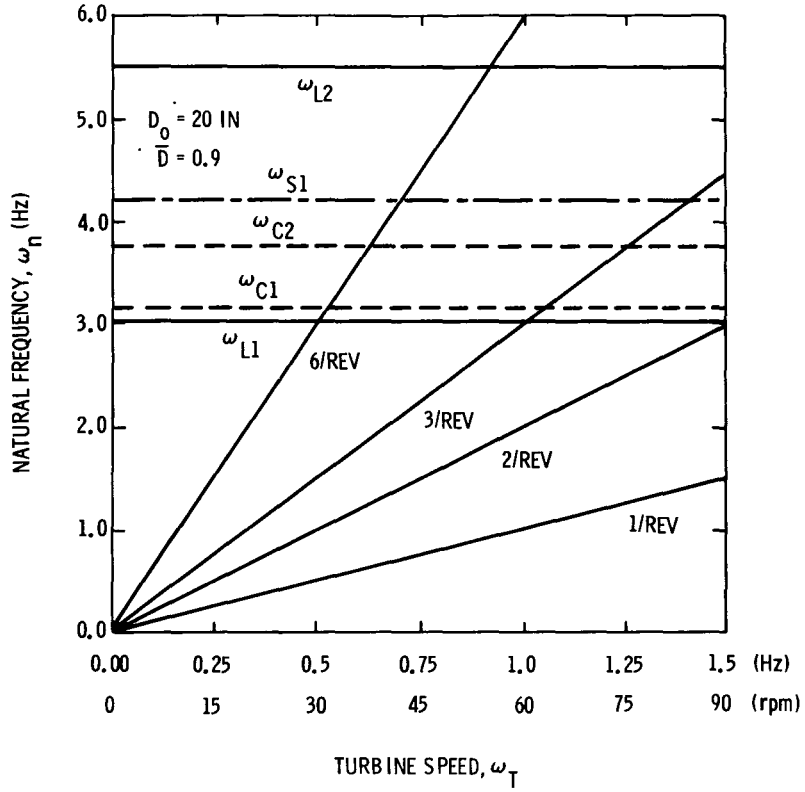

Figure 23

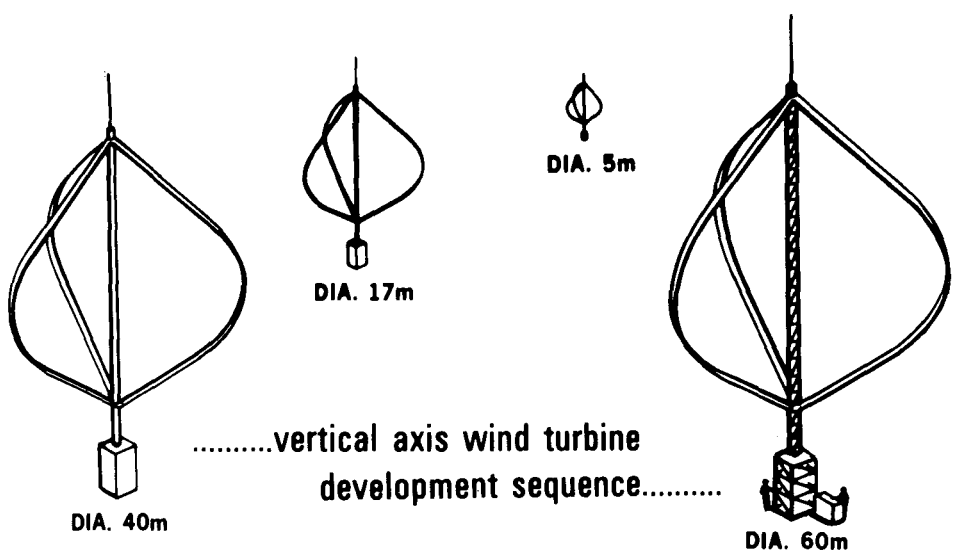

DIA.(m)	5	17	40		60
MAX POWER (KW) wind speed at 18 MPH	1.6	20	150	AND/OR	350
wind speed at 25 MPH	4.4	50	350	AND/OR	1000

Figure 24

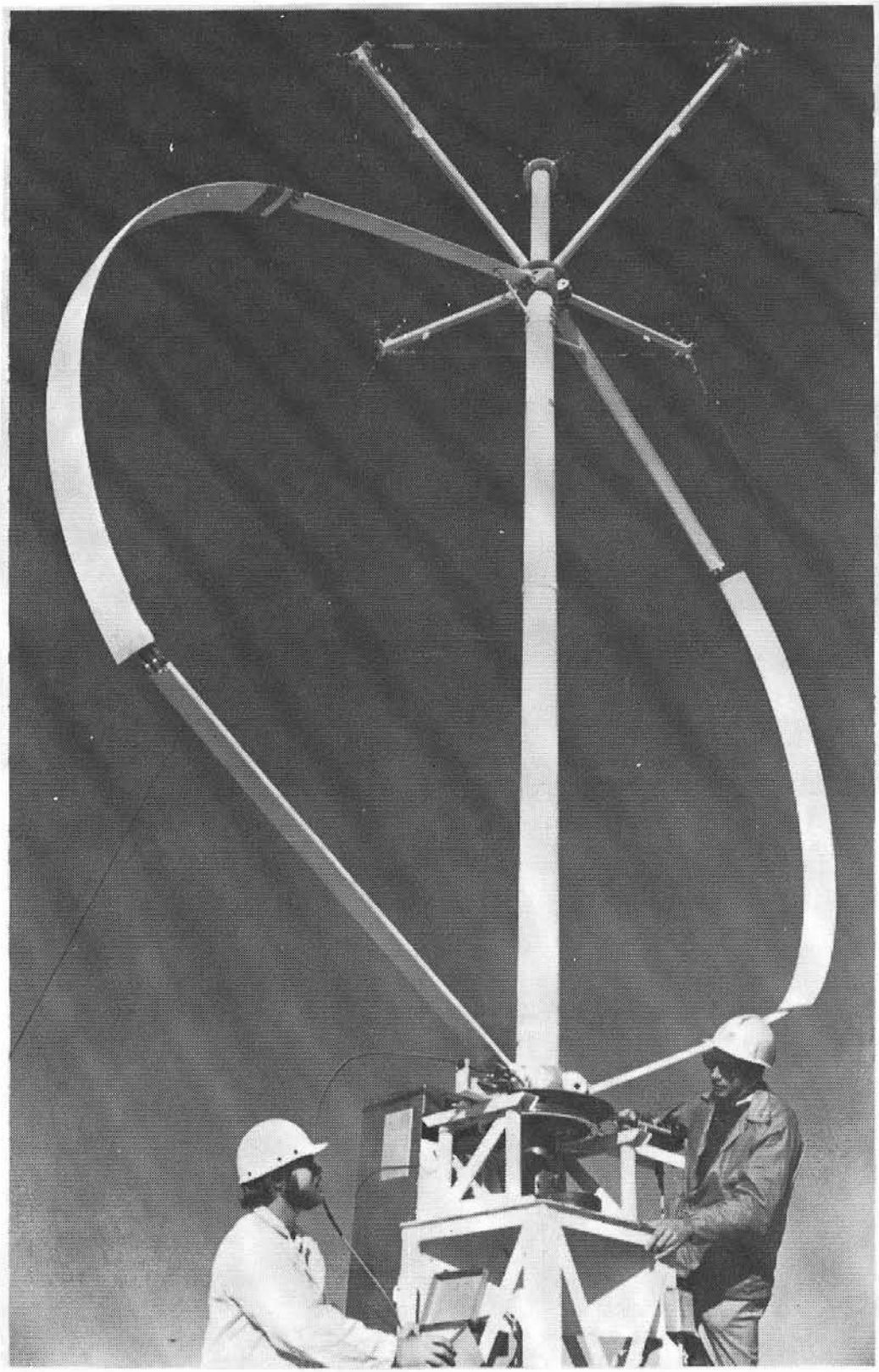

Figure 25

ELECTRIC POWER RESEARCH INSTITUTE PROGRAM

Piet Bos, EPRI

(This paper had not been received by press time)

CANADIAN WIND ENERGY PROGRAM

R.J. Templin and P. South
Low Speed Aerodynamics Laboratory
National Research Council of Canada

1. INTRODUCTION

The extent to which wind energy may be able to contribute to Canada's future energy needs is at present uncertain, and is likely to remain so for several years to come. In the meantime, since our research and development effort is necessarily small, it has been aimed at applications that look promising within about the next decade. Most of these are in geographic regions where annual average wind speeds are high, and where the costs of electricity generation from fossil fuels is already high, and likely to increase with time.

Applications studies or experimental projects are in progress at several Canadian universities, in federal and provincial government agencies, and in most of the provincial power authorities. At least two Canadian companies (Dominion Aluminum Fabricating, Limited, Toronto and Bristol Aerospace Ltd., Winnipeg) have recently begun to manufacture vertical-axis wind turbines.

This paper does not attempt to do justice to most of these separate programs, but will concentrate on the vertical-axis turbine work which has been carried out at NRC in support of our largest experimental project: the Magdalen Islands turbine, which it is hoped will begin operation later this year.

2. MAGDALEN ISLANDS 200 kW TURBINE

A large vertical-axis wind turbine is under construction at Dominion Aluminum Fabricating, Limited, Toronto, under contract to the federal government, at a contract price of $230,000. The turbine is scheduled to be delivered this summer to the Magdalen Islands, which are a part of the Province of Quebec, where it will be erected and operated by the provincial power authority, Hydro Quebec. Connection to the island grid system is scheduled for late autumn.

The Islands are a single island chain, about 40 miles long, joined together by sand dunes, and located almost in the geographic centre of the Gulf of St. Lawrence in the eastern coastal region. The population of about 13,000 is presently supplied with electricity from a diesel plant of 26MW total capacity. It has been estimated that the present cost of generating power is about 6 cents/kW-hr., of which about 3 cents is the cost of diesel fuel. Hydro Quebec's pricing policy is such that the islanders are charged the same rates as in the rest of the province - about 2 cents/kW-hr.. The average annual wind speed at Cap aux Meules, the island capital, is about 19 mph (8.5m/sec.), and so it is not surprising that the research laboratories of Hydro Quebec had been studying the economic feasibility of wind energy for this and other similarly isolated locations during the past few years. Five of Canada's ten provinces border on the Gulf, and some of them are also examining wind energy applications.

Some of the turbine design parameters are as follows. The two-bladed rotor equatorial diameter is 80 ft. (24.4m) and the axial height is 120 ft. (36.6m). The height-to-diameter ratio of 1.5 was chosen to provide guy-wire clearance from the blades without central column overhang, and hence to minimize column bending moments. As compared with h/d = 1.0, the supporting tower height is also reduced for a given rotor center height above ground. The tower height from ground levelto tower bearing is 30 ft. (9.1m). Two, rather than three blades were chosen, in spite of the fact that overall aerodynamic loading will have larger cyclic components. The choice of two blades reduces manufacturing costs, and because the rotor can be assembled flat and erected as a complete unit, erection costs are reduced. Blade chord is 2 ft. (0.61m), yielding a value of 0.1 for the solidity parameter NC/R. This choice was mainly the result of cost optimization, taking into account various methods of blade manufacture. Each blade is supported by two horizontal struts extending horizontally outward from the central column to about 60 percent of the rotor equatorial radius.

The turbine will drive a 200 kW three-phase induction generator which also serves as the starting motor, and will thus operate symbiotically with the island power network. The control system has been designed by Hydro Quebec, and is described in Ref. 1. Nominal operating rotor speed is approximately 40 rpm. Normal and emergency stopping, whether manual or automatic, will be by means of a mechanical brake, but

emergency overspeed protection is provided by centrifugally actuated aerodynamic blade spoilers.

The Magdalen Islands site, already equipped as a wind laboratory for testing large-scale transmission lines, is located about 13 miles (21km) from the diesel plant. The annual energy produced by the wind turbine is estimated to be approximately 600,000kWh. The estimated cut-in wind speed is 12 mph (5.4m/sec.) and the rated wind speed is 30 mph (13.4m/sec.).

The remainder of this paper will summarize the experimental and theoretical work carried out by NRC during the past two years, mainly in support of the design of the 200 kW turbine. Wherever possible, results of aerodynamic measurements are presented in non-dimensional form to render them applicable to turbines of different scale and blade configuration.

3. VERTICAL-AXIS ROTOR PERFORMANCE PREDICTION

The method generally used at NRC to compute vertical-axis rotor performance is the computerized single stream tube theory described in Ref. 2, together with airfoil data for the appropriate Reynolds number. A multiple stream tube theory (Ref. 3) has been developed by the Sandia Laboratories, and it may be of interest to this workshop to summarize a comparison between the two theories and some experimental measurements carried out in the NRC 30 ft. (9.14m) V/STOL wind tunnel on a 15 ft. (4.6m) diameter commercial vertical-axis turbine, built by Dominion Aluminum

Fabricating, Limited. The comparison is shown in Figure 1.

The experimental data points in Figure 1 were obtained from measurements carried out on a 3-bladed rotor having extruded aluminum blades of 6-inch (15.2cm) chord. A constant wind speed of approximately 22 ft./sec. (6.7m/sec.) was used throughout the measurements, so that rotational speed was varied, and blade Reynolds number, based upon tangential speed at the equator ranged from approximately 0.2×10^6 to 0.6×10^6. The apparent blade parasite drag coefficient, C_{DO}, was measured by driving the rotor on its torque balance in still air over the same range of rotational speed. It varied from about 0.0117 at the highest speed to about 0.015 at the lowest speed.

Two curves in Figure 1 show the results of the single stream tube theory of Ref. 2, one of which has been calculated for a constant value of $C_{DO} = 0.012$, and the other with C_{DO} variable, as determined from the still air spin-up tests just described.

It will be seen that agreement between experimental and theoretical values of C_P is excellent, especially in the variable - C_{DO} case. In a similar comparison with earlier wind tunnel tests, given in Ref. 2, the agreement was relatively poor, in the range of blade tip speed ratio around 3 to 4, where blade stalling occurs, and some doubt about the accuracy of blade airfoil data in this region was expressed. In the present case, two-dimensional aerofoil data were obtained by measurements carried out on an actual

section of the aluminum aerofoil extrusion in the NRC 3 ft. (1m) low speed wind tunnel over a range of Reynolds number representative of the rotor test conditions. These data, in the form of the normal force coefficient C_N and the chordwise gross thrust coefficient $C_T + C_{DO}$ are listed in Table I, as a function of aerodynamic angle of attack α.

The third theoretical curve of Figure 1 was computed for the same airfoil data, with $C_{DO} = 0.012$, using the Sandia DART multiple stream tube program of Ref. 3, and is not in good agreement with the measurements at high values of the tip speed ratio. Conceptually it would seem that the multiple stream tube theory ought to represent an improvement over the simple single stream tube theory of Ref. 2, and indeed some experimental data presented in Ref. 3 indicates this is so. It may be that we have here some interesting material for the Society for Irreproducible Results. However, it might be pointed out that in the comparison shown here and also in Ref. 3, the multiple stream tube theory was found to underestimate the value of C_P at high values of the speed ratio $R\Omega/V$. A possible explanation is that in this region the multiple stream tube theory yields values of the induced flow velocity retardation at the centre of the rotor disk that are well above the limit (one-half of the ambient wind speed) for which the momentum theory is valid. Corresponding values of the induced velocity are not as extreme in the single stream tube theory because they are averaged over the entire disk area. It must be admitted, however, that this suggestion is conjectural.

4. SPOILER AERODYNAMICS

Various forms of aerodynamic spoilers have been used for overspeed control on vertical-axis rotors at NRC for several years. Generally they are centrifugally self-actuating at a pre-set rotational speed, but their mechanical design will not be described here since this depends upon the intended application. An aerodynamically effective type, requiring only small area to cancel positive power generation over the whole operating speed ratio range, consists of one or more small-area plates, hinged at the blade trailing edge so that, when open, the plane of the spoiler is normal to the airfoil chord plane, which approximately bisects the spoiler area. Several wind tunnel measurements of their effectiveness have been made on two different 3-blade rotors. One of these had an equatorial radius of 12 ft. (3.66m), (Ref. 4) and the other was the commercial rotor already described.

Figure 2 summarizes the results of these measurements, in coefficient form. Most of the data collapses close to a line having the equation

$$\Delta C_P = 1.5 \frac{A_S}{A}\left(\frac{R_S}{R}\right)^3 \left(\frac{R\Omega}{V}\right)^3$$

where ΔC_P is the increment of power coefficient ($C_P = \frac{\text{Power}}{\frac{1}{2}\rho V^3 A}$) given by the spoilers, A_S is total spoiler area, A is the rotor swept area, R_S and R are respectively the radius from the rotor axis to the spoiler location and the rotor equatorial radius. $R\Omega/V$ is the rotor tip speed ratio. It can be shown that this relation is equivalent to the power required to rotate the spoilers alone in still air at a radius R_S, if

their parasite drag coefficient were assumed to be 1.5, based on their area.

Those data points in Figure 2 which fall below the line apply to spoilers of small chord relative to the airfoil chord, and at low values of the speed ratio, where the turbine blades are stalled.

5. BLADE FLUTTER

Some time ago the Sandia Laboratories discovered during wind tunnel tests that a violent blade flutter mode could occur on 3-bladed rotors, and that the critical flutter rotational speed was almost independent of wind speed; flutter could occur in still air if the rotor was driven to the critical speed.

The same apparent mode of flutter has been confirmed with a 2-blade rotor model of 60 inches (1.52m) height in the NRC 6x9 ft. (1.83x2.74m) low speed wind tunnel at a critical rotational speed that was essentially independent of wind speed. Steel and aluminum blades were installed on this model with a range of chords and thicknesses shown in Figure 3. Because it was impossible at this scale to construct hollow metal airfoil blades, most of the blades were of flat strap form, but in one series of measurements solid extruded airfoils of NACA 0012 section were used.

Although very large flutter amplitudes could always be made to occur at sufficiently high rotational speeds, it was found that the first onset of flutter occurred at somewhat lower speeds, and thus it was necessary to determine the

critical speed with some care. This was done by observing reflected light from the polished blade surfaces.

When flutter occurs it consists of combined blade bending (plunging) and torsional degrees of freedom. A simple analysis indicated that blade coriolis accelerations were probably a factor coupling the two degrees of freedom, that high values of the blade natural frequency in torsion (ω_α) were important in avoiding flutter, and that the ratio of ω_α to the natural frequency in blade plunge (ω_h) should be well above unit. Since the effective blade torsional natural frequency is lowered if the central column is torsionally weak, it follows that the column design must be stiff. Assuming high column torsional stiffness, it can be shown that ω_α is proportional to

$$\frac{t}{\ell c}\sqrt{\frac{G}{\rho_B}} \text{ (neglecting rotational speed effects)}$$

where t = airfoil thickness

c = airfoil chord

G = shear modulus of blade material

ℓ and ρ_B are as previously defined

A similar non-rotating reference value of ω_h can be defined, which is proportional to

$$\frac{k}{\ell^2}\sqrt{\frac{E}{\rho_B}}$$

so that the ratio of the two reference natural frequencies, ω_α/ω_h, is proportional to

$$\frac{\ell t}{k c}\sqrt{\frac{G}{E}}$$

In the wind tunnel flutter models, this parameter was

varied from 133 to 300. Another dimensionless parameter which could affect the reduced flutter speed is the blade-to-air density ratio

$$\frac{\rho_B A_B}{\frac{\pi}{4}\rho c^2}$$

where A_B is the blade material cross-section area. The density parameter was varied over approximately a 10:1 range, as shown in Figure 3.

Measured flutter speeds were reduced to the non-dimensional form

$$\frac{U_c \ell}{t}\sqrt{\frac{\rho_B}{G}}, \text{ which is proportional to } \frac{U_c}{\omega_{\alpha c}}$$

where U_c = blade tangential velocity at flutter onset.

This quantity is plotted versus the density ratio in Figure 5, from which it is seen that the flutter speed is relatively insensitive to blade density ratio, and is significantly raised by the addition of supporting struts. Over the wind-to-blade speed ratio range $V/U = 0$ to 0.7, airspeed had little effect on flutter speed.

The form of the flutter parameter indicates that, for geometrically and structurally similar rotors, the critical blade flutter speed is independent of rotor scale. With metal blades attached to a torsionally rigid column, especially with blade bracing, the aeroelastic model tests have indicated that other factors will usually dictate a greater blade section thickness than that required to avoid flutter.

6. STOPPED-ROTOR BLADE BUCKLING

Unless the blades of a vertical-axis rotor are of very

light weight construction, centrifugal tension under normal operating condition is generally high in comparison with the aerodynamic compressive load on the upwind blade, and hence the most critical blade buckling case occurs under high winds when the rotor is stopped with one blade upwind. In this condition the combined gravitational and aerodynamic loads can produce stresses that are above critical.

A simplified analysis suggests that for rotors with constant-chord stressed-skin blades the important non-dimensional parameters are,

aerodynamic buckling: $B_A = \frac{q_c h \ell^2}{\tau E k^2}$, and

gravitational buckling: $B_G = \frac{\rho_B \ell^2 g}{E k^2}$

where q_c = critical wind dynamic pressure

h = rotor height

ℓ = blade length

τ = total airfoil skin thickness

E = modulus of elasticity

k = airfoil radius of gyration in bending

ρ_B = blade material

g = acceleration of gravity

For a family of geometrically and structurally similar rotors, the aerodynamic buckling parameter is independent of scale, but the gravitational parameter increases linearly with scale, indicating the increasing severity of gravitational effects with increasing rotor size.

A family of rotor models was constructed with blades made of thin ribbons of steel and aluminum, and these were

tested with the rotors not rotating in a low speed wind tunnel. The models ranged in rotor height from 10 to 30 inches (25.4cm to 76.2cm). The blades were unbraced, and braced at two different locations. Two values of rotor height-to-diameter ratio were used. It was found that the most critical azimuth angle for blade buckling was with one blade directly upwind. The results of the wind tunnel buckling measurements are summarized in Figure 4.

The critical value of the aerodynamic buckling parameter was found to be sensitive to the gravitational parameter only over a limited range. If $\sqrt{1/B_G}$ is reduced to a low value, B_A drops sharply and will approach zero, indicating gravitational collapse at no wind speed. However, increasing $\sqrt{1/B_G}$ above 0.1 has no further effect on the buckling wind speed, especially if the blades are braced with horizontal struts to at least 0.5R. Figure 5 shows an example of the relationship between solidity per blade (C/R) and rotor size that is required for $\sqrt{1/B_G}$ to exceed 0.1 with a particular configuration. In this figure the effect of ice loading was calculated by assuming that ice was evenly distributed over the blade, and had mass but no stiffness. Even with low solidity per blade, large rotor sizes are possible without incurring gravitational or aerodynamic buckling.

In order to maintain the required value of the aerodynamic buckling parameter B_A, there will be a minimum permissible solidity per blade (C/R) that will depend upon the ratio of blade skin thickness to airfoil chord. Relatively

thick-walled structures, such as aluminum extrusions make possible the use of low-solidity blading such as that on the Magdalen Islands turbine, for which C/R = 0.05. Figure 4 also shows that horizontal blade bracing struts to 0.5 or 0.7R approximately double the critical buckling wind speed.

7. TWO-BLADE ROTOR DYNAMIC LOADS

7.1 Cyclic Drag and Side Loads

One of the disadvantages inherent in the choice of a two-bladed configuration for the large 200 kW vertical-axis turbine is that the rotor has large cyclic drag and cross-wind force components. Both components would be expected to have a principal frequency equal to twice the rotor rotational frequency.

In order to measure these components, the 60-inch (1.52m) flutter model described in Section 5 was mounted in the wind tunnel with its upper bearing supported in a two-component strain gauge balance rigidly attached to the tunnel roof. The dynamic drag and side force balance output were transmitted to a Hewlett-Packard Fourier Analyzer to determine the amplitude of the various frequency components. The most significant components occurred at frequencies of 2, 4 and 6 times rotational frequency. These data are plotted in coefficient form in Figure 6 and 7 versus the wind-to-blade velocity ratio V/U, for a rotor solidity NC/R of 0.1.

The dynamic force coefficients, based upon the square of blade velocity, are defined on the graphs.

7.2 Cyclic Torque

For a two-bladed vertical-axis rotor, the aerodynamic torque generated is near zero when the blades are moving directly up- and down-wind, and reaches a maximum at one-quarter revolution from this position. Thus the main component of torque ripple, when the blades remain largely unstalled, occurs at a frequency of twice the rotational frequency, and its half-amplitude is roughly 100% of the mean torque. This ripple magnitude would be unacceptable in most applications if it were allowed to feed through the energy conversion system. It would also lead to large out-of-plane bending moments at the blade roots, if the blades were assumed to be rigid. Fortunately, rotor elasticity and the slip characteristics of an induction generator can greatly attenuate the magnitude of this ripple, and can also react into the rotor structure in such a way as to attenuate the blade root moments (provided that the rotor has one, or two blades, but not three). In effect, the large aerodynamic torque ripple is reacted by small-amplitude cyclic acceleration and deceleration of the blades as they rotate.

In order to experimentally investigate torque ripple and blade dynamic stresses more accurately than would have been possible on small wind tunnel models, a one-quarter scale aeroelastic model of the Magdalen Islands turbine design, with hollow aluminum extruded blades, was constructed by

Dominion Aluminum Fabricating, Limited as a part of the contract for the full-scale system. The model rotor height was 30 ft. (9.14m) so that it would just fit into the NRC 30 ft. tunnel. A photo of this model in the tunnel is shown in Figure 8.

Since the blockage of this rotor in the tunnel was too large for accurate wall interference corrections to be made to tunnel velocity, no precise power coefficient calibration could be carried out. Wall effects were reduced to some extent by operating the tunnel with an open roof, but in any case the purpose of the tests was to determine maximum values of torque ripple, blade stresses, etc. over the full range of velocity ratio, and hence no accurate determination of wind speed was required. The turbine was coupled to a three-phase induction motor-generator to permit operation at nearly constant rotational speed.

The maximum rotor shaft torque ripple half-amplitude was found to be about 12 percent of maximum mean torque, thus confirming the large attenuation that was expected. If required, further reduction in output torque ripple could be achieved by introducing a flexible shaft coupling, and a tuned fly-wheel, provided that care is taken to avoid the additional resonant frequencies that are introduced by mechanical filtering. Although theoretical analysis has indicated the feasibility of these refinements, an analysis carried out by Hydro Quebec for the Magdalen Islands transmission system has shown that, without further filtering, the maximum line voltage ripple will

remain well below a permissible value of ± 0.05 percent, at maximum wind power input.

7.3 Blade Stresses

Resistance strain gauges were attached at 28 locations on the blades, struts and central column of the 30 ft. (9.14m) aeroelastic rotor model to measure dynamic stress levels. No significant dynamic stresses were measured under normal operating conditions at wind-to-blade speed ratios less than 0.25, for which the blades remain unstalled. At ratios greater than 0.25, resonances could be excited in the out-of-plane "butterfly" mode of the blades when the natural frequency of this mode was an odd multiple of the rotational frequency. The most significant stress occurred at the trailing edge of the blades, immediately outboard of the strut attachment point. Some data from this location, presented in Figure 9, in the form of a stress coefficient $S/\frac{1}{2}\rho U^2$, where S is the peak-to-peak dynamic stress and U is the blade equatorial speed, shows the effect of adding friction damping at the attachment point of the struts to the blades. An analysis of these data shows that satisfactory dynamic stress levels can be maintained on the full-scale rotor.

Most of the dynamic stress data were taken with a relatively stiff support at the upper rotor bearing, the natural frequency of the upper mount being about four times the normal operating rotational frequency. A few runs were made with a softer upper mount having a natural frequency of 1.25 and 1.5 times rotational frequency. With this softer

mount the blade stress levels were generally reduced, although insufficient data were taken to explore the effect in detail.

8. WIND ENERGY IN A MIXED POWER SYSTEM

A probability model has been developed to examine some of the problems of adding random energy from large-scale wind plants to existing power networks that are required to supply energy on demand to a load of known characteristics. The model does not address certain engineering problems such as system stability and control, and is not useful for studying behaviour over short time intervals; it deals with integrated energy over periods that are assumed to span at least one year.

A diagrammatic description of the model is shown in Figure 10. It consists of four components:

(a) A load, representative of certain communities and regions in Canada which, because of geographic location, are supplied with electricity by local oil-fired plants. The load characteristics are given in the model by one or more demand curves representing different types of days during the year (e.g. winter week-days). A pair of such curves is shown in box (a) in the figure. The quantity H(L) is the number of hours per day during which the demand power is at or above a given level L.

(b) A storage unit, into which energy can be pumped during base load periods, and discharged during peaking operation, with a specified percentage loss. The effect of storage in modifying the load demand curve as "seen" by the

power plants is shown for a typical case in box (b). Large-capacity seasonal storage is not modelled.

(c) A wind plant, which may consist of any number of turbine units of total installed power P_{max}. It is assumed that the fluctuations in available wind power are statistically uncorrelated with short-period fluctuations in demand, although seasonal correlation is allowed for. During each season, the availability of wind power up to P_{max} is assumed to be random, but to have a known probability distribution. Typical distributions, computed for contstant-speed vertical-axis turbines in the Gulf of St. Lawrence region are shown in box (c). The shape of these curves is a function of turbine performance and wind speed probability distribution. They contain a spike of finite area at $P_w = 0$, signifying that there is a finite probability that there will be no wind power. The probability distribution p_w is scaled so that

$$\int_{P_w = 0}^{P_{max}} p_w \cdot dP_w = 1 \text{ (including the spike at } P_w = 0)$$

(d) A thermal power plant, capable of supplying energy on demand. Its demand curve is as shown in box (d).

An enlarged version of this box is shown in Figure 11(a). The upper boundary of the shaded area is the storage-modified demand curve for a particular day-type (e.g. winter week-days). The average demand curve as "seen" by the thermal plant is the curve labelled $H_T(L)$, and it can be shown to be given by the integral equation in the diagram, which involves the wind power probability distribution p_w. The diagram has been drawn

for a large value of the installed wind power P_{max}. If P_{max} is greater than the base load demand, some wind energy must be discarded (or not generated) because there will be occasions when available wind power is higher than demand. The shaded area below the H axis represents the average daily amount of this "lost" wind energy. A computer analysis of the system model has been carried out, with the following results.

For the one situation so far investigated (eastern Canadian coastal regions) the seasonal variation in available wind energy closely matches the seasonal variation in electricity demand. Thus, although seasonal storage was not modelled, there appears to be little need for it.

Figure 11(b) shows the effect of installed wind plant capacity on the partition of annual energy supply between the wind and thermal plants, when the system has no storage capacity. The wind energy that must be discarded does not represent a large percentage loss until total wind plant capacity approaches the system peak power, or until the wind is supplying about half the total energy demand.

The addition of storage, cycled daily by charging during low demand periods and discharged during peaking operation, serves two purposes: it can reduce the required thermal plant installed capacity, and may recover a part of the discarded wind energy. Whether the first of these (peak-shaving) is worthwhile depends upon the relative capital costs of the storage and thermal plants, and this is relatively

independent of the wind part of the system. With regard to the recovery of "lost" wind energy, our analysis has shown that the wind energy recovered into storage was surprisingly small — not more than about 10% of the discarded energy. If storage is to be useful for reliable peak-shaving, then it must be charged partly by thermal plant energy, and it was found that unless the storage exchange efficiency is greater than about 80% the storage losses would exceed the recovered wind energy.

It therefore appears that, in a system of the type analyzed, there may be little to be gained by the use of either long-term (seasonal) or short-term (daily) storage, but that significant fuel savings can be achieved by the addition of wind energy up to about half the system demand.

The economic savings can be substantial. For example, industrial estimates of the production cost of the 200 kW vertical-axis turbine system are about $120,000 per unit, including installation. If annual interest rates are assumed to be 3% greater than the inflation rate over a 25-year lifetime, the present value of this cost is about $150,000. Assuming an annual maintenance cost of 3% of the capital cost, increasing at the inflation rate, the present value of the wind energy costs is $240,000, and at a production rate of 600,000 kW-hr/yr., the cost of the 25-year energy is 1.6 cents/kW-hr. in present-value terms. At current fuel oil prices in eastern Canada (approaching 50 cents per Imp. gallon) the fuel component of diesel-electricity is about 3.0 cents/kW-hr.

9. CONCLUSION

Several aspects of recent work at the National Research Council of Canada on the development of vertical-axis turbines have been reviewed. Most of this work, during the past year or more, has been in support of the design of a 200 kW unit now being built for experimental operation on the Magdalen Islands in the Gulf of St. Lawrence. Results of small and large scale aeroelastic wind tunnel model experiments have confirmed that very large scale vertical-axis wind turbines are feasible, especially if designed for normal operation at constant rotational speed. A computer model of a simple mixed power system has indicated that substantial cost savings may be possible by using wind energy in Canadian east coast regions.

REFERENCES

1. R.D. McConnel, M. Fortin, B. Piché and J.H. VanSant. "An Experimental 200 kW Vertical Axis Wind Turbine for the Magdalen Islands". Paper to be delivered at the 11th Intersociety Energy Conversion Engineering Conference, Sept. 12-17, 1976.

2. R.J. Templin. "Aerodynamic Performance Theory for the NRC Vertical-Axis Wind Turbine". National Research Council of Canada Laboratory Technical Report, LTR-LA-160. June 1974.

3. James H. Strickland. "The Darrieus Turbine: A Performance Prediction Model Using Multiple Stream-tubes". Sandia Laboratories Energy Report SAND 75-0431, October 1975.

4. P. South and R. Rangi. "An Experimental Investigation of a 12 ft. Diameter High Speed Vertical Axis Wind Turbine". National Research Council of Canada Laboratory Technical Report LTR-LA-166. April 1975.

TABLE I

Values of Airfoil Normal Force Coefficient and Gross Thrust Coefficient Used in Performance Prediction of Small Scale Rotors

Angle of Attack α(deg)	Normal Force Coefficient CN	Gross Thrust Coefficient $C_T + C_{DO}$
0	0	0
1	0.10	0.0016
2	0.20	0.0066
3	0.30	0.0148
4	0.40	0.0262
5	0.50	0.041
6	0.60	0.059
7	0.70	0.0804
8	0.80	0.105
10	1.00	0.145
12	1.05	0.185
12.5	1.05	0.190
12.6	0.85	0.070
15	0.80	0.040
20	0.77	-0.024
30	1.18	-0.037
40	1.50	-0.040
50	1.80	-0.038
60	1.94	-0.0136
80	2.08	0.040
100	2.05	0.138
120	1.85	0.156
140	1.51	0.154
150	1.17	0.131
160	0.78	0.089
170	0.77	0.016
172	0.80	0.017
180	0	0.030

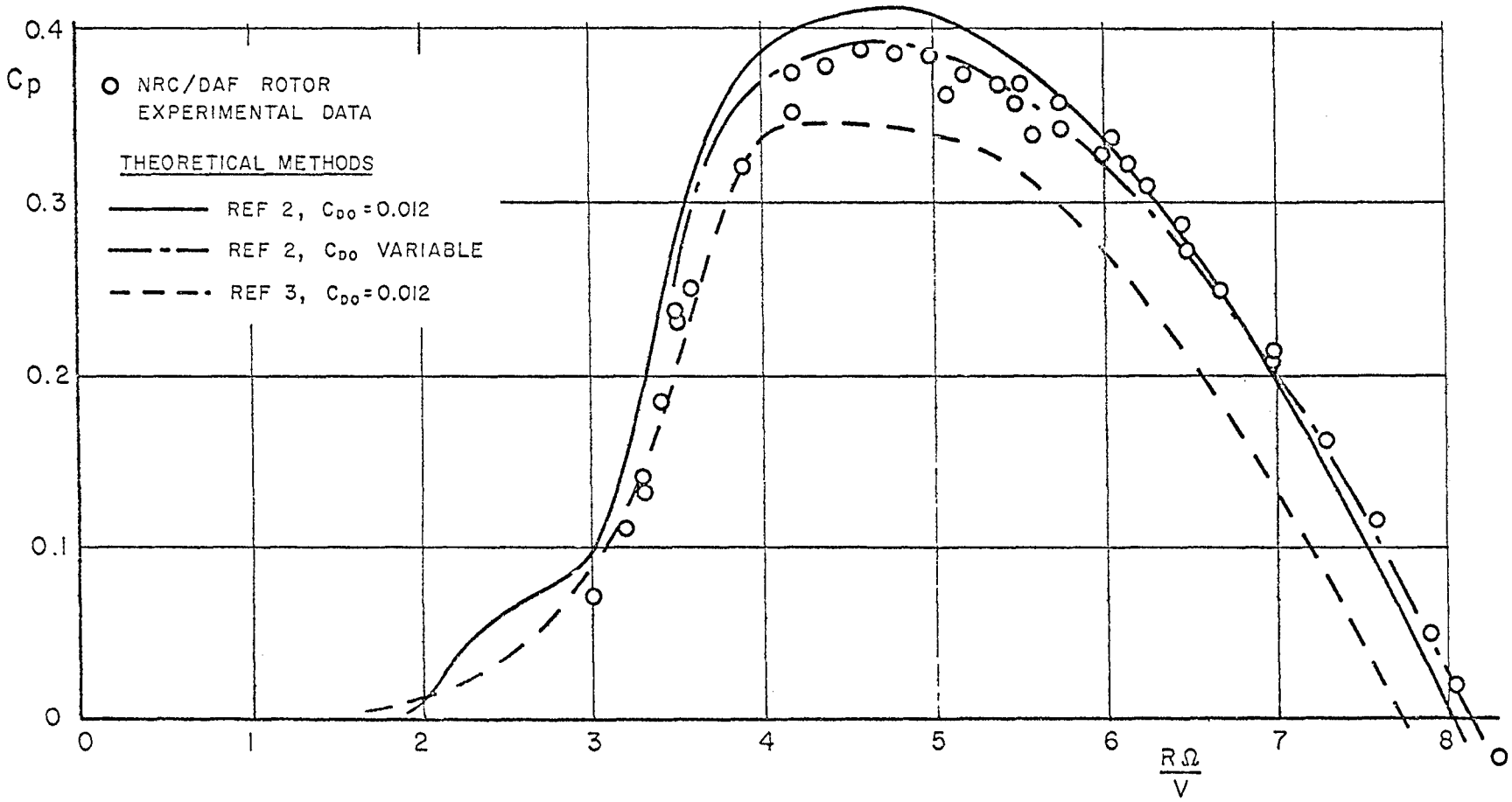

FIG 1 COMPARISON OF PERFORMANCE THEORIES
WITH PRODUCTION ROTOR CALIBRATION

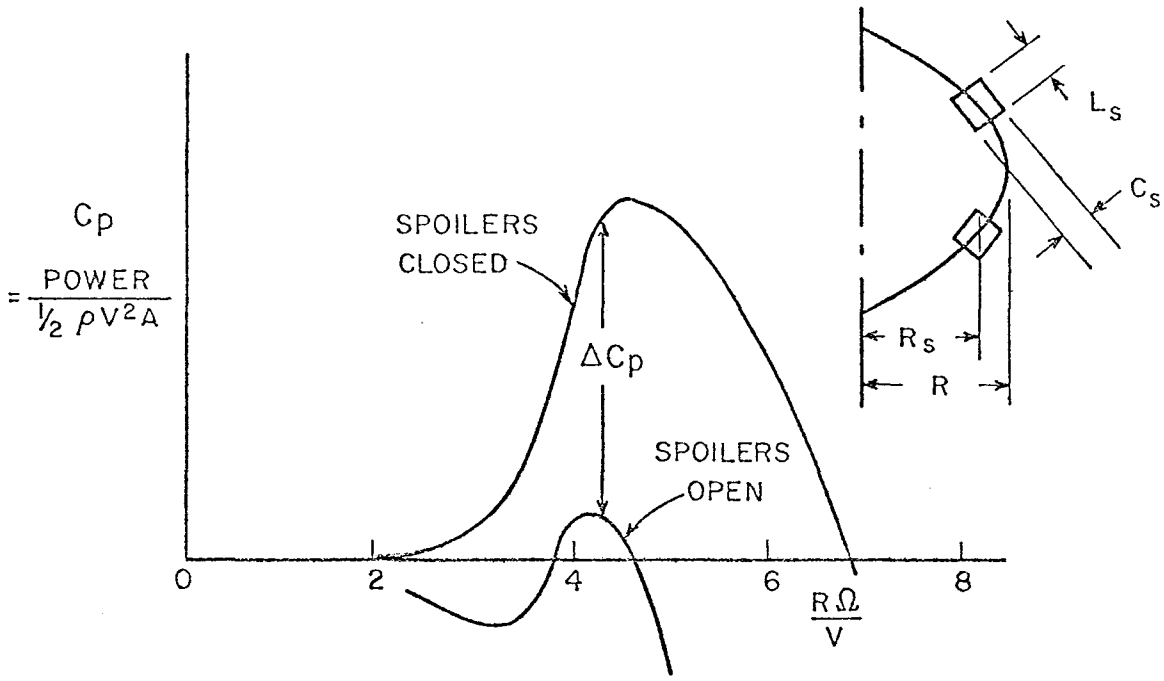

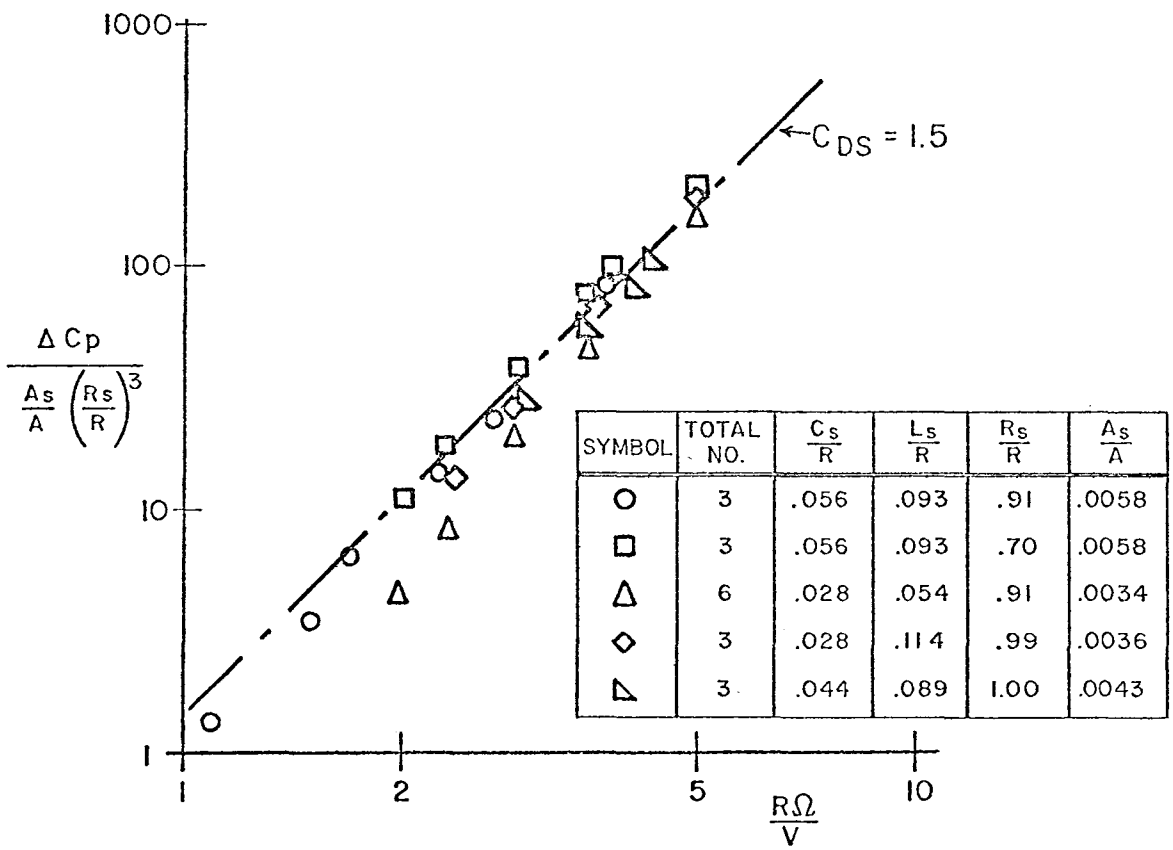

SYMBOL	TOTAL NO.	Cs/R	Ls/R	Rs/R	As/A
○	3	.056	.093	.91	.0058
□	3	.056	.093	.70	.0058
△	6	.028	.054	.91	.0034
◇	3	.028	.114	.99	.0036
◺	3	.044	.089	1.00	.0043

FIG 2 MEASUREMENTS OF SPOILER EFFECTIVENESS ON 3-BLADE ROTORS

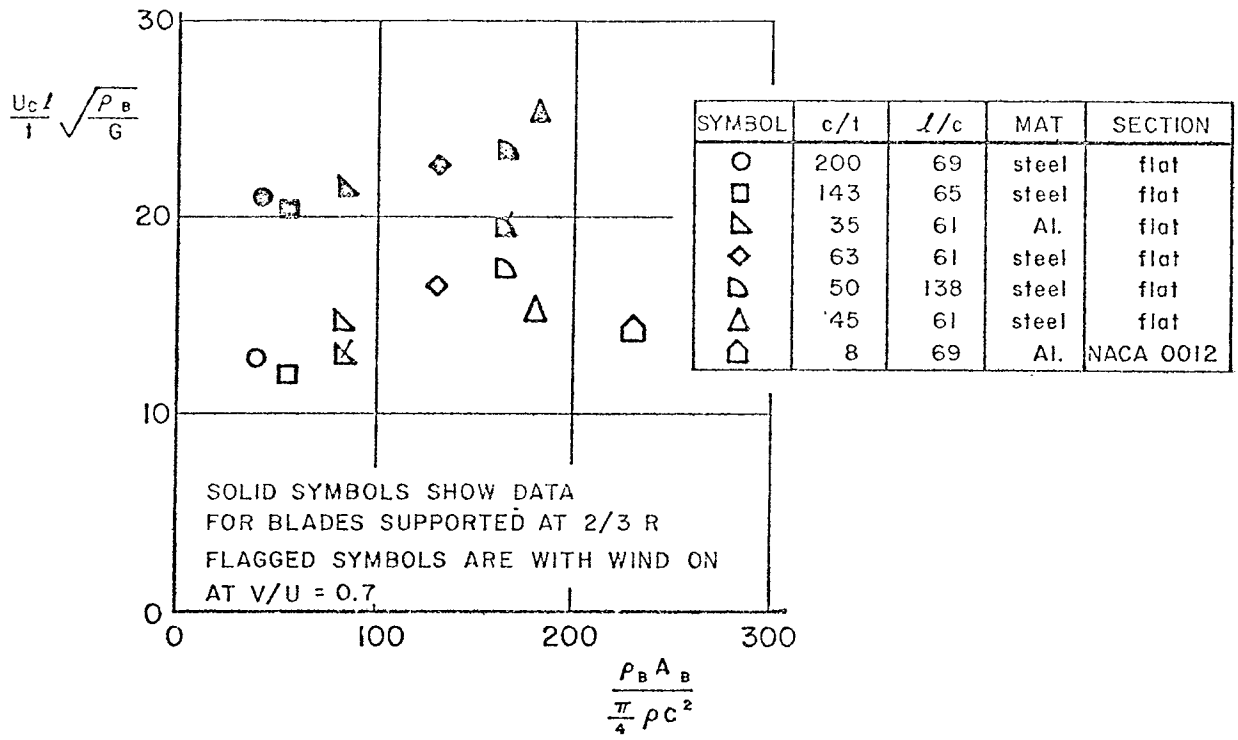

FIG 3 VARIATION OF BLADE FLUTTER PARAMETER WITH DENSITY RATIO FOR TURBINE WITH h/d = 1.5

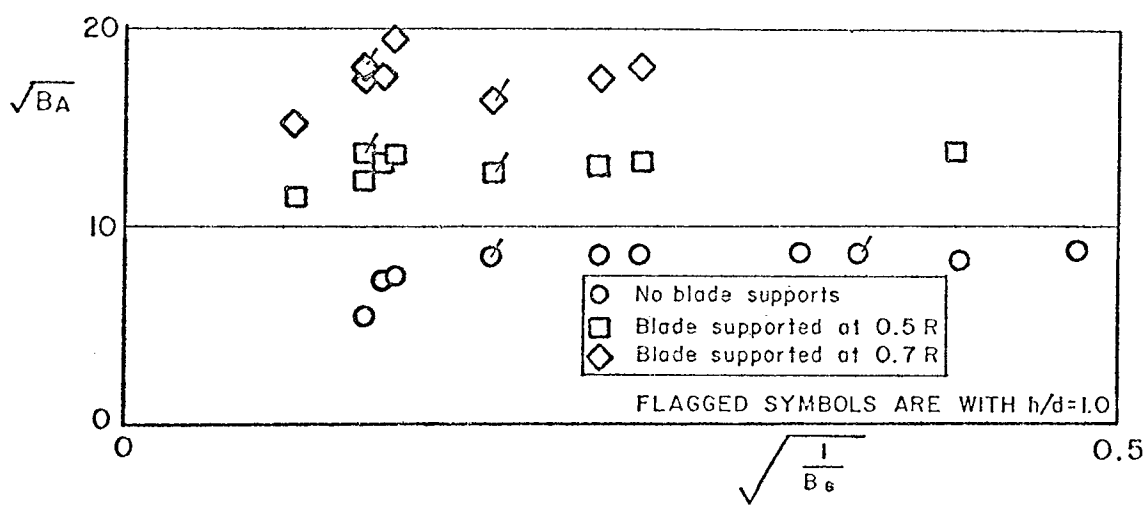

FIG 4 VARIATION OF BLADE AERODYNAMIC BUCKLING PARAMETER WITH GRAVITATIONAL BUCKLING PARAMETER FOR ROTOR WITH h/d=1.5

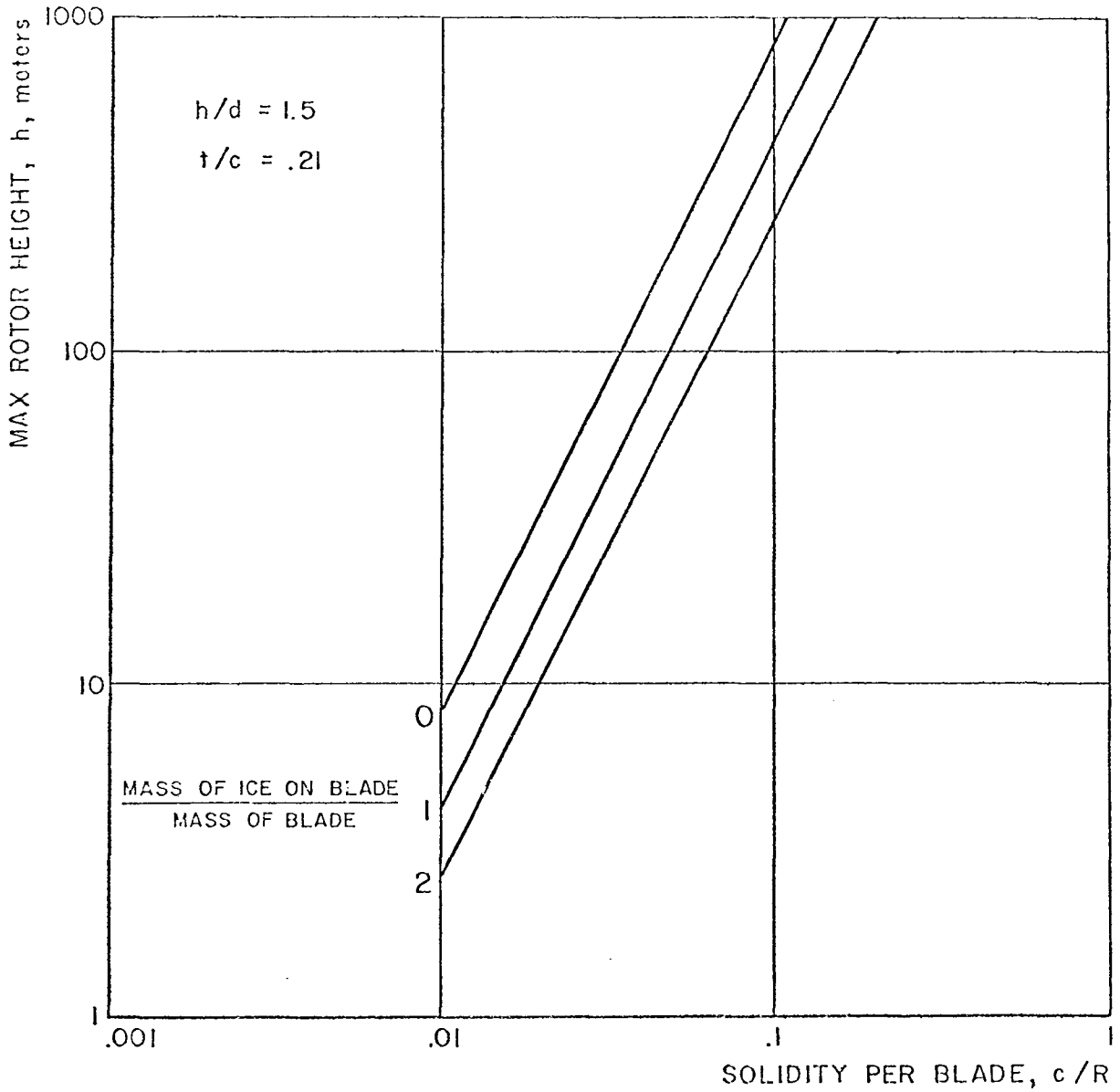

FIG 5 VARIATION OF MAXIMUM PERMISSIBLE ROTOR HEIGHT WITH SOLIDITY PER BLADE FOR CONSTANT SECTION HOLLOW METAL BLADES

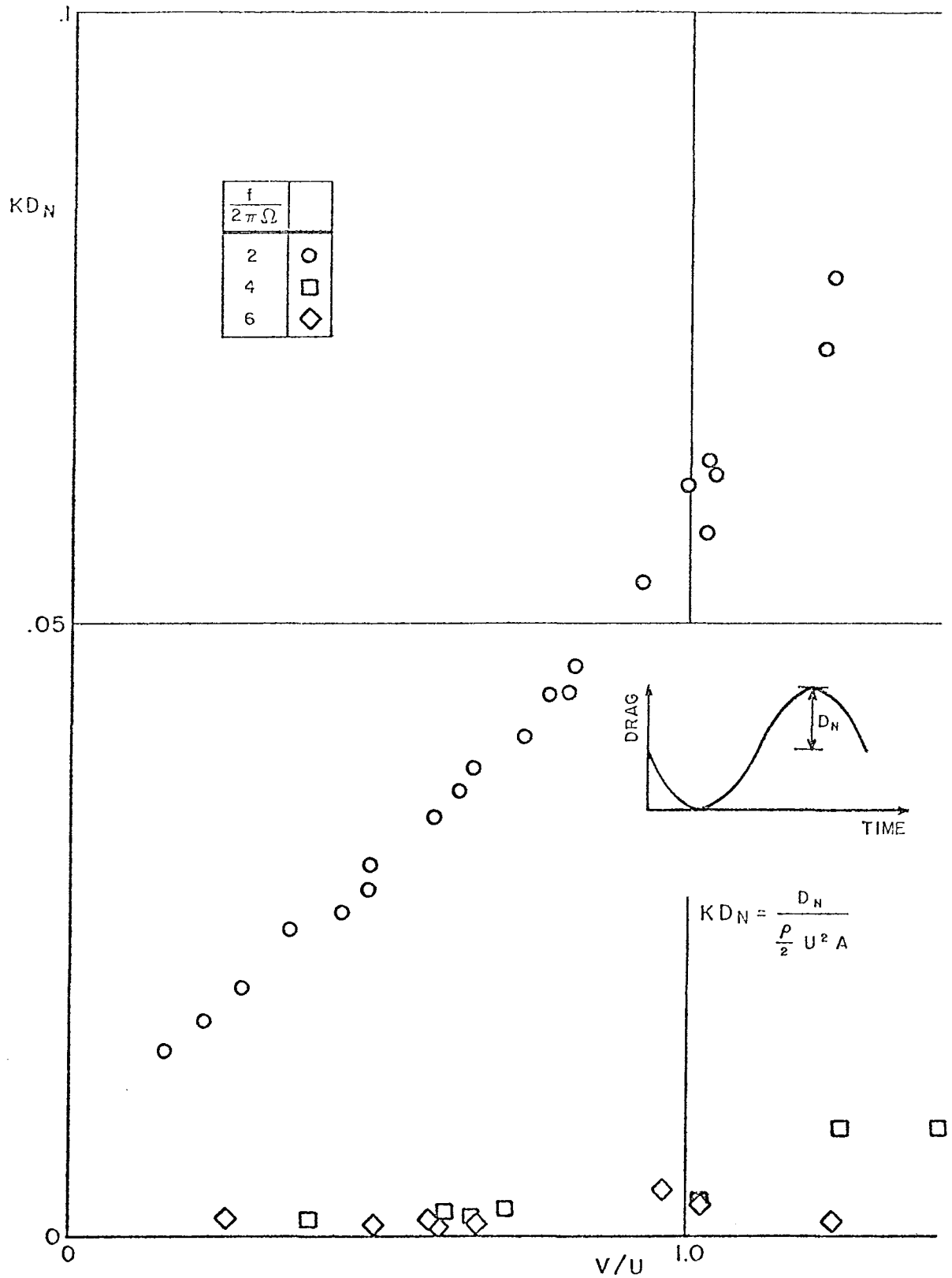

FIG 6 AMPLITUDE OF DYNAMIC DRAG FORCE ON A TWO BLADE ROTOR

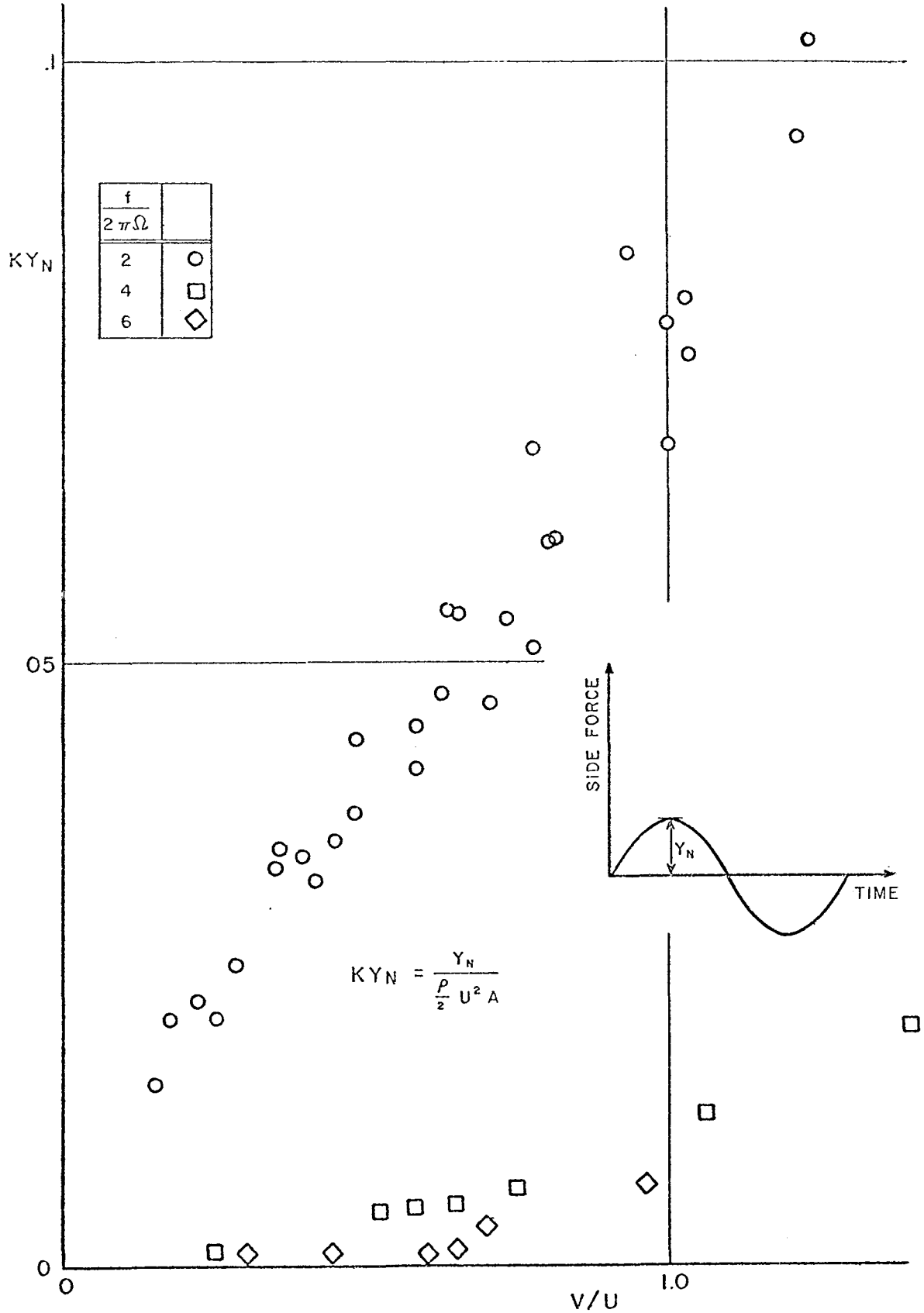

FIG 7 AMPLITUDE OF DYNAMIC SIDE FORCE ON A TWO BLADE ROTOR

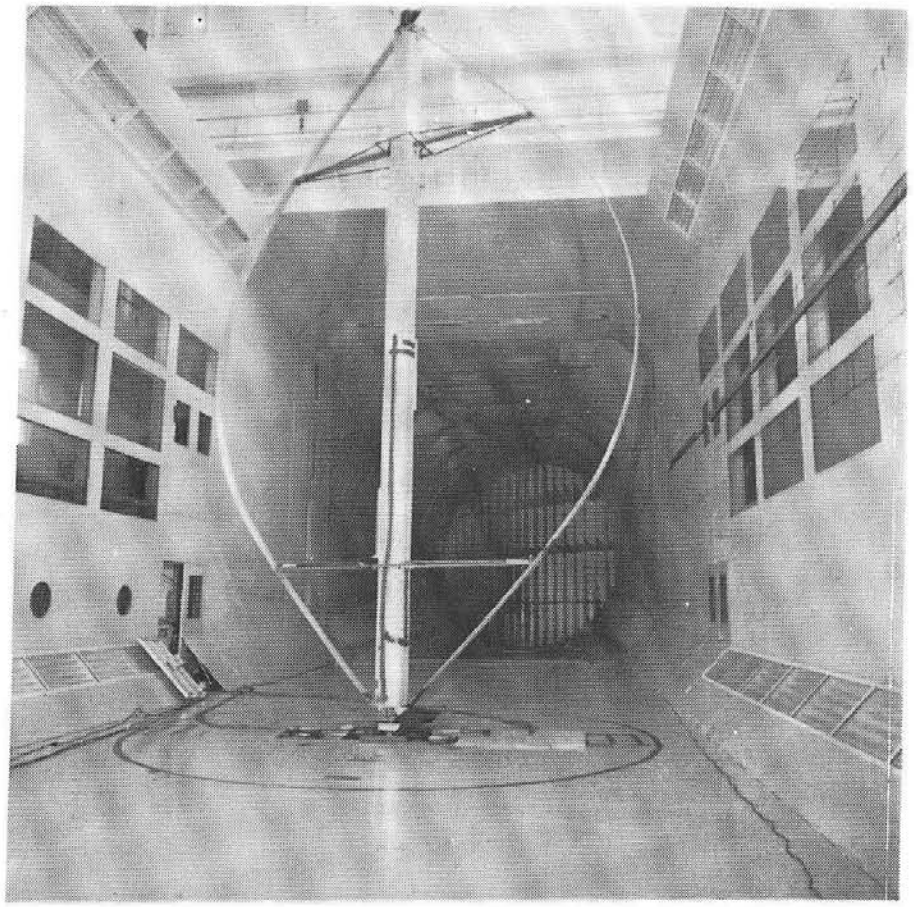

FIG 8 9x6M TURBINE IN NAE 9x9M WIND TUNNEL

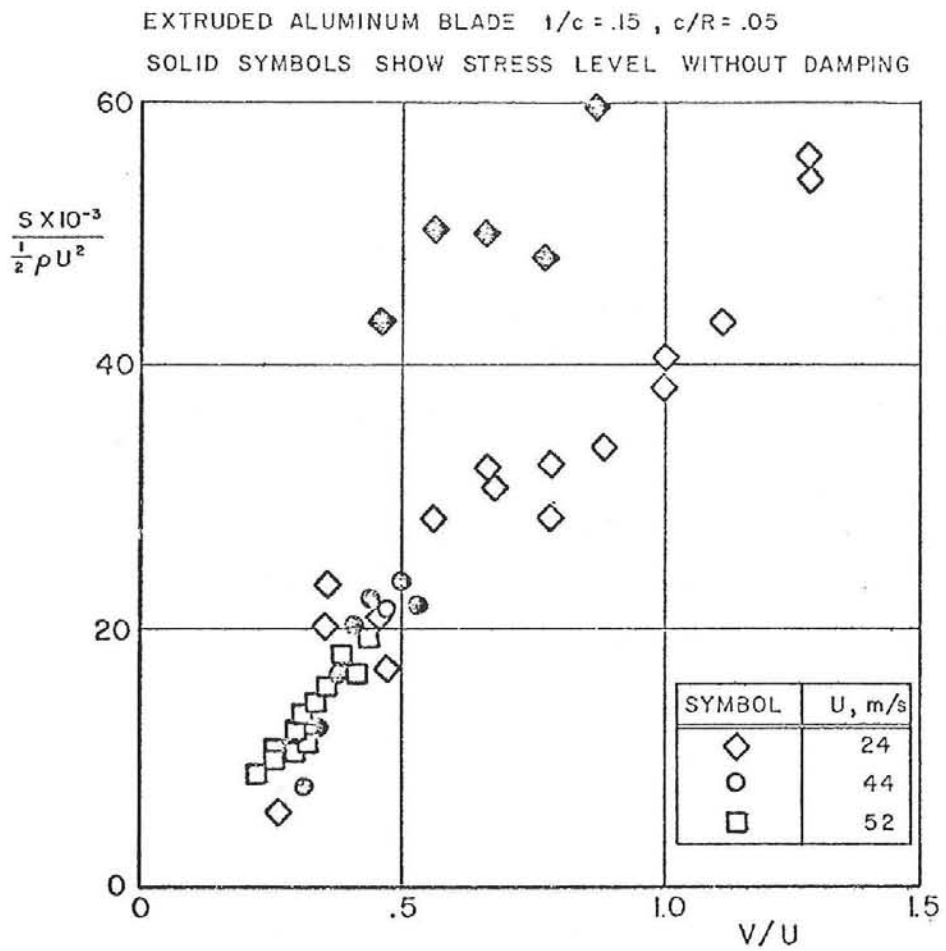

FIG 9 PEAK-TO-PEAK AMPLITUDE OF DYNAMIC TENSILE STRESS AT TRAILING EDGE OF BLADE

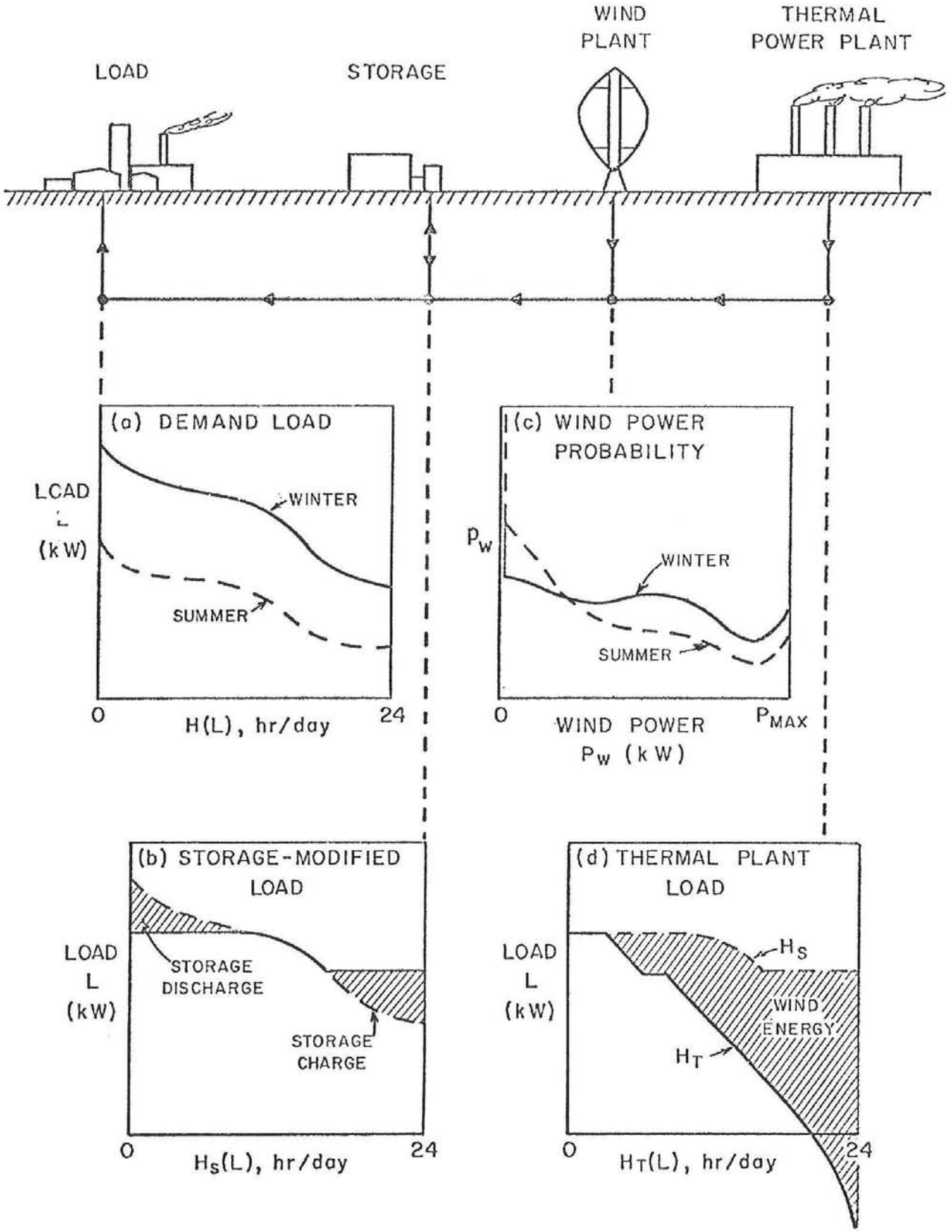

FIG 10 MIXED POWER SYSTEM DESCRIPTION

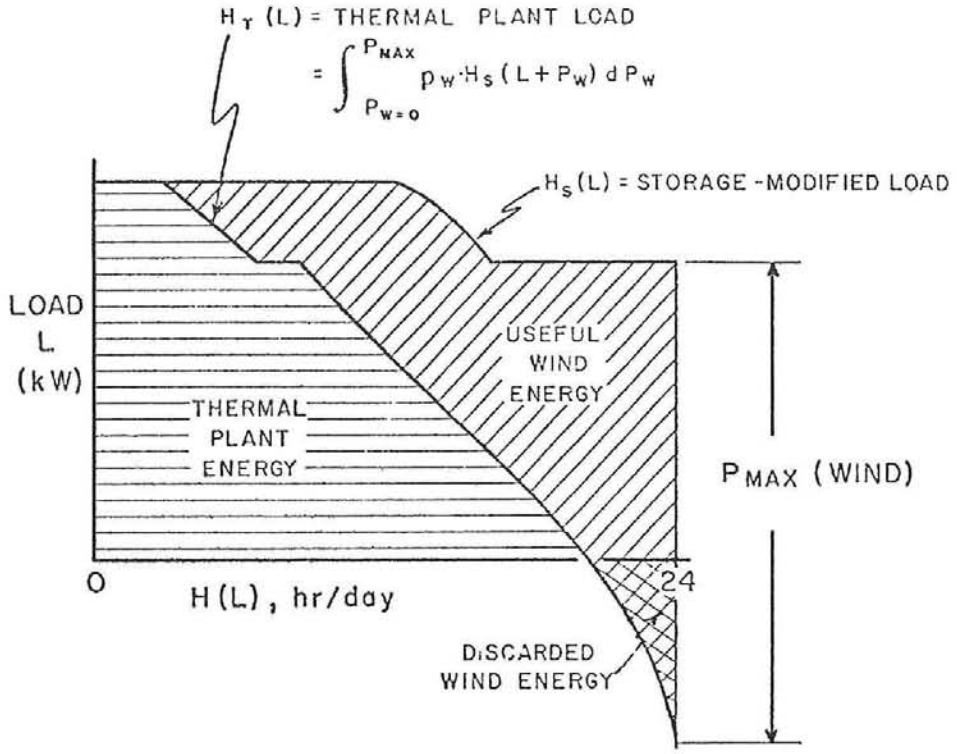

(a) PARTITION OF ENERGY SUPPLY DURING A TYPICAL DAY

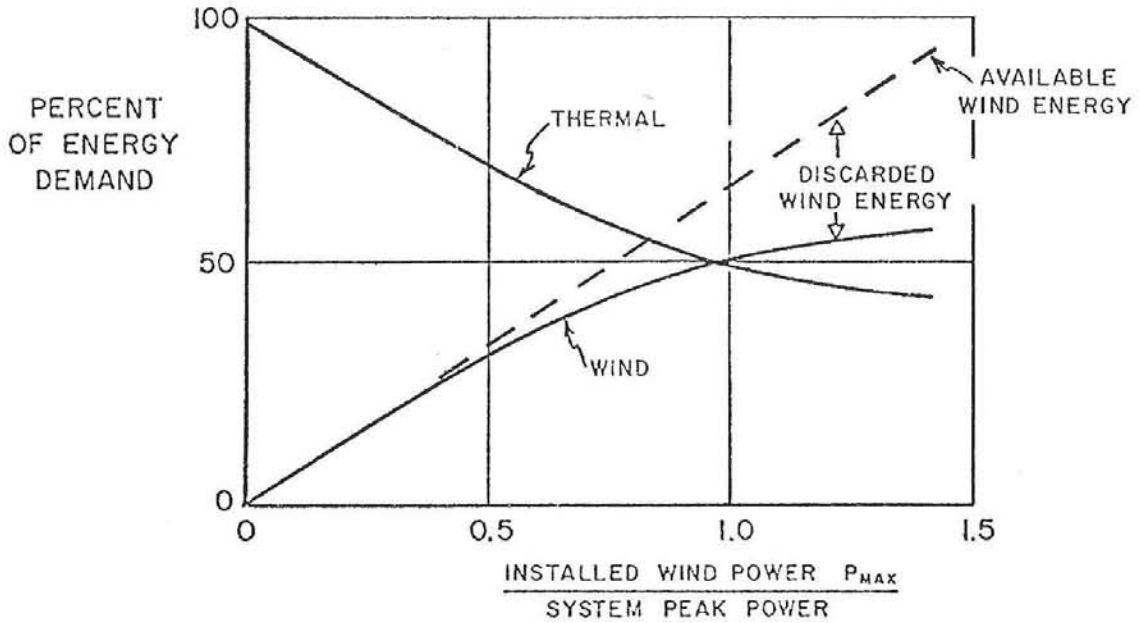

(b) PARTITION OF ANNUAL ENERGY SUPPLY

FIG 11 PARTITION OF ENERGY IN MIXED POWER SYSTEM

SYSTEM DESIGN - 17-METER RESEARCH TURBINE

Emil G. Kadlec

Sandia Laboratories

SYSTEM DESIGN - 17-METER RESEARCH TURBINE

The purpose of this paper is to familiarize you with the 17-meter research turbine design. Several of the succeeding speakers will refer to the 17-meter system, so an understanding of the purpose, design approach and current design will be helpful.

The purpose of the 17-meter design is two-fold: 1) to provide a test bed for system performance and response, and 2) to provide a test bed for component evaluation.

Analytic studies and development have been conducted concurrently with the system design. This analytic effort as developed was used to guide and support the 17-meter design. The design, in turn, will be used to evaluate the adequacy of the analysis. These analytic efforts are systems analysis, aerodynamics, electrical, and structural.

The approach was to design and fabricate a system which was large enough to require vigorous analysis and which could be scaled up. Optimization was not a goal, but flexibility was. Commercially available components were used wherever possible to reduce cost, effort, and time. Since the 17-meter system is a test bed, instrumentation is built into the system and components are mounted in a non-compact, easily accessible arrangement.

An artist's conception of the 17-meter system is shown in Figure 1. While this figure is not entirely consistent with the design, salient features of the design are depicted. As can be seen, struts have been added to modify the blade resonant characteristics and affect the additional gravity loads which are inevitable with scaleup. An aerodynamic study was conducted which indicated a substantial effect if struts were arbitrarily shaped. As a result, the struts have the same cross section as the blades. The blade shape is the straight-circle-straight approximation of the troposkein shape (spinning rope shape).

Since cable tensions can affect system resonant frequencies, load cells are included in the cable system and can be seen in Figure 1. The general arrangement of the base support tower and components can also be seen.

Figure 2 is a block diagram of the 17-meter system showing the major elements. While the general arrangement and interaction are self-apparent, a few words of explanation are appropriate.

The blade instrumentation referred to will be strain gage information measured at several locations. This information will be transmitted from the rotating parts by a radio frequency link as indicated or by slip rings. Both approaches are being pursued.

The brake, which will be discussed later, is coupled directly to the rotary tower so that braking torque is not transmitted through any component or coupling.

The auxiliary start motor (50 HP) applies torque through the synchronous generator and not as shown directly to the speed increase. An electrically-controlled clutch couples the start motor and the synchronous generator.

The general specifications are shown in Figures 3 and 4. It should be noted that the turbine can be operated with 1, 2 or 3 blades which will allow testing at several solidities. In addition, tests may be conducted without struts should the structural response fall within acceptable limits.

The brake characteristics are listed in Figure 5. Two separate systems are being designed. One system will be used for normal operations, both in synchronization and in shutdown. The other will be an emergency system which will utilize stored energy so that it will be operable in case of loss of power. Both the torque and energy dissipation capabilities of the system exceed the conservatively calculated requirements.

The arrangement of power train components is shown in Figure 6. Flexible couplings are used on both sides of both torque transducers. The couplings are of the no-slack, elastic design to provide protection from high amplitude transients to the torque transducers. The speed increase consists of three elements (Figures 6 and 7): a three-stage planetary, a right-angle drive, and a timing belt drive. The three-stage planetary and the right-angle drive are fixed ratio. Ratio changes are accomplished by pulley changes in the timing belt drive.

The design of major items is almost completed. Most of the long lead time orders have been placed and delivery dates are compatible with the schedule shown in Figure 8. The order for the blade design was placed with Kaman Aerospace in early February. Delivery is scheduled for the first week of October. The speed increase elements are either ordered or procurement activity is currently underway.

Since promised delivery dates have not been received for all the items, the schedule may be changed. However, reasonable procurement time has been allowed for all items and the expectation of meeting the schedule is high.

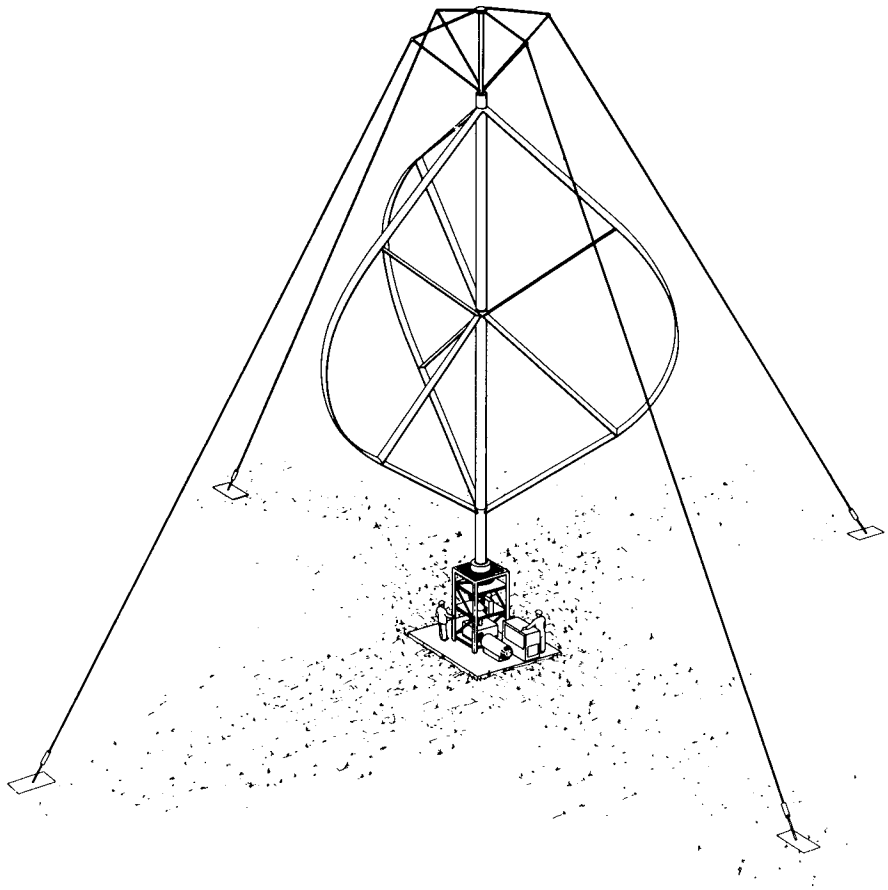

Figure 1

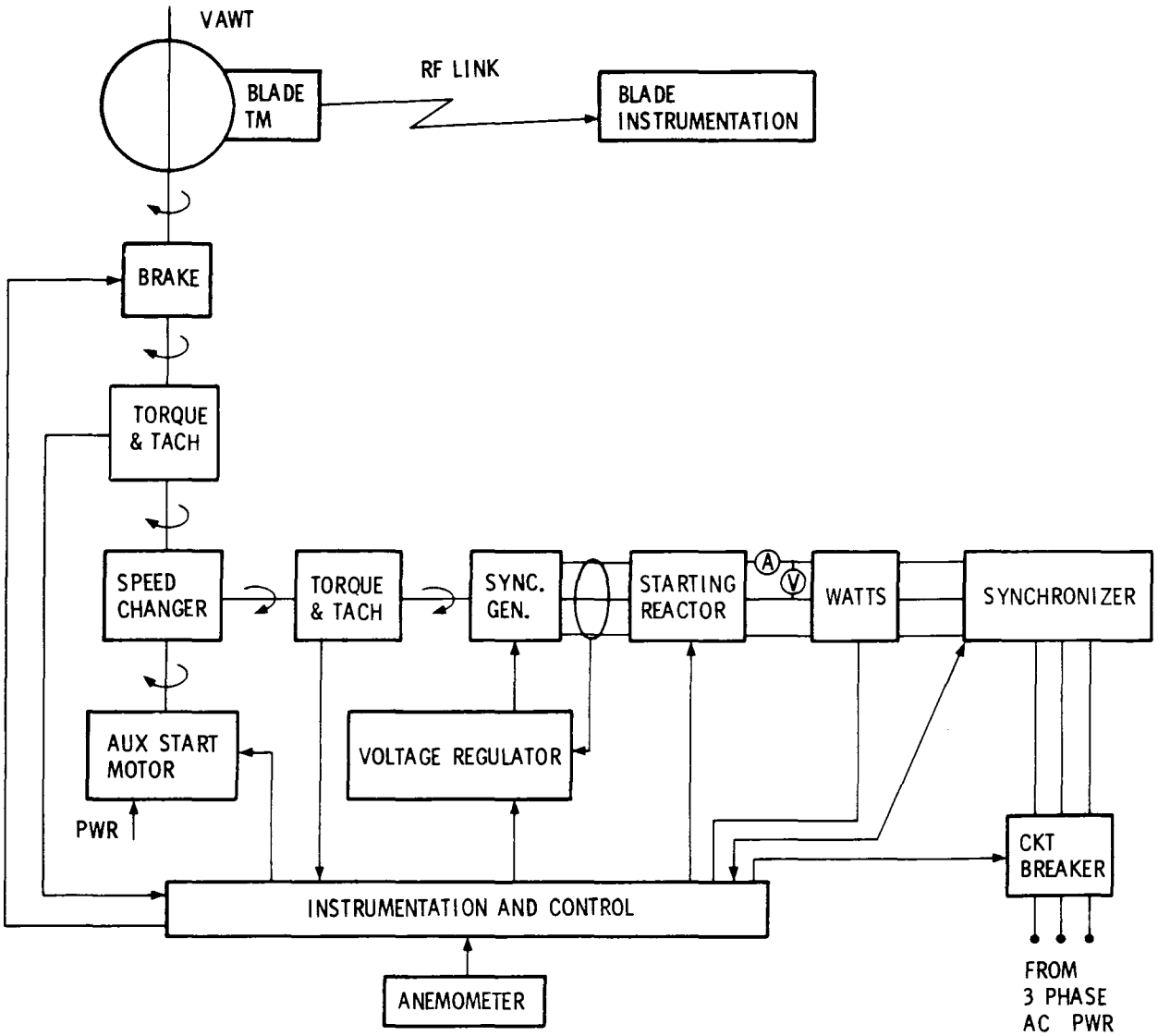

Figure 2. Synchronous Windpower System

17 METER DARRIEUS
GENERAL SPECIFICATIONS

DIAMETER METERS	17M
NUMBER OF BLADES	1, 2 OR 3
BLADE SECTION	NACA 0012
BLADE SHAPE	STR-CIRCULAR-STR
CHORD LENGTH	.533 METERS, 21 INCHES
TURBINE SWEPT AREA	180 SQ. METERS, 1937 FT^2
SOLIDITY	.07 PER BLADE

Figure 3

17 METER DARRIEUS
GENERAL SPECIFICATIONS

POWER:	
TURBINE POWER KW	70
GENERATOR OUTPUT KW	60
GENERATOR RPM	1800
RATED WIND SPEED MPH	32
CUT-IN WIND SPEED MPH	10
CUT-OUT WIND SPEED MPH	60
TURBINE RPM AT RATED POWER	45.4
DIRECTION OF ROTATION (LOOKING DOWN)	CCW

Figure 4.

BRAKES

TYPE	DISC
OPERATION	HYDRAULIC
DISC DIAMETER	30 INCHES
NO. OF CALIBERS	4 PER SYSTEM
TORQUE PER SYSTEM	53,000 LB FT
ENERGY DISSIPATION PER SYSTEM	3×10^6 FT LBS

Figure 5

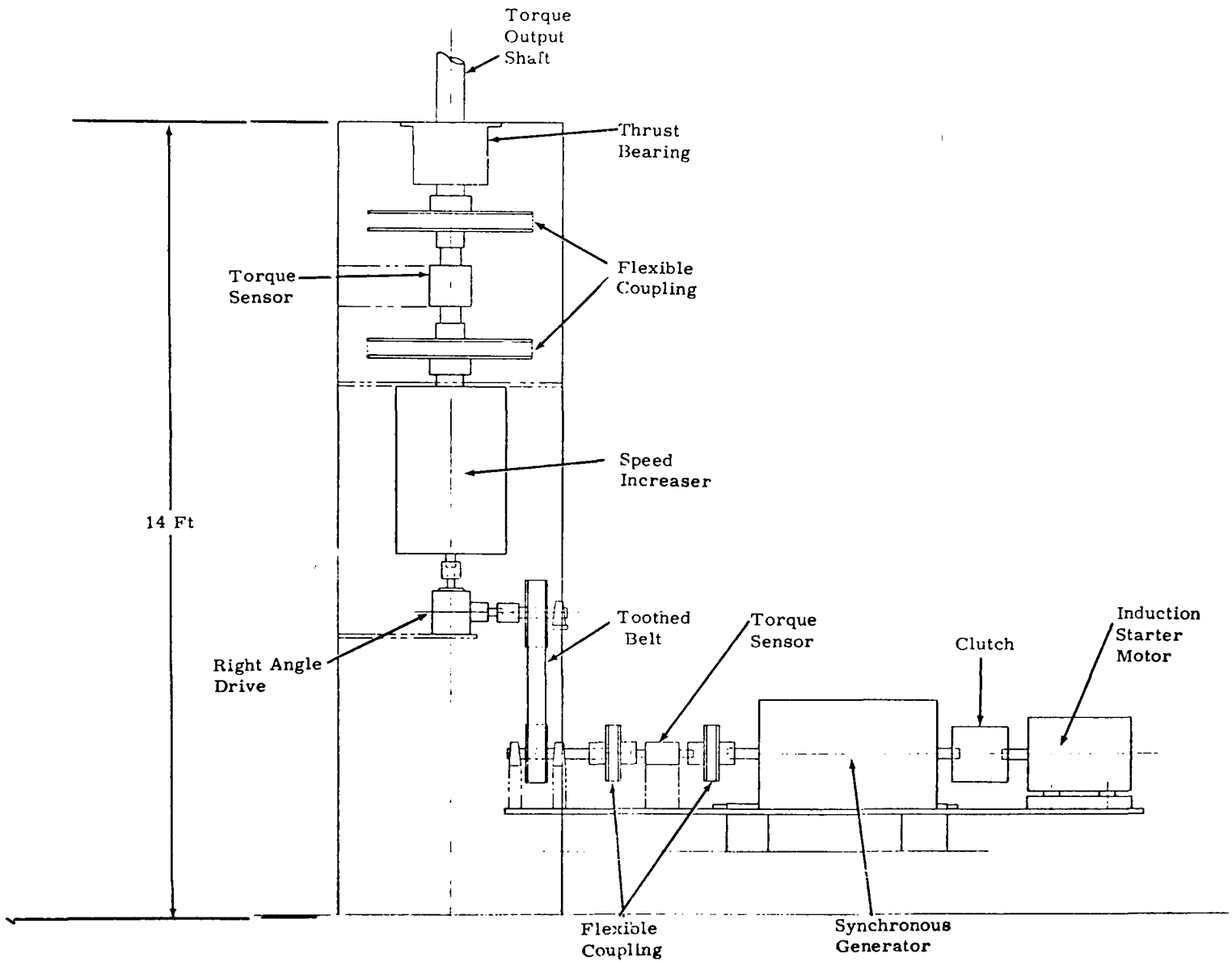
Torque
Output
Shaft
Thrust
Bearing
Flexible
Coupling
Torque
Sensor
Speed
Increaser
14 Ft
Toothed
Belt
Torque
Sensor
Clutch
Induction
Starter
Motor
Right Angle
Drive
Flexible
Coupling
Synchronous
Generator

Figure 6

SPEED INCREASER

- 3 STAGE PLANETARY

  42.9 : 1 RATIO

  13500 LB FT TORQUE CAPABILITY

- RIGHT ANGLE DRIVE

  1 : 1 RATIO

- TIMING BELT DRIVE

  4 INCH BELTS

  YIELD TURBINE SPEEDS

  30 THRU 54 RPM

Figure 7

17 METER SCHEDULE

COMPLETION OF MAJOR ITEM DESIGN	MAY 31
START OF TURBINE ASSEMBLY	AUG. 16
COMPLETION OF BASE ASSEMBLY & TOWER ERECTION	SEPT. 30
START OF SUB SYSTEM CHECKOUT	OCT. 1
COMPLETION OF SUB SYSTEM CHECKOUT	NOV. 15
BLADE ERECTION	NOV. 15-24
FIRST TURN	NOV. 30
PRELIMINARY TESTS	NOV. 30-JAN. 3
STRUCTURAL AND PERFORMANCE TESTS	JAN.77-JAN.78

Figure 8

System Engineering - Performance Considerations

W. N. Sullivan - Sandia Laboratories

The main thrust of Sandia's wind energy program has been directed toward the development of large vertical-axis Darrieus wind turbines. It is planned to maintain these turbines at constant RPM by connection to a utility grid through a synchronous generator.

The existing performance characteristics of the Darrieus turbine had an influence on the decision to pursue this synchronous application. Specifically, the ability of the Darrieus turbine to self-regulate in the synchronous mode, thereby eliminating costly aerodynamic controls, is viewed as a definite advantage over more conventional systems.[1,2,3]

This paper will briefly review the known performance characteristics of the Darrieus with emphasis on comparing the performance of this turbine with state-of-the-art horizontal axis machines. Also, the potential advantages gained by using the Darrieus turbine in an asychronous (variable RPM) mode are discussed.

Power Coefficient

A collection of power coefficients for various turbines[4-7] is shown in Figure 1. It is seen that the Darrieus is a high speed turbine, with performance peaking at a tip speed ratio of around 5. The peak output is about 10% less than a typical high performance propeller-type turbine. The tip speed ratios at peak power for the latest generation of low-solidity horizontal-axis turbines[8]

are in the vicinity of 10-12, and thus such horizontal axis machines will rotate at proportionally higher speeds than Darrieus turbines. The Darrieus is not generally self-starting, though this is not considered to be a major disadvantage for utility grid applications where electrical power and hardware are readily available for starting.

Synchronous Performance Characteristics

The narrow nature of the C_p curves for the Darrieus turbine leads to a torque vs. wind speed characteristic for a fixed RPM shown in Figure 2. The peak in torque output which occurs permits unregulated operation, provided the synchronous generator is sized with a rating above this peak torque.

The broadness of the C_p curve for a horizontal-axis turbine leads to an output torque which continually increases with wind speed (Figure 3). Due to this effect, aerodynamic controls are generally used to limit turbine output at a fixed power rating above the rated wind speed.

System Performance

It appears that the most reasonable single measure of turbine performance is not the power coefficient, or the torque vs. wind speed characteristic, but rather the net annual energy collected by the turbine/generator system at a given wind site. A means for evaluating this net energy collection is shown graphically in Figure 4. The family of curves shown represents a turbine

output duration for a site with a particular wind power duration. The area under each of these duration curves is the net system output per unit of turbine area. The turbine RPM evidently determines the required minimum generator size for unregulated operation of the Darrieus. Typically, a unique RPM is selected which maximizes the net energy output per unit swept area.

A similar graphical process can be applied to horizontal axis turbines (Figure 5), the major difference being the institution of regulated performance above the rated wind speed. For such turbines, this rated wind speed and the turbine RPM are selectable operational parameters. A unique choice of both of these parameters exists which maximizes the energy collected per unit of swept turbine area.

Performance Comparisons

Figure 6 shows the torque vs. RPM characteristics for three different systems, all with the same turbine area. The performance parameters in each case were choosen to maximize the net energy output in a 12 MPH average wind environment.[8] The Darrieus performance characteristics are from Sandia Wind Tunnel results,[7] and the horizontal axis data are from a Kaman Aerospace prediction[8] for a low solidity (2%), high performance two-bladed turbine. The third configuration is a "perfect" asychronous Darrieus type, where the RPM is varied to maintain the turbine at the maximum C_p for wind speeds below the rated speed (see Figure 7).

It is clear from Figure 6 that the optimized torque vs. wind speed curves differ considerably for these three system types. However, the differences in net energy collection are much less pronounced. The horizontal axis turbine in the synchronous mode produces about 7% more energy than the Darrieus, due primarily to its higher maximum C_p. This small difference should be weighed against the relative simplicity of the vertical axis system and the uncertainties which exist in the accuracy of the power coefficients and wind speeds used in the calculations. In addition, it remains to allow further aerodynamic development of the Darrieus with the goal of improving its performance.

The hypothetical improvement following from the asynchronous operation of the Darrieus (21% better than synchronous) is difficult to judge. The operation of any large rotating machine at variable RPM introduces many new structural and electrical problems which have not yet been addressed. More investigation is undoubtedly needed to assess whether or not the 21% improvement is worth the considerable complexity introduced by variable RPM systems.

Summary and Conclusions

In terms of overall system performance, the Darrieus vertical axis turbine as it now exists appears competitive with horizontal axis designs. A performance penalty of about 7%

is incurred by the Darrieus, which is offset by its ability to operate without aerodynamic controls. The ultimate judgment of these two approaches must, of course, include a careful accounting of the economic advantages associated with each design.

REFERENCES:

1. J. F. Banas, E. G. Kadlec, W. N. Sullivan, Application of The Darrieus Vertical-Axis Wind Turbine to Synchronous Electrical Power Generation, SAND75-0204, April 1975.

2. J. F. Banas, E. G. Kadlec, W. N. Sullivan, Methods for Performance Evaluation of Synchronous Power Systems Utilizing the Darrieus Vertical-Axis Wind Turbine, SAND75-0165, April 1975.

3. Sandia Vertical-Axis Wind Turbine Program Technical Quarterly Report, October-December, 1975, SAND76-0036, April 1976.

4. J. F. Banas, W. N. Sullivan, Engineering of Wind Energy Systems, SAND75-0530, January 1976.

5. T. Baumeister, L. S. Marks, Standard Handbook for Mechanical Engineers , Sixth Edition, McGraw-Hill Book Company, N. Y., 1958.

6. R. J. Templin, Aerodynamic Performance Theory for the NRC Vertical-Axis Wind Turbine, National Research Council of Canada, LTR-LA-160, June 1974.

7. B. F. Blackwell, R. E. Sheldahl, L. V. Feltz, Wind Tunnel Performance Data for the Darrieus Wind Turbine with NACA 0012 Blades, SAND76-0130, May 1976.

8. Design Study of Wind Turbines, 50kW - 3000kW, for Electric Utility Applications, Kaman Aerospace Report R-1382, February 1976.

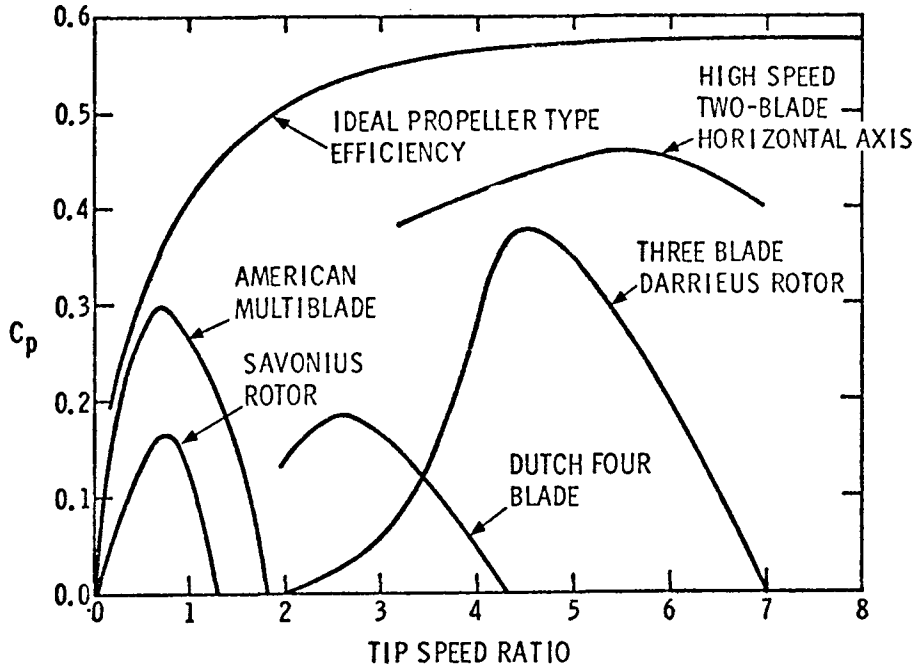

Figure 1 - Power Coefficients for Various Turbines

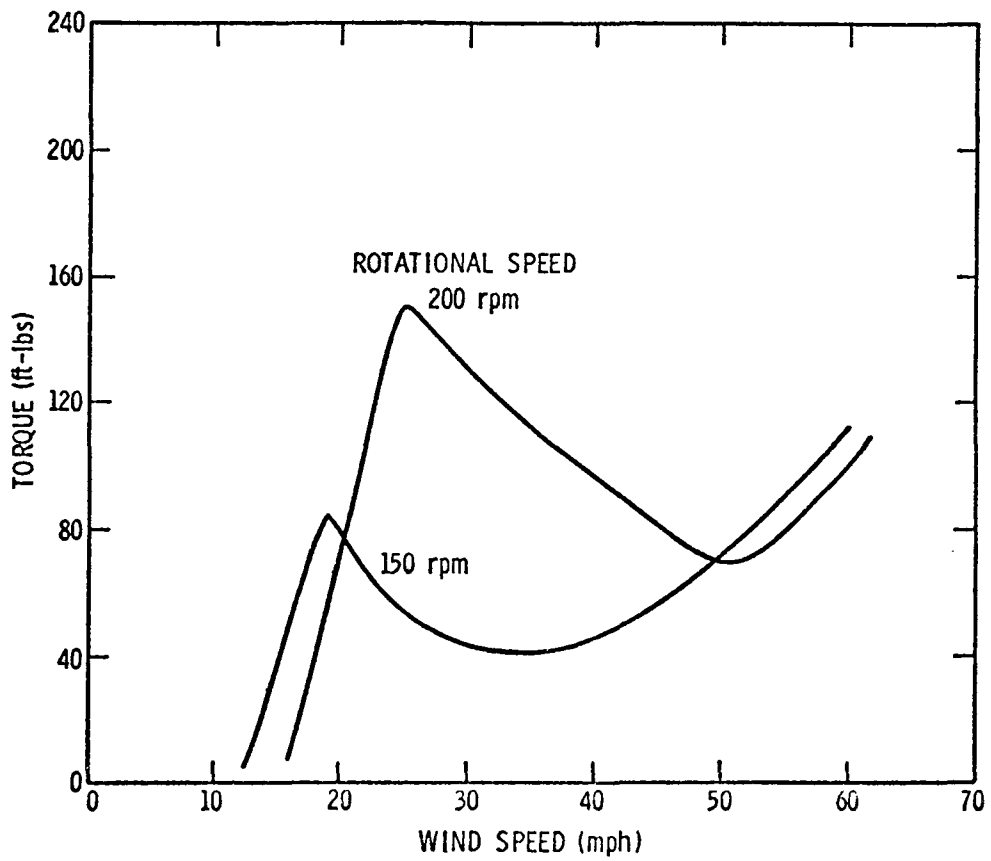

Figure 2 - Torque vs. Wind Speed Characteristic for a Darrieus Turbine

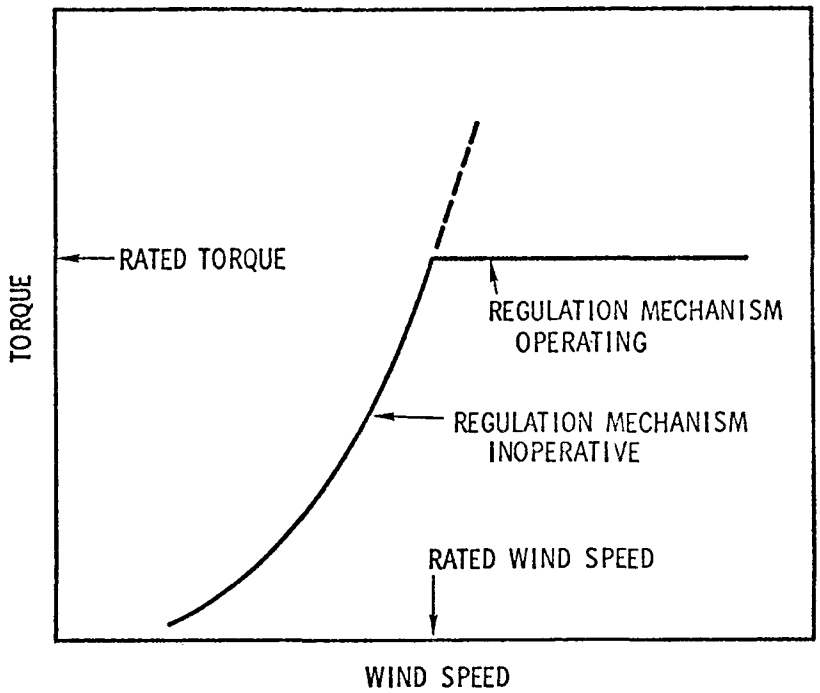

Figure 3 - Torque vs. Wind Speed Characteristic for a Typical Horizontal Axis Turbine

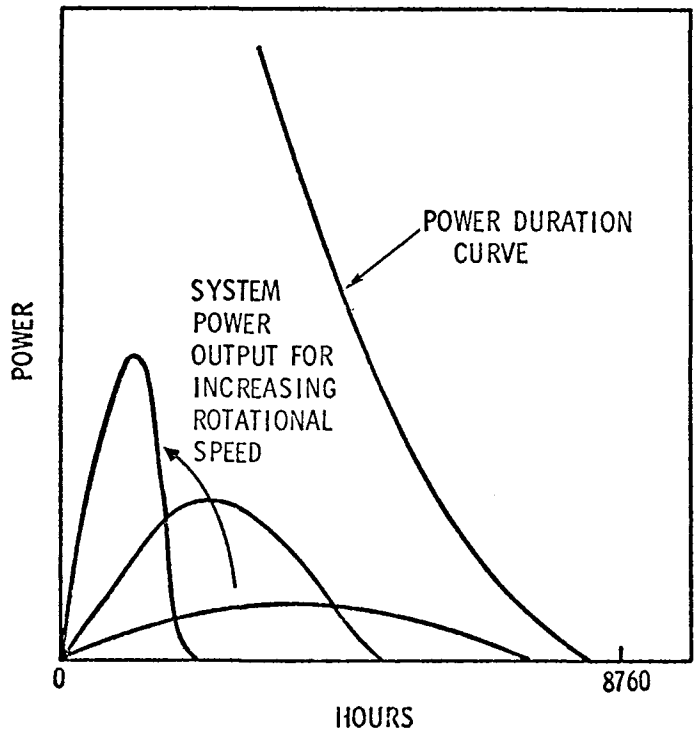

Figure 4 - Relation Between Turbine Output and Wind Power Duration at a Site

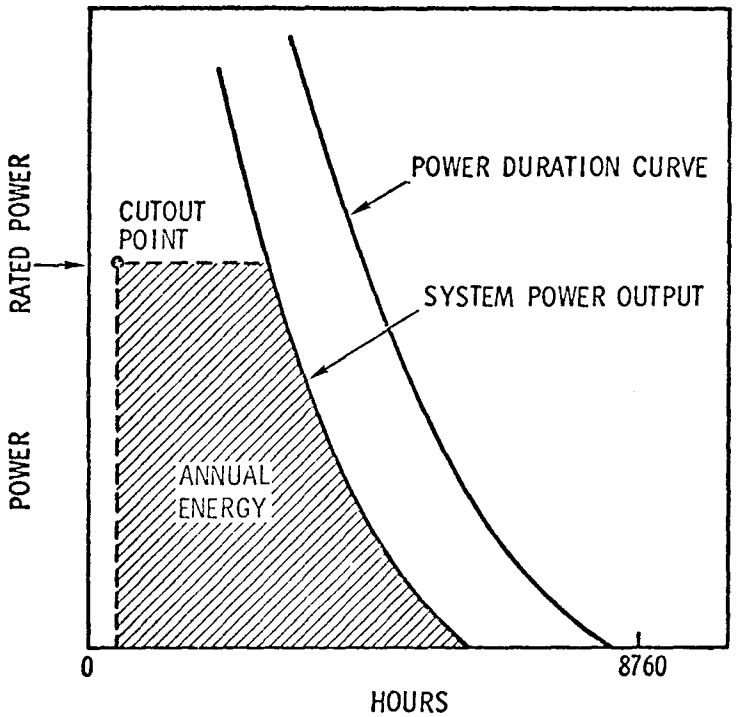

Figure 5 - Horizontal Axis Turbine Site Performance

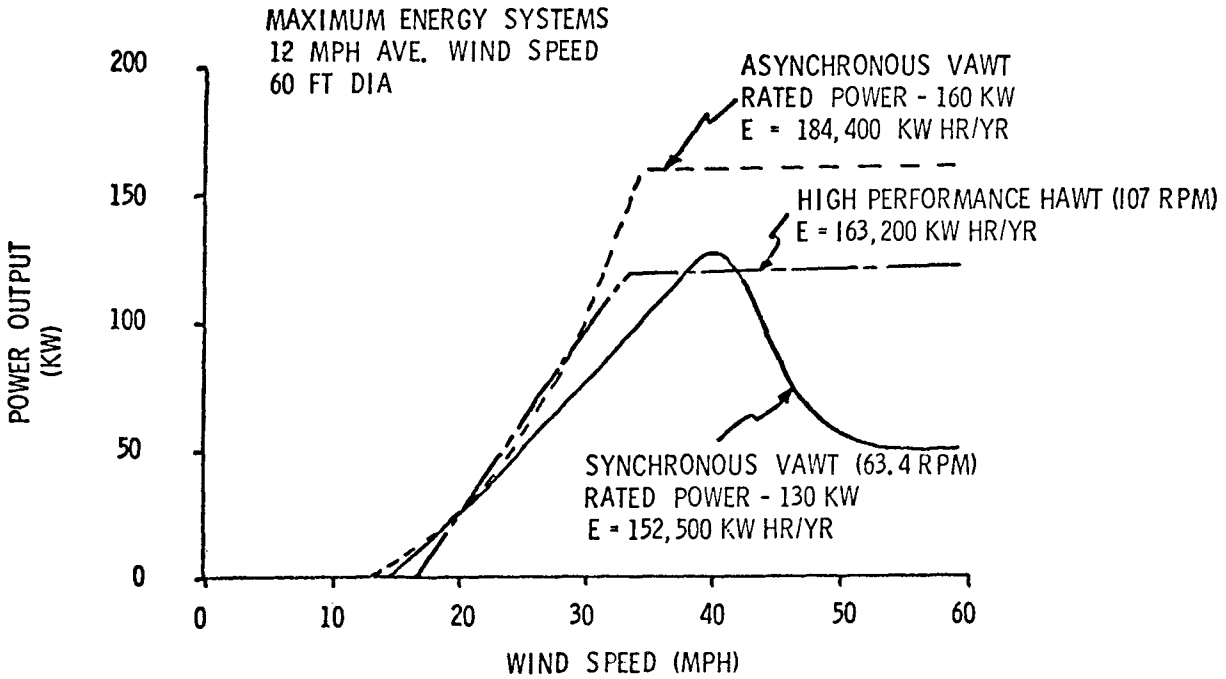

Figure 6 - Comparison of Optimized Torque vs. Wind Speed Characteristics, 12 MPH average Wind Speed

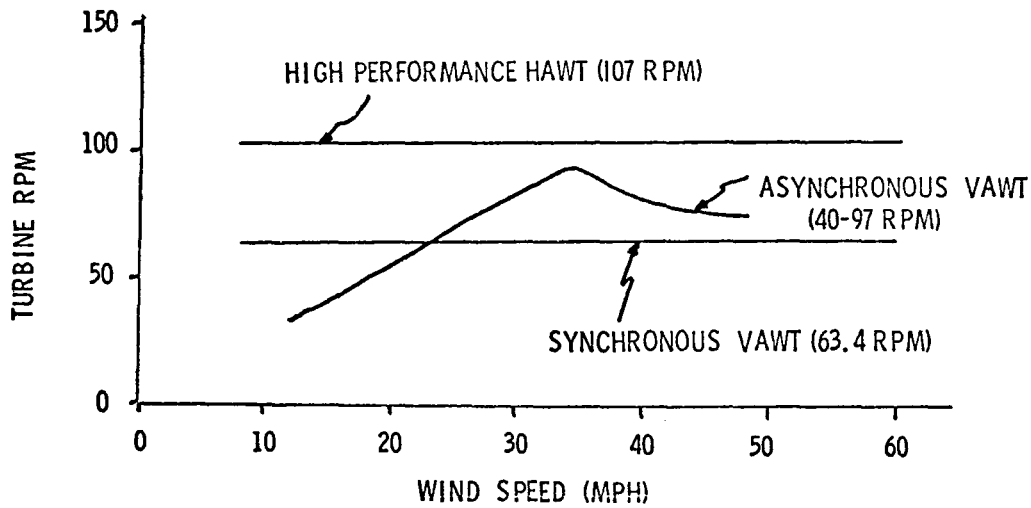

Figure 7 - RPM Variations for Optimized Systems

ECONOMIC CONSIDERATIONS

James Banas

Sandia Laboratories, Albuquerque, New Mexico 87115

The objectives of economic studies are twofold. First, to identify tradeoffs and trends among system design parameters which lead to the definition of scale-up systems. Second, to identify the cost of optimum systems in order to determine the role of the vertical-axis windturbine in wind power. Since the VAWT is in early stages of development, an iterative process is visualized to meet the above objectives wherein the economics of VAWT systems are continuously updated as new performance and cost data becomes available. This paper summarizes economic studies performed to date with emphasis on trends related to system design, for example, in the areas of aerodynamics and structures. The effects of potential component cost savings are also indicated.

The economics of wind power generation systems involve a complex interplay of both cost and performance parameters. For example, aerodynamic studies indicate that parameters such as solidity, height-to-diameter ratio, and turbine configuration can produce a wide variety of performance characteristics. In an attempt to build intuition leading to the definition of economically attractive systems, the effect of various features of the power coefficient on simple economic indicators have been investigated.

Early analyses have indicated that turbine cost and transmission cost are the two major contributors to total system cost. Turbine cost can, to some degree, be related to the swept area of the turbine. Transmission cost is related to the rated output torque of the turbine. Thus, it would appear reasonable to use as measures of energy cost the terms E/A and E/T_R where E is the annual energy output, A is the turbine swept area, and T_R is the rated torque. These "economic indicators" are relatively easy to evaluate so that a wide range of postulated systems can be investigated.

A particular functional form for the turbine power coefficient has been selected and is depicted in Figure 1. Features of interest are the maximum power coefficient $C_{P_{max}}$, the tip speed ratio corresponding to the maximum efficiency λ_M, the tip speed ratio at zero efficiency λ_R, the tip speed ratio at which power reaches a maximum with respect to windspeed λ_K, and an exponent $N \geq 3$ which defines the turbine power output for high wind speeds.

Figures 2 and 3 show a typical result from computations of E/A and E/T_R as functions of RW/λ_M and λ_K/λ_M. The parameters x and η are used to characterize the efficiency of the transmission and generator. Several observations can be made as follows:

1. E/A and E/T_R increase with $C_{P_{max}}$, that is, higher efficiency means more energy extracted from the wind;
2. E/T_R increases with λ_M, that is, rated torque for a given rated power can be decreased by increasing λ_M which is a measure of turbine rotational speed;
3. E/A and E/T_R reach maxima with respect to $R\omega/\lambda_M$, that is, if ω is small, power is small which implies little energy, furthermore, if ω is large, power is large but corresponding wind speeds are rare which implies little energy;
4. E/A and E/T_R when maximized by $R\omega/\lambda_M$ also achieve maxima with respect to λ_K/λ_M, that is, if λ_K/λ_M is small, component efficiency at reduced loads becomes small, furthermore, if λ_K/λ_M is large, turbine efficiency is reduced;
5. Although not demonstrated in Figs. 2 and 3, the exponent N should be close to 3 in order to achieve a constant power - wind speed relationship; finally λ_R/λ_M should be large so that the turbine efficiency characteristic is broadened.

Using an economic model which accounts for the actual costs of the turbine, transmission, and generator indicates that a value of λ_M/λ_M intermediate to the values of Figs. 2 and 3 should be chosen. It should be noted that this value will depend on the relative component costs but is around 1.

The foregoing discussion has indicated that several features of the power coefficient can substantially influence the economics of wind power systems. Results from aerodynamic studies suggest, however, that these features do not vary independently. For example, Fig. 4 shows power coefficients for several values of turbine solidity calculated with the single-streamtube aerodynamic performance model. While λ_M is increasing, as desired, with decreasing solidity, $C_{P_{max}}$ is decreasing. Coupling of the features is similarly obtained from variations of the other aerodynamic design parameters.

Fig. 5 shows a flow chart of the economics model. This model has been structured to accept updated cost and performance data as it becomes available. Power coefficient as a function of tip speed ratio, turbine solidity, and Reynolds number is based on extrapolations of both wind tunnel test data and aerodynamic performance model predictions. Also included in the model are component efficiences and costs. In particular, the turbine cost has been made to depend on solidity σ, number of blades, N, and radius R according to $\frac{\sigma^{1.2}R^{2.2}}{N^{0.2}}$. If resonances and centrifugal loads are only considered, the blade wall thickness need not grow with scale-up and cost would be proportional to R^2. However, aerodynamic loads appear to require some increase of thickness. For the examples which follow, cost was arbitrarily made proportional to $R^{2.2}$.

A reference case, formulated to illustrate results of the economic analysis, includes the following:

1. Turbine cost is increased to reflect use of struts which have the same cross-section as the blades;
2. Blade cost is $10/lb. based on roll-formed steel construction;
3. Site median wind speed is 12 mph.

Fig. 6 shows energy cost for optimum systems with rated power up to 1000 kW. Turbine diameter and rotational speed are noted for the 500 kW and 1000 kW systems. For rated power below about 200 kW energy cost is rising rapidly and these systems would not appear to be cost effective. For rated power above 200 kW energy cost is judged relatively constant within the accuracy of the model. The selection of solidity equal to 0.1 and number of blades equal to 3 is discussed in the following paragraphs.

Low solidities are attractive because of decreased blade cost and increased tip speed ratios. However, as solidity is decreased, the maximum power coefficient is reduced. Fig. 7 shows the variation of energy cost with solidity when the number of blades is fixed at three. As anticipated an intermediate value of solidity results in the lowest energy cost.

A given solidity can be achieved by varying the number of blades and chord/radius ratio. As depicted in Fig. 8, solidity is linearly dependent on chord/radius for a fixed number of blades. By increasing the number of blades the required value of chord/radius is reduced which tends to reduce the Reynolds number. This last point is important since it appears from wind tunnel test data that λ_K/λ_M is decreasing as Reynolds number is increasing, thereby reducing energy output. Structural requirements must be considered to determine how small chord/radius can get. Alternatively, the limits on chord/radius can be used to determine the required number of blades. This is illustrated in Fig. 9 which shows the variation of energy cost with chord/radius and number of blades. A minimum value for chord/radius of say .06 results in the choice of 2 blades although 3 blades would give a lower energy cost at a chord/radius of .03.

Three areas for potential cost reduction are the blades, the struts and the transmission. Fig. 10 shows relative to the reference case the individual effect of 1) reducing the blade cost to $5/lb., 2) halving the transmission cost and 3) eliminating the struts. It can be seen that each cost reduction has a substantial effect on energy cost. Figs. 11 and 12 show the combined effects of these cost reductions on energy cost for site median wind speeds of 12 mph and 18 mph respectively.

Further effort is needed with regard to definition of aerodynamic performance, structural requirements, and component costs. Currently, aerodynamic performance is based on extrapolations of wind tunnel data over an order of magnitude in Reynolds number although trends of analytic predictions are consistent with these extrapolations. Structural requirements must be defined for scale-up systems. Finally, cost of components such as the turbine, tower, and transmission must be defined in more detail. It is anticipated that design, fabrication, and testing of the 17m turbine system will provide much of the needed information.

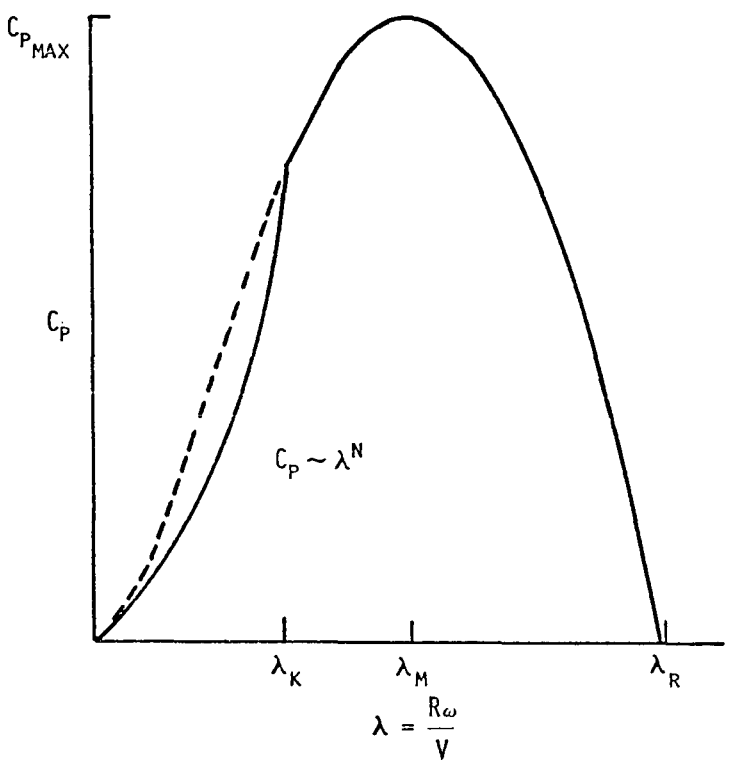

Figure 1. Model Power Coefficient

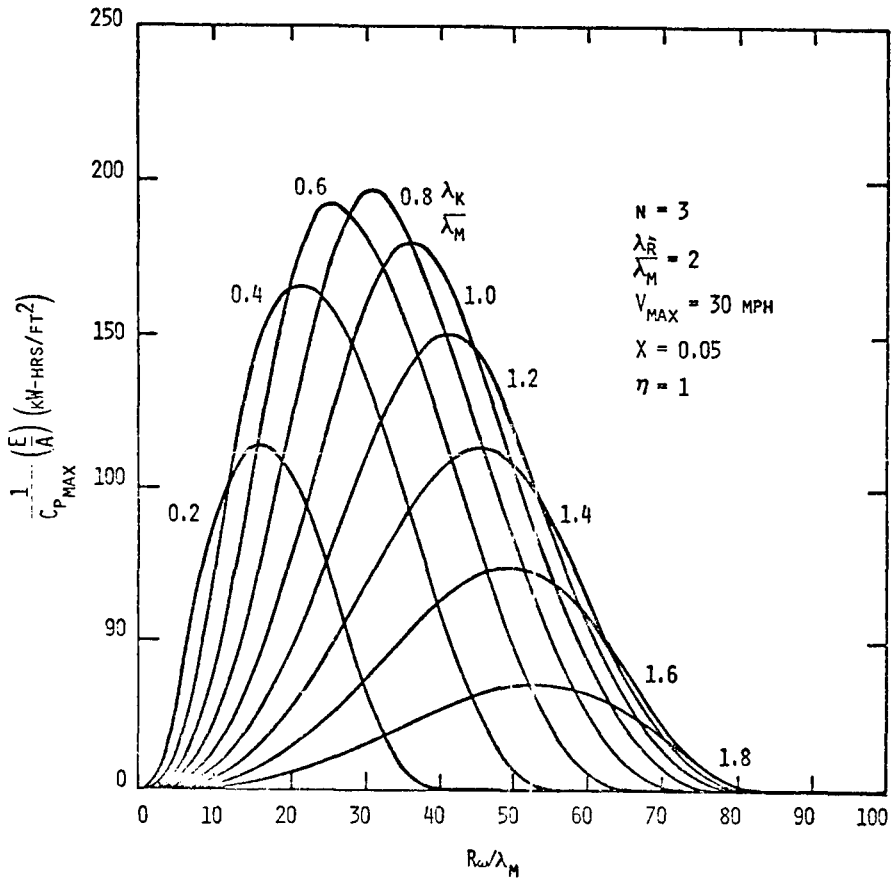

Figure 2. Energy Per Unit Swept Area

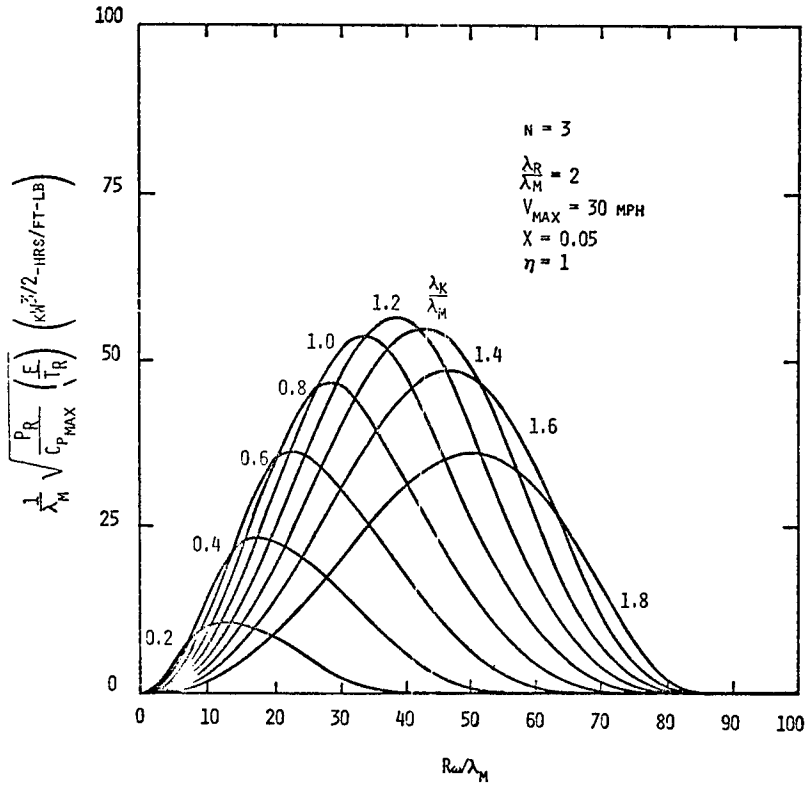

Figure 3. Energy Per Unit Rated Torque

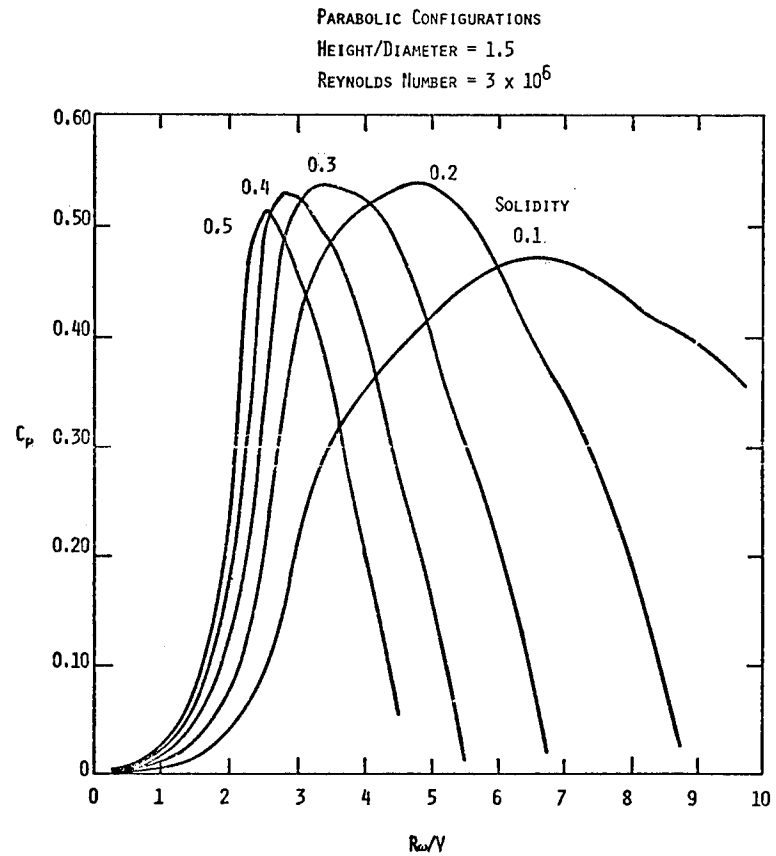

Figure 4. Power Coefficients from Aerodynamic Model

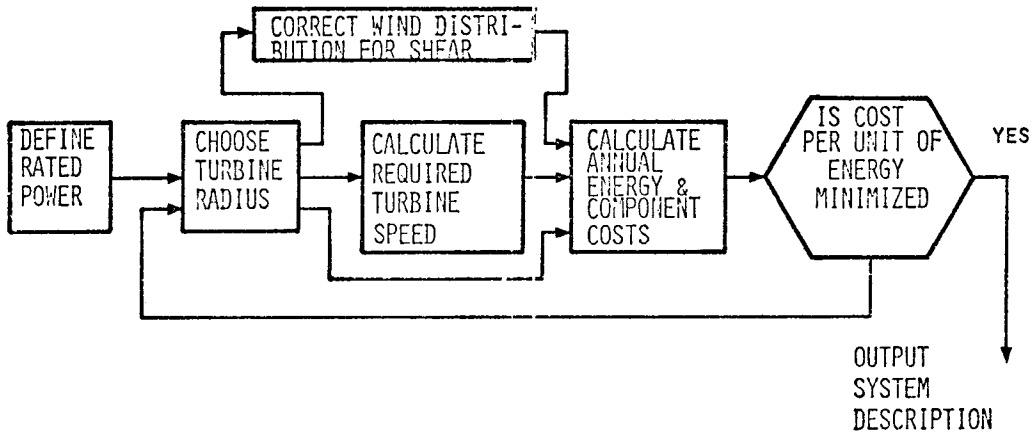

Figure 5. Flow Chart of Economics Model

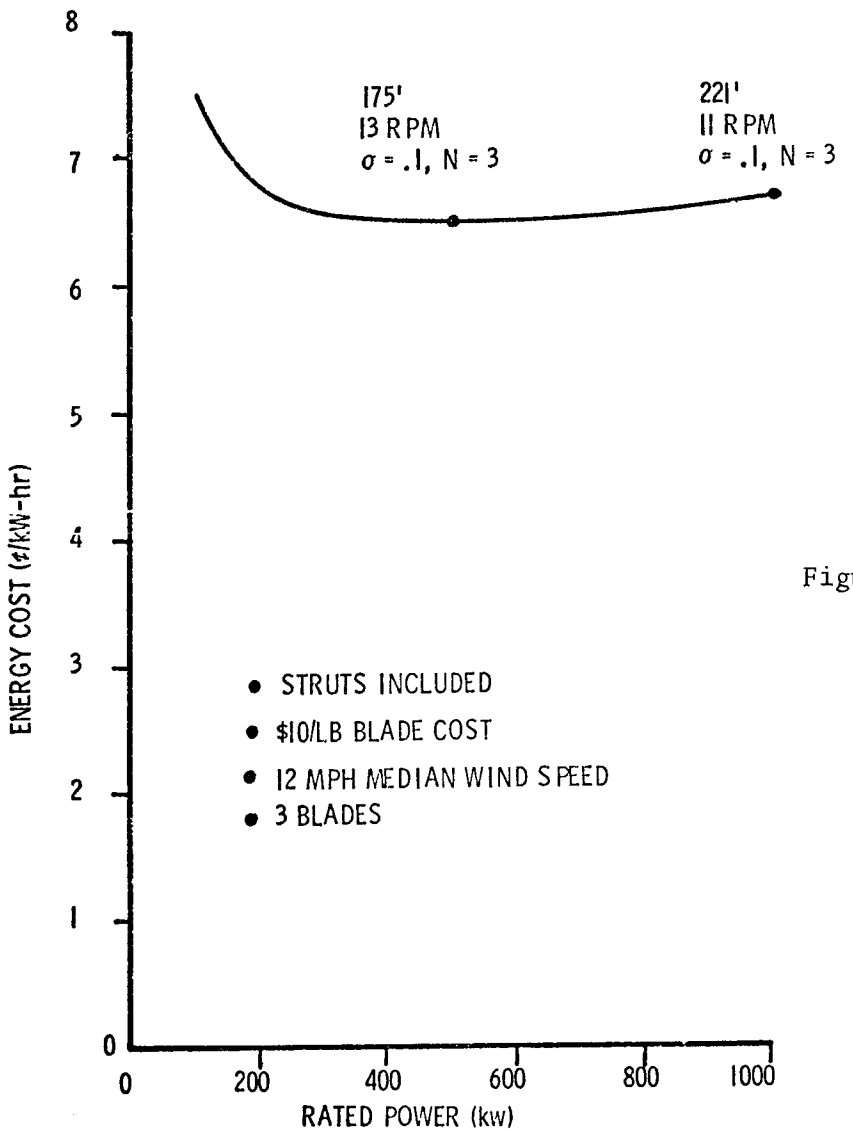

Figure 6. Reference Cost Case

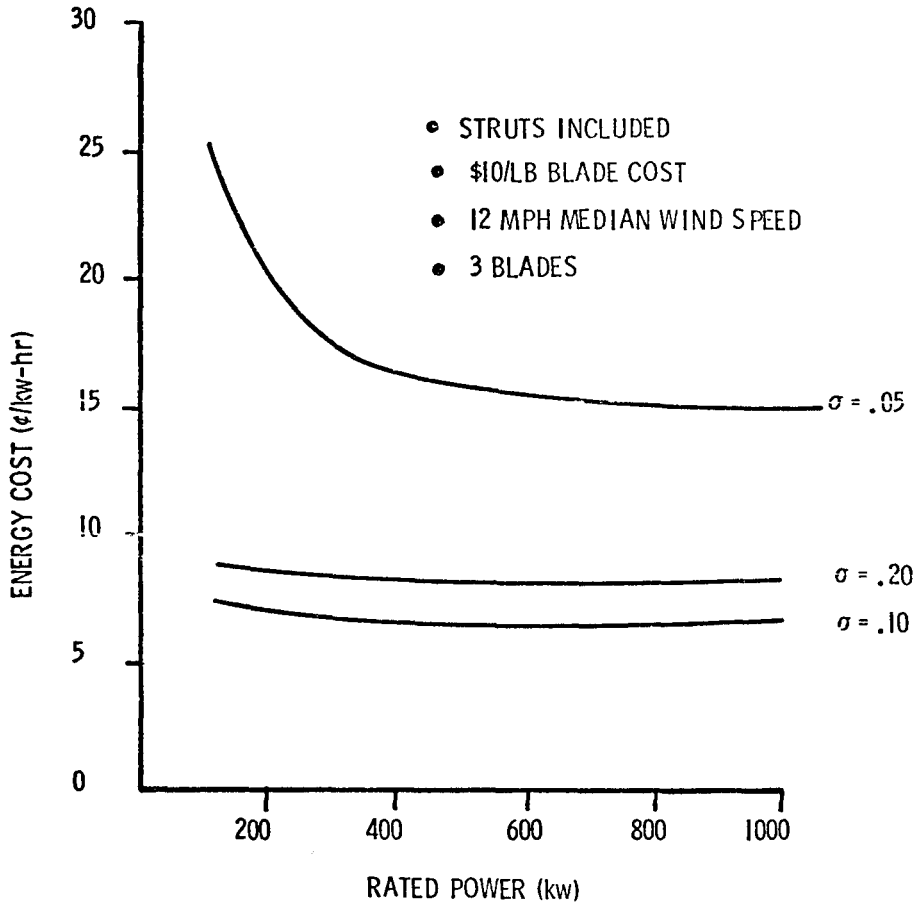

Figure 7. Variation of Energy Cost with Solidity

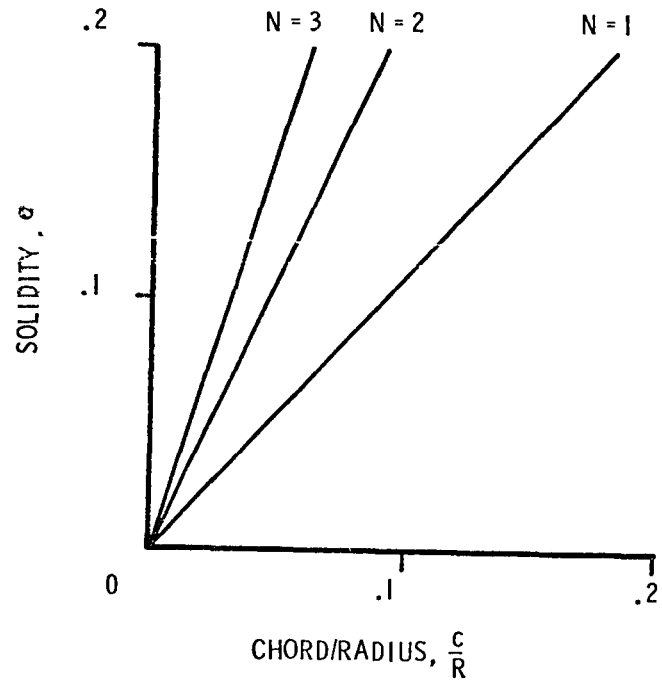

Figure 8. Variation of Solidity with Chord/Radius

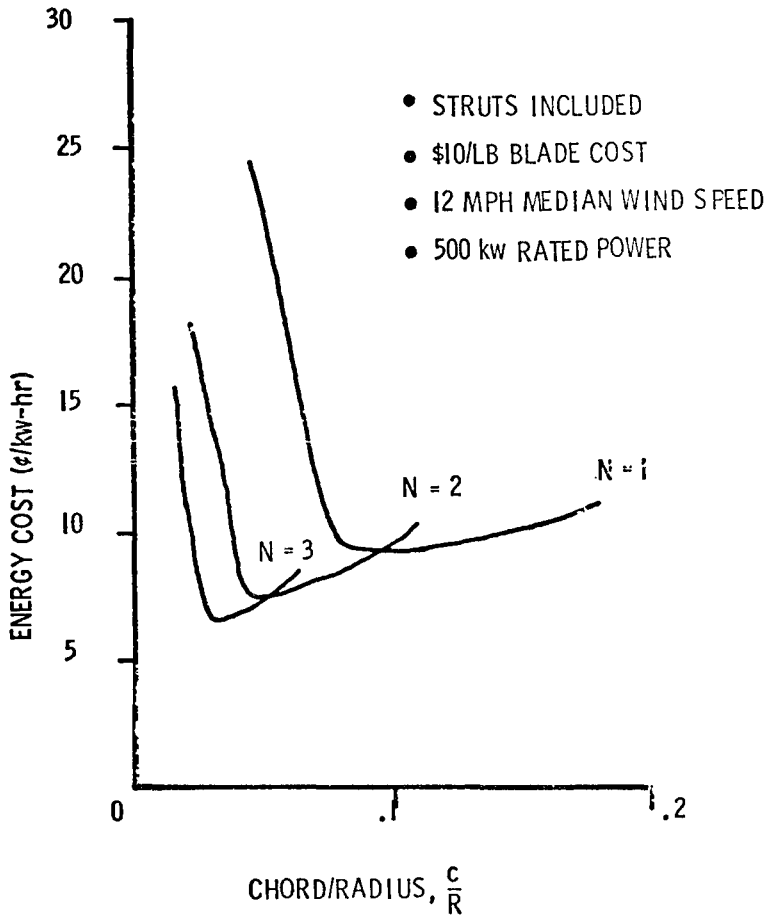

Figure 9. Variation of Energy Cost with Chord/Radius

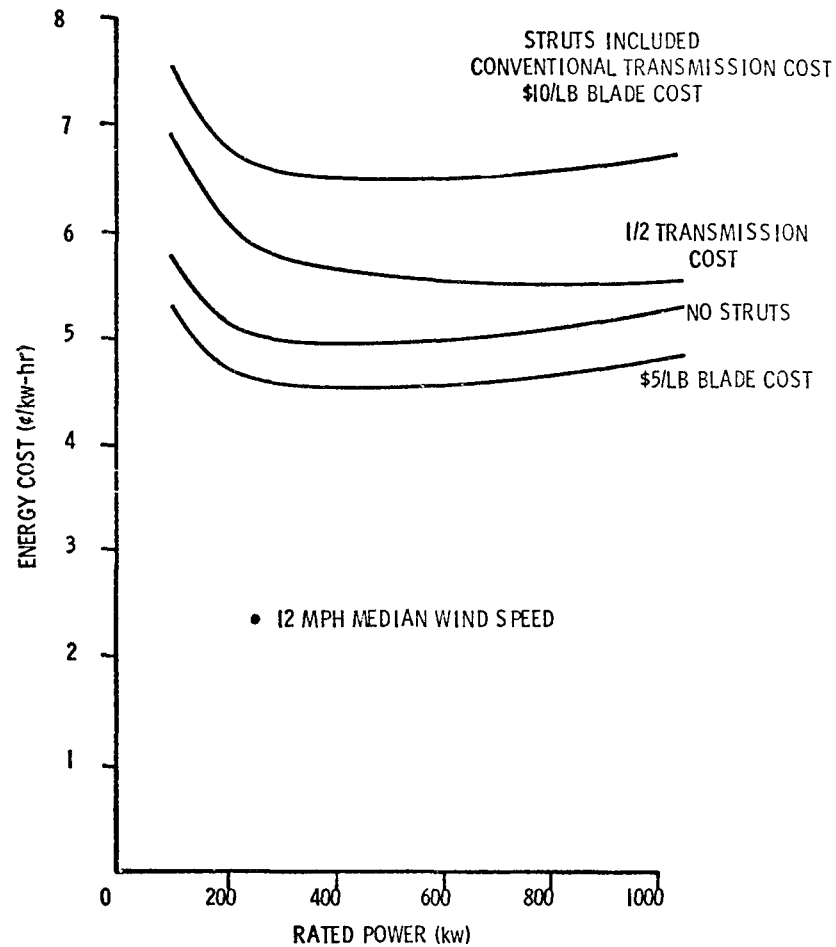

Figure 10. Effects of Component Cost Reductions

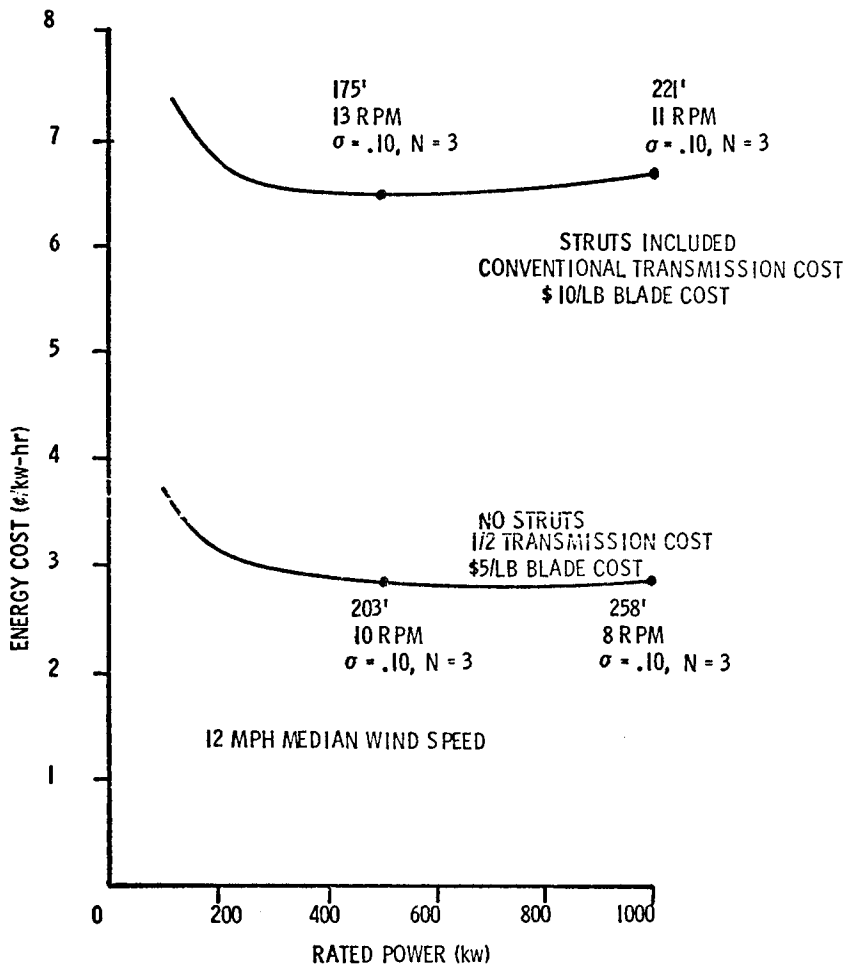

Figure 11. Combined Effects of Potential Cost Reductions

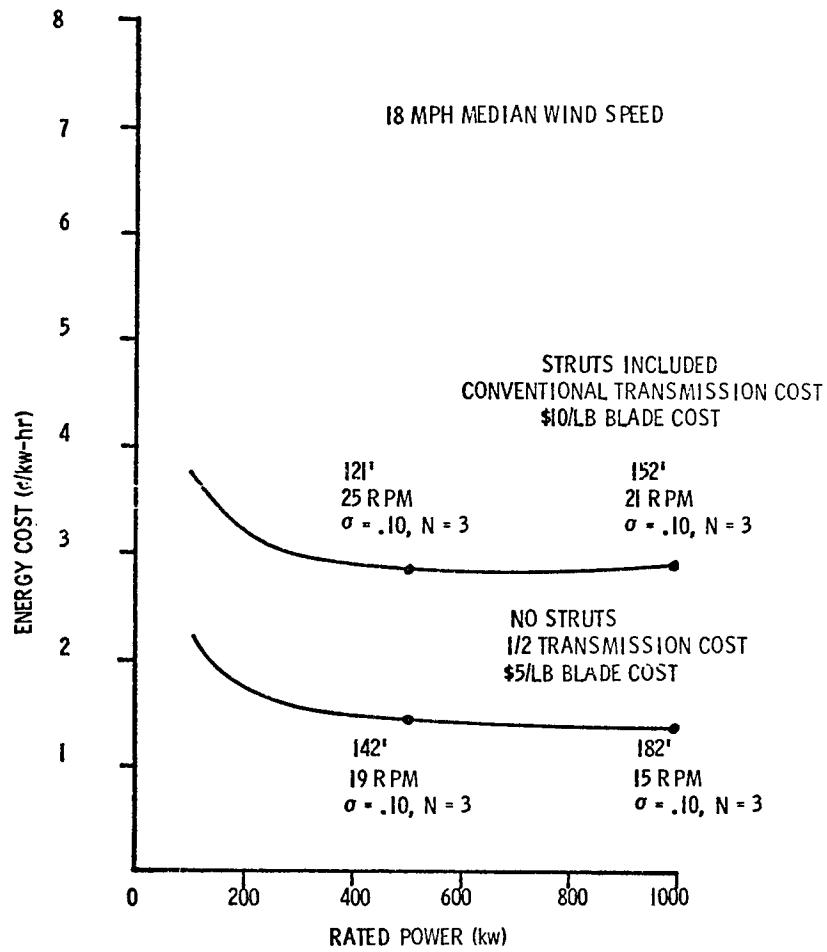

Figure 12. Combined Effects of Potential Cost Reductions

AERODYNAMICS OF THE DARRIEUS TURBINE

J. H. STRICKLAND

Assistant Professor, Mechanical Engineering
Texas Tech University
Lubbock, Texas

This paper describes an analytical performance prediction model for the Darrieus turbine. This model is shown to predict the performance of small scale rotors, for which test data is available, with reasonable accuracy. It displays a marked improvement over older methods in which the "induced velocity" through the rotor is considered to be constant. The model is capable of predicting the overall rotor power output and the distribution of aerodynamic forces along the rotor blades. The model can be used to study the effects of rotor geometry variations such as blade solidity, blade taper, and variations in rotor height to diameter ratios. In addition, spacial variations in freestream velocity such as that produced by atmospheric wind shear can be handled by the model. This model should be particularly useful in the design and optimization of large scale rotors for which test data is not available. Scale effects can be predicted based upon high Reynold's number airfoil data.

INTRODUCTION

Recent interest in the Darrieus Turbine as a wind energy conversion device [1-5] has resulted in a need for an adequate performance prediction model. Such a model is necessary so that large scale rotor systems can be properly engineered and optimized. This model must accurately predict the performance of small scale rotors, for which test data is currently available, if there is to be any hope of predicting the performance of large scale rotors whose blade Reynold's numbers are more than an order of magnitude greater.

There are several approaches, directed toward the formulation of a model, which one might take. One could, for instance, attempt a solution using vortex theory, which has been used successfully in propellor and wing design as well as for some vertical axis wind machines [6]. However, because of the complex structure of the resulting vortex system applicable to the Darrieus Turbine configuration, the computer time required to effect such a solution appears to be excessive. Another approach which has recently been used by R. J. Templin [7] is to visualize the rotor as being enclosed in a single streamtube. As this streamtube passes through the rotor, the wind velocity is assumed to be everywhere constant. In other words the induced velocity through the rotor is constant. The forces on the airfoil blades are then computed, using this uniform velocity. The wind velocity in the streamtube at the rotor is then related to the undisturbed freestream velocity by equating the drag force on the rotor to the change in fluid momentum through the rotor. While this approach affords a great deal of simplicity and predicts overall performance

rather well for lightly loaded blades, it is incapable of adequately predicting information which requires a more precise knowledge of wind velocity variations across the rotor. These variations become increasingly large as blade solidities and blade tip speeds increase. In addition, it does not appear that wind shear effects can be incorporated into the model.

A somewhat more sophisticated model than the single streamtube model is one in which a series of streamtubes (actually stream filaments) are assumed to pass through the rotor. The same basic principles which were applied to the single streamtube are now applied to each of the multiple streamtubes. The multiple streamtube model gives rise to a velocity distribution through the rotor which is a function of the two spacial coordinates perpendicular to the streamwise direction. The multiple streamtube model, while still somewhat inadequate in its description of the flow field, does predict overall performance very well, yields a more realistic distribution of blade forces, and can be used to study wind shear effects.

This paper consists of the development and utilization of the multiple streamtube model. The basic aerodynamic model is first developed along with a description of a suitable iterative solution technique. An associated computer analysis which is given the acronym DART for DARrieus Turbine is documented in Ref. [13]. The DART model is exercised to provide comparison with test data and the single streamtube model. Effects of solidity and Reynold's number variations on overall performance are then investigated along with the effects of wind shear. In addition, the aerodynamic blade forces as a function of blade position are presented for a specific case.

AERODYNAMIC MODEL

The performance analysis is based upon a simplified aerodynamic model which is an adaptation of Glauerts blade element theory [8]. Basically, this theory utilizes the streamwise momentum equation, which equates the streamwise forces on the airfoil blades to the change in fluid momentum through the rotor. Computations are performed for a series of streamtubes which pass through the rotor. In Fig. 1 a typical streamtube is shown. The cross-sectional area of the streamtube is given by $\Delta h\ r\ \Delta\theta \sin\theta$, where Δh is the vertical height of the streamtube. The streamtube cross-sectional area is assumed to be constant as it passes through the rotor, although in reality it will increase somewhat. The fluid velocity through the streamtube at the rotor is denoted by U and is a function of the angle θ and the vertical coordinate Z.

Momentum Considerations

Since energy is extracted by the blade elements as they pass through the streamtube, the rotor streamtube velocity U is less than the undisturbed freestream velocity U_∞. The time averaged streamwise momentum equation can be used in conjunction with Bernoulli's equation to relate the velocities U and U_∞ and the average streamwise force $\bar{F}_X$ exerted by the blade elements as they pass through the streamtube. This expression can be written as:

$$\bar{F}_X = 2\ \rho\ A_S\ U(U_\infty - U) \tag{1}$$

where ρ is the fluid density and A_S is the streamtube cross-sectional area as defined previously.

The average force $\bar{F}_x$ in the streamtube can be related to the streamwise force F_x exerted by an individual blade element as it passes through the streamtube by noting that each of N blade elements spend $\Delta\theta/\pi$ percent of their time in the streamtube. Therefore the average force becomes:

$$\bar{F}_x = NF_x \frac{\Delta\theta}{\pi} \tag{2}$$

Eliminating $\bar{F}_x$ from equations 1 and 2 yields:

$$\frac{NF_x}{2\pi\rho r\Delta h \sin\theta U_\infty^2} = \frac{U}{U_\infty}\left(1 - \frac{U}{U_\infty}\right) \tag{3}$$

For convenience, the left hand side of equation 3 is denoted by F_x^*

$$F_x^* = \frac{NF_x}{2\pi\rho r\Delta h \sin\theta U_\infty^2} \tag{4}$$

Blade Element Forces

As can be seen from equation 3, the streamwise force exerted on the blade elements by the fluid must be found to obtain the ratio of rotor streamtube velocity to undisturbed freestream velocity. In addition, the force F_t, which acts along the chord line of the airfoil and tangential to the blade element flight path, must be found in order to compute the torque and power being produced by the element as it passes through the streamtube. A complete set of aerodynamic forces on a blade element would include not only the force F_t which is tangent to the airfoil chord line and F_n, which is normal to the chord line, but also the force along and the moment about the spanwise coordinate axis. The spanwise force is neglected since it does not contribute to the torque

produced by the blade element and contributes only slightly to the resultant force F_x. The pitching moment about the aerodynamic center of the airfoil is essentially zero, except at large angles of attack. In any event, the pitching moment on the blade element as it passes through the downstream portion of the streamtube is of opposite sign and of equal magnitude (within the limitations of this model). Therefore, it is of no consequence for calculation of rotor performance.

The two forces F_n and F_t, along with their resultant force F_x in the streamwise direction, are shown in Fig. 2. From this figure, it is seen that the resultant streamwise force F_x is given by:

$$F_x = -\left(F_n \sin\beta \sin\theta + F_t \cos\theta\right) \tag{5}$$

The forces F_t and F_n can be expressed in terms of the fluid density ρ, the plan area of the airfoil $\Delta h C \sin\beta$, where C is the airfoil chord length, and the relative velocity U_R of the fluid moving onto the airfoil

$$\begin{aligned} F_t &= 1/2\ C_t\ \rho\ \frac{\Delta h C}{\sin\beta}\ U_R^2 \\ F_n &= -1/2\ C_n\ \rho\ \frac{\Delta h C}{\sin\beta}\ U_R^2 \end{aligned} \tag{6}$$

The coefficients C_t and C_n are related to the more common airfoil lift and drag coefficients C_L and C_d by:

$$\begin{aligned} C_t &= C_L \sin\alpha - C_d \cos\alpha \\ C_n &= C_L \cos\alpha + C_d \sin\alpha \end{aligned} \tag{7}$$

where α is the angle of attack between the airfoil chord line and U_R.

Combining equations 4, 5, and 6, the non-dimensional streamwise force F_x^* can be written as:

$$F_x^* = \frac{NC}{4\pi r} \left(\frac{U_R}{U_\infty}\right)^2 \left(C_n - C_t \frac{\cos\theta}{\sin\theta\sin\beta}\right) \tag{8}$$

Relative Velocity Vector

The angle of attack and associated relative velocity in the plane of the airfoil cross section can be obtained from consideration of Fig. 3. The angle of attack α is given by:

$$\mathrm{Tan}\alpha = \frac{U\sin\theta\sin\beta}{U\cos\theta + U_t} \tag{9}$$

where U_t is the tangential speed of the airfoil blade element. The relative velocity U_R in the plane of the airfoil cross section is obtained from the identity:

$$U_R \sin\alpha = U\sin\theta\sin\beta \tag{10}$$

Solution of the Momentum Equation

Defining an interference factor by:

$$a \equiv 1 - \frac{U}{U_\infty} \tag{11}$$

and using this notation in conjunction with equations 3 and 4, the streamwise momentum equation can be written as:

$$a = F_x^* + a^2 \tag{12}$$

Equation 12 forms the basis for an iterative solution of the streamtube momentum equation. The function F_x^* is a rather complex function of "a"

making an explicit solution for "a" all but impossible. The procedure for carrying out computations on a specified streamtube begins by setting "a" equal to zero. The angle of attack α can then be computed from equation 9. Lift and drag coefficients can then be obtained from airfoil data and the relative velocity U_R can be obtained from equation 10. The non-dimensional force F_x^* is next computed using equation 8. Using the present value of "a" and F_x^* in the right hand side of equation 12 a new value of "a" can be computed. The value of U/U_∞ can be obtained from equation 11. This process is repeated starting with the calculation of α until the desired accuracy in "a" is obtained.

This process yields the value of U/U_∞ for the streamtube. Normally, convergence is rapid. For example, it has been found that computer processing time averages about 4×10^{-3} seconds per streamtube with a convergence error of less than 1.0×10^{-3} on "a".

Rotor Power Coefficient

Once the streamtube momentum equation has been solved, the torque produced by a rotor blade element as it passes through the streamtube can be obtained by:

$$T_s = 1/2\ \rho r C_t\ \frac{C\Delta h}{\sin\beta}\ U_R^2 \qquad (13)$$

In order to obtain the total torque on a blade for a particular value of θ, T_s must be integrated or summed over the number of blade segments N_s making up the blade. Each blade segment is assumed to be of a length $\Delta h/\sin\beta$ with T_s being calculated at the center of each element.

The torque on a complete blade is thus given by:

$$T_B = \sum_{1}^{N_s} T_s \tag{14}$$

To obtain the average torque produced on the rotor by all of the N blades, the value of T_B must be time averaged and multiplied by N. If values of T_s are obtained at N_t values of θ in increments of $\pi/(N_t-1)$, then the average rotor torque becomes:

$$\bar{T} = \frac{N}{N_t} \sum_{1}^{N_t} \sum_{1}^{N_s} T_s \tag{15}$$

For all of the work presented herein, calculations were made at every 10° intervals in θ and at intervals in Z equal to one-tenth of the rotor height, where Z is measured from the rotor base along the vertical axis. Therefore, $N_s = 10$ and $N_t = 19$.

The rotor power coefficient in terms of the average rotor torque is given by:

$$C_p = \frac{\bar{T}\omega}{1/2\rho \sum_{1}^{N_s} 2r\Delta h U_\infty^3} \tag{16}$$

where ω is the angular speed of the rotor. Combining equations 13, 15 and 16, one obtains:

$$C_p = \frac{\sum_{1}^{N_s} \sum_{1}^{N_t} \left[\frac{NC}{2R\sin\beta} \frac{U_t}{U_\infty} \left(\frac{U_R}{U_\infty}\right)^2 C_t \right]}{N_t \sum_{1}^{N_s} \frac{r}{R}} \tag{17}$$

where R is the equatorial radius of the rotor.

DISCUSSION OF RESULTS

In order to test the accuracy of the DART model, predictions were made for two rotor configurations which were recently tested by Sandia Labs in the LTV wind tunnel [13]. Comparisons were then made between the DART model and the single streamtube model using identical airfoil data. The DART model was then used to predict solidity and Reynold's number effects for rotors with constant chord blades, height to diameter ratios equal to 1.0, and uniform freestream velocities. The blade span line as shown in Fig. 1 was taken to be a sin curve, which closely approximates a Troposkien [14]. The effects of atmospheric wind shear on the power coefficient curve were investigated and finally, the variation of blade forces with respect to blade position were examined.

Comparison with Test Results

Wind tunnel tests of two six foot diameter Darrieus rotors were conducted in the LTV wind tunnel in May, 1975 [13]. Both a two bladed rotor with a value of NC/R = 0.18 and a three bladed rotor with a value of NC/R = 0.27 were tested. The aluminum rotor blades were NACA 0012 airfoils. The tests were conducted with freestream velocities of 7.0, 9.0, and 11.0 meters per second. For the 9 meter per second wind speed, blade Reynold's numbers on the rotor tip range from about 0.10×10^6 to 0.36×10^6 for tip to wind speed ratios of 2 and 7 respectively. Data to be used in the DART model were selected from Ref. [9] for the NACA airfoil for a blade Reynold's number of 0.30×10^6 (data is unavailable for Reynold's numbers as low as 0.10×10^6). The drag coefficient at zero angle of attack was also obtained from Ref. [9] at the test Reynold's number. Data from Ref. [9] is shown in

Fig. 4 and Table 1. For large angles of attack, greater than about 30°, the data in Ref. [10] was used (see Fig. 5). Values of C_n and C_t are given in Table 2 and shown in Fig. 6 for a blade Reynold's number of 0.3×10^6 as well as for 3.0×10^6. Fig. 7 shows the relatively good agreement between wind tunnel measurement of the rotor power coefficient and the DART model predictions using data for a blade Reynold's number of 0.3×10^6. The failure to agree exactly on the left hand portion of the curves is at least partially due to the difference in blade Reynold's numbers between test and analysis. The DART prediction of C_p would be expected to be higher in this region since increasing the blade Reynold's number tends to delay aerodynamic stall. Unfortunately, airfoil data is not available at the low Reynold's numbers, consistent with the test Reynold's numbers, on the left hand side of the C_p curve. On the right hand side of the curve, the test Reynold's numbers at the rotor tip and the Reynold's numbers used in the DART analysis are nearly the same. The DART prediction is again somewhat high which may be in part due to blade Reynold's numbers toward the rotor hub which are again less than that used in the analysis.

Comparison with Single Streamtube Model

Also shown in Fig. 7 is a comparison between C_p predicted by the DART model and the single streamtube model. As is typical, agreement between the models is quite good at low tip to wind speed ratios. This is due to the fact that for lightly loaded blades (i.e. low tip to wind speed ratios or low solidities) the distribution of rotor streamtube velocities is reasonably uniform and is almost equal to the freestream velocity. For highly loaded blades, on the other hand, the distribution

Wind tunnel data		Corrected for "still air" conditions	
Test Reynold's Number	Test C_{DO}	Effective Reynold's Number	Adjusted C_{DO}
170,000	.0128	449,000	.0105
330,000	.0084	871,000	.0065
660,000	.0091	1,740,000	.0075
1,340,000	.0090	3,540,000	.0077
2,380,000	.0085	6,280,000	.0073
3,180,000	.0080	8,400,000	.0069

Tab. 1 DRAG COEFFICIENT C_{DO} AT ZERO ANGLE OF INCIDENCE
(From NACA TR586)

$R_e = 0.3 \times 10^6$ $C_{Do} = .0085$			$R_e = 3.0 \times 10^6$ $C_{Do} = .0081$		
α	C_n	$C_t + C_{Do}$	α	C_n	$C_t + C_{Do}$
0.0	0.000	0.0000	0.0	0.000	0.0000
2.0	.200	.0061	2.0	.200	.0066
5.0	.499	.0393	5.0	.498	.0421
7.5	.765	.0910	10.0	.987	.1670
10.9	.850	.1230	15.0	1.396	.3560
11.0	.860	.0810	17.5	1.497	.4320
15.0	.834	.0560	18.0	1.326	.1890
17.5	.821	.0230	20.0	1.136	.0940
21.0	.815	-.0300	25.0	1.042	-.0110
30.0	1.160	-.0500	30.0	1.160	-.0500
40.0	1.500	-.0500	40.0	1.500	-.0500
50.0	1.750	-.0300	50.0	1.750	-.0300
60.0	1.950	-.0100	60.0	1.950	-.0100
70.0	2.050	.0100	70.0	2.050	.0100
80.0	2.080	.0500	80.0	2.080	.0500
90.0	2.060	.0900	90.0	2.060	.0900
100.0	2.040	.1250	100.0	2.040	.1250
110.0	1.950	.1500	110.0	1.950	.1500
120.0	1.850	.1500	120.0	1.850	.1500
130.0	1.700	.1500	130.0	1.700	.1500
140.0	1.500	.1500	140.0	1.500	.1500
150.0	1.170	.1400	150.0	1.170	.1400
154.0	1.000	.1250	154.0	1.000	.1250
160.0	.780	.1000	160.0	.780	.1000
164.0	.720	.0600	164.0	.720	.0600
168.0	.740	.0450	168.0	.740	.0450
170.0	.760	.0400	170.0	.760	.0400
172.0	.850	.0250	172.0	.850	.0250
175.0	.500	.0250	175.0	.500	.0250
180.0	0.000	.0250	180.0	0.000	.0250

Tab. 2 Normal and tangential force coefficients for NACA 0012

of rotor streamtube velocities is extremely non-uniform and the uniform rotor velocity approximation is invalid. Fig. 8 depicts an example of the variation of streamtube velocities through the rotor with a solidity of 0.3 operating at a tip to wind speed ratio of 3.5 and a blade Reynold's number of 0.3×10^6. The single streamtube model predicts a uniform value of rotor wind speed to freestream velocity of 0.756.

Solidity and Reynold's Number Effects

Fig. 9 characterizes the effect of solidity on the C_p curve at blade Reynold's numbers of 0.3×10^6 and 3.0×10^6. The variation of X_m with Reynold's number is dominated by the skin friction drag coefficient. On the other hand, variation of X_s with Reynold's number is dominated by profile drag due to aerodynamic stall. A more detailed description of individual C_p curves can be obtained from Ref. [13].

Wind Shear Effects

In order to evaluate the sensitivity of the Darrieus turbine to atmospheric wind shear the common 1/7 power freestream velocity profile was used [11-12]. The bottom of the rotor was assumed to be at ground level resulting in the relationship

$$\frac{U_\infty}{U_{\infty c}} = \left(\frac{2Z}{H}\right)^{1/7} \tag{18}$$

where $U_{\infty c}$ is the freestream velocity upstream of the center or equator of the rotor. The quantity Z/H is the ratio of the height above the base of the rotor to the overall rotor height.

Fig. 10 shows a comparison between power coefficient curves for a rotor with and without wind shear present.

The difference between the two curves is small when the centerline or equatorial freestream velocity at Z/H = 0.5 is used as the basis for computing C_p and U_T/U_∞. If, however, the freestream velocity at a height of Z/H = 0.45 is used, the C_p curves with and without wind shear are virtually identical.

Examples of blade aerodynamic forces are shown in Figure's 11 through 14. In Figures 11 and 12 the "flap" (normal) and "lead" (tangential) forces at the equator are non dimensionalized using the freestream velocity U_∞. Thus, one can visualize in these figures the start up process in a constant wind environment. As the tip to wind speed ratio increases, the region over which the airfoil is stalled decreases. Eventually the stall region disappears and the aerodynamic forces vary smoothly as the blade changes position. Figures 13 and 14 depict the same flap and lead forces which are non dimensionalized, this time, with respect to the rotor tip speed. Thus in these figures, the effect of a varying wind speed on a rotor operating at constant angular speed is displayed. The primary thing to be noted here is that as the wind speed increases, very sharp peaks begin to appear. This effect is more dramatic for large Reynold's numbers and should therefore be carefully considered in the design of large rotors.

Conclusions and Recommendations

In conclusion, the multiple streamtube model appears to be a substantial improvement over the single streamtube model in that; it more precisely predicts measured values of C_p, it more precisely predicts distributed effects such as blade forces and rotor wake velocity distributions, and it is adaptable to inclusion of spatial

variations in freestream velocity. On the other hand, the model is inadequate in describing many of the details of the flow field such as are related to streamtube distortions and interactions. The most serious deficiency is that, under conditions of large solidity and high tip to wind speed ratios, the simple momentum considerations inherent in the model break down. This deficiency is more severe in the single streamtube model.

The present DART model can be used to make investigations concerning blade aerodynamic force distributions for examination of rotor structural and vibration problems. In addition, these blade force distributions can be used to assess the transient behavior of a rotor during a single period of revolution. A more extensive investigation of the effects of windshear, including vertical distributions different from the 1/7 power profile as well as horizontal distributions, can be undertaken. A study using symmetrical airfoil data other than that for the NACA 0012 can be undertaken to investigate the effect on C_p.

With minor modification to the DART program, a systematic study of the effects of blade taper or non-uniform blade chord distributions can be made. An investigation of the effects of various spanwise blade shapes can also be made in conjunction with both straight and tapered blade chord distributions. In addition the potential of non-symmetrical airfoils can be examined.

Investigations which would require more extensive modification of the DART model might include; the inclusion of mast wake effects, the modification of the momentum equation for cases when it breaks down, and inclusion of some of the effects of streamtube distortion and interaction.

REFERENCES

1. Blackwell, B. F. and Feltz, L. V., "Wind Energy - A Revitalized Pursuit," Sandia Laboratory Report SAND75-0166, March (1975).

2. Banas, J. F., Kadlec, E. G., and Sullivan, W. N., "Methods for Performance Evaluation of Synchronous Power Systems Utilizing the Darrieus Vertical-Axis Wind Turbine," Sandia Laboratory Report SAND75-0204, April (1975).

3. Wilson, R. E., and Lissaman, P. B. S., Applied Aerodynamics of Wind Power Machines, Oregon State University, May (1974).

4. Strickland, J. H., Ford, S. R., and Reddy, G. B., "The Darrieus Turbine; A Summary Report," Proceedings of the 2nd U. S. National Conference on Wind Engineering Research, p. V-2-1, Colorado State University, June (1975).

5. South, P., and Rangi, R., "Preliminary Tests of a High Speed Vertical Axis Windmill Model," National Aeronautical Establishment of Canada Report LTR-LA-74, March (1974).

6. Larsen, H. C., "Summary of a Vortex Theory of the Cyclogiro," Proceedings of the 2nd U. S. National Conference on Wind Engineering Research, p. V-8-1, Colorado State University, June (1975).

7. Templin, R. J., "Aerodynamic Performance Theory for the NRC Vertical-Axis Wind Turbine," National Research Council of Canada Report LTR-LA-160, June (1974).

8. Glauert, H., The Elements of Aerofoil and Airscrew Theory, The Macmillan Co., New York, (1943).

9. Jacobs, E. N., and Sherman, A., "Airfoil Section Characteristics as Affected by Variations of the Reynold's Number," NACA Report No586, 23rd Annual NACA Reports 577-611, (1937).

10. Riegels, F. W., Aerofoil Sections, Translated from German by D. G. Randell, Butterworths, London, (1961).

11. Davenport, A. G., "The Dependence of Wind Loads on Meteorological Parameters," Proc. Wind Effects on Buildings and Structures Conference, International Research Seminar, University of Toronto Press, (1968).

12. Reed, J. W., Maydew, R. C., and Blackwell, B. F., "Wind Energy Potential in New Mexico," Sandia Laboratory Report SAND74-0071, July (1974).

13. Strickland, J. H., "The Darrieus Turbine: A Performance Prediction Model Using Multiple Streamtubes," Sandia Laboratory Report, SAND75-0431, July (1975).

14. Blackwell, B. F. and Reis, G. E., "Blade Shape for a Troposkien Type of Vertical Axis Wind Turbine," Sandia Laboratory Report, SLA-74-0154, April (1974).

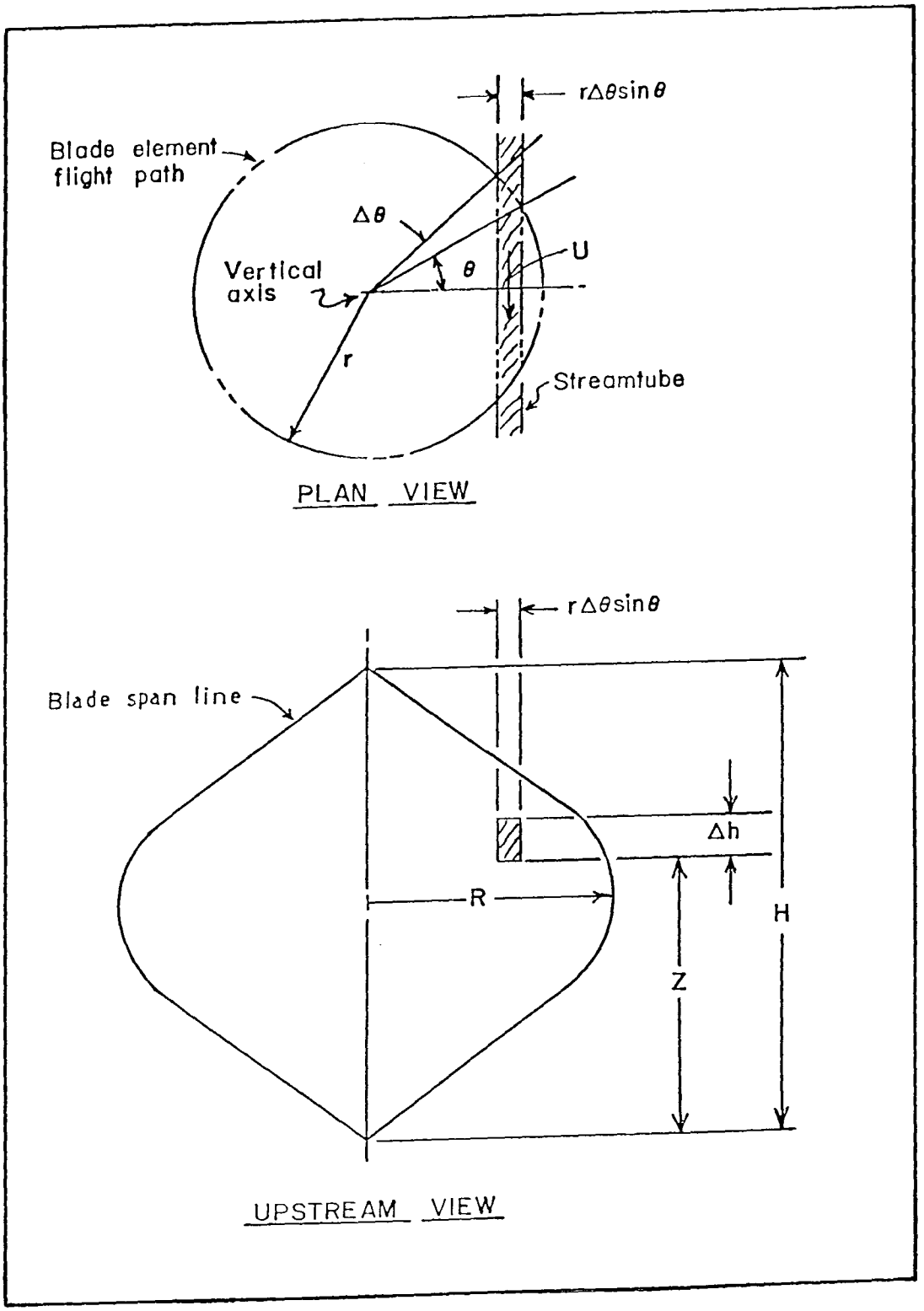

Fig. 1 Typical streamtube passing through the rotor

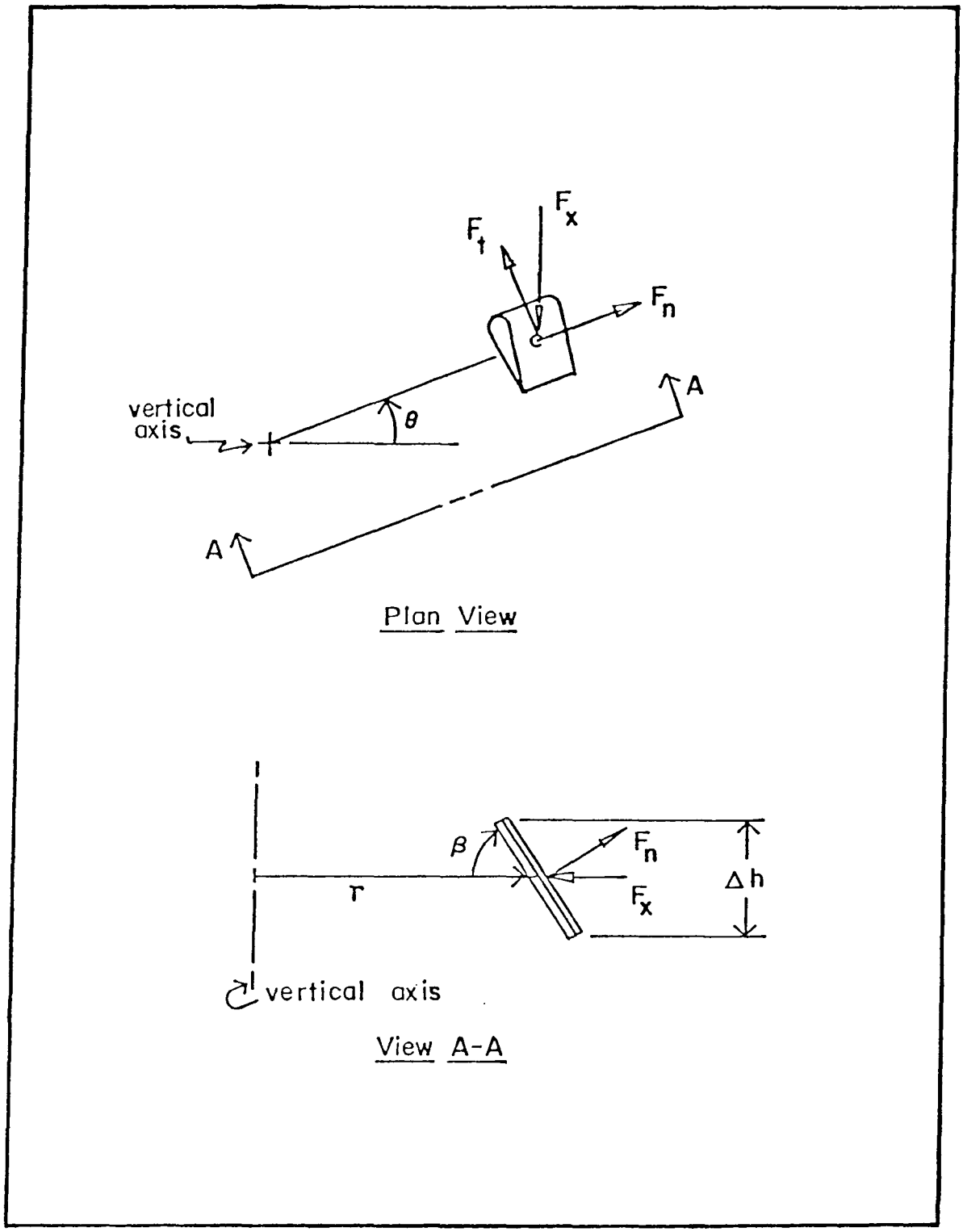

Fig. 2 Blade element forces

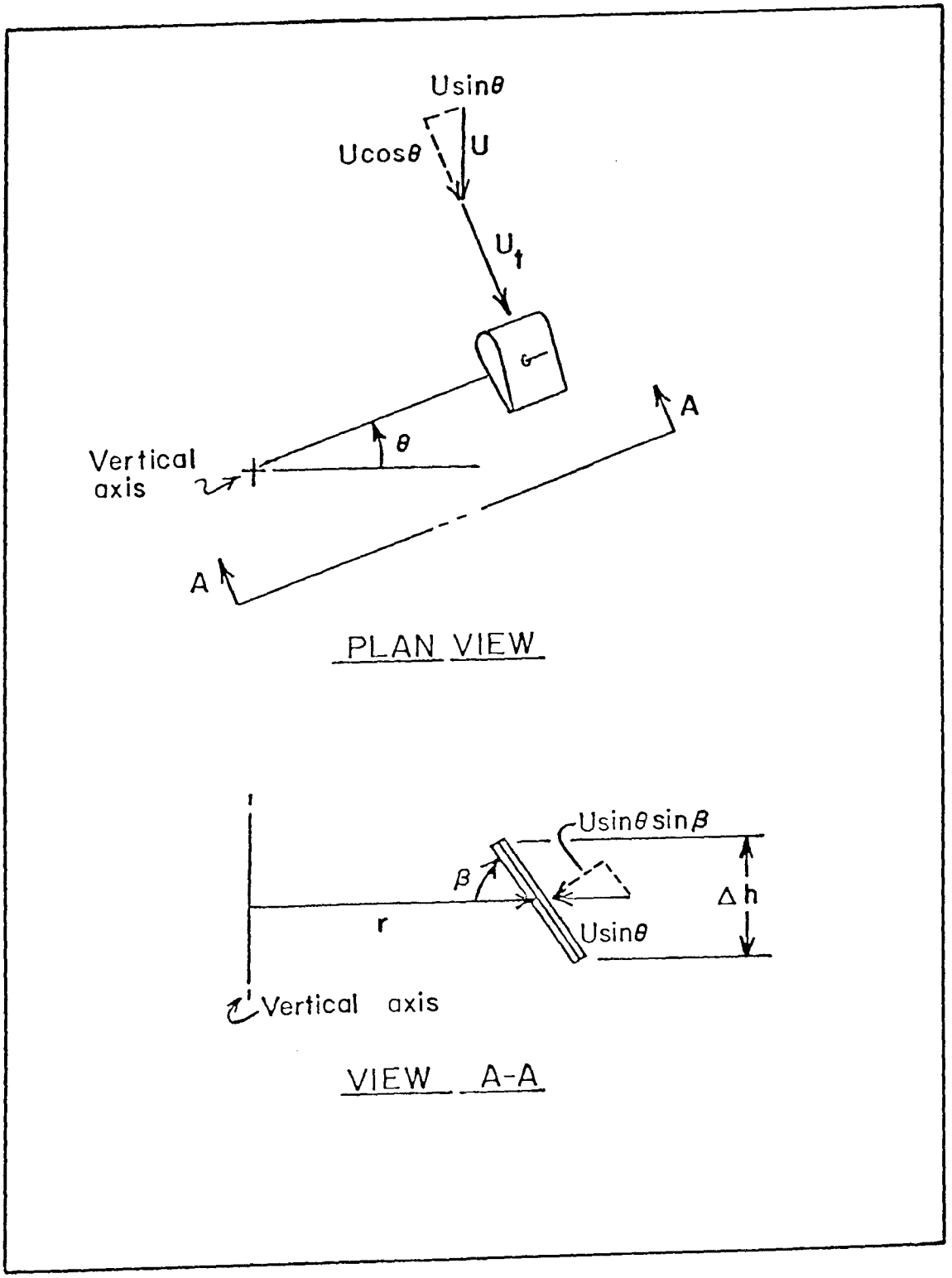

Fig. 3 Relative velocity vector

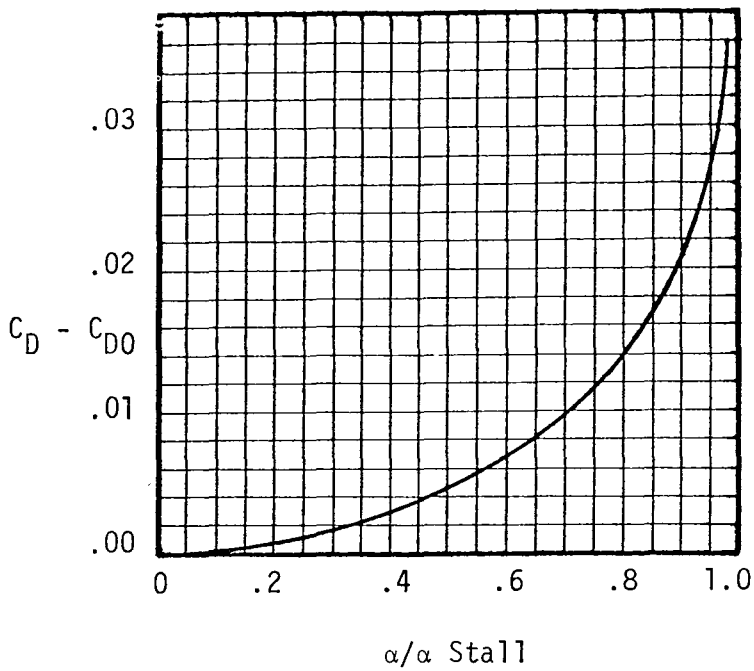

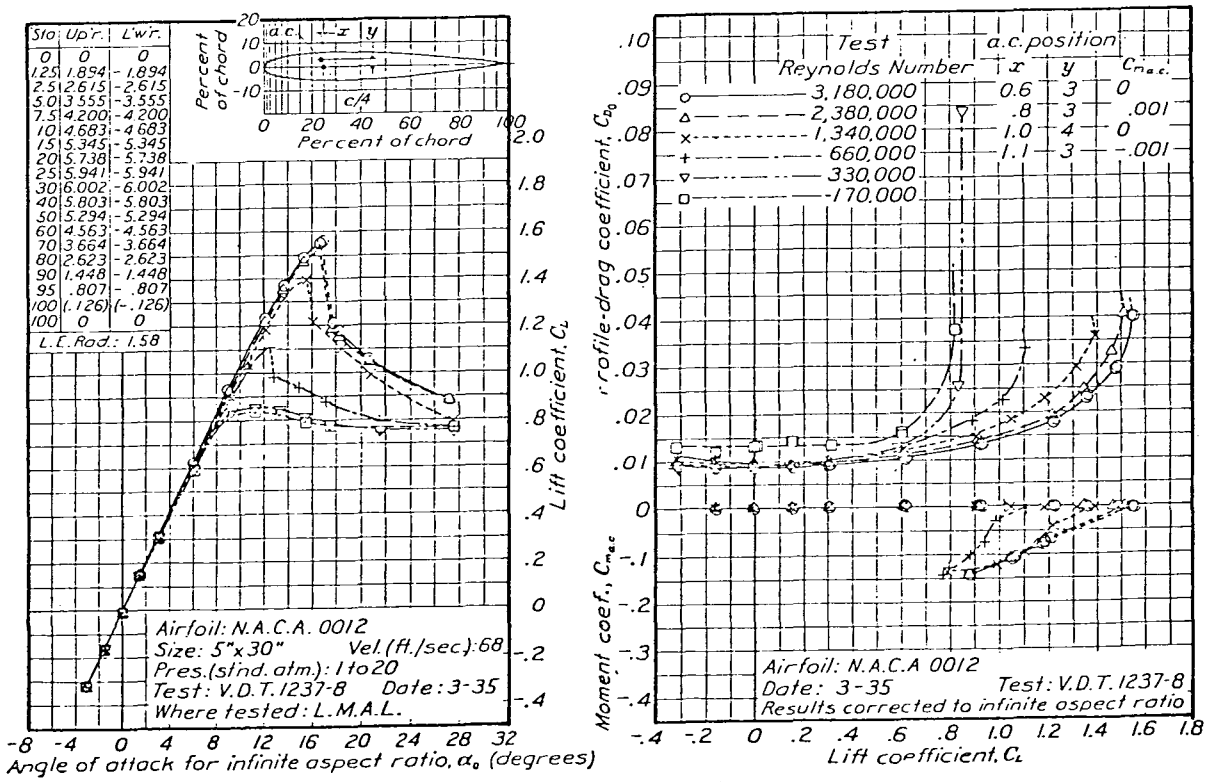

FIGURE 3.—N. A. C. A. 0012.

Fig. 4 Airfoil data from NACA TR586

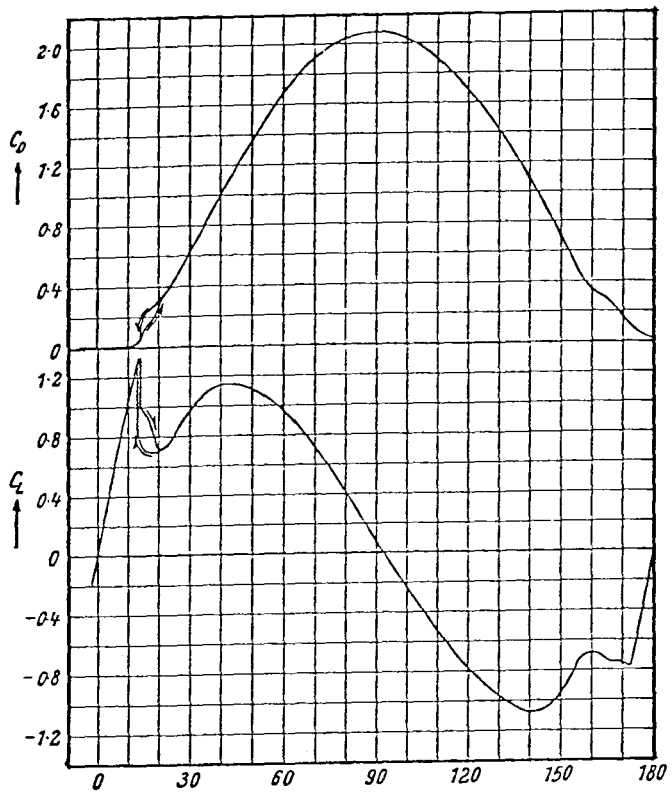

Fig. 12.105a. NACA 0012. $R = 1{\cdot}8.10^6$. Wind tunnel: TDT. [N 3361]

Fig. 5 Airfoil data from Ref. [10]

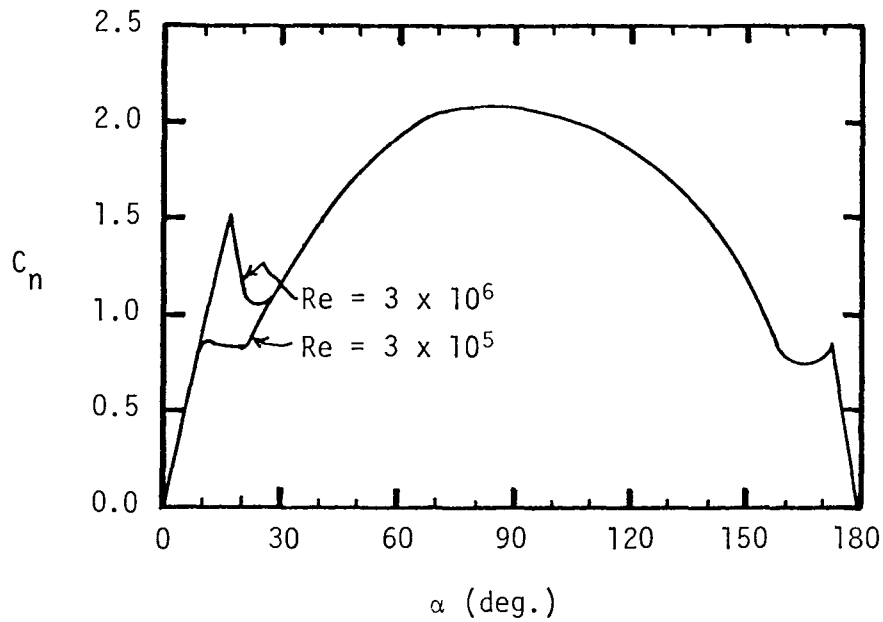

Normal Force Coefficient
For NACA 0012 Airfoil

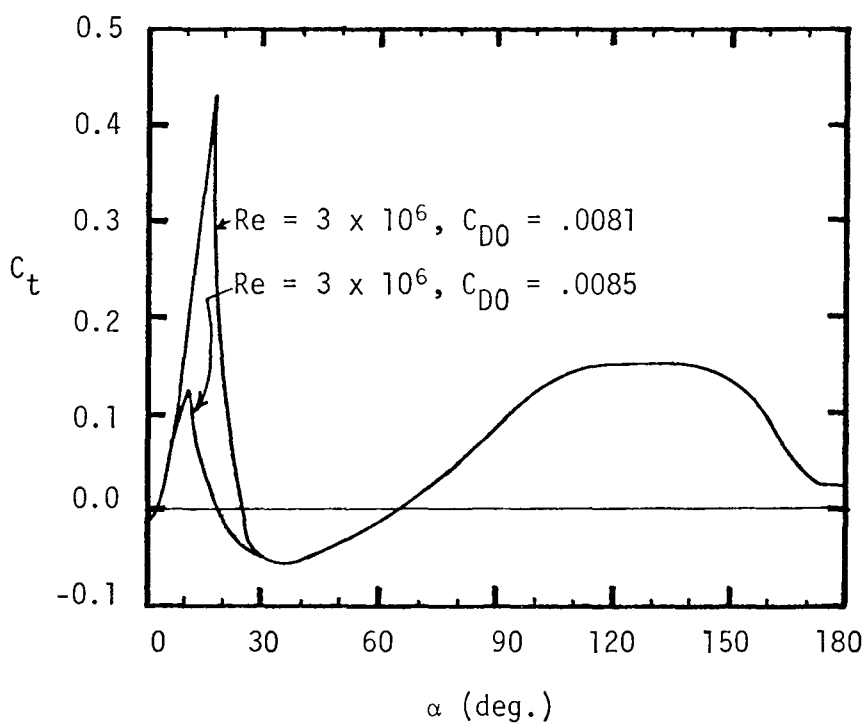

Tangential Force Coefficient
For NACA 0012 Airfoil

Fig. 6 Normal and tangential force coefficients for NACA 0012

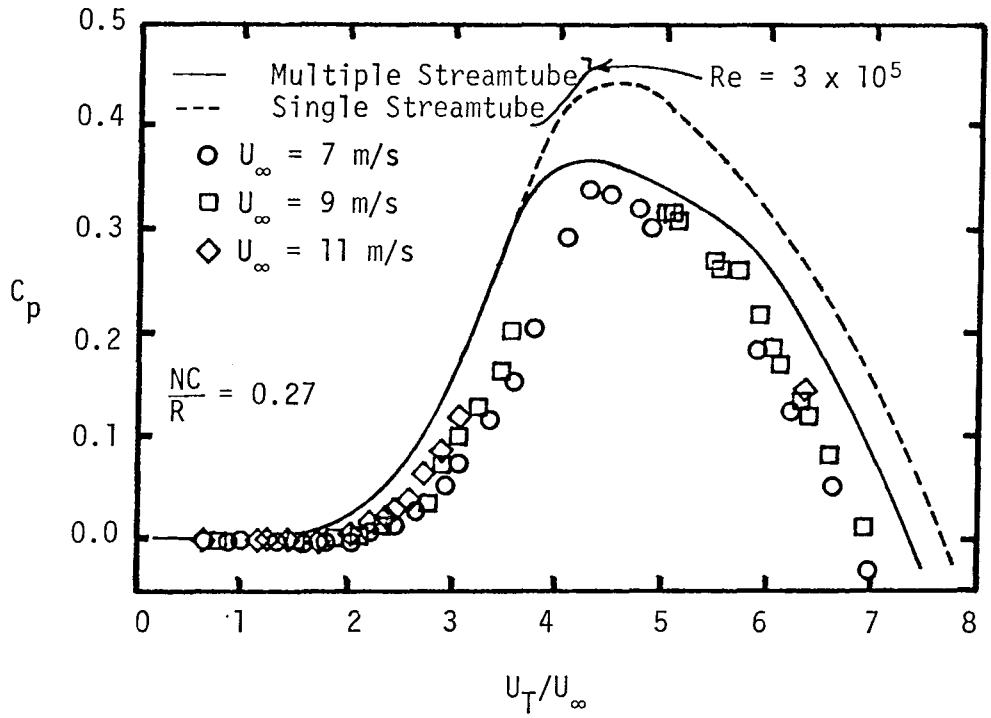

Fig. 7 Comparison of Single-Streamtube Model and Multiple-Streamtube Model with Experimental Data (Sandia 2m rotor)

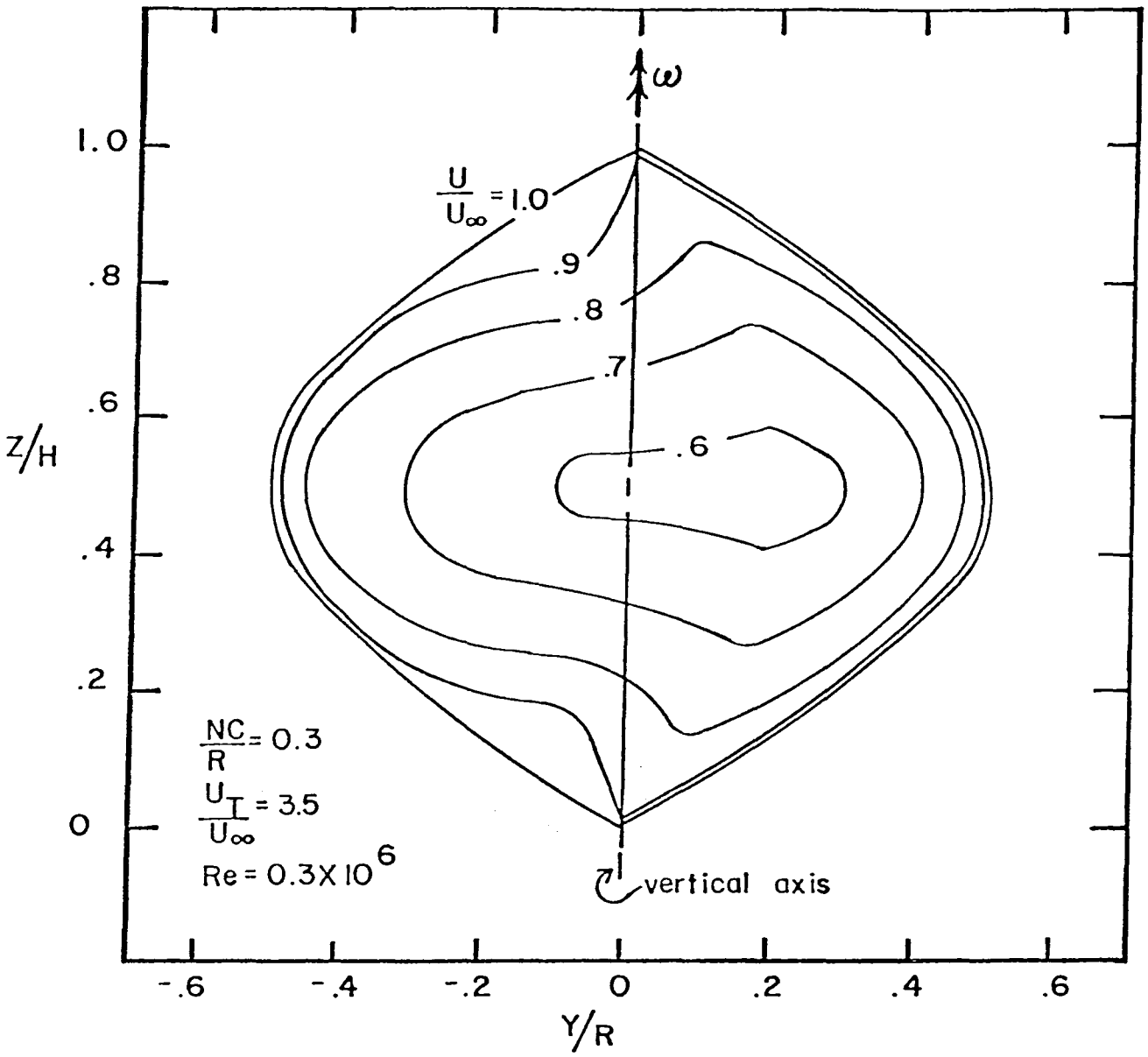

Fig. 8 Variation of streamtube velocities through the rotor (view looking upstream through the rotor)

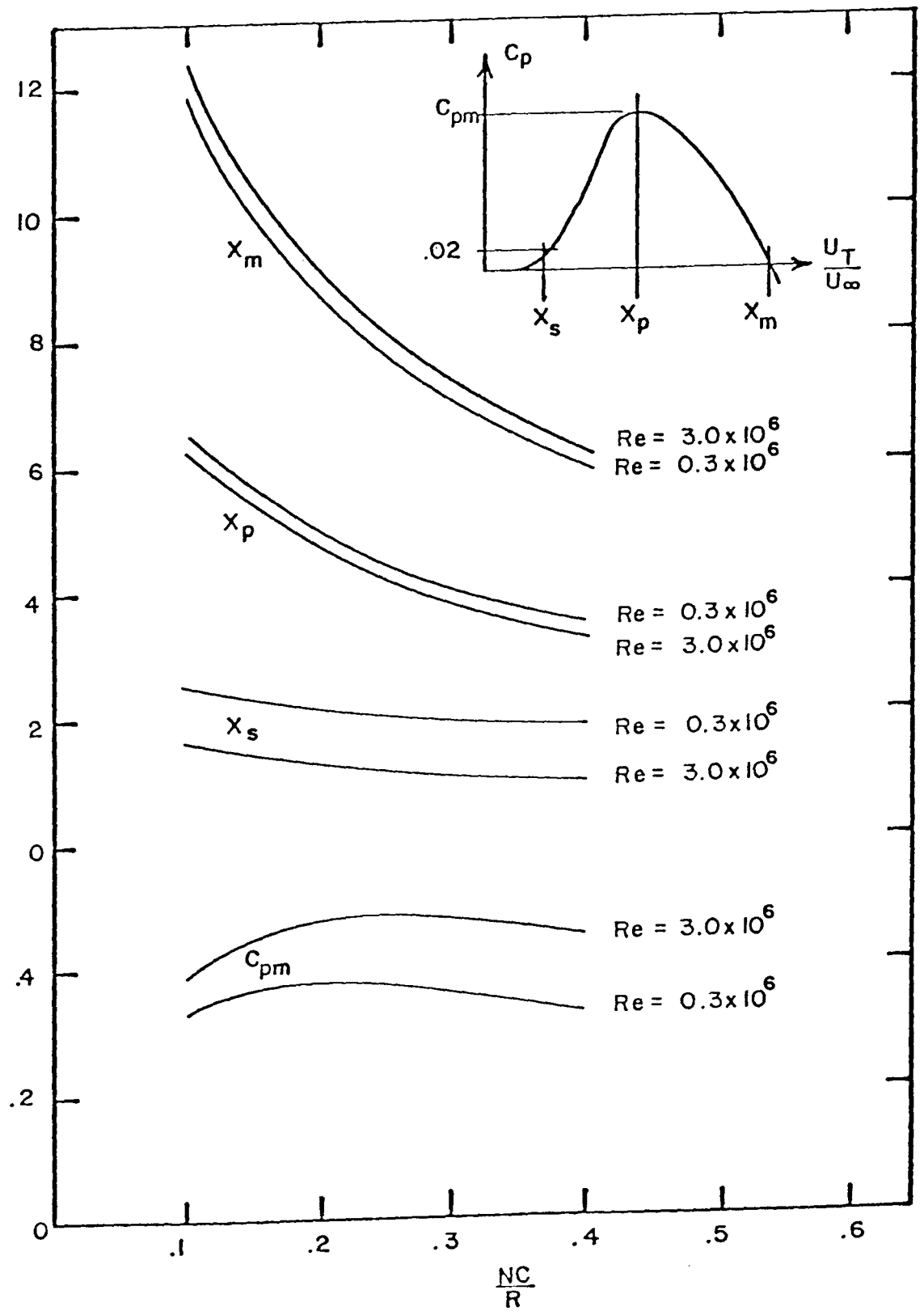

Fig. 9 C_p curve characterization

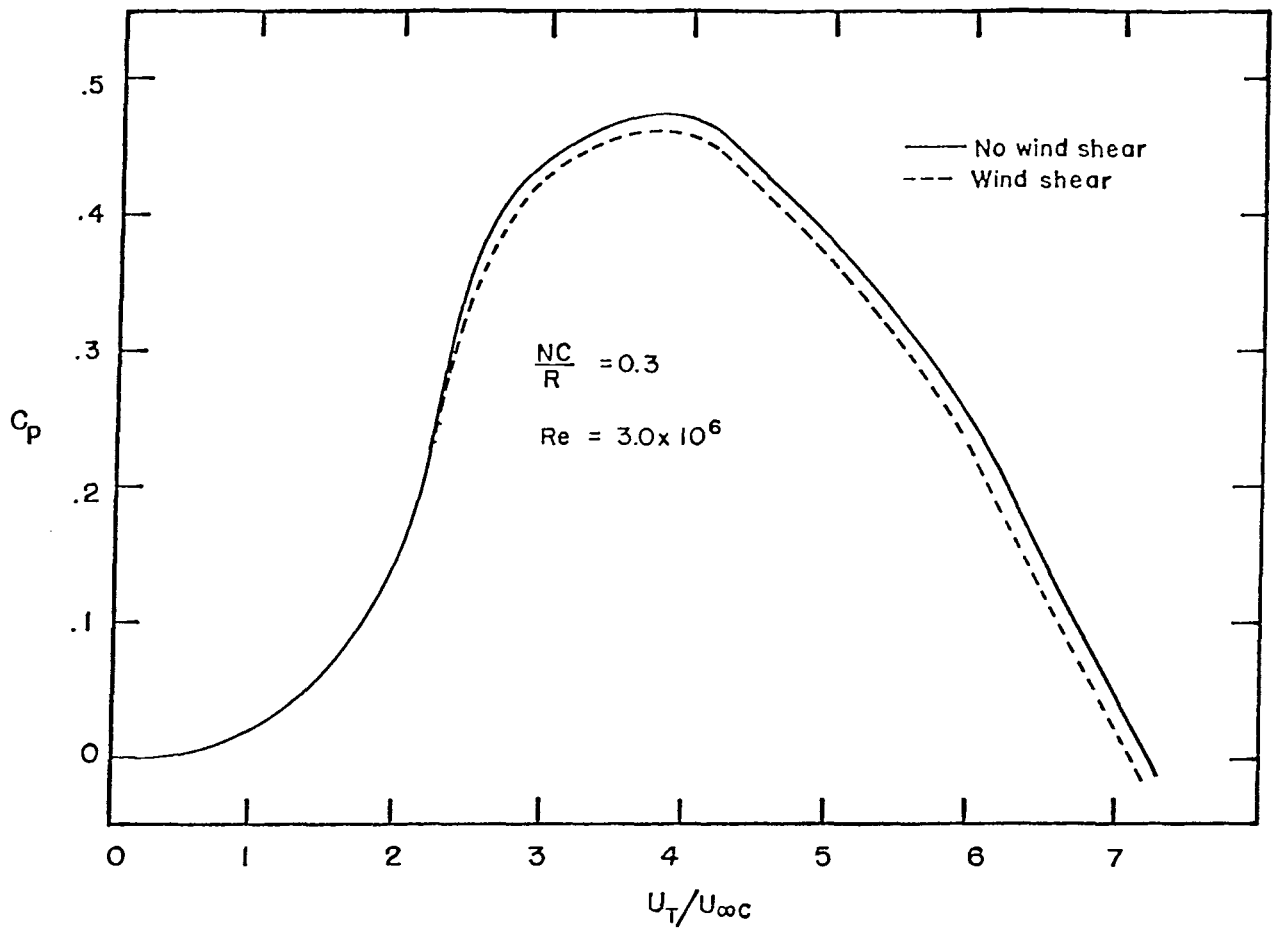

Fig. 10 Effect of wind shear on rotor performance

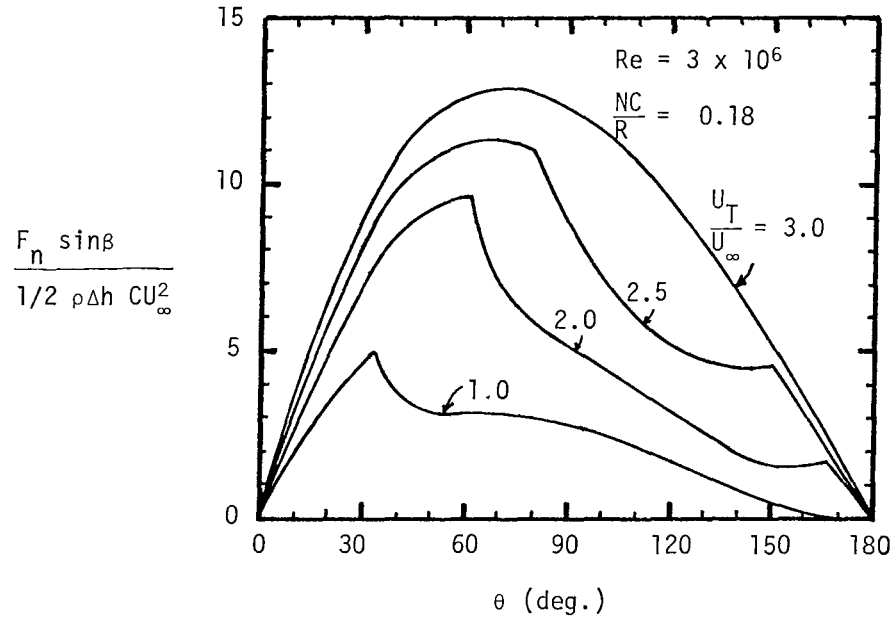

Fig. 11 U_∞ Normalized Equatorial Flap Force

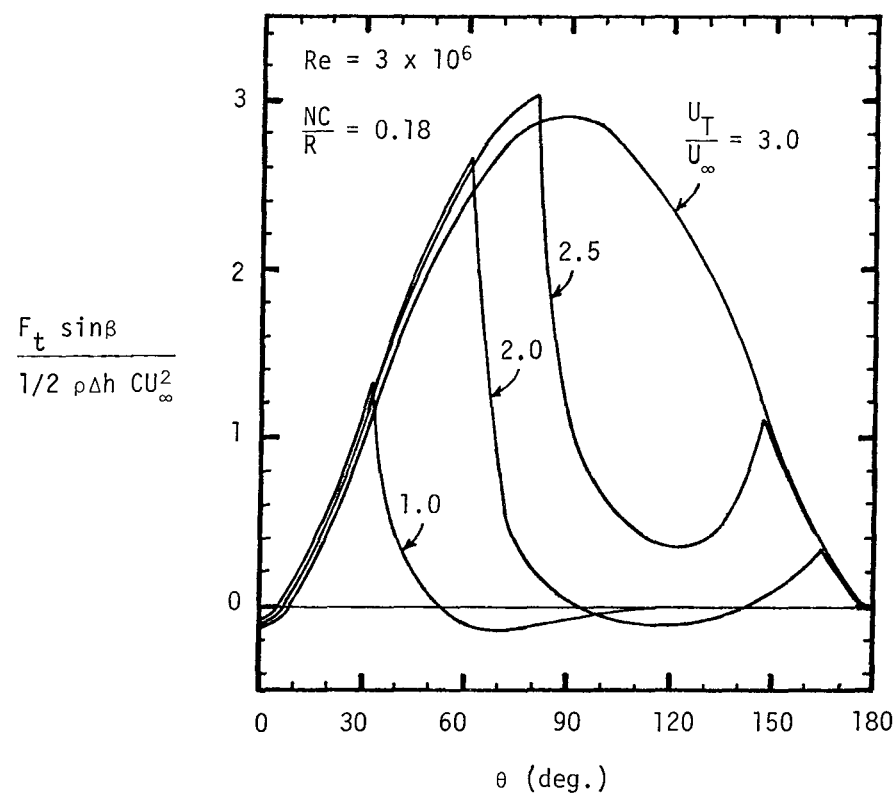

Fig. 12 U_∞ Normalized Equatorial Lead Force

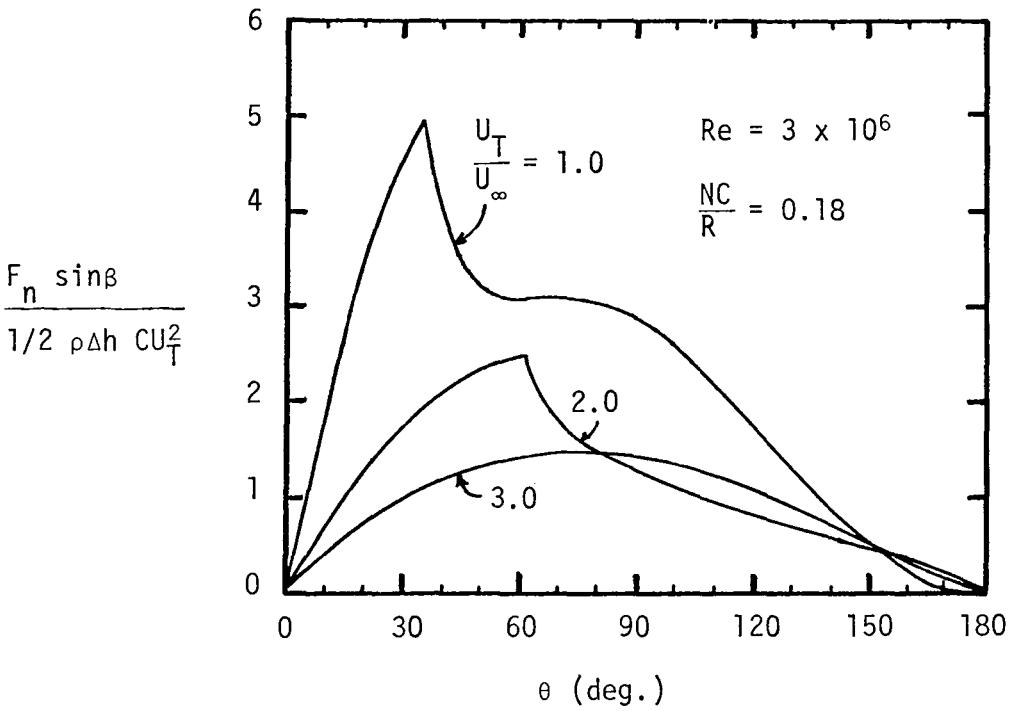

Fig. 13 U_T Normalized Equatorial Flap Force

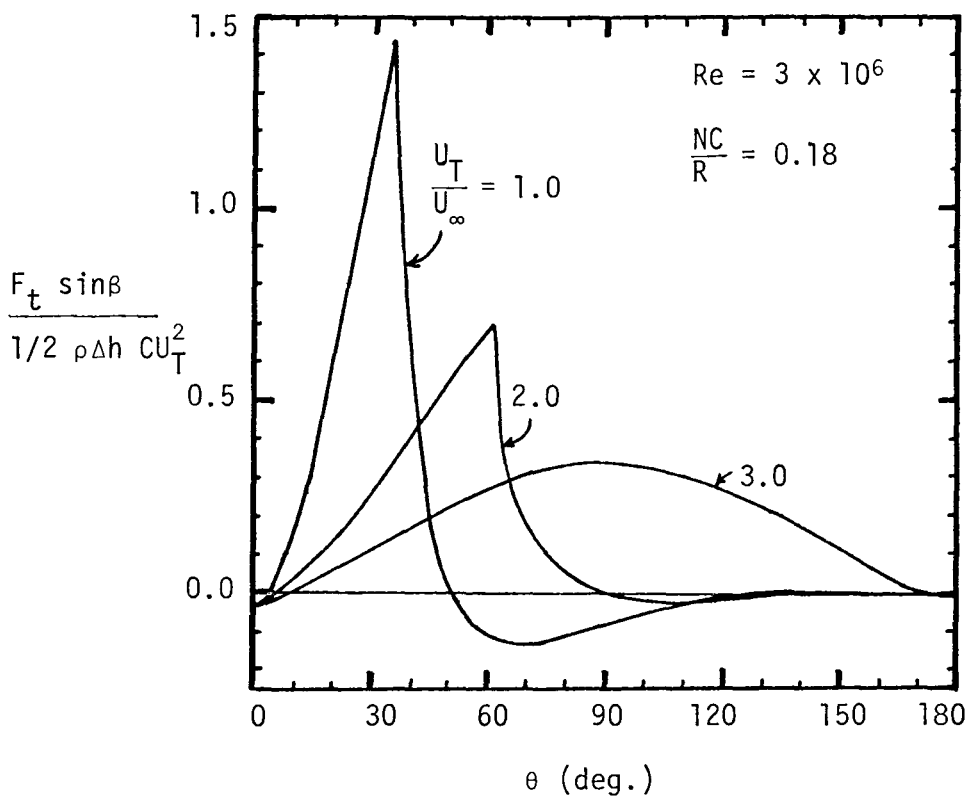

Fig. 14 U_T Normalized Equatorial Lead Force

Selected Wind Tunnel Test Results for the Darrieus Wind Turbine

B. F. Blackwell and R. E. Sheldahl
Sandia Laboratories, Albuquerque, N. M. 87115

Introduction

The previously published experimental performance data for the Darrieus turbine are contained in a series of National Aeronautical Establishment/National Research Council of Canada (NAE/NRC) reports [1-5] and a recently published NASA report [6]. In order to verify some of the earlier findings, expand the range of some of the pertinent parameters, and provide a comprehensive data base for the development of computer models in the prediction of aerodynamic performance and loads, Sandia Laboratories undertook an extensive wind tunnel test program. The purpose of this paper is to summarize the primary results from the test program conducted at the Vought Corporation, Vought Systems Division Low Speed Wind Tunnel.

Test Models, Instrumentation, and Facility

Figure 1 presents a typical 2-m-diameter test model located in the 4.6- x 6.1-m (15- x 20-ft) wind tunnel test section. The turbine consists of the rotating components (tower and blades) held by bearings in the upper collar and in the lower support structure. The upper collar is restrained by steel cables with a predetermined tension and are affixed to the walls of the test section. The blades were machined from a high-strength aluminum alloy (7075-T6) to the NACA 0012 airfoil section specification as a flat ribbon and then formed to the desired curved shape.

The rotating tower is attached to the power and instrumentation train (Fig.2), which consists of a precision torque and rotation transducer, a right-angle gear transmission with a 2:1 gear ratio, and a speed-controlled 5-hp electric motor/generator. Also included are several shaft flexible couplings. The torque and rotation transducer was a commercially available Lebow Model 1404-200. The 2:1 gear box allowed a better match between wind turbine and load characteristics. The motor/generator speed was controlled by a Morse VLT-5 AC adjustable speed

controller. (The significance of maintaining a specified turbine rotational speed is discussed in a subsequent section.) Figure 3 is a schematic of the turbine, instrumentation, and load system.

The Vought Systems Division Low Speed Wind Tunnel [7] is a horizontal single-return, tandem test section, closed-circuit facility. The facility contains a rectangular 2.1- x 3.0-m (7- x 10-ft) test section with a rectangular 4.5- x 5.1-m (15- x 20-ft) test section 11.9 metres long located upstream of the 2.1- x 3.0-m test section. The upstream test section has a windspeed range of 3-23 m/s. Figure 1 shows the wind turbine in the 4.6- x 6.1-m section; the photograph was taken looking downstream into the contraction region of the 2.1- x 3.0-m test section. Controls for both the wind turbine and the wind tunnel are located behind the windows shown on the right side of the photograph. The windows provided visual observation of the turbine and also allowed video and camera coverage.

Test Procedure and Matrix

The general character of the torque/speed curves for the Darrieus turbine must be fully understood for proper design of an experimental setup that will define the performance over the tip-speed ratio range of interest. For example, consider the experimental torque/speed curve shown in Fig. 4. If the turbine is started under no external load, it will simply accelerate to the runaway-condition which is in excess of 700 rpm. Suppose an external load of 88 in-lbf is applied. What will be the new equilibrium rotational speed? Both 365 and 540 rpm correspond to a load of 88 in-lbf. From elementary stability considerations, it can be shown that the 365-rpm condition is unstable. In fact, all regions where the slope of the torque/speed curve is positive are unstable if uncontrolled. In order to obtain performance data in the unstable regions, some type of control system had to be devised. The system shown schematically in Fig. 3 accomplished the purpose of maintaining a fixed rotational speed independent of tunnel speed.

Since the Darrieus turbine is a lift device, one would expect that the performance is a function of Reynolds number. If a single Reynolds number is to be associated with a particular freestream velocity and turbine rotational speed, what are the appropriate length and velocity scales? The obvious length scale is the blade chord; however, the velocity scale is not so obvious since the velocity

of the wind relative to the blade depends both on angular position of the blade and on location along the blade length. If one observes the primary torque-producing portion of the blade (near equatorial plane) operating at high tip-speed ratios, it appears that the most appropriate velocity scale is the blade tip speed ($R\omega$). This suggests that configurational changes—such as chord, number of blades, airfoil section, etc—can be more readily compared at constant Reynolds number, where the length and velocity scales are blade chord (c) and tip speed ($R\omega$).

$$Re_c = \frac{cR\omega}{\nu} \tag{1}$$

Consequently, the tip-speed ratio for a given test configuration was varied as a result of tunnel speed changes while a constant rotational speed (and hence Reynolds number) was maintained. The constant rotational speed method of testing has the additional advantage of better simulating the synchronous grid application of the Darrieus turbine.

Although the primary test method employed involved constant turbine speed with variable tunnel speed, additional data were taken at constant tunnel speed with variable turbine speed. The complete test matrix is presented in Table I. Five different configurations—consisting of three different chords and two different numbers of blades—were tested at a variety of turbine and tunnel speeds.

Test Results

The test results are presented in terms of power coefficient as a function of tip-speed ratio:

$$C_p = \frac{Q\omega}{\frac{1}{2}\rho V_\infty^3 A_s} \tag{2}$$

$$X = \frac{R\omega}{V_\infty} \quad . \tag{3}$$

The blade geometry is characterized by the solidity, which is the ratio of total blade planform area* to rotor swept area.† Figure 5 shows the influence of Reynolds number on power coefficient for a solidity of 0.3. An increase in Reynolds number by a factor of 3 produces a 30% increase in maximum power coefficient. Increasing the Reynolds number also increases the tip-speed ratio range where useful power is produced. The tip-speed ratio where the power coefficient is a maximum decreases with increasing Reynolds number. This is thought to be due to the fact that stall occurs more abruptly at the higher Reynolds numbers.

Figure 6 presents power coefficient data for a solidity of 20%, which is the solidity chosen for the Sandia 17-m turbine. The trends with Reynolds number are similar to those for the 30% data.

The peak power coefficient for any configuration tested was found to be approximately 0.34. At first glance, this might appear to be considerably below the often-quoted number 0.4-0.45 for $(C_p)_{max}$, of a well-designed horizontal-axis wind turbine. However, the Reynolds number for the horizontal-axis performance calculations is generally not stated, and these results are obviously Reynolds-number-dependent also. Utilizing the peak power coefficient in Fig. 6 and extrapolating to the Reynolds number of 1.2×10^6, the peak C_p for the Sandia 17-m design was conservatively estimated to be 0.45. This is clearly in the same ball park as horizontal-axis designs at comparable Reynolds numbers.

Figure 7 presents the effect of solidity on performance at a nominal Reynolds number of 1.5×10^5. The most noticeable influence of solidity is that the runaway-condition tip-speed ratio increases with decreasing solidity. For a synchronous application where the tip-speed ratio varies over a wide range, power can be produced over a greater windspeed variation for a given turbine rotational speed. The tip-

*The blade planform area for a constant chord blade is the number of blades times blade chord times blade length.

†A rotating blade of the Darrieus turbine sweeps out a volume which is symmetric about the axis of rotation; this is called the swept volume. The area common to the swept volume and to a plane containing the axis of rotation is called the swept area.

speed ratio at which the power coefficient is a maximum increases with decreasing solidity. If it is desired to maximize the power coefficient, a solidity in the range 0.2-0.25 should be chosen.

Numerous theoretical models for Darrieus turbine performance have been proposed. In the majority of these models, the only effect of the number of blades is through the solidity parameter. This implies that for a given swept area the performance of a two-bladed system is the same as that of a three-bladed system provided that the product (Nc) remains constant. In order to verify this hypothesis, a two-bladed and a three-bladed configuration, both with a solidity of 20%, were tested at the same Reynolds number. The results are shown in Fig. 8. It appears that the three-bladed configuration is slightly better than the two-bladed one. The difference seems to be most pronounced in the tip-speed ratio range 3-4. No satisfactory explanation for this effect has been found.

Figure 9 compares performance data for two of the Sandia configurations tested at constant freestream velocity with NRC data presented by South and Rangi.[5] The NRC test conditions were 50- to 250-rpm turbine speed and 3.05- to 6.1-m/s (10- to 20-ft/s) tunnel speed. The NRC data exhibit a slightly higher $(C_p)_{max}$ occurring at a higher tip-speed ratio and a lower tip-speed ratio for the runaway condition. Discrepancies between the two data sets obviously exist.

Figures 10 and 11 present a comparison of theoretical calculations with experimental data for solidities of 0.3 and 0.13, respectively. The model, which is a multiple streamtube computer code, has been described by Strickland.[8] The Strickland[8] model utilized airfoil section data at a single constant Reynolds number, whereas the calculations presented in Figs. 10 and 11 were performed by utilizing the local chord Reynolds number and with section data tabulated as a function of Reynolds number. The agreement between theory and data is quite good for the left-hand side of the power coefficient curve. For the relatively low tip-speed ratio range, the blades are "lightly loaded" and the theory has the most validity. The poor agreement between theory and data on the right-hand side of the power coefficient curve can be attributed to the fact that the model assumes that the downwind portion of the rotor sees the same induced velocity field as the upwind portion of the rotor.

Addition experimental data for the Darrieus turbine can be found in Blackwell et al.[9]

References

1. P. South and R. S. Rangi, "Preliminary Tests of a High Speed-Vertical Axis Windmill Model," National Research Council of Canada, LTR-LA-74, March 1971.
2. P. South and R. S. Rangi, "A Wind Tunnel Investigation of a 14-ft Diameter Vertical-Axis Wind Turbine Developed at the National Research Council, Ottawa, Canada," Agricultural Engineer, pp. 14-16, February 1974 (see also American Society of Agricultural Engineers, Paper No. PNW 73-303).
4. R. J. Templin, "Aerodynamic Performance Theory for the NRC Vertical-Axis Wind Turbine," National Research Council of Canada, LTR-LA-160, June 1974.
5. P. South and R. S. Rangi, "An Experimental Investigation of a 12-ft Diameter High Speed Vertical Axis Wind Turbine," National Research Council of Canada, LTR-LA-166, April 1975.
6. R. J. Muraca and R. J. Guillotte, "Wind Tunnel Investigation of a 14' Vertical Axis Windmill," National Aeronautics and Space Administration, NASA TM X-72663, March 1976.
7. J. W. Holbrook, "Low Speed Wind Tunnel Handbook," LTV Aerospace, AER-EOR-12995-B, February 1974.
8. J. H. Strickland, "The Darrieus Turbine: A Performance Prediction Model Using Multiple Streamtubes," Sandia Laboratory, SAND 75-0431, October 1975.
9. B. F. Blackwell, L. V. Feltz, and R. E. Sheldahl, "Wind Tunnel Performance Data for the Darrieus Wind Turbine with NACA 0012 Blades," Sandia Laboratories, SAND 76-0130, May 1976.

TABLE I

Darrieus Rotor Tests in the Vought Systems Division

Low Speed Wind Tunnel

Run No.	Configuration Number	No. of Blades	Solidity (%)	Rotor Speed (rpm)	Wind Velocity (m/s)	Chord (cm)	Chord Reynolds Number
1	1	3	30	180	Variable	8.815	104,000
2	1	3	30	267	Variable	8.815	150,000
3	1	3	30	500	Variable	8.815	290,000
5	1	3	30	Variable	11	8.815	Variable
6	1	3	30	Variable	9	8.815	Variable
7	2	3	25	216	Variable	7.346	101,000
8	2	3	25	320	Variable	7.346	151,000
9	2	3	25	600	Variable	7.346	278,000
10	2	3	25	Variable	11	7.346	Variable
11	2	3	25	Variable	9	7.346	Variable
13	3	3	20	270	Variable	5.877	101,000
14	3	3	20	400	Variable	5.877	154,000
15	3	3	20	525	Variable	5.877	200,000
16	3	3	20	Variable	9	5.877	Variable
17	3	3	20	Variable	7	5.877	Variable
18	4	2	20	180	Variable	8.815	106,000
19	4	2	20	267	Variable	8.815	156,000
20	4	2	20	350	Variable	8.815	204,000
21	4	2	20	500	Variable	8.815	290,000
22	4	2	20	Variable	9	8.815	Variable
23	4	2	20	Variable	11	8.815	Variable
24	5	2	13	Variable	7	5.877	104,000
25	5	2	13	270	Variable	5.877	155,000
26	5	2	13	400	Variable	5.877	200,000
27	5	2	13	525	Variable	5.877	Variable
28	5	2	13	Variable	9	5.877	Variable

$A_s = 2.5944\ m^2$

$R = 0.9798\ m$

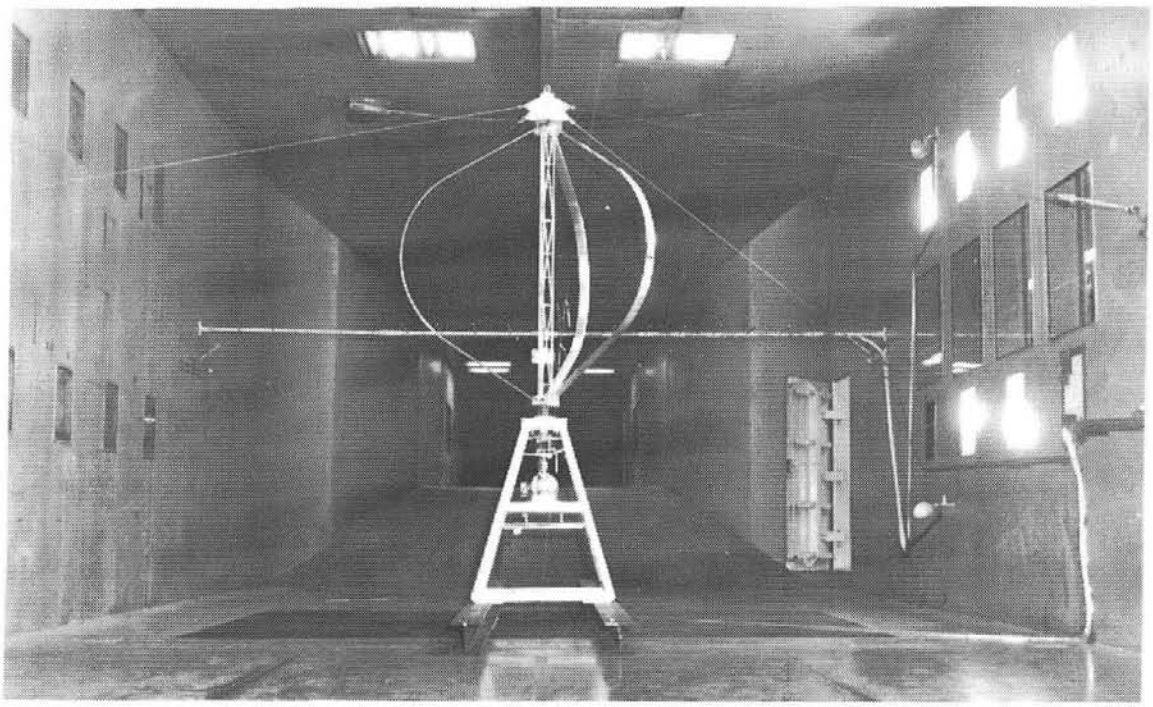

Fig. 1. Photograph of 3-m model in wind tunnel.

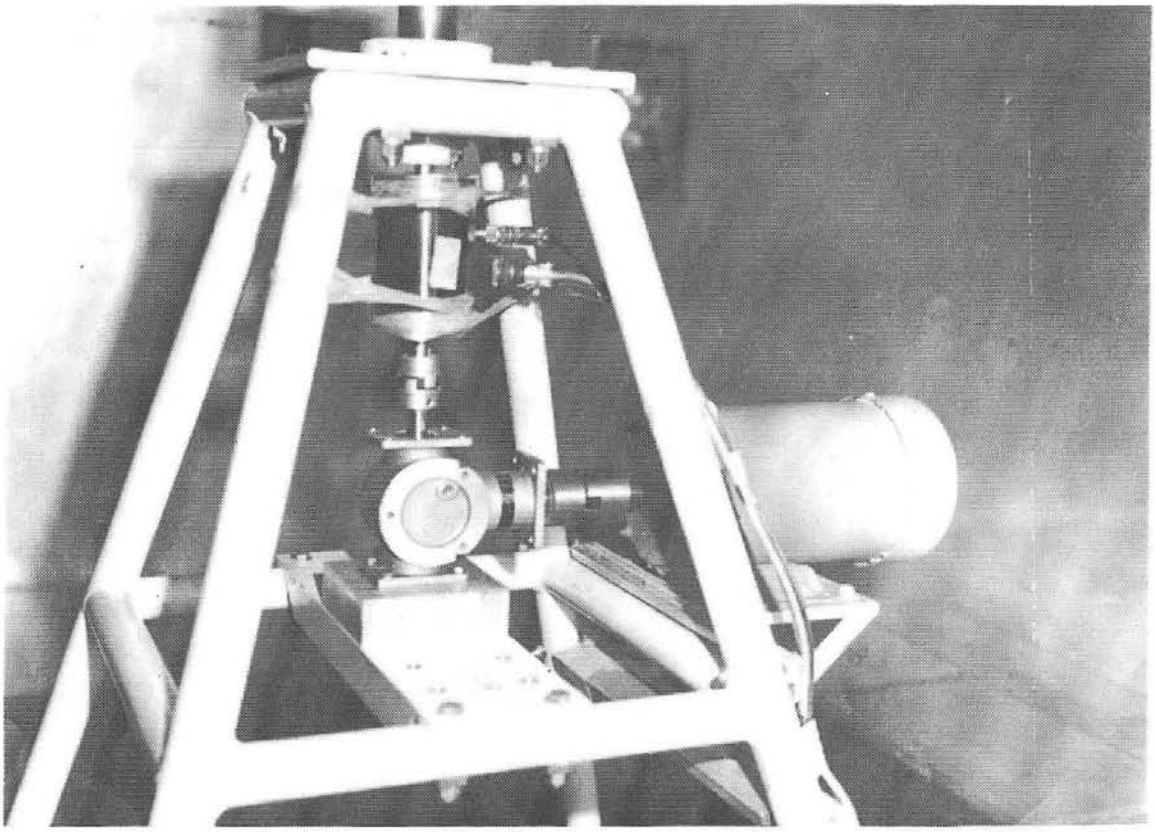

Figure 2. Photograph of torque meter, gear box, and motor/generator.

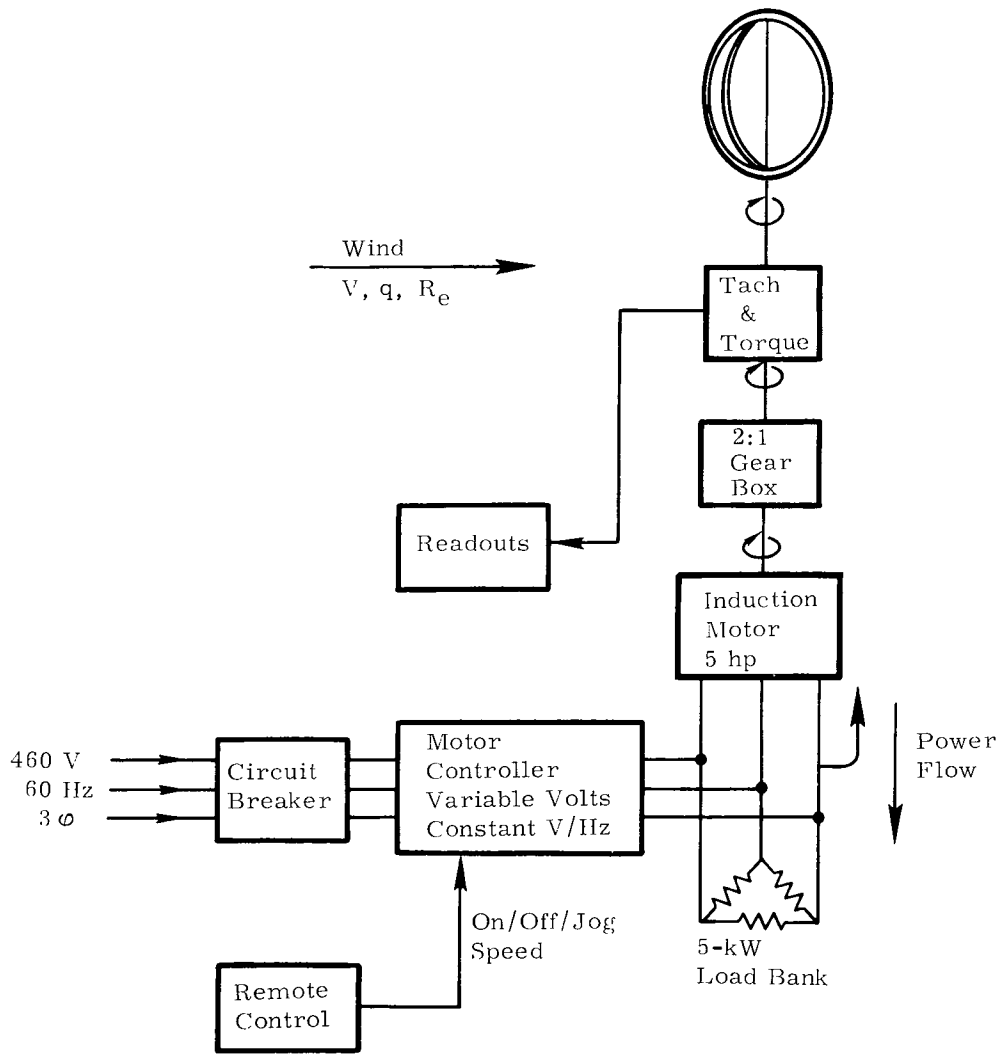

Fig. 3. Schematic of test setup

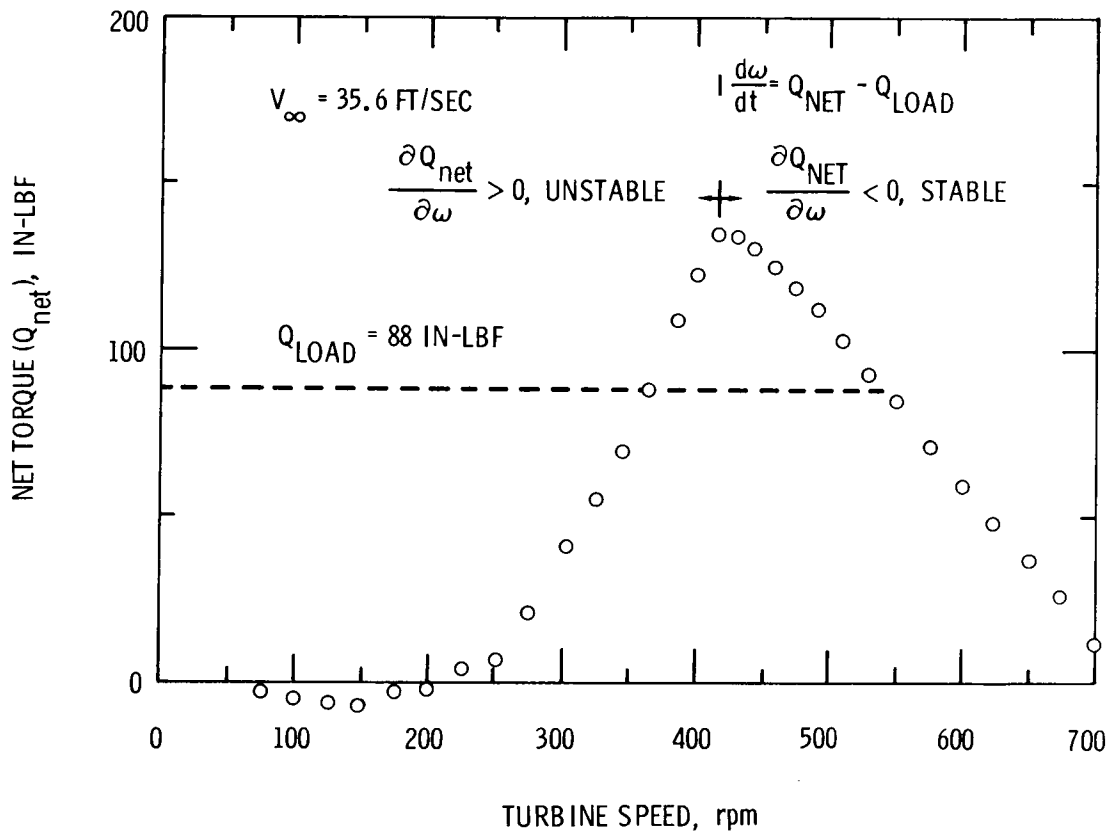

Fig. 4. Representative torque vs. rpm curve.

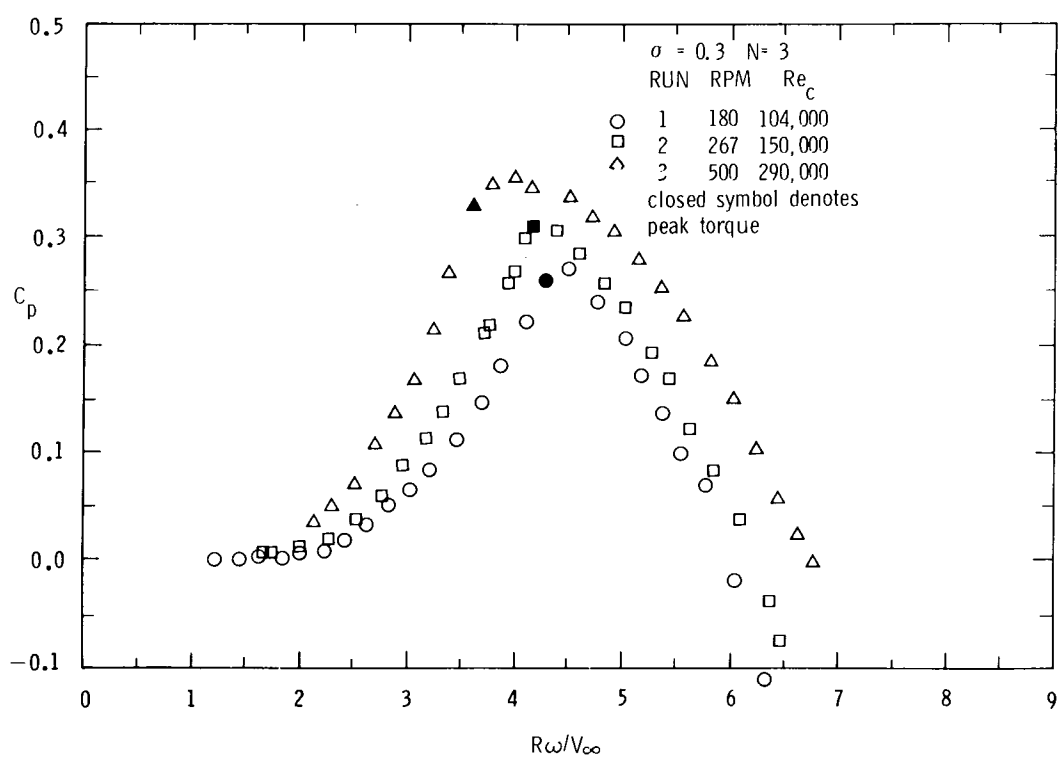

Fig. 5. Influence of Reynolds number on power coefficient for solidity of 0.3.

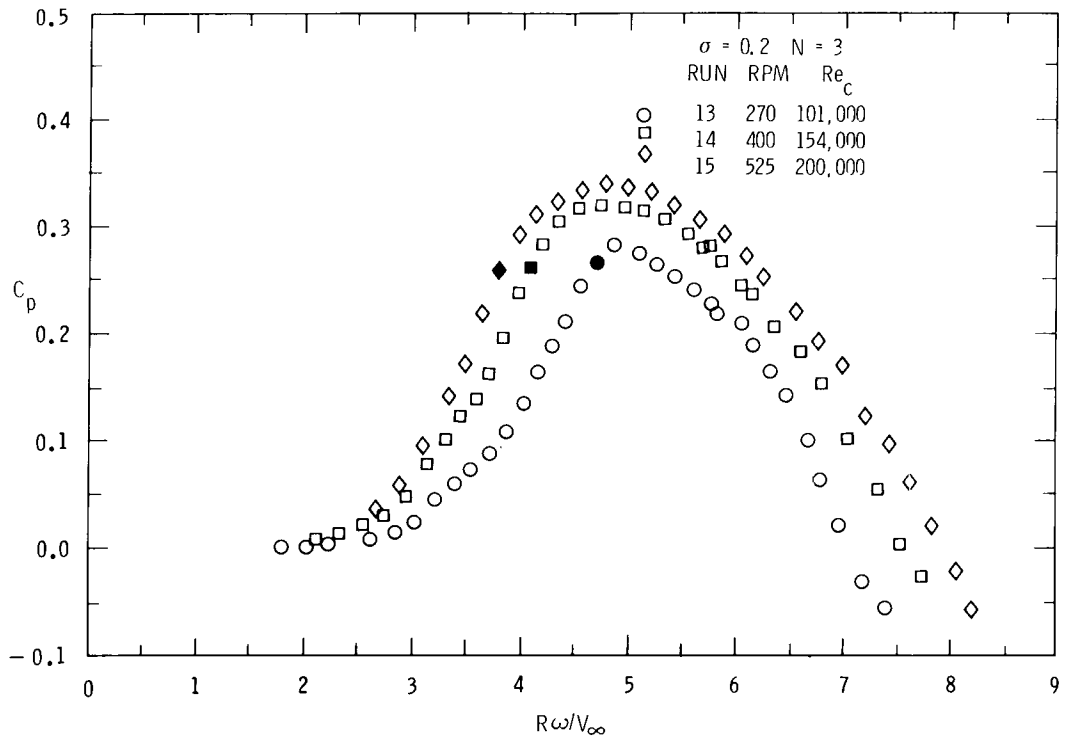

Fig. 6. Influence of Reynolds number on power coefficient for solidity of 0.2.

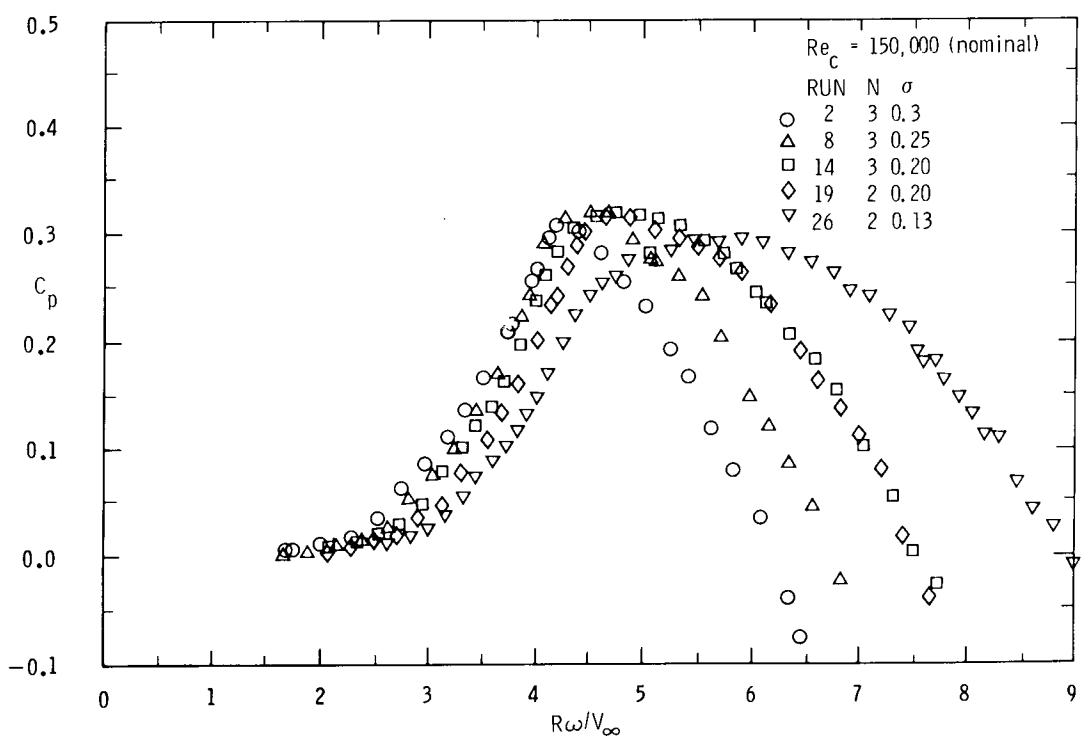

Fig. 7. Influence of solidity on power coefficient for nominal Reynolds number of 150,000.

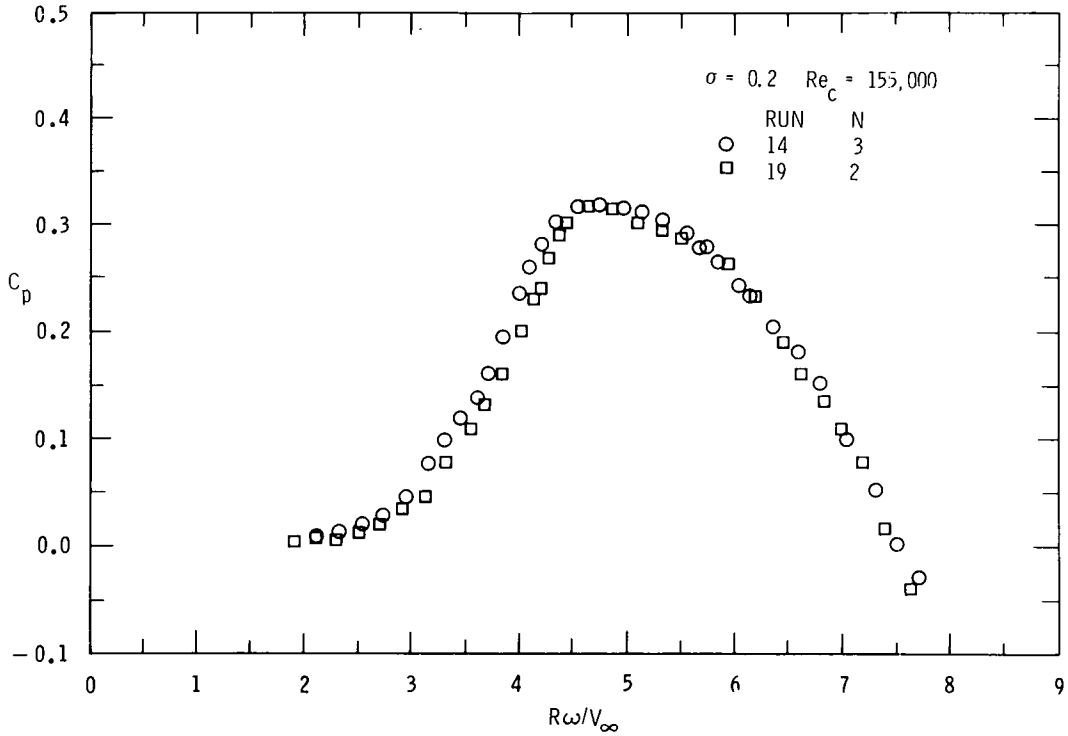

Fig. 8. Influence of number of blades on power coefficient for solidity of 0.2 and Reynolds number of 155,000.

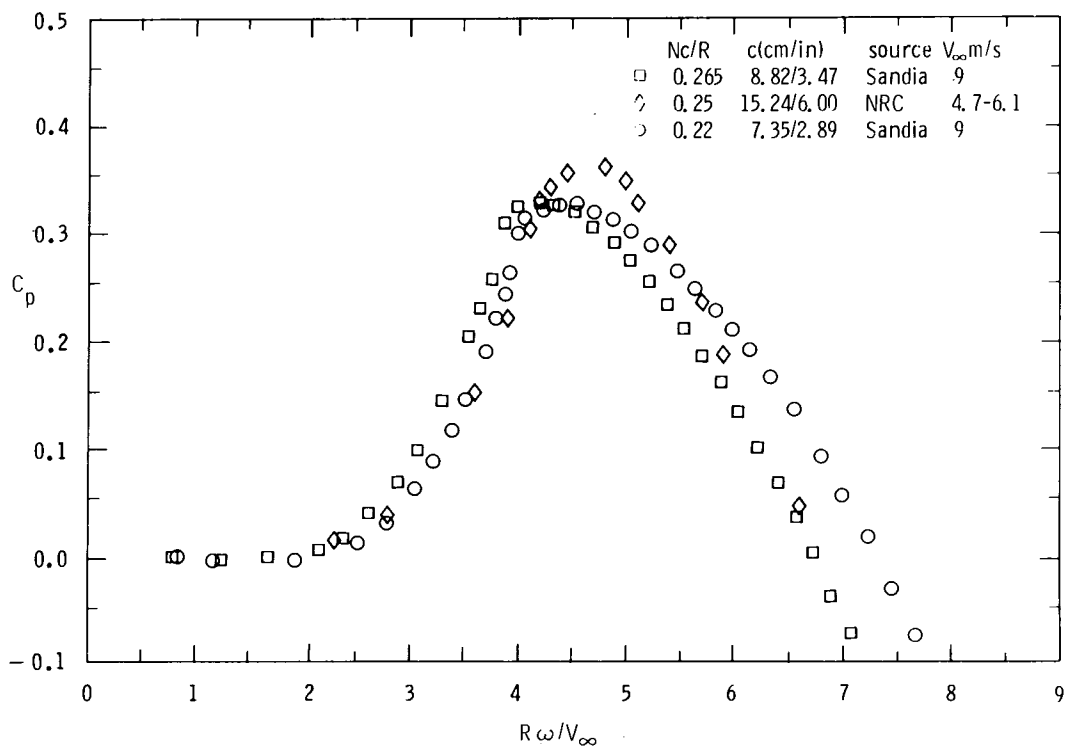

Fig. 9. Comparison of Sandia and NRC data.

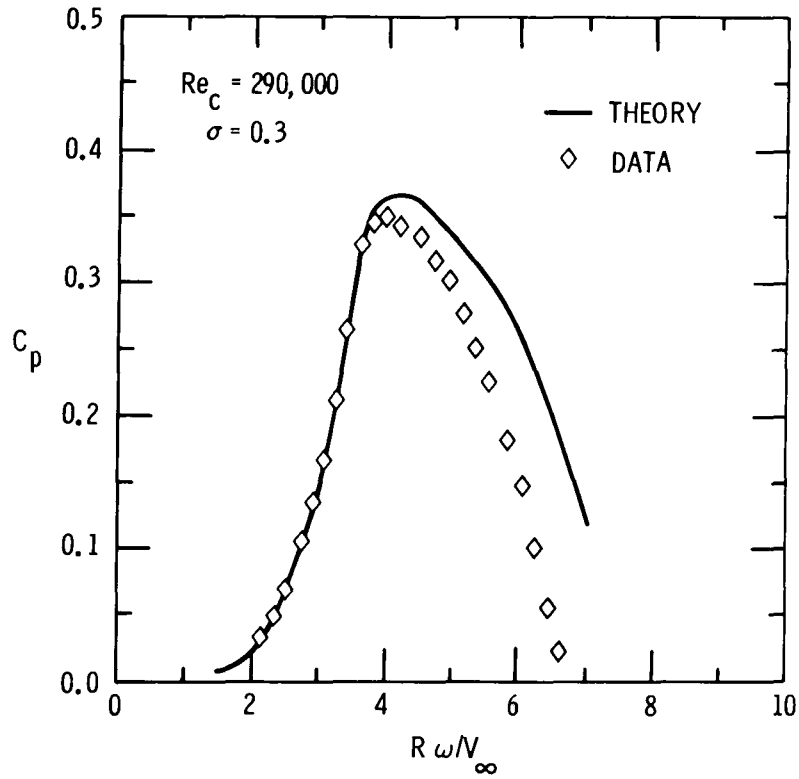

Fig. 10. Comparison of theoretical model with data for solidity of 0.3 and Reynolds number of 290,000.

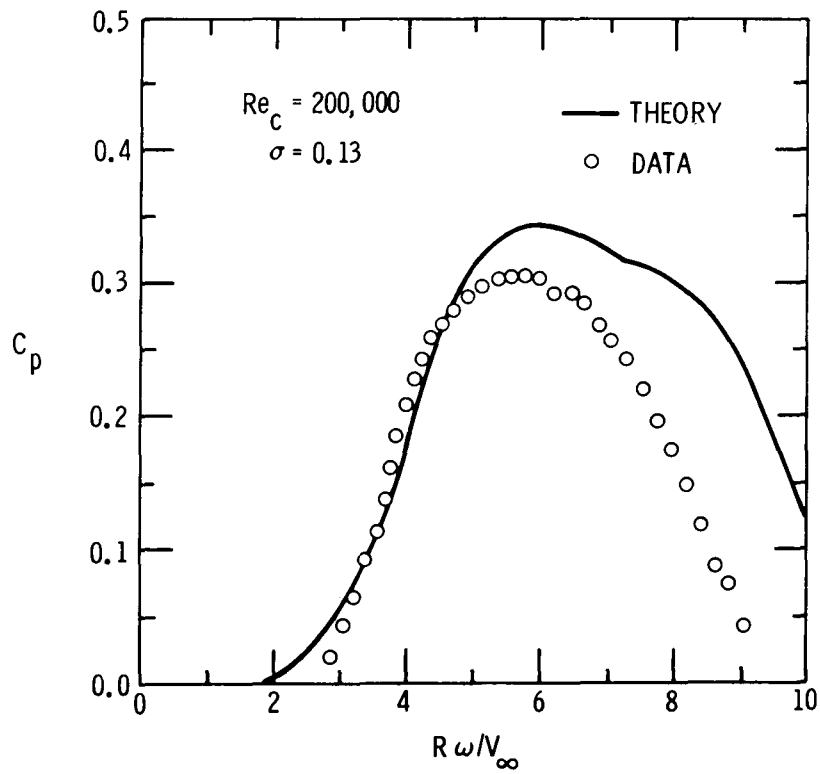

Fig. 11. Comparison of theoretical model with data for solidity of 0.13 and Reynolds number of 200,000.

Aerodynamic Characteristics of Four Symmetrical Airfoil Sections through 180 Degrees Angle of Attack at Low Reynolds Numbers
(Preliminary Data Report)

Robert E. Sheldahl
Ben F. Blackwell
Sandia Laboratories, Albuquerque, N. M. 87115

Symbols

c	-	Airfoil chord length
c_a	-	Section axial force coefficient
c_d	-	Section drag coefficient
c_ℓ	-	Section lift coefficient
R	-	Rotor radius
Re_c	-	Chord Reynolds Numbers, $\frac{\rho_\infty Uc}{\mu_\infty}$
U	-	Relative velocity
V_∞	-	Free stream wind velocity
X_∞	-	Tip speed ratio, $\frac{R\omega}{V_\infty}$
α	-	Angle of attack
θ	-	Angle of rotation about the turbine vertical axis
μ_∞	-	Free stream viscosity
ρ_∞	-	Free stream density
ω	-	Turbine angular velocity

Introduction

When analytical work began on the vertical axis wind turbine, it became immediately apparent that the amount of available data for symmetrical airfoil sections was limited. The section data requirements for application to vertical axis wind turbines are broader in scope than what the aircraft industry usually concerned itself with when obtaining such data. Figure 1 shows the range of angle of attack the airfoil at the equatorial plane of a Darrieus turbine is exposed to for various tip-speed ratios. At low tip speed ratios, it is even possible to be at an angle of attack approaching 180 degrees. In operation, with a tip speed ratio in excess of 2.0, the angle of attack can exceed 25 degrees. Portions of the airfoil closer to the axis of rotation will see even greater angles of attack. This figure shows only one-half of the revolution; the second half will be similar except the angles of attack will be negative. The airfoil is then subjected to a continually changing angle of attack cycling from positive to negative back to positive as it revolves about the vertical axis. This particular figure is for the 17-metre turbine but results are similar for turbines of all sizes. The requirements here call for section data for angles of attack to 180 degrees and data for both increasing and decreasing angle of attack showing airfoil hysteresis.

As the angle of attack changes, so does the Reynolds number. In Fig. 2, the Reynolds number is shown as a function of the rotation angle for several tip speed ratios. Again, this is for the 17-metre system at a fixed rotational speed of 46 rpm (4.82 rad/sec) and a blade chord of approximately 0.5 metre. In operation with a tip speed ratio in excess of 2.0, the Reynolds number range is from 0.5×10^6 to 2×10^6. Scaled down turbines will also have lower Reynolds numbers proportional to chord length. A Sandia 2-metre wind tunnel model operated over a range of Reynolds numbers from 0.1 to 0.3×10^6 in a recent wind tunnel test. The requirements here calls for section data over a very wide Reynolds number range. Data for the very low Reynolds numbers, less than 0.5×10^6, are required to compare the solutions from computer models with the data from wind tunnel model tests.

These requirements are generally out of the range of most published airfoil section data. Examples of published data for symmetrical airfoil sections are presented in References 1 and 2. Since the NACA-0012 is one of the more popular symmetrical airfoils, because of its favorable lift to drag ratio, there is generally more data available for that airfoil. Due to its popularity, it was a logical first choice for the vertical axis wind turbine. It is yet to be proven that the NACA-0012 airfoil is the optimum for application to this type of turbine.

Sandia Laboratories contracted with Wichita State University to construct four different symmetrical airfoil sections and to test the models at angles of attack to 180 degrees for three different Reynolds numbers. One of the Reynolds numbers was to be as low as could be obtainable and still be within the operational range of their facility and balance system. The purpose of these tests was to obtain needed section data for the NACA-0012 airfoil over the angle of attack range of interest at as low a Reynolds number as possible. In addition to help answer the question of the optimum airfoil for the turbine, similar section data for a thinner (NACA-0009) and thicker (NACA-0015) airfoil was deemed necessary. Also, a non-standard airfoil, a modified-0012 designated NACA-0012H, was tested. At this time, the information presented in this report must be considered preliminary and subject to revision.

Airfoil Section Models

The four symmetrical airfoil models were constructed of aluminum to standard wind tunnel model tolerances by Wichita State University. All models had a 6-inch (15.24 cm) chord with a 3-foot (0.91 m) span. These models were of standard airfoil cross-section, NACA-009, -0012 and -0015. Geometries for these three airfoils can be found in Reference 3. The fourth airfoil was a non-standard airfoil. It was a modification of the NACA-0012 provided by Raymond M. Hicks of NASA/Ames Research Center.[4] The modification was designed with the aid of a computer program to increase $c_{\ell_{max}}$ of a given airfoil by reducing the leading edge pressure spike associated with subsonic airfoils. The resultant airfoil was still 12% thick and has been designated NACA-0012H. The geometry for this airfoil is presented in Table I.

Facility

The airfoils were tested in the Walter H. Beech Memorial Wind Tunnel at Wichita State University.[5] It has a 7 x 10-foot (2.13 m x 3.05 m) test section fitted with floor to ceiling 2-dimensional inserts for testing 2-dimensional airfoil sections. These inserts in the center of the test section act as flow splitters to form a separate test section 3 feet (0.92 m) wide by 7 feet (2.13 m) tall. Part of the total airflow in the wind tunnel goes through the 3 x 7 foot section and part flows by each side. The 3 x 7 foot section is separately instrumented with pitot-static probes for the determination of the flow conditions within that section. A wake survey probe was installed in the wind tunnel on a separate series of tests to obtain the airfoil section drag at low angles of attack for all airfoil models.

Tests

The airfoil models were attached to the end plates in the walls of the 2-dimensional inserts. These end plates are the attachments to the angle of attack control mechanism and the facility balance system. The models were tested at three Reynolds numbers, nominally 0.35×10^6, 0.50×10^6 and 0.70×10^6, through angles of attack of 180 degrees. The angle of attack control mechanism has an approximate range of 60 degrees which required that the model be re-oriented on the end plates three times to complete the full range of angles of attack to 180 degrees. This allowed for some overlap of data near 40, 90 and 130 degrees.

Data for each airfoil was first obtained over the range of -24 degrees to +32 degrees (increasing α) and then from +32 degrees to -24 degrees (decreasing α) for the three Reynolds numbers. This was done to obtain the hysteresis loop in the region of airfoil stall. Full range data all were obtained with increasing angles of attack to 180 degrees. Lift, drag and moment data were obtained from the balance system. All the data were corrected for wake and solid blockage, bouyancy, upwash and wind turbulence factor.[6] The turbulence factors used to correct the Reynolds numbers to 0.35×10^6, 0.50×10^6 and 0.70×10^6 were 1.38, 1.29, and 1.13 respectively. All of the tests reported here were performed on aerodynamically smooth airfoils. A separate test of the NACA-0015 airfoil with transition strips was

conducted. The strips were of No. 80 carborundum grit glued to a strip approximately 0.1-inch (0.25 cm) wide located approximately at the 17% of chord station. The results with the strips were similar to the data without transition strips and thus were inconclusive and not presented here.

Results

The section coefficient of lift data for the four airfoils are shown in Figs. 3 through 6 for the angles of attack from -24 to +24 degrees at nominal Reynolds numbers of 0.35×10^6 and 0.70×10^6. Each airfoil cross-section is sketched in the figures. These figures include data obtained for both increasing and decreasing angle of attack and demonstrate the extent of the lift coefficient hysteresis for each airfoil. The lift coefficient for the NACA-0009 airfoil shown in Fig. 3 reaches a maximum of approximately 0.8 near 10 degrees angle of attack. There is not a significant drop in lift past stall nor is there any significant hysteresis. Data for the NACA-0012 is shown in Fig. 4 and we see that $c_{\ell_{max}}$ has increased to 1.0 for positive angles and to -1.08 for negative angles with a hysteresis loop most pronounced for negative angles.

The NACA-0012H lift data are presented in Fig. 5 showing a dramatic improvement in lift characteristics over the NACA-0012. The maximum lift coefficient approaches $\pm$ 1.2 at the higher Reynolds number condition. Note the larger size of the hysteresis in the lift data near positive and negative stall angles. The dashed line in the sketch shows the curvature of the standard NACA-0012 airfoil. The lift data for the NACA-0015, Fig. 6, is similar to the NACA-0012H. The maximum lift coefficient for the -0015 is slightly less than that for the -0012H, but stall is less abrupt and occurs at a slightly greater angle of attack. Figure 7 is a composite of the previous four figures showing the lift data for the four airfoils at a Reynolds number of 0.7×10^6. Data shown are for increasing angle of attack for positive angles and decreasing angle of attack for negative angles. This shows the increased performance of the NACA-0012H and the favorable performance of the NACA-0015.

Figures 8 through 11 show the full range section lift coefficient data for the four airfoils. All data were taken with the angle of attack increasing. The data

for all the airfoils beyond 25 degrees angle of attack are similar. At an angle of 40 to 45 degrees, the lift coefficient for a -0009 airfoil is greater than 1.1 and with increasing airfoil thickness, the lift coefficient decreases to 1.05 but generally speaking, the effect of Reynolds number (in the range of 0.35×10^6 to 0.70×10^6) the airfoil geometry has little effect on the lift coefficient in the angle of attack range of 25 to 180 degrees.

The section drag coefficients for a NACA-0012 airfoil is shown in Fig. 12 over the angle of attack range of -24 to +24 degrees. The minimum drag coefficient near zero lift is approximately 0.004. The data for the drag coefficients were obtained by the balance system and corrected by data obtained in the angle of attack range of positive to negative stall by a wake survey method.[4] This corrected the force data for drag on the end plates. Figures 13 through 16 present in expanded scale, the drag coefficients for the airfoils as obtained from force measurements and from wake surveys. These figures show the magnitude of correction required for the force data to conform to the "more accurate" wake survey method of obtaining drag data. The full range section drag coefficients for the four airfoil sections are shown in Figs. 17 through 20. These data are similar for all angles greater than 20 degrees. At 90 degrees, the drag coefficient of approximately 1.8 is near Hoerner's value of 1.98 for a 2-dimensional flat plate.[7]

The component of force that makes a vertical axis wind turbine work is the chord wise or axial force. The axial force coefficient for the NACA-0012 airfoil is shown in Figure 21 for angles of attack from -24 to +24 degrees. It is desirable to increase the area under the positive portion of the curve for both positive and negative angles of attack and to minimize the negative axial force coefficients near zero angle of attack. Figures 22 through 24 show the full range axial force coefficients for the NACA-0012, -0012H and -0015 airfoil sections. The important thing to note is the larger area under the curve before airfoil stall for the -0012H and -0015 when compared to the -0012. Intuitively this should provide for better performance from a wind turbine using either one of these than the presently used NACA-0012 airfoil. Note that the axial force coefficient is obtained by:

$$c_a = c_\ell \sin \alpha - c_d \cos \alpha$$

Data obtained in this manner beyond 20 degrees becomes very scattered because the results are obtained by taking small differences of larger numbers. It must be emphasized that the data presented here is preliminary and subject to change as more careful analysis is given to the test results.

Conclusions

Aerodynamic Section data over a wide range of angles of attack at Reynolds numbers of 0.35×10^6, 0.50×10^6 and 0.70×10^6 has been obtained for four symmetrical airfoils. The data presented here is preliminary and is subject to revision as more careful analysis is given to the test results. The low values of minimum drag for the airfoils are of concern and will require careful scrutinization. The hysteresis in the coefficient of lift data obtained by quasi-steady state methods points out the advisability of including it in computer solutions of vertical axis wind turbine performance. This hysteresis is much more pronounced with the thicker airfoils, i.e., the NACA-0012H and NACA-0015. The data presented here are the start of a data base which will be extremely useful in the analysis of vertical axis wind turbines. It is intended to extend the data base with additional tests of a NACA-0012 airfoil with a 15-inch (38.1 cm) chord at Reynolds numbers of 0.70×10^6 to 2×10^6 so that section data are available in the operating Reynolds number range for the Sandia Laboratories 17-metre system.

References

1. Eastman N. Jacobs and Albert Sherman, Airfoil Section Characteristics as Affected by Variations of the Reynolds Number, NACA Report No. 586, 1937.
2. Laurence K. Loftin, Jr., and Hamilton A. Smith, Aerodynamic Characteristics of 15 NACA Airfoil Sections at Seven Reynolds Numbers from 0.7×10^6 to 9.0×10^6, NACA TN 1945, October 1949.
3. Ira H. Abbott and Albert E. von Doenhoff, Theory of Wing Sections, McGraw-Hill Book Co., Inc., New York, 1949.
4. Private Communication, Raymond M. Hicks, NASA, Ames Research Center, Moffett Field, CA. 94035.

5. Information for Users of the Walter H. Beech Memorial Low-Speed Wind Tunnel, Wichita State University Aeronautical Engineering Department, July 1966.

6. Alan Pope and John J. Harper, Low-Speed Wind Tunnel Testing, John Wiley & Sons, Inc., New York, 1966.

7. Sighard F. Hoerner, Fluid Dynamic Drag, S. F. Hoerner, Midland Park, New Jersey, 07432, 1965.

TABLE I
Coordinates for the Modified
NACA-0012 (NACA-0012H) Airfoil

x/c	± y/c	x/c	± y/c
0.0	0.0	0.275	0.06048
0.005	0.01438	0.299	0.06002
0.010	0.02074	0.349	0.05951
0.020	0.02925	0.399	0.05808
0.030	0.03522	0.449	0.05588
0.040	0.03982	0.500	0.05294
0.050	0.04351	0.550	0.04952
0.060	0.04655	0.600	0.04563
0.080	0.05121	0.650	0.04133
0.100	0.05454	0.700	0.03664
0.125	0.05740	0.750	0.03160
0.150	0.05924	0.800	0.02623
0.175	0.06033	0.850	0.02053
0.200	0.06087	0.900	0.01448
0.225	0.06100	0.950	0.00807
0.250	0.06084	1.000	0.00126

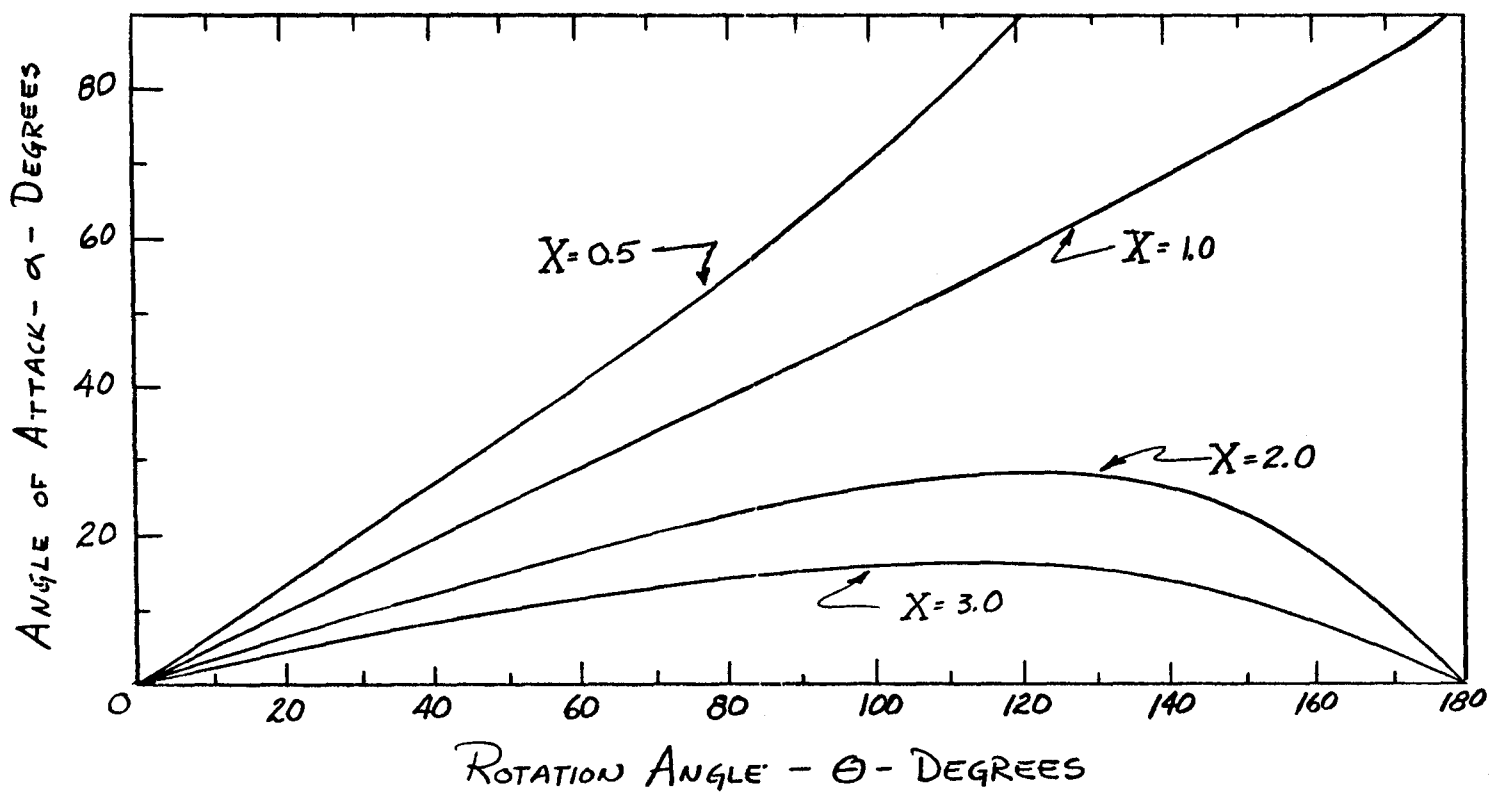

Figure 1. Equatorial Plane Angle of Attack Variation for the 17-Metre Turbine at a Rotational Speed of 46 rpm (4.82 rad/s).

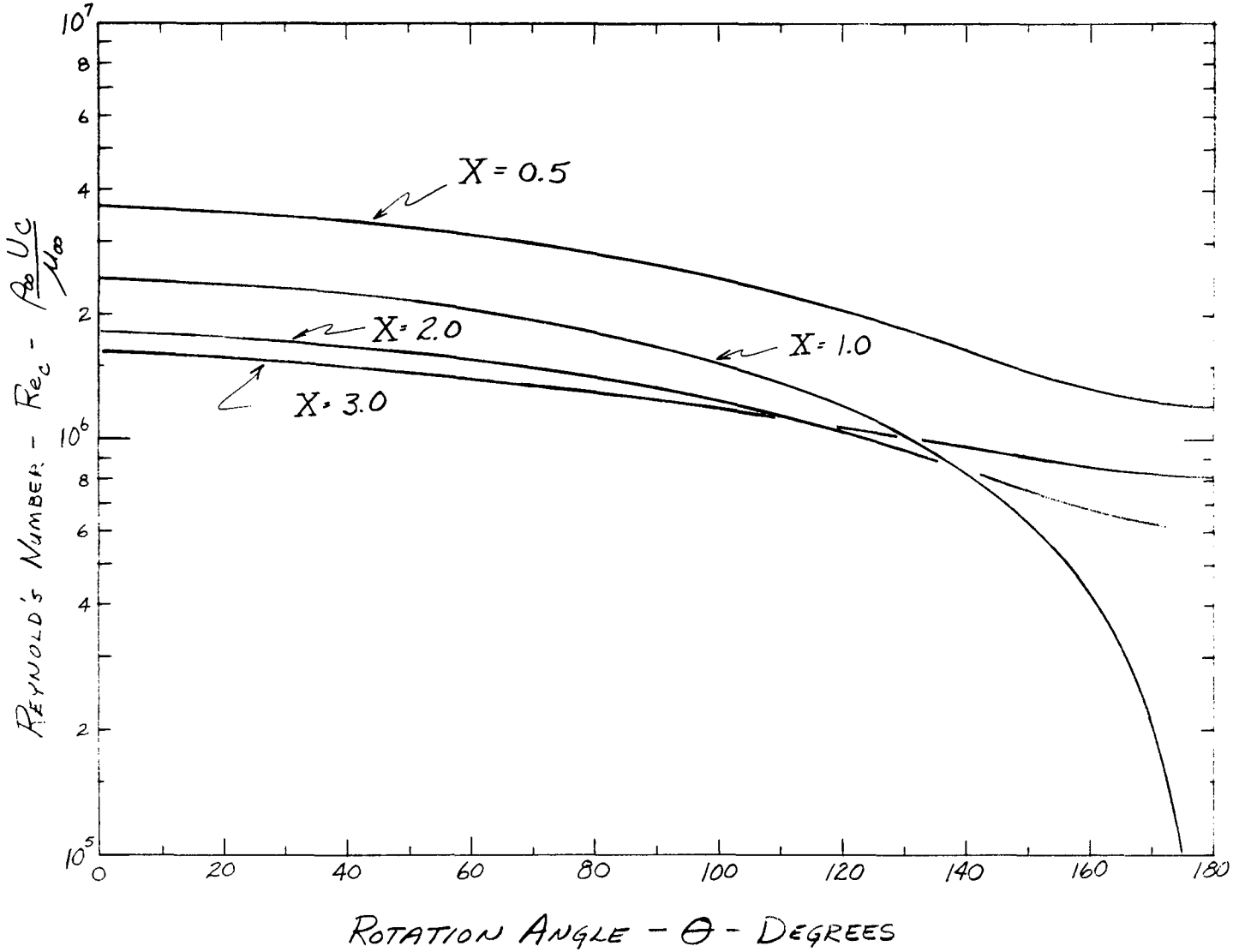

Figure 2. Variation of the Chord Reynolds Numbers at the Equatorial Plane of the 17-Metre Turbine at a Rotational Speed of 46 rpm (4.82 rad/s).

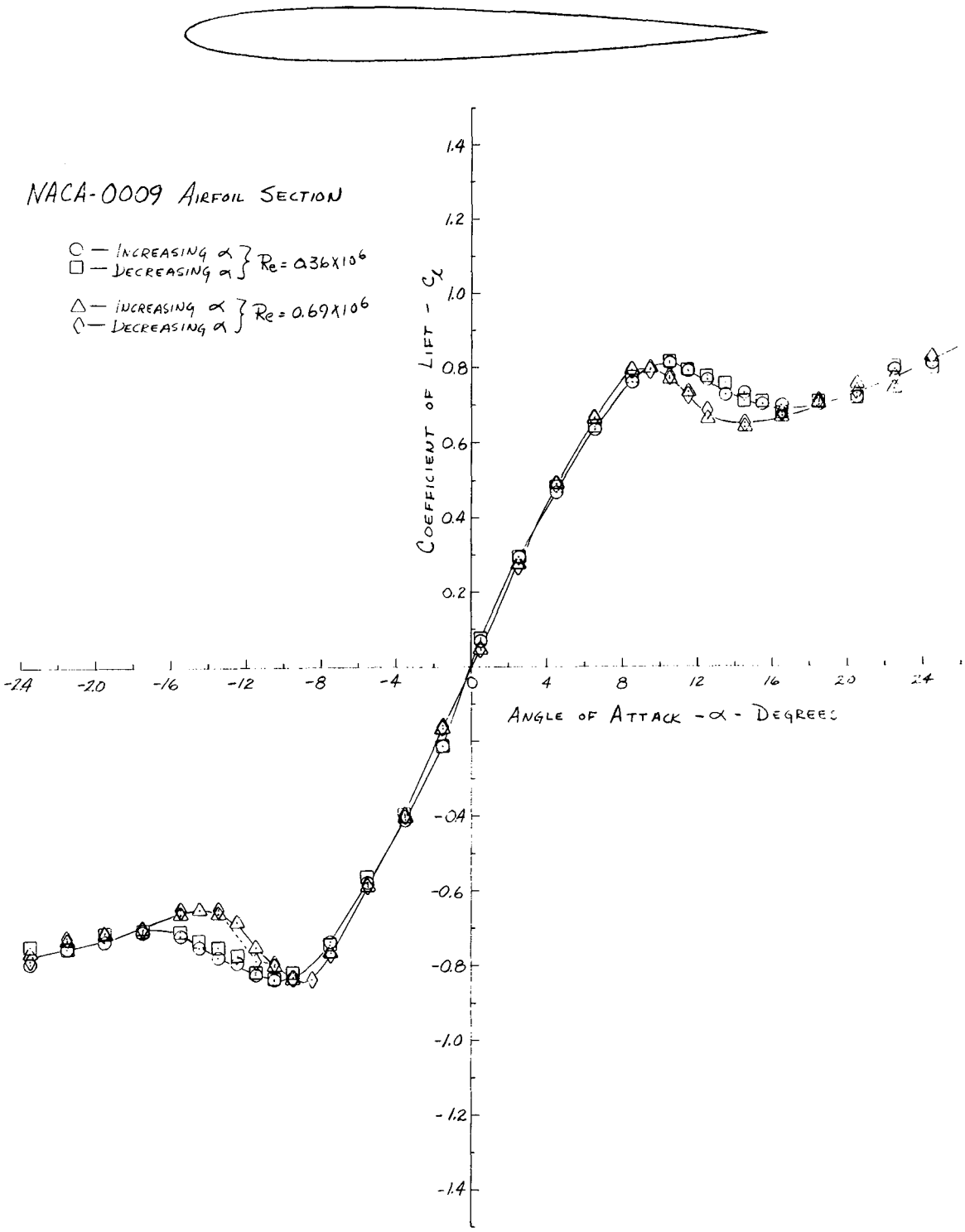

Figure 3. Section Lift Coefficients for the NACA-0009 Airfoil at Reynolds Numbers of 0.36×10^6 and 0.69×10^6.

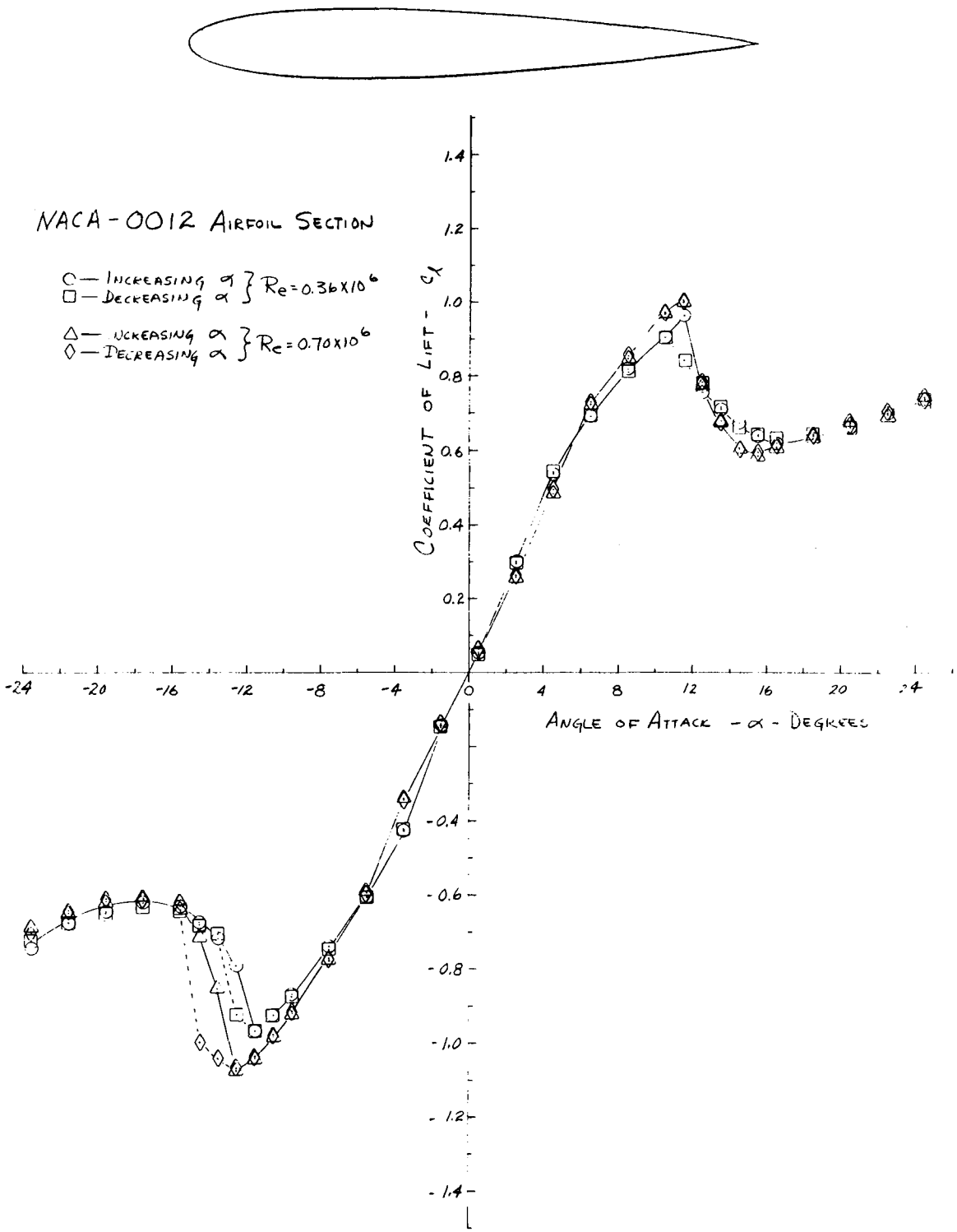

Figure 4. Section Lift Coefficients for the NACA-0012 Airfoil at Reynolds Numbers of 0.36×10^6 and 0.70×10^6.

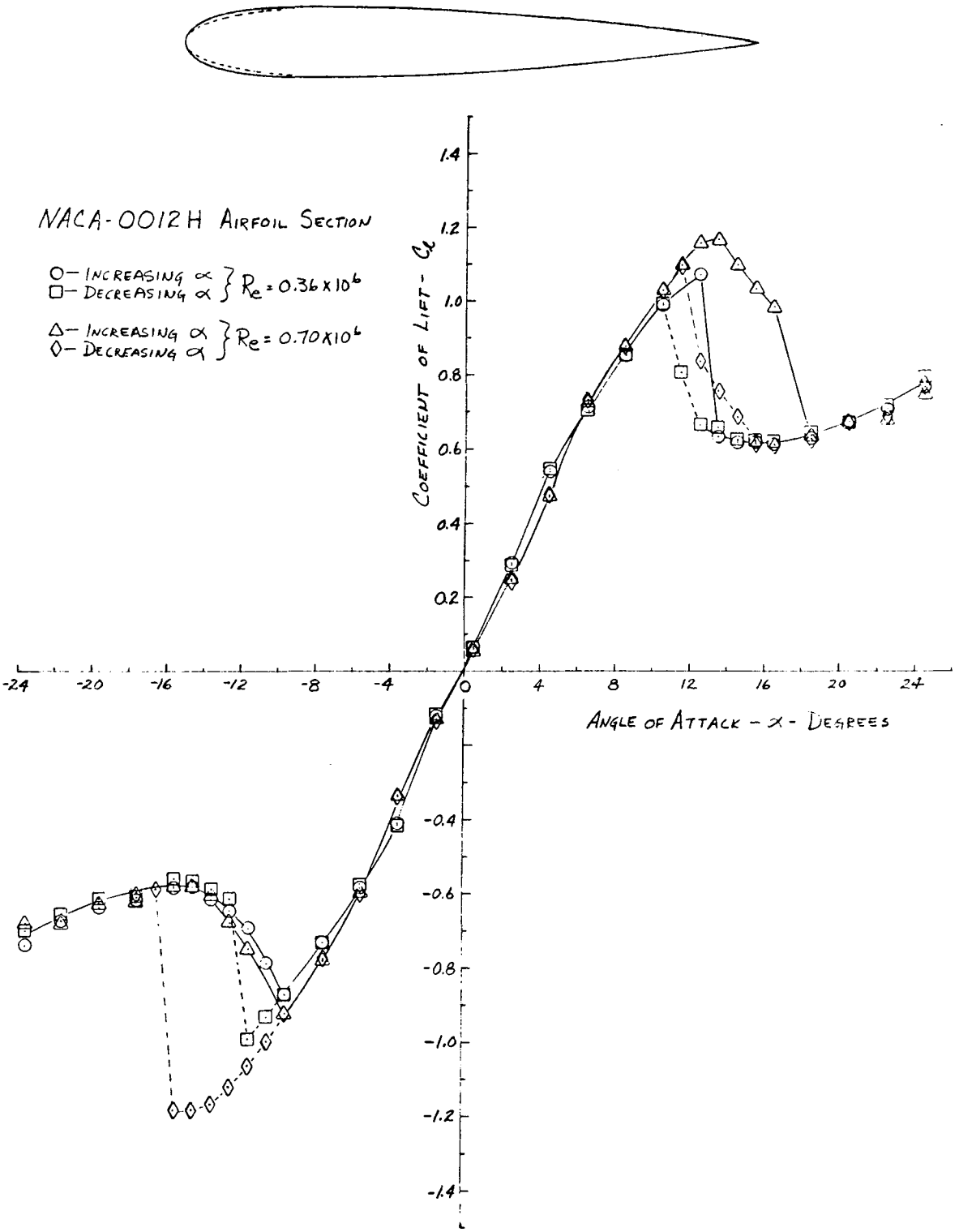

Figure 5. Section Lift Coefficients for the NACA-0012H Airfoil at Reynolds Numbers of 0.36×10^6 and 0.70×10^6.

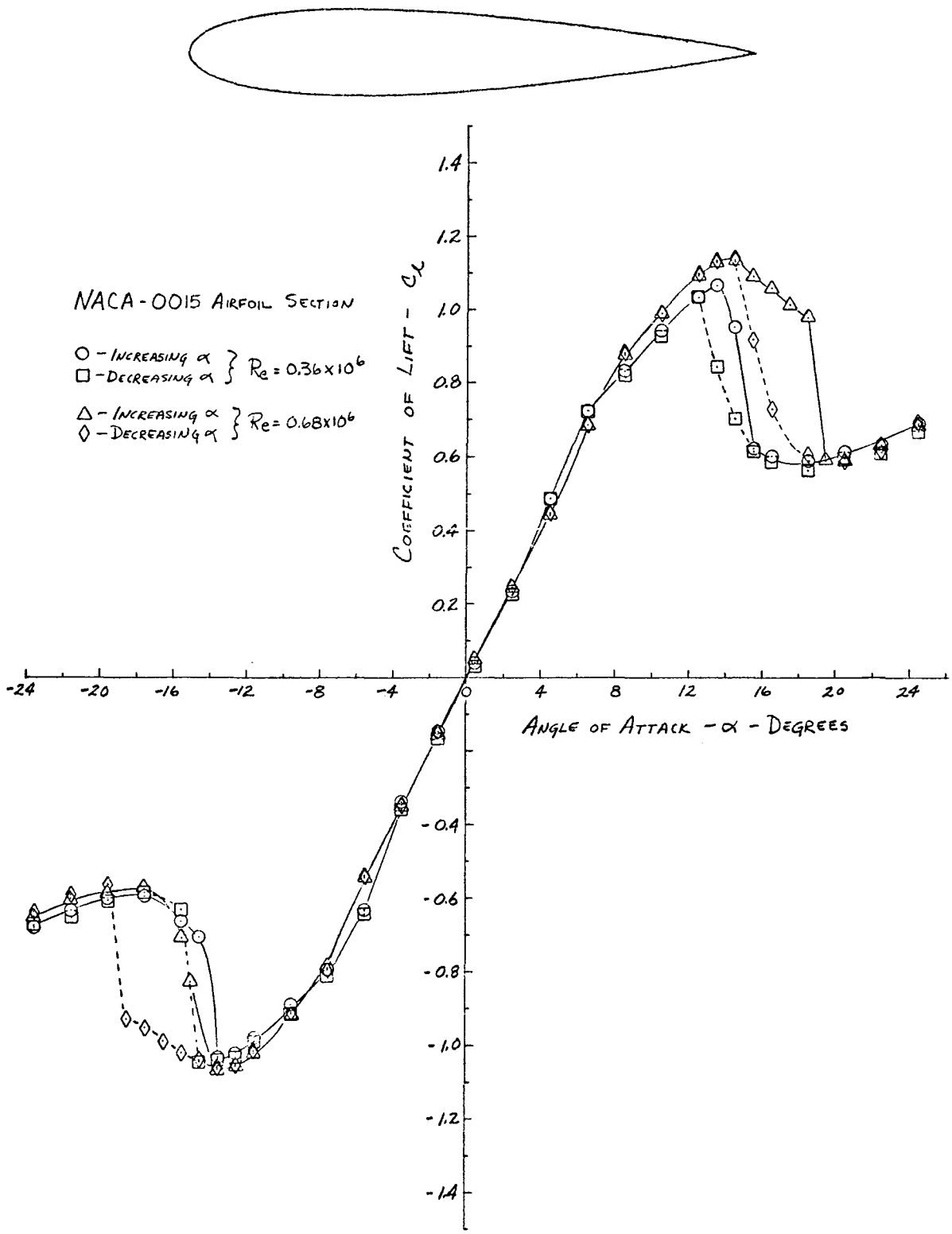

Figure 6. Section Lift Coefficients for the NACA-0015 Airfoil at Reynolds Numbers of 0.36×10^6 and 0.68×10^6.

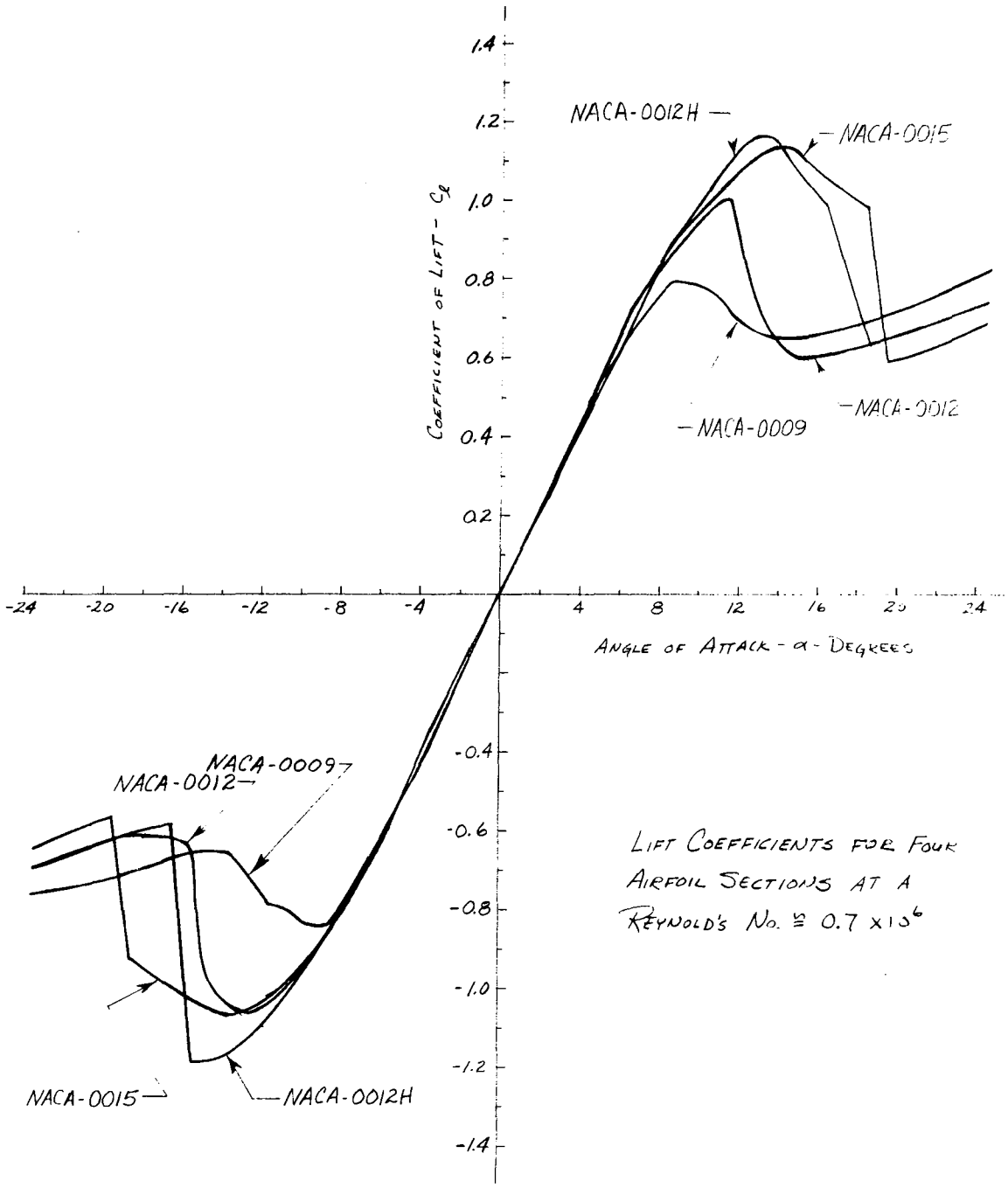

Figure 7. Section Lift Coefficients for Four Airfoil Sections at an Approximate Reynolds Number of 0.70×10^6.

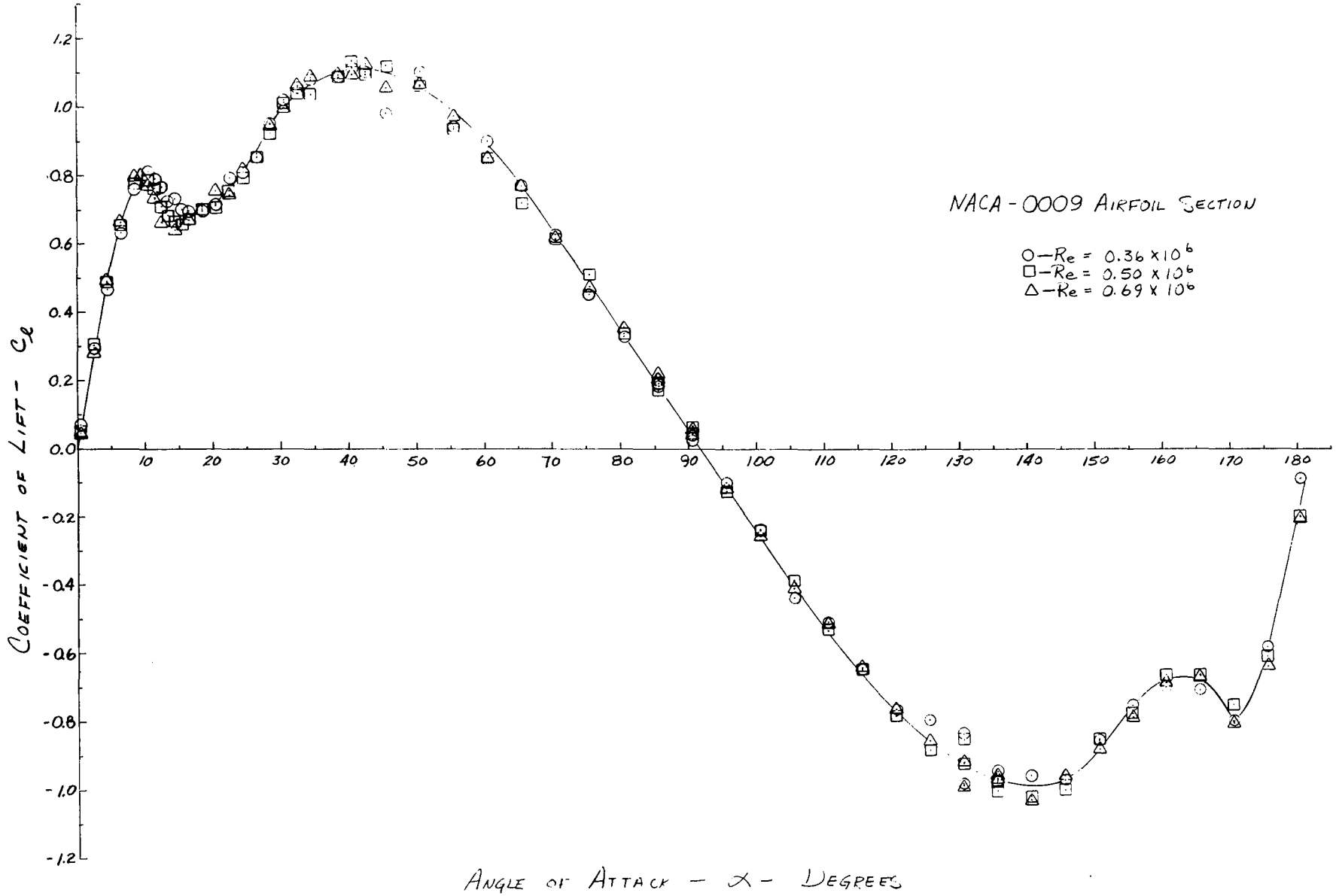

Figure 8. Full Range Section Lift Coefficients for the NACA-0009 Airfoil at Reynolds Numbers of 0.36×10^6, 0.50×10^6 and 0.69×10^6.

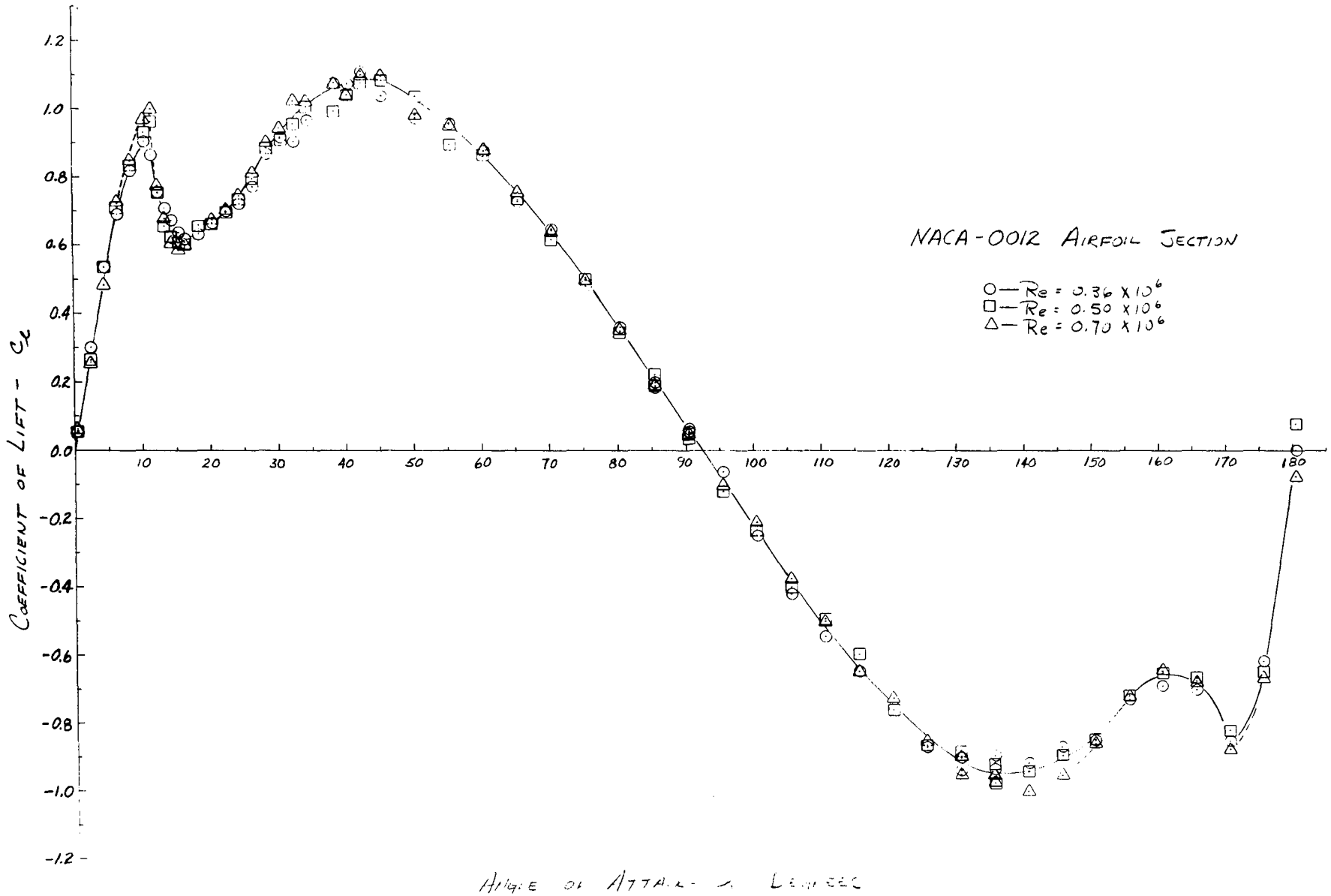

Figure 9. Full Range Section Lift Coefficients for the NACA-0012 Airfoil at Reynolds Numbers of 0.36×10^6, 0.50×10^6 and 0.70×10^6.

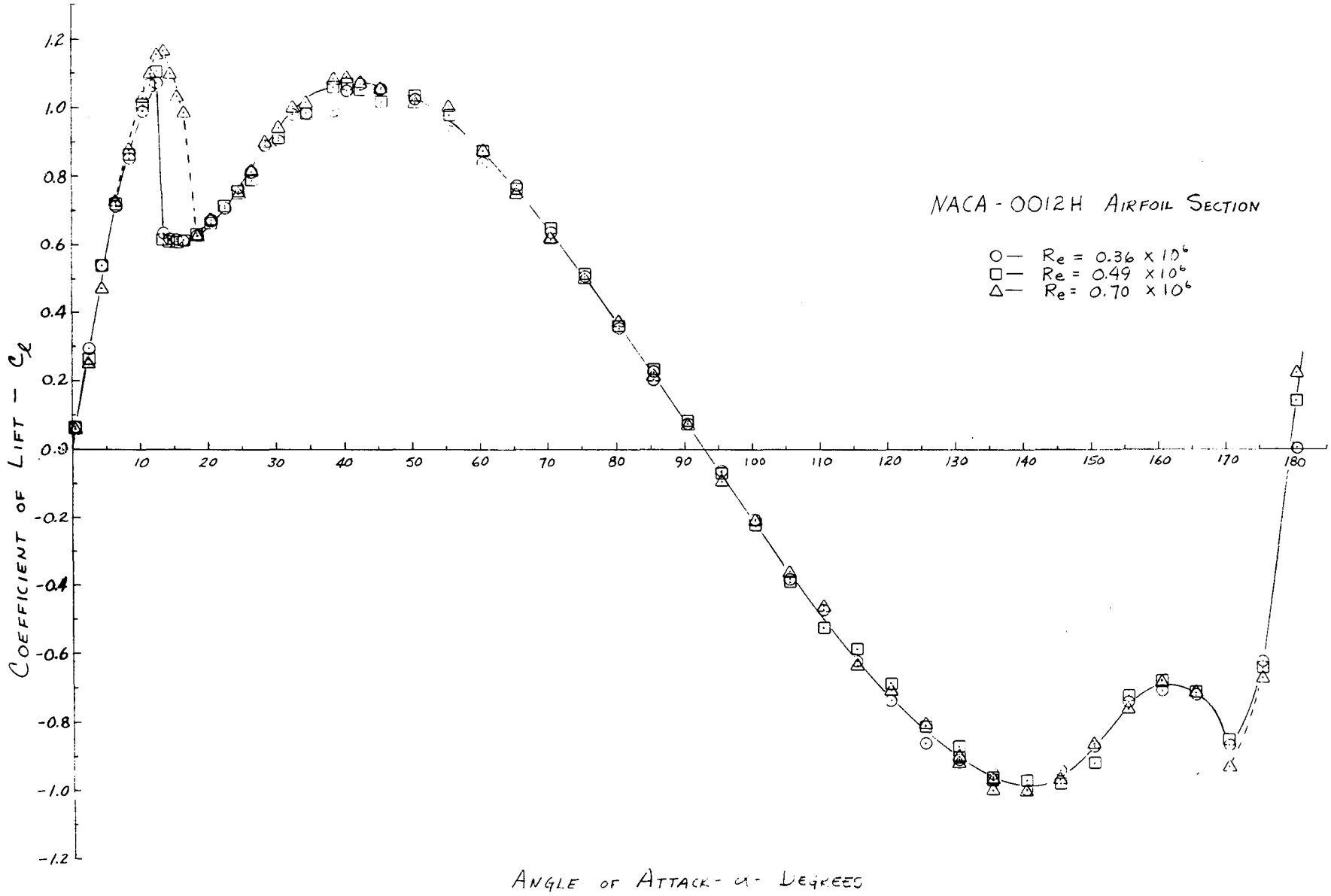

Figure 10. Full Range Section Lift Coefficients for the NACA-0012H Airfoil at Reynolds Numbers of 0.36 x 10^6, 0.49 x 10^6 and 0.70 x 10^6.

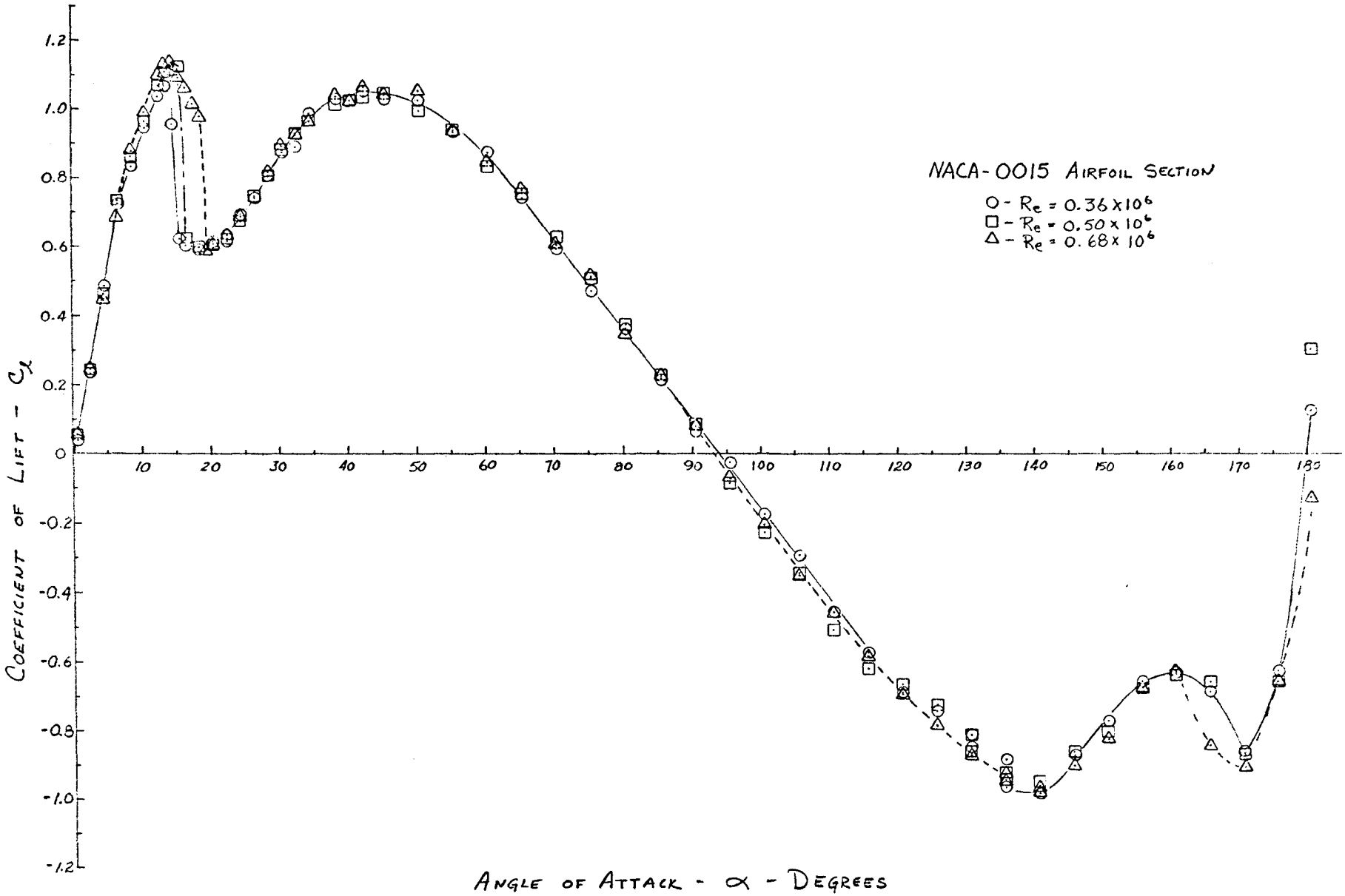

Figure 11. Full Range Section Lift Coefficients for the NACA-0015 Airfoil at Reynolds Numbers of 0.36×10^6, 0.50×10^6 and 0.68×10^6.

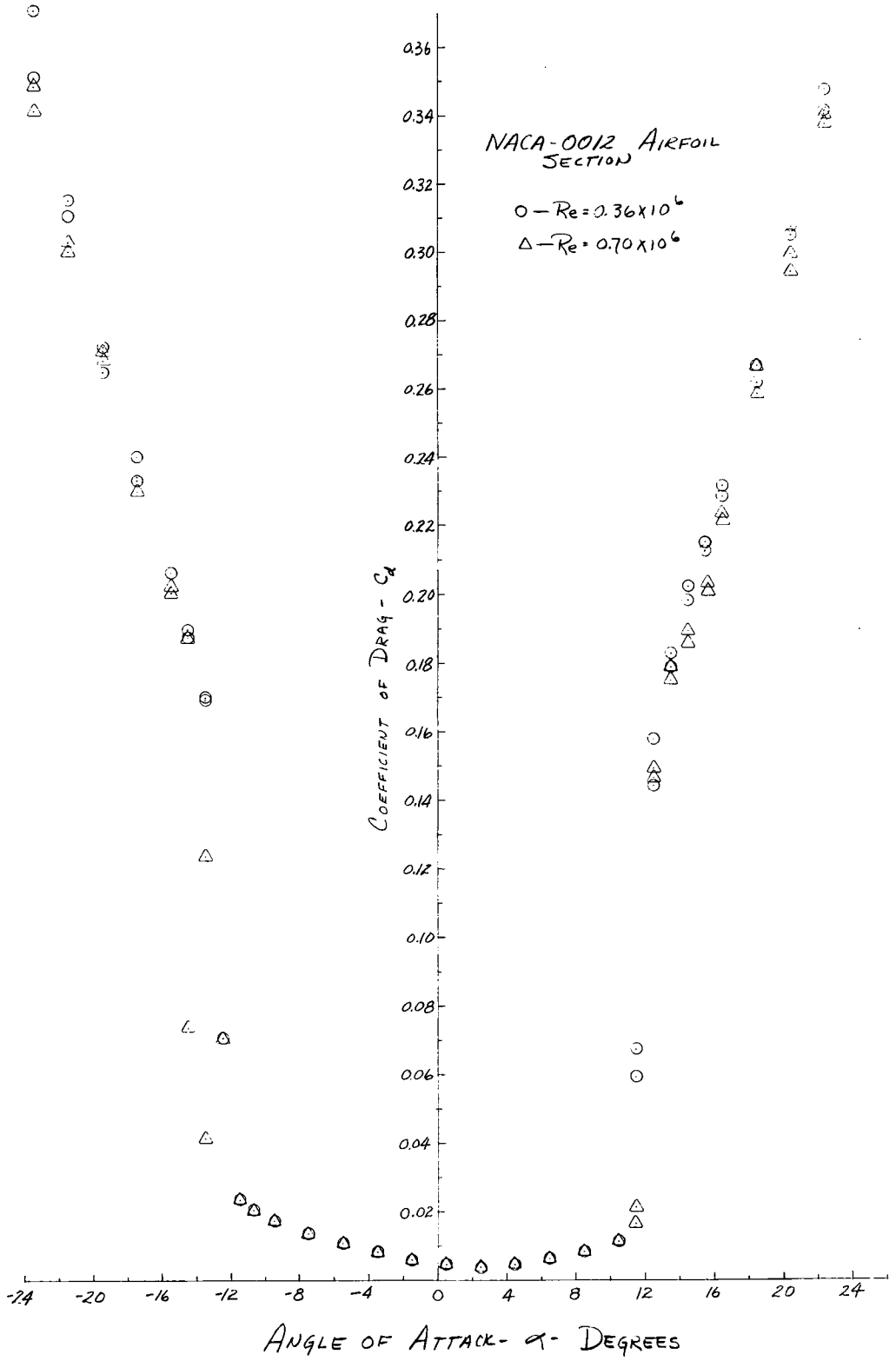

Figure 12. Section Drag Coefficients for the NACA-0012 Airfoil at Angles of Attack from -24 degrees to +24 degrees and Reynolds Numbers of 0.36×10^6 and 0.70×10^6.

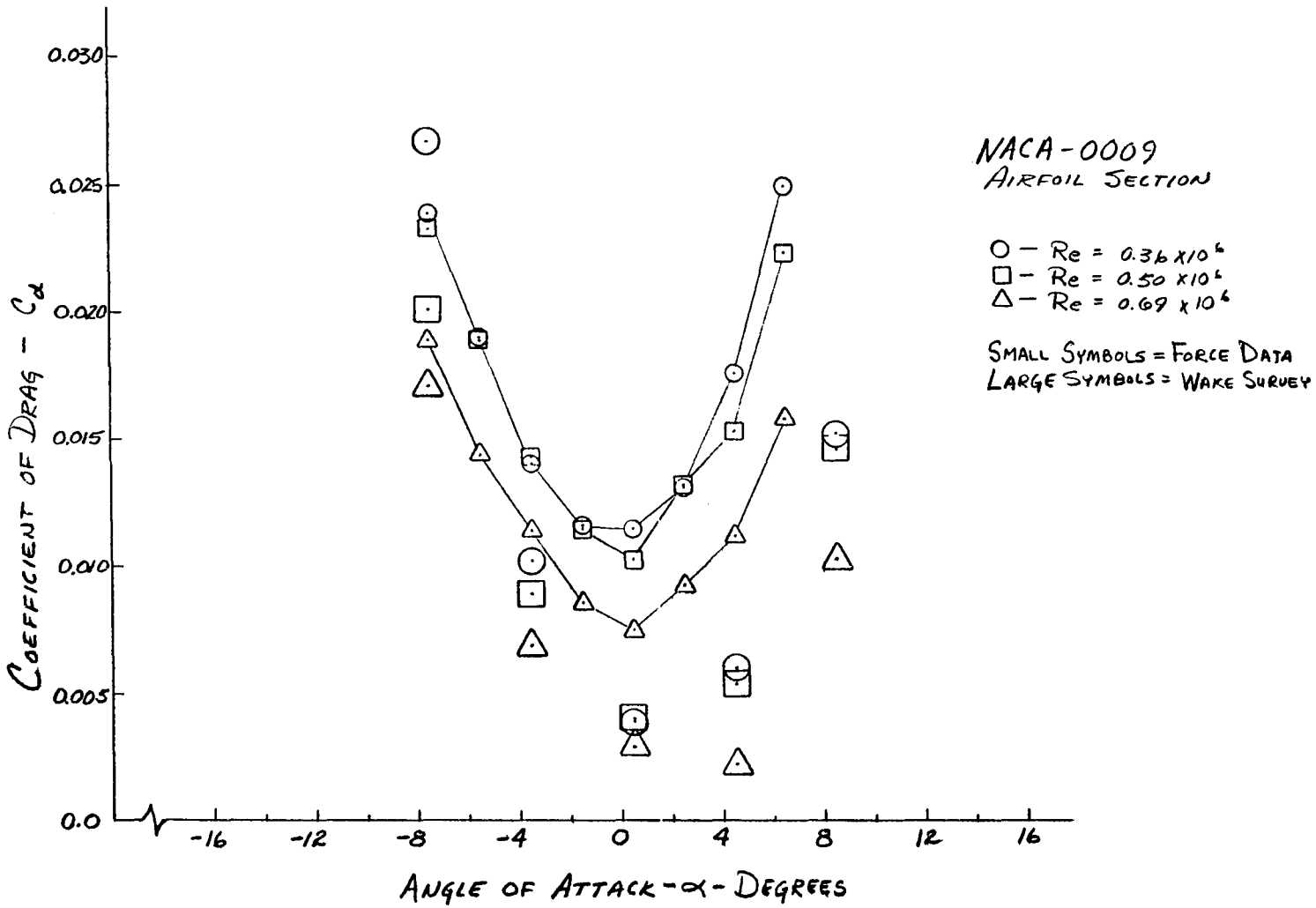

Figure 13. Section Drag Coefficients for the NACA-0009 Airfoil at Small Angles of Attack and Reynolds Numbers of 0.36×10^6, 0.50×10^6 and 0.69×10^6.

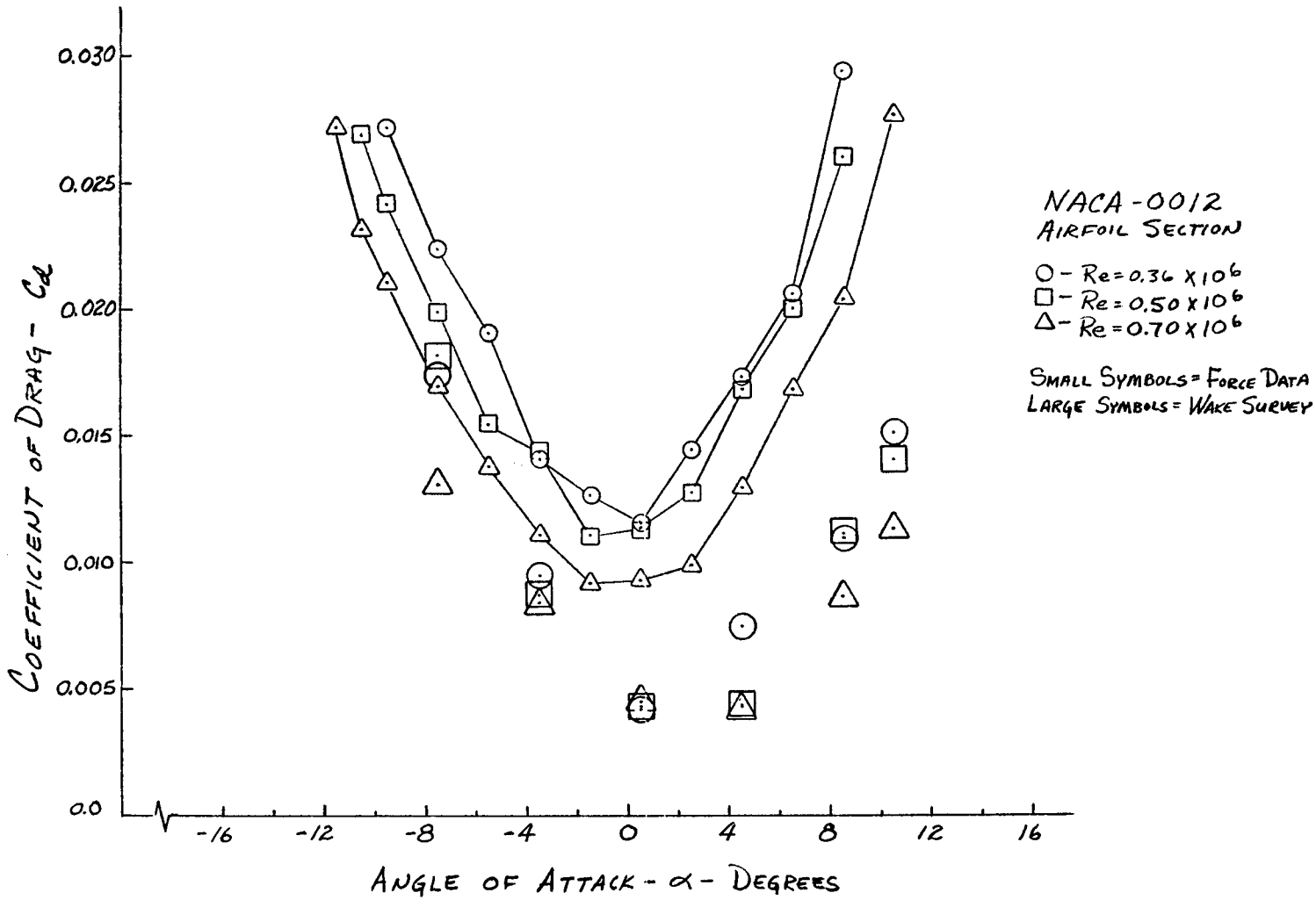

Figure 14. Section Drag Coefficients for the NACA-0012 Airfoil at Small Angles of Attack and Reynolds Numbers of 0.36×10^6, 0.50×10^6 and 0.70×10^6.

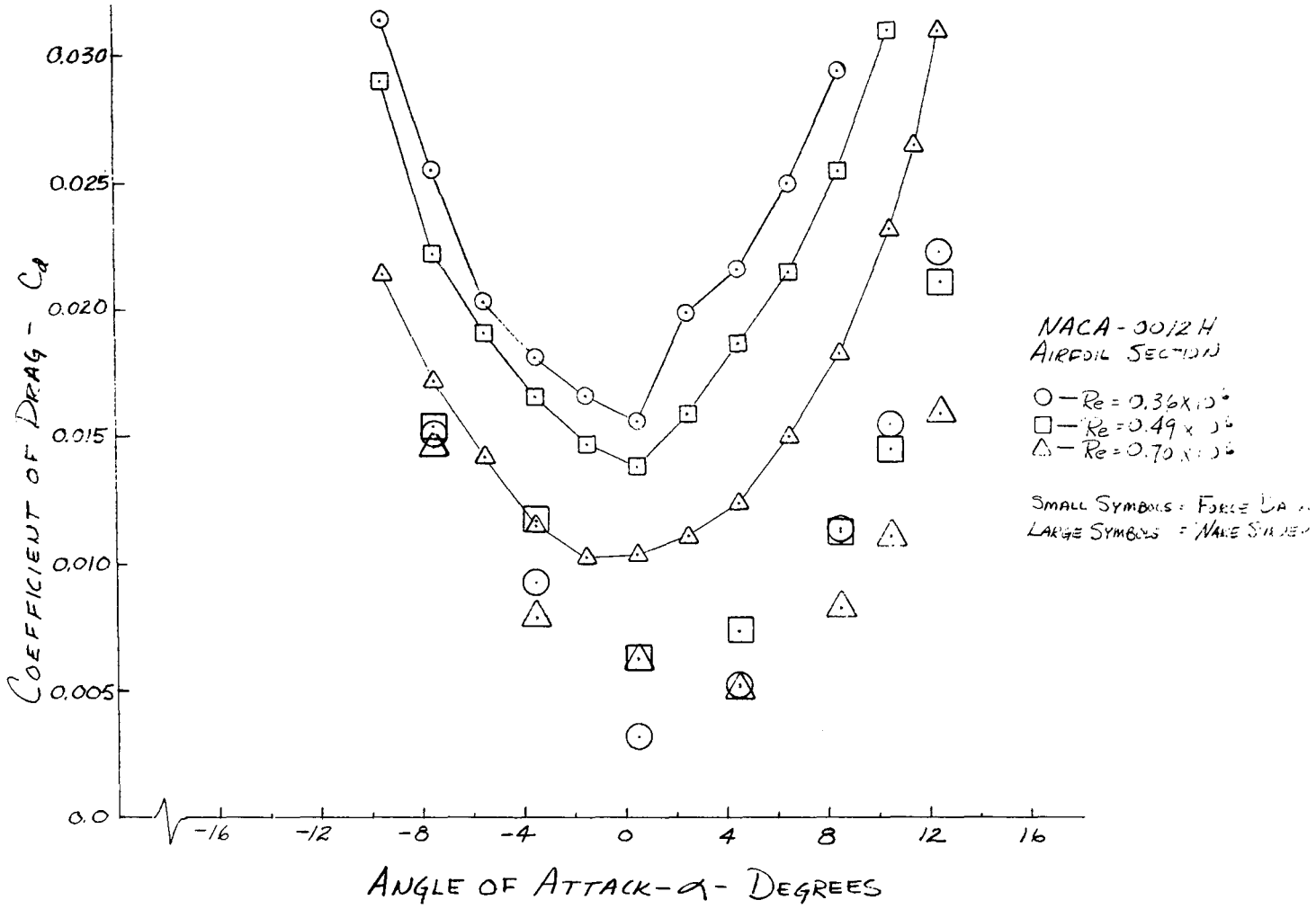

Figure 15. Section Drag Coefficients for the NACA-0012H Airfoil at Small Angles of Attack and Reynolds Numbers of 0.36×10^6, 0.49×10^6 and 0.70×10^6.

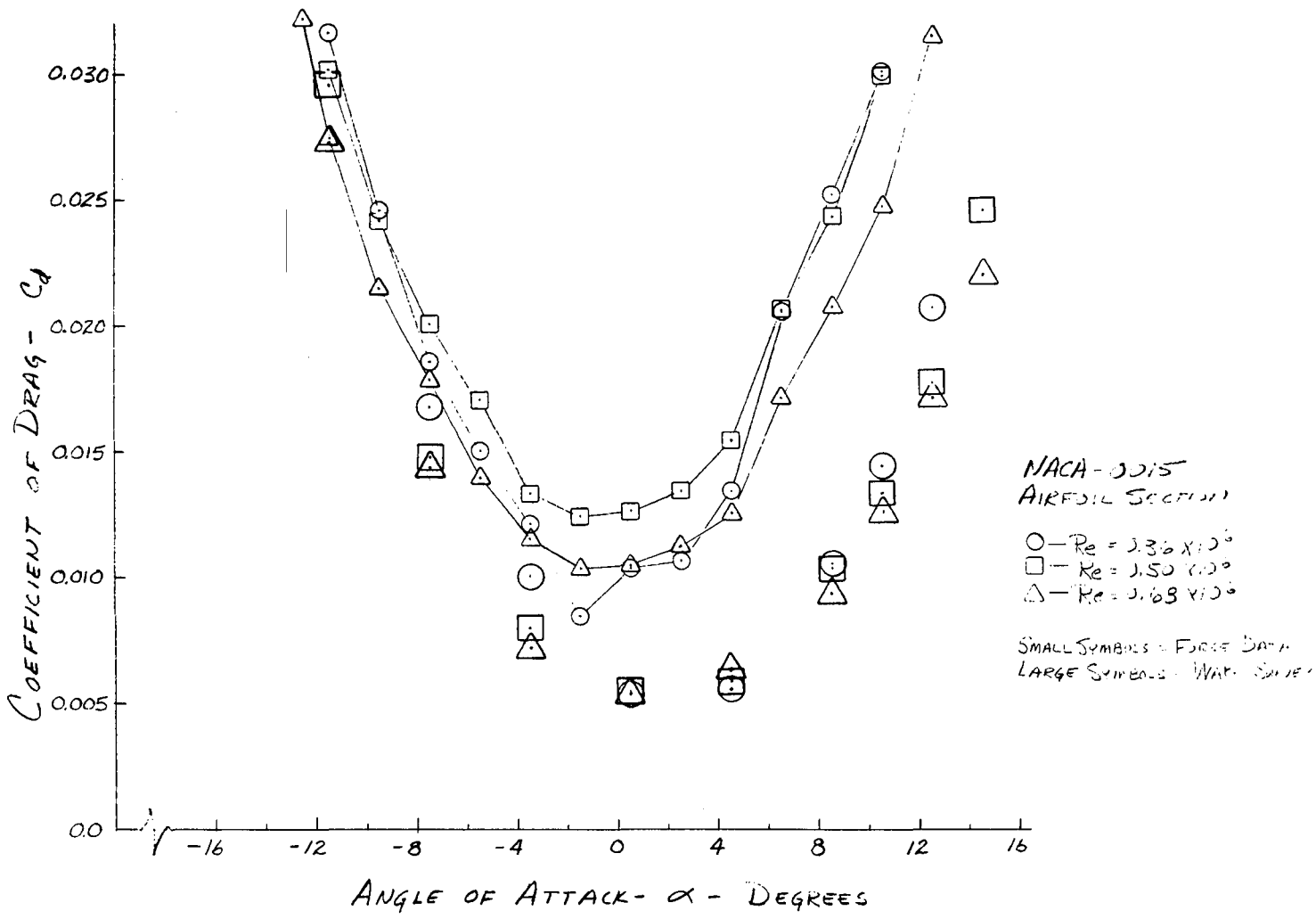

Figure 16. Section Drag Coefficients for the NACA-0015 Airfoil at Small Angles of Attack and Reynolds Numbers of 0.36×10^6, 0.50×10^6 and 0.68×10^6.

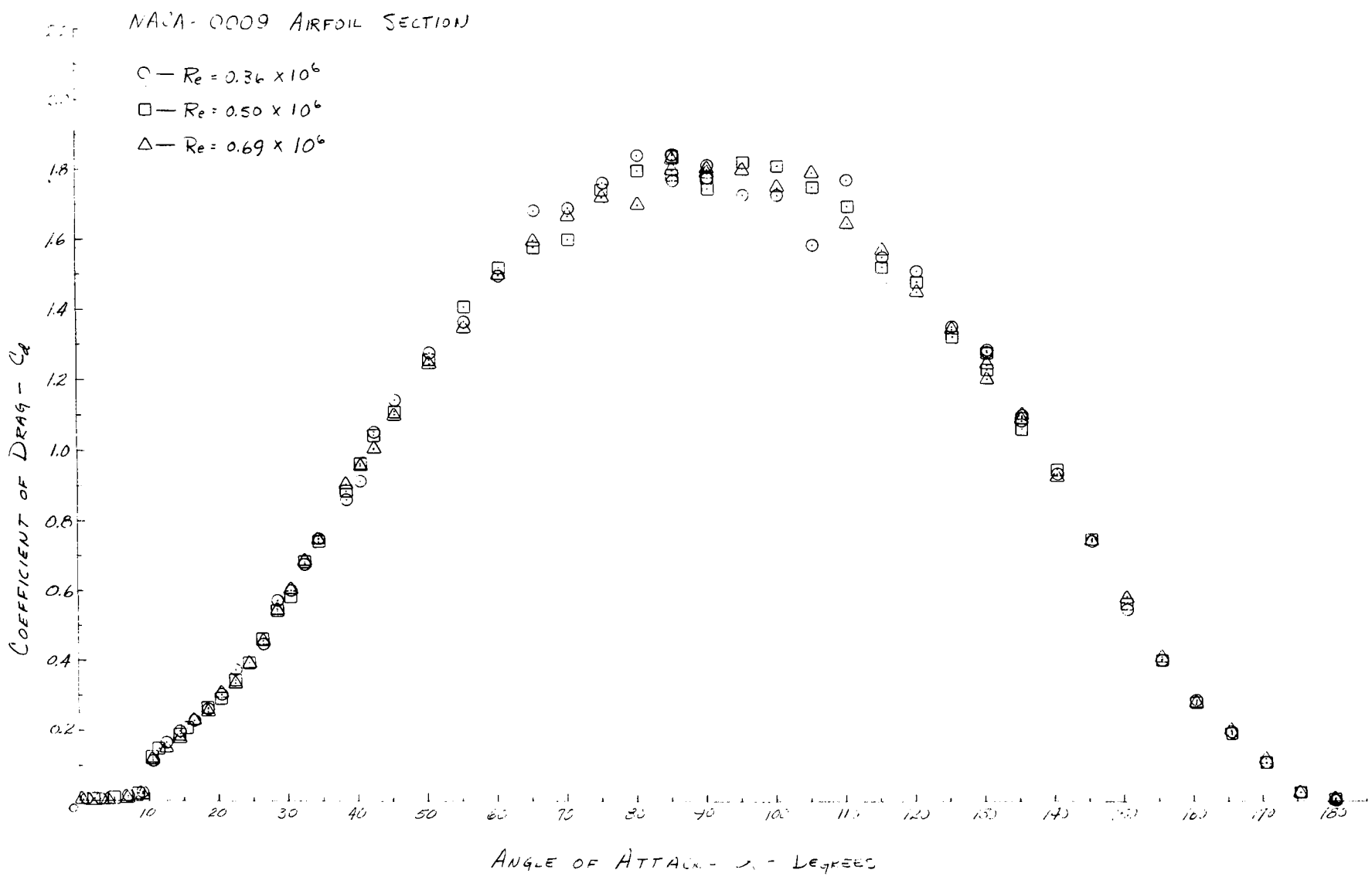

Figure 17. Full Range Section Drag Coefficients for the NACA-0009 Airfoil at Reynolds Numbers of 0.36×10^6, 0.50×10^6 and 0.69×10^6.

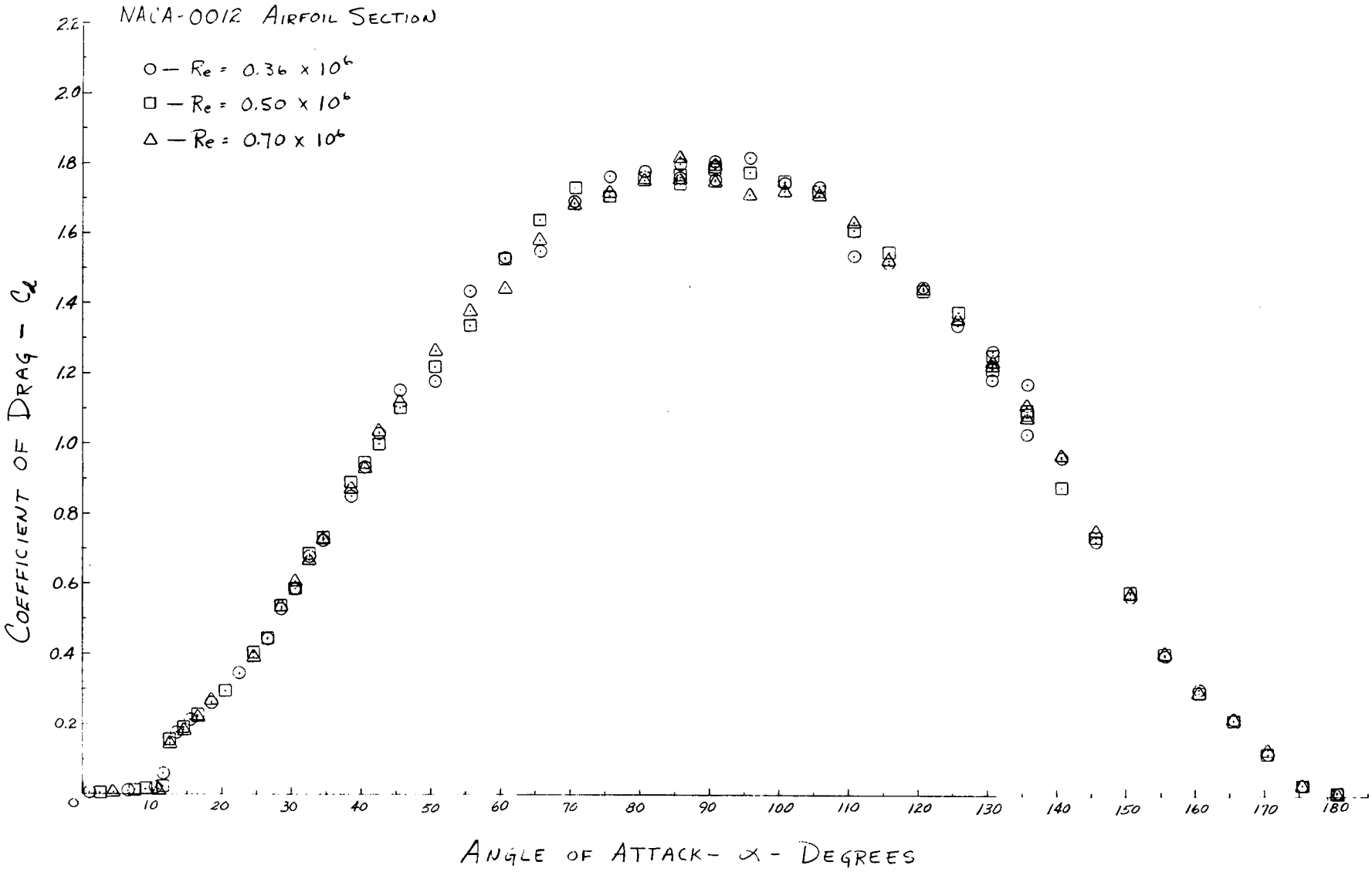

Figure 18. Full Range Section Drag Coefficients for the NACA-0012 Airfoil at Reynolds Numbers of 0.36×10^6, 0.50×10^6 and 0.70×10^6.

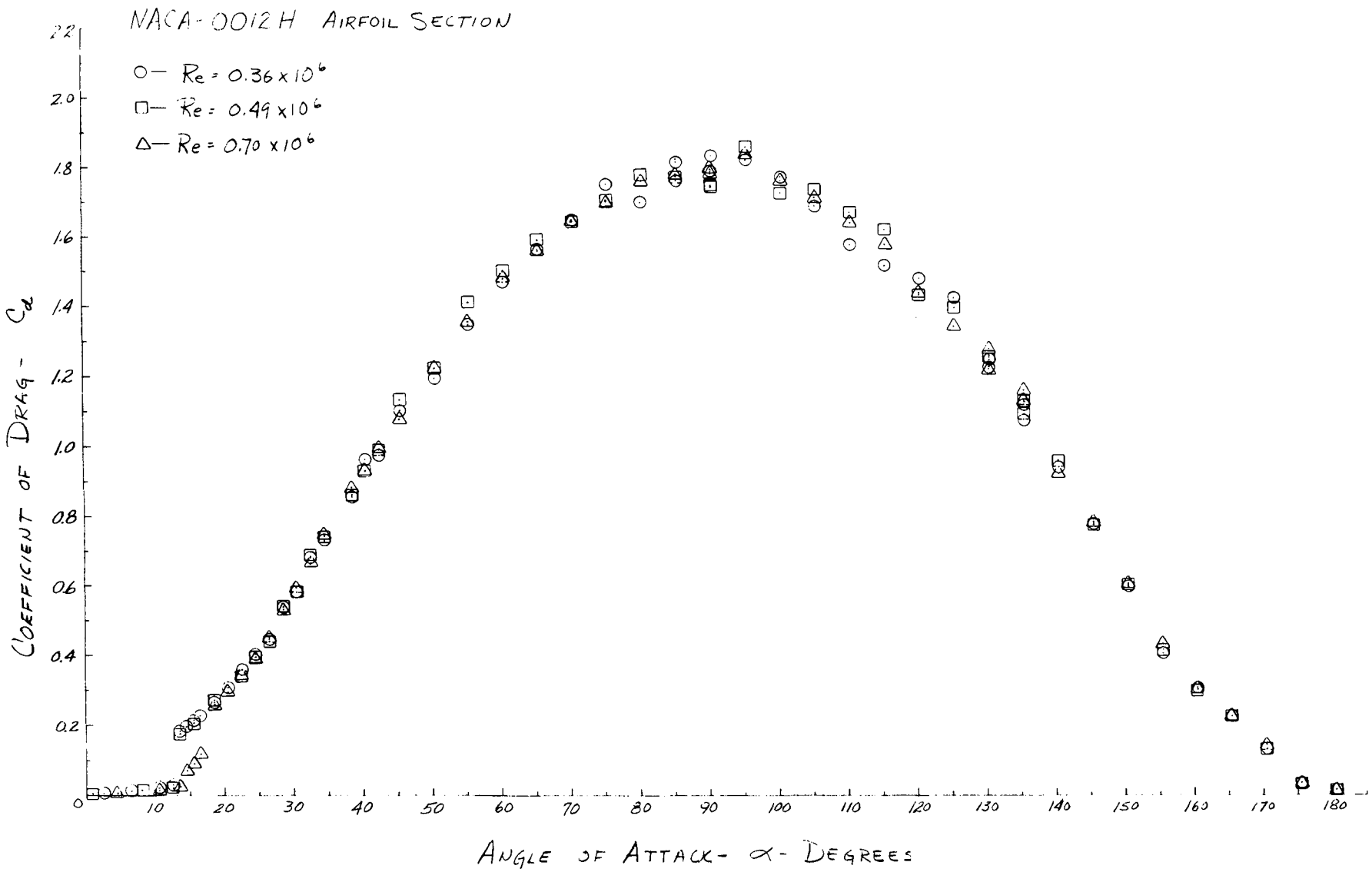

Figure 19. Full Range Section Drag Coefficients for the NACA-0012H Airfoil at Reynolds Numbers of 0.36 x 10^6, 0.49 x 10^6 and 0.70 x 10^6.

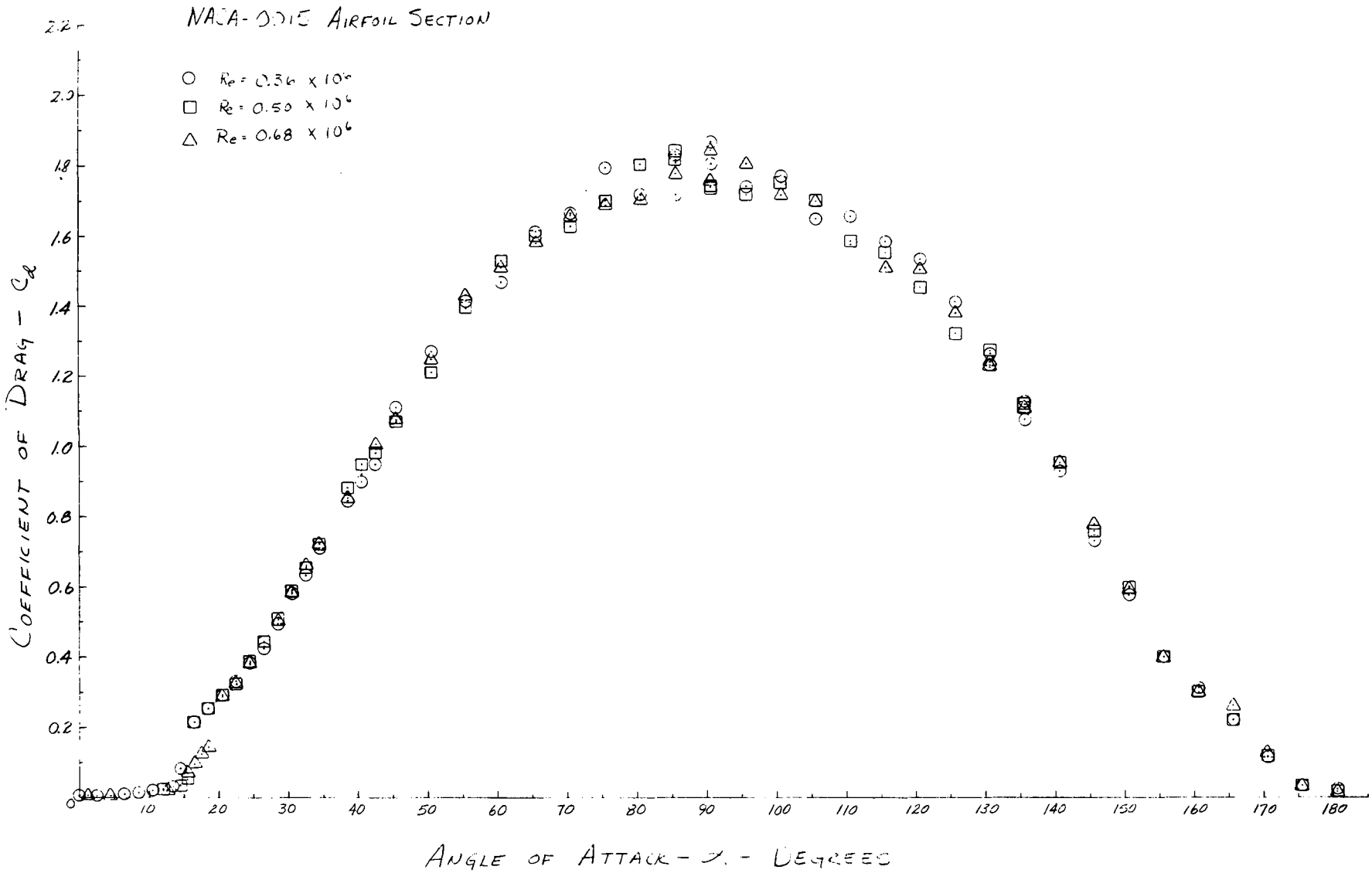

Figure 20. Full Range Section Drag Coefficients for the NACA-0015 Airfoil at Reynolds Numbers of 0.36×10^6, 0.50×10^6 and 0.68×10^6.

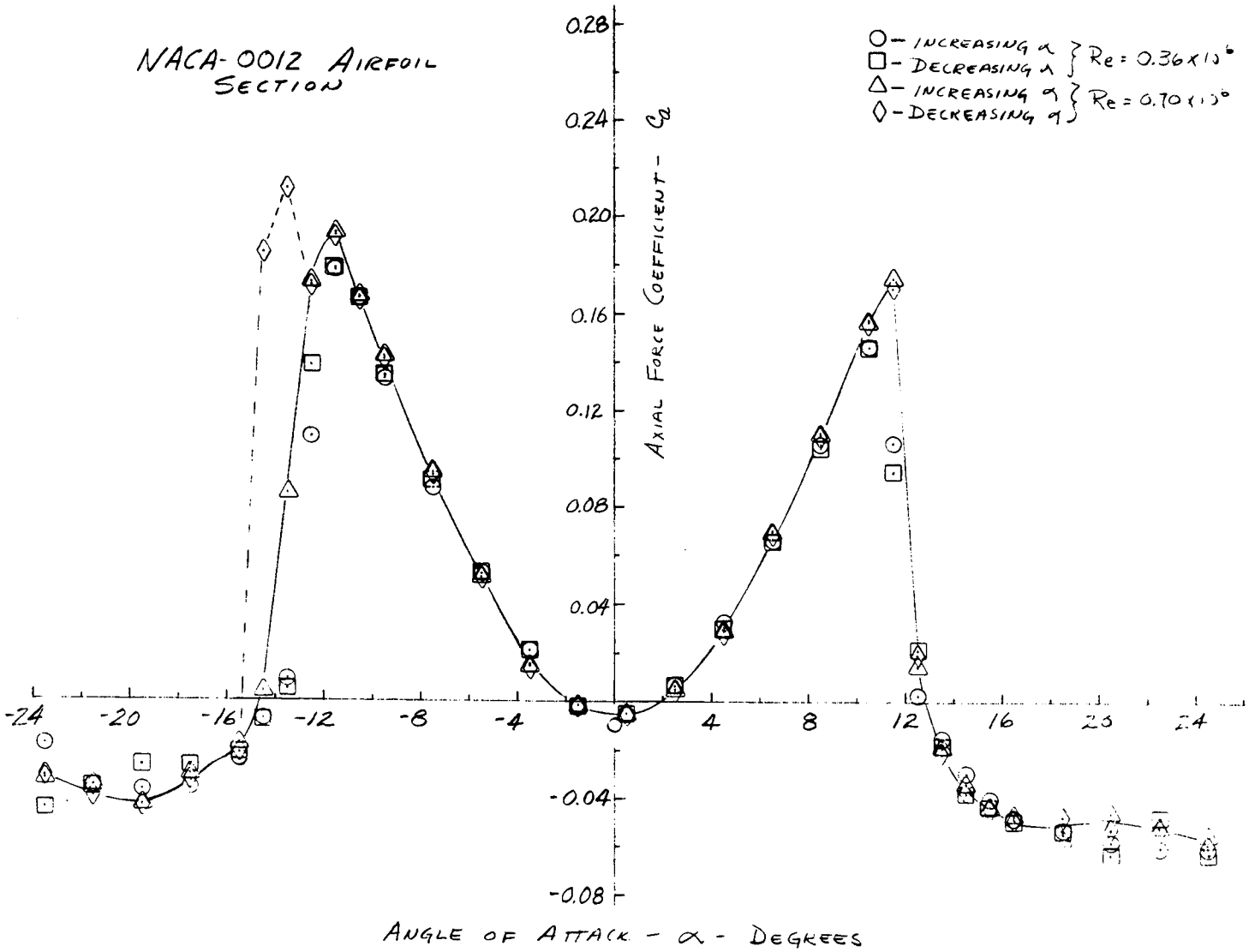

Figure 21. Section Axial Force Coefficients for the NACA-0012 Airfoil at Angles of Attack from -24 degrees to +24 degrees and Reynolds Numbers of 0.36 x 10^6 and 0.70 x 10^6.

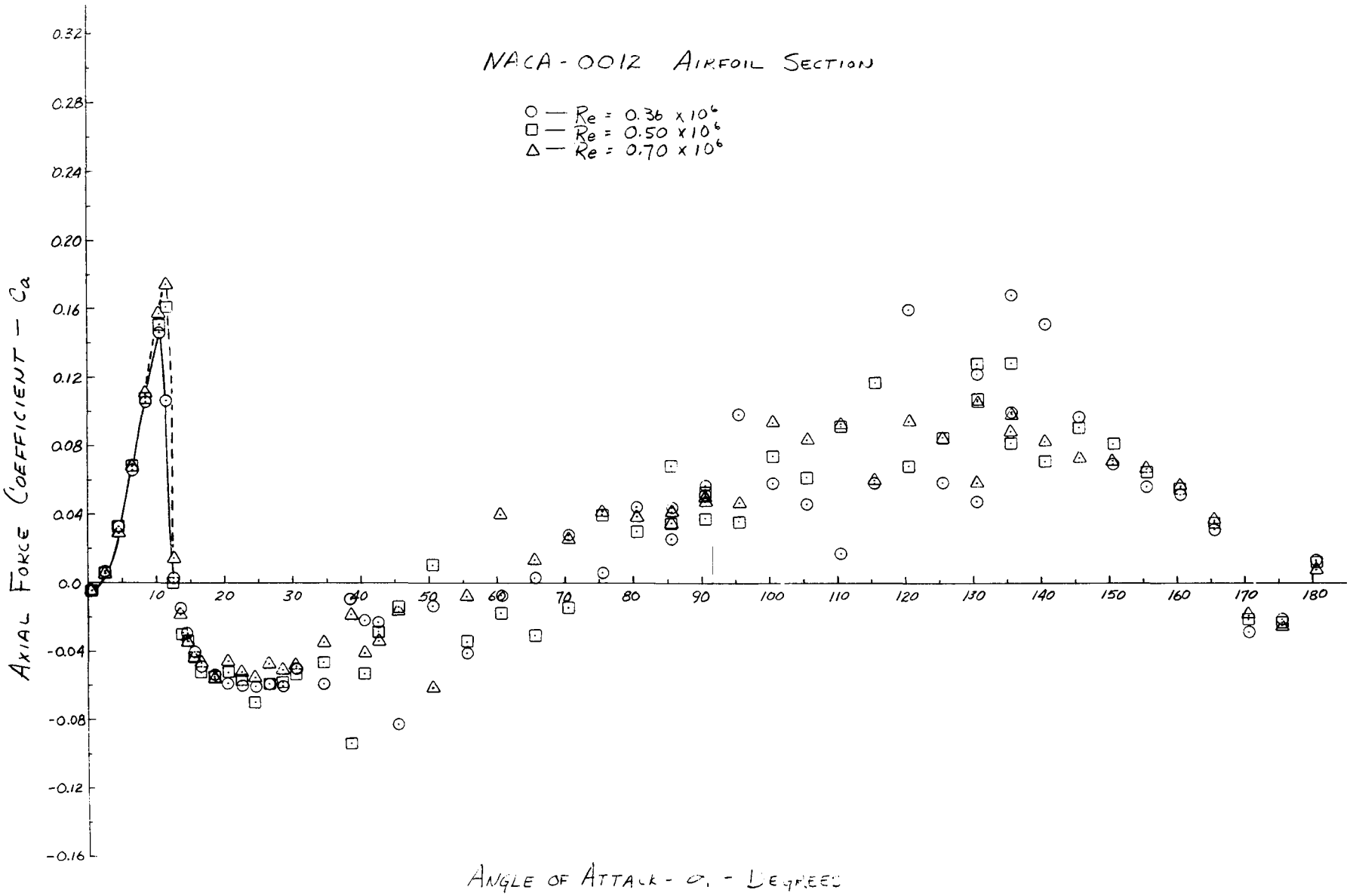

Figure 22. Full Range Section Axial Force Coefficients for the NACA-0012 Airfoil at Reynolds Numbers of 0.36×10^6, 0.50×10^6 and 0.70×10^6.

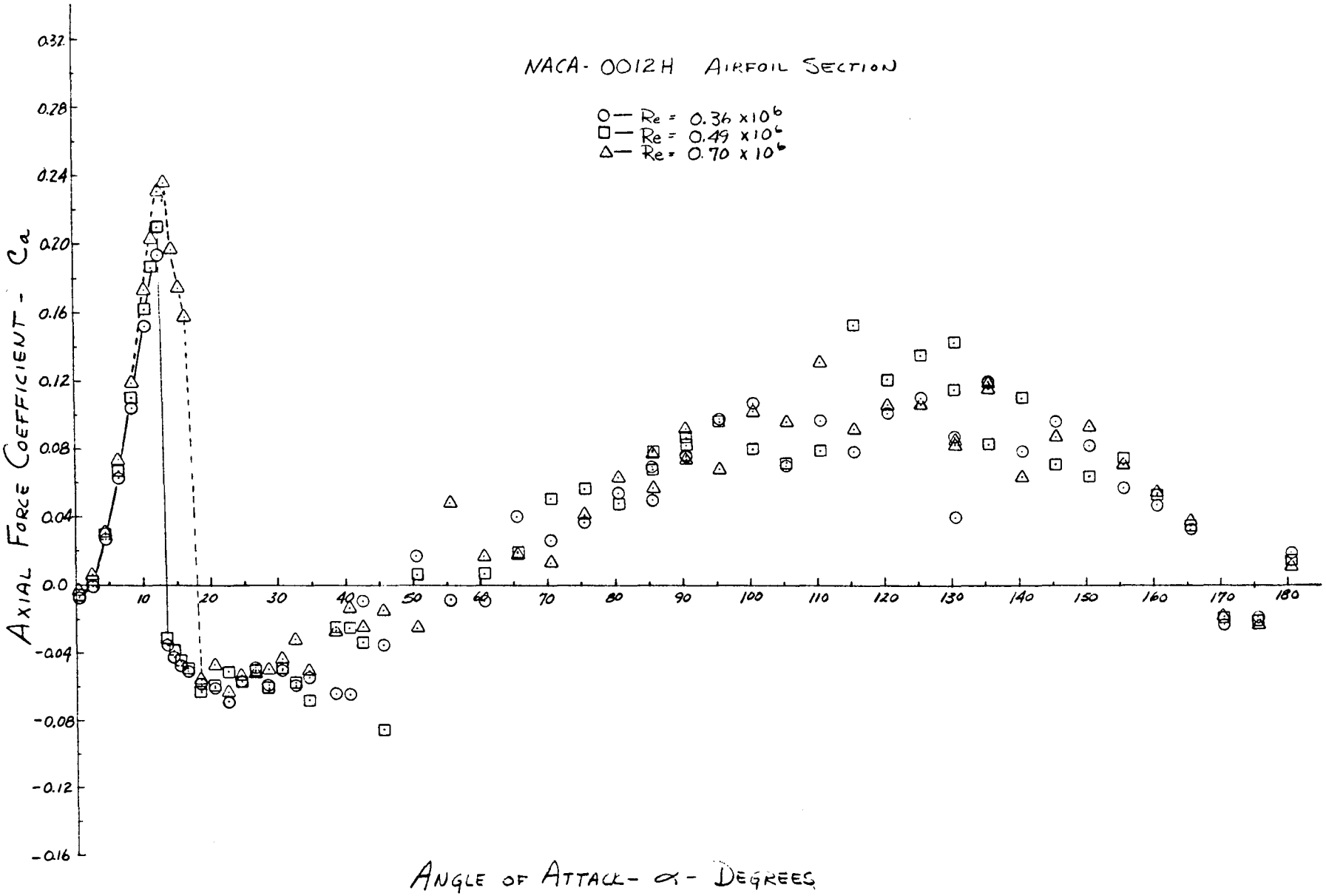

Figure 23. Full Range Section Axial Force Coefficients for the NACA-0012H Airfoil at Reynolds Numbers of 0.36×10^6, 0.49×10^6 and 0.70×10^6.

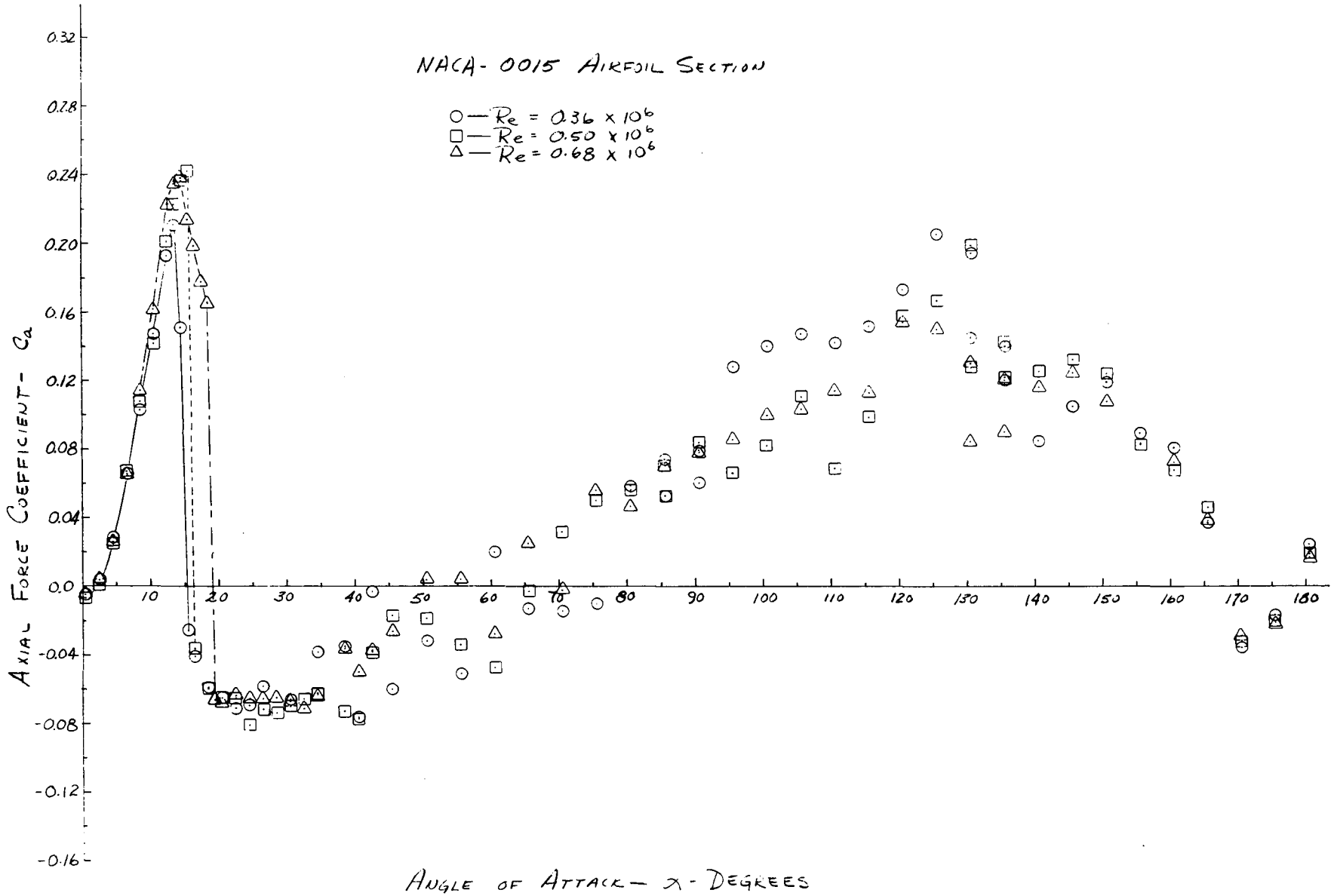

Figure 24. Full Range Section Axial Force Coefficients for the NACA-0015 Airfoil at Reynolds Numbers of 0.36×10^6, 0.50×10^6 and 0.68×10^6.

5-M Turbine Field Testing

W. N. Sullivan - Sandia Laboratories

The 5-M turbine (actually designed as, and previously designated as a 15 foot diameter unit) has recently undergone a series of operational field tests. This test series was initiated to see if field data could possibly be used to measure the performance of the 5-M turbine and to develop standardized techniques applicable for the 17-M test program.

Test Configuration

The 5-M turbine was converted to operate at almost constant RPM by connecting a 1725 RPM induction motor to the turbine with a two stage belt-type speed increaser. By selecting various pulley diameters, a range of synchronous turbine speeds between 87.5 and 175 RPM is available. The turbine shaft torque is measured with a Lebow strain gage torquemeter located between the first and second transmission stages.

The constant speed operation is desirable so that the wind-applied torque on the blades can be equated to the measured shaft torque, avoiding the need to account for the angular acceleration of the turbine. Calculations* have shown that failure to account for inertial effects due to "slip" in the induction motor (causing about a 1% RPM variation in the turbine as load changes) does not introduce unacceptable scatter in the results. Cup-type anemometers have been used for wind velocity measurements. The most

* See the "Sandia Vertical-Axis Wind Turbine Program Technical Quarterly Report" SAND76-0036 (April 1976). for additional details.

successful anemometer location, in terms of correlating output torque to wind speed, has been immediately upstream of the turbine, within two diameters of the machine. The "ideal" location remains to be found and is a subject of continuing investigation.

Data Reduction Schemes

The overall objective is to measure wind speed and turbine torque, and attempt to correlate these two variables. Anemometer readings taken from a weather tower about 100 yds from the turbine were used in initial test runs. It was found, however, that the direct correlation between measured torque and wind speed was very weak or nonexistent. The situation visibly improved when the anemometer was moved to a close-in (two turbine diameters) upstream location. But, simply plotting wind speed and torque points taken every .5 sec* still did yield very scattered results (Figure 1). A smoothing technique consisting of averaging torque and wind speed over a 5 sec. interval improved the situation considerably, although the data still exhibit much uncertainty. In figures 2 & 3, these averaged data are shown which indicates a definite trend which is apparently repeatable for the two different wind speed distributions shown.

---

* The time interval selected was based on an estimate of the best frequency response of the turbine and instrumentation.

Another scheme (the "method of bins") has received most of our attention because it has the advantage of indicating the velocity distribution associated with the wind record during the test. In this method, the velocity is divided into discrete bins of equal width, normally taken to be 2 MPH. Each data pair is assigned to a bin associated with the velocity, and the corresponding torque is averaged with values previously accumulated in the bin. By keeping track of the number of points in each bin, the velocity distribution may be calculated. Typical results from this technique are shown in Figure 4, for a 175 RPM operating condition generated from about 3 minutes of data, sampled at .5 sec intervals. Results for an expanded data base taken over several different days lead to the even smoother results of Figure 5 for 150 RPM operation. This curve was constructed from approximately 30 minutes total running time.

The effect of RPM variations is shown clearly in Figure 6, where there is a pronounced increase in output with increasing RPM, as is expected for turbines of this type.

The C_p curve may be readily derived from the torque data, although uncertainties in velocity measurements tend to be amplified by the necessity to cube the velocity in the calculation. The peak C_p (Figure 7) for the 150 RPM data is much lower than anticipated (about .25). This effect is due either to poor aerodynamic performance of this particular turbine, systematic errors in the measurement process, or both.

Concluding Remarks

The method of bins can evidently produce a repeatable measure of turbine performance which is at least qualitatively accurate. More refinement is needed in understanding anemometer placement and data sampling techniques to put this technique on a firmer foundation. Data taken in the field should be attempted on a turbine which has also been wind tunnel tested so that the cumulative effect of uncertainties can be determined. Finally, the process should be automated at the site, so that the lost time between data collection and analysis could be eliminated.

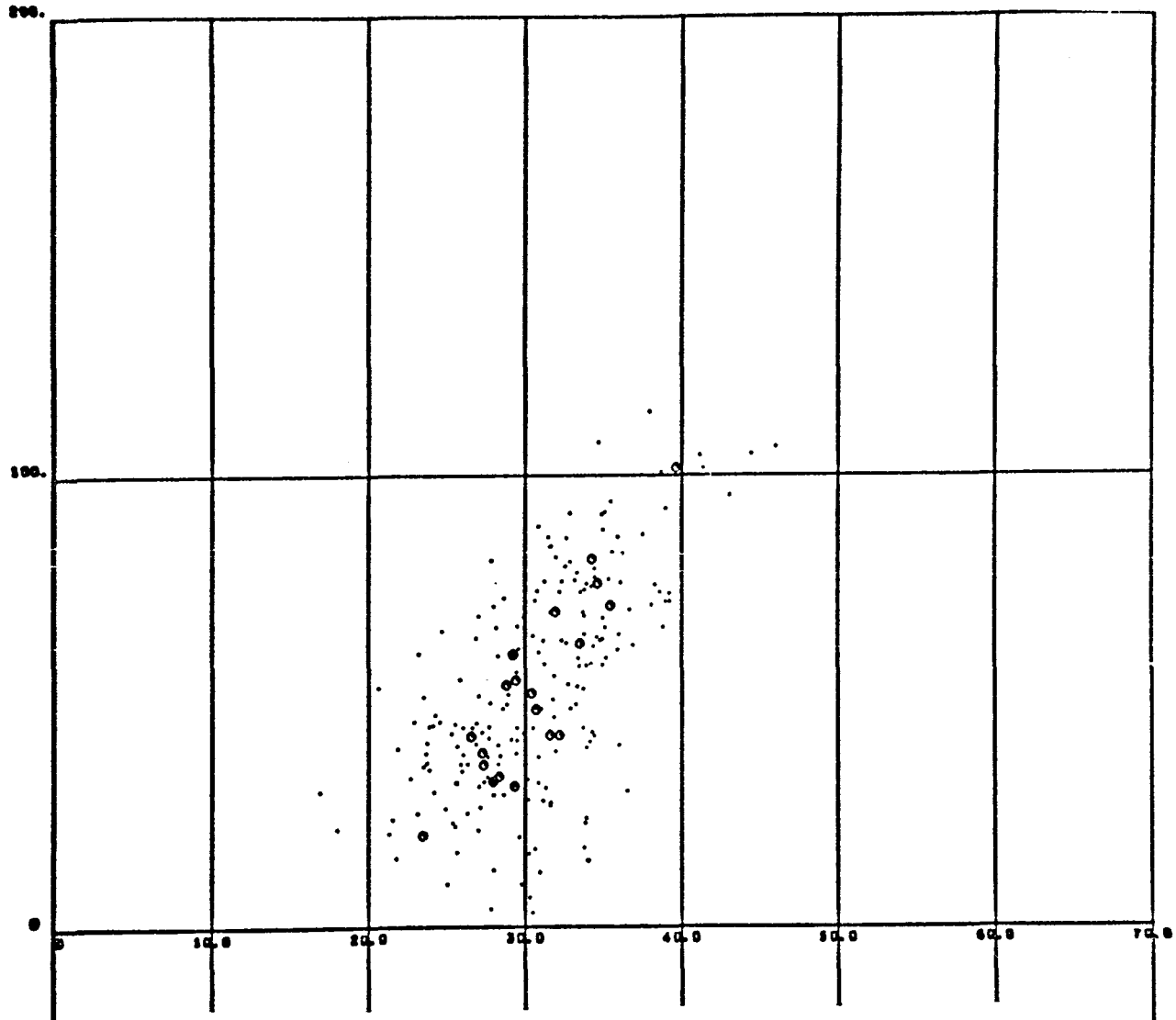

Figure 1. Pointwise Torque and Velocity Data (175 RPM) Sampled at .5 sec Intervals. Circular Points are for 5 sec. Averages.

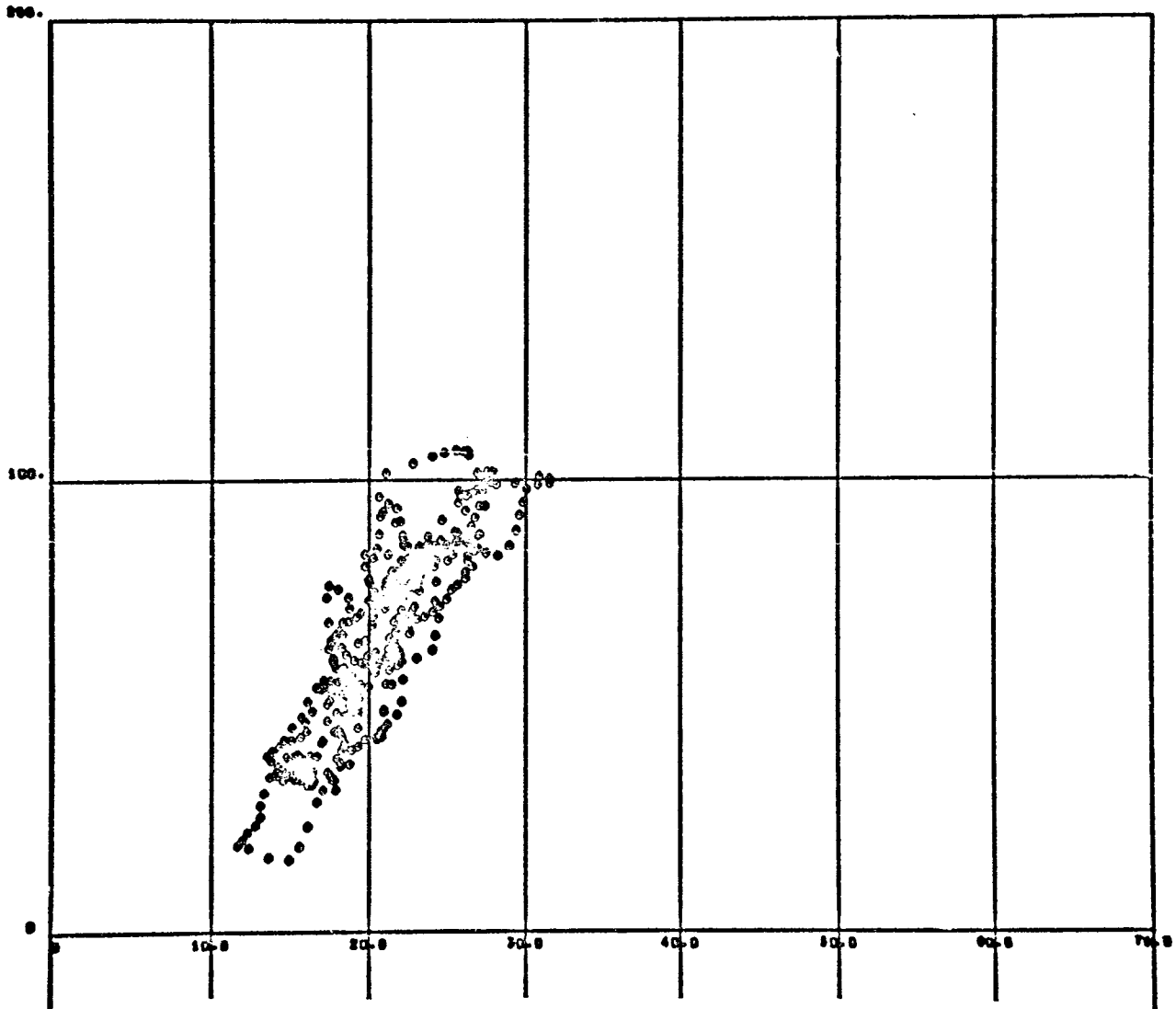

Figure 2. 5 sec. Averaged Data, 175 RPM, Approximately 3 Minutes of Data (175 RPM)

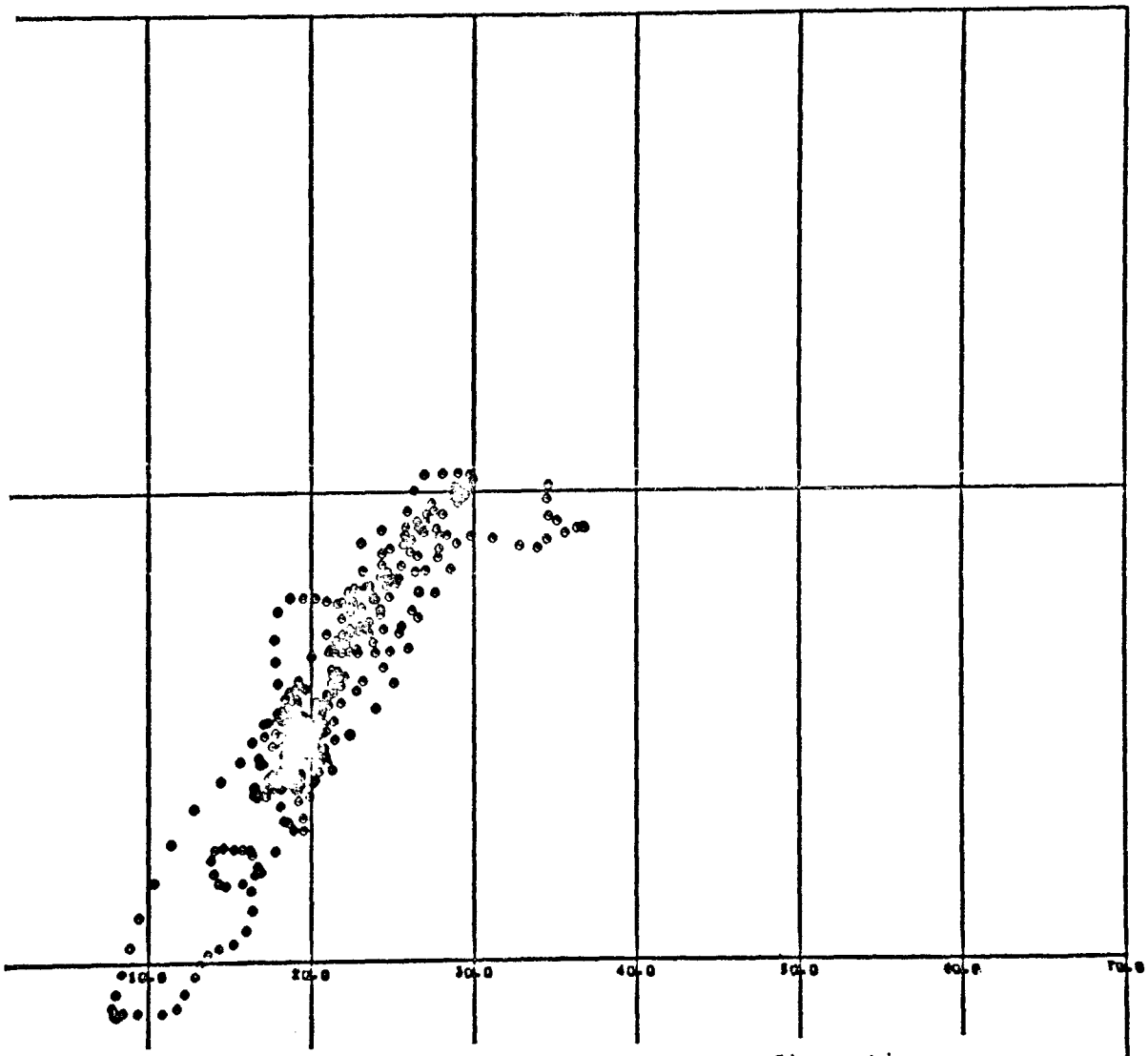

Figure 3. Repeatability Test, Same Configuration as Figure 2 with a Different Wind Speed Record.

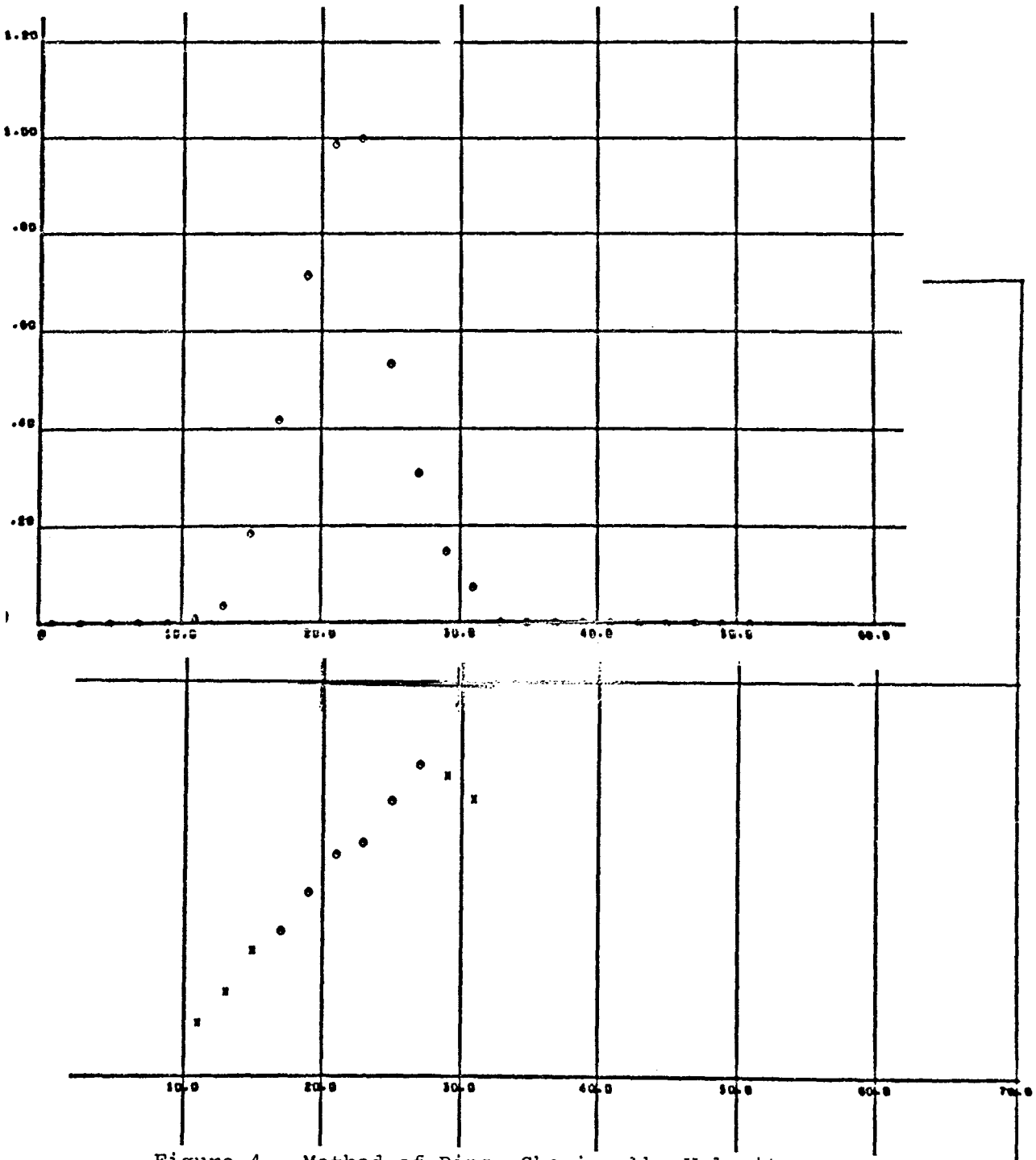

Figure 4. Method of Bins, Showing the Velocity Distribution (Upper Points) and Torque vs. Velocity for 175 RPM Operations.

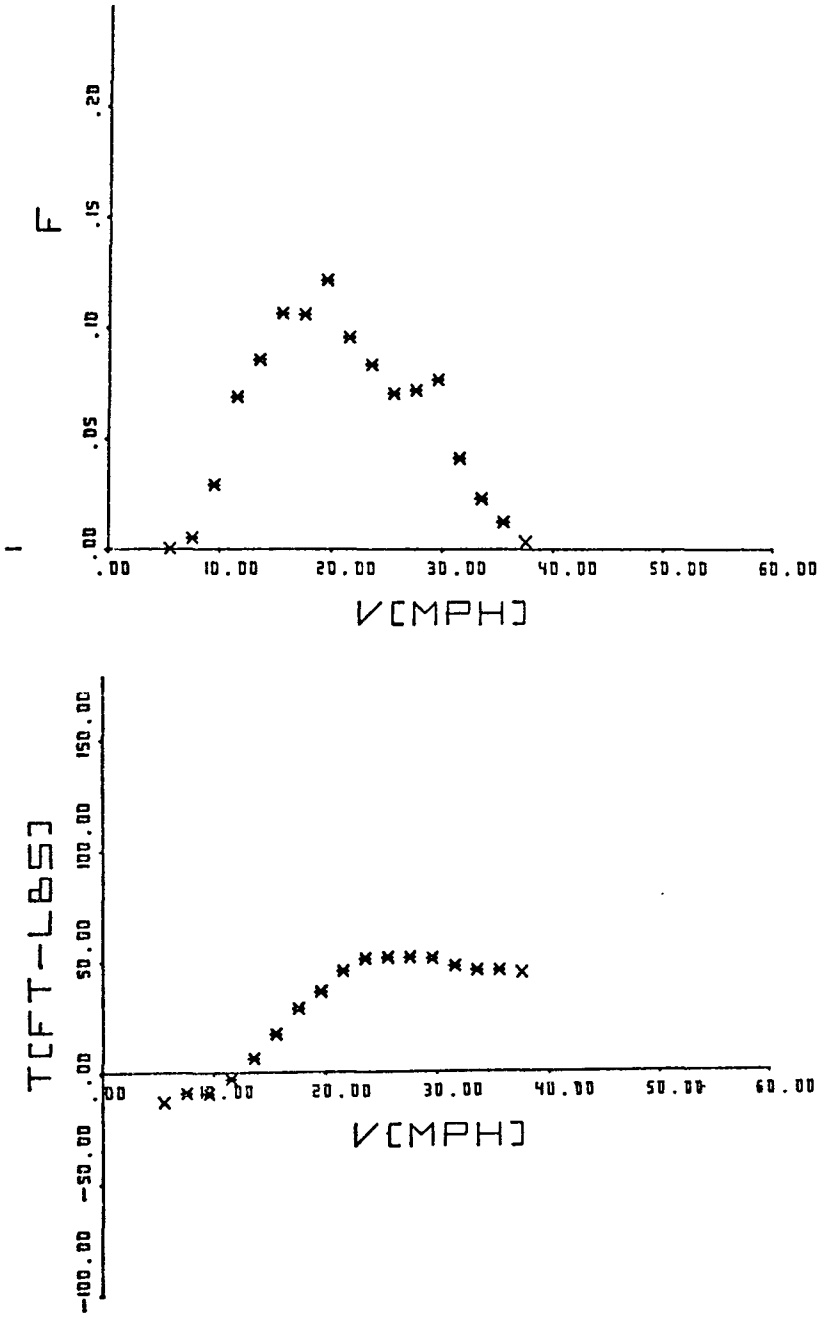

Figure 5. Method of Bins with an Expanded Velocity Distribution for 150 RPM Operations.

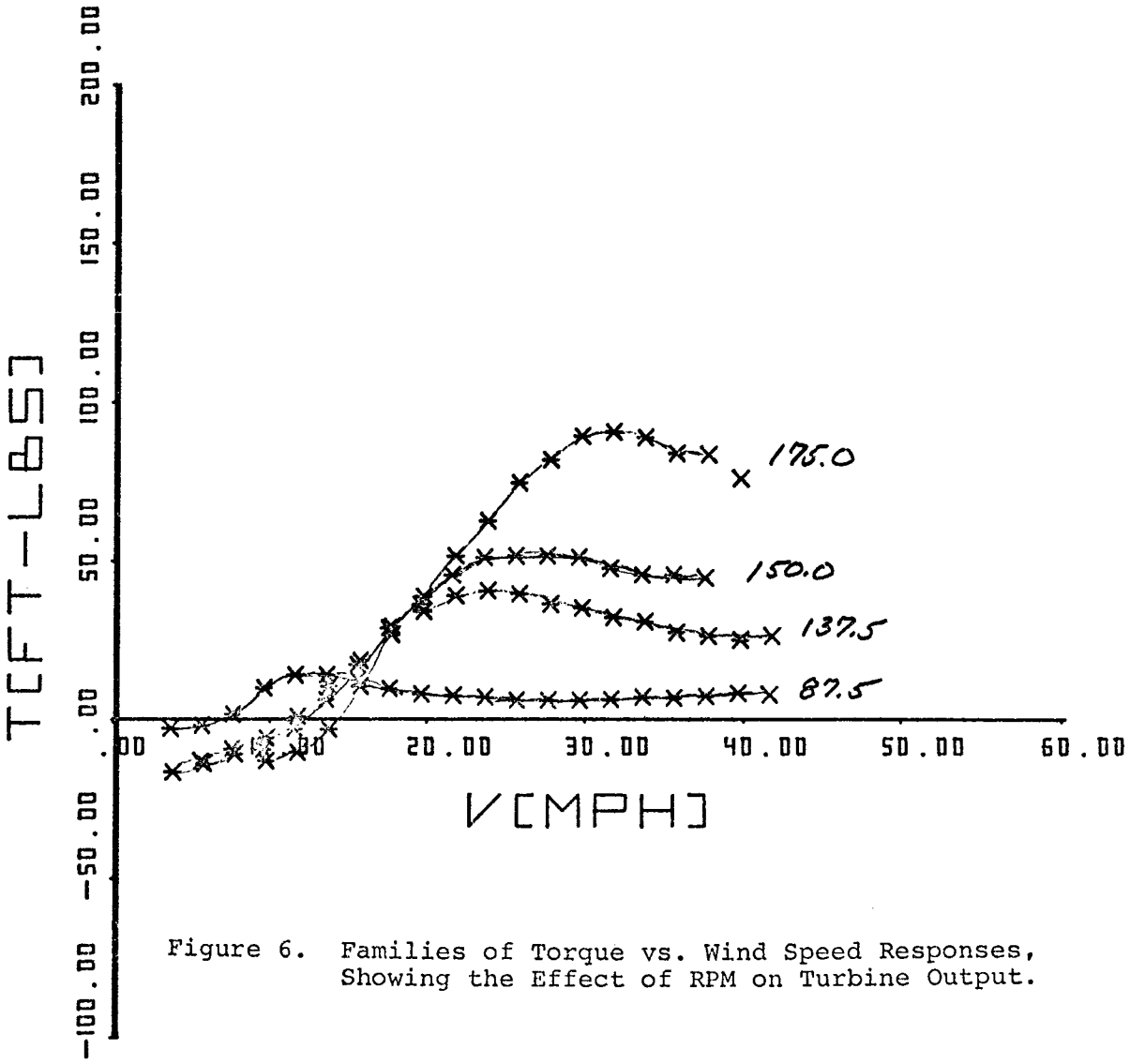

Figure 6. Families of Torque vs. Wind Speed Responses, Showing the Effect of RPM on Turbine Output.

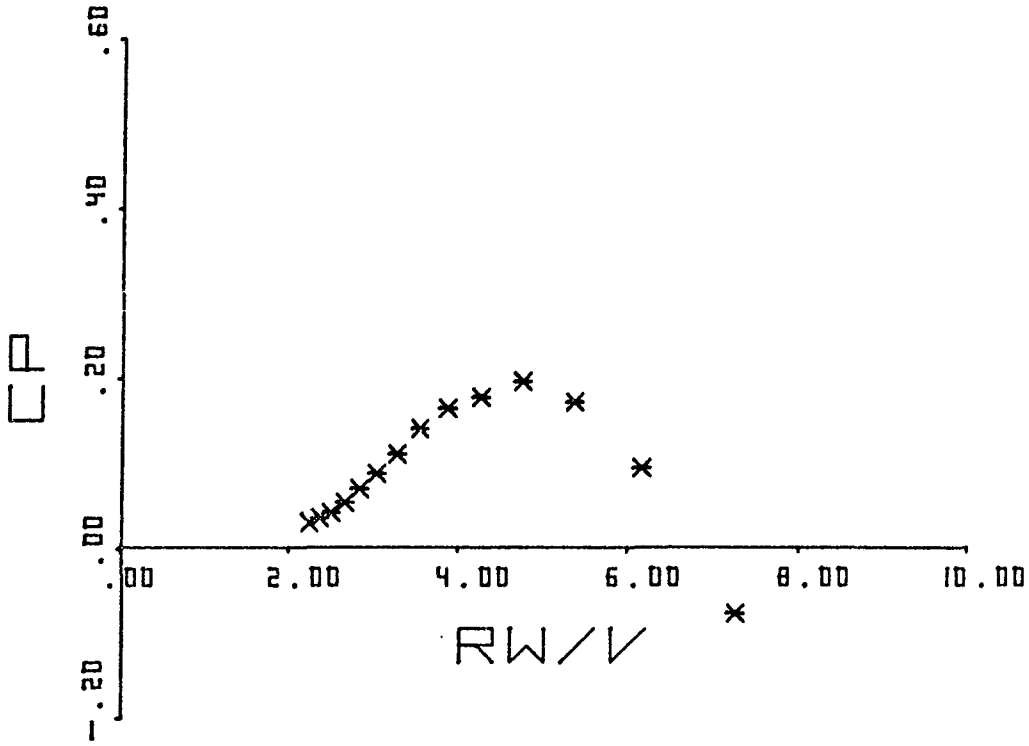

Figure 7. Power coefficient, Calculated from the 150 RPM Data of Figure 5.

PERFORMANCE PREDICTION FOR THE 17-m TURBINE

James Banas, Sandia Laboratories, Albuquerque, New Mexico

Early in the program a matrix of potential turbine sizes and maximum output power levels was defined. This matrix was suggested by an overall system design philosophy of constructing a system which is large enough to generate significant power levels and to present design problems associated with large systems yet small enough to have a reasonable probability of success. These considerations led to the selection of a 17-m diameter turbine, using troposkien or troposkien-approximation blades. This paper describes the utilization of aerodynamic data along with models for the other system components to estimate the performance of the 17-m turbine system, leading to selection of the generator capacity and the gear ratios for the speed increaser. Input/output relationships for the components are combined to estimate maximum system output power as a function of turbine rotational speed. In addition, the percentages of time that wind speed would be expected to exceed the wind speeds required for positive and maximum power are calculated. The basic system components are the synchronous generator, the speed increaser, and the wind turbine. Generator capacities of 30 kW and 60 kW are considered for comparative purposes.

Generator -- The generator rotational speed is chosen to be 1800 RPM. Although lower speeds are available, step-up to 1800 RPM will require gear ratios appropriate to larger systems. Representative efficiencies under various load conditions are shown in Table I.

TABLE I

Percent Efficiencies of Synchronous Generators
(1800 rpm)

	Load		
Rating	4/4	3/4	2/4
30 kW	88.9	87.2	83.0
60 kW	90.6	89.3	85.9

A linear relationship between input and output power can be used to approximate these efficiency characteristics which are given by

$$P_{out} = 0.957\ P_{in} - 2.30\ \text{kW (30-kW generator)}$$
$$P_{out} = 0.958\ P_{in} - 3.47\ \text{kW (60-kW generator)}$$

where P_{in} and P_{out} are in units of kilowatts.

Speed increaser -- Losses at rated load in a 6-to-1 transmission stage amount to about 2 percent of rated load. The assumption is made that this loss is approximately constant. Since the speed increaser for the 17-m system will involve a stepup of approximately 36 to 1, the losses are 4 percent of rated load which is dependent upon the generator size. The input/output power relationship for the speed increaser is given by

$$P_{out} = P_{in} - 1.35\ \text{kW (30-kW generator)}$$
$$P_{out} = P_{in} - 2.65\ \text{kW (60-kW generator)}$$

where P_{in} and P_{out} are in units of kilowatts.

Wind Turbine -- The wind turbine performance characteristic of interest for the synchronous (i.e., constant rotational speed) application is the variation of power with wind speed. Turbine power is usually expressed by

$$P = 1/2\ \rho A V^3\ C_p \left[\frac{R\omega}{V}\right]$$

where the power coefficient, C_p is a function of the tip speed to wind speed ratio, $R\omega/V$. Although the required characteristic can be generated from this equation, a more useful form is given by

$$P = 1/2\ \rho A\ (R\omega)^3\ K\left[\frac{V}{R\omega}\right] .$$

where

$$K = \frac{C_p\left[\frac{R\omega}{V}\right]}{\left(\frac{R\omega}{V}\right)^3} .$$

The function K depends on the advance ratio, $V/R\omega$ and also on the properties of the wind turbine and the flow. For example, Figure 1 shows the variation of K with advance ratio derived from wind-tunnel test data for a Darrieus turbine with a solidity of 0.2 and 3 blades of NACA-0012 cross section. As is most appropriate for constant rotational speed operation, the Reynolds number is based on tip speed and chord length.

For a given value of Reynolds number, Figure 1 indicates that K achieves a maximum with respect to advance ratio; that is, power achieves a maximum with respect to wind speed. The advance ratio at which $K = K_{max}$ is related to the wind speed for maximum power. The advance ratio at which $K = 0$ is the inverse of the "runaway" tip speed ratio; for a system with no losses, this value of advance ratio is related to the wind speed

above which positive power is generated. These three parameters are used to estimate the performance of the 17-m system. The curves in Figure 1 further indicate a substantial Reynolds number dependence. Figures 2 through 4 show the variation of K_{max},

$$\left(\frac{V}{R\omega}\right) K = K_{max}, \text{ and } \left(\frac{V}{R\omega}\right) K = 0$$

with Reynolds number for the wind tunnel test data. These figures also show predictions from the single streamtube and multiple streamtube aerodynamic codes.

Results -- Figure 5 shows maximum system output power as a function of turbine rotational speed. With a 30-kW generator, rated output power corresponds to a turbine rotational speed of 36 rpm and a wind speed of 22 mph. With a 60-kW generator, rated output power corresponds to a turbine rotational speed of 43.5 rpm and a wind speed of 28 mph.

At selected points on the curves of Figure 5 are noted two percentages. These are percentages of time for which the wind speed exceeds certain values and are based on yearly wind statistics for Albuquerque at a height of 48 feet above the ground. The larger is the percentage of time for which the wind speed exceeds the value for positive output power at the given turbine rotational speed. The smaller is the percentage of time for which the wind speed exceeds the value for maximum output power at the given turbine rotational speed; this percentage can be approximately doubled for the windiest month and halved for the calmest month. Thus, the numbers indicate that, for fractions of time exceeding 25 percent, positive system output power would be generated, while for fractions of time of the order of a few percent, maximum system output power would be generated.

The system will be used to deduce aerodynamic performance characteristics in anticipation of scale-up. Turbine rotational speeds have been selected to cover a wide range of Reynolds numbers, since both the wind tunnel test data and the aerodynamic codes indicate a strong dependence of performance on Reynolds number. Figure 6 shows the intervals of Reynolds number spanned by experimental data from the wind tunnel tests, the 5-m turbine tests, and the suggested 17-m turbine tests. Since the differences in efficiency between the 30 kW and 60 kW system are not substantial and the 60 kW system allows a greater interval of rotational speeds, a 60 kW generator has been selected for the 17-m turbine.

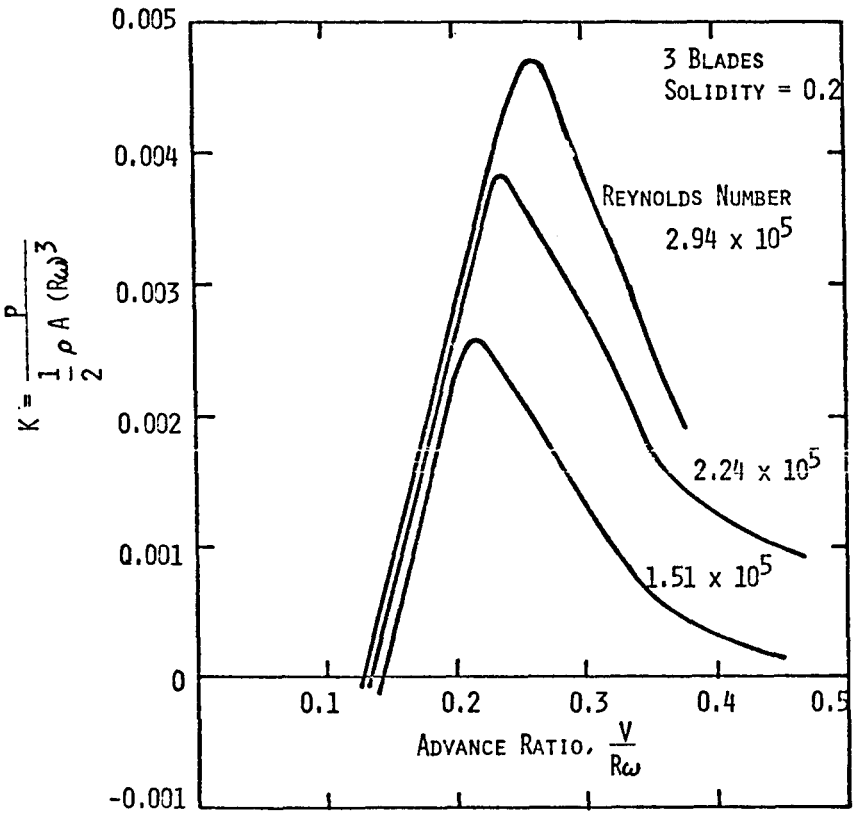

Figure 1. Wind Turbine Performance Characteristics

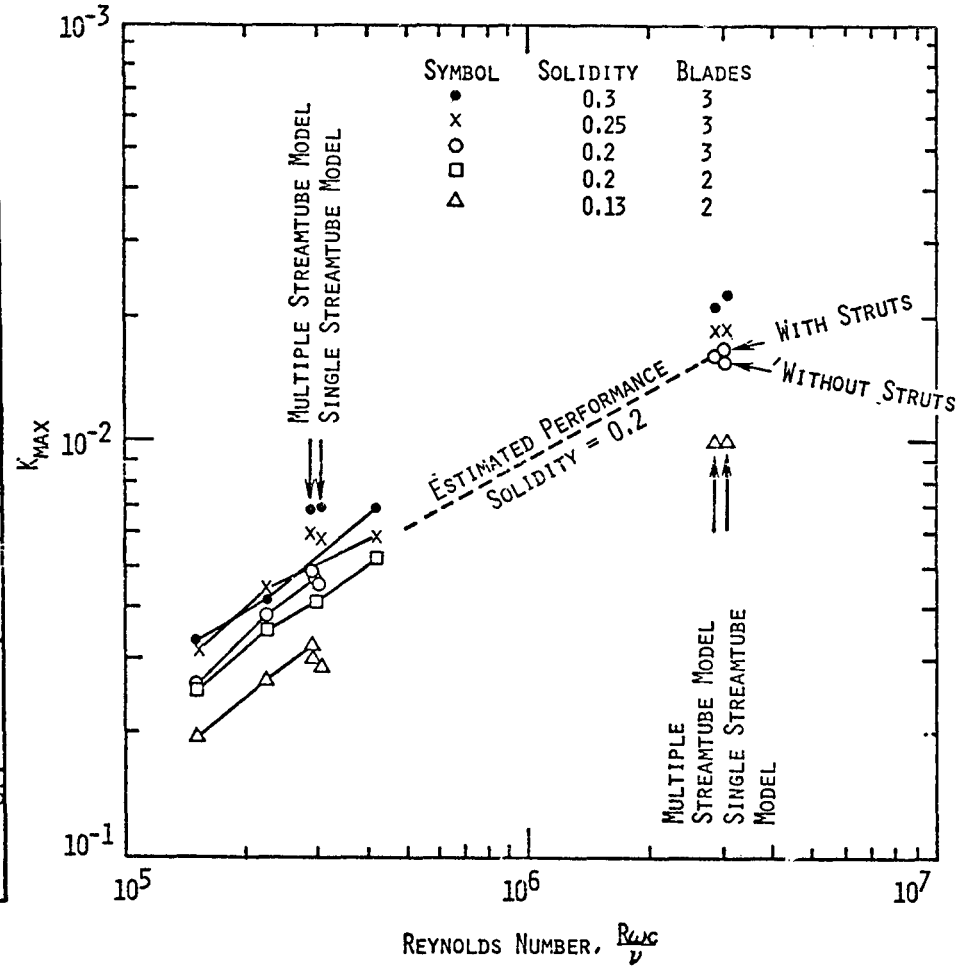

Figure 2. Variation of K_{max} with Re

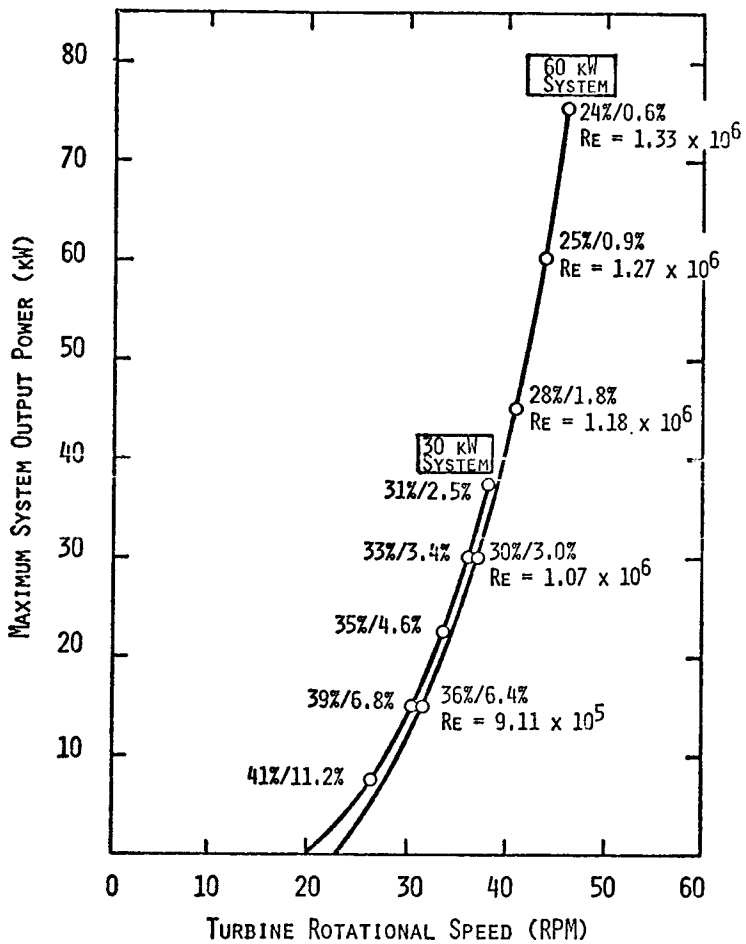

Figure 5. Performance of the 17-m System

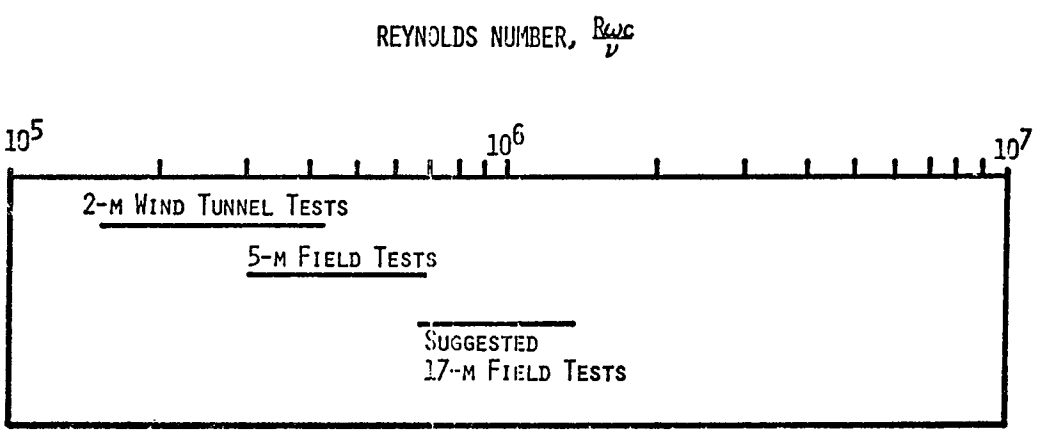

Figure 6. Reynolds Numbers for Experimental Data

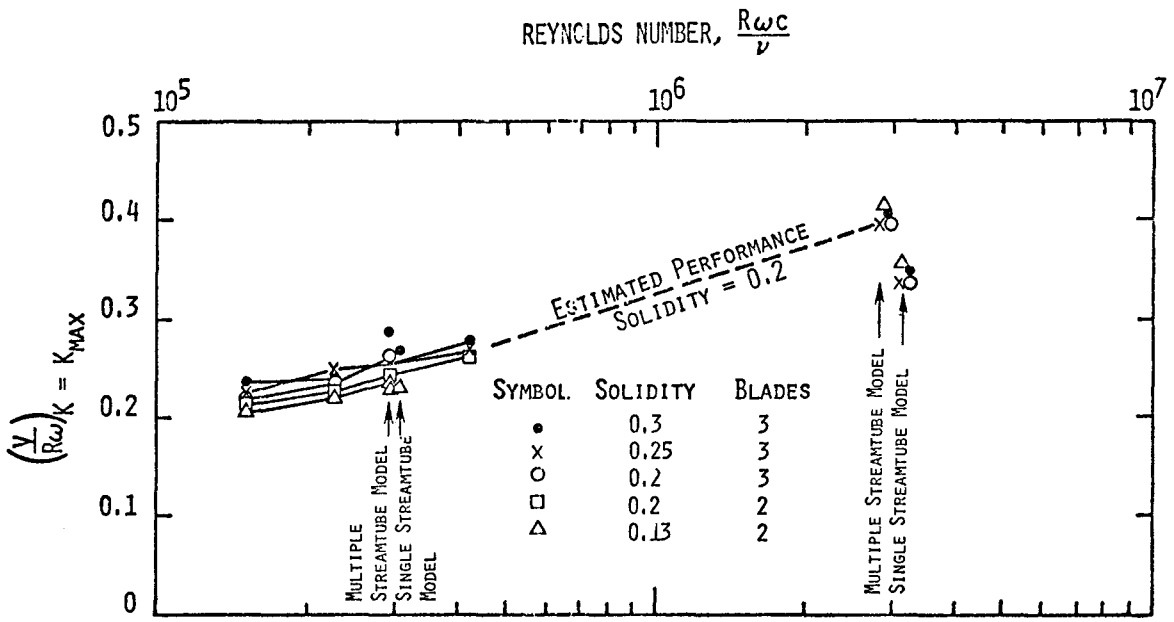

Figure 3. Variation of $\left(\frac{V}{R\omega}\right)$ $K = K_{max}$ with Re

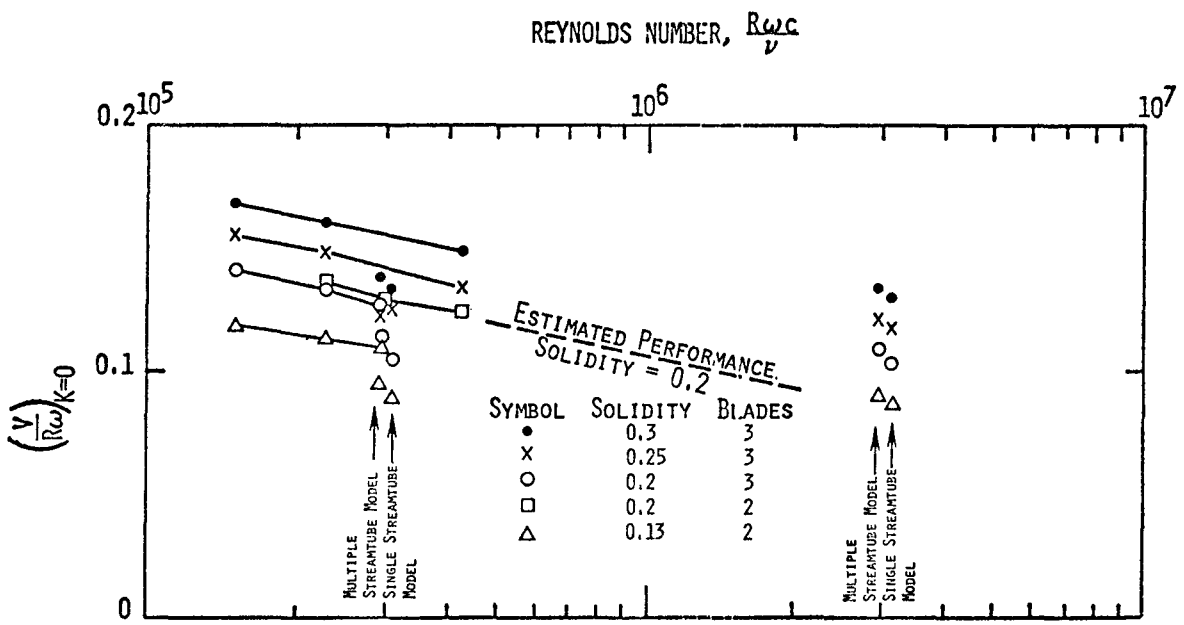

Figure 4. Variation of $\left(\frac{V}{R\omega}\right)$ $K = 0$ with Re

STRUCTURAL OVERVIEW

Sandia Laboratories

R. C. Reuter, Jr.

INTRODUCTION

Whenever advanced hardware involves large, periodic loads, low natural frequencies and many interacting components, the probability of encountering structural problems is high. The Darrieus vertical axis wind turbine being developed here at Sandia is typified by these features. The helicopter and horizontal axis wind turbine industries have provided a basis from which some understanding of structural problems can be drawn: however, the vertical axis turbine is sufficiently different from either of these structures that it requires a new technology all its own. Obvious differences include the curved blades, attached at both ends, the possibility of discrete, intermediate support (i.e., struts), large aerodynamic load variations, relatively small tower loads and dynamic tower-blade coupling. The existence of structural problems associated with the Darrieus VAWT has also been highlighted by firsthand experience here at Sandia. A small, 2 meter wind tunnel model suffered a blade support tower collapse due to local buckling. Blade resonances and instabilities have been observed on this model. Coupled tower tie down vibrations have been observed in the 2 meter model and a 15 meter field turbine. These are examples of structural problems that can affect turbine performance and life, and which deserve attention to the extent that they are understood and hopefully eliminated.

The VAWT structural program at Sandia has three natural objectives: 1) to understand the problems and their solutions, 2) to aid and support design, and 3) to assist in system cost evaluation. Presently being emphasized are strength requirements necessary to meet performance conditions, stiffness requirements for control of natural frequency locations, fatigue requirements for safety and low life cycle costs, and also aeroelasticity affects which couple structural behavior with aerodynamics.

DETAILS OF THE VAWT STRUCTURAL PROGRAM

Sandia's structural program features an experimental phase and an analytical phase which are complimentary in nature. The analytical phase is further divided into developmental activities and applied activities. Recognizing that hardware design is the ultimate goal, the developmental portion of the analytical phase, which generates the tools required by applied analysis, plays a supportive role. Component and system design follows.

Experimental Phase

The experimental program consists of experience gained from the design, erection and operation of two existing machines, the 2-m wind tunnel model and the 5-m field turbine. Both of these machines have operated successfully with structural analysis supporting design and providing explanations for observed phenomena. These phenomena consist largely of the locations of blade and system resonant frequencies and instabilities, and their sensitivity to various system parameters. Bench tests have also been used to measure blade non-rotating natural frequencies. The major portion of the experimental program is yet to come. It consists of the acquisition of structural data during turbine operation. Telemetry instrumentation packages are currently being designed for use on these field turbine and/or the 17-m, 60 kW turbine, depending upon time of completion. Eventually both turbines (and possibly the 2-m model) will be instrumented for comparison with analytical predictions of strain levels, mode shapes, natural frequencies and modal participation.

Analytical Phase

The main thrust of the structural program to date has been with analytical development and applied analysis related to design and evaluation of the 2-m and 5-m turbines and the design of the 17-m turbine.

Of primary concern is the evaluation of the aerodynamic loads, [1], which begins with a characterization of blade aerodynamic properties as a function of spacial position and operating conditions such as wind properties and turbine speed. The next step is to convert these loads to usable structural loads for design of the blades, tower and related hardware. This is an important part of the program since it affects practically every turbine component including tie down, support and input-output hardware, and fastening and attachment systems.

In recognition of potential problems associated with the adequacy of turbine blade strength and stiffness properties, a considerable effort has been devoted to analytical characterization of blade response to complex aerodynamic and structural loading, [2]. Two general purpose codes have been developed for this purpose. The first allows only in-plane motion, however, it has the capability of including important effects such as gravity, aerodynamic and centrifugal loads, point loads due to attachment hardware and the presence of support struts. The second code is more general in that out-of-plane motion is permitted so that in and out-of-plane coupling effects are accounted for. The second code will have an iterative procedure for evaluation of aeroelastic effects. Both codes have been used for present and future turbine design evaluation and performance limit definition.

After some effort had been directed toward blade support tower design, it became apparent that the support tower and blades had similar dynamic properties. This suggests strong coupling possibilities between the blades and support tower. Also, recognizing the potential involvement of relatively soft tie down systems, another general purpose code was implemented for analysis, [3]. This code treats the entire system - blades, tower, tie down and the resulting coupling - and has been used for both static and dynamic analysis. Of particular interest have been the results of the eigenvalue analysis which predicts mode shapes and correspond-

ing frequencies for the system. It has become clear that certain "blade" modes are significantly effected by tower compliance (e.g. the first symmetric out-of-plane mode), demonstrating the need for more than uncoupled component analysis for design. Another contribution of this approach has been the discovery of certain system (or composite) modes -- assymetric modes which are not present when blades and support tower are analyzed separately. The presence of these modes has raised questions concerning the possibility of exciting them at operational speeds or during start up. Answers will come from the modal participation analysis, [3], being conducted to determine the frequency content and modal participation factors of blade response to the oscillating aerodynamic forces. This analysis will be performed for a variety of tip speed ratios.

Another important aspect of blade analysis is the characterization of aerodynamic instabilities. Early wind tunnel testing with torsionally soft blades that were not mass balanced demonstrated the presence of a serious instability. The general problem of blade instability is being addressed by Professor N. D. Ham, [4]. Thus far both a simplified structural model and a more rigorous aeroelastic model have been developed.

Finally, there are numerous turbine components which must be analyzed for design adequacy and interaction with other components of the system. Many of these problems were handled through analytic, or closed form approaches, [5,6]. The blade support tower and tie down system are examples of components which need individual attention for preliminary design and coupled analysis for final design.

Current Activities

The above describes the basic elements of Sandia's VAWT structural program as it has evolved over the past several years. While many of the general activities are continuing, current activities are largely directed toward design and evaluation of the forthcoming 17-m turbine. Kaman Aerospace Corporation, Bloomfield, Connecticut is supplying the blades for this turbine, [7]. Evaluation and performance limit definition of these blades is receiving considerable attention, as is the system analysis of frequencies, mode shapes and modal participation. These results may influence final selection of operating speeds and wind conditions. Other activities commensurate with the 17-m erection schedule include component design and evaluation, turbine imbalance evaluation, [5] and analysis of blade instabilities, [4].

CONCLUDING REMARKS

Even with an extensive and inclusive structural analysis and evaluation program, there are always uncertainties associated with the actual performance of the hardware. If this were not true, production line hardware could be manufactured directly from the designer's desk without the need for mock ups, prototype and other developmental test bed hardware. Practical experience, however, has demonstrated the advantages of complimentary experimental and theoretical efforts, particularly when advanced hardware and technology is involved. Uncertainties associated with the 17-m turbine include modal excitation response,

blade and system instabilities, fatigue characteristics, aerodynamic loads and design (cost) evaluation. Through field experience with the 17-m turbine and a related analytical program, these uncertainties will be transformed to understood phenomonology.

REFERENCES

1. Sullivan, W. N., "Structural Loads", Proceedings of the Vertical Axis Wind Turbine Technology Workshop, May 18-20, 1976, Albuquerque, N.M.

2. Weingarten, L. I., "Blade Structural Analysis", Ibid.

3. Biffle, J. H., "System Structural Response", Ibid.

4. Ham, N. D., "Aeroelasticity", Ibid.

5. Rodeman, R., "The Effects of System Imbalance", Ibid.

6. Reuter, R. C., Jr., "Tower Analysis", Ibid.

7. Barzda, J., "Blade Design and Fabrication - 17-m", Ibid.

Structural Loads for the 17m Darrieus Turbine

W. N. Sullivan, Sandia Laboratories

The main purpose of the structural load effort at Sandia is to provide a realistic load input to the structural analysis programs which have been developed to examine the 17m turbine. There are three major load systems which act on this turbine: gravitational, centrifugal, and aerodynamic. This paper will consider only the aerodynamic loads, as the gravitational and centrifugal loads are well understood and can be routinely input to an analysis.

The aerodynamic loads given in the following figures were calculated using the single streamtube* aerodynamic model. More recently, the more sophisticated multiple streamtube model, including local Reynolds number variation along the blade, has been applied to calculate loads. Preliminary results with the new model suggest that the loads predicted by the single streamtube model are too high by as much as 50%, although the cyclic variations are qualitatively accurate. For future calculations, we intend to put more reliance on the multiple streamtube model.

We believe that the loads predicted by either the multiple or single streamtube model do reflect the major aerodynamic loads acting on the turbine. However, certain effects are lost in the model simplifications and assumptions. These lost effects include tower and blade shadows, perturbations due to vortex shedding, and dynamic blade stall effects. Future efforts are planned for quantifying the significance of these simplifications.

* See the "Sandia Vertical Axis Wind Turbine Program Technical Quarterly Report" SAND76-0036 for additional details.

Blade Loadings

Figure 1 shows the maximum magnitudes of aerodynamic forces in the in-plane (in the plane defined by the blade and the turbine axis, directed normal to the blade--these are also referred to as "flap" forces) and out-of-plane (normal to the in-plane forces--also referred to as "lead-lag" forces) directions. The magnitudes shown are for that portion of the blade at the maximum distance from the axis of rotation. The blade loads decay approximately linearly with radius as the turbine hub is approached.

The time dependence of the blade loads is demonstrated in Figure 2 in terms of the net radial force (F_2) and twisting moment (M_1) resultants at the blade root. By normalizing these resultants with respect to their maxima over a cycle, the curves become a function only of the tip speed ratio. The erratic behavior of the loads for tip speed ratios less than 3 is due to the periodic stalling of the blades.

Tower Resultants

The net force resultants on the tower are easily obtained by summing the root loads from the individual blades. The direction and cyclic variation of the downwind tower force resultants are represented by the polar plots in Figs. 3 & 4, for three and two-bladed turbines, respectively. The radial coordinate of these traces represents the relative magnitude and direction changes of the tower force resultant during rotation. It is noteworthy that the three-bladed turbine at tip speed ratios greater than 3.0 has an essentially constant force resultant. The peak magnitudes of the force resultants are summarized in Fig. 5.

The net twisting moment on the tower also varies considerably with rotational angle, except for the three-bladed turbine at tip speed ratios above three. The twisting moment variations are summarized in Figures 6 and 7.

Conclusion

The aerodynamic models currently available provide a reasonable starting point for defining the appropriate loads seen by the turbine structure. More refinements would be desirable, coupled with experimental data from operating turbines to ensure that the load models contain all the most important effects.

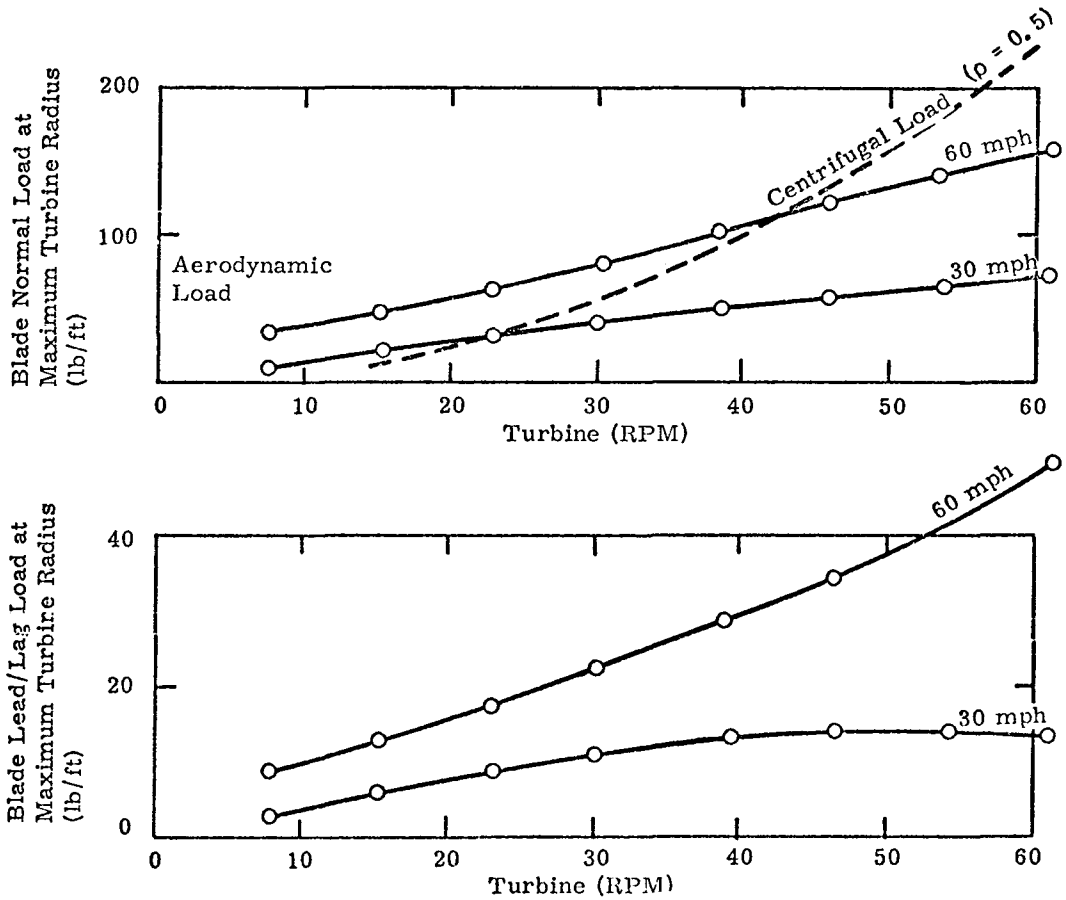

Figure 1. Aerodynamic and Centrifugal (For Blade Specific Gravity of .5) Blade Loads.

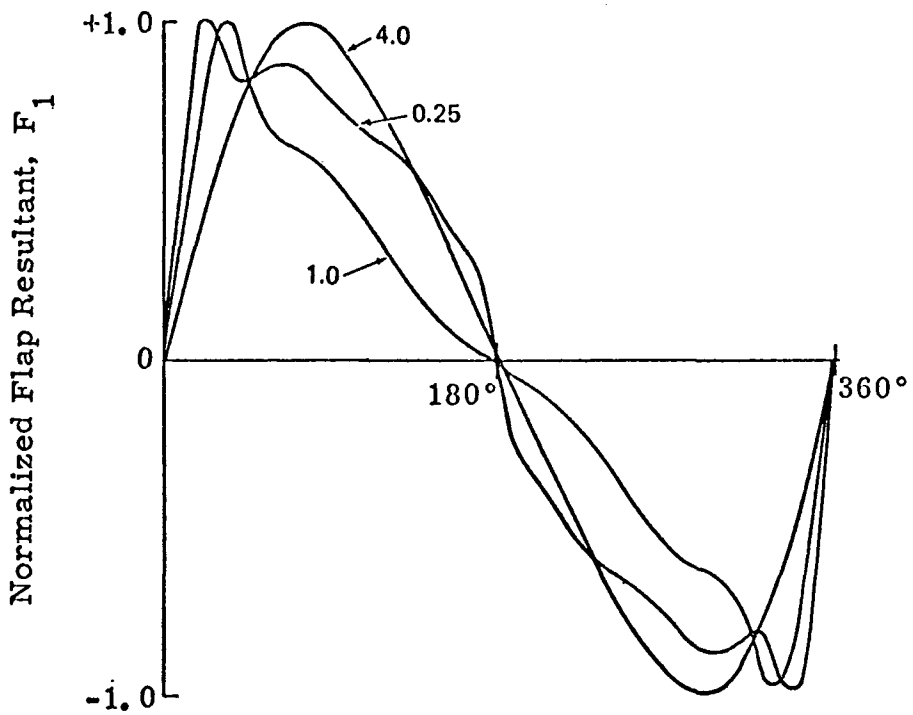

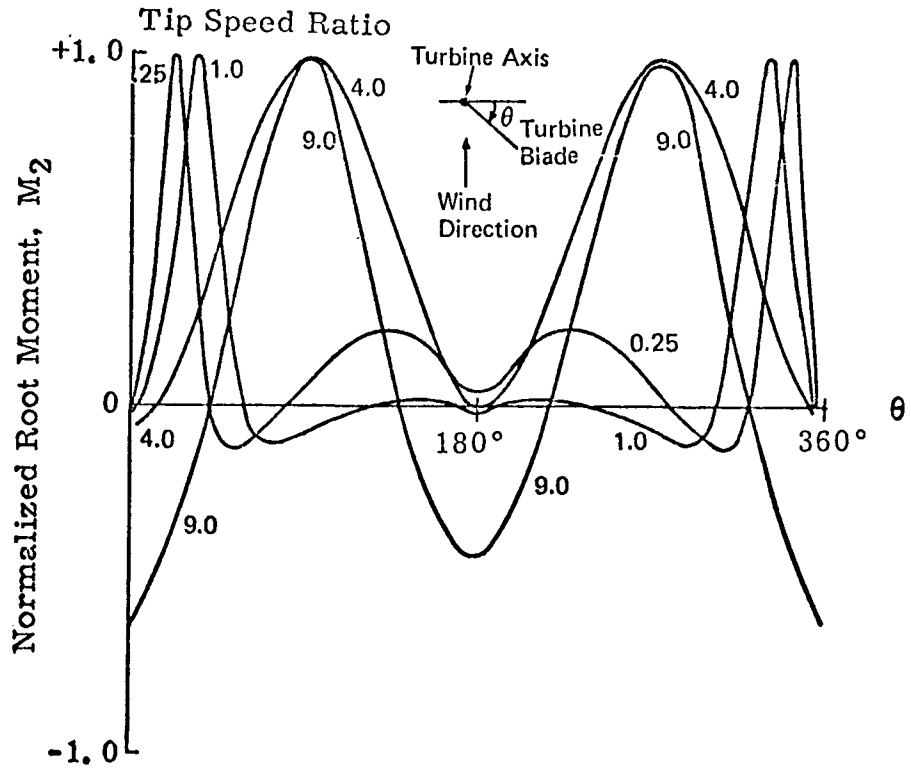

Figure 2. Blade Root Resultants, Demonstrating Time Variations of Blade Loads Due to Turbine Rotation

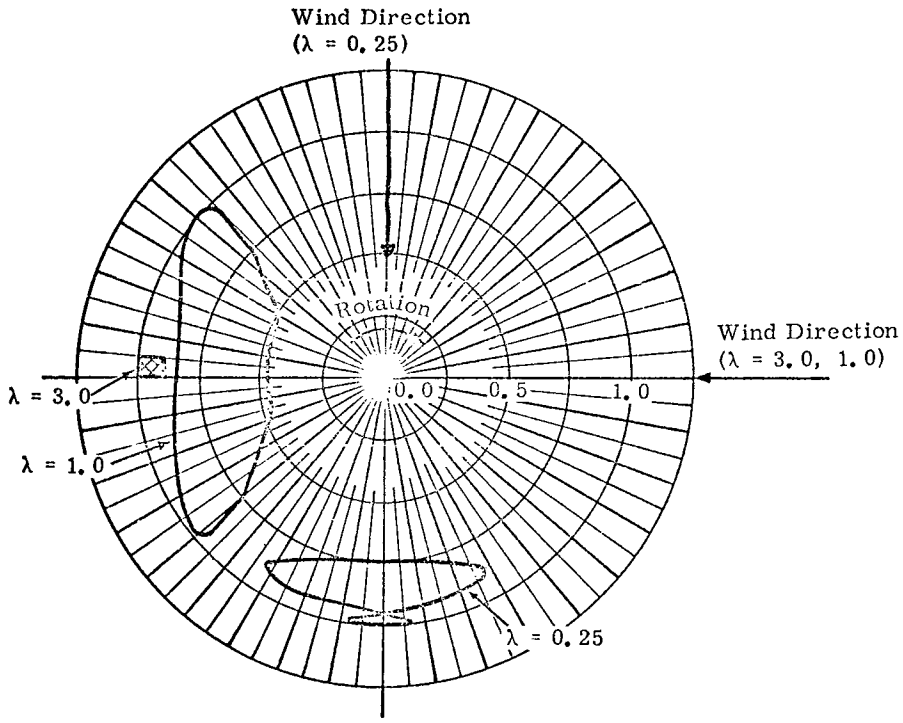

Figure 3. Force Polars for Three-Bladed Rotor

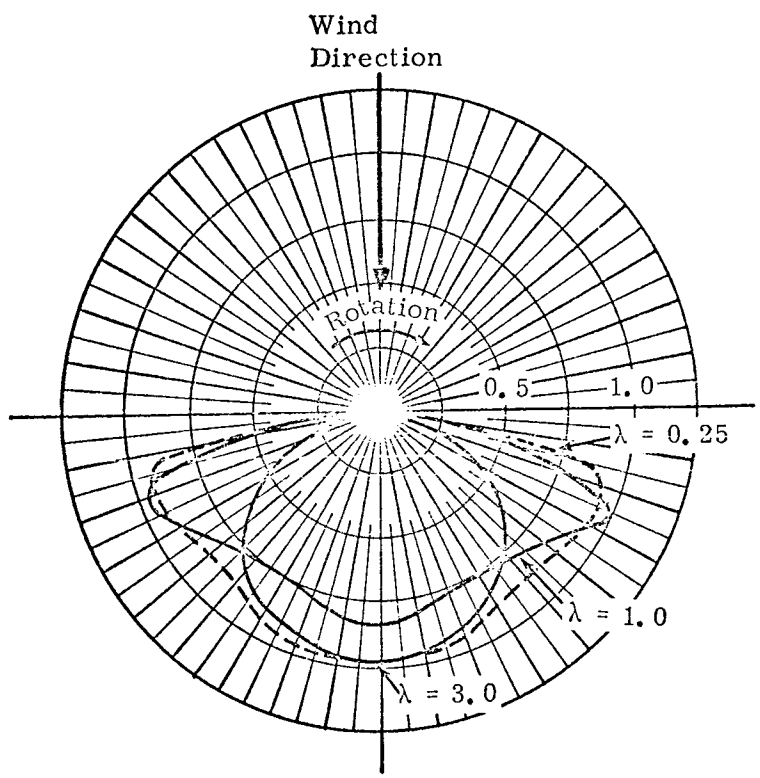

Figure 4. Force Polars for Two-Bladed Rotor

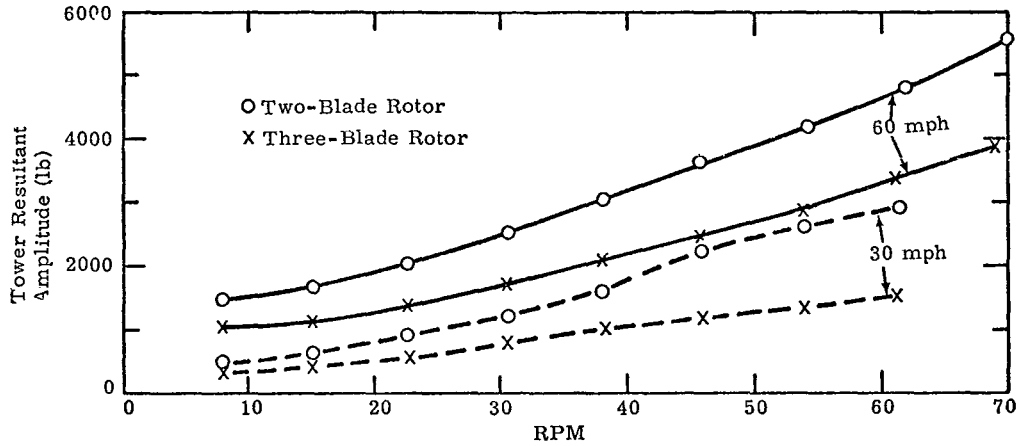

Figure 5. Tower Resultant Magnitude

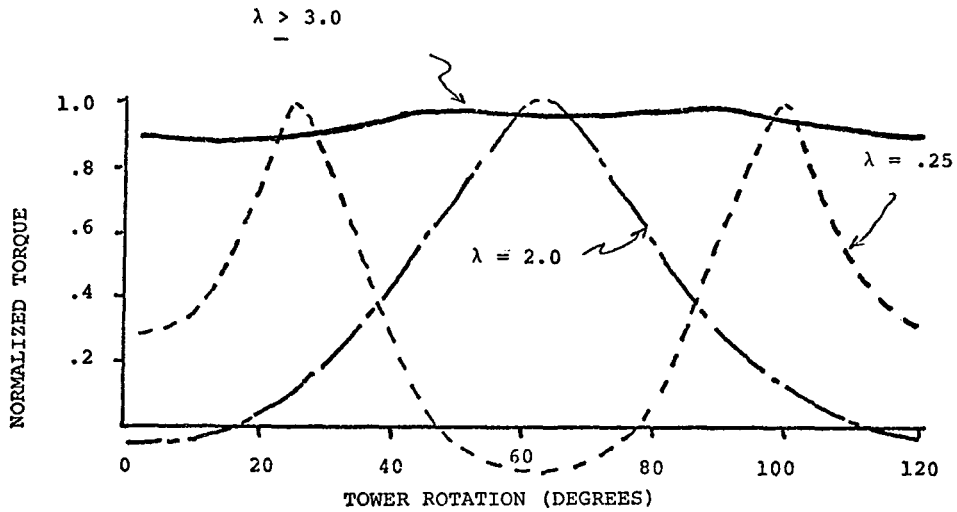

Figure 6. OUTPUT SHAFT TORQUE VARIATIONS - THREE-BLADE DARRIEUS ROTOR

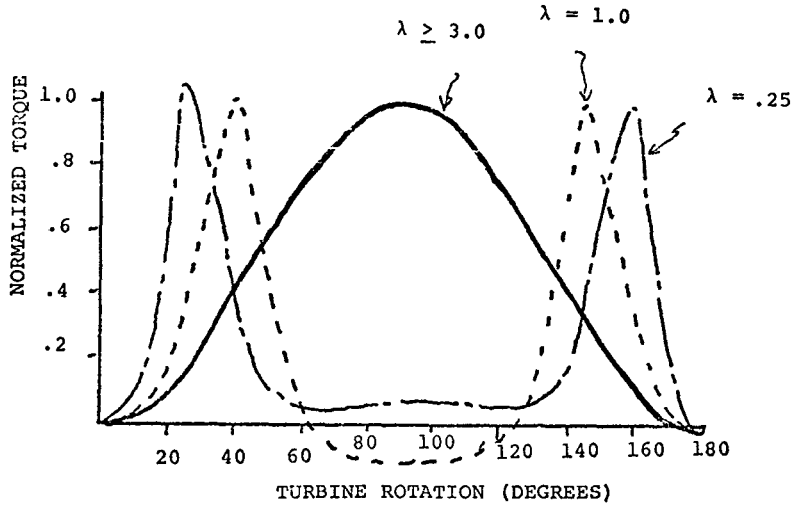

Figure 7. OUTPUT SHAFT TORQUE VARIATIONS - TWO-BLADE DARRIEUS ROTOR

BLADE STRUCTURAL ANALYSIS

L. I. Weingarten & D. W. Lobitz

Sandia Laboratories

INTRODUCTION

Vertical-axis wind turbine blade structural analyses have been conducted at Sandia Laboratories since mid-1974. The initial motivation was the necessity to determine the effect of a non-troposkien shaped blade on the stress distribution. The 5-meter wind turbine built by Sandia during 1974 had blades constructed of two straight and one circular-arc section which was a small deviation from the troposkien. It had been shown previously (Reference) that the stresses in a troposkien were completely tensile under the action of only centrifugal forces. An early version of the general purpose, nonlinear, finite element code, MARC, was used to simulate behavior for a wide range of turbine rotational speeds. A significant result was that the stresses in the blade were not purely tensile but did have significant bending stresses. In fact, onset of material yielding as a result of bending was predicted at a speed slightly over 300 RPM. Consequent examination of the blades, which had been run up to approximately 375 RPM, showed a small permanent deflection in the portion predicted by the code. Since that time this code has been used to predict stresses and natural

frequencies of the blades of various wind turbine models, including, the wind tunnel model and the 17-meter turbine.

FINITE ELEMENT CODE CAPABILITY

As previously stated, the primary workhorse in the structural analyses of the blades has been the general purpose finite element code, MARC. Two different beam elements were selected from the element library to carry out this analysis. The first, a curved beam element with four degrees of freedom (two displacements and two rotations) at each node, was used for analyses where motion occurred only in the plane of the blade.* For motion involving combined in-plane and out-of-plane deformations, a straight beam element with six degrees of freedom (three displacements and three rotations) at each node was used. Using the nodal point tying features of MARC, models of the hinges present in the blade assembly were formed. The large displacement capability of this code which incorporates the effects of geometric nonlinearities was utilized to, among other things, accurately model the centrifugal stiffening in the blades. The natural frequencies and corresponding mode shapes of the blades were obtained through the use of a package for eigensystem analysis which exists in the code.

---

* For the purpose of this paper, in-plane motion is defined as motion in the plane formed by the tower axis and the locus of the centers of gravity of the blade cross-section. Out-of-plane motion is motion in the plane of rotation.

The finite element model loading initially consisted of only centrifugal forces. Later the effects of gravity and aerodynamic forces normal to the chordline were incorporated. These forces produce motion only in the plane of the blade. Presently, the finite element model has been extended to include out-of-plane motion resulting from out-of-plane aerodynamic loads.

ANALYSIS DETAILS

The analysis presented in this paper addresses the blade which is being designed and built by Kaman for Sandia's 17-meter wind turbine. As shown in Figure 1, the blade consists of two straight sections and a center circular section. Struts are included between the blade and the shaft to provide additional support. The geometric properties used in the analysis are also given in Figure 1. The struts have the same cross-section as the blade, which is shown in Figure 2. The load-carrying portion of the blade is a 6061-T6 aluminum leading-edge D-section and trailing-edge spline. The cross-section is described in more detail elsewhere in the workshop by J. Barzda of Kaman. The material and elastic properties of this blade are tabulated in Table I.

EI_1 (flatwise flexural stiffness)	31.63×10^6 lb-in^2
EI_2 (chordwise flexural stiffness)	1246×10^6 lb-in^2
EA (longitudinal stiffness)	52.16×10^6 lb
W (linear density)	0.572 lb/in
GJ (torsional stiffness)	25.06×10^6 lb-in/rad.

TABLE I - BLADE ELASTIC PROPERTIES

To date, the blade structural analyses include the following loading configurations:

1) O RPM, O MPH wind,gravity included

2) O RPM,150 MPH wind,gravity included

3) 52.5 RPM, 60 MPH wind, gravity neglected (normal operating condition)

4) 75 RPM, 80 MPH wind, gravity neglected (runaway condition)

The blade deflections for the first configuration are shown in Figure 3. The ground is to the left in the figure and deflections are magnified by a factor of 10. The maximum stresses are approximately 1700 psi which are well below yield.

The second loading configuration represents severe gust loading with the wind turbine in a parked mode.

Figure 4 shows the deflection for an inward-directed 150 mph wind. The deflection shown is actual. Stresses induced in the blade and struts are high, the maximum being approximately 20000 psi, but are less than yield. However, there are large compressive forces in the straight sections, which may lead to a buckling problem. This is presently being studied and it may provide an upper limit for a gust which the turbine can withstand.

As outlined, the third and fourth loading configurations neglect gravity. Without gravity the blade model can be simplified since by symmetry considerations only half the blade need be modeled.

An investigation was performed on a blade rotating at 75 RPM (a runaway condition), with and without gravity to determine the effects of this omission. Results showed that there was less than 10% difference in maximum stresses. This indicates that for relatively high rotational speeds, gravity can be neglected.

Results presented here for the third and fourth loading configurations are restricted to the blades assembly with struts. One reason for this is that analyses of blade models without struts indicated that stresses in the spline of blade, caused by out-of-plane loads, were well above the yield point of 6061-T6 aluminum. The inclusion of the struts alleviates these high stresses as is shown in Table II.

In each case, quasi-static analyses were completed for three different blade positions. The first designated by (C-A) corresponds to the point in the cycle where the aerodynamic forces are maximal with the radial component directed in the opposite direction of the centrifugal forces. The symbol (C + A) denotes the case where the aerodynamic forces are also maximal, but the radial component is in the direction of the centrifugal forces. The position designated by (C) corresponds to the case where aerodynamic forces are zero.

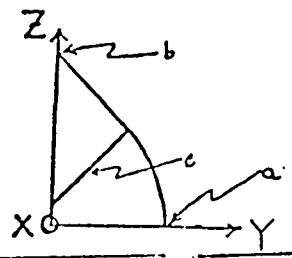

LOAD CONDITION	X DISP. PT. a (in.)	Y DISP. PT. a (in.)	Z TWIST PT. a (deg.)	MAX. STRESS (Ksi.)	MAX. STRESS LOCATION
52.5 RPM, 60 MPH					
I) C - A	5.29	0.60	-2.15	16.52	b
II) C + A	4.66	1.42	-1.84	16.56	b
III) C only	0.00	1.09	0.00	9.51	c
75 RPM, 80 MPH					
I) C - A	9.16	1.14	-3.73	29.11	b
II) C + A	7.38	2.40	-2.85	28.05	b
III) C only	0.00	1.97	0.00	16.18	c

TABLE II - Example Deformation & Stress Results

For the normal operating condition in Table II (52.5 RPM, 60 MPH) the maximum out-of-plane displacement is 5.29", with a corresponding angle of twist of -2.15°. Deformations of this magnitude are not thought to significantly degrade turbine performance, although further attention is being devoted to this area. A maximum stress of 16.56 Ksi occurs at the root of the blade in the splines. The stress at this point varies from this maximum down to a minimum stress of 1.04 Ksi twice per cycle. Using this data along with similar results for other operational speeds and winds, life cycle estimates for a particular wind turbine site can be obtained.

For the runaway condition, (75 RPM, 80 MPH) performance degradation is not an issue, nor is fatigue since the number of cycles at this condition is assumed to be low. The main concern is that blades do not yield. The results shown in Table II show the maximum stress to be less than the yield value of 35 Ksi for 6061-T6.

The results for these last two loading configurations are thought to be on the conservative side. For example, the aerodynamic loads used do not take into account Reynolds number effects which may reduce the loads by as much as a factor of two. Also, the aerodynamic loads are actually dynamic and the blades may not have time to respond fully to these time-varying forces.

Dynamic results predicted by the MARC code are depicted in Figures 5, 6, and 7. These results are restricted to motion in the plane of the blade. The blade analyzed has similar, but not identical, properties as that of Figures 1 and 2. The purpose here is to show the stiffening effect of the struts. Figure 5 shows the lowest two frequencies and corresponding mode shapes for an unstruted blade. Figure 6 corresponds to the similar modes in a struted blade. The effect of struts in increasing blade stiffness is readily apparent. However, the presence of struts introduces two additional modes corresponding to principally strut motion. For this design, they occur at about 3.6 and 3.8 Hz, as seen in Figure 7. Still, the presence of struts increases the lowest natural frequency for in-plane motion by approximately a factor of two.

The preliminary results presented in this paper show that a software capability exists for analyzing the struted and unstruted blades for Sandia's vertical-axis wind turbine. They also show that the Kaman-designed blades are structurally adequate for the loading conditions addressed. However, further analyses are planned to provide more insight into the structural adequacy of the blades for these as well as other loading conditions. These include fatigue and buckling studies.

Reference

Blackwell, B. F., and Reis, G. E., "Blade Shape for a Troposkien Type of Vertical-Axis Wind Turbine," SLA-74-0154, Sandia Laboratories, Albuquerque, New Mexico, 1974.

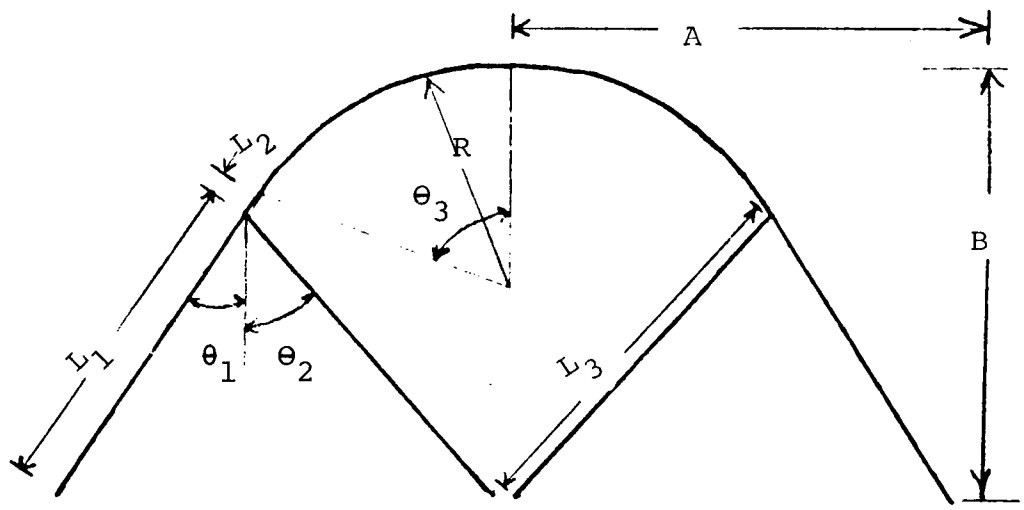

R	=	220.0 in	L_3	=	272.07 in
A	=	329.24 in	θ_1	=	33.24°
B	=	325.47 in	θ_2	=	41.12°
L_1	=	245.07 in	θ_3	=	56.76°
L_2	=	13.0 in			

Distance from blade attachments to tower centerline = 14 in

FIGURE 1 -WIND TURBINE BLADE GEOMETRY

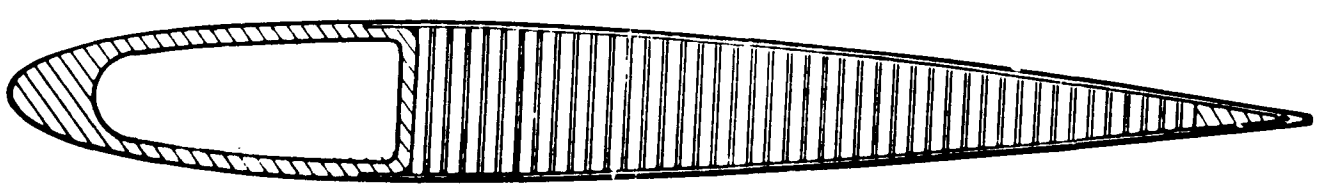

FIGURE 2 - KAMAN BLADE CROSS-SECTION

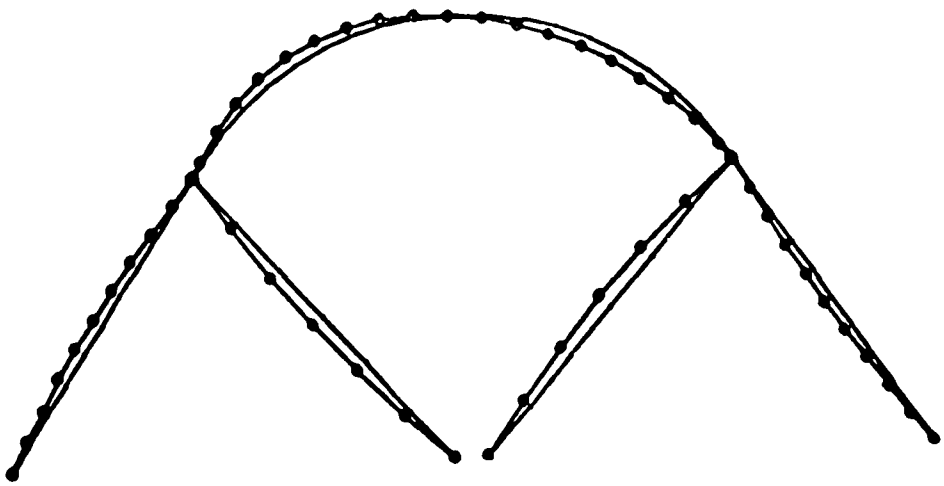

DEFLECTION (10X)

O RPM-GRAVITY

FIGURE 3 - NON-ROTATING IN-PLANE DEFORMATION

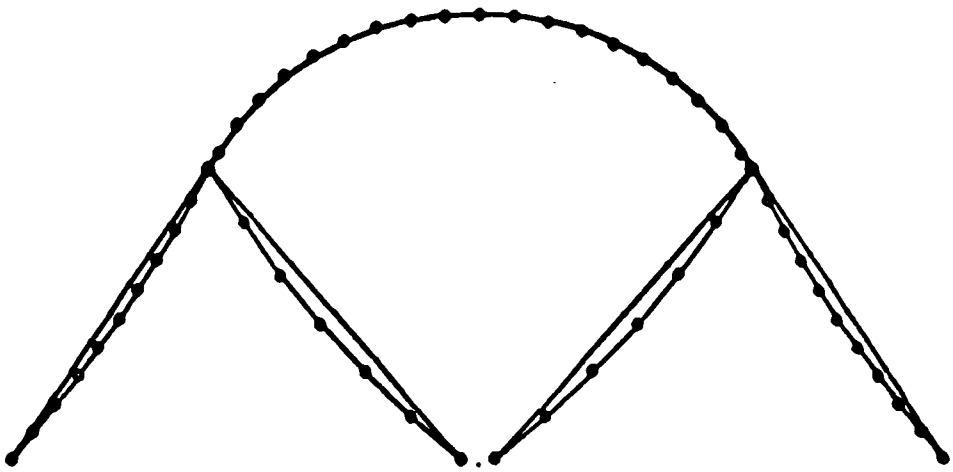

DEFLECTION

O RPM-GRAVITY-150 MPH WIND, DIRECTED TOWARDS TOWER

FIGURE 4 - NON-ROTATING IN PLANE DEFORMATION WITH SEVERE GUST

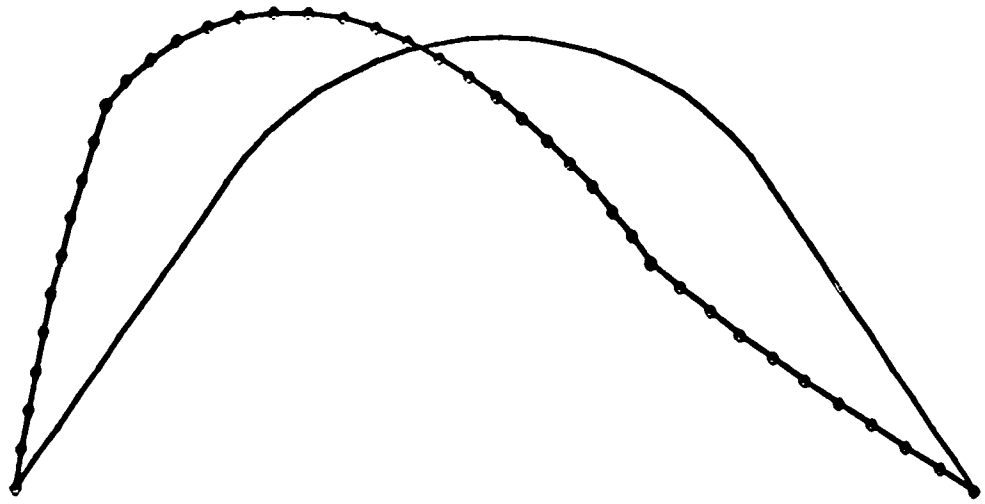

1.931 Hz - 75 RPM - NO STRUTS

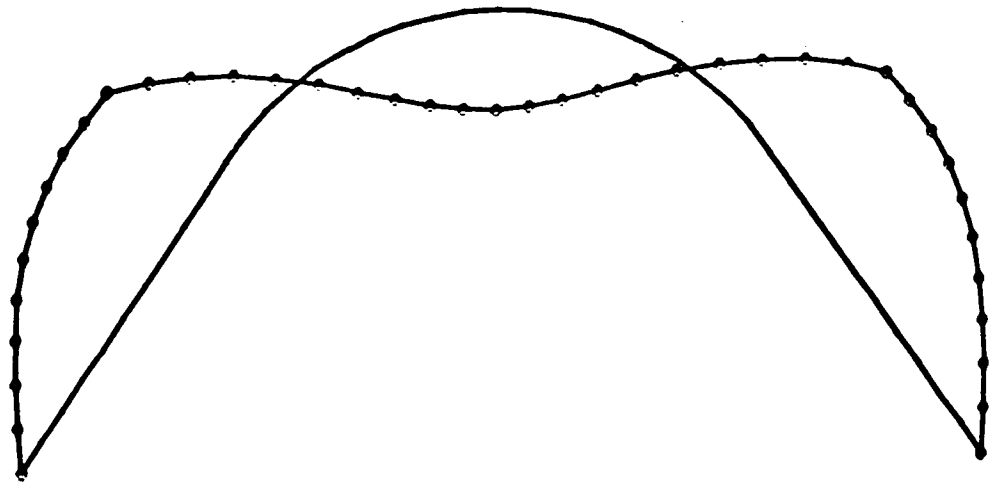

3.694 Hz - 75 RPM - NO STRUTS

FIGURE 5 - UNSTRUTED BLADE MODES AND NATURAL FREQUENCIES

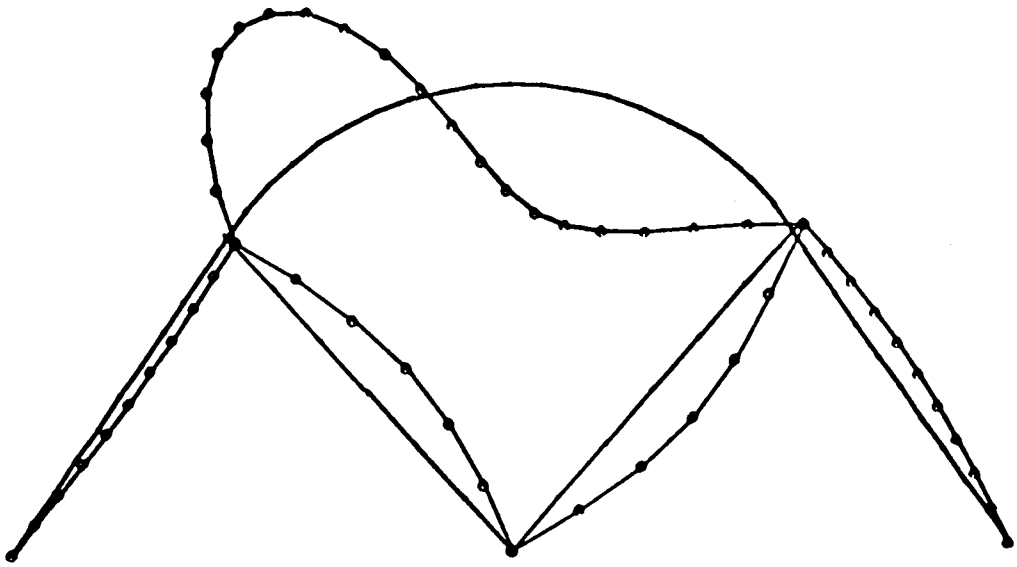

5.461 Hz - 75 RPM - STRUTS

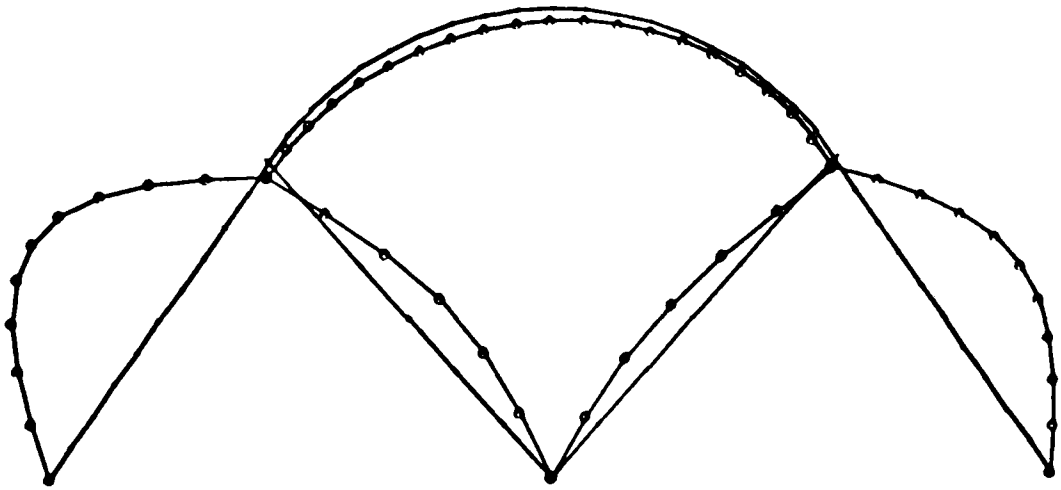

6.322 Hz - 75 RPM - STRUTS

FIGURE 6 - STRUTED BLADE MODES AND NATURAL FREQUENCIES

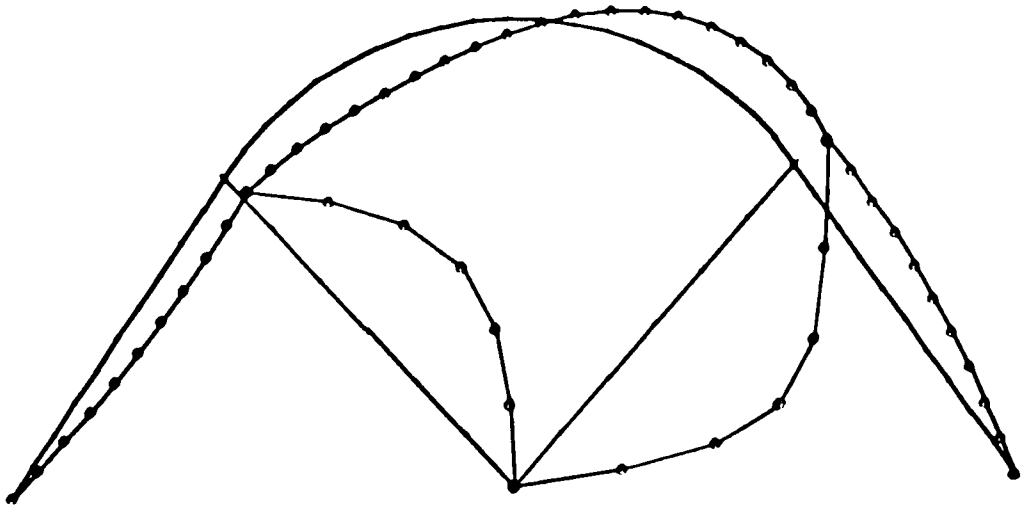

3.604 Hz - 75 RPM - STRUTS

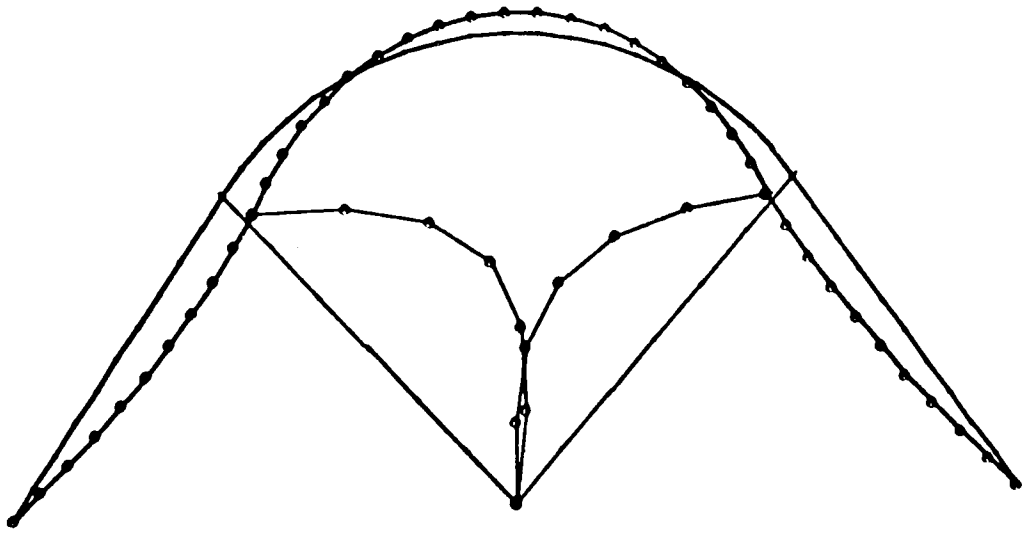

3.797 Hz - 75 RPM - STRUTS

FIGURE 7 - STRUTED BLADE MODES AND NATURAL FREQUENCIES

Question:

What effect would icing have on the blades?

Answer:

The ice would act as added mass but no structural stiffening to the blade. Results to date show a large margin of safety in the Kaman blades for gravity induced stresses, so that icing should not effect present design. The effect of icing during operation could be more significant because the ice will effectively change the airfoil shape and resultant stresses due to aerodynamic loads.

TOWER ANALYSIS

Sandia Laboratories

R. C. Reuter, Jr.

NOMENCLATURE

d	truss tower element diameter
D_i	tubular tower inside diameter
D_o	tubular tower outside diameter
$\overline{D}$	D_i/D_o
E	Young's modulus
G	shear modulus
ℓ	truss tower bay length
L	total tower length
R	truss tower radius
W_{tu}	weight of tubular tower
W_{tr}	weight of truss tower
α	angle formed by intersection of truss tower cross brace elements with horizontal plane
ρ	weight density of tower material

TOWER ANALYSIS

Introduction

During the course of Sandia Laboratories' wind energy program, two wind turbines have been built and operated with no apparent problems resulting from blade support tower design. The smaller turbine, a two meter model, has a prismatic, triangular cross section truss tower, and the larger one, a 5 meter turbine, has a tubular tower. Since no sustaining problems have arisen from either tower design, the rationale for selection of a truss tower or tubular tower is still uncertain. The purpose of this report is to enhance tower selection rationale by establishing some design guidelines for VAWT blade support towers, and to review the specific design for the tower of the forthcoming 17 meter turbine.

A review of the requirements placed in a VAWT blade support tower reveals that they must, 1) support axial, torsional and bending loads, and 2) have axial, torsional and bending stiffness components high enough to minimize deflections and maximize natural frequencies. Axial loads are a result of axial components of centrifugal and aerodynamic forces at the blade roots, axial components of tie-down loads, tie-down hardware weight and blade weight. Torsional loads are due primarily to chordwise aerodynamic loads on the blades and flexural loads result from radial components of centrifugal and flat wise aerodynamic blade loads and tower drag. In addition to implying strength and buckling requirements, these loads are time varying and, therefore, represent potential forcing functions for natural modes of vibration of the tower. Since it is undesirable to have turbine component or system natural modes at or near operating frequencies, it is necessary to impose stringent stiffness requirements on the turbine components. In this way, vibrations during start-up and operation are minimized.

In addition to satisfying strength and stiffness requirements, the blade support tower must be as light weight, inexpensive and as pleasing to look at as possible.

In order to develop tower selection rationale, comparisons are made first between a truss and tubular tower on the basis of equivalent stiffness components. The initial objective is to minimize weight. The truss towers are always prismatic, triangular cross-section space frames with cross bracing in one direction only, as illustrated in Figure 1. This configuration was selected for several reasons: 1) it is similar to an existing turbine tower (2 meter model), 2) to minimize costs, towers must be as simple as possible, and 3) general conclusions will not change with truss tower construction changes. The material used is steel because of relatively low cost and essentially constant strength and stiffness to weight ratios compared to lighter weight materials.

Analysis & Numerical Results

In order to perform numerical evaluations of tubular and truss tower stiffness components, it is necessary to express these quantities in terms of the design parameters. For the tubular tower the axial, torsional and flexural stiffness components respectively are given by

$$\left(\frac{EA}{L}\right)_{tu} = \frac{E\pi D_o^2(1 - \bar{D}^2)}{4L} \qquad (1)$$

$$\left(\frac{GJ}{L}\right)_{tu} = \frac{G\pi D_o^4(1 - \bar{D}^4)}{32L} \tag{2}$$

$$(EI)_{tu} = \frac{G\pi D_o^4(1 - \bar{D}^4)}{64} \tag{3}$$

where the subscript, tu, designates tubular. Stiffness components for the truss tower are considerably more complicated because of the larger number of design parameters and the complicated way that truss elements interact. Expressions for the truss stiffness components were derived using beam theory and elementary principles of elasticity; these derivations will be treated under separate cover. The axial, torsional and bending stiffness components for the truss tower are

$$\left(\frac{EA}{\ell}\right)_{tr} = \frac{3EA}{\ell} + \frac{36EI\cos^3 a\left[\left(\frac{\ell^2 A}{12I}\right)(1 + \cos a) + \sin^2 a\right]}{\ell^3\left[\left(\frac{\ell^2 A}{12I}\right)\sin^2 a\cos a + \cos^4 a(1 + \cos a) + \sin^2 a(1 + \cos^2 a)\right]} \tag{4}$$

$$\begin{aligned}\left(\frac{GJ}{\ell}\right)_{tr} = {} & 3\left[1 + \left(\frac{4EI\tan^2 a}{GJ}\right)\right]\frac{GJ}{\ell} \\ & +3\left\{\frac{\left[\left(\frac{A\ell^2}{12I}\right)\sin^2 a + \cos^3 a(1 + \cos a)\right]}{\left[\left(\frac{A\ell^2}{12I}\right)(1 + \cos^3 a) + \sin^2 a\cos^3 a\right]}\left(\frac{EA\ell^2}{GJ}\right)\frac{\tan^2 a}{12}\right. \\ & \left. + \left[\cos^2 a + \left(\frac{EI}{GJ}\right)^2\sin^2 a\right]^{\frac{1}{2}}\sin(90 - \beta + a)\right\}\frac{GJ\cos a}{\ell}\end{aligned} \tag{5}$$

where $\beta = \tan^{-1}\left(\frac{EI\tan a}{GJ}\right)$

$$(EI)_{tr} = 3EI\left[2 + \frac{13}{3}\tan^2 a\left(\frac{\ell}{d}\right)^2\right] \tag{6}$$

where $A = \frac{\pi d^2}{4}$, $I = \frac{\pi d^4}{64}$, $J = \frac{\pi d^4}{32}$ and the subscript, tr, designates truss. The truss radius, R, and bay length, ℓ, are related by

$$R = \frac{\ell \tan a}{\sqrt{3}}$$

Since tower weights are also of concern, they are included as

$$(W)_{tu} = \frac{\pi D_o^2 \rho L}{4} \left(1 - \bar{D}^2\right) \tag{7}$$

$$(W)_{tr} = \frac{3A \rho L}{4} \left(1 + \frac{1}{\cos a} + \tan a\right) \tag{8}$$

where L is the total tower length and will be an integral number of truss bay lengths.

Numerical comparisons of the tubular and truss tower are made by selecting a truss geometry, calculating one of the stiffness components, e.g. the axial component, equating the tubular stiffness expression to this result and calculating the tubular geometry necessary to achieve an equivalent stiffness component. These tubular and truss tower geometries are then used in (7) and (8) and the ratio, $(W)_{tu}/(W)_{tr}$ is formed. Results are presented with this ratio as the dependent variable (on the ordinate) and the particular stiffness of interest as the independent variable (along the abscissa). This produces a numerical relationship between the ratio of the weights of tubular and truss towers that have equivalent stiffness components, and the value of the stiffness. Families of curves are generated by varying truss tower geometry. The process is repeated for each component of stiffness. Figures 2, 3, and 4 show results for the axial, torsional and flexural stiffness components, respectively. Three truss element diameters and three bay lengths are considered in each figure. Stiffness changes are accomplished by varying the truss radius as indicated schematically in each figure.

Figure 2 demonstrates that for any axial stiffness required, a tubular tower will always weigh less than a truss tower with an equivalent stiffness. Therefore, if total weight is of primary concern, towers designed by axial stiffness requirements should be tubular.

Conclusions drawn from Figures 3 and 4 are the reverse of the above. For equivalent torsional stiffnesses or equivalent flexural stiffnesses, a truss tower can always be designed which will weigh less than the equivalent tubular tower. In some cases the weight savings is substantial. Therefore, if total weight is of primary concern, towers designed by torsional or flexural stiffness should be truss towers.

Often, as in the case of the vertical axis wind turbine, total tower weight is not the only concern. Size (diameter) is also important. Figures 5 through 9 display relationships between tubular and truss tower sizes when particular stiffness components are equal. For these results, $\bar{D}$ of the tubular tower is taken as 0.9.

Figure 5 shows how the tubular tower diameter varies with the truss tower radius, for various truss element diameters, when the two towers have equal axial stiffnesses. Results are practically independent of bay length, except at small R, because the cross bracing becomes ineffective as R/L becomes large. This also causes the independence of D_o as R increases.

Figures 6, 7, and 8 display the dependencies of D_o upon R for three truss element diameters when the towers have equal torsional stiffnesses. Results depend somewhat upon bay length, but the major observation is that truss radius increases very quickly with tubular diameter. In other words, the radius of a truss tower is very large compared to the diameter of a tubular tower with the same torsional stiffness. Similar conclusions are drawn from the results shown in Figure 9 where the dependence of D_o upon R is illustrated for towers with equal bending stiffnesses. Three truss element diameters are considered and results are independent of bay length.

General conclusions thus far suggest that if tower design is controlled by axial stiffness requirements, tubular towers are favored for minimum weight with no particular advantage or penalty concerning size. If tower design is controllea by torsional or flexural stiffness requirements, truss towers offer a considerable weight savings over equivalent tubular towers at the expense of size.

17 Meter Tower Design

In the design of the blade support tower for the Sandia 17 Meter VAWT, tower size (diameter) is a concern if it becomes too large. A large diameter tower would consume blade length near the axis of rotation (and thus narrow the C_p curve), result in greater wind blockage and possibly become unsightly. It is necessary, then, to specify stiffness requirements for the 17-m turbine, design a tubular and truss tower to meet these requirements and compare them on the basis of weight, size, and appearance. This process is typified by results given in Figure 10 where tubular tower weight is plotted versus tubular tower outside diameter, for various inside diameter-to-outside diameter ratios, $\bar{D}$. The intersecting curves labeled "bending" and "torsion" represent the minimum tower designs for insuring that the lowest bending and torsional modes are above 4.5 hz. This frequency, 4.5 hz, is the result of requiring that natural frequencies be at or above 3/rev plus 20% at a turbine speed of 75 rpm. If the tower is assumed to be pinned at both ends, its lowest bending frequency is given by

$$f_1 = 1.56 \left[\frac{gEI}{wL^4} \right]^{\frac{1}{2}}$$

where w is the tower weight per unit length and g is the acceleration of gravity. Solving for EI with $f_1 = 4.5$ gives

$$EI = \frac{8.32 w L^4}{g} \tag{9}$$

The "bending" curve in Figure 10 is obtained by finding tubular tower geometries ($\bar{D}$ and D_o) which satisfy (9) for a tower length of 55 ft.

The first torsional mode is assumed to be that which causes uniform twist in the tower. Half of the blade polar moment of inertia is lumped at the top and half at the bottom of the tower. The "torsion" curve of Figure 10 is obtained by finding tubular tower geometries ($\bar{D}$ and D_o) which satisfy

$$GJ = 40.5 \pi^2 L \bar{J}_B \tag{10}$$

where $\bar{J}_B$ is half the total polar mass moment of inertia of three turbine blades.

Any tubular tower with geometry corresponding to points to the right of the cross-hatched portions of the bending and torsion curves of Figure 10 will satisfy the bending and torsional stiffness requirements. These configurations represent an overdesign for axial stiffness. A minimum weight, tubular tower is selected from Figure 10, (i.e., $\bar{D} = 0.9$ and $D_o = 20$ inches) Refering back to Figures 6 through 9, it is seen that to achieve the same stiffnesses as the 20 in. O.D. tubular tower with a truss tower, a truss radius of approximately 60 inches would be required (extrapolation of Figure 8). This corresponds to a truss tower face width of approximately 9 feet.

Because of the large diameter (10 feet) of the circle circumscribing the truss tower required to meet the bending and torsional stiffness requirements, the tubular tower was selected for the 17-m turbine. The diameter of the required truss tower is approximately 18% of the diameter of the turbine, a number judged to be in excess of desirable.

With reference to Figure 10, the location of the "bending" and "torsional" curves are high, implying design conservatism. The bending stiffness requirement would be lowered in the event that the base of the tower is not pinned, but clamped (yet free to rotate about its axis). The torsional stiffness requirement would be lowered by considering that actually less than half the blade polar mass moment can be ideally placed at each end of the tower. These over specifications imply that a smaller, lighter weight tubular tower could be used to meet more rigorous requirements. This, however, is not the case when one considers not just the natural frequencies of the tower by itself, but what effect the tower stiffness has on other turbine component frequencies. Other major turbine components which are likely to have low, troublesome natural frequencies are the blades. Since the blades are attached directly to the tower, tower stiffness will affect blade frequencies, and visa versa. In order to determine the extent of this tower-blade coupling, a model analysis was performed on the turbine system [1]. Some of the results of this analysis are presented in Figure 11 where natural frequencies are plotted versus turbine speed, where the tower is characterized by $\bar{D} = 0.9$ and $D_o = 20$ inches. Since the design goal is to locate natural frequencies above the 3/rev line, the 20 inch tubular tower again appears as a minimum design. This conclusion is based on expected maximum operating speeds of 45-50 rpm.

The blade support tower for Sandia's 17-m VAWT will therefore be a steel, tubular tower with an outside diameter equal to 20 inches and a wall thickness equal to 1 inch. This tower is over designed for strength and buckling resistance as indicated by Figures 12 through 15. Figures 12 and 13 display column and wall buckling critical axial loads and torsional critical loads versus tubular tower diameter for various values of $\bar{D}$. Maximum axial load and torque expected in the tower are 4.0×10^4 lbs. and 3.0×10^5 in.-lbs., respectively. Figures 14 and 15 display critical axial, torsional loads and bending moments based on working stresses of 10^4 psi. A wide margin of conservatism exists.

Summary

These are many facets to the design of an inexpensive, effective and attractive blade support tower for a vertical axis wind turbine. A stiffness approach has been described in this report. This approach precluded any real concern for strength and buckling resistance because of inadvertent conservatism in these areas. The

major issue, once stiffness requirements were established, was whether to recommend a tubular or truss blade support tower. The general conclusion was that with design controlled by bending or torsional stiffness, a truss tower will provide the lightest weight structure. This weight savings, although potentially substantial, was accomplished at the expense of overall tower size. Since the truss tower necessary to meet the requirements of the 17 meter turbine was judged to be too large in diameter, a tubular tower was selected and sized.

---

[1] Biffle, J. H., "System Structural Responce", Proceeding of the Vertical Axis Wind Turbine Technology Workshop, May 18-20, 1976, Albuquerque, N.M.

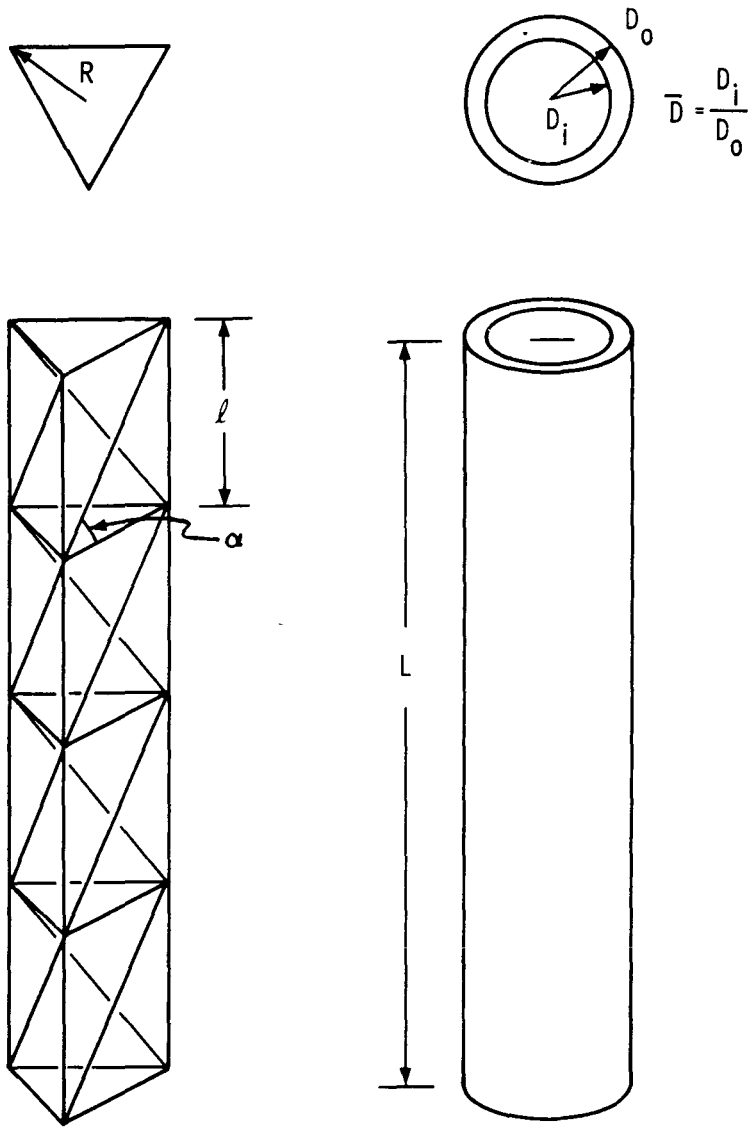

Figure 1. Tubular and Truss, Blade Support Tower Geometries.

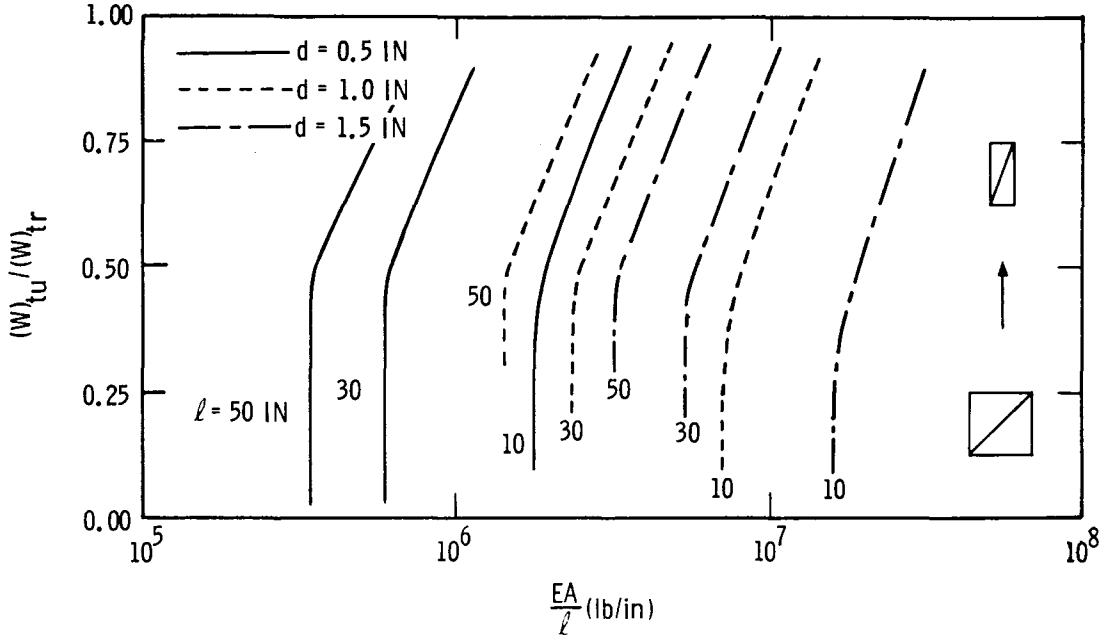

Figure 2. Ratio of the Weights of Tubular and Truss Towers Which Have Equivalent Axial Stiffnesses.

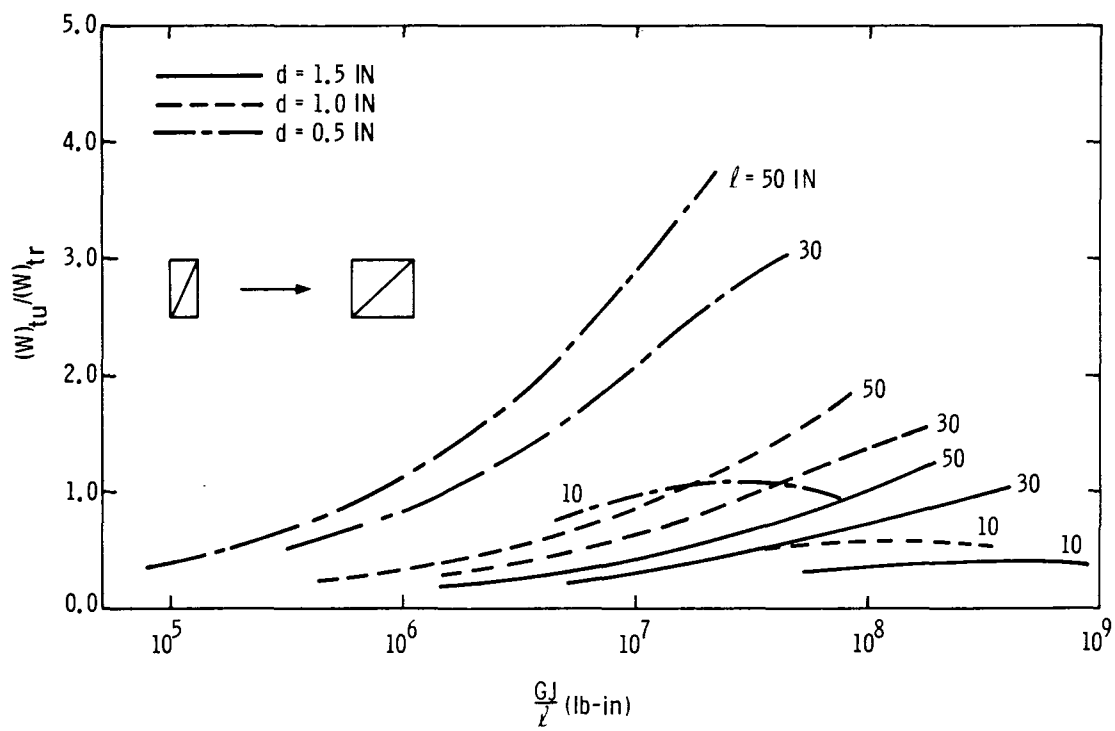

Figure 3. Ratio of the Weights of Tubular and Truss Towers Which Have Equivalent Torsional Stiffnesses.

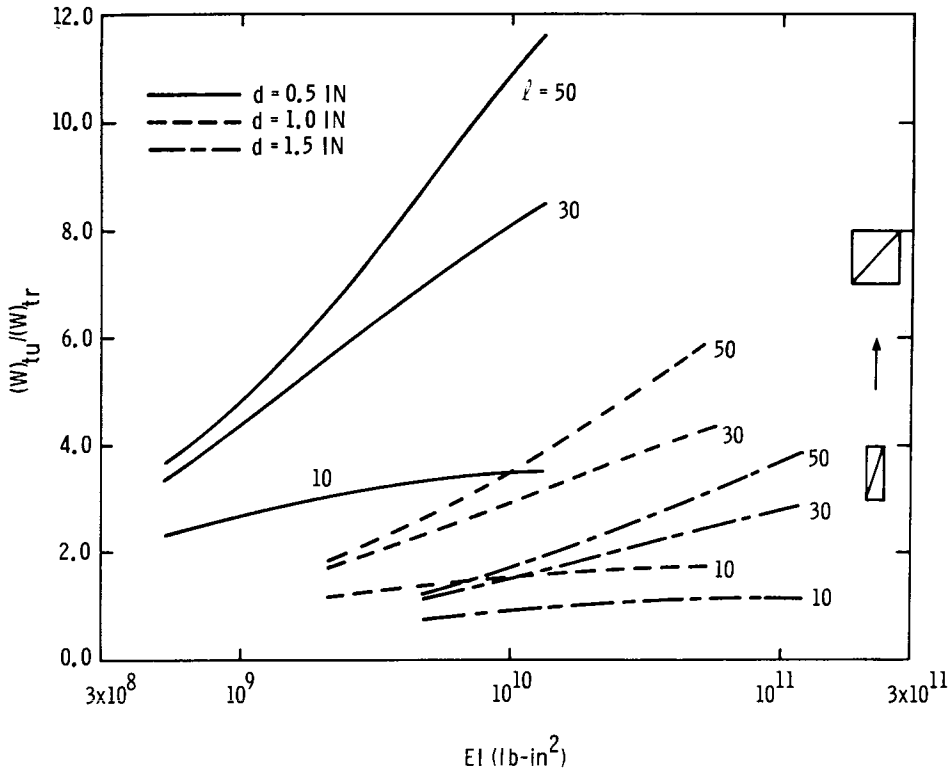

Figure 4. Ratio of the Weights of Tubular and Truss Towers Which Have Equivalent Bending Stiffnesses.

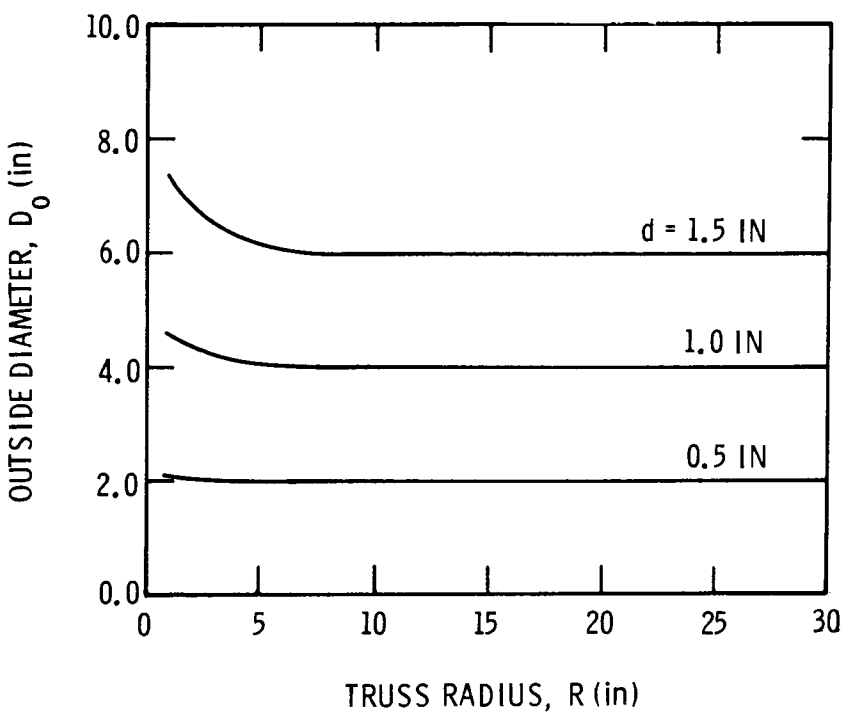

Figure 5. Relationship Between the Geometries of Tubular and Truss Towers that Have Equivalent Axial Stiffnesses.

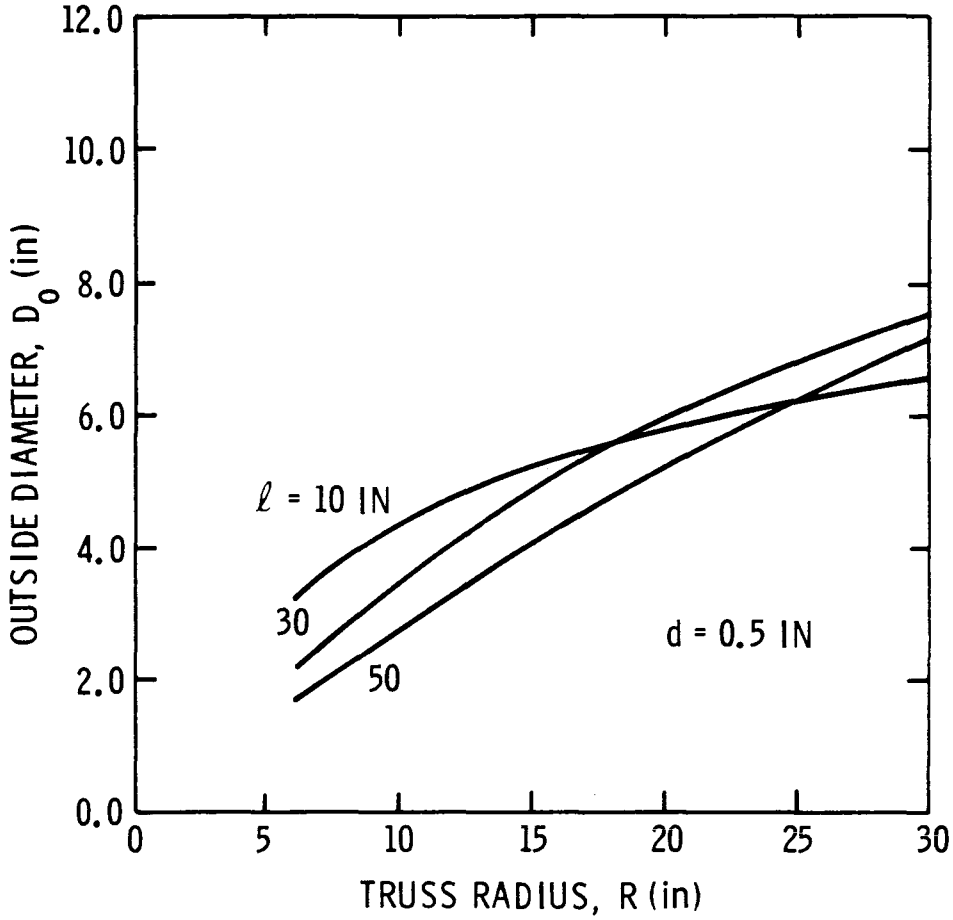

Figure 6. Relationship Between the Geometries of Tubular and Truss Towers that Have Equivalent Torsional Stiffnesses.

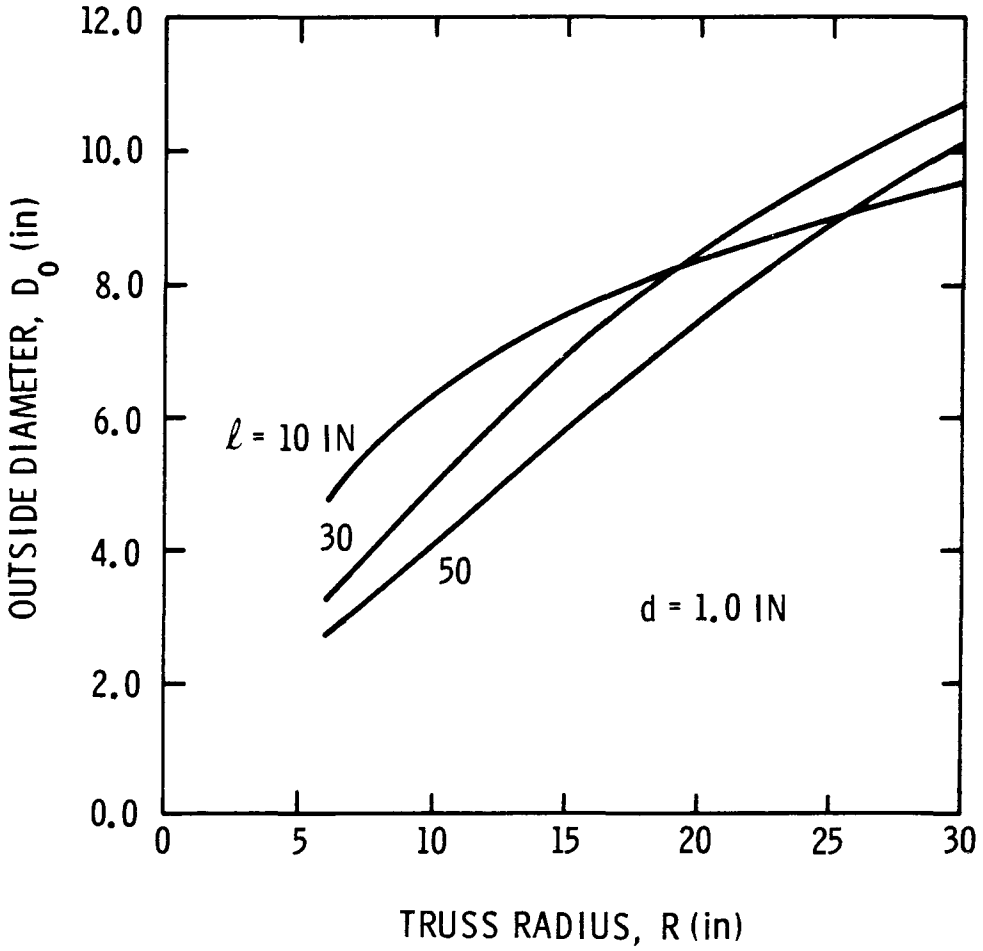

Figure 7. Relationship Between the Geometries of Tubular and Truss Towers that have Equivalent Torsional Stiffnesses.

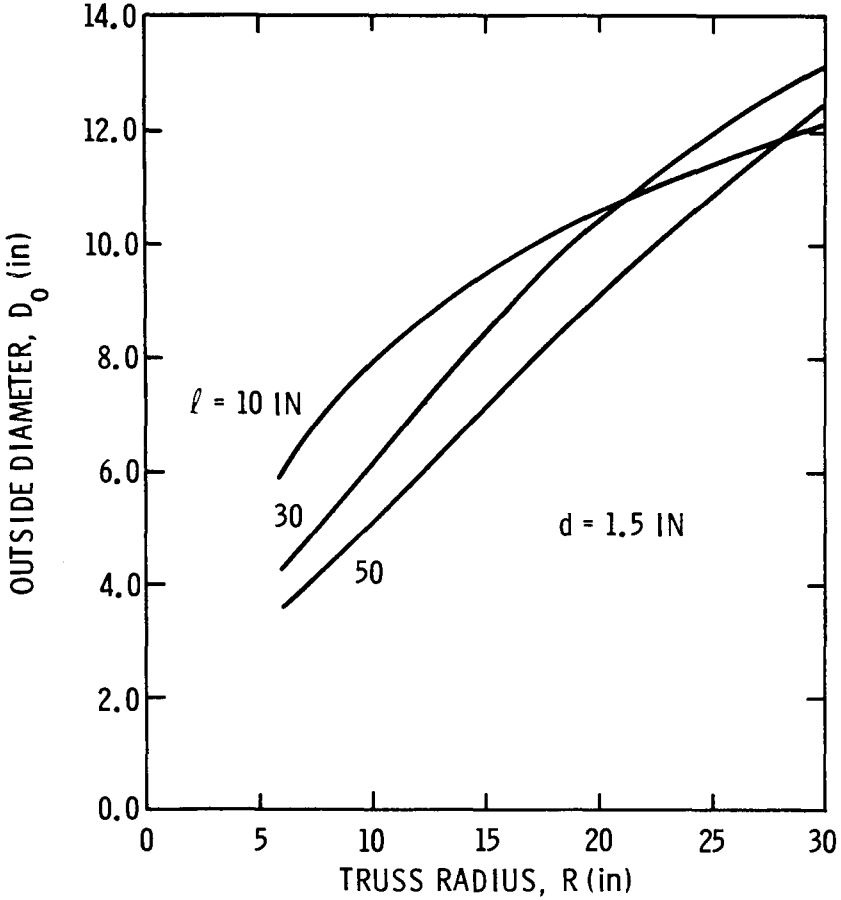

Figure 8. Relationship Between the Geometries of Tubular and Truss Towers that Have Equivalent Torsional Stiffnesses.

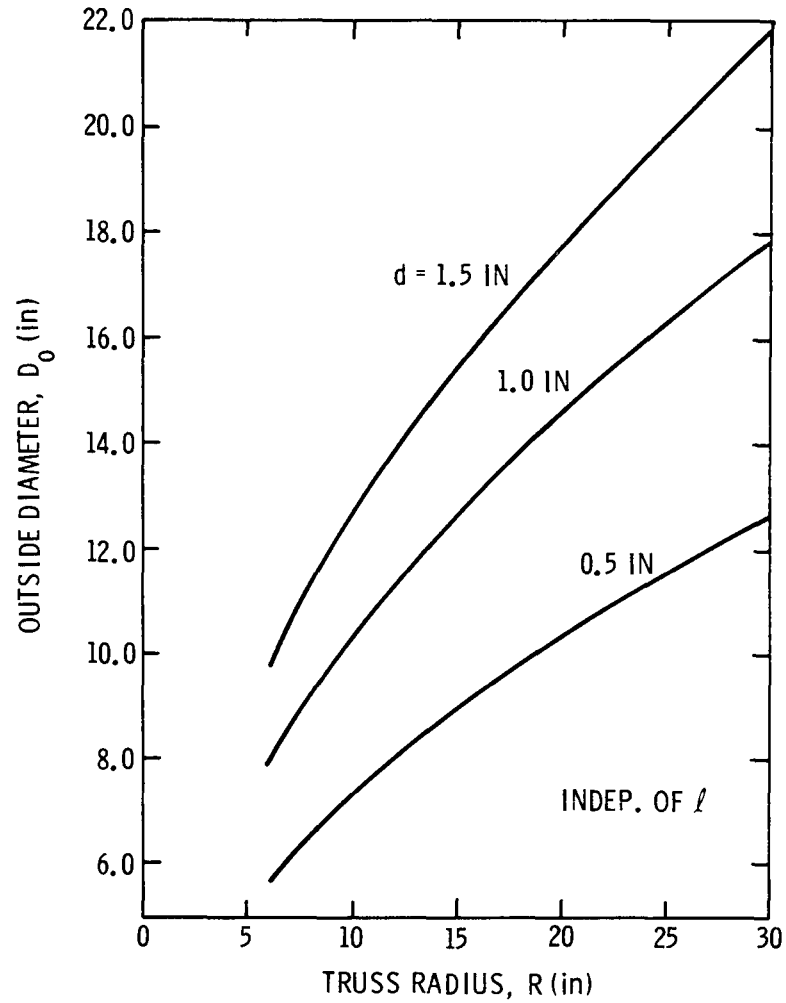

Figure 9. Relationship Between Geometries of Tubular and Truss Towers that Have Equivalent Bending Stiffnesses.

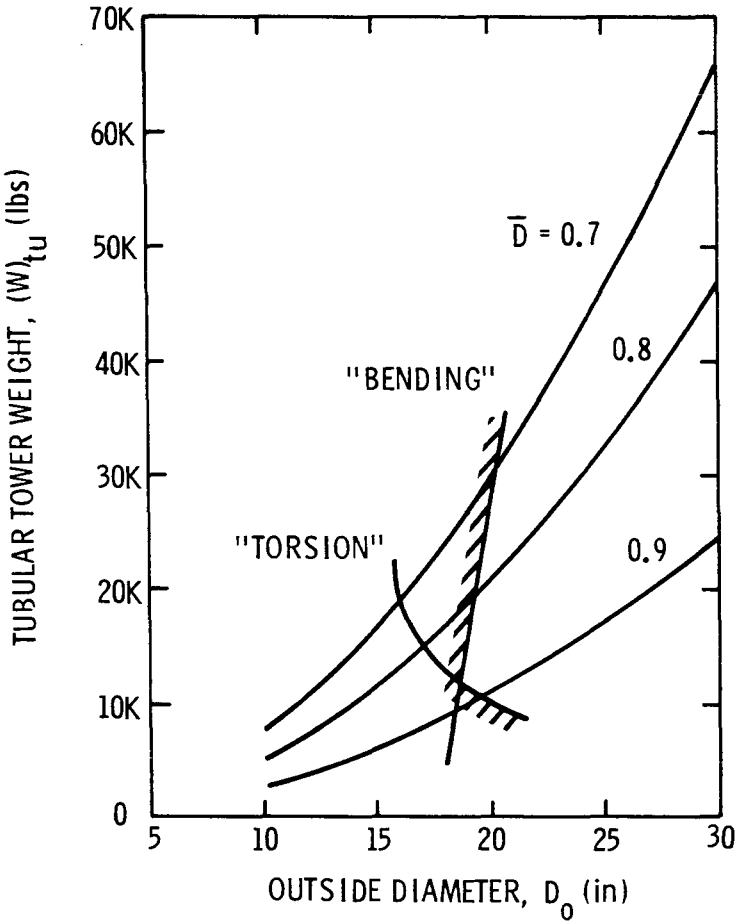

Figure 10. Minimum Weight Design Curves for Tubular Towers.

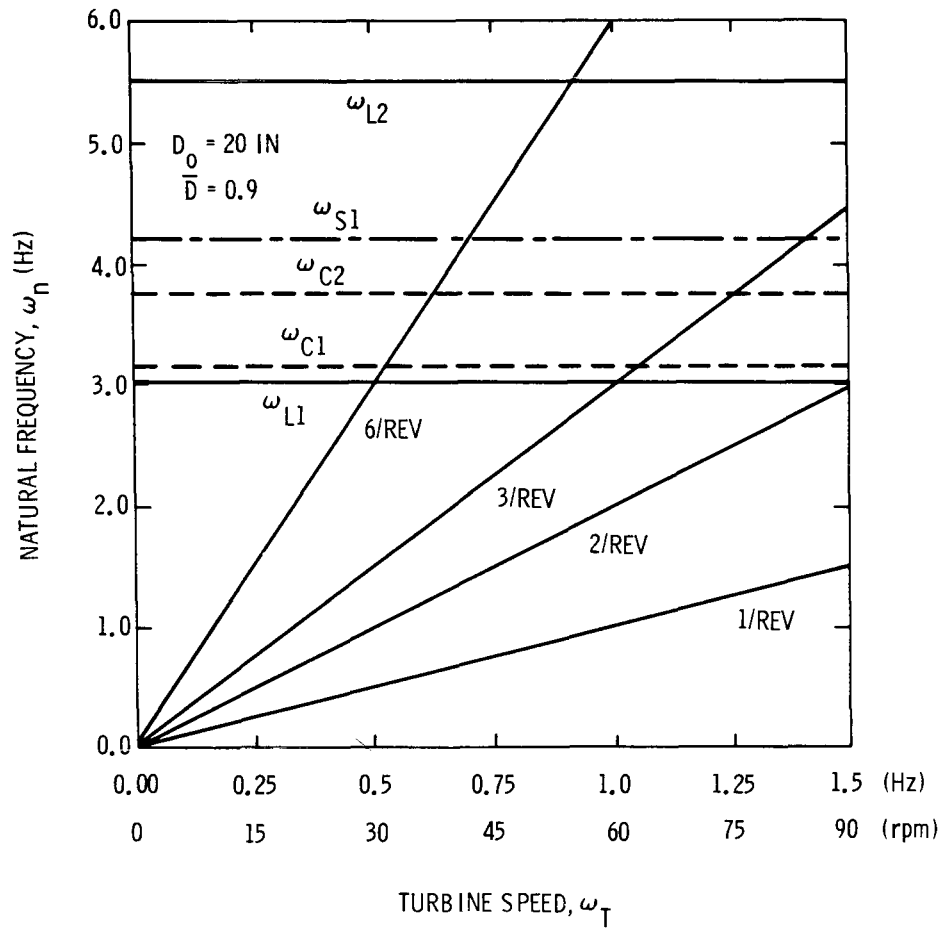

Figure 11. Turbine Component and System Natural Frequencies Versus Rotational Speed.

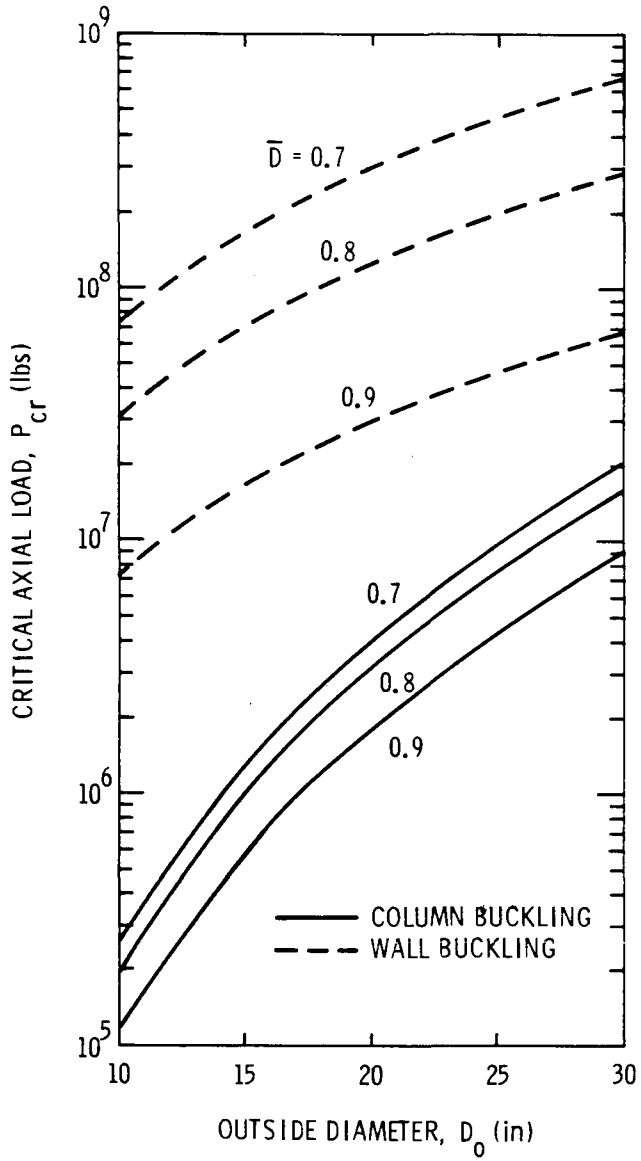

Figure 12. Critical Column and Wall Buckling Loads as a Function of Tubular Tower Geometry.

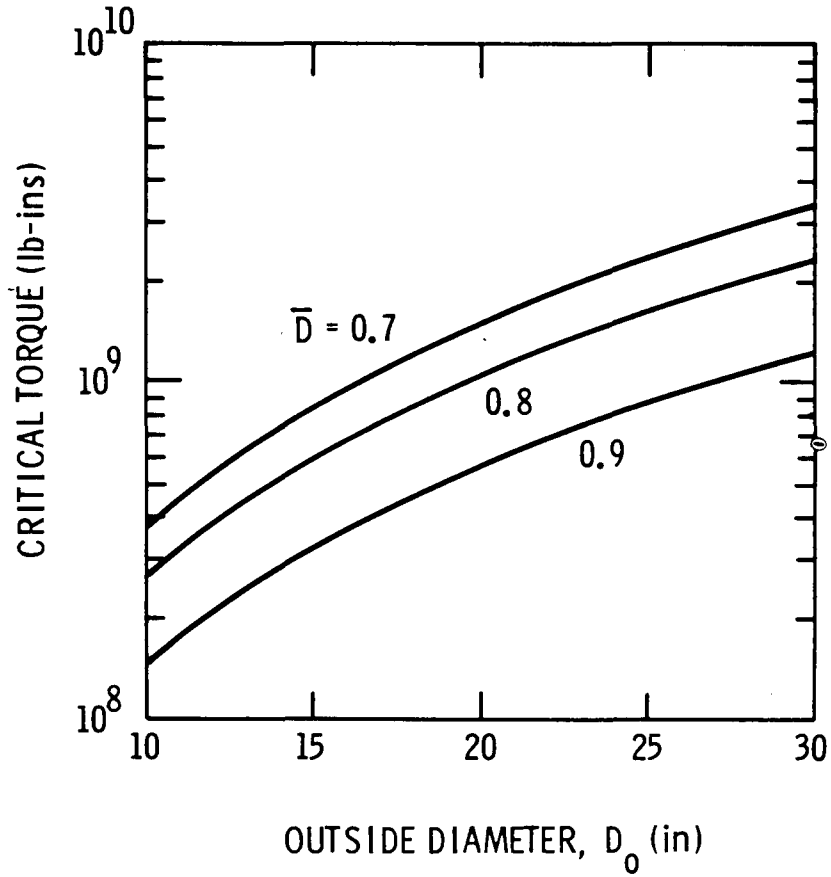

Figure 13. Critical Torsional Buckling Loads as a Function of Tubular Tower Geometry.

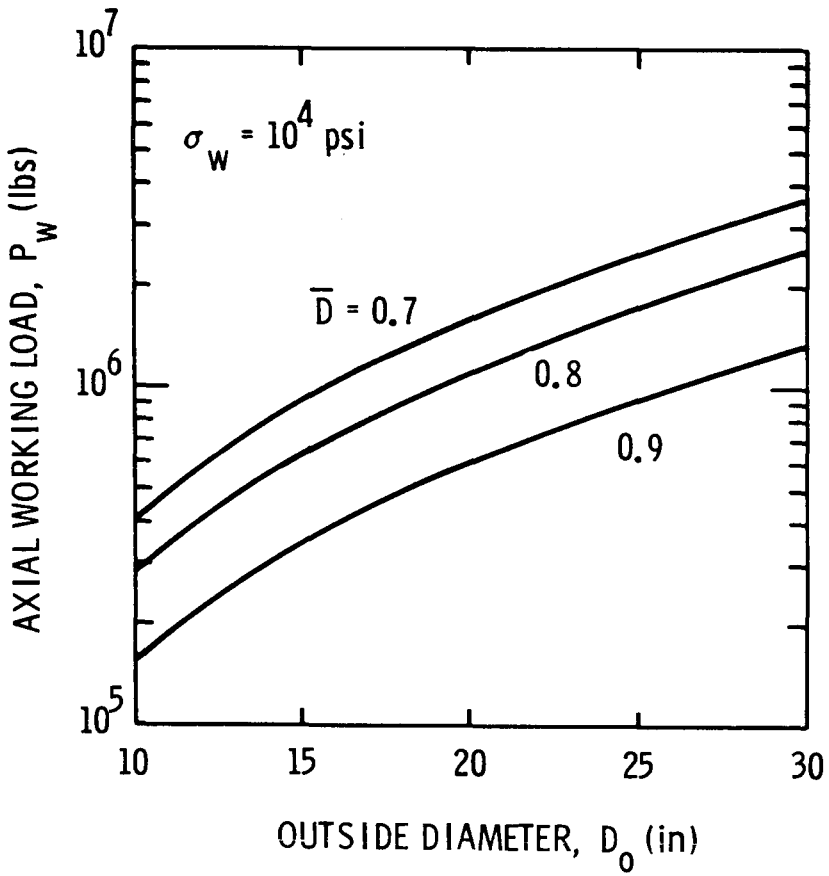

Figure 14. Axial Working Loads as a Function of Tubular Tower Geometry.

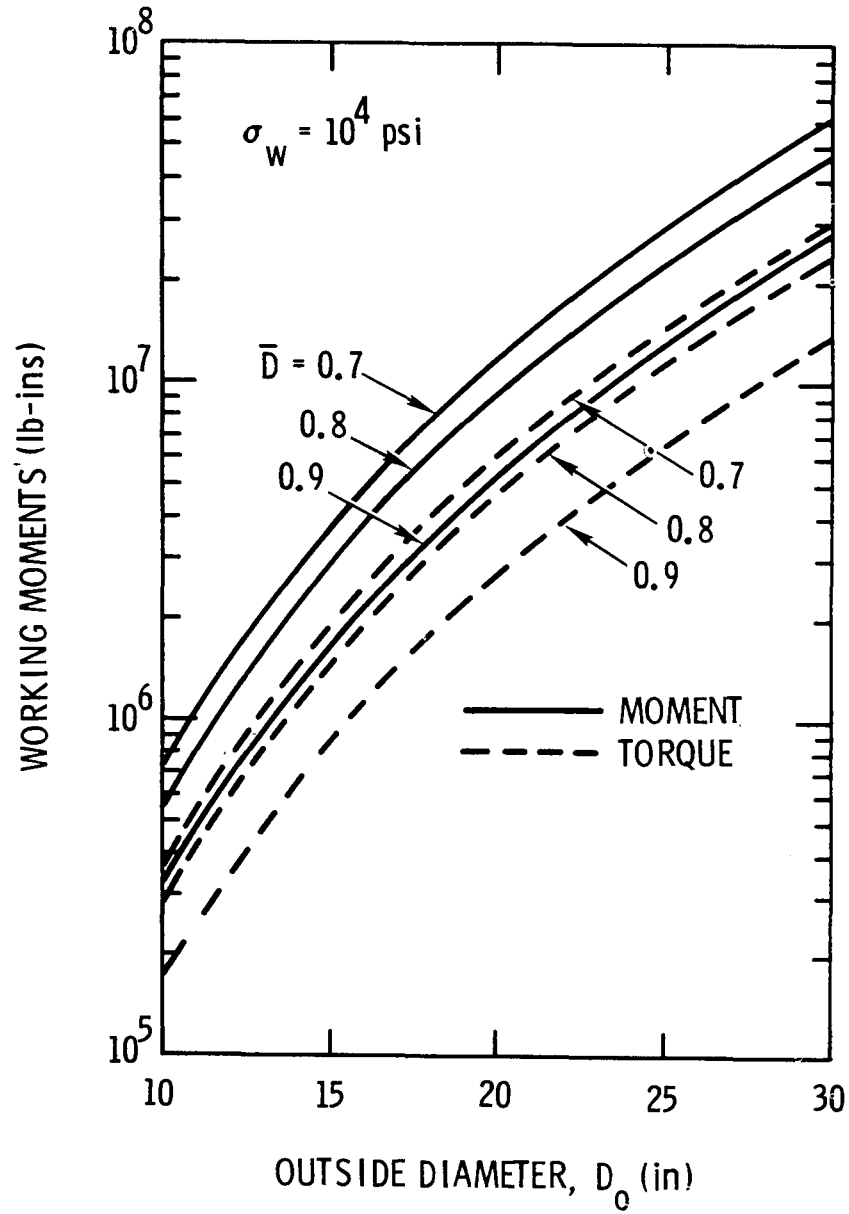

Figure 15. Working Moments and Torsional Loads as a Function of Tubular Tower Geometry.

SYSTEM STRUCTURAL RESPONSE

J. H. Biffle

Sandia Laboratories
Division 1281
Albuquerque, New Mexico 87115

Introduction

The 17 meter vertical axis wind turbine (VAWT) system was analyzed to determine the mode shape and frequencies of the structure. Changes in the design such as tower stiffness, 2 and 3 blade configuration, with and without struts and bearing designs for the tower are to be considered. The significance of the various natural modes and frequencies are to be determined by comparison to the frequency content of the applied forces.

Finite Element Model

To first determine the mode shape and frequencies, the structure was modeled for the finite element SAP4(1) computer program. SAP4 is a linear elastic general purpose program for analyzing structures. A three-dimensional beam element was used throughout the model which is shown in Figure 1. Since a lumped mass matrix is used, the number of elements necessary to obtain approximately 10% accuracy of the first harmonic bending frequency of each section was used. There are six elements in each steel tower section, six elements in each strut, five elements in each inner blade section, and eight elements in each outer blade section. The cables attached to the four outriggers were modeled with a stiffness of 8182 lb/inch in the axial direction of the cable to simulate the axial stiffness of the cables. Since the

natural frequencies of the cables was very much lower than the rest of the structure, the cables were not modeled with beam elements. The blades are labled A, B, and C for identification on subsequent plots. At Joint D the flexibility was specified as being either the continuous tower stiffness or pinned, i.e., no moment carrying capacity.

When the turbine is operated, sufficient axial forces are generated in the beam elements to affect the bending stiffness. The effect is caused by the nonlinear terms in the strain-displacement equations. If it is assumed that the displacements are small, then the effect can be included in the linear analysis as initial tension in the beams comprising the blades and struts. A nonlinear analysis is first performed, in this case by L. I. Weingarten (2). A stiffness matrix is added to the linear stiffness matrix for each beam which is of the form

$$\underset{\sim}{K}_{NL} = \frac{T_p}{L} \begin{bmatrix} \underset{\sim}{I}_3 & -\underset{\sim}{I}_3 \\ -\underset{\sim}{I}_3 & \underset{\sim}{I}_3 \end{bmatrix}$$

Where T_p is the initial tension, L is the length of the beam and I_3 is a 3 x 3 identity matrix.

The displacements are arranged as

$$\underset{\sim}{u}^T = \left[u_1^i \; u_2^i \; u_3^i \; u_1^j \; u_2^j \; u_3^j \right]^T$$

where 1, 2, 3 are local coordinate directions of the element, and i, j refer to the two nodes defining the beam. The above stiffness matrix was an addition to the SAP4 code.

Response

Some of the mode shapes predicted for the 70 m VAWT are shown in Figures 2 through 12. The deformations of various parts of the structure can be seen by comparing the three views of a normalized mode shape to the correspond undeformed shape shown in Figure 2. Sufficient displacements have been added to the underdeformed structural shape to be able to visualize the mode shape.

Figure 3 shows a predominately low frequency mode where the blades are bending out of their plane and all in the same direction. The value of the frequency associated with the mode depends on the torsional stiffness of the tower. For blade geometry 1, Table 1, using a 20" O.D., 19" I.D. tower; a 15" O.D., 14" I.D. tower and a 10" O.D., 9" I.D. tower with preliminary initial tensions 1, Table 2, the frequencies were 2.59, 2.40 and 2.07 Hz respectively. Using blade properties 2 and the 20" tower the frequency was 3.04 Hz.

Figure 2 is the second mode of the frequency and shape shown in Figure 3; a blade bending and torsion mode out of the plane of the blade. Only the blade properties primarily affect the predicted frequency. For blade 1 the frequency is 4.90 Hz and for blade 2 the frequency is 5.52 Hz.

Figures 5, 6 and 7 are views of a mode shape in which two blades move asymmetrically with respect to the other blade. The mode appears throughout the frequency spectrum and is usually the lowest frequency mode. It is influenced greatly by the tower bending stiffness and whether or not Joint D is pinned. Figure 5 shows a response when the tower does not bend appreciably. Figure 6 shows a result when the tower bends and also there is strut motion. Figure 7 shows the results when the structure is pinned at Joint D.

There is a set of modes associated with predominately strut motion as shown in Figure 8. The value of the frequency is influenced by the initial tensions in the struts, i.e., at what rpm the turbine is operated. With blades 1, initial tensions 1 give 5.00 Hz. With blades 2, initial tensions 2, a frequency of 4.2 Hz is obtained. If there is no initial tension the frequency is 2.72 Hz with blades 1.

Figure 9 shows the response of a mode characterized by outer blade motion in the plane of the blade. The mode frequency is dominated by the initial tension of the blade. With initial tensions 2, blade 2, the frequency is 5.44 Hz.

Figure 10 is a node characterized by inner blade motion in the plane of the blade. For blade 2 and initial tensions 2, a frequency of 5.9 Hz is predicted.

The significance of the mode shapes and frequencies depends upon the actual loads on the structure. Work is underway to predict which mode shapes and frequencies are the most important to the successful operation of the turbine, i.e., at what rpm can the turbine be successfully operated without structural problems. A modal participation factor will be calculated in the following manner. The following norm N of X_i--the response of the structure in the i'th mode, ϕ_i, at the frequency ω_i due to the time dependent aerodynamic forces on the blades--will be calculated.

$$N = \sum_{\Delta\omega} x_i^{*T}(\omega)\ x_i(\omega)$$

The number of frequencies needed to predict the response should become apparent from the analysis. Also some physical reasoning will probably have to be used to access the significance of the different modes.

Conclusions

The results so far have led to the use of the 20 inch tower to stiffen the system in torsion and in bending. The magnitude of the frequencies are also greatly affected by the constraints conditions at Joint D. For this reason, the joint will be made with a bearing capable of carrying moment loads. The lowest predicted frequency at 75 rpm should be about 3.0 Hz which is the mode shape in Figure 3 and in future designs will be changed by blade geometry.

References

1. Bathe, K., Wilson, E. L., and Peterson, F. E., "SAP4--A Structural Analysis Program for Static and Dynamic Response of Linear Systems," Earthquake Engineering Research Center, University of California, Berkeley, California, Report No. EERC 73-11, June 1973, Revised April 1974.

2. Weingarten, L., "Blade Structural Analysis," Proceedings of ERDA Vertical-Axis Wind Turbine Technology Workshop, Albuquerque, NM, May 18-20, 1976.

TABLE 1

Blade and Strut Properties

A in^2	Ixx in^4	Iyy in^4	J in^4	E lb/in^2	G lb/in^2	ρ $lb\ sec^2/in^4$
			Blade 1			
34.98	468.1	22.4	62.4	1.41×10^6	5.43×10^5	4.03×10^{-4}
			Blade 2			
34.98	836.2	21.2	43.7	1.49×10^6	5.74×10^5	4.03×10^{-4}

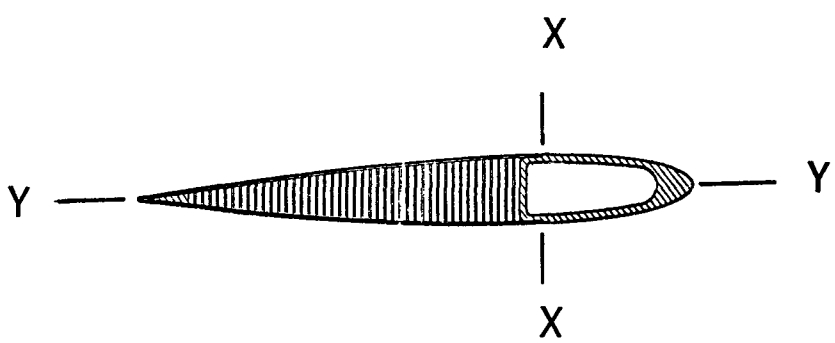

Blade Cross Section

TABLE 2

Initial Tensions, lbs

Item	Number	Load	
		At Tower	At Blade
Strut	1	7,500	10,000
	2	4,634	4,073
		At Tower	At Strut
Inner Blade	1	10,000	7,500
	2	11,223	8,892
		At Strut	At Center
Outer Blade	1	7,500	5,000
	2	8,892	4,940

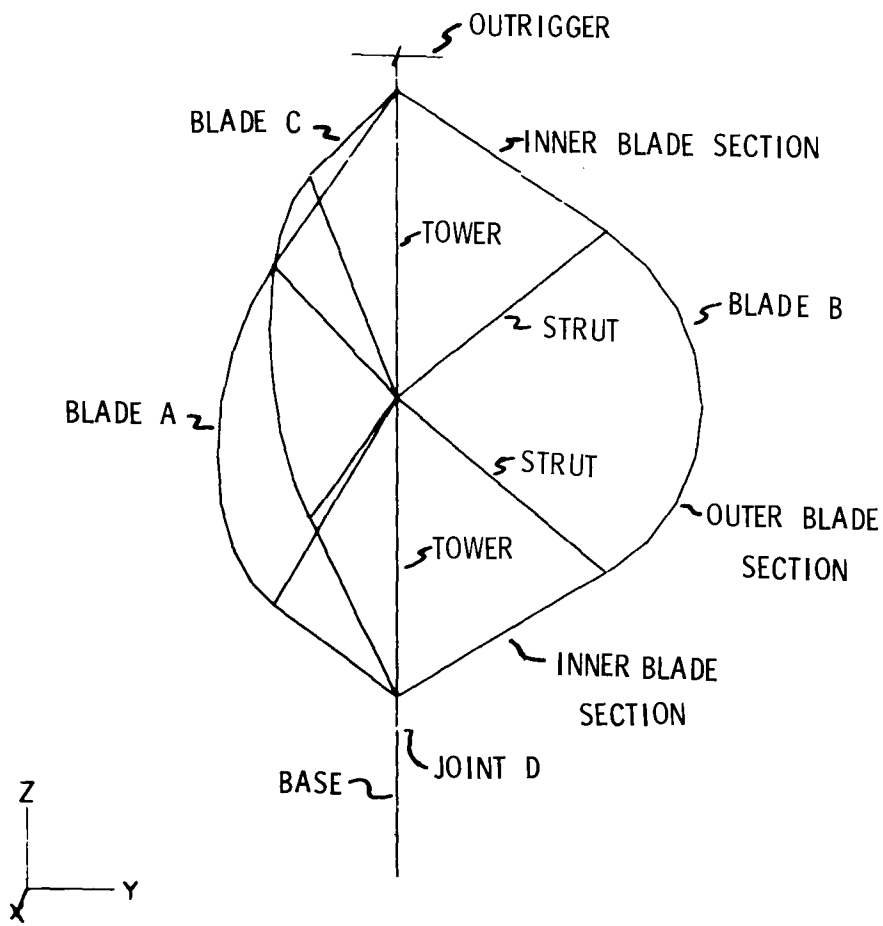

Figure 1. Finite element model of VAWT with 3 blades, struts and 4 cable outriggers.

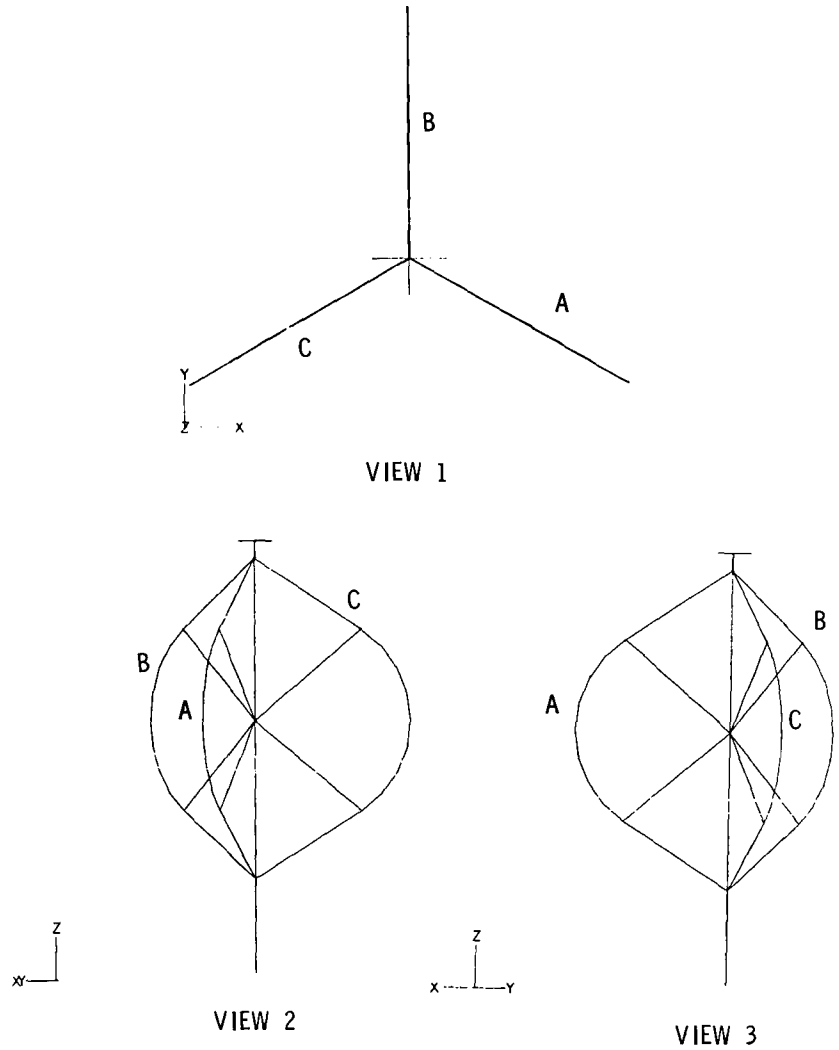

Figure 2. Isometric Views of Underformed VAWT

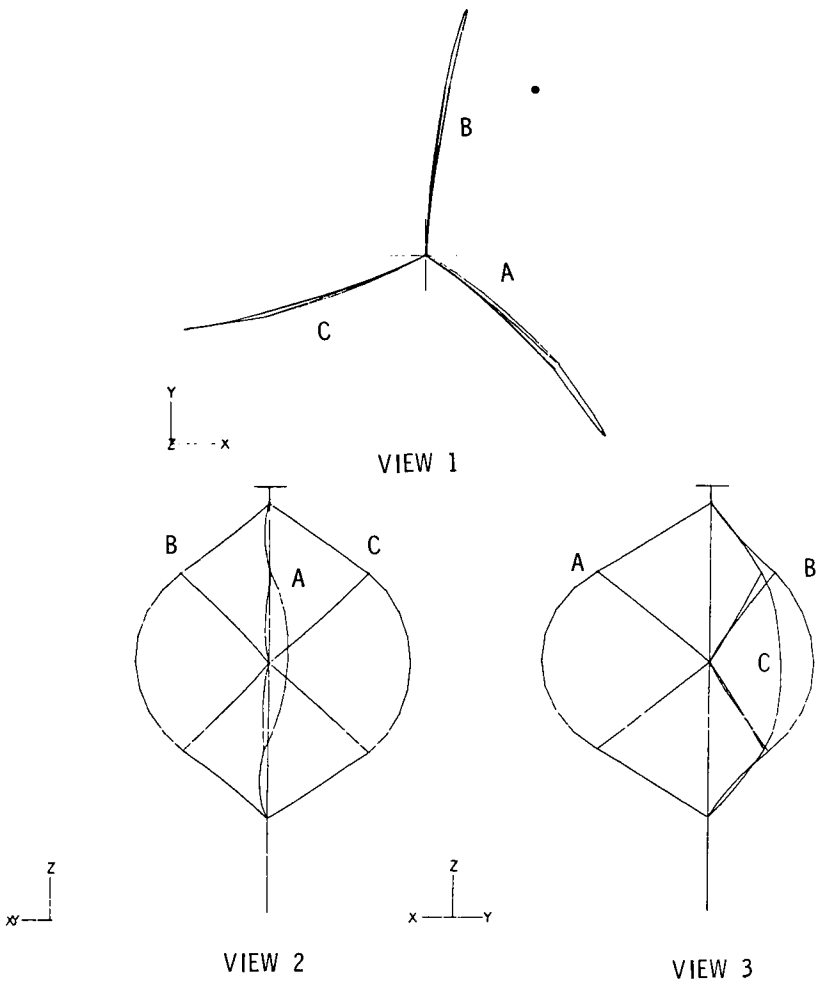

Figure 3. Isometric views of first symmetric out of plane bending mode of blades.

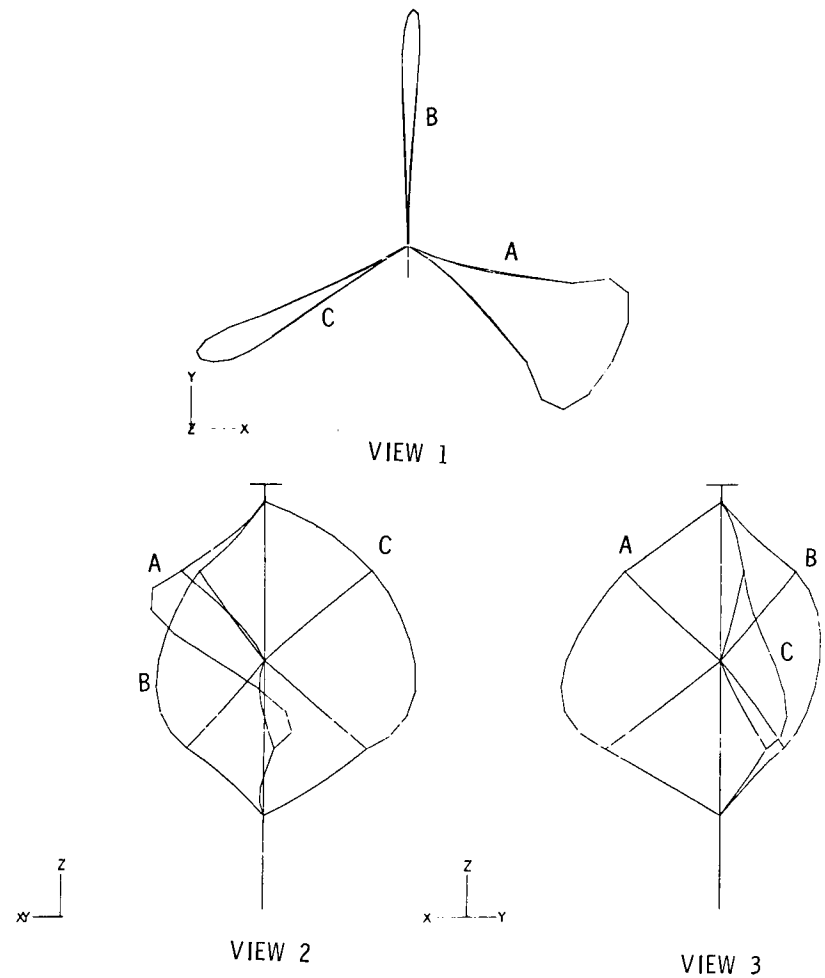

Figure 4. Isometric view of second symmetric out of plane bending mode of blades.

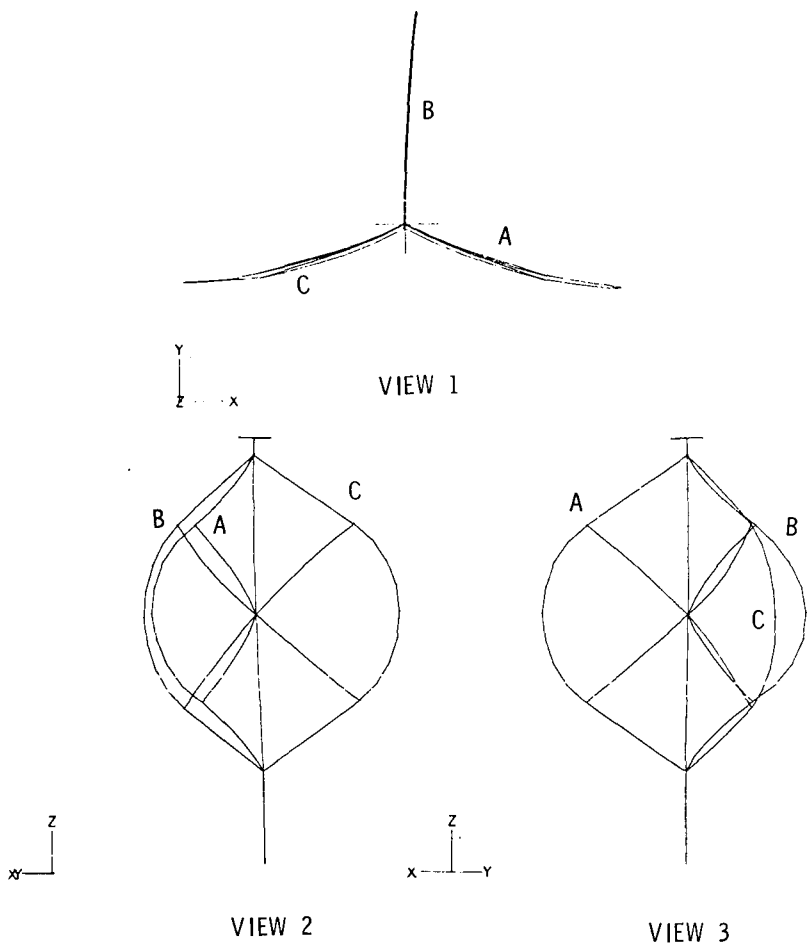

Figure 5. Isometric views of asymmetric out of plane bending mode of blades.

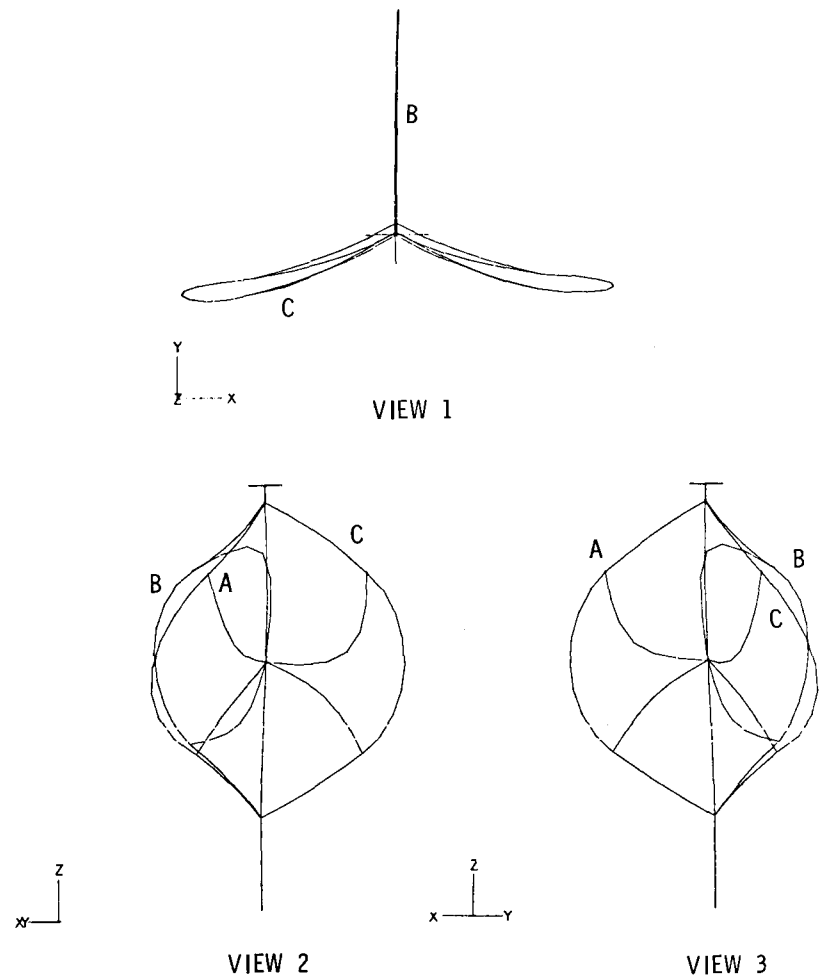

Figure 6. Isometric view of asymmetric of plane bending mode of blades with strut and tower motion.

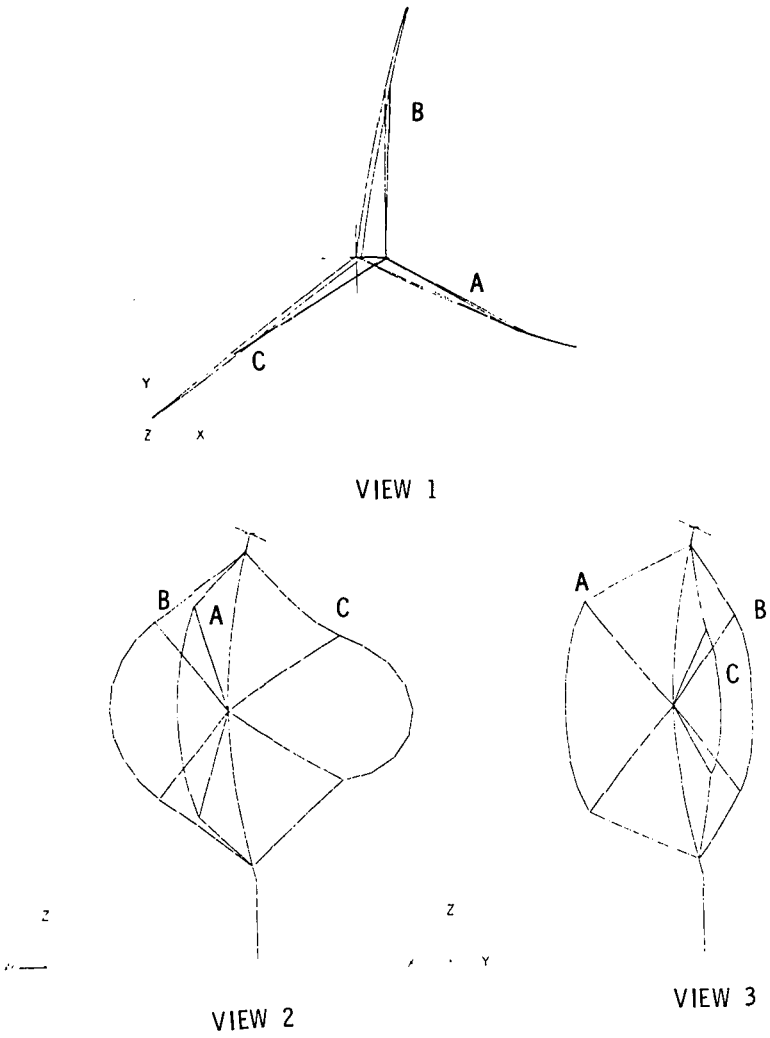

Figure 7. Isometric view of first asymmetric out of plane bending mode of blades with tower bending.

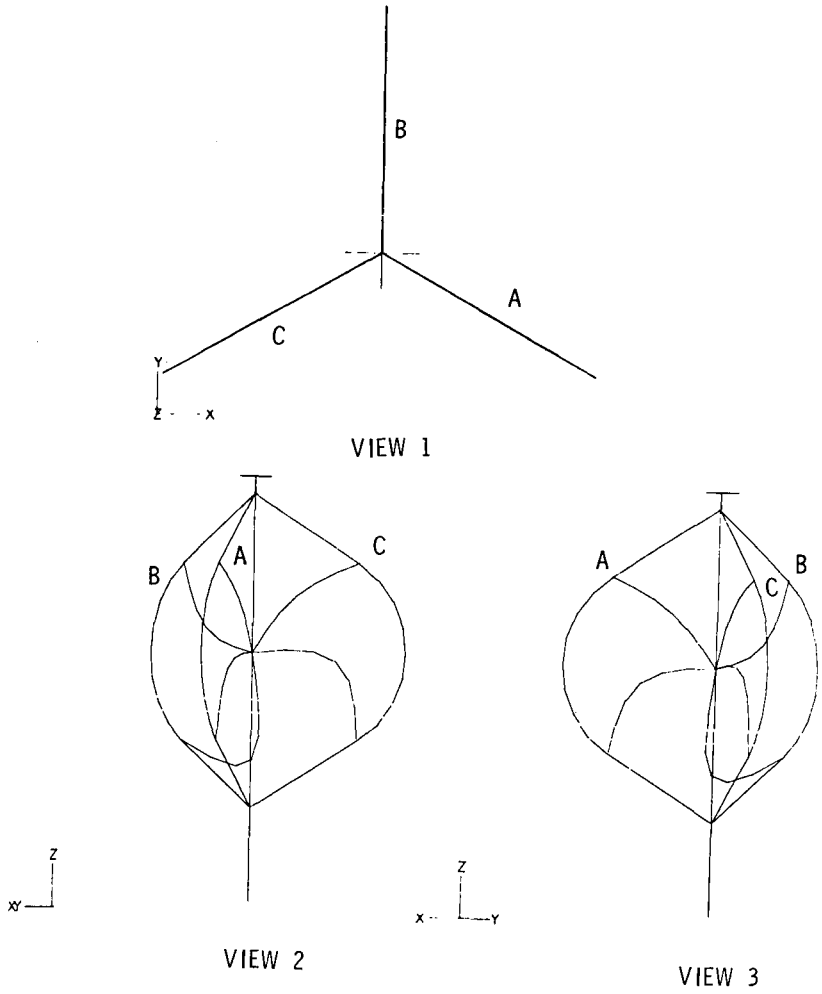

Figure 8. Isometric view of a mode dominated by strut motion.

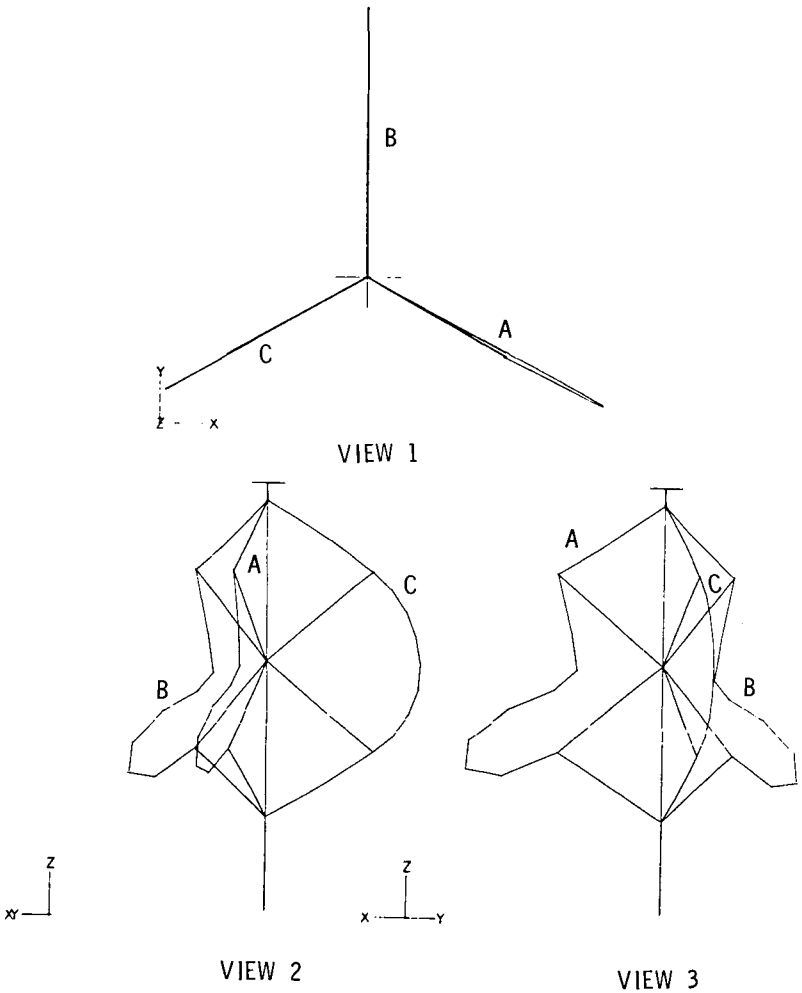

Figure 9. Isometric view of mode dominated by center section in-plane blade motion.

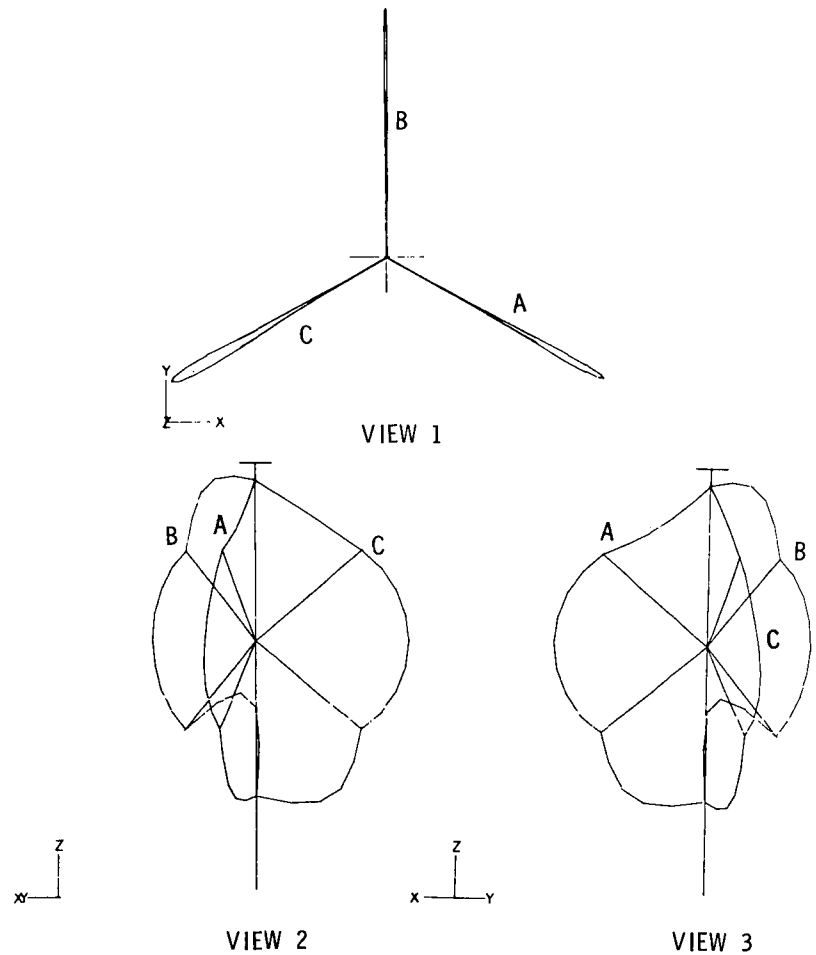

Figure 10. Isometric views of mode dominated by outer section in-plane blade motion.

THE EFFECTS OF SYSTEM IMBALANCE

Ronald Rodeman
Sandia Laboratories
Albuquerque, New Mexico 87115

Dynamic Loading Due to Imbalance

The VAWT is to be designed to be capable of smooth operation over a wide range of speeds and loads. This design will almost certainly result in the mass center of the system being displaced from the geometric center of the rotating shaft. This eccentricity will result in forces applied to the bearings of the shaft which could have a pronounced effect on their lives. If the shaft turns at a frequency below the first lateral natural frequency of the VAWT the motion will be stable and the mass center will precess at a rate equal to the turning of the shaft.

However, at turning speeds beyond the first lateral natural frequency it is possible for the system to undergo an unstable motion in which the mass center of the system precesses at a speed different from that of the shaft. This general motion is termed nonsynchronous precession in the literature and is a type of self-excited motion that is damping dependent. This motion is not at all like the general orbiting of the shaft at the rotor critical speed, and can lead to destruction of the bearings or the shaft.

Analysis

The VAWT is a complex structure with many significant normal modes. To determine if the effects of imbalance were critical for the 17M turbine a simplified model was constructed. This model, shown in Figure 1, is known as the Jeffcott model in the literature; it con-

sists of a centrally located unbalanced disk attached to a massless elastic shaft. The parameters for the model were computed by calculating the effective mass and stiffness for the wind turbine.

The effective mass is that value of mass located at the center of the shaft such that its kinetic energy will equal the system kinetic energy. The effective stiffness is equal to the reciprocal of the center deflection of the VAWT due to a unit load applied at the center.

As can be seen in Figure 1, there are three degrees of freedom associated with this model: δ-deflection of the rotor center from the origin, ϕ-the precession angle, and β-the phase angle. There is also a damping force which is developed at the bearings and is due to the frictional force developed between two mating surfaces undergoing relative sliding. For the simplified case where the rotor centerline deflection δ is constant this force is given as

$$F = - C_r \delta (\dot{\phi} - \omega)$$

where C_r is a damping coefficient. This force is developed only if the whirl speed $\dot{\phi}$ is different than the rotational speed ω. When the whirl speed is smaller than the rotational speed, the damping force becomes a source of excitation and energy is added to the system causing the whirl amplitudes to increase.

Results

The steady state response of the model was obtained for the case of synchronous precession, i.e., $\dot{\phi} = \omega$. The normalized amplitude factor (δ/e) versus the rotor speed ratio is shown in Figure 2. The lateral natural frequency was estimated to be approximately

4 Hz and the maximum turning speed is 1.25 Hz (75 RPM). From the response curve of Figure 2 it is seen that at this speed ratio there is very little amplification. The maximum force transmitted to the bearings computed using the maximum eccentricity was shown to be small for this rotor speed ratio. It was also found that the onset of non-synchronous precession, which corresponds to the self-excited motion, would not occur until the turning speed ω was three times the first lateral natural frequency. Therefore, at the present turning speeds the 17M VAWT will not be significantly affected by mass imbalance.

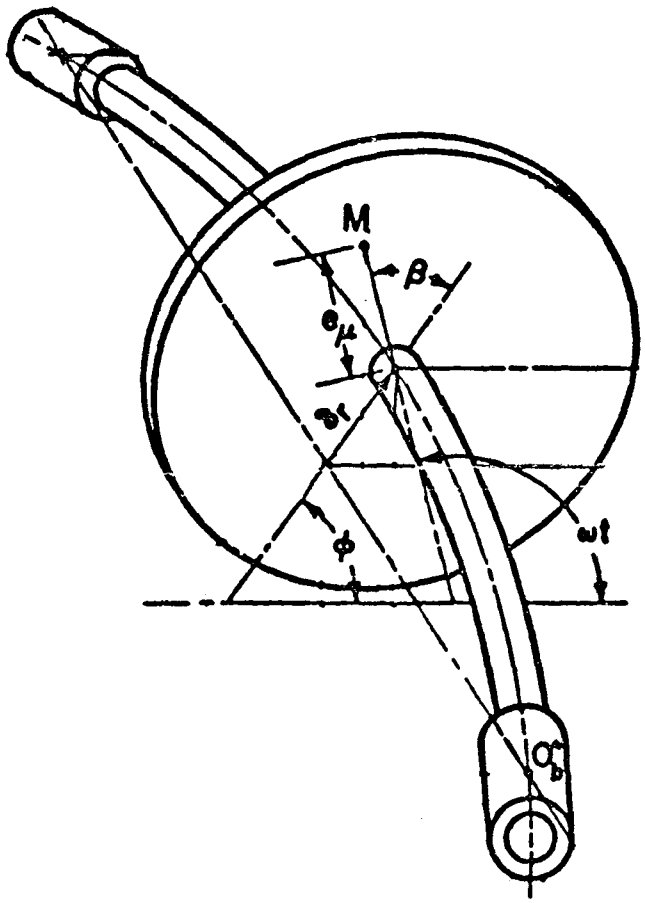

FIG. 1 JEFFCOTT MODEL

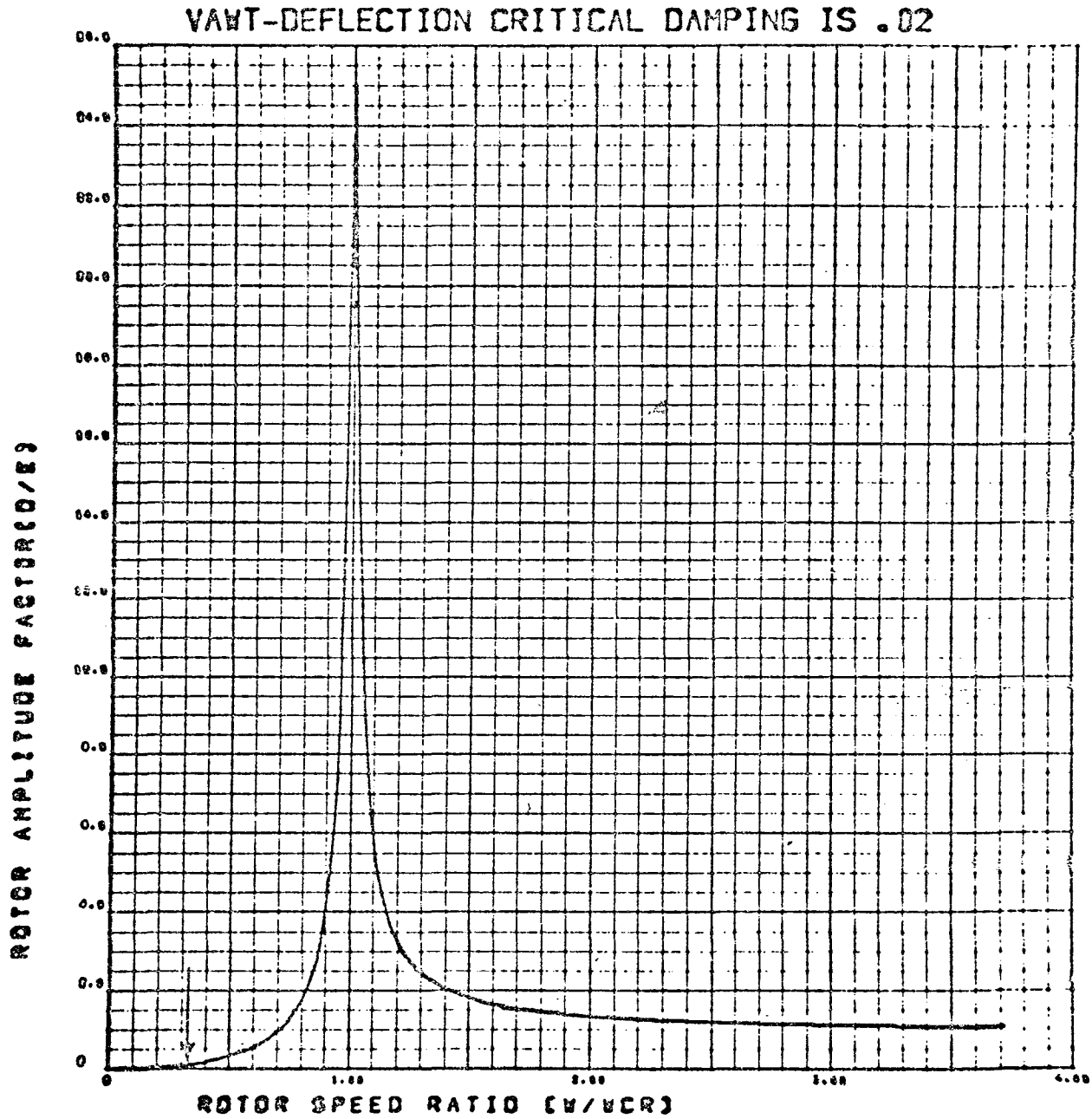
VAWT-DEFLECTION CRITICAL DAMPING IS .02
ROTOR AMPLITUDE FACTOR(D/E)
ROTOR SPEED RATIO (W/WCR)
0
1.00
2.00
3.00
4.00

FIGURE 2

AEROELASTIC ANALYSIS OF THE TROPOSKIEN-TYPE WIND TURBINE

Norman D. Ham
Department of Aeronautics and Astronautics, Massachusetts Institute of Technology

1. Introduction

The troposkien type of vertical-axis wind turbine, Reference 1, embodies flexible curved blades connected at each end to the top and bottom of a vertical shaft which permits the blades to rotate about the vertical axis under the action of the wind. The curve of each blade is approximately that of a troposkien; i.e., the shape taken by a flexible cable of uniform density and cross section whose ends are attached to two points on a vertical axis, when it is spun at a constant angular velocity about the vertical axis. In this manner the bending stresses in the blades are reduced to a minimum.

The testing of such devices has indicated that under certain conditions, serious vibrations of the blades can occur, involving flatwise bending, torsion, and chordwise bending. It is the purpose of this report to perform an aeroelastic analysis of the stability of the coupled bending and torsional motion of such blades with a view to determining the cause of these vibrations and a means of suppressing them. The emphasis of the analysis is on obtaining physical understanding, rather than exact numerical results.

2. Blade Bending Modes and Frequencies

Consider the rotating blade of the troposkien-type rotor shown in Figure 1. The bending moment at x is given by

$$M(x) = \int_x^{\ell/2} [y(\xi)\Omega^2 - \ddot{y}(\xi)]\, m(\xi)(\xi - x)\, d\xi - H[y(\ell/2) - y(x)]$$

where Ω = rotor rotational speed

$m(\xi)$ = rotor blade mass at ξ per unit of x-distance

H = blade tension force at mid-span

ℓ = distance between the two ends of the blade

Differentiating the bending moment equation twice with respect to x,

$$\frac{\partial^2 M(x)}{\partial x^2} = y(x)\Omega^2 m(x) - \ddot{y}(x)\ m(x) + H\frac{\partial^2 y}{\partial x^2}$$

From the theory of elasticity for the bending of slender beams,

$$M(x) = EI\ \frac{\partial^2 y}{\partial x^2}$$

Therefore

$$\frac{\partial^2 M(x)}{\partial x^2} = \frac{\partial^2}{\partial x^2}\ [EI\ \frac{\partial^2 y}{\partial x^2}]$$

Then neglecting the structural bending stiffness of the blade in comparison with the stiffening effect of the centrifugal force, the approximate blade bending equation of motion is

$$H\ \frac{\partial^2 y}{\partial x^2} + \Omega^2 m(x) y - m(x)\ddot{y} = 0 \tag{1}$$

Note that $m(x)\ dx = m(s)\ ds$, where s = arc length along the blade, and $m(s) = m$, a constant. Then

$$m(x) = m\ \frac{ds}{dx} = m\sqrt{1 + (\frac{dy}{dx})^2}$$

Equation (1) is the equation of the vibrating blade: the steady-state case is described and solved in Reference 1. For present purposes, consider the equation which results when it is assumed that $y = y(\theta)$:

$$H\ \frac{\partial^2 y}{\partial \theta^2}\ (\frac{\partial \theta}{\partial x})^2 + \Omega^2 m(\theta) y(\theta) - m(\theta)\ddot{y}(\theta) = 0 \tag{2}$$

Let $x = R - R\cos\theta$ (i.e., blade is a semi-circular arc)

$$y = \sum_{n=1}^{\infty} y_n(\theta)\ g_n(t)$$

Equation (2) becomes, after separation of variables,

$$\frac{1}{R^2}\ \frac{y_n''}{y_n} = \frac{m}{H}\ \frac{\ddot{g}_n}{g_n} - \frac{\Omega^2 m}{H} = -\lambda_n^2 \qquad n = 1, 2, \ldots$$

for the nth modal eigenvalue λ_n and $m(\theta) = \frac{m}{\sin^2\theta}$.

Then $$y_n'' + R^2\lambda_n^2 y_n = 0 \tag{3}$$

and $$\ddot{g}_n + (\frac{H}{m}\lambda_n^2 - \Omega^2)\, g_n = 0 \tag{4}$$

Assume a solution for equations (3) and (4) for free vibration in a vacuum:

$$y_n = R \sin n\theta\, \bar{g}_n\, e^{i\omega_n t}$$

Then $\lambda_n = n/R$

$$\omega_n = [\frac{H}{m}(\frac{n}{R})^2 - \Omega^2]^{1/2} \qquad n = 1, 2, \ldots \tag{5}$$

Assume that the blade is constructed in the shape given by n = 1:

$$y_1 = R \sin\theta \tag{6}$$

In this case, the bending frequency given by equation (5) is zero for n = 1:

$$\omega_1 = [\frac{H}{m}(\frac{1}{R})^2 - \Omega^2]^{1/2} = 0$$

Therefore $H = R^2\Omega^2 m$.

Then from equation (5),

$$\omega_n = [n^2 - 1]^{1/2}\,\Omega \qquad n = 2, 3, \ldots \tag{7}$$

Equation (7) yields frequencies that compare closely with those from Reference 2, as shown in Figure 2 for a blade of uniform mass distribution.

The corresponding mode shapes are

$$y_n = R \sin n\theta \qquad n = 2, 3, \ldots \tag{8}$$

Equation (6) is an approximate representation of the troposkien blade shape discussed in Reference 1. Equations (7) and (8) are the frequencies and mode shapes for small amplitude vibrations of the blade whose undisturbed shape is given by equation (6).

3. Blade Torsion/Chordwise Bending Modes and Frequencies

Reference 3 describes the elastic motion of a partial slender ring perpendicular to its own plane in terms of coupled torsion and chordwise bending.

Equation (5) of Reference 3 is the eigenvalue equation for torsion/chordwise bending free vibration of elastic rings:

$$\beta_n^{VI} + 2\beta_n^{IV} + \beta_n'' = \lambda_n \left(k\beta_n'' - \beta_n\right) \tag{9}$$

where β_n = nth torsion mode shape

$k = \frac{GK}{EI_2}$

GK = torsional stiffness of ring section

EI_2 = chordwise bending stiffness of ring section

λ_n = nth eigenvalue for ring torsion

Solution of this equation leads to the complicated expressions for the mode shapes given in Reference 3. It is proposed to use the following simple expressions for the mode shapes of the blade:

$$\beta_n(\theta) = \sin n\theta \qquad n = 2, 3, \ldots \tag{10}$$

Note that n = 1 corresponds to a mode requiring blade extension.

It is now necessary to determine if the approximate mode shapes given by equation (10) correspond to eigenvalues that are close to the values given in Reference 3. Substituting equation (10) in equation (9) given the characteristic equation

$$n^6 - 2n^4 + n^2(1 - k\lambda_n) - \lambda_n = 0$$

Solving for λ_n,

$$\lambda_n = \frac{n^6 - 2n^4 + n^2}{kn^2 + 1} \tag{11}$$

Taking k = 0, the following result is obtained for the case n = 2:

$$\lambda_n = 36, \qquad \lambda_n^{1/2} = 6$$

This value is within ten percent of the value shown in Figure 3 of Reference 3. Note that for n = 1, $\lambda_n = 0$ since blade extension is not permitted in the analysis of Reference 3.

Equation (11) for the non-rotating partial ring is used to calculate approximate coupled chordwise bending/torsion frequencies for the troposkien-type blade:

$$\bar{\omega}_{n_o} = \lambda_n^{1/2} \sqrt{\frac{GK}{mR^4}} \qquad n = 2, 3, \ldots \tag{12}$$

Now consider the effects of centrifugal force shown in Figure 3. Including the components of centrifugal force in equations 9(b) and 9(d) of Reference 3, where $v \triangleq z$ is the chordwise bending displacement,

$$v^{IV} - R\beta'' - k(v'' + R\beta'') = \frac{mR^4}{EI_2}\left(\ddot{v} - \underline{v\Omega^2} + \underline{\frac{H}{mR^2} v''}\right) \tag{13}$$

$$v'' - R\beta + k(R\beta'' + v'') = 0 \tag{14}$$

for free vibration in a vacuum; the new terms are underlined. Note that in equations 9(a) to 9(d) of Reference 3, in-plane forces do not affect torsion/chordwise bending and out-of-plane forces do not affect in-plane bending.

Following the solution of equations (14) and (16) in Reference 3, the eigenvalue equation (9) of the present report is unchanged, while the time history as given by equation (14) of Reference 3 becomes, approximately,

$$\ddot{T}_n + (\bar{\omega}_{n_o}^2 + (n^2-1)\Omega^2)T_n = 0 \tag{15}$$

in the absence of viscous damping and external forces.

Then the approximate coupled chordwise bending/torsion frequencies

for the rotating troposkien-type blade are

$$\bar{\omega}_n = [\bar{\omega}_{n_o}^2 + (n^2-1)\Omega^2]^{1/2} \qquad n = 2, 3, \ldots \tag{16}$$

where $\bar{\omega}_{n_o}$ is given by equation (12).

The corresponding mode shapes are given by equation (10).

4. Blade Equations of Motion

Consider equation (2) describing blade flatwise motion. Assume a solution in terms of normal modes:

$$y = \sum_{n=2}^{\infty} y_n(\theta)\, g_n(t)$$

Substituting in equation (2),

$$\sum_{n=2}^{\infty} m y_n(\theta)\, \ddot{g}_n(t) = \sum_{n=2}^{\infty} H \frac{y_n''(\theta)}{R^2 \sin^2\theta}\, g_n(t) + \sum_{n=2}^{\infty} \Omega^2 m y_n(\theta) g_n(t) \tag{17}$$

Assume free vibration in a vacuum in the nth blade bending mode:

$$g_n(t) = \bar{g}_n\, e^{i\omega_n t}$$

Therefore

$$-m\omega_n^2\, y_n\, \bar{g}_n e^{i\omega t} = H \frac{y_n''}{R^2 \sin^2\theta}\, \bar{g}_n\, e^{i\omega t} + \Omega^2 m y_n\, \bar{g}_n e^{i\omega t}$$

or $$-m\omega_n^2 y_n = H \frac{y_n''}{R^2 \sin^2\theta} + \Omega^2 m\, y_n$$

Then equation (17) becomes

$$\sum_{n=2}^{\infty} m y_n(\theta)\, \ddot{g}_n(t) + \sum_{n=2}^{\infty} m\omega_n^2\, y_n(\theta)\, g_n(t) = 0 \tag{18}$$

where $y_n(\theta) = R \sin n\theta \qquad n = 2, 3, \ldots$

$\omega_n = [n^2 - 1]^{1/2}\, \Omega \qquad n = 2, 3, \ldots$

Adding the Coriolis force due to chordwise bending and the aerodynamic lift force, as shown in Figures 3 and 4, equation (18) becomes

$$\sum_{n=2}^{\infty} m y_n\, \ddot{g}_n + \sum_{n=2}^{\infty} m\omega_n^2\, y_n g_n + \sum_{n=2}^{\infty} 2m\Omega z_n \dot{f}_n = \frac{1}{R}\frac{dL}{d\theta} \sin\theta \tag{19}$$

where the modal expression for blade chordwise bending is written as

$$z = \sum_{n=2}^{\infty} z_n(\theta)\ f_n(t) \tag{20}$$

The modal equation for chordwise bending is

$$\sum_{n=2}^{\infty} m z_n(\theta)\ \ddot{f}_n(t) + \sum_{n=2}^{\infty} m\bar{\omega}_n^2 z_n(\theta)\ f_n(t) = 0 \tag{21}$$

where $z_n(\theta) = R \sin n\theta$

$$\bar{\omega}_n = [\bar{\omega}_{n_o}^2 + (n^2-1)\Omega^2]^{1/2} \qquad n = 2,\ 3,\ \ldots$$

since z_n and β_n are coupled (see Section 3). Adding the Coriolis force due to flatwise motion, as shown in Figure 3, and neglecting unsteady chordwise aerodynamic forces, equation (21) becomes

$$-\sum_{n=2}^{\infty} 2m\Omega y_n \dot{g}_n + \sum_{n=2}^{\infty} m z_n \ddot{f}_n + \sum_{n=2}^{\infty} m\bar{\omega}_n^2 z_n f_n = 0 \tag{22}$$

Multiplying equations (19) and (22) by $R \sin n\theta$ and integrating from 0 to π, the coupled equations of motion in the nth mode are obtained:

$$I_n \ddot{g}_n + I_n \omega_n^2 g_n + 2I_n \Omega \dot{f}_n = \int_o^{\pi} R\sin\theta \sin n\theta \frac{dL}{d\theta}\, d\theta \tag{23}$$

$$-2I_n \Omega \dot{g}_n + I_n \ddot{f}_n + I_n \bar{\omega}_n^2 f_n = 0 \tag{24}$$

where

$$I_n = \int_o^{\pi} mR^2 \sin^2 n\theta\, d\theta$$

Following Reference 4 and Figure 4, the aerodynamic lift for the wind turbine rotating in <u>still</u> air at constant rotational speed Ω is

$$\frac{1}{R}\frac{dL}{d\theta} = -\frac{1}{8}\rho a c^2\, \Omega y_1 \dot{\beta} - \frac{1}{2}\rho a c \Omega y_1 C(k)\,[\dot{y} \sin\theta + \Omega y_1 \beta + (0.5c - x_A)\dot{\beta}]$$

where ρ = air density

a = blade section lift curve slope

c = blade chord

β = blade twist angle (positive nose down) $\equiv \frac{\beta}{z} z$ (see Fig. 3)

y_1 = blade undisturbed shape = R sinθ

C(k) = Theodorsen's lift deficiency function

x_A = distance from section aerodynamic center to blade elastic axis, positive when A.C. is forward.

Neglecting the $\dot{\beta}$ terms since c << R, multiplying by R sin nθ and dividing by $I_n\Omega^2$, there results

$$\frac{1}{I_n\Omega^2}\int_0^{\pi} \sin\theta \sin n\theta \frac{dL}{d\theta}\, d\theta = -m_{\dot{g}}\dot{g}_n - m_\beta C_n f_n$$

where $C_n = \frac{R\beta}{z} = -\frac{n^2(1+k)}{1+kn^2}$ from equation (14).

$$m_{\dot{g}} = \frac{\gamma}{2}\overline{C(k)}\ \frac{\int_0^{\pi}\sin^3\theta \sin^2 n\theta\, d\theta}{\int_0^{\pi}\sin^2 n\theta\, d\theta} = m_\beta$$

$$\gamma = \frac{\rho acR}{m}$$

$\overline{C(k)}$ = mean value of C(k) evaluated at $\theta = \frac{\pi}{4}, y_1 = 0.707R$

and the contributions of modes other than the nth are neglected.

Dividing equations (23) and (24) by $I_n\Omega^2$ and including the aerodynamic term,

$$\frac{\ddot{g}_n}{\Omega^2} + m_{\dot{g}}\frac{\dot{g}_n}{\Omega} + \nu_n^2 g_n + 2\frac{\dot{f}_n}{\Omega} + m_\beta C_n f_n = 0 \tag{25}$$

$$-2\frac{\dot{g}_n}{\Omega} + \frac{\ddot{f}_n}{\Omega} + (1+iG)\bar{\nu}_n^2 f_n = 0 \tag{26}$$

where $\nu_n = \frac{\omega_n}{\Omega} = [n^2 - 1]^{1/2}$ n = 2, 3, ...

$\bar{\nu}_n = \frac{\bar{\omega}_n}{\Omega} = [(\frac{\bar{\omega}_{n_o}}{\Omega})^2 + (n^2-1)]^{1/2}$ n = 2, 3, ...

G = structural damping coefficient

These are the flutter equations for the wind turbine rotating in still air.

5. Calculation of Flutter and Divergence Boundaries

Assume the following solutions to equations (25) and (26):

$$g_n = \bar{g}_n \, e^{\nu\Omega t} \tag{27}$$

$$f_n = \bar{f}_n \, e^{\nu\Omega t} \tag{28}$$

where $\nu = \frac{\sigma}{\Omega} + i\,\frac{\omega}{\Omega}$. Assume at present that $\overline{C(k)} = 1$ and $G = 0$.

Substitution of equations (27) and (28) in equations (25) and (26) results in two coupled homogeneous algebraic equations. For a solution to exist, the determinant of coefficients must vanish; i.e.,

$$\begin{vmatrix} (\nu^2 + m_{\dot{g}}\nu + \nu_n^2) & (2\nu + m_\beta C_n) \\ -2\nu & [\nu^2 + \bar{\nu}_n^2] \end{vmatrix} = 0$$

Expanding the determinant yields the characteristic equation of the system:

$$A\nu^4 + B\nu^3 + C\nu^2 + D\nu + E = 0$$

where the coefficients are combinations of the system parameters. Then by Routh's criteria for system stability

$$A,\ B,\ C,\ D,\ E \geq 0 \tag{29}$$

and $$BCD - AD^2 - B^2E \geq 0 \tag{30}$$

It is now possible to determine the values of $\bar{\nu}_n^2$ required to satisfy conditions (29) and (30) for a given blade configuration. Since

$$\bar{\nu}_n^2 = \left(\frac{\bar{\omega}_{n_o}}{\Omega}\right)^2 + (n^2-1)$$

the values of rotational speed at which flutter or divergence will occur are then specified for a given non-rotating torsional frequency $\bar{\omega}_{n_o}$.

In the present case, the characteristic equation is

$$\nu^4 + m\dot{g}\nu^3 + (4 + \nu_n^2 + \bar{\nu}_n^2)\nu^2 + m\dot{g}(\bar{\nu}_n^2 + 2C_n)\nu + \nu_n^2\,\bar{\nu}_n^2 = 0$$

Applying condition (29), flutter occurs when

$$\bar{\nu}_n^2 = -2C_n$$

or using equation (16), when

$$\left(\frac{\bar{\omega}_{n_o}}{\Omega_F}\right)^2 = -2C_n - (n^2-1) \tag{31}$$

Applying condition (30), flutter occurs when

$$\bar{\nu}_n^2 = \frac{2C_n^2 - 4C_n - C_n\,\nu_n^2}{2 - C_n}$$

or using equation (16), when

$$\left(\frac{\bar{\omega}_{n_o}}{\Omega_F}\right)^2 = -2C_n - \frac{2(n^2-1)}{2 - C_n} \tag{32}$$

where $C_n = -\dfrac{n^2(1+k)}{1+kn^2}$ as discussed in Section 4.

Note that equation (31) is the critical case.

6. Discussion of Results

Equation (7) for blade flatwise bending frequency of the first flatwise mode (n = 2) is plotted in Figure 5 for the two-meter blade and in Figure 6 for the seventeen-meter blade. Also shown are blade torsion-chordwise bending frequencies of the first torsion-chordwise mode (n = 2).

The blade flatwise and torsion-chordwise bending frequencies for both blades approach one another as rotational speed is increased, but resonance between these modes does not occur in the operating range. The resonance between the second bending mode and the first torsion/chordwise mode shown in Figures 5 and 6 is not critical since these modes are orthogonal and therefore are not coupled. This is true for all higher bending modes.

Equation (31) for blade flutter is plotted in Figure 7 for both blades in terms of rotational speed at flutter and torsion/chordwise coupling coefficient C_n. The instabilities are seen to be sensitive to this parameter, which has a theoretical value of about -4 for the first mode (n = 2). Substantial 2/rev vibration of the two-meter blade in modes similar to those described by equations (8) and (10) occurred experimentally in the 200 to 300 rpm range. This result suggests that a practical value of the coupling coefficient C_n may be between -2 and -3. If so, then the seventeen-meter blade without struts would be expected to flutter in the 50 to 75 rpm range.

The theoretical analysis indicates that blade instabilities can be suppressed by increasing the blade torsional stiffness. Figure (8) shows the effect of torsional stiffening on theoretical rotational speed at flutter for the two-meter blade, and a value for C_n of -2.0. The flutter speed varies nearly linearly with the square root of the torsional stiffness. It is suggested that experimental confirmation of the effect of varying torsional stiffness on the rotational speed for blade flutter be obtained using the two-meter model.

7. Conclusions and Recommendations

The analysis of this report indicates that the troposkien-type blade is subject to flutter instabilities. These instabilities can be suppressed at a given rotational speed by increasing the blade torsional stiffness.

It is recommended that these results be confirmed by experimental investigation of the effect of increasing the torsional stiffness of the two-meter model blades on the rotational speed at which blade instability occurs.

It is also recommended that further analysis be conducted to determine the effect of the incident wind on blade aerodynamics and response, and to investigate the effect of bracing struts on the stability of the seventeen-meter model.

References

1. Blackwell, B.F., and Reis, G.E., "Blade Shape for a Troposkien Type of Vertical-Axis Wind Turbine", Sandia Laboratory Report 74-0154, April 1974.
2. Weingarten, L.I., and Nickell, R.E., "Nonlinear Stress Analysis of Vertical-Axis Wind Turbine Blades", Sandia Laboratory Report 74-0378, April 1975.
3. Ojalvo, I.U., "Coupled Twist-Bending Vibrations of Incomplete Elastic Rings", International Journal of Mechanical Sciences, 4, Pp.53-72, 1962. (See Appendix A).
4. Miller, R.H., and Ellis, C.W., "Blade Vibration and Flutter", Journal of the American Helicopter Society, 1, 3, July 1956.

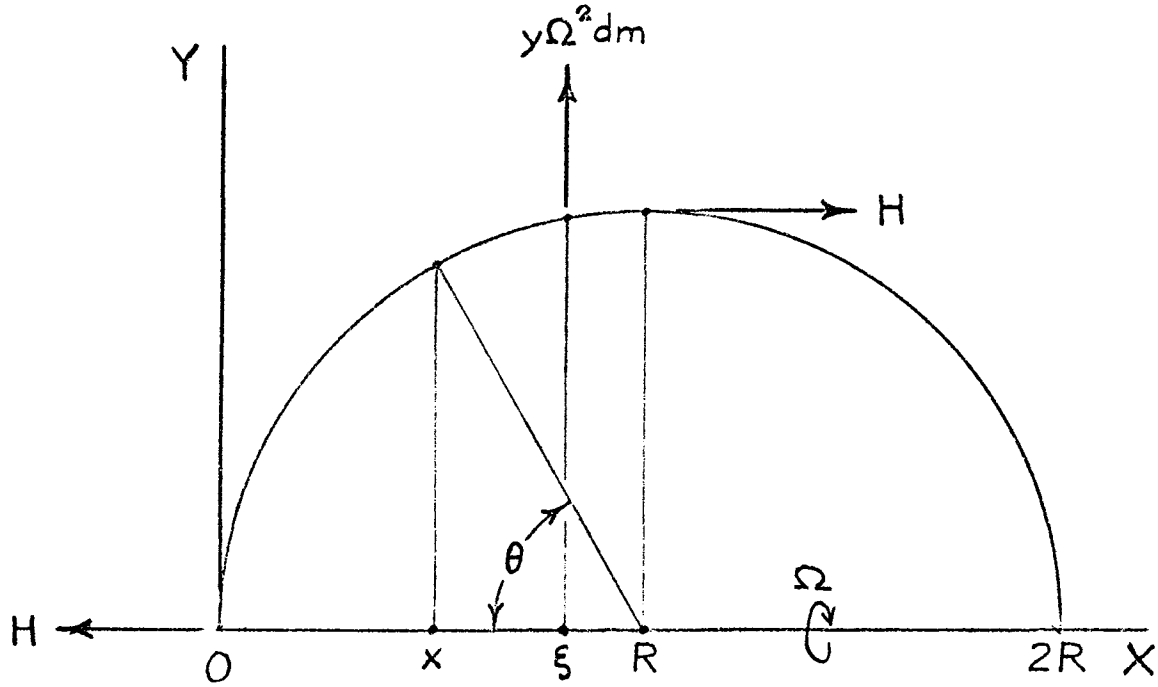

FIGURE 1. BLADE GEOMETRY

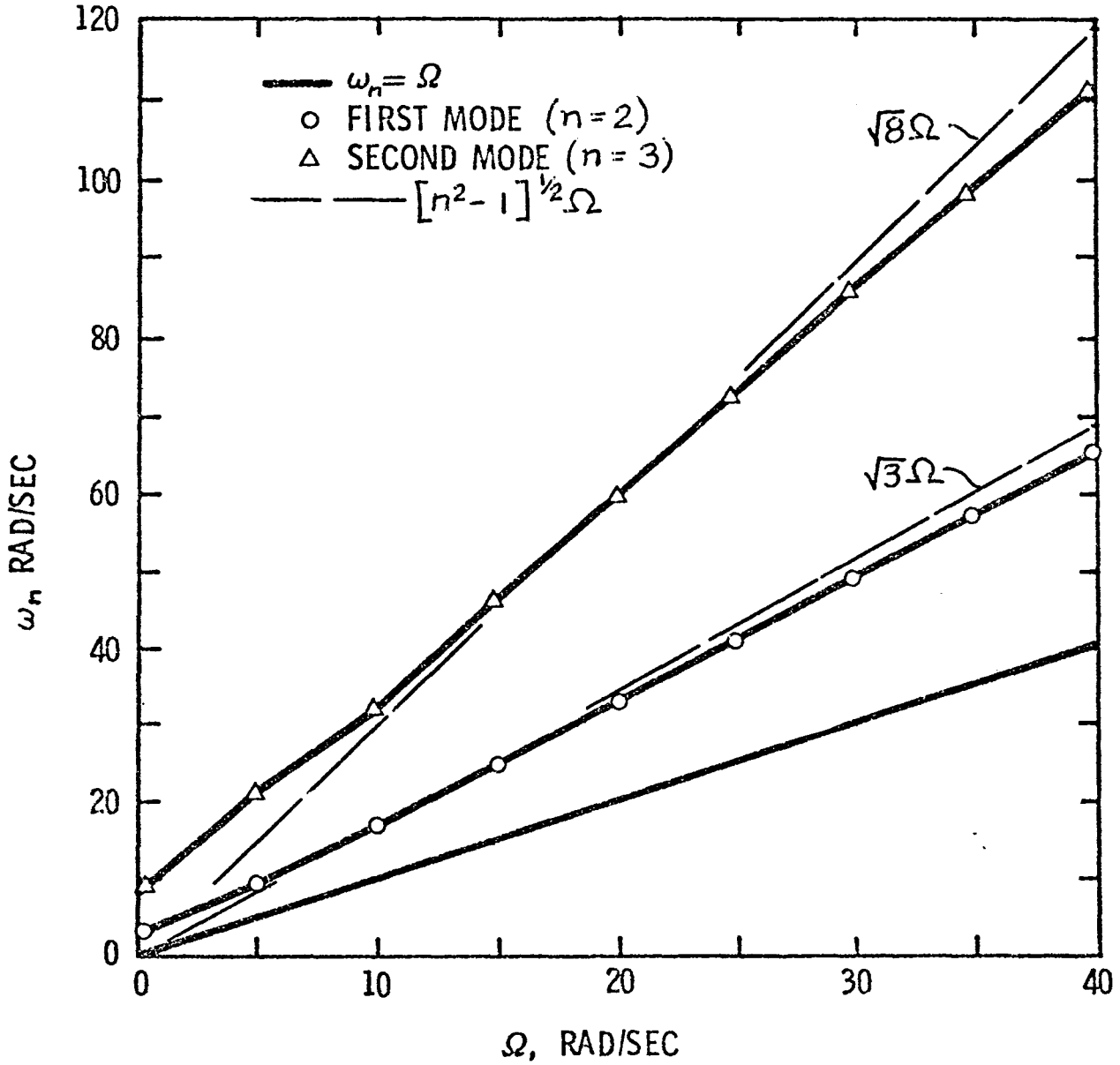

FIGURE 2. Natural Frequency Spectrum (First Two Modes), ω_n vs. Angular Velocity, Ω.

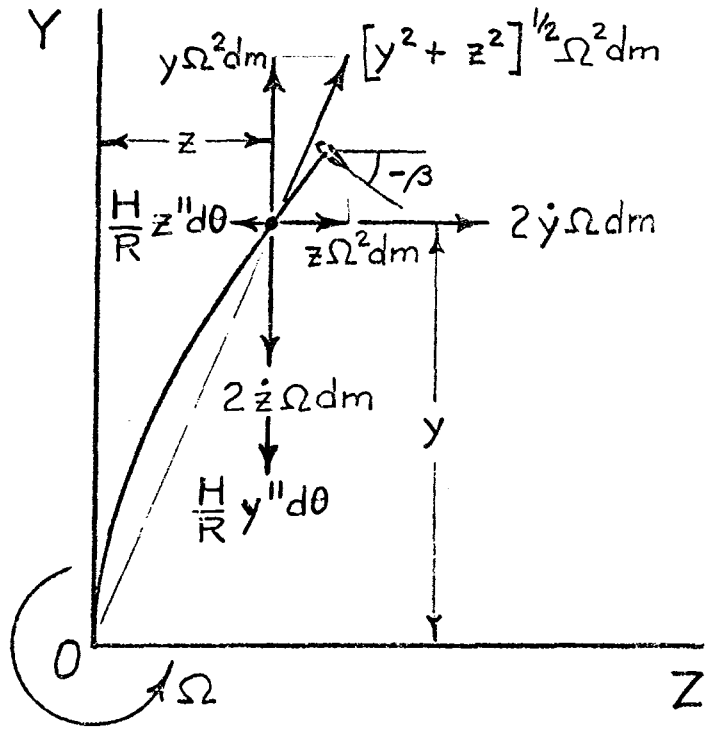

FIGURE 3. BLADE DYNAMICS

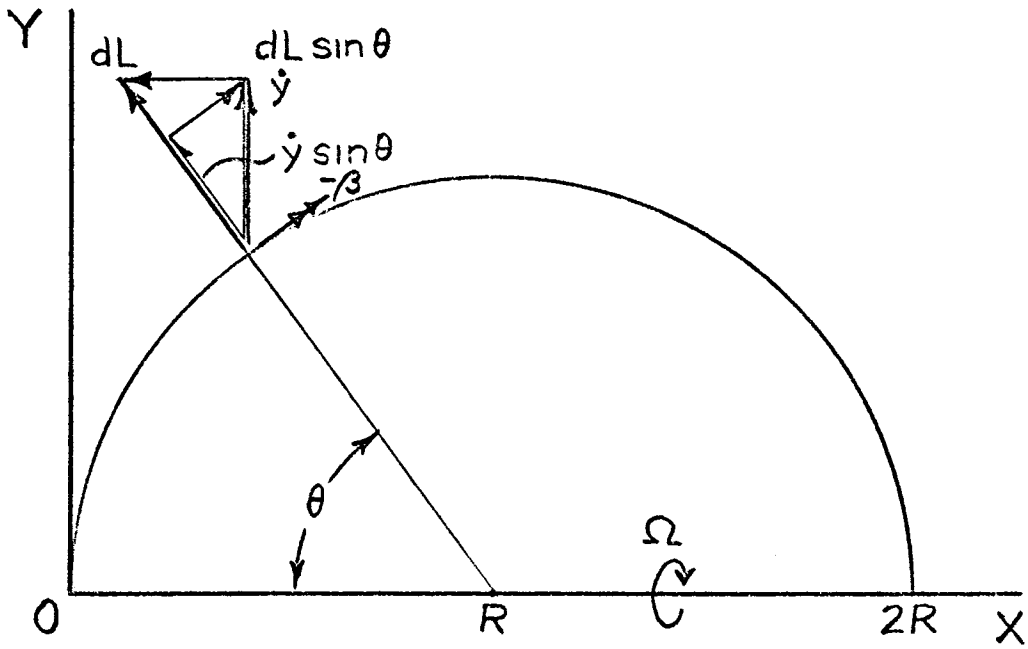

FIGURE 4. BLADE AERODYNAMICS

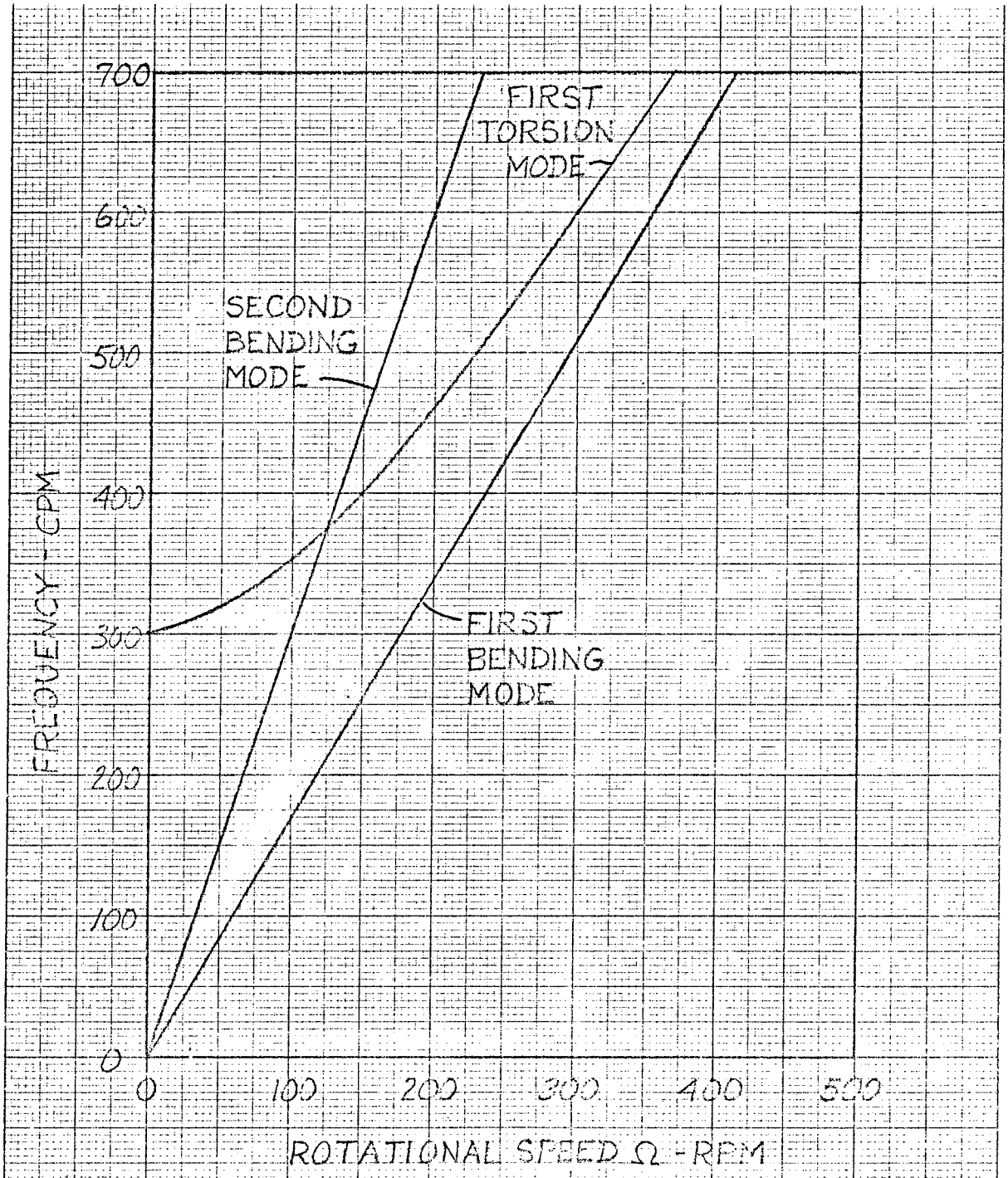

FIGURE 5. FREQUENCY DIAGRAM: TWO-METER BLADE

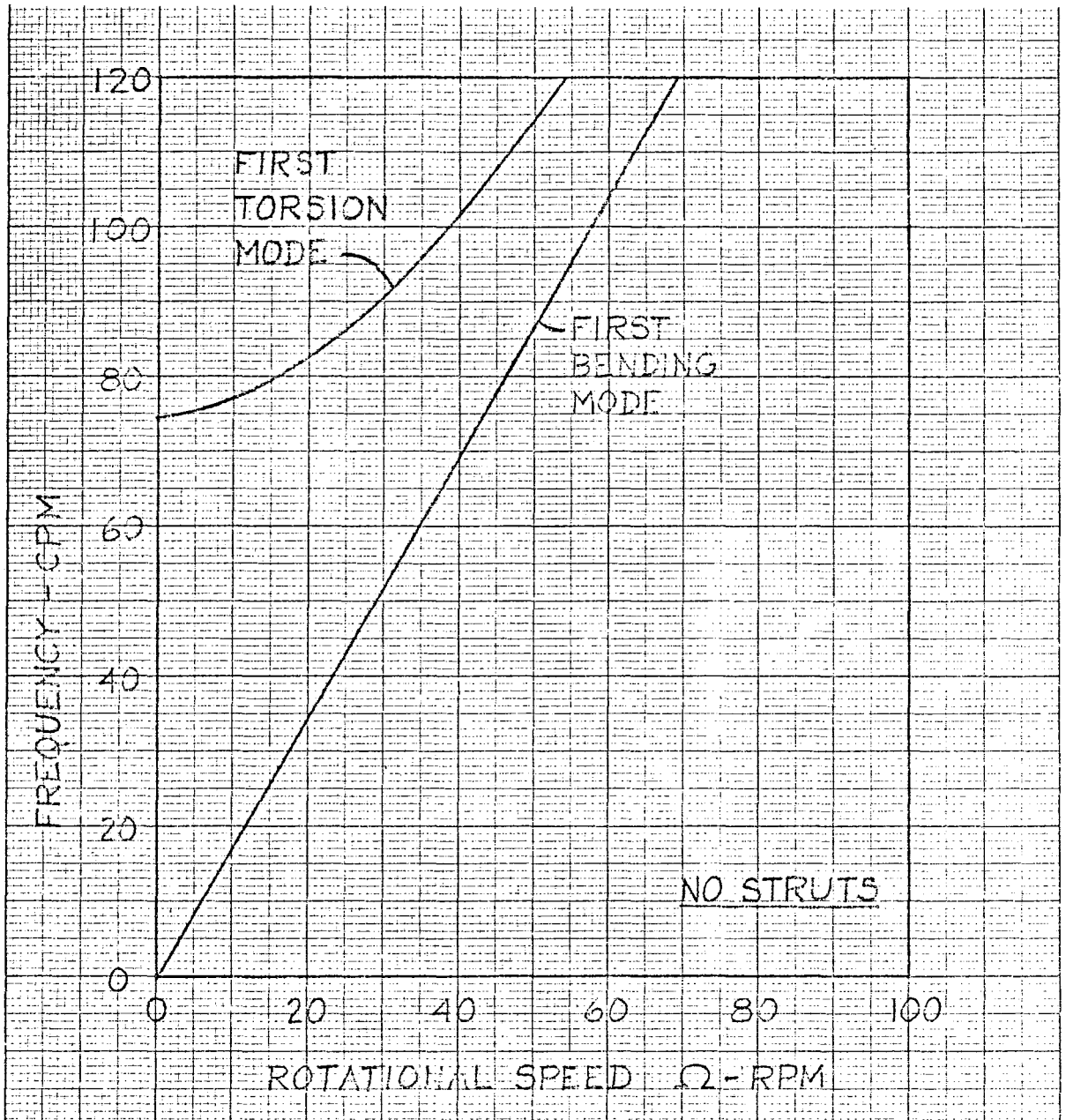

FIGURE 6. FREQUENCY DIAGRAM: SEVENTEEN-METER BLADE

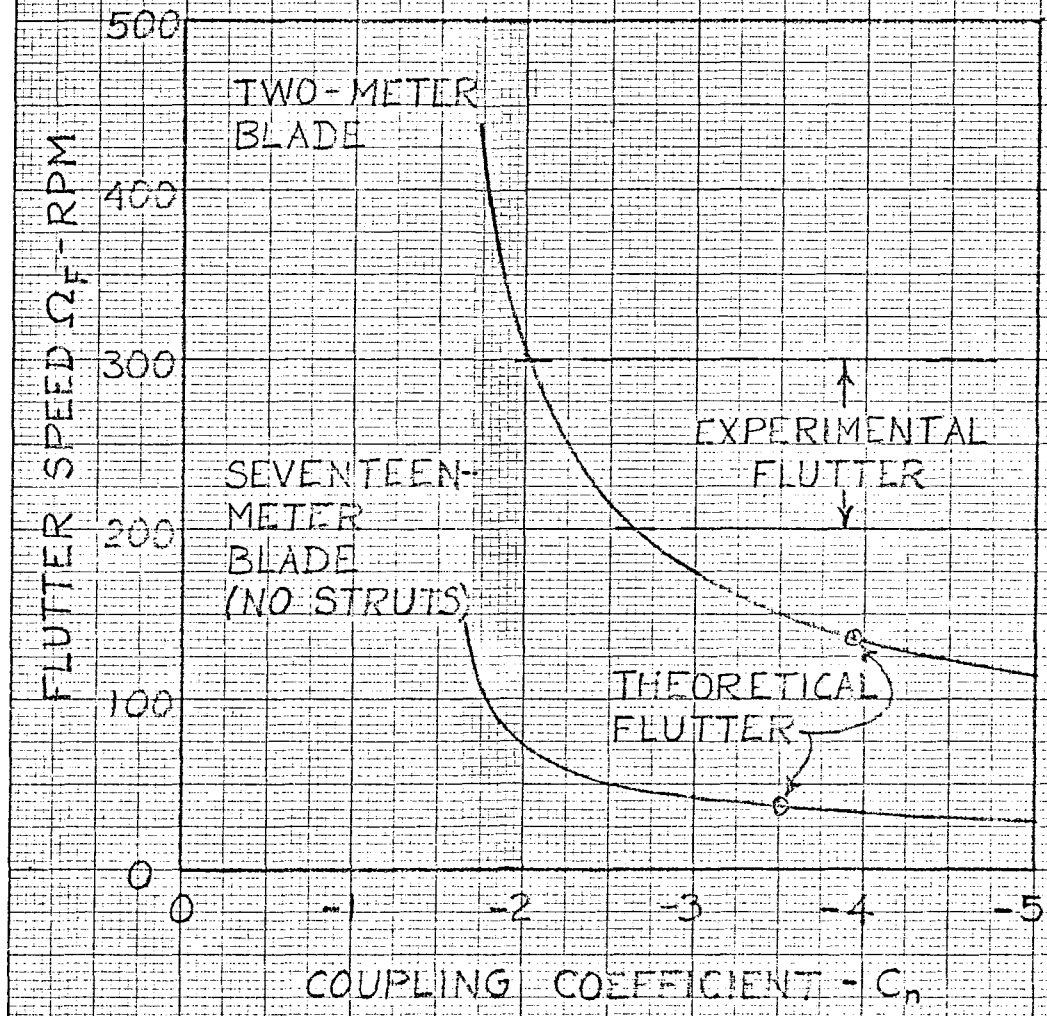

FIGURE 7. EFFECT OF COUPLING COEFFICIENT ON FLUTTER SPEED

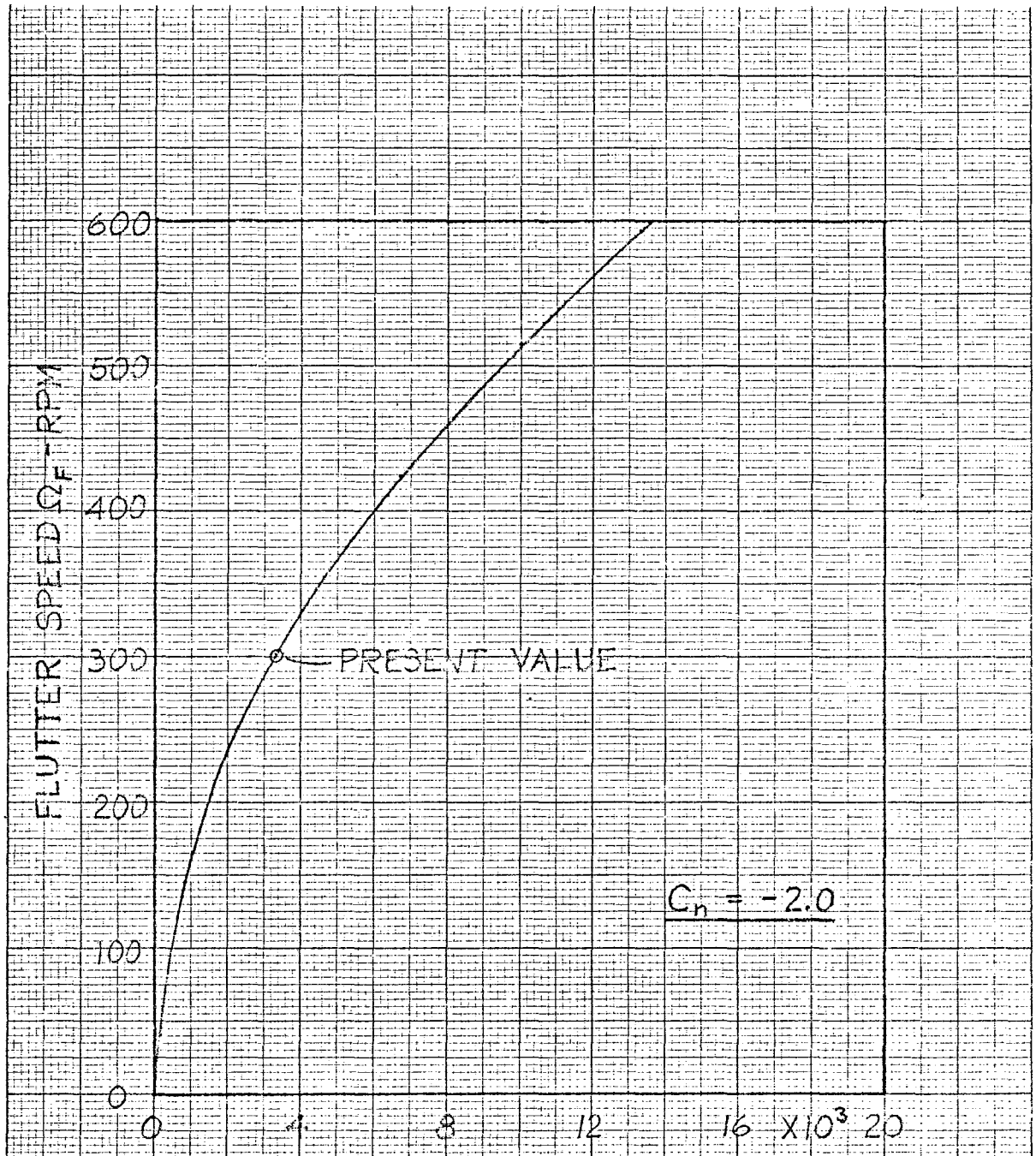

FIGURE 8. EFFECT OF TORSIONAL STIFFNESS : TWO-METER BLADE

BLADE DESIGN AND FABRICATION - 17-METER VAWT*

Justin J. Barzda
Chief of Systems Research
Kaman Aerospace Corporation
Bloomfield, Connecticut

Abstract

Sandia Laboratories is planning to erect and operate an experimental 17-meter vertical axis wind turbine (VAWT) power generation system. The subsystems are being designed for fabrication. The subject of this paper is the design and fabrication of rotor blades for the turbine. The rotor will have three blades with 0012 airfoil and 21-inch chord. The blades will be stiffened with support struts. The design criteria, structural design, supporting engineering analysis, and fabrication methods are discussed.

Introduction

The Federal government is presently committed to develop alternative clean, cost competitive sources of energy. The Energy Research and Development Administration (ERDA) is the lead Federal agency in this development.

Wind energy is one of the sources of interest. Numerous wind energy conversion systems are being funded for demonstration and evaluation as part of the development program.

One of the concepts of interest is the vertical axis wind turbine (VAWT) which accepts wind from any direction, eliminating the need for a yaw mechanism in the system. Blade pitch control may not be required either. Thus, the VAWT system design may be simpler than that of the horizontal-axis turbine systems.

To evaluate the competitiveness of VAWT systems, ERDA has funded Sandia Laboratories to erect and operate a 17-meter VAWT power generation system. The system will serve as a research facility to experimentally demonstrate and evaluate aerodynamic, structural, and system design concepts.

Kaman Aerospace Corporation was awarded the contract to design and fabricate the turbine rotor blades. Sandia is designing and providing all other subsystems, including the turbine support tower.

*Work being performed under Sandia Laboratories Contract No. 02-7427.

Design Criteria

The basic design criteria and guidelines specified by Sandia are as follows. The rotor will be 17-meters (approximately 56 feet) in height and maximum diameter. Basic geometry is shown in Figure 1.

The edge view profile of the blades should approximate a troposkien*, a shape favorable structurally. An acceptable approximation is two straight segments connected to a middle circular arc segment.

Blade cross section is to be NACA 0012 airfoil shape. Chord length, approximately 0.5 meters, is to be constant along the entire length of the blade.

The blades should survive aerodynamic, dynamic, centrifugal, and gravity loads for rotational speeds up to 75 rpm in wind gusts up to 80 mph. It is also desired that, stopped, the blades survive hurricane wind forces.

Blade natural frequencies must be high enough to avoid two- and three-per-revolution excitation.

The blades should also withstand repeated angular accelerations and decelerations during free run and braking. The brake rating will be approximately 50,000 pound-feet torque.

Blade Design

General - Blades for the 17-meter rotor will be long slender structures supported at the ends. The structures must be relatively light for low cost and installation handling. But they must be strong and stiff enough in edgewise bending to withstand start up and braking decelerations and provide proper edgewise frequencies, have sufficient torsional stiffness to preclude blade flutter from aerodynamic loads, and be flexible enough flatwise to allow the structure to assume a near-troposkien shape when rotating so that steady centrifugal loads primarily load the structure in tension.

After evaluating these essential requirements, Kaman proposed to adapt and use for the VAWT application an existing rotor blade structure which Kaman developed for the UH-1H helicopter under U. S. Army contract. The structure, shown in Figure 2, has been tested and proven. Use of this field repairable blade structure saves engineering and tooling efforts and cost and minimizes development risks.

* Shape assumed by a rope, in the absence of gravity, when spun about an axis containing the end support points.

Blade Shape and Size - For portability, handling ease, and transport convenience during manufacture, delivery, and site erection, the blades will be made in three segments - a curved center section and two end straight sections. The curved section span will be 31.8 feet, and the arc height 9.2 feet. The straight section will be 20.4 feet long. Weights, respectively, will be about 300 pounds and 185 pounds.

To meet the natural frequency requirement, struts will be used to stiffen the basic blade. The strut structures, 22.7 feet long, will be similar to the blade straight sections. Their provision is conservatively tentative until operational experience is obtained. If satisfactory dynamic behavior can be demonstrated without them, struts would be eliminated from future systems to reduce costs.

When assembled, the sections will form a Darrieus-type rotor conforming essentially to Sandia's specified geometry. The blade and strut cross sections will be NACA 0012 along their entire length, excepting the end attachment areas. The blade strut intersections will be faired to minimize drag and power loss.

Blade Cross Section - The blade structure being adopted for the VAWT is shown in Figure 3. It consists of a durable and abrasion tolerant extruded aluminum leading edge spar, non-corrosive polyamide (Nomex) paper honeycomb core afterbody, fiberglass afterbody skins, and a rugged aluminum trailing edge spline. Extrusions will be 6061-T6 aluminum alloy.

The design was the winning candidate of six final configurations studied by Kaman for the U. S. Army for less expensive helicopter blades. The advanced design blade was to have a lower life cycle cost, be more tolerant of damage, and be more field repairable than existing operational blades.

The field repairable blade structure best met these objectives. Kaman believes that the design and features will also well serve the VAWT application.

The structure is rugged, durable, and damage tolerant. The heavy-walled leading edge spar allows deeper blending of nicks and erosion damage. The composite afterbody is highly repairable. Kaman has developed and demonstrated tools and techniques for field repair of damage up to and including through holes up to 7 inches in diameter.

The low operating stresses in the prime structural members, the anti-corrosion design, and degree of repairability should assure a long service life.

Interconnections - The design of the connecting fittings at the blade - strut interfaces and tower attachments have the following design features and objectives:

1. All end fittings are attached in a like manner to the blade and strut structures.

2. Each end fitting system consists of:

   - a honeycomb-closure rib fitting of machined aluminum alloy.

   - load distribution skin doublers - four sheets of .010 inch aluminum alloy extending from the leading edge to the trailing edge on both surfaces, conforming to the airfoil contour, and bonded to the basic structure.

   - hinge fittings of heat treated 4340 steel, cadmium plated for corrosion protection, attached to the leading and trailing edge extrusions with flush head fasteners.

3. Double pin attachments are provided in the outboard ends of the blade straight sections to:

   - facilitate erection assembly - straight sections and struts can be mounted and pinned before installation of the curved segments.

   - permit repositioning of the strut up to horizontal, if desired.

4. Weight attachments for static and dynamic balancing are provided within the closure ribs at the blade-strut interfaces.

Engineering Analyses

Engineering analyses are in process to verify the blade components structural integrity, determine blade natural frequencies and dynamic behavior, and calculate the physical and mechanical characteristics.

Although the Darrieus-type rotor was first demonstrated in the 1920's, published analyses and data to predict rotor performance, blade loadings, and inflows are scarce. As a result, Kaman wrote and developed its own computer codes for much of the analyses.

Loads Prediction - Rotor performance and operational blade loads are being calculated with the Darrieus Rotor Elemental Airloads and Moments (DREAM) program, a detailed blade element analysis, developed by Kaman. The program:

- modifies the inflow velocity to account for extraction of energy.

- calculates turbine output power using the modified inflow.

- calculates blade normal and chord forces distribution along the span as a function of azimuth and operating conditions.

The analysis defines the elemental section angle of attack along the span and around the azimuth, uses straight line approximations of NACA 0012 airfoil lift and drag coefficient curves for angles of attack through 180 degrees and includes body forces due to gravity and centrifugal fields. Rotation is counter-clockwise, viewed from above. 0 degree azimuth is downwind on the rotor centerline vertical plane.

Figure 4 presents calculated power coefficients (C_p) versus tip speed ratio ($\Omega R/V_\infty$) and shows a comparison with experimental data[1]. Calculated coefficients approximate the experimental values, but spread over a wider range of tip speeds. The correlation is considered satisfactory for Kaman's design needs.

Figure 5 is a plot of the calculated aerodynamic loading normal to the blade elements at 75 rpm and 80 mph wind for the 50 deg azimuth position where loading is approximately maximum outward (positive). Maximum inward (negative) loading occurs 80 deg later. Both maximums are about 175 lb/ft span at the equatorial element.

Stress Analysis - The predicted aerodynamic loadings, combined with gravity and centrifugal forces, were used to establish reactions, external and internal loads, and moments in the blade and strut structures. Detail stress analyses are in process on the structural components for:

- normal operation at 50 rpm in 30- and 60-mph winds.
- runaway operation at 75 rpm in 80-mph wind gusts.
- deceleration at 50,000 lb-ft braking torque.
- locked rotor gusts loadings up to 150 mph.

Fifty rpm is the planned maximum normal operating speed. Rotational speed will be regulated to this level by the power load or the torque brake. The runaway speed of 75 rpm represents an overspeed design margin, allowing time for the brake to become effective in sudden wind velocity increases.

The stress analysis will verify structural adequacy and fatigue life of the newly designed interconnecting end attachment fittings and the blade basic structure being adapted for the VAWT application.

While the basic structure appeared suitable in preliminary design, if the analysis shows insufficient strength or inadequate life, it is believed the shortcoming would be local and readily strengthened with reinforcement or modification.

Dynamic Analysis - Natural frequencies for the curved blade, straight sections, and struts are being determined by the MacNeal-Schwendler Corporation under a subcontract. It was expedient and economical to use their proprietary computer program, SADSAM. The program was readily adaptable for the VAWT system analysis.

The determinations, nearing completion, are being made with a fully-coupled flatwise, chordwise, and torsion dynamic analysis. Each blade component is represented by multiple beam finite elements and lumped masses at the junctions between elements as shown in Figure 6. Flap hinges are assumed at the blade-strut interfaces and tower attachment points.

The mathematical model also includes centrifugal stiffening and coriolis effects. The latter is significant for VAWT turbines compared to propeller-type rotors.

It has already been determined that support struts are needed to stiffen the blades in flatwise bending. Without struts, the blade natural frequency is below two hertz. The struts raise frequency to over five hertz.

Fabrication

Since the design definition and supporting analyses are only in the final stage of completion, fabrication is yet to begin.

Manufacture of the straight blade sections and struts will be relatively straightforward. Techniques, procedures, and experience developed and acquired by Kaman in the manufacture of helicopter blades can be directly applied.

Detail components such as the spar and trailing edge spline, honeycomb after-body core, skin plies, doublers, and connecting fittings will be fabricated to their preassembly configuration.

The spar, spline, afterbody core, and skins will be laid up and assembled with adhesives in the bonding "clean room" on the bonding tool, a contoured mold mounted on a stiff base structure. The mold forms one surface of the section. The other surface will be shaped by a thin aluminum caul plate curved and held in place by a vacuum bag. The bag applies bonding pressure during the cure cycle. This layup is then placed into an autoclave to cure the high temperature adhesive at 250°F for 60 to 90 minutes and 25-30 psi pressure.

End "load distribution" doublers are then bonded to the primary structure in a secondary bonding operation using low temperature cure adhesive.

The structures will then be completed with the installation of end fittings to the spar and trailing edge spline. Fittings will be positioned into place in a jig for proper orientation and alignment, then secured with high strength flush fasteners.

Fabrication of the curved sections is more complex because of the size and shape. The curved section is too large to fit into the autoclave. The structure will have to be bonded with low temperature cure adhesives in an assembly room environment. Forming techniques for bending the heavy walled spar and trailing edge spline within acceptable tolerances have to be perfected.

ALCOA will be fabricating and forming the extrusions. They have bent some spar specimens in trial forming with success. Prime concern was to avoid buckling and twist. The 6061-T6 specimens formed to the desired radius without twisting and closely matched the design bend radius. The final pieces will, however, have to be formed in the T4 temper, then aged to the T6 temper for maximum strength properties and residual stress relief. Specimen pieces in the T4 temper are being prepared for trial forming to evaluate formability in the softer temper. The achievements thus far give confidence that successful forming techniques will be developed.

Fabrication of the curved sections will differ from the straight structures in another respect. The composite afterbody will be made up of sections or trailing edge pockets bonded to the spar and unitized with the trailing edge spline. The section-to-section joints will be sealed with fiberglass splice strips. This approach, used successfully on helicopter blades, was selected to expedite prototype units fabrication.

Tooling for the afterbody fabrication will be smaller, more manageable, and less expensive for sections than for a very large homogeneous piece. Sections will facilitate assembly of the afterbody to the spar by permitting minor adjustments for mating and contour discrepancies.

The afterbody sections, one at a time, will be assembled with adhesive in the bonding tool, then cured in the autoclave just as were the straight section assemblies.

Assembly of the curved section will begin with positioning and securing of the curved spar nose down on the floor assembly jig. The afterbody sections will then be mated, aligned, and bonded to the spar one at a time. Heat lamps will be used to cure the low temperature cure adhesive. A dummy spline, referenced to the spar, will be used to align the section trailing edge for proper camber and trailing edge curvature. When all sections have been bonded to the spar, the dummy will be removed, and the permanent spline inserted and bonded to the structure. Bond assembly will be completed with the addition of end doublers.

All sections and end connecting fittings will then be weighed and selectively matched and coded into blade assemblies so that assembly weights will match as closely as possible. Weight will be added to the lightweight blades to bring all blade weights within 0.3 percent of each other.

The structures will be completed with the installation of the end connecting fittings to the spars and trailing edge splines. The blade sections will be positioned and aligned on a floor plane to simulate their installed relationship, and secured. The fittings will be fitted and aligned, then secured with high strength flush fasteners. This preinstallation alignment should facilitate site erection.

Conclusion

The 17-meter VAWT system will be the first of its size to be erected and demonstrated in the nation. Engineering judgment has to be used to anticipate the structural requirements and dynamic behavior because past experience to draw on is limited. Sandia's guidelines provide a sound starting point. Kaman believes its proposed blade structure will serve the needs of this prototype research power generation system. The engineering knowledge developed in the design and data acquired in experimental operations should provide a sound basis for engineering of blade structures for future systems and improving cost competitiveness.

References

1. Banas, J.F., Sullivan, W.N., ENGINEERING OF WIND ENERGY SYSTEMS, Sandia Laboratories, Albuquerque, N.M., SAND 75-0530, January 1976.

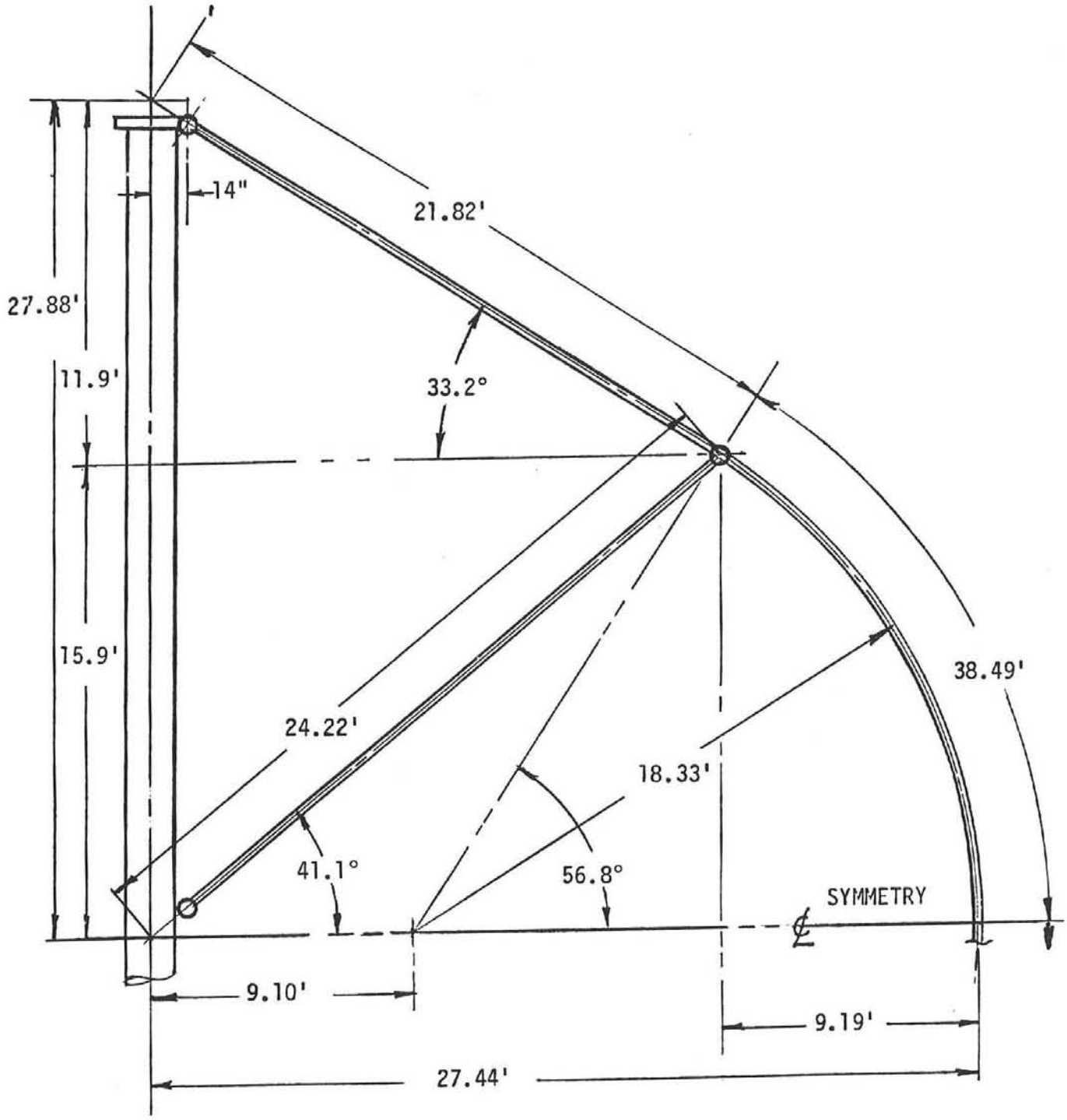

Figure 1. 17-m VAWT Rotor Geometry

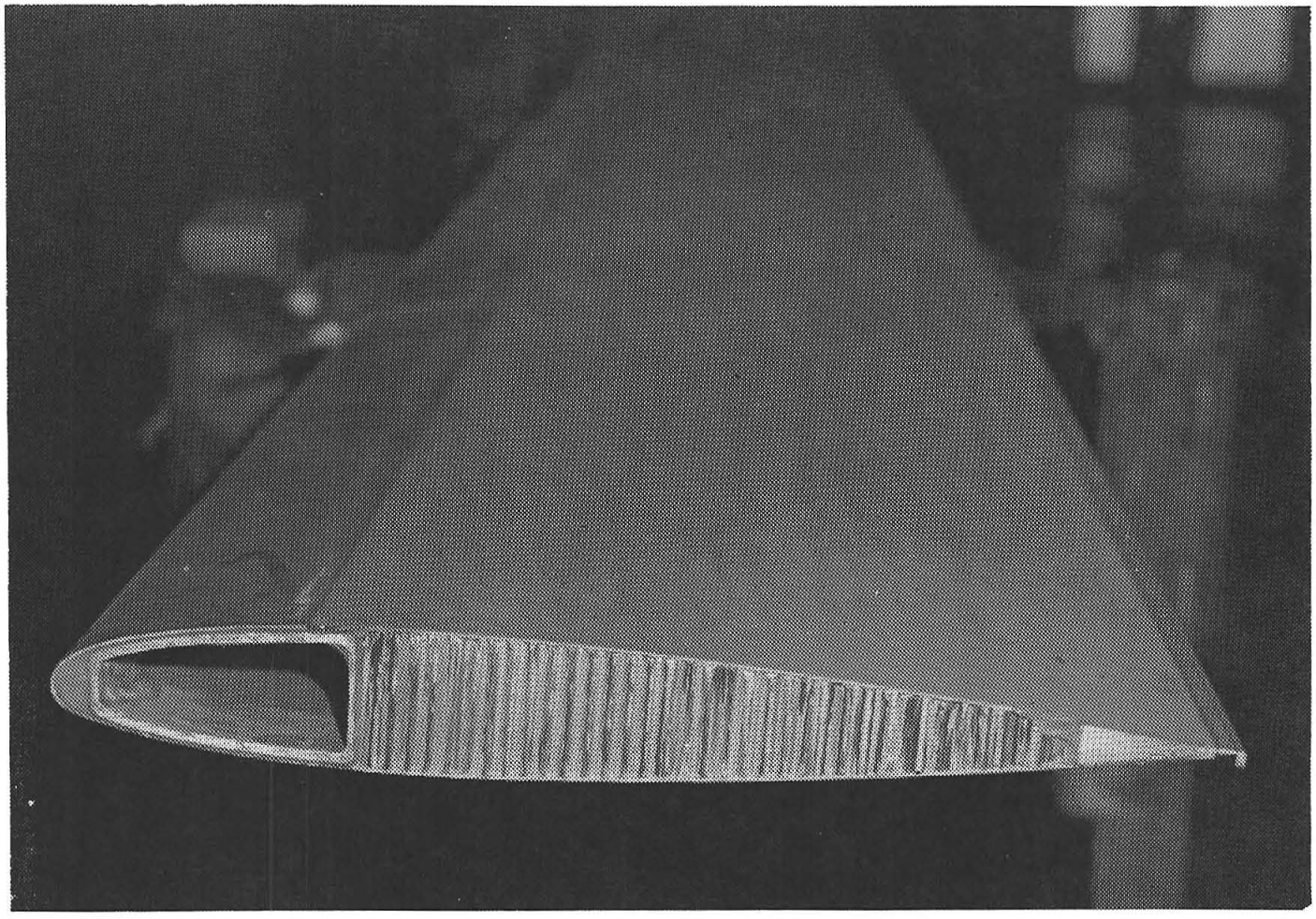

Figure 2. Field Repairable Blade for UH-1H Helicopter

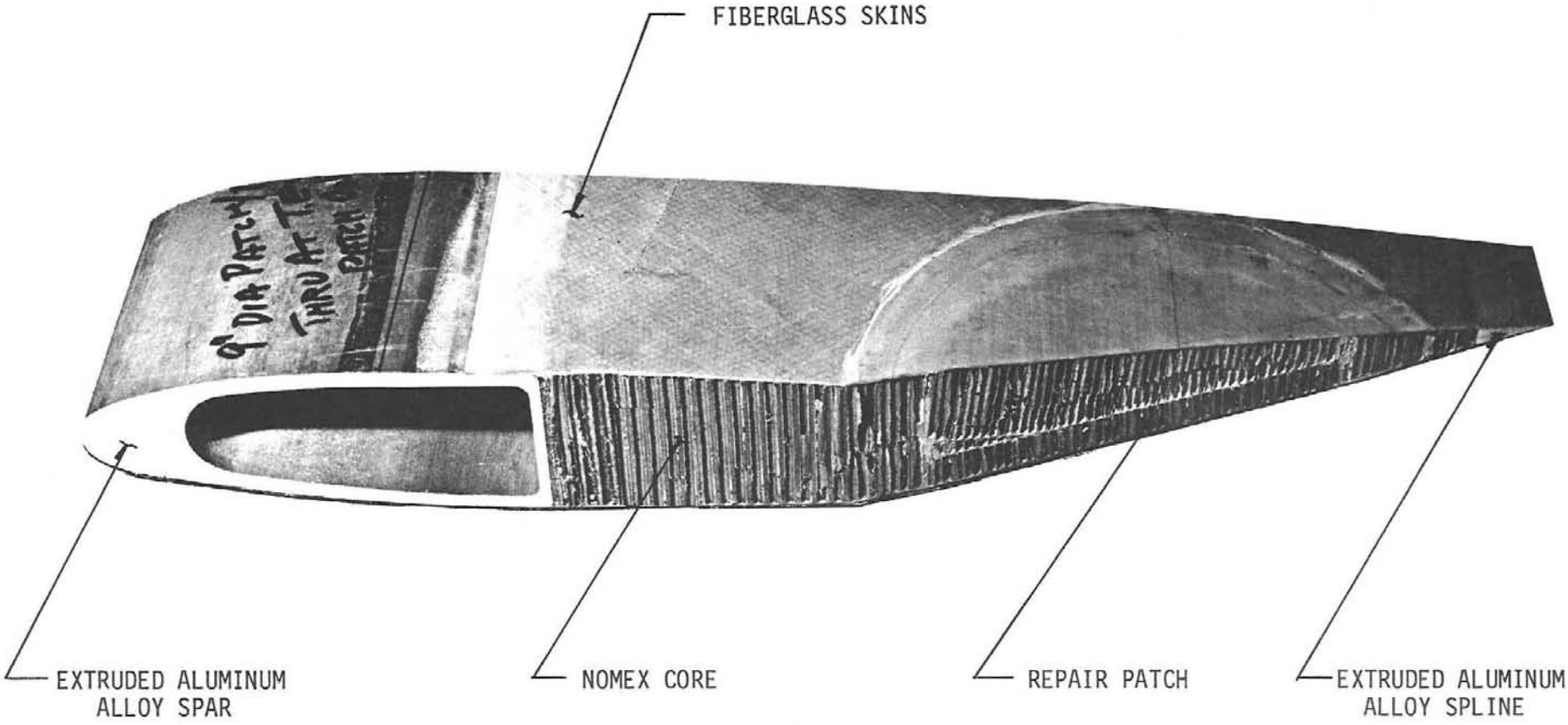

Figure 3. Blade Structure Features

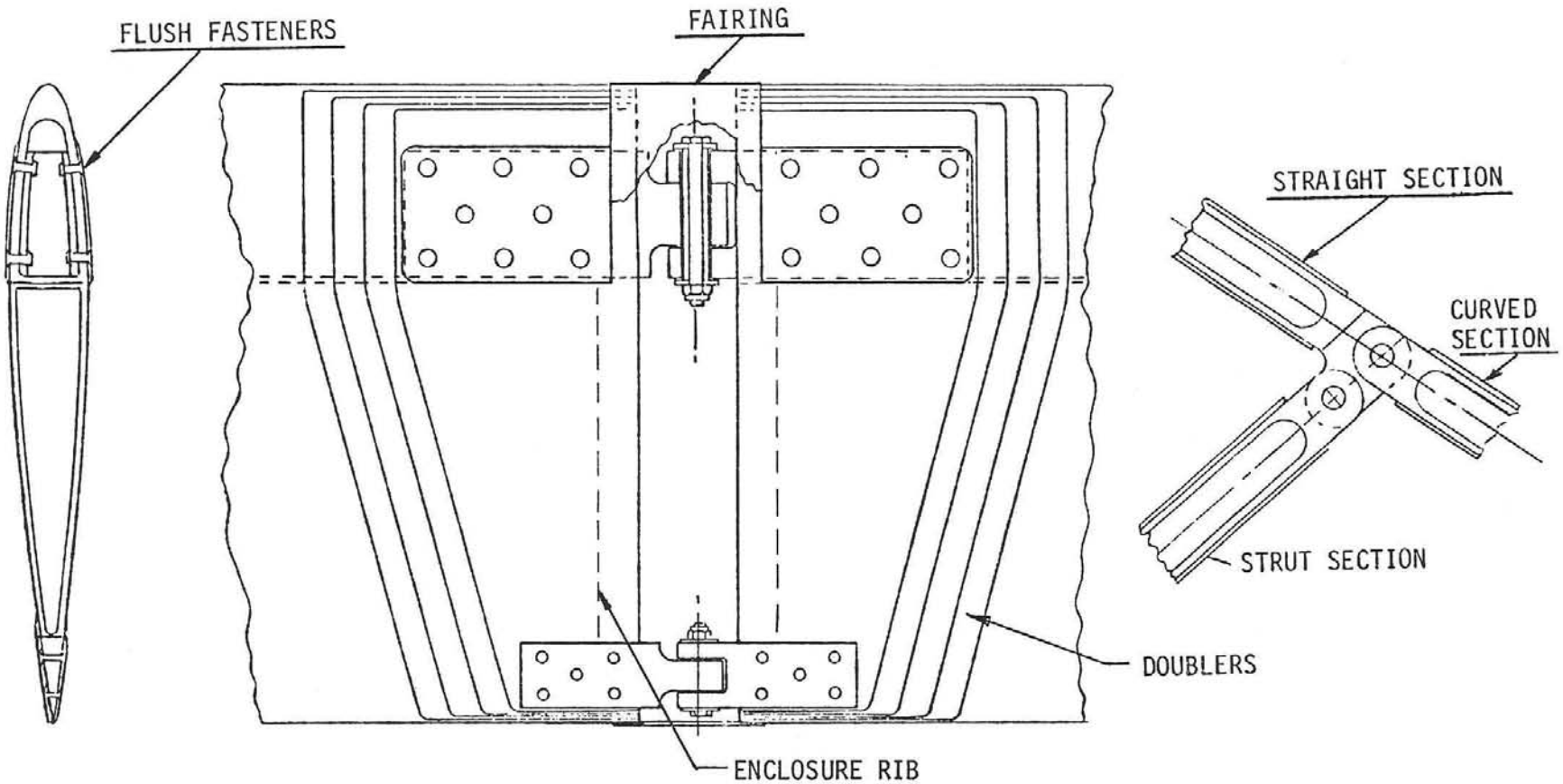

Figure 4. Blade-Strut Connection Details

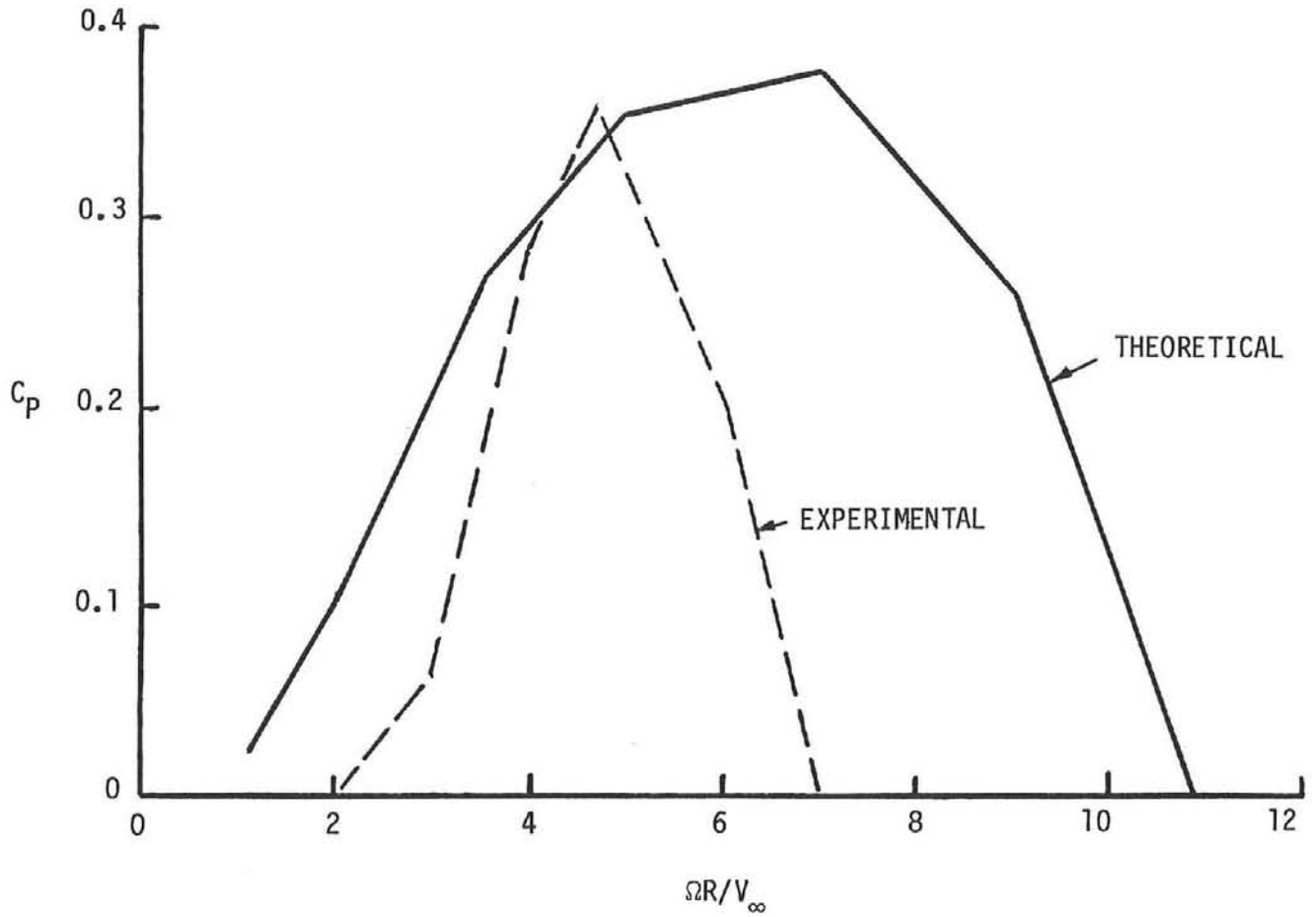

Figure 5. Power Coefficient vs Tip Speed Ratio

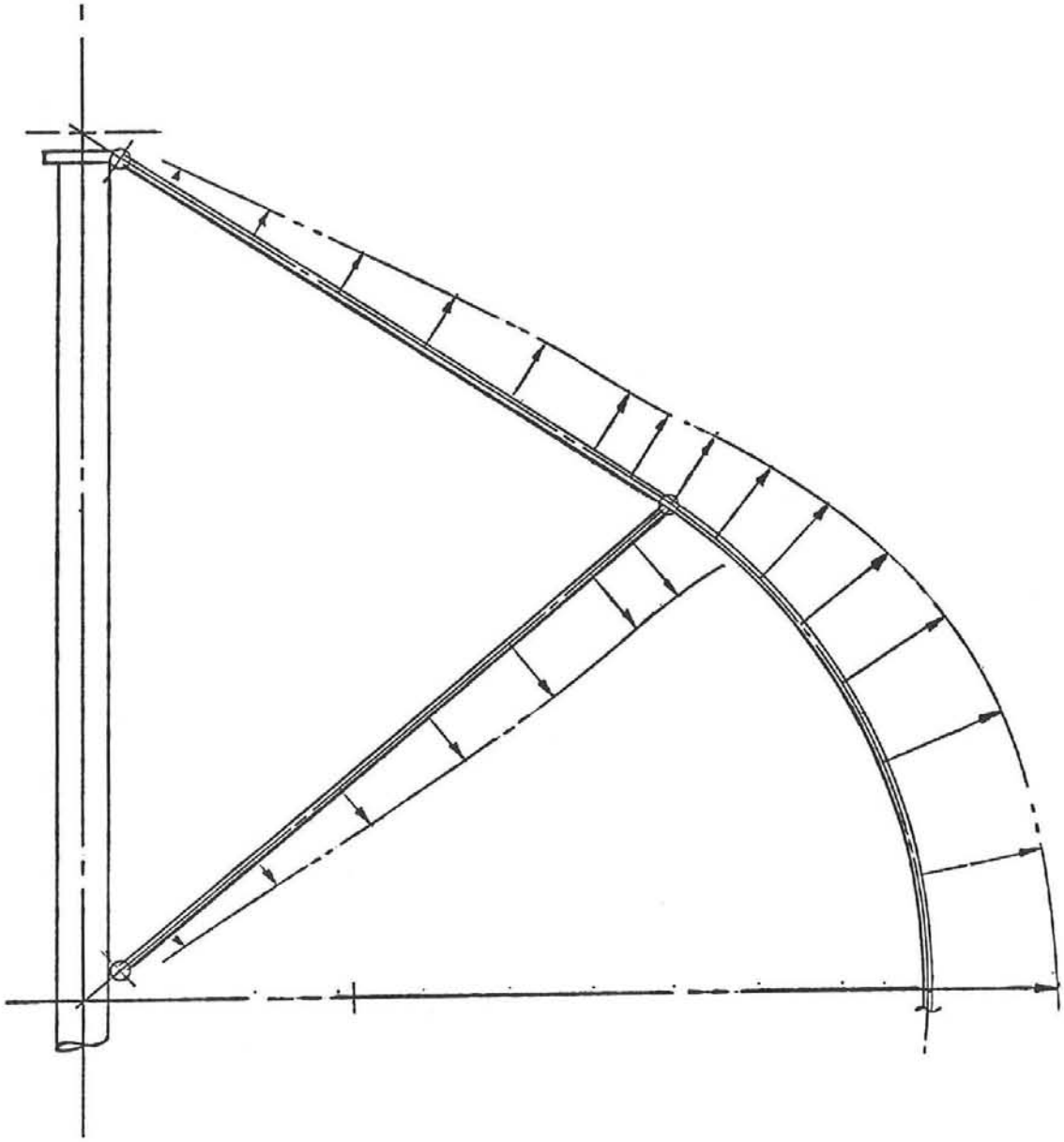

Figure 6. Blade Normal Force Distribution

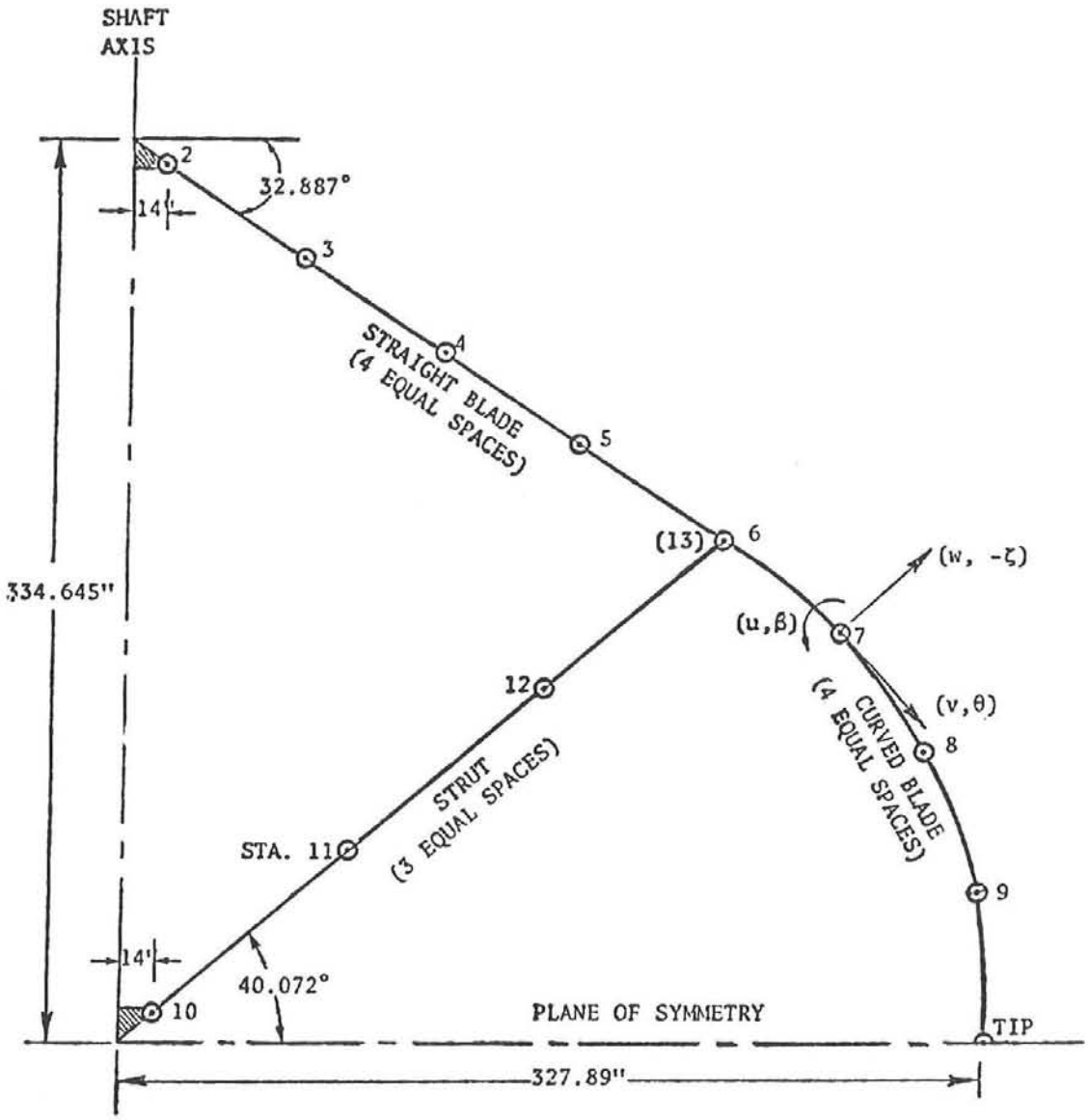

Figure 7. Dynamic Model

Figure 8. Formed Specimen Spars

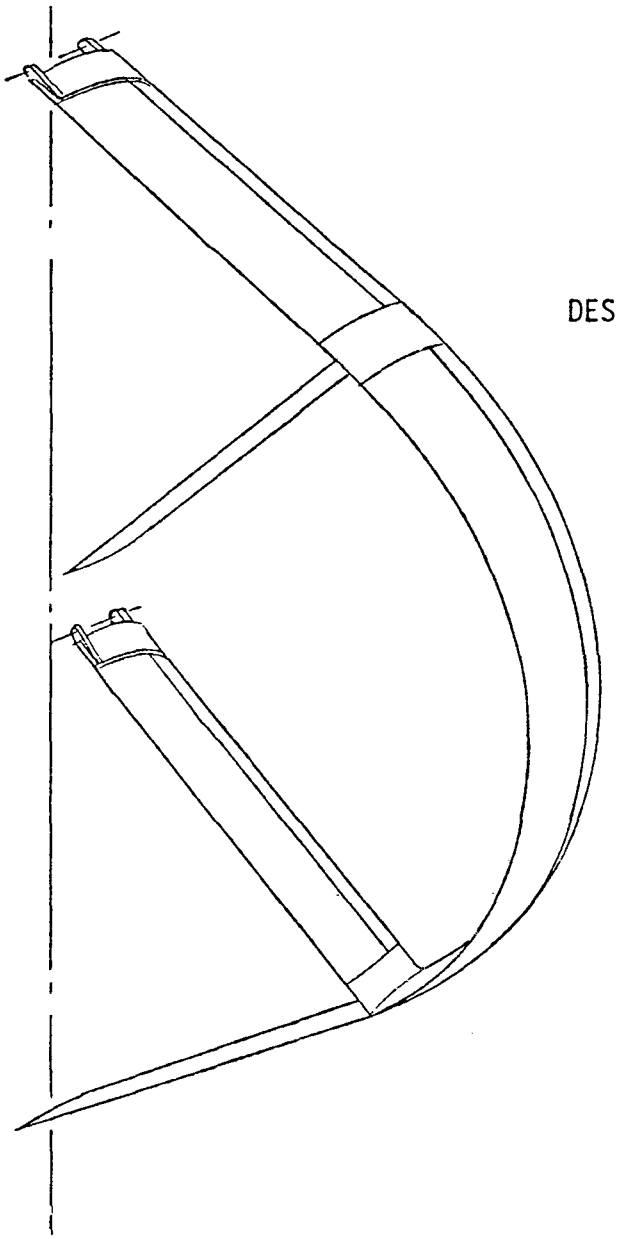

DESIGN AND FABRICATION OF VAWT BLADES

CONTRACT 02-7427

KAMAN AEROSPACE CORPORATION

LOW-COST BLADE DESIGN CONSIDERATIONS

Louis V. Feltz
Sandia Laboratories, Albuquerque, NM 87115

Introduction

ERDA has funded Sandia Laboratories to evaluate the potential of the Darrieus wind turbine. Since the preliminary studies have corroborated the claims—by Sandia and by others—that this turbine design is an attractive alternative to conventional propeller systems, the next step is to establish hardware designs that are attractive from both operational and economic considerations. This paper addresses one important component of such a design: the wind turbine blade.

It is recognized by those involved with wind energy conversion that the development of a low-cost blade design which will provide acceptable performance along with longevity of operation is crucial to a successful, cost effective wind energy program.

Attention to reducing the blade cost can have a decided effect in reducing the total system cost. Consequently, a major effort must be directed to developing a low-cost blade for the Darrieus turbine. Several approaches toward accomplishing this goal are discussed.

Low-Cost Blade Program Approach

A contract has been awarded to Kaman for the engineering and production of a set of prototype Darrieus blades for a 17-m system. In contrast to that approach, the studies described herein attempt to identify and continually upgrade blade designs that appear promising from a primarily economic viewpoint. The goal of this effort is to establish several low-cost blade designs.

The present in-house approach is to consider an overview of manufacturing processes and materials and to identify designs that appear to be economically attractive. These selected blade designs will then be refined by Sandia with the assistance of the appropriate manufacturing industry. Finally, a detailed design definition (drawings, procedures, etc) will be offered to competing manufacturers for a fabrication-only contract.

The fabrication-only-contract approach has two primary advantages:

- Details affecting blade design arise from an involvement and a familiarity with the entire Darrieus turbine program. It must be emphasized that the design of a Darrieus wind turbine blade is a highly interactive process and that the continuous updating of the design inputs encourages having both the input determination and the design activity within the same agency. The Darrieus turbine engineering activity is rapidly expanding, but the transfer of this technology is not instantaneous despite the honest and best efforts of the participants.

- Providing a completed blade design widens the pool of potential manufacturers (who may not possess the required analytical and engineering capabilities for a "turnkey" contract).

It is believed that this approach will be attractive to the many potential manufacturers who either do not have or cannot accumulate the various technical specialties required for the design of the blade. Furthermore, if given a specified production quantity along with the blade design, the manufacturer will establish the most accurate cost projection that can be made.

Sandia's responsibility to ERDA for establishing a low-cost Darrieus blade design can be fulfilled in various other ways. It can consist of Industry response

to a request for proposal which includes some of the engineering responsibility along with the charge of fabricating the blade. Such an approach was deemed warranted for the first set of blades for the 17-m turbine. The time scale proposed for this first large turbine indicated the desirability of incorporating both the analytical and manufacturing specialties of the helicopter industry. Although the cost of this task was established by open competition, it cannot be said that the establishment of a very-low-cost, production-quantity blade design constituted the foremost priority. It is hoped that this contractual effort will be extended to include blade designs with cost as a prime consideration.

Finally, a procedure will be established whereby unsolicited proposals concerning <u>any</u> phase of the design or manufacturing of the turbine components will be encouraged. At present, such an approach that includes the blade design effort may be premature; however, it will be both practical and profitable once an adequate blade design data base has been accumulated. This approach has already proved its worth in the selection of a geared increaser drive for the 17-m Darrieus turbine.

Design Process

It has been suggested that, because of the rapid pace of the overall Darrieus turbine engineering activities, the design function should not yet be separated from these related activities. This philosophy is expanded herein, along with the author's interpretation of the designer's task.

Although the hardware designer may be considered an integrator, a collator, or an innovator, his essential task is that of absorbing the assembled design inputs and establishing the definition of a hardware item that can be uniquely interpreted. The results of his effort usually constitute a set of manufacturing drawings and processes. Testing and acceptance criteria may also be included.

The apparent ease of the simplistic approach presented above is seldom, if ever, realized. Complications arise because the input requirements for a "real world" design are rarely determined to the degree of precision desired. This can

be demonstrated by considering various inputs to the Darrieus turbine blade design. A comprehensive list of general design inputs is presented in Table I.

TABLE I

Turbine Blade Design Inputs

- Function
- Operational Requirements
- Production Quantity
- Load Requirements
- Economics
- Service Aspects
- Manufacturing Considerations
- Geometry and Properties
- Mass and Properties
- Materials
- Time Restrictions
- Contractual Considerations

Most of the listings of Table I can be greatly expanded. Indeed, many of these topics have already been covered in considerable detail by others. What should be emphasized here is that there are many questions concerning these design input criteria which we have not (yet) answered. Progress toward the solutions is proceeding at Sandia and at other facilities. A brief glimpse of how several of the design input factors may influence the blade design follows.

Even the basic function of the design may be a subject for conjecture. It would appear to most observers that the function of a wind turbine is to be capable of converting the energy of a natural windstream to a form more useful to man. However, earlier prototype design goals—such as "Thou shalt not fall" or "Thou shalt appear beautiful to the beholder"—may have strong political implications. These latter considerations sometimes seem to approach, in importance, the basic energy conversion function.

A determination of loads should include any influence that stresses the blade material. For some very simple problems, loads can be determined with great accuracy. For a new technology involving both complex shapes and complex loadings, it

would be naive to suppose that the material stresses could be everywhere determined with a great degree of accuracy. Instead, what is hoped to be an amount of conservatism is included in the design. As ignorance of a particular area diminishes, so also can the conservatism. The load determinations for the Darrieus blades are being continually updated.

The economic considerations are an obviously fluctuating item. A recent addition that is relevant to this topic is energy economy.

- How long will it take to recover the energy expended in producing the wind machine?
- How much additional energy can be expected?
  (The importance of the consideration of this energy economy is becoming evident.)

The service provided by and required for the wind machine involves many considerations.

- Does a remote siting requirement or the projected high cost of operating labor presuppose a machine that requires infrequent attention? (Perhaps it is advantageous to build an extremely low-cost machine that has a relatively shorter predicted life.)

The manufacturing considerations, which are extensive, involve such items as a production machine's capacity both in size and in numbers of the produced parts. The manufacturing technology level required permeates this consideration.

- Are the production requirements so stringent as to direct the task only to the aerospace industry?

The shape and size of an item always constitute one of the more basic design considerations. Blades for wind machines of the sizes being considered are so

large that segmenting at the manufacturing stage with subsequent assembly at the turbine site will be required.

- How much deviation from an established ideal shape (blade curve or airfoil) is deemed acceptable?

Of all the input considerations for a typical design task, it is the author's belief that the materials selection area is the most neglected.

- What material or materials are indicated?

Time considerations are always included. Inflexible project completion dates are always perplexing to those who are last in a series of interdependent events, especially when many of the earlier tasks have been permitted to slip. Unfortunately, this situation is a rule more than an exception in a complicated design task unless exceptional management is employed.

- What is the actual time allowed for the completion of the design?

After the design inputs have been considered individually, all of them must be considered concurrently. New difficulties now emerge as a result of inherent conflicts, sometimes completely divergent effects, of the various input criteria. These dilemmas can be addressed only by assigning weighted values to each of the inputs. These values, in turn, must be established by an honest appraisal of the intended function of the design. Also, cost trade-offs, which are very difficult to satisfy completely, are now required. Cost considerations are involved with each of the many design input factors. Perhaps only Industry's response to a request for proposal can establish precise costs.

Often, establishing a particular design is made more difficult because of the lack of a particular essential specialty under the design agency's roof. Here at Sandia, and probably also within much of the aerospace industry, this shortcoming may be the familiarity with low-cost, high-production manufacturing methods.

Mass-production techniques having cost as a foremost consideration are not our forte. We must rely on conferral with the manufacturing industries concerning this proficiency.

A similar dilemma may exist within the manufacturing processing. Can a single supplier accomplish each specialty technique required for the production of the low-cost blade? If not, each of the individual processes must be assigned legally identifiable boundaries, and the inevitable horse trading that occurs becomes more difficult and more costly.

The determination of the input factors—especially for an emerging technology—is an ongoing process. One is never fully satisfied with the answer obtained. However, the timely completion of a design requires that, at some point in time, the best information available be used. Frequently, only a "quasi-freeze" of the inputs is granted to the designer.

The above consideration of parallel efforts in the actual design along with the design input determinations requires that the proposed design be flexible enough to absorb these changes without the undertaking of a major redesign. The potential of emerging materials and manufacturing processes supports this concept of design flexibility.

It has been suggested that the designer's function can vary from a straightforward task to one that is incredibly complex. The difficulties of objectively applying each of the input criteria into the final design have been involved. When the subjectivity of assigned relative values is introduced, a later assessment of sound engineering of a particular design must always consider these values in the context of the time at which they were made. A "best design" appraisal may well depend on whether the observer agrees or disagrees with value assignments.

Existing Designs

A new design should, at some time during the process, include a consideration of what others have already accomplished in similar or related projects. Various

designs for small turbines (5 m or less in diameter) have been produced. Many of the features of these designs are refreshingly innovative. Selected features of these smaller blade designs are also applicable to the design of much larger blades. Furthermore, there are strategic advantages in advancing a particular design if certain of its features have already been practically demonstrated on a smaller scale system.

Many of the blades known to have been produced are shown in Figs. 1a and 1b. The designs can be categorized by the manner in which the blade structure is loaded. Figure 1a presents those designs in which all of the blade material is load-carrying. Figure 1b presents those designs wherein the structure required for establishing the aerodynamic shape is, in varying degrees, parasitic on the load-carrying structure. No further detailed comparison of the various features of each design will be made except in later discussions of those features considered pertinent to the full-scale (17-m) blade designs.

Proposed 17-m Blade Designs

Three provisional blade designs proposed for the 17-m turbine are shown in Figs. 2, 3, and 4. These blades have identical external geometries. It is also presumed that each design can be constructed to accommodate the structural requirements. Descriptions of these designs are accompanied by examples of how the weighting of selected values of the input criteria, especially the production quantity anticipated, can affect the selection of a particular design. The proposed construction methods and materials of each design, along with the manufacturing technology level involved as related to the expected production quantities, will be emphasized. Also, features of prior blade designs that have contributed directly to the 17-m blade designs will be acknowledged.

The design in Fig. 2 is an all-steel, welded monocoque structure. The shapes are produced (in straight sections) by roll-forming from continuous strip sheet metal stock. The roll-forming element of this design was accomplished on a small scale in the NRC design. The NRC researchers in fact, produced their own roll-forming tooling to accomplish this task in their wind tunnel maintenance machine shop. After being roll formed to contour, each individual component is then stretch formed into the troposkien blade curve. The components are then joined by automatic seam welding into an integral blade assembly, and the end attachments are added by welding. There are no cross chord structure components (ribs) except the surface skin. The hinge end fixtures are of weldable investment-cast steel; e.g., AISI 4130 alloy. The investment casting process will provide for substantial savings both in machining and in material costs. The joint (end attachment) structural efficiency can be made very high by welding.

Each of the sheet metal components of this design is a low-alloy weldable steel that is also resistant to corrosion. The entire structure is considered to be load-carrying. The finished blade would be given extended service life by the addition of a protective coating to further retard any corrosion tendencies. The production of raw steel is considered to be relatively energy efficient when compared to competing structural materials. Use of primarily machine processes will afford excellent reliability and reproducibility.

Costs of blades produced by this approach can be projected with acceptable accuracy. If the anticipated high costs of tooling could be ignored, this design would be projected to be the least costly of all the designs so far considered. Of course, tooling costs cannot be ignored; therefore, this relatively large expense must be diluted (cost per blade consideration) by the production of a very large number of blades.

It appears that production from this design will require processing by four separate suppliers. The manufacturability was established by contacting individually the roll-forming and stretch-forming industry specialists. The welding of the components into the finished assembly and the investment casting of the end attachments are more widely understood to be state-of-the-art processes.

The second design, shown in Fig. 3, employs a different approach to the structural loading. It provides an acceptable design for the situation where very large quantities of blades cannot be anticipated. Tooling costs will be minimal, but the labor costs will be quite high. Material costs will probably be higher than for an all-steel blade design.

The technology level required for the production of this blade is lower than that required for the metal monocoque blade. This approach could be significant in that it might offer employment to those in sluggish manufacturing areas. If large production quantities can be projected, the bottom-line cost for this design is anticipated to be higher than for the monocoque design because this one is inherently labor intensive. Conversely, for low production the cost per blade will be significantly lower because the tooling costs for this design can be minimal.

The blade loads are accommodated primarily by a steel backbone similar to the earlier Sandia and NAL designs for smaller turbines. The aerodynamic shape is established by the rigid-foam airfoil halves, which are bonded to the steel backbone. A smooth fiberglass aerodynamic skin also provides impact resistance; e.g., for hail. With regard to structural load capacity, both the foam and the skin are largely parasitic on the steel backbone.

The manufacturing sequence is fairly simple. The backbone is constructed from inexpensive and easily obtainable mild-steel pipe or tube. The pipe elements would be welded to each other as shown in Fig. 3, forming a structural "strap" or "ribbon." This strap would then be bent to the desired blade curvature, and end attachments similar to those of the first design would be attached by welding. Lengths of rigid polyurethane foam would then be bonded to the strap. These foam airfoil segments could either be formed to shape from slabs or be molded to the desired shape. Flat, foam airfoil shapes could probably be used because the anticlastic* tendency of rigid foam is very low. The foam segments would be split along the chordal line (airfoil centerline) to facilitate assembly.

---

*Anticlastic behavior is the tendency for a material to curve about an axis that is transverse to the axis about which it is being bent. The degree of severity of this behavior is indicated by the value of the Poisson ratio.

If deemed necessary for providing additional torsional ridigity, structural fiberglass ribs could be interdigitated between the foam segments along the blade. Finally, a fiberglass skin would be bonded to the structure either by use of preformed skin segments or by the wet layup technique. The finished assembly would be smoothed to the aerodynamic finish desired, and an abrasion-resistant finish would be applied.

Individual blades might need to be selected (or modified) for the blade set in order to achieve a tolerable dynamic mass balance. The reproducibility of the blades (accuracy of form, weight etc) will not be so good for this design as for the monocoque design but it may still meet the operational requirements of the turbine. The anticipated departure from an "ideal" geometry will probably be acceptable, inasmuch as preliminary analytic studies have indicated that blade angles of up to 2° will not significantly degrade the turbine performance.

In the two preceding designs are presented the possibilities of using what are considered to be practical upper and lower boundaries of the existing manufacturing technology. The final design, shown in Fig. 4, is included as an illustration of how features from both the high-technology and low-technology approaches can be combined into a single design. The pictorial representation of the components included in this third design is not intended to be so specific as the details of the first two designs but, rather, to present a design approach involving various technology levels.

In this approach, certain high-level technology components would be furnished to an assembly team which might possess considerably lower fabricating skills. This team would construct a finished blade structure by assembling the components, using only elementary techniques. This particular approach would permit either the more critical blade components or the entire blade being furnished to the assemblers in kit form.

The precision of a blade could be assured by the machine processing of critical components and by the supplying (on a loan basis) of such special fixturing as deemed necessary for accurate assembly. Utilizing a trained blade fabrication

technician to assist in the assembly might also be advisable. The assembly labor would be drawn from the location of the user. Although Fig. 4 shows specific materials — laminated wood for the leading edge, paper honeycomb for the aft filler, and fiberglass skin — the individual components would be selected on a merit basis. The same approach might yield a design with an extruded aluminum D-spar leading edge, polyurethane rigid foam filler, and bonded-metal skins. Many of the features of the various blade designs for small turbines could be considered applicable to this design philosophy.

Obviously, no complete appraisal of each blade that might be produced by such an iteration of the various components exists. Such an approach may be prescribed, however, if the anticipated production quantity is too low or too high for the first and second design respectively, approaches presented. This design must have a production that is high enough to introduce such high-technology components as the laminated-wood leading edge or an aluminum extrusion D-section. If very high production is anticipated, a design similar to that of Fig. 2 might prove to be the optimum approach.

This third design approach, like that of Fig. 3, has the advantage of allowing assembly at or near the turbine site. This would minimize such shipping concerns as the size and bulk of the blades and the protection to be furnished en route. Also, it would employ the local labor force, a consideration which might foster the acceptance of wind machines by the community.

Design Option Selection

It has been suggested that the selection of a design approach for the large turbine blades may depend primarily on the number of units anticipated. It does not follow that the other design inputs in Table I are of lesser importance but, rather, that the other requirements are considered as having already been satisfied in the three designs presented. As can probably be surmised, each of the other individual input requirements is accomplished with varying degrees of success for these three designs.

The overriding consideration of all the design input factors must be that of cost of the wind turbine system consistent with its acceptable performance. It must be reiterated, however, that the turbine blade costs will be based very strongly on the production quantity anticipated.

Unfortunately, this determination of the anticipated production quantity is difficult to ascertain in a free market economic system. It's the familiar chicken/egg paradox. The potential buyer will not commit himself until he finds out how much the workable wind system will cost. The producer, on the other hand, cannot furnish his most attractive cost until he has counted his buyers.

It may be necessary (as is being attempted in Canada) to build purchaser confidence by successful use and demonstration of wind systems by government agencies. If this should become necessary, the initial numbers established for a production target might be based entirely, or at least primarily, on the needs of these agencies.

Conclusions

It was stated at the outset of this paper that the design of the turbine blades is crucial to the performance and economic success of the Darrieus wind turbine endeavor. It is candidly acknowledged that the determination of many of the input criteria required for accomplishing this task has not yet been completed and that the information turnover in this area is considerable. It was also suggested that the design approaches and the design team assemblage are strongly influenced by the procedure and timing of the Darrieus turbine technical data bank accumulation. Several contractual approaches appear to have merit for accomplishing low-cost blade designs.

Although many of the design inputs are not yet rigidly established, it is considered that reasonable values may be selected so that the establishment of the hardware definitions may proceed. Several tentative blade designs appear to meet the goal of acceptably low cost. Each utilizes some features that have already been included in earlier demonstrations, and each of these designs may also be considered a target design for some specific production quantity.

The cost of each of the proposed designs can be lowered when the presumed conservatism of the existing design inputs is minimized. The eventual "bottom-line" cost of any design will depend on the modified design inputs and also on emerging manufacturing techniques. This cost will be presented by those specialists of the manufacturing industries required by the selected designs. Although the selection of a particular design will depend heavily on the production quantity anticipated, it is believed that a technically viable and economically attractive design consistent with any given production quantity can be established.

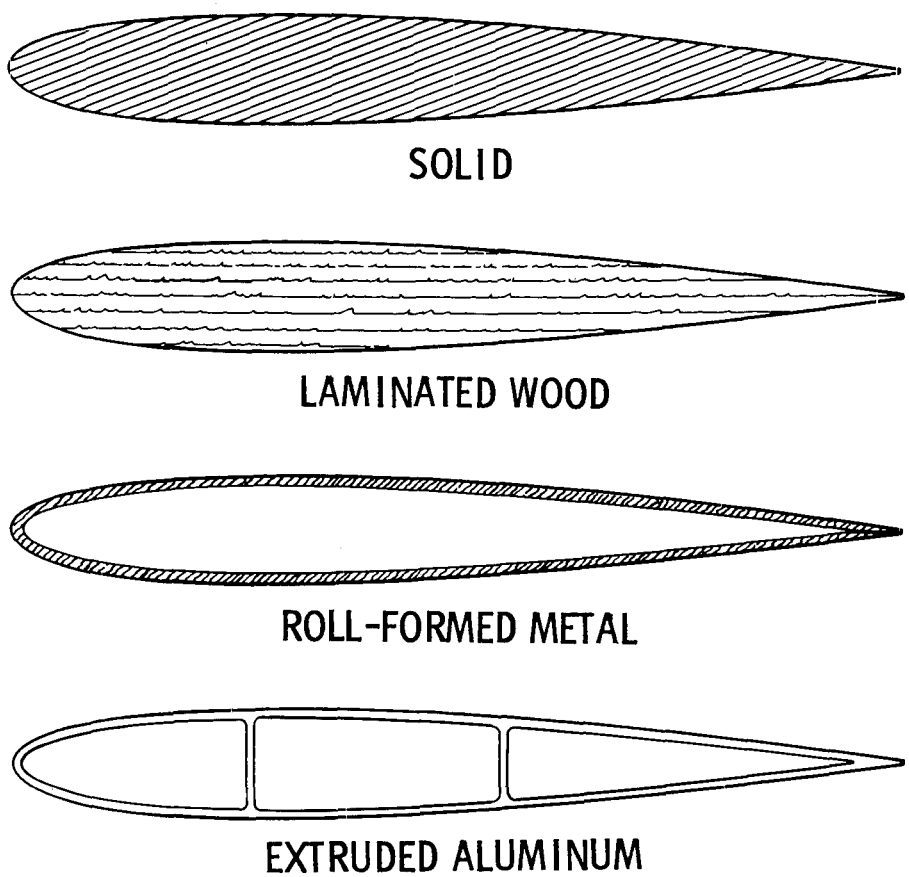

SANDIA (ALUMINUM), VETTER (PLASTIC)

SANDIA

NATIONAL RESEARCH COUNCIL (CANADA)

DOMINION ALUMINUM (CANADA)

Figure 1a. Existing Designs (Fully Loaded)

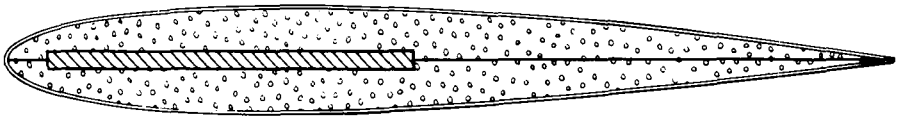

STEEL/FOAM/FIBERGLASS

SANDIA

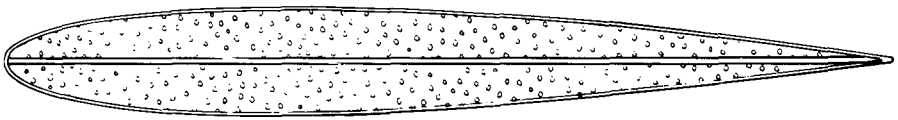

ALUMINUM/FOAM/FIBERGLASS

RESEARCH & DESIGN INSTITUTE

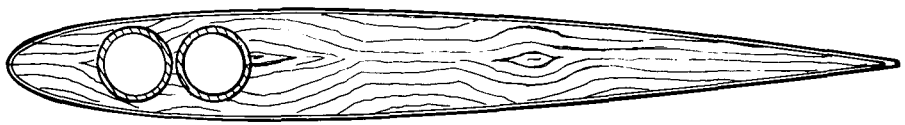

STEEL/WOOD/FIBERGLASS

NATIONAL AERONAUTICS LABORATORY (INDIA)

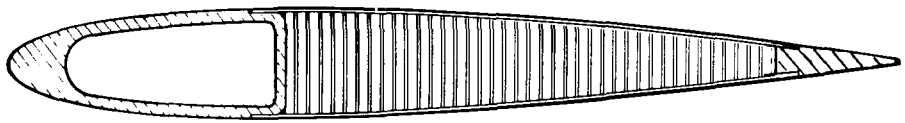

ALUMINUM EXTRUSION/PAPER HONEYCOMB/FIBERGLASS

KAMAN

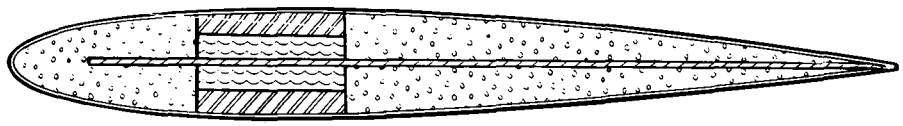

ALUMINUM/STYROFOAM/FIBER/ HEAT SHRINKABLE FILM SKIN

TEXAS TECH

Figure 1b. Existing Designs (Backbone Loaded)

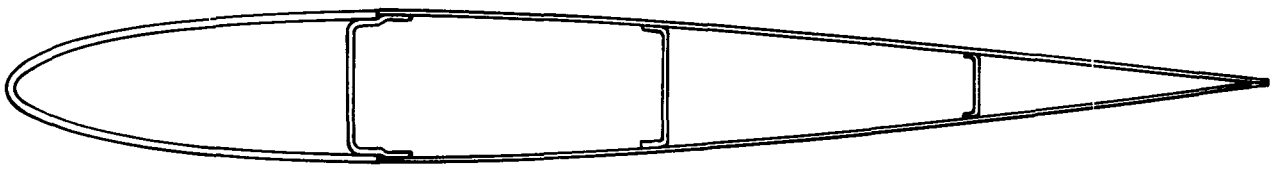

FEATURES:

- ROLL-FORMED COMPONENTS
- AUTOMATIC SEAM WELDS
- LOW-ALLOY STEEL
- STRETCH-FORMED TO CURVE
- INVESTMENT-CAST END FIXTURES
- HIGH TECHNOLOGY - HIGH VOLUME

Figure 2. Proposed Low-Cost Design No. 1

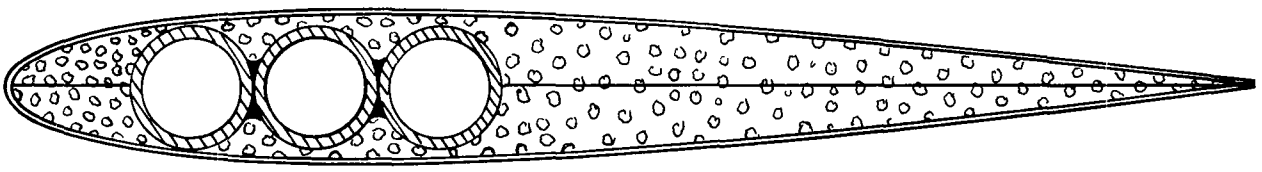

FEATURES:

- COMMERCIAL TUBING BACKBONE
- BACKBONE BENT TO SHAPE
- MOLDED OR FORMED FOAM AIRFOIL SEGMENTS
- FIBERGLASS RIBS INTERDIGITATED
- FIBERGLASS SKIN - HAND LAYUP
- WELDED END FIXTURES
- LOW TECHNOLOGY - LOW VOLUME
- LOW TOOLING COSTS

Figure 3. Proposed Low-Cost Design No. 2

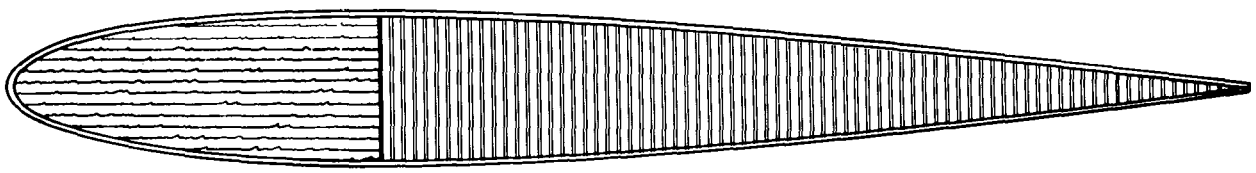

FEATURES:

- WOOD LAMINATED
- HONEYCOMB AFT SECTION
- FIBERGLASS RIBS
- FIBERGLASS SKIN
- BONDED END ATTACHMENTS
- TECHNOLOGY MIX (by components)
- MEDIUM VOLUME DESIGN

Figure 4. Proposed Low-Cost Design No. 3

ELECTRICAL POWER SYSTEM

SANDIA LABORATORIES

ANTHONY F. VENERUSO

ELECTRICAL POWER SYSTEM

This system performs the mechanical-to-electrical power conversion for the wind turbine and interfaces with the electrical distribution system. For large scale applications, this distribution system is typically the utilities' power grid. On the other hand, small scale applications may be situated in remote areas where the windpowered electric system is completely independent of any utility. In any case, there are many approaches to windpowered electric generation. However, all of these approaches may be categorized as to whether the windturbine rotates at constant or variable speed. The constant speed approaches are generally implemented with standard induction or synchronous generators while the variable speed systems typically employ electronic switching systems and special purpose generators to achieve constant electrical output voltage and frequency while the wind turbine's speed may be varying.

The basic approach to the electrical power system for the Vertical Axis Windturbine (VAWT) has been to use standard induction machines with all the VAWT's built and tested. Other machines have also been of interest in this endeavor. For example, automotive type alternators have been used in small scale systems tests with the 5 meter VAWT and a 60 kw synchronous generator being designed and built along with an induction machine for the 17 meter VAWT to be used as a general purpose cost effective electrical power testbed for operation of the VAWT in conjunction with the utility systems.

The induction machine is ideally suited to constant speed operation with the VAWT for the following reasons: first of all, the VAWT is not self starting. Some auxilliary means must be used to spin up the turbine to a speed where it can begin to extract energy from the wind. Once running at a suitable constant

speed, the turbine's output rises as the wind's speed increases until a peak is reached at which point the turbine's output begins to level off and then drops as the wind increases further. The induction machine is a perfect compliment to this VAWT behavior. As shown in Figure 1, the induction machine starts off as a motor, providing a drive torque for the VAWT. As the machine comes up to speed, the torque reaches a peak and then rapidly passes through zero torque at the synchronous speed of the induction machine. Thus far, this is the characteristic that most people associate with induction motors. However, if there is a prime mover such as the VAWT, external to the induction machine, then the torque vs speed curve indicates the induction machine will behave like a generator converting mechanical energy from the VAWT to electrical energy fed back into the electrical grid. This generator effect continues as the machine is spun faster and faster until a peak is reached then the generator's output drops. To match an induction machine with a VAWT, the primary requirements are to match the operating speeds and peak torque and power levels of the induction machine and VAWT. Figure 1 displays the effect of increasing rotor resistance upon the slope of the torque versus speed characteristic. By choosing the proper slope the operating speed of the VAWT can be held within a desired band, such as $\pm$ 5%, over the range of expected wind speeds. Finally, some pragmatic reasons for using the induction machine are that for sizes up to about 100 kw, it is the most cost effective, rugged, and readily available electromechanical converter known since its invention in 1888 by Galileo Ferraris and Nicola Tesla.

Among the drawbacks which must be recognized for induction machines are their poor power factor and possible unstable behavior as generators in a wind-powered network. As the name might imply, the induction machine appears to the electrical network as a large inductance and is therefore characterized by a lagging power factor, which is to say the current lags the voltage and this reactive current, which produces no useful work, must circulate through the

distribution network. Concerning the instability question, under certain conditions two or more induction machines in a network may interact and transfer massive amounts of power back and forth. Both of the above drawbacks can be corrected in practice by suitable design of the machines together with passive capacitor banks for power factor correction or use of a synchronous generator with an induction motor start capability.

Figure 2 shows a block diagram of the single phase electrical power system on the 5 meter turbine presently in operation and on view during the workshop tour of the wind facility. This single phase system uses a standard capacitor start induction motor as both a motor and a relatively constant speed generator as an expedient until three phase electrical power is installed at the test site. The three phase power block diagram is shown in Figure 3.

A block diagram of the electrical power system for the wind tunnel test is shown in Figure 4. Here a standard three phase, 5 HP induction motor is driven by a commercially available variable speed drive. This drive produces a variable output voltage while holding the ratio of voltage to freauency constant. By this means the synchronous operating speed can be selected by a dial on the motor controller. The induction machine then establishes a relatively constant speed for the VAWT. If the machine is extracting energy from the windstream, the 5 kw load bank absorbs the energy from the VAWT. On the other hand, if the machine is driving the VAWT, the motor controller supplies the necessary power while maintaining a constant, but selectable speed.

Figure 5 lists the topics in electrical power systems to be considered specifically for the VAWT. The performance ground rules for design of the starting system on the 17 meter system are given in Figure 6. Figure 7 gives a mathematical model with which the starting torque, T_m, can be computed. The total power required to start the turbine is considered in Figure 8. In starting the VAWT, power is dissipated in mechanical friction, aerodynamic drag, and in

accelerating the mass moment of inertia up to operating speed. The results of this analysis are shown in Figure 9 where a 50 HP induction motor is selected for starting the turbine. This size machine is also suitable for electrical power tests as an induction generator.

One problem in spinning up a large inertia, such as the VAWT, is the long time during which the induction machine is drawing surge current on the order of five times its rating as shown in Figure 10. Since heat dissipation in the motor is proportional to the square of the current, the machine would dissipate 25 times more heat during startup than at normal running speed. To prevent motor burnout, a series reactance starter is inserted into the circuit during startup to limit the surge current. This reactor starter is being used rather than the more standard reduced voltage autotransformer because the reactor starter offers a simpler, lower maintainance, and more cost effective approach for motor starting the VAWT than an autotransformer of suitable size.

Figure 11 presents the major arguments for using a synchronous generator with the VAWT. In addition to the items listed, a synchronous and an induction generator are approximately equal in cost for sizes of about 500 kw or more.

The basic ideas of synchronization for the synchronous generator are given in Figure 12 and a mathematical model for the induction start motor is shown in Figure 13. To achieve synchronism and prevent turbine speed runaway, this math model is used to derive a very simple relation between the VAWT's performance parameter k_w and the required slope, k_m, of the induction motor's torque versus speed curve near synchronism. As a backup, the mechanical brakes can also be used to assist synchronization as shown in Figure 14.

The results of these analysis are given in terms of the generator specification shown in Figure 15 and the autosynchronizer considerations shown in Figure 16. A block diagram of the electrical power system for the 17 meter VAWT is shown in Figure 17. All the items within the dashed line are being designed and built by

Kato Engineering of Mankato, Minnesota, to stimulate a partnership between industry and ERDA in electrical power systems for windpower technology.

Items for future investigation:

1. A minimum cost transmission/generator combination which takes advantage of the VAWT's ability to accomodate large power conversion equipments located at ground level under the turbine.
2. Small scale systems and systems autonomous from the electric utility.
3. Variable speed systems in which the VAWT is operated at quasi-constant speed over a range of permissible speeds depending on average wind conditions to maximize total kwh converted.
4. Addressing electric utility interface questions such as identifying special fault correcting equipment and analyzing and correcting any instabilities in networks containing a number of induction or synchronous generator equipped VAWT's.

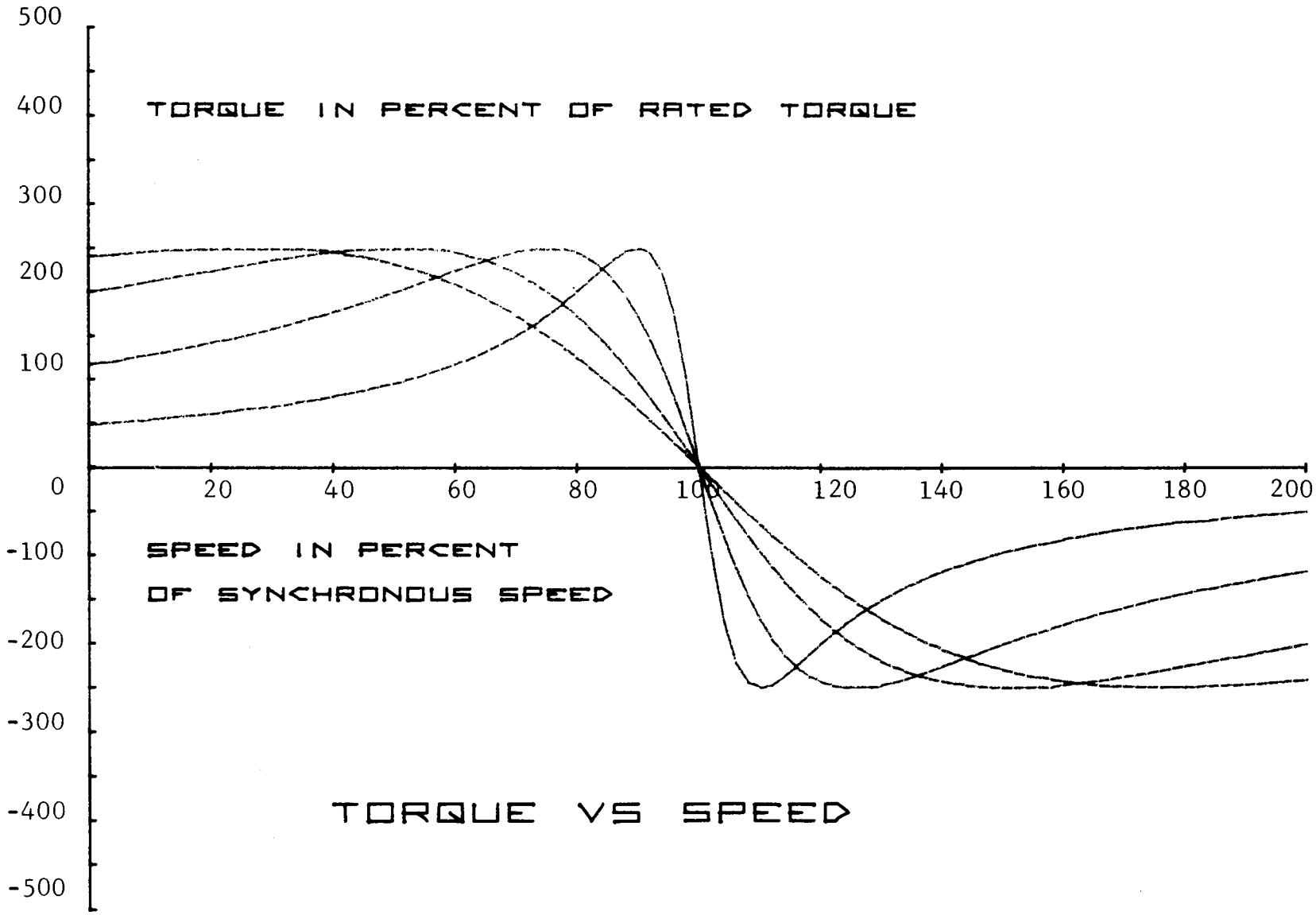
500
400
300
200
100
0
-100
-200
-300
-400
-500
TORQUE IN PERCENT OF RATED TORQUE
20
40
60
80
100
120
140
160
180
200
SPEED IN PERCENT
OF SYNCHRONOUS SPEED
TORQUE VS SPEED

Figure 1

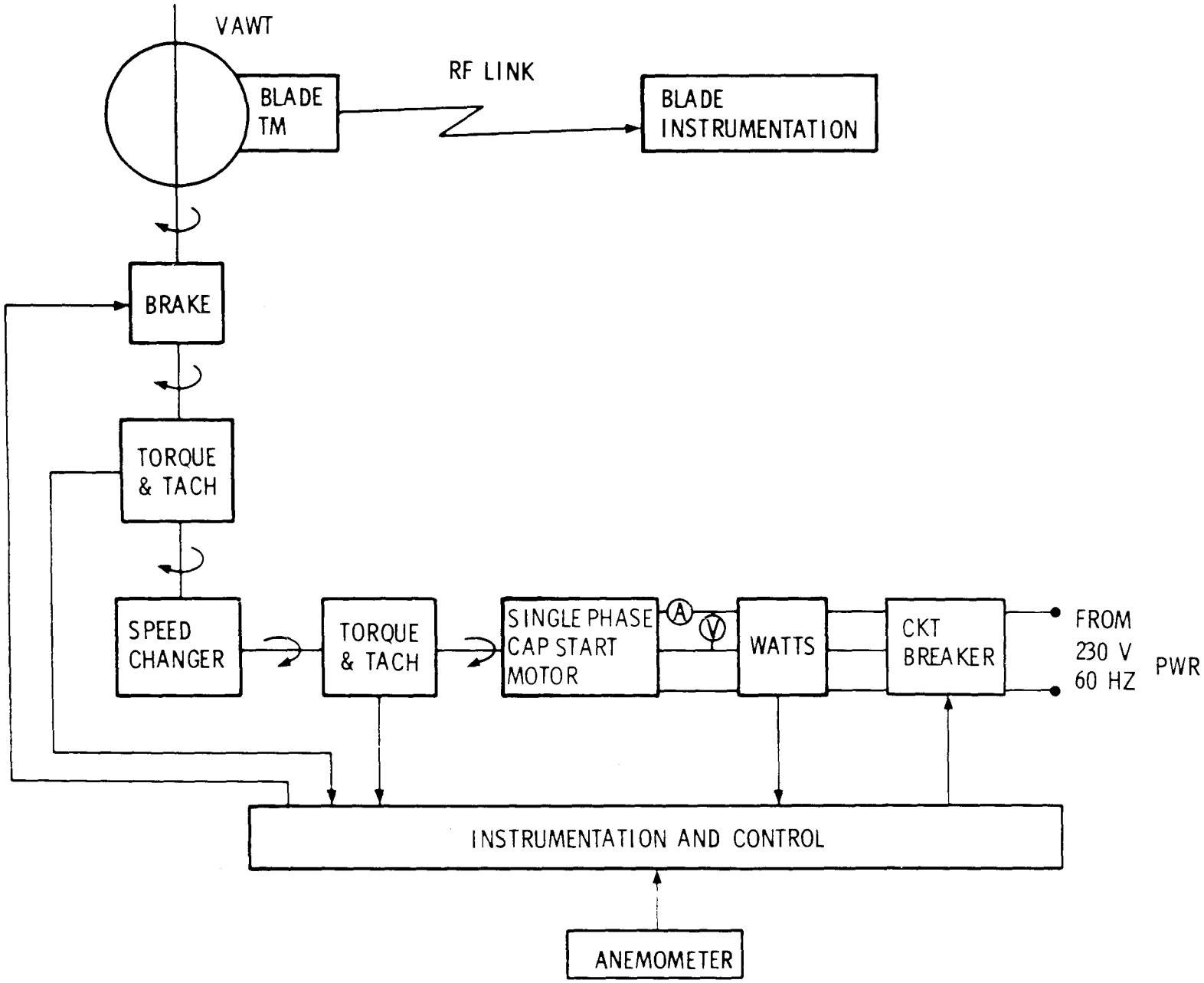

Figure 2. Single Phase Windpower System

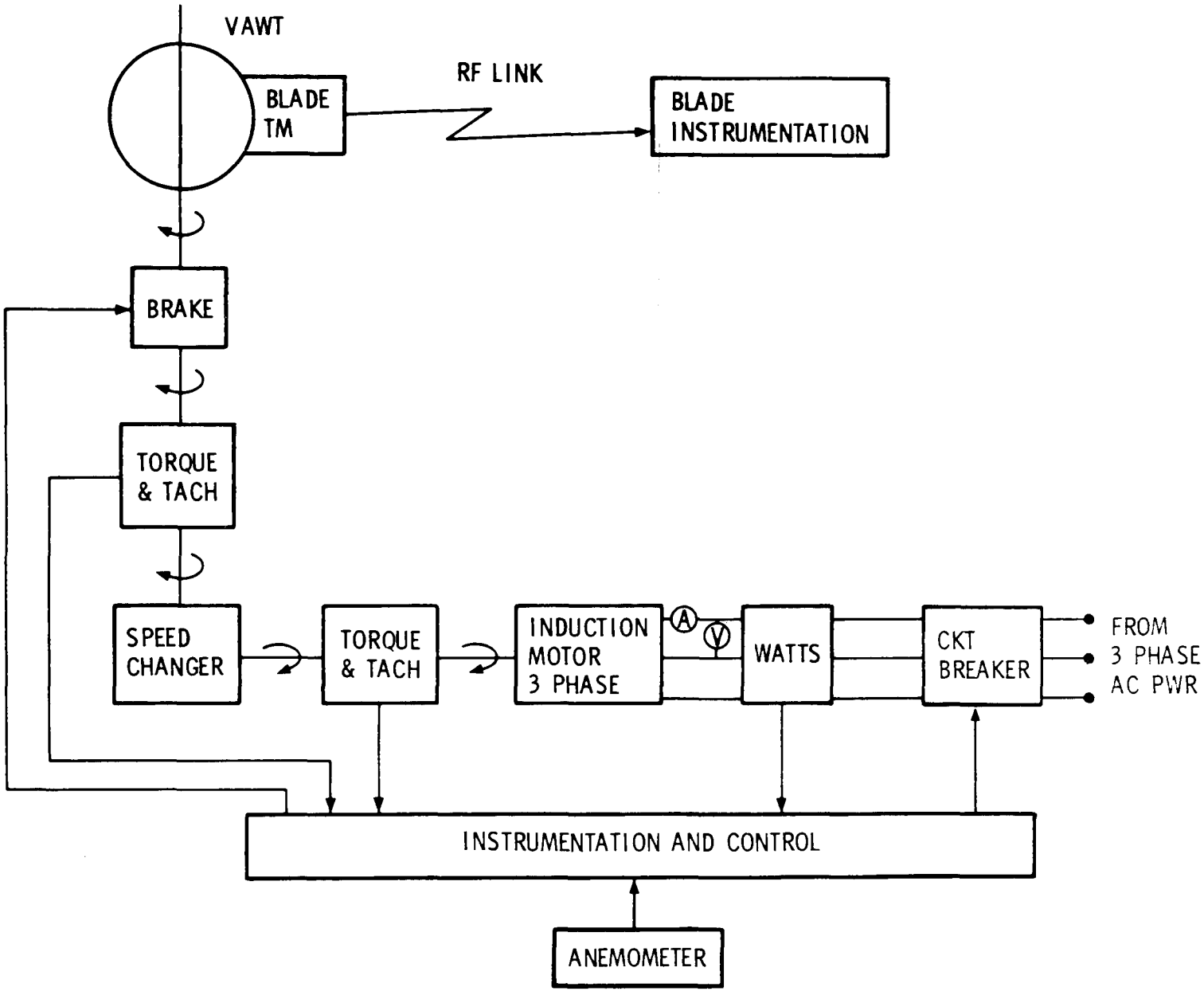

Figure 3. 3-Phase Induction Windpower System

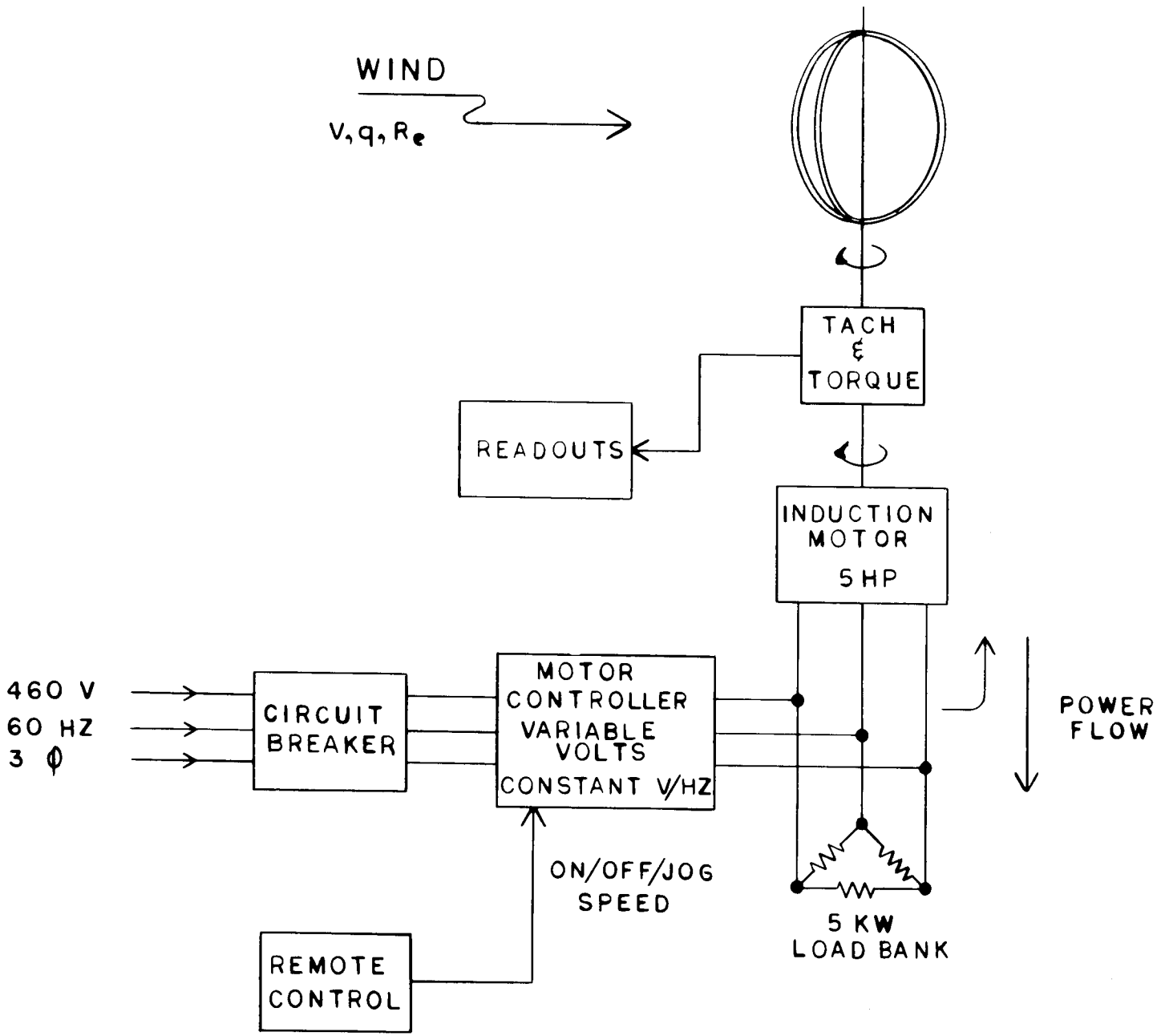

Figure 4. Wind Tunnel Test of VAWT

ELECTRICAL POWER SYSTEMS

CONSIDERATIONS FOR VAWT:

- STARTING
  - GROUNDRULES
  - MOTOR REQUIREMENTS
- CONSTANT SPEED OPERATION
  - GENERATOR CHARACTERISTICS
  - SYNCHRONIZATION
  - STABILITY
- UTILITY INTERFACE
- SAFETY

Figure 5

STARTING THE VAWT

PERFORMANCE GROUNDRULES:

1. STARTUP TURBINE (0 → 41 RPM) IN 30 SECONDS WITH $V_{WIND} = 0$
2. GENERATOR IS NOT ENERGIZED
3. CONSTANT STARTUP TORQUE
4. SPEED RATIO = 43.9
5. 1800 RPM SYNC SPEED GENERATOR

Figure 6

STARTING THE VAWT

STARTING TORQUE:

$$T_M = \dot{\omega}_M I_{EQ} \qquad (1)$$

ASSUME $\dot{\omega}_M$ = CONSTANT,

IE $$\dot{\omega}_M = \frac{\omega_S}{T_S} \qquad (2)$$

THEN $$T_M = \frac{\omega_S I_{EQ}}{T_S} \qquad (3)$$

MODEL:

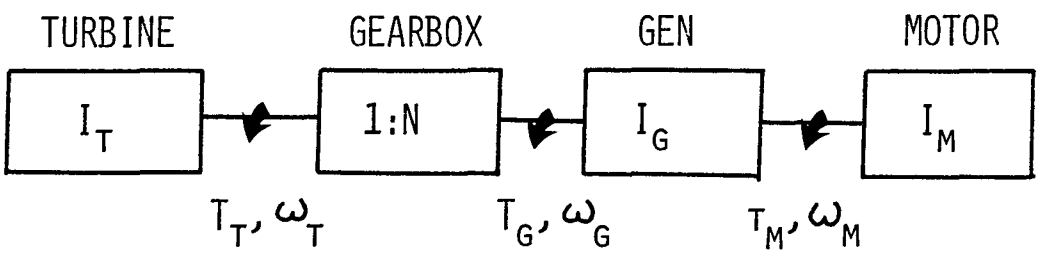

$$I_{EQ} = I_G + I_M + \frac{I_T}{N^2} \qquad (4)$$

Figure 7

STARTING POWER

$$P_{TOTAL} = \underbrace{P_I}_{\text{INERTIA}} + \underbrace{P_A}_{\text{AERO}} + \underbrace{P_F}_{\text{MECH FRICTION}} \qquad (1)$$

INERTIA

$$P_A = I_{EQ}\,\omega_S^2 / T_S \qquad (2)$$

AERODYNAMIC DRAG

$$P_A = .54\,\rho\, C_{DO}\; c\,\omega_S^3\, R^4\, N \qquad (3)$$

WHERE

ρ = AIR DENSITY

C_{DO} = DRAG COEFFICIENT

c = CHORD LENGTH

R = BLADE RADIUS

N = NUMBER OF BLADES

MECHANICAL FRICTION

$$P_F = \frac{(1-\eta)\,P_{OUT} + P_C}{\eta} \qquad (4)$$

WHERE

η = GEAR BOX EFFICIENCY

P_{OUT} = OUTPUT POWER FROM GEARBOX

P_C = POWER LOSS AT COUST SPEED & $P_{OUT} = 0$

Figure 8

STARTING THE VAWT

DESIGN EXAMPLE:

$I_T = 18000$ SLUG FT^2

$I_G = 4$ SLUG FT^2

$I_M = 1.5$ SLUG FT^2

$R_S = 41$ RPM

$T_S = 30$ SECONDS

$N = 43.9$

$P_I = 31.95$ HP

$P_A = 4.9$ HP

$P_F = 5$ HP

$P_{TOTAL} = 41.85$ HP

$T_{START} = 93$ FT LB

CHOOSE 50 HP MOTOR WITH MIN TORQUE = 210 FT LB

Figure 9

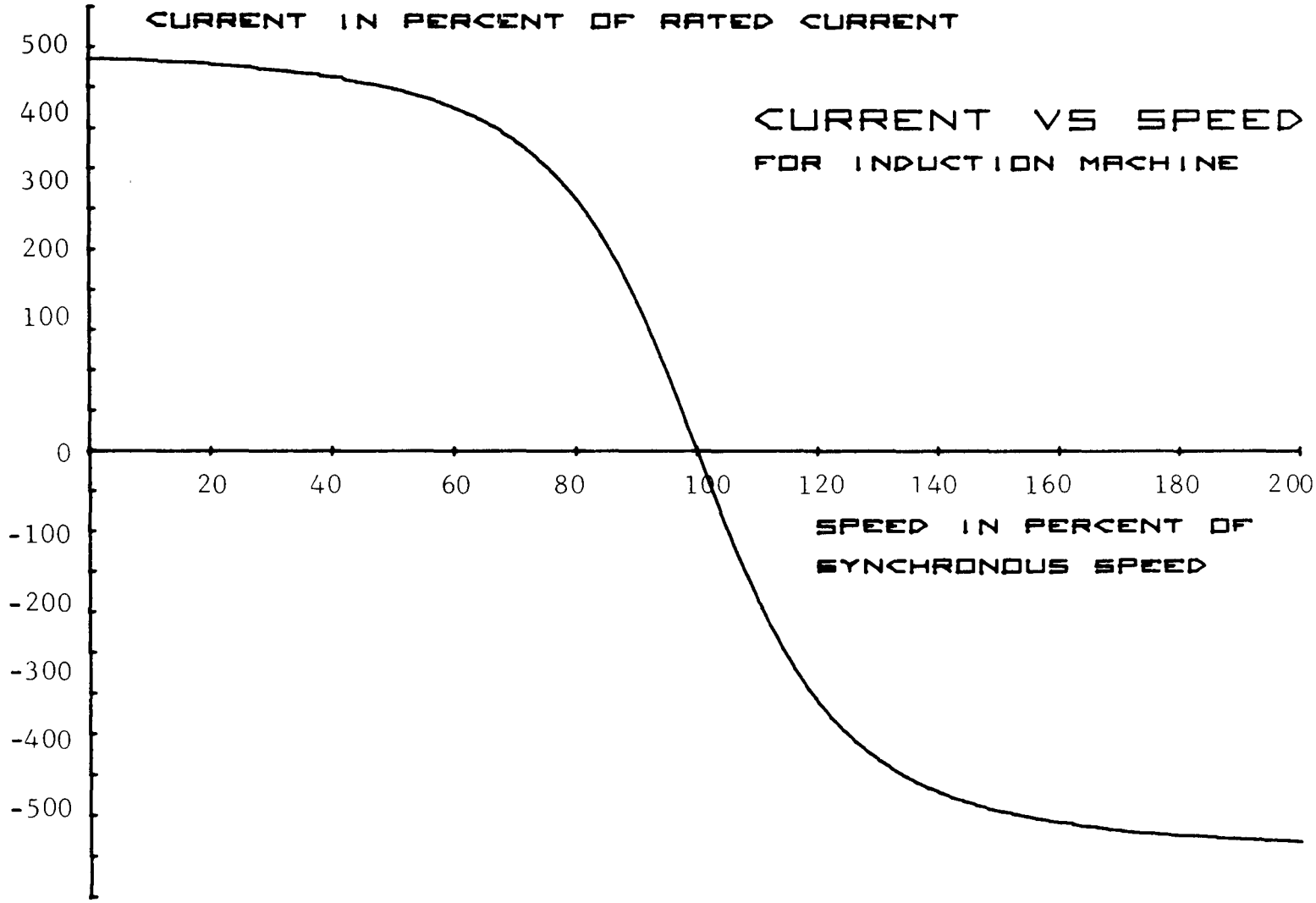
CURRENT IN PERCENT OF RATED CURRENT
500
400
300
200
100
0
-100
-200
-300
-400
-500
20
40
60
80
100
120
140
160
180
200
CURRENT VS SPEED
FOR INDUCTION MACHINE
SPEED IN PERCENT OF
SYNCHRONOUS SPEED

Figure 10

- Necessary control is provided by synchronizing network as long as generator rating is not exceeded.
- Magnitude of the structural vibrations problem is reduced in that only a single rotational speed must be considered to avoid coincidence with potentially destructive resonant frequencies.
- Equipment can be used for power factor compensation.
- Synchronous generators are standardized hardware.

Figure 11. Features of Synchronous Power Generation

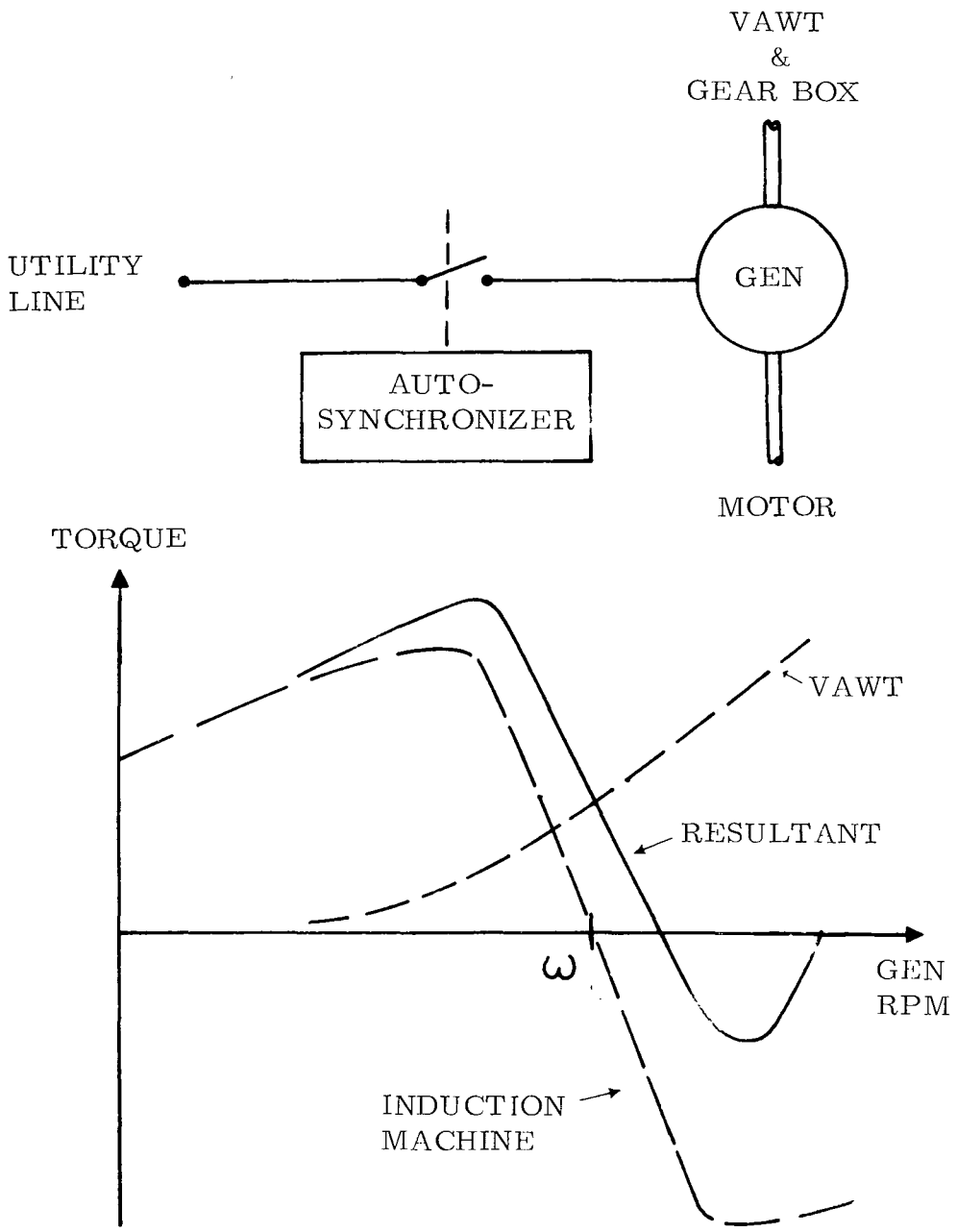

Figure 12. Synchronization

SYNCHRONIZATION

MATH MODEL

$$I_{EQ}\dot{\omega}_M = \underbrace{\frac{K_W \omega_M^2}{N^3}}_{\text{WORST CASE DRIVEN VAWT}} - \underbrace{K_M(\omega_M - \omega_S)}_{\text{INDUCTION MACHINE}} \qquad (1)$$

DRIVE TORQUE

TO PREVENT RUNAWAY

$$\dot{\omega}_M = 0 \text{ OR } K_M > \frac{4K_W \omega_S}{N^3} \qquad (2)$$

FOR $N = 38.71$, $\omega_S = 188.5\ \text{SEC}^{-1}$, $K_W = 638$ FT LB SEC

$$\frac{4\ K_W \omega_S}{N^3} = 8.3 \qquad (3)$$

AND

$K_M = 48$ FT LB SEC FOR 50 HP MOTOR

Figure 13

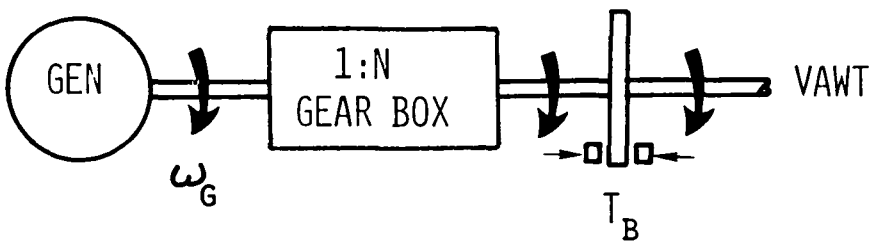

MATH MODEL

$$T_{BMIN} = \frac{K_W \omega_S^2}{N^2} - I_{EQ}\, \dot{\omega}_{GMAX} N \qquad (1)$$

SOLUTIONS

TO LIMIT $\dot{\omega}_G = \omega_{GMAX} / T_{BMIN} = 2{,}940$ FT LB

TO HOLD $\omega_G = \omega_S$, $T_{BSYNC} = 15{,}230$ FT LB

TO REVERSE $\dot{\omega}_G = -\dot{\omega}_{GMAX} = 39{,}530$ FT LB

BRAKE DESIGN $T_B = 50{,}000$ FT LB

Figure 14. Mechanical Brake

TYPE	-	BRUSHLESS SYNCHRONOUS
SPEED	-	1800 RPM
ELECTRICAL	-	60 kW, 3 PHASE, 60 Hz, 0.8 POWER FACTOR, 277/480 VOLT OUTPUT Y CONNECTED
MECHANICAL	-	TWO BEARING, HORIZONTAL MOUNT DRIPPROOF GUARDED ENCLOSURE
PROTECTIVE SERVICES	-	GROUND FAULT PROTECTION, OVERCURRENT, OVERVOLTAGE, LOSS OF PHASE, LOSS OF SYNCHRONIZATION

Figure 15. General Specifications

REQUIRE:

$\pm 15^{0}$ ELECTRICAL AND $\pm$ .5 HZ FOR 0.1 SEC

ASSUMING:

$$\omega_G = \omega_S + \dot{\omega}_G T$$

WORST CASE RESULT

FREQ: $\Delta F_G = 0.42$ HZ

PHASE: $\Delta \theta_G = +15^{0}$

Figure 16. Autosynchronizer

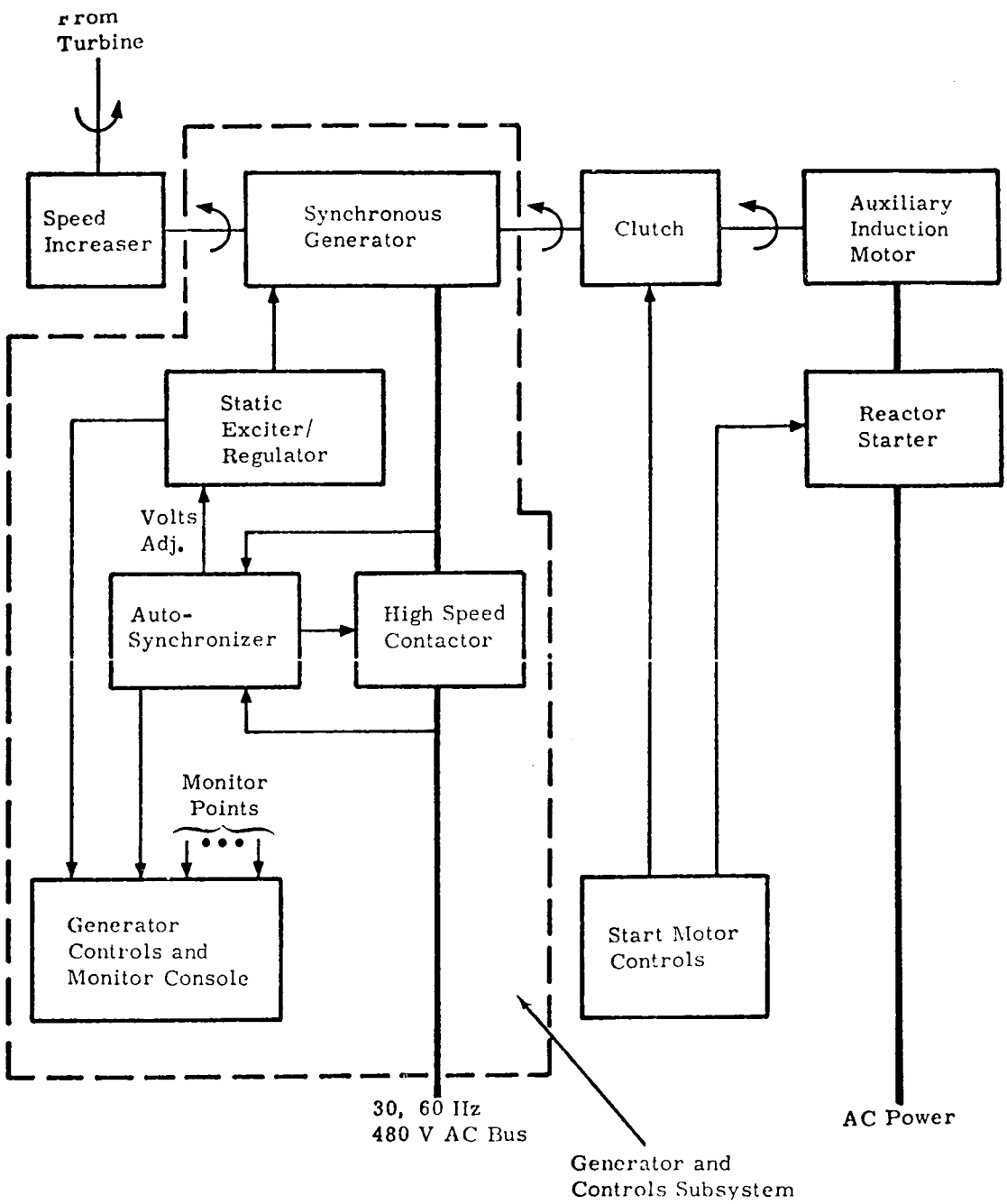

Figure 17. Electrical Subsystem for 17 Meter VAWT

AUTOMATIC CONTROL AND DATA ACQUISITION

SANDIA LABORATORIES

ANTHONY F. VENERUSO

Automatic Control and Data Acquisition

The primary goal of automatic control and data acquisition for the wind turbine program is to minimize the manpower costs of operation by having cost effective automation capable of operating and monitoring the complete wind turbine system independently of on-site personnel. To achieve this goal Sandia Laboratories' Wind Turbine Test Facility is equipped with a microprocessor system and a number of peripheral electronic devices which interface the processor with the turbine's power systems, operating sensors, anemometers, and output recording devices. The microprocessor is a recent development in solid state electronics which enables a miniature but complete digital computer to be built in the form of integrated circuits in very small, inexpensive package. The revolutionary personal programmable calculators as well as "smart" test instruments were made possible because of the development of these inexpensive microprocessors.

The equipment in the test facility consists of a TI Silent 700 teleprinter, a set of control and instrumentation racks and a power control console. The microprocessor based automation is achieved with a paper tape punch, reader, an Intel Intellec-80 microcomputer, and an ICOM dual floppy disk magnetic data storage system. Signal conditioning is performed by a DORIC 100-channel analog-to-digital converter. The power control console contains all the operating controls and instrumentation for the 5-hp induction machine to operate the 5-meter VAWT.

Figure 1 is a simplified block diagram of a microprocessor system for automatic control of the VAWT. In essence the microprocessor is an intelligent automatic operator which runs the start motor, generator, or brakes as a function of the wind conditions and the state of the VAWT.

Figure 2 shows a simplified program flowchart for the microprocessor VAWT control. One advantage of this approach is that the operation is governed by software written into a programmable read only memory (PROM) which can be programmed to carry out all the required measurements and performance checks to ensure safe, reliable, efficient operation of the wind turbine. Changes to the program can be made simply by erasing the PROM and reprogramming it.

Basically, the program shown in Figure 2 determines when to run the VAWT based on the wind's speed history. If sufficient wind speed is observed for a sufficient time then the turbine is started. If the wind's speed falls below an acceptable level for more than a prescribed time the turbine is shut down. Both the wind speed and time criteria for running are programmable and different values may be chosen depending on the site and particular turbine characteristics. Once the turbine is running the microprocessor monitors sensors such as bearing and generator temperatures, structural vibration, turbine shaft speed, and electrical power. If an unusual condition is observed the system will notify responsible personnel. If a malfunction occurs, the system will execute an orderly shutdown. A microprocessor wind turbine controller which displays the above functions was demonstrated in yesterday evening's display.

Figure 3 displays block diagrams of wind instrumentation systems based on the conventional manual method and an automated data acquisition approach. In the manual approach the anemometer and wind turbine torque data are stored on a strip chart recorder. The chart recorded is then digitized and the data is stored on magnetic tape for input to a computer for data processing and output plotting. This approach has a number of severe drawbacks. First, the strip chart recording is not appropriate for taking accurate data over extended periods of time. The amount of chart paper required for long runs is enormous and the accuracy obtained is inversely related to the paper's speed because of ink smear and noise. Once the long lengths of recordings are made the information must be digitized for computer processing. This procedure requires extensive, time consuming, manual labor.

The automated approach alleviates the above problems by performing the analog to digital (A/D) conversion directly from the test instruments. The digital data is processed by a microprocessor and recorded onto a paper tape, magnetic cassette, or fed directly to a large computer via a phone link. A further step may be taken by using digital instruments to eliminate the A/D converter entirely. This approach will be discussed further by Jack Reed in the next presentation.

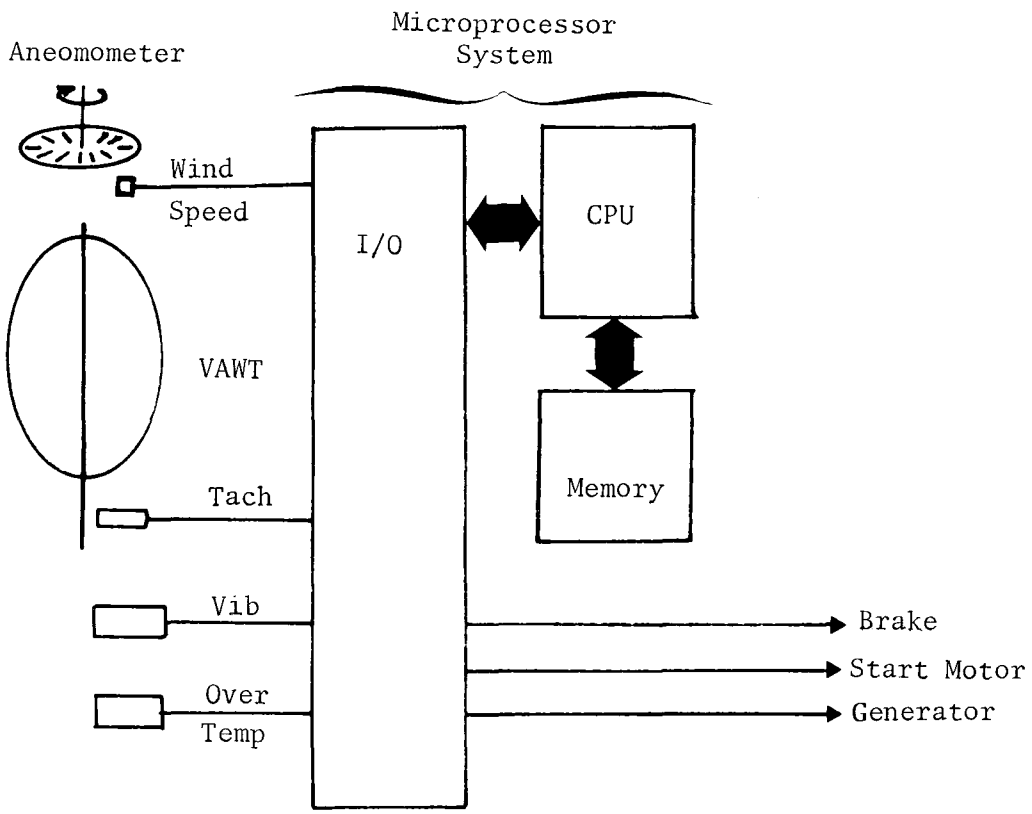

Figure 1. Automatic Control of VAWT

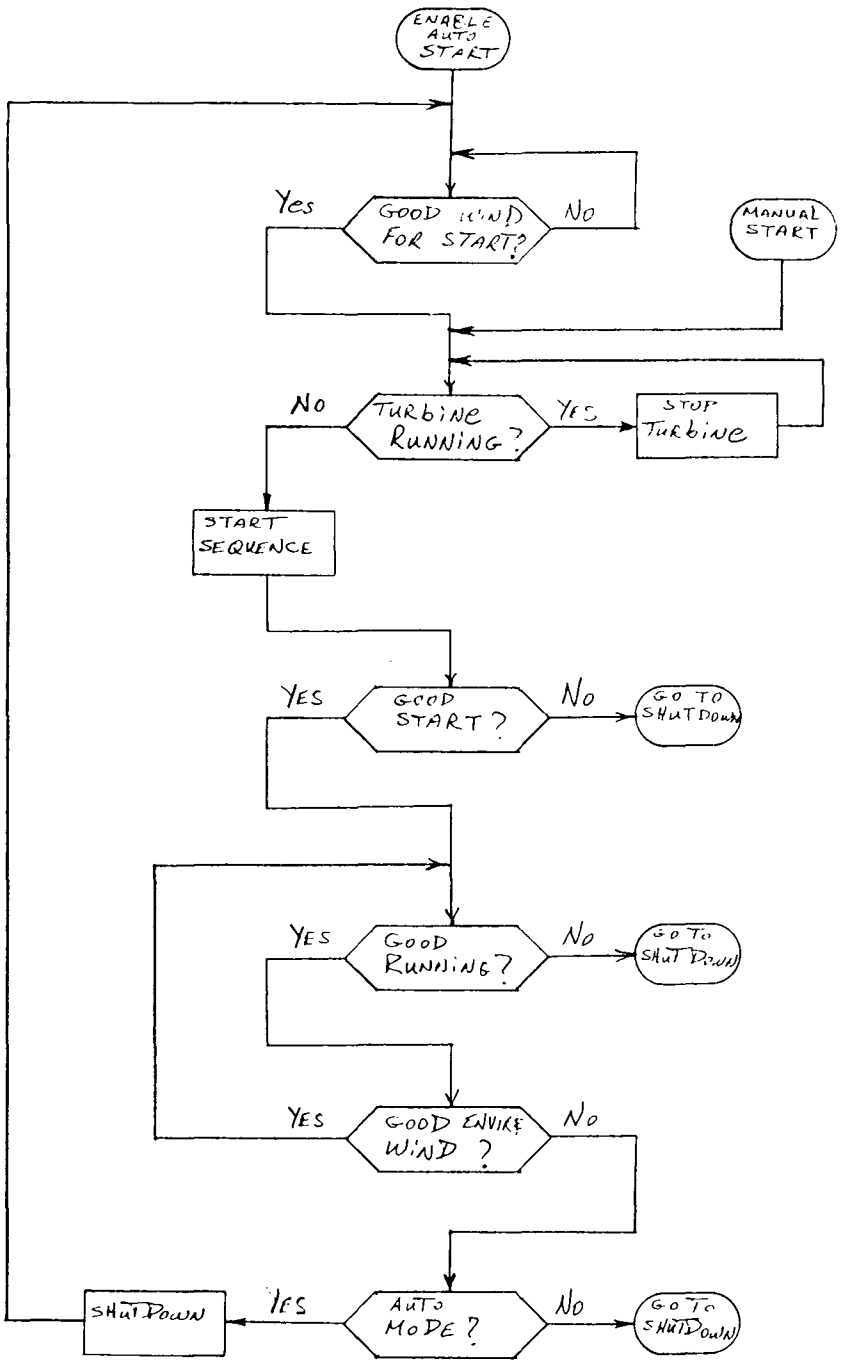

Figure 2. Microprocessor Program Flowchart for VAWT

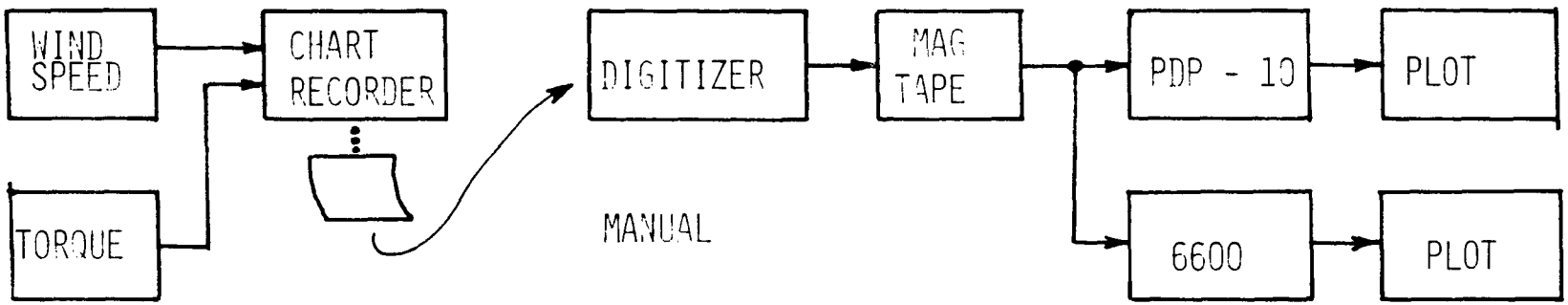

INSTRUMENTATION

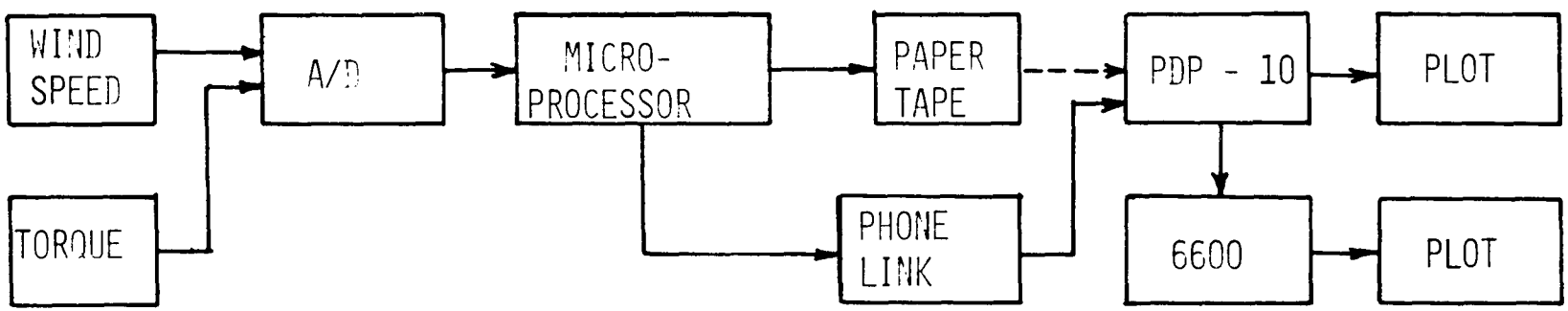

Figure 3

ANEMOMETRY DATA AND PROCESSING

Jack W. Reed
Environmental Research Division - 5443
Sandia Laboratories
Albuquerque, New Mexico

ABSTRACT

Turbulent wind characteristics are described as they affect both measurements and interpretations of data acquired at the Sandia Vertical-Axis Wind Turbine Laboratory. It is proposed that a similar, but inexpensive, universal wind observation system be developed for installation at the various projected wind turbine experiment demonstration, and power generation sites. This system would depend primarily on recently developed micro-processor technology. It would have the capability to serve all conceivable wind data needs, from structures vibration analyses through wind power assessment, to routine climatological studies. The more complex evaluations, involving time series spectral analyses, would require interfacing with large computer centers.

ANEMOMETRY DATA PROCESSING

Introduction

Special requirements for wind characteristics detail, beyond simple hourly meter readings as provided by weather service observations, have been a special concern of the AEC, now ERDA, for many years [1]. In particular, the spread of pollutants in our atmosphere is largely governed by the intensity of atmospheric turbulence, on short time scales that are not detected by ordinary rugged airport anemometers. Measurement at these needed high frequencies generated a great quantity of data, so that a substantial investment in recording and data reduction equipment was necessary for each experimental site. Special anemometers with low friction and momentum were also necessary, and these delicate sensors were often abused by the winds they observed, so their records are often incomplete in relatively high wind speed periods. Fortunately, pollution episodes are most severe in light winds, so adequate data for these problems were usually obtained. But such detailed observations were restricted to a small number of expensive, specialized programs, and their results are not sufficiently general for application to of other modern problems, such as high-rise building response or wind power turbine evaluations.

With recent advances in pocket calculators and similar micro-processors, as well as magnetic tape cassette recorders, it appears time for a radical

change in anemometer data handling that will allow complete wind characterization with relatively inexpensive installation.

We have developed a prototype data acquisition and pre-processing system for our turbine lab at Sandia to do the necessary work, but we have not yet attempted to synthesize an inexpensive, commercial system. In my opinion, that ought to be done soon by the established wind instruments business community.

In this presentation, wind spectral characteristics will be described, and a high-frequency cut-off will be justified that allows greatly simplified data processing. A model for data pre-processing by mini-computer, implemented at Sandia, will be shown that suggests inexpensive commercial replication. Output recordings could be simply processed for wind power evaluations or collected at a large computer center for spectral analyses for various applications to turbine engineering dynamics.

Wind Characteristics

Wind is never steady, but varies continuously and on a continuum of time scales with some examples illustrated in Figure 1. These time scales range from Brownian motion of air molecules at about 3 GHz in sea level air, to interglacial frequencies of 300 fHz. Fortunately, a complete characterization, or spectrum of wind variation only requires definition by observation up to a moderate high-frequency range, above which turbulence theory provides an adequate extrapolation method. On the low frequency end, spectral estimates depend on the length of available record, but it is not always necessary to have a long record at a specified location for a wind turbine. Weather Service records, even at considerable distance, may adequately show annual cycles as well as climatic changes from year to year, or decade to decade.

A frequently referenced wind spectrum by Van der Hoven [2] is reproduced in Figure 2, in normalized form that gives the wind variance (m^2s^{-2}), or σ^2, at each wave number, n, or frequency, at Brookhaven National Laboratory, on

Long Island, New York. A notable spectral peak occurs at about 0.01 per hour, from the synoptic-scale storms shown on the weather map with 4-5 day recurrences. A peculiar local feature here is a 12-hour period peak, rather than a diurnal peak at 24 hours as found at most locations. The so-called "mesoscale gap," centered near 1 hour, shows there is very little wind oscillation with this periodicity, or wavelength of 10-50 km.

The peak on the right near 1-minute period is important to turbulence and diffusion phenomena. In rough terrain, such as here at Sandia Laboratories, this peak is shifted to a lower frequency with about 20-minute periodicity, apparently in result of the nearby mountain dimensions with 5-20 km extents. Spectral peak amplitude for other sites or special cases (this illustration reflects data collected during a hurricane passage , which emphasizes the amplitude,) depend on a combination of factors that include wind speed, terrain roughness, and atmospheric thermodynamic stability or temperature lapse rate. At frequencies higher than this peak, however, many experiments have clearly shown that the spectra decays in proportion to the five-thirds power of frequency, as predicted by Kolmogorov [3]. An example, from a recent report by Berman [4], is reproduced in Figure 3, but without the normalization of Figure 1, and in double-log coordinates. This particular spectrum was obtained from shipboard tethered balloon measurements during the Global Atmospheric Research Program (GARP) expedition in the South Atlantic. The very high-frequency peak at 0.12 Hz is a spurious result of rolling motion on that particular ship. Other published spectra from fixed measuring systems show the five-thirds law, once established, is valid to higher frequencies.

Thus, it appears that a definition of the mesoscale high-frequency peak, under various air mass or weather conditions, is all that is needed on the high-frequency end, for any practical purpose. Measurements at

3-4 per minute should be adequate to define this peak. Variances at all lower frequencies may be obtained by simply smoothing these data, to a limit defined by the period of record.

Complete spectral analyses of long records are exeedingly complex and time consuming by ordinary mathematical techniques [5]. On the other hand, fast Fourier transform (FFT) methods have now been derived [6] that allow inexpensive data reduction, but require large computer storage and data handling capacities. Such processing is well beyond the current potential of microprocessor systems. Our Sandia instrumentation is designed to do some pre-processing of raw wind sensor outputs, to store results on a simple magnetic tape cassette recorder, and then play back this tape into our CDC-6600 computer network for time series analysis and spectrum construction.

From a spectrum, it is a relatively simple matter for any of the various components engineers to reconstruct a wind "noise" record for a frequency band of specific concern. Vibration analyses of blade and structure components are primarily concerned with frequencies above about 1 Hz, which can be obtained by Kolmogorov's extrapolation. Large turbine systems will effectively filter out most such high-frequency wind effects through their slow momentum response. Thus problems of dynamic loads on shafts, gears, and electrical generators, as well as interfaces to electric power grids will be addressed through analysis of another, and lower, frequency band. At even lower frequencies, problems of diurnal, weekly and annual variations in supply and demand can likewise be assessed from spectral evaluations. Obviously, problems with inter-annual variations of wind, and

associated economic impacts of wind power drouths or climate changes, will require use of data from existing established observing stations with long periods of record.

The point we intend to make is, however, that a universal state-of-the-art anemometry system can now be assembled that collects all the useful wind data, for whatever purpose, of wind energy assessment, turbine dynamics, building response, or pollution dispersion evaluation. Mass production would bring its cost into competition with analog paper recorder systems. By simple computer instructions at one or more available computer centers, each specific user's analysis requirements could be served. In addition, a user who "discovers" that he needs more detail than he originally estimated can always recover it from a total record. He no longer would need to buy new gear and start over in recording. Finally, new users from other fields of study would be able to use these archived collections. If numerous recording sites are used under a variety of exposures, we would no longer be restricted to re-analysis of scarce data collected in selected spots where someone had sufficiently funded interest to field a special research project.

Wind Speed Sensors

The most common basic method for wind speed measurement is the familiar cup anemometer, shown by schematic in Figure 4. It rotates almost proportionally to wind speed, with the cup center travelling at about 0.3-0.4 of the wind speed [1]. Anemometer sensitivity is regularly stated in terms of a "distance constant," or the length of air column passage required to register (1-1/e) or 63% of a changed speed. Since

typical rugged airport anemometers have 5m distance constants, they allow good records of 15 second oscillations in $4ms^{-1}$ speeds. With "micrometeorological" sensors, typical distance constants are 1m, allowing adequate detail of even $0.3ms^{-1}$ speeds.

Popular systems use light-chopper discs on the cup shaft to generate digital sensor outputs. Postulating a requirement for accuracy of 15-second readings, an average speed from 5 readings per second would be accurate to about 10% of the standard deviation for the sample of 75 readings. In turn, this translates to about 16 pulses per revolution of the cups, on 7.5cm arms, that begin to turn at $0.5ms^{-1}$.

Software in several vest-pocket portable mini-calculators furnishes automatic sums and sums of squares of number sequences, such as these 75 observations. These sums could then be recorded in much less tape space than is required for an original analog recording. More generally useful output could be obtained by simultaneous digital sensing of wind direction. Each speed vector should be resolved into two orthogonal components, and these two series registered into the pre-processor statistical program. This avoids errors and difficulties of definition of polar coordinate variances, that are obtained by many existing systems. As shown in Figure 5, this would still allow evaluation for direction variability, which may be essential to those wind turbine systems that are sensitive to wind direction. In addition, results can be translated by computer into along-wind and cross-wind turbulence parameters of interest to pollution trackers. Finally, some provision should be made for temporary data storage, so that accumulations would be transferred to a recorder at intervals. Thus, the recorder would not be running and drawing power continuously. None of this pre-processing appears to present any difficult problem, according to micro-computer specialists.

Recording

If it is assumed that a total wind vector observation is required, then there would be four values recorded every fifteen seconds, $\bar{u}$, $\bar{v}$, σu, and σv, or the respective sums from which they are derived. If 3-digit accuracy is maintained, this requires nearly 10^6 digits recorded in two weeks, as shown in Table I. At least one commercial cassette storage unit, as a hand calculator accessory, has capacity for 9000 13-digit numbers, but it appears inadequate by nearly an order of magnitude for storing a two-week collection, which may be a reasonable period for servicing each reorder. On the other hand, the required numbers may be expressed as 3.23×10^6 binary bits. If a simple cassette recorder is assumed to record 5 kHz for 30 minutes, that would be 9×10^6 cycles (bits), and possibly adequate with necessary timing and parity checks. With a high density two-hour tape capacity of 3.6×10^7 bits, there would be room for two or three levels of anemometry on a tower.

There are obvious possibilities for data compression techniques to further reduce tape storage requirements. At even the windiest sites, such as Nantucket Shoals, Massachusetts, wind speed exceeds $10ms^{-1}$ only 40% of the time and 60% of the reports would require only two decimal digits in reporting. With few exceptions, standard deviations could also be reported in two digits. This would give a net 25% reduction in capacity needs, over 30% reduction at windy continental sites such as Lubbock, Texas. An actual evaluation of digital bit requirements based on some typical wind distributions may be necessary to establish just what requirements really need to be met at various prospective turbine sites.

Another data compression scheme is one that looks at the last measurement and, based on the relative change that occurred, decides

TABLE 1

"TOTAL" WIND OBSERVATIONS.

$$\{u, \sigma_u, v, \sigma_v\}$$

Every 15 seconds, with 3-digit decimal accuracy.

DECIMAL					BINARY
12	digits	per	15 seconds	or	40 digits (bits)
48	"	"	minute	"	160 "
2,880	"	"	hour	"	9,600 "
69,120	"	"	day	"	230,400 "
483,840	"	"	week	"	1,612,800 "
967,680	"	"	fortnight	"	3,225,600 "

Magnetic Tape Memory Capacity

Commercial Decimal Example		5 kHz 30-minute binary tape	
9000	13-digit numbers	5,000	bits per second
117,000	digits	300,000	" " minute
		9,000,000	" " 30-minutes

whether a new observation needs to be recorded. The accuracy statistics for this decision making have not been worked out but it certainly seems promising. In spite of the opening contention that wind is never unchanging, there are many times when it appears to be relatively constant. Particularly at night, very low speeds in orographic drainage flows may only vary by small amounts over hours. It does not seem unreasonable to expect that a factor of two or three reduction in data acquisition volume could be achieved by this technique.

There is great interest in recording at more than one height, for various reasons. We feel that the change of wind with height above ground is adequately understood in relatively flat terrain [7] so that only a single level observation is necessary. But for installations in rough country, where our understanding is much poorer, multiple sensor levels appear to be needed for the near future at least. This would, of course, double the data handling capacity requirement.

There is, also, an alternative of using multiple cassette recorders, since they can be quite inexpensive. A redundant system, properly programmed, could also be valuable in case of failure, or in case of a week of extraordinary wind speeds and variabilities.

Poor Man's Micro-Met Wind System

The following proposition indicates a package that ought to be developed by commercial instrument suppliers, to serve all wind data user's needs, in particular the turbine site survey requirements. The $2000 total price tag, for a system diagrammed in Figure 6, has been declared naive, radical, and unrealistic by some of those who are invovled in supplying equivalent performance systems for $20-$25K. One immediate contention was that a cost reduction to $6K was the best that could possibly

be expected. On the other hand, the only things lacking in this cost breakdown are the wire and software linkage. Wire is negligible in cost, and software is a one-shot expense that would be amortized to a few percent of total cost. With concerted pressure (or support, possibly) by the wind energy establishment at least, it would seem totally reasonable that some anemometry supplier could profitably produce this package.

Time Series Analyses

A primary concern to wind turbine projects is an assessment of available wind power. This only requires elementary analysis of the wind records, essentially a summation of speeds cubed. Long time digital records are also needed to assess economic benefits, by comparison of supply and demand functions. Similar evaluations will eventually be needed for storage system capacity designs. It is not obvious that these calculations would benefit by spectral analysis methods. Direct numerical comparisons seem most reasonable.

On the other hand, considerable advantage to analysts of turbine-generator dynamics would result from time series spectral analysis techniques. In particular, bivariate spectral analyses, applied as a "historical filtering problem" [5], will allow optimized solutions $\tilde{L}$, for the process

$$X(t) = L[Y(t)],$$

shown in Figure 7, where a response (turbine) function, $X(t)$, results from an input (wind) function, $Y(t)$, that has been affected by a linear filter, L. The solution for $\tilde{L}$ is a frequency-dependent attenuation (or amplification), whose source or sources can be appropriately attributed to components of the turbine-generator system. With this tool, the effects

of component modification on the total system can be identified and fine-tuned for maximum cost effectiveness.

Not all turbine installations will require this analysis of their wind records, but it will doubtless be most useful to many of our early projects of proof testing. On the other hand, with use of the universal wind system described earlier, all the data that are needed will be available at little cost, so this analysis can be made when unexpected requirements arise.

Data Processing

It may be possible to do some elementary processing with field computers or data preprocessors. For example, wind power integration would be simply obtained from any of several programmable tape-fed portable calculators. These now cost only a few hundred dollars, and will probably drop further in price.

Evaluations of long-term characteristics would most economically be performed by large computer centers. A mail-order tape analysis system could be developed to operate like photo-film processing centers. Various programs for analysis could thus be centrally available, responsive to immediate demands from specific users. In rough estimate, it would appear that the owner of a $2000 anemometry tower system could expect an annual bill of $500 for tapes, postage, and processing, even including some spectral analyses.

Summary

Wind varies on a near-infinite continuum of time scales, but a finite wind observing system can only obtain data from a limited frequency band.

Fortunately, high frequency turbulence above about 0.01 Hz, may be derived through theoretical models, and very low frequency variations below about 3×10^{-8} Hz may be estimated from long-term weather station records. Thus, use of a micro-processor computer system allows 5 Hz readings to be appropriately resolved into cartesian coordinate winds, statistical summations to be performed at 0.07 Hz, and results stored in a small magnetic tape cassette. Data fidelity is only slightly limited by the response of the selected anemometer or wind vane and the length of operation.

Some linear evaluations, for wind power, for example, may also be performed on-site by this computer. Calculations of power spectra require large computers for analysis, however, so data reduction for some requirements of structures design or specialized research must be done at a central computer facility. Also, very long records would most economically be digested by a large computer. Once a uniform data acquisition system is put into operation, a mail-order computer center could do any of the reductions, depending only on the user's needs.

References

1. Slade, D. H., ed., Meteorology and Atomic Energy, USAEC, Washington, D. C. July 1968.

2. Van der Hoven, I., "Power spectrum of horizontal wind speed in the frequency range from 0.0007 to 900 cycles per hour", J. Meteor., 14, 160-164, April 1957.

3. Kolmogorov, A. N., "The local structure of turbulence in incompressible viscous fluid for very large Reynolds numbers", Dokl. Akad. Nauk SSSR, 30, 301-335, 1941.

4. Berman, E. A., "Measurements of temperature and downwind spectra in the "Buoyant Subrange" ", J. Atmos. Sc., 33, 495-498, March 1976.

5. Koopmans, L. H., The Spectral Analysis of Time Series, Academic Press, New York, 1974.

6. Cooley, J. W., and Tukey, J. W., "An algorithm for the machine calculation of complex Fourier series", Math. Comput., 19, 297-301, 1965.

7. Reed, J. W., "Wind Power Climatology of the United States", SAND 74-0348, Sandia Laboratories, June 1975.

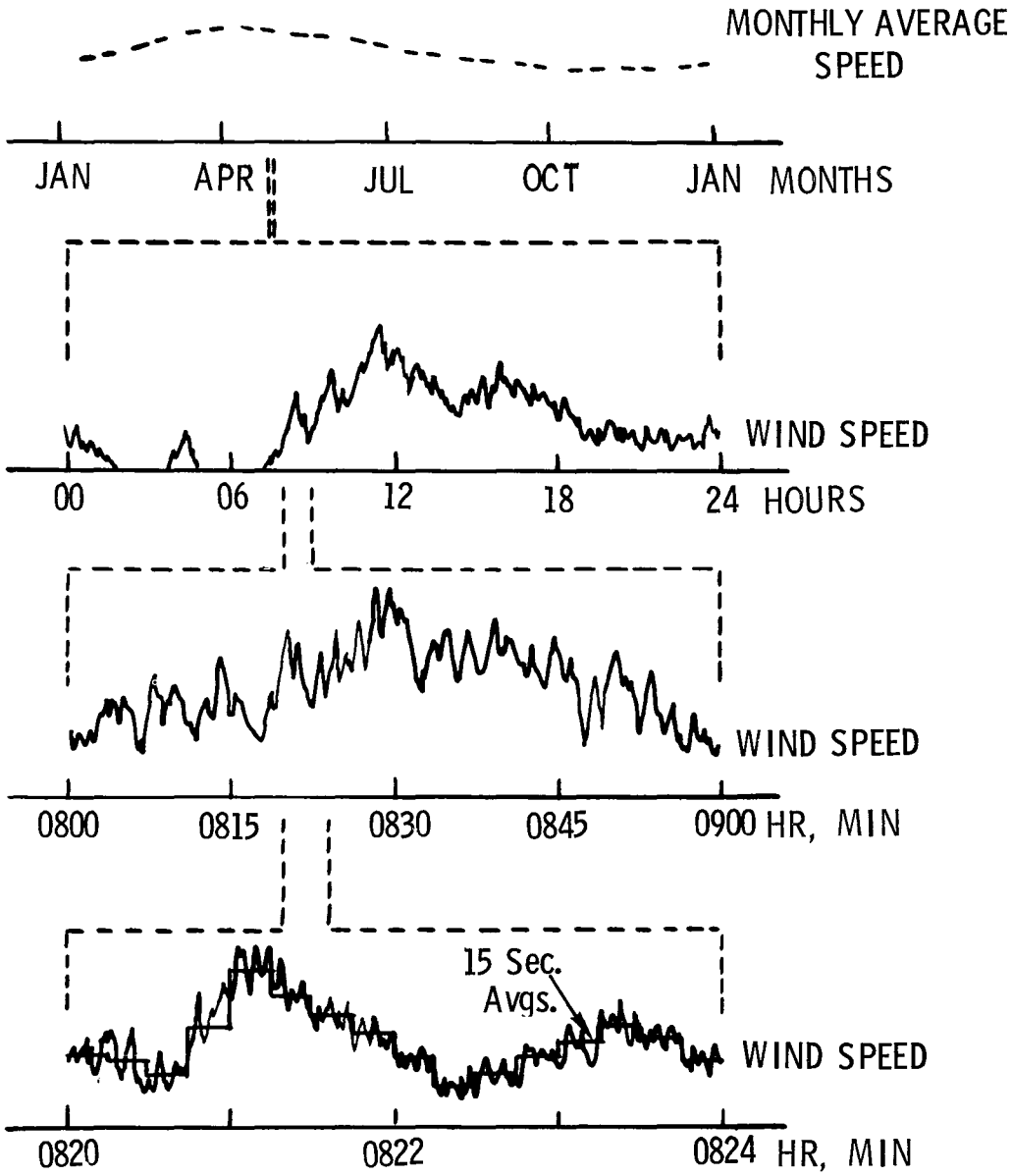

Figure 1. Wind Speed Records on Expanding Time Scales

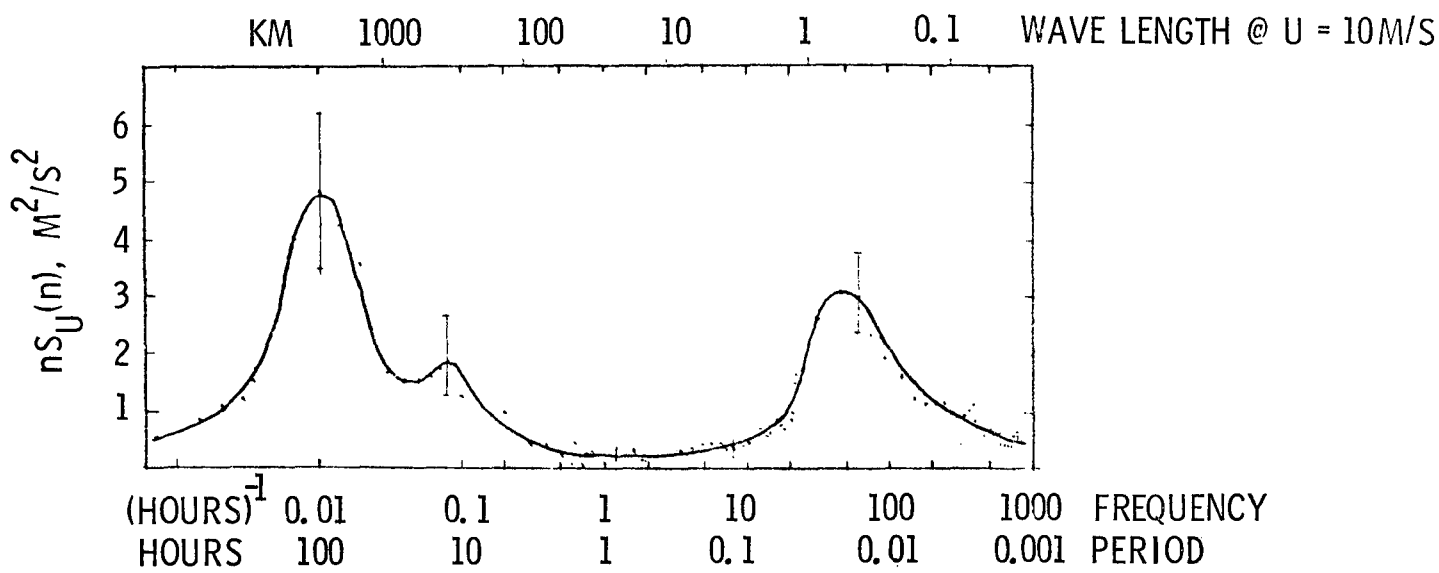

Figure 2. Horizontal Wind Speed Spectrum BNL, 1955, 100 M Height

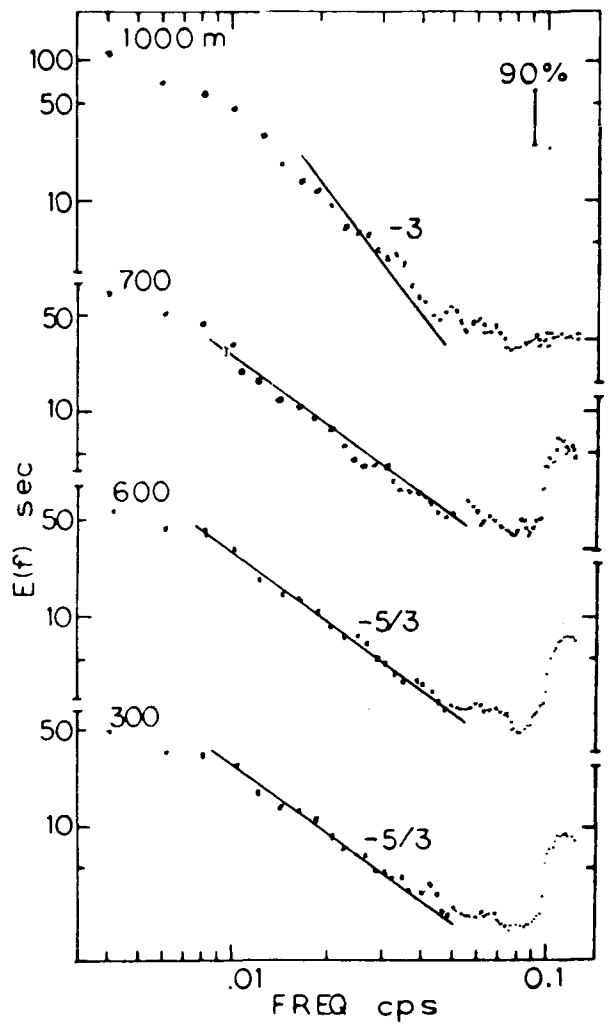

Figure 3. Wind Spectra at Four Heights Over Water, From Berman (Ref. 4)

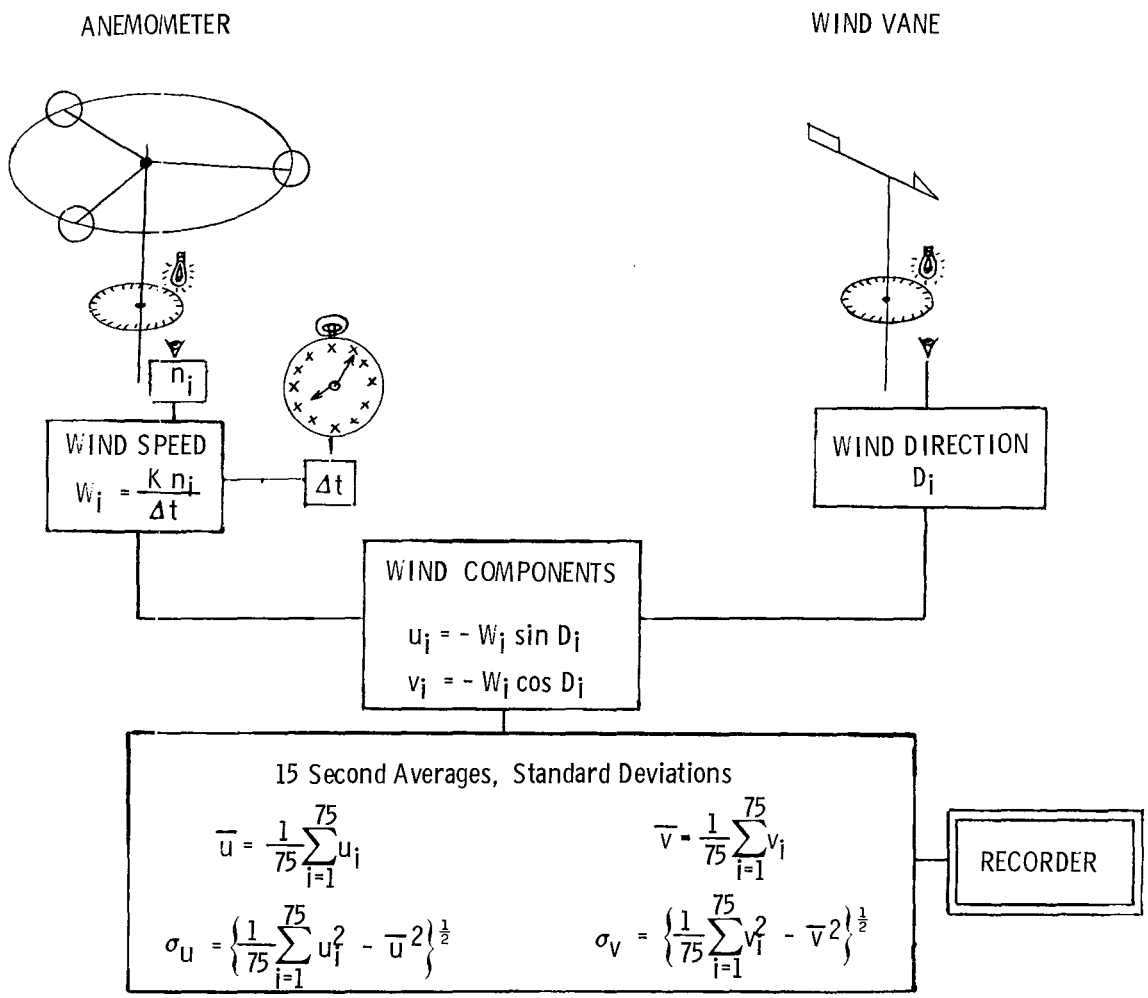

Figure 4. Wind Observing System and Preprocessing Equations

IF POLAR COORDINATE WINDS ARE REQUIRED

$$\overline{W} = (\overline{u}^2 + \overline{v}^2)^{\frac{1}{2}}$$

$$\begin{cases} \overline{D} = \arctan(\overline{u}/\overline{v}) + 360^0, & \text{if } \overline{v} < 0 \\ \overline{D} = \arctan(\overline{u}/\overline{v}) + 180^0, & \text{if } \overline{v} > 0 \end{cases}$$

DOWNWIND AND CROSSWIND VARIANCES

$$\sigma_W^2 = \frac{\sigma_u^2 \overline{u}^2 + \sigma_v^2 \overline{v}^2}{\overline{W}^2}$$

$$\sigma_c^2 = \frac{\sigma_u^2 \overline{v}^2 + \sigma_v^2 \overline{u}^2}{\overline{W}^2}$$

TURBULENCE INTENSITY

$$I_W = \frac{\sigma_W}{\overline{W}} = \frac{(\sigma_u^2 \overline{u}^2 + \sigma_v^2 \overline{v}^2)^{\frac{1}{2}}}{\overline{u}^2 + \overline{v}^2}$$

$$I_c = \frac{\sigma_c}{\overline{W}} = \frac{(\sigma_u^2 \overline{v}^2 + \sigma_v^2 \overline{u}^2)^{\frac{1}{2}}}{\overline{u}^2 + \overline{v}^2}$$

IF CONVENTIONAL SIGMA-METER EQUIVALENT IS NEEDED

$$\hat{D} = \left(\sum_{i=1}^{75} D_i\right) / 75$$

$$\text{SIGMA} = \left\{(1/75) \sum_{i=1}^{75} D_i^2 - \hat{D}^2\right\}^{\frac{1}{2}}$$

Figure 5. Equations (contd)

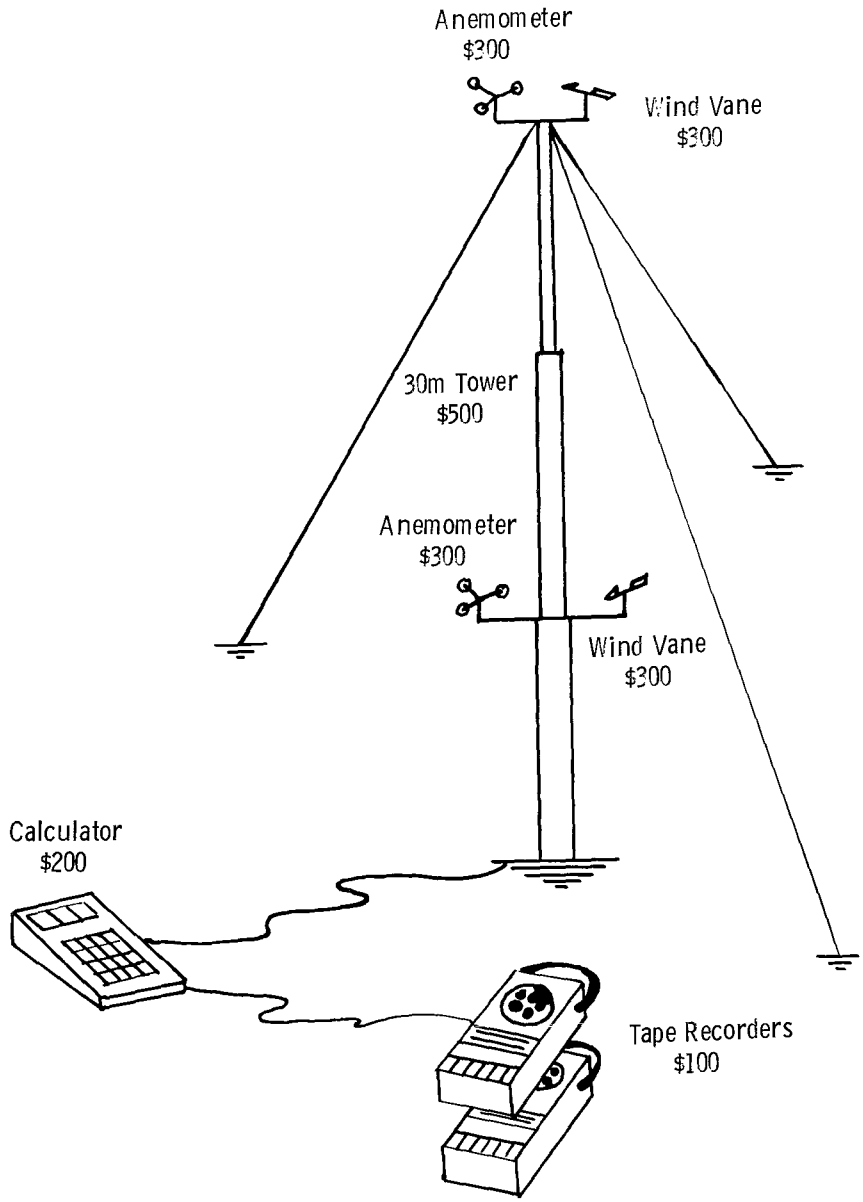

Figure 6. Poor-Man's "Micro-Met" Wind System

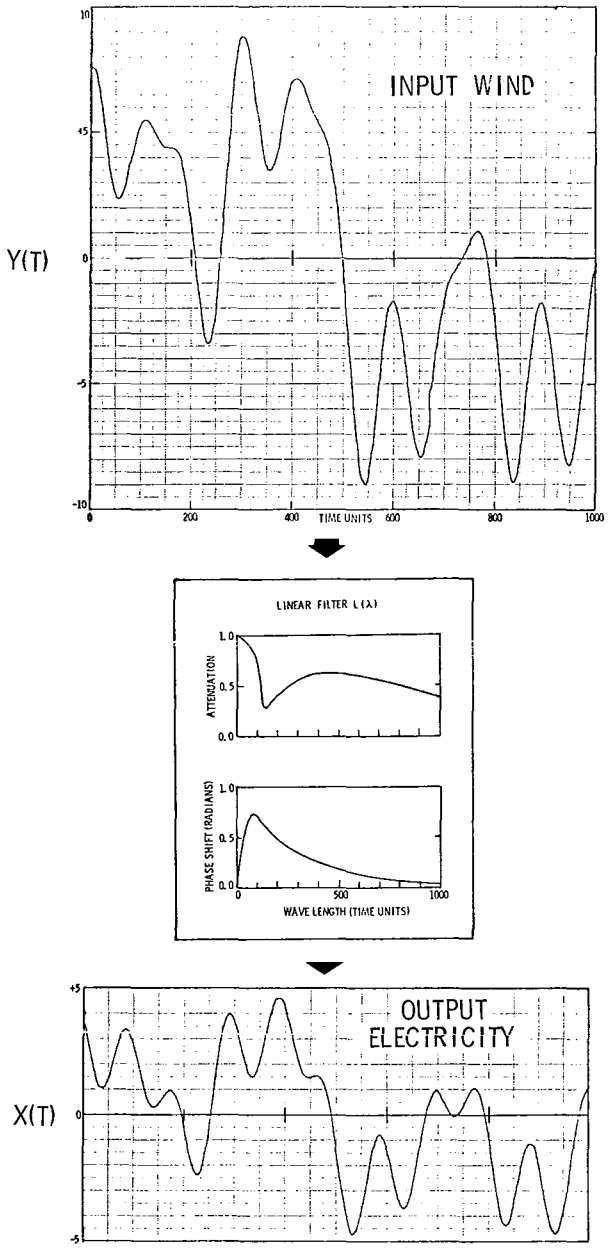

Figure 7. Schematic Effects of Filtering on a Wind Record

BANQUET ADDRESS

Wednesday, May 19, 1976

Wind Power, Fact or Fantasy

W. Lyle Donaldson
Senior Vice President
Southwest Research Institute

WIND POWER, FACT OR FANTASY

The critical need for additional energy sources is apparent to all of us, yet there is disagreement among the people of this nation as to which way we should go both politically and technically to keep our energy problem from turning into disaster. Conflicting views by technical experts and inaccurate media presentations have much of the general public confused. Typical of this type of reporting is an article appearing in San Antonio's Express-News of Sunday, May 16, 1976 titled Wind Pumps. Quoting from this feature story -

> "There are well over a million of them in Texas and their spinning blades and windlashed tail vanes are as much a part of the state's rural vistas as the cattle they help to support." ----

> "A NASA report sent to Congress recently estimated that 50 per cent of the nation's 1985 electricity needs could be supplied by wind generators placed on the Great Plains - power equivalent to about 140 billion gallons of gasoline."

In my opinion the million wind mills in Texas is a gross exaggeration and the 1985 date for that amount of power from wind generators completely unrealistic. I am sure the NASA report has been completely misquoted and I am positive that this is not a NASA viewpoint. Such reporting does produce enough believers so that political obstacles are created in formulating a cohesive national energy program.

I am an enthusiastic believer in the ability of wind generators to make a real contribution to our energy needs and the facts being presented at this conference strongly substantiate this belief. You wind power experts are certainly to be commended on the accomplishments since the conference in Washington a year ago.

If ERDA's primary objective for wind power is to have wind generators make a real energy contribution (and I believe this to be the case), then the electric utility industry (either privately or publicly owned) must be the target user. Failing to sell this industry on wind power use will probably relegate the usefulness of the national program to the small and medium sized machines for use in isolated installations.

The power that could be generated from all of these machines would probably never amortize the cost of the research program, although there would be social benefits. Maybe a market study is needed!

For this reason my talk tonight is concerned with the strategy of getting wind generators into commercial use by electric utilities. Fortunately a recently issued NBS report by Arthur D. Little, Inc., titled Federal Funding of Civilian Research and Development will give us some guidance. This report states "Countless examples show that R&D cost is a small part of the total cost of bringing technological innovation into the market place. This fact is often overlooked by federal policy makers in both the executive and legislative branches. It is one of the reasons why many U. S. companies with proven records of developing and marketing new products often shun federal R&D funds, and why so many federal R&D products are shelved."

The study of this report further finds

> "that commercial innovation is most likely to succeed when convergence of a number of factors takes place."

These factors are:

1. Technical knowledge
2. User needs
3. Advocate or champion
4. Resource availability
5. Favorable "Risk Factors"
6. Timing.

Let's consider each of these factors in the light of our wind power program.

1. Technical Knowledge - ERDA is providing this information through R&D as well as demonstration projects. There are still gaps to be filled but I am sure ERDA has these well targeted. For example, the mean time to removal (MTR) of the main rotor blades

on many of the helicopter types is under 500 hours. Practical wind power systems cannot from a maintenance standpoint afford a similar MTR. Blade technology must be improved. The technical knowledge factor must be reasonably complete if commercialization is to take place, but this factor alone will not assure success.

2. User Need - The need exists for energy, but the utility engineer must be convinced that wind power is a solution.

3. Advocate or Champion - Certainly ERDA and this group are advocates of wind power - but it would be helpful if a few advocates would appear among electric utility personnel. I would caution that an attempt to oversell tends to turn off utility executives. A case in point is the newspaper article quoted earlier.

4. Resource Availability - There is plenty of wind!

5. Favorable Risk Factor - The use of wind power generators must be economically viable and there is only one cost to consider

LIFE CYCLE COST PER KWH

Since there will be much uncertainty concerning maintenance costs, manpower requirements, and outages, government action in addition to R&D and demonstration programs will probably be needed to effect commercialization. Possibilities include tax incentives, subsidies, and low interest loans. There are other possibilities and at this time I am not suggesting an approach, but I do suggest that ERDA and others should begin to consider the possibilities and start working with Congress and other agencies to provide appropriate incentives. The decontrol of fuel prices would certainly stimulate the introduction of new energy sources. There is still another important factor that must not be overlooked. That is the price of OPEL oil. We forget that the price of this oil (which costs the Arabs about $.60 per barrel to get out of the ground) can be lowered in price as well as raised in price. This is an overhanging threat to any substantial investment in any energy source where the incentive to introduce the source is a small energy cost advantage. This applies equally well to shale oil production and solar energy. A simple example is your own willingness to invest your savings in a company whose sole product is energy produced from an unproven source at a marginal cost advantage.

6. Timing - This factor is particularly important to wind power. If we don't move promptly and accurately with our needed development, other energy sources may become commercialized to the point that investor money would be difficult to obtain and utility bias would oppose the introduction of wind power. If the factors converge correctly, we will have wind power systems providing substantial energy to utility grids within the next decade.

We need to help this convergence along a bit and to do so we need to understand the target industry better. Few people familiar with the intimate details of wind energy conversion have adequate knowledge of the utility industry. As a start let's consider a few facts.

The first fact about the utility industry that requires serious effort to absorb, is the sheer magnitude of the numbers involved. The public and private electric utility systems in the United States represent a total generating capacity of more than 300,000 MW of electrical power. With this capacity, they delivered a total of nearly 2 trillion KWH of energy to their millions of commercial, residential and industrial consumers last year. This is almost 10,000 KWH for every man, woman and child in the United States. Based on the current efficiency factors of the average generating plants in the United States, this represents the fuel equivalent of about 20×10^{15} BTU, or 3-1/2 billion barrels of oil if all these plants had been fueled petroleum. This is about equal to the total of our oil imports and represents a current annual value, at import prices, of more than 50 billion dollars.

The second fact that characterizes the electric utility industry is its enormous complexity. The combination of thousands of generating plants of all types, integrated into a veritable web of transmission, subtransmission, and distribution lines, must equate supply and demand requirements of overwhelming diversity, meeting consumer needs instantaneously and without restriction. Equipment failures, outages, and even natural disasters must not greatly impair the overall ability of the utility to meet its commitments. Indeed its product is the life blood of American industry, and for that matter, of the American standard of living. Fuel must be available, with reserve and backup capability, under all reasonably predictable circumstances. Few industries in the world have met their commitments as well.

Finally, the third fact difficult for even technical persons outside the industry to comprehend, is the enormous size of the machinery involved in generating utility power. A coal-burning, steam turbine generator plant with a capacity of 400 MW is currently only of average size. Many nuclear fuel plants have capacities of 1,000 MW or even more, and a 200 MW gas turbine generator is considered a small machine, relegated to peaking chores.

Faced with these three principal characteristics of the utility industry for the first time, the wind power expert is likely to feel a sense of hopelessness, to stand back aghast, and to decide that wind power is a small boy sent to do a man's job. As we all know, the largest conceivable wind conversion machine, confined to the imagination of the very daring, might have a capacity of 5 MW. Almost certainly a practical machine, with its cost and other tradeoffs, will be little larger than 1 MW, and there is a possibility that the most cost effective scheme will utilize even smaller machines, perhaps of 100 KW or so. The largest wind generator in the world today, which has been described to us at this meeting, is the ERDA-NASA 100 KW horizontal-axis machine, and those of us who have seen it know that it can hardly be classified as small, at least not in a structural sense.

If the wind power expert has some things to learn about the utility industry, the utility engineer, first exposed to wind energy as a serious energy possibility, is in for his share of assimilation and shock. Generation capacity represents the first area of disenchantment he is likely to experience. It is simply difficult for him to believe that fooling around with machines of this miniscule capacity can possibly be worth the trouble.

A second area of difficulty is the uncertain nature of the wind. Strangely enough, it is here that common ground can be most easily reached. Utility engineers have long recognized the ability of their systems to absorb the output of intermittent generating sources. Systems inherently must have the capacity to follow demand, and obviously it makes no difference whether a drop in demand is caused by reduced load, or increased output from a remote intermittent generator. Connected to the utility network in relatively small numbers, wind generators can be operated in a run-of-the-wind mode, supplying power to the network in response only to the wind. The conventional base-load and peaking generators will then follow the overall load requirements as set by demand and wind generators. Perhaps from one to as much as 10% of a utility's total capacity might be made up

of wind generators operating in this manner, directly conserving fuel when the wind is favorable. It is in this context that wind generators should first be integrated with utility networks, leaving for the future questions about energy storage. Studies recently completed at Southwest Research Institute indicate that there are presently no identifiable elements which make attractive the concept of wind generator-storage combinations that provide uniquely favorable characteristics as utility elements. Rather from every aspect, wind generators should be considered separately from storage, each on its own merits.

A third and serious area of disenchantment for the utility engineer is the matter of cost. Wind generated electricity may be fuel-free, but it is not cheap. The best estimates made by a number of relatively independent sources, including the Southwest Research Institute study, indicate that the most cost-effective conventional wind turbine generators of the horizontal axis propellor type can probably be built to produce electricity for from 2 to 3 cents/KWH in an area of good to excellent winds such as the Texas Panhandle. The investment cost for such a machine in production quantities, would run from $450 to $600/KW, making the cost of a 1 MW machine a half million dollars or more. It must be stated that there are great uncertainties in these cost estimates, and by the time the first machines are actually built and running it is quite likely that actual costs will be greater. Consider for a moment the cost of producing power in recently built plants and I quote from Electrical World's 19th Steam Station Cost Survey. Thirty modern stations from all parts of the country except New England were considered. Nuclear plants accounted for 18.6% of the total capacity of the survey and only one gas plant was included.

Quoting from the survey -

	19th Survey	18th Survey
Total busbar energy cost, Mills/KHH	15.09	7.99
Fixed charges, Mills/net KWH	7.58	3.78
Operating costs*, Mills/net KWH	7.51	4.21

The purpose of presenting this information is to show that fixed charges increased in the same percentage range as operating cost and

*Fuel costs were 82.2% of operating costs for the 19th Survey and 82.6% of operating costs for the 18th Survey.

this fact must not be overlooked in projecting the cost of wind power systems.

One of the coal stations listed in this survey has a busbar energy cost of 30.46 mils/KWHV. Clearly, wind generators show promise, but it is unlikely that utilities will devote much energy to immediate wind power implementation until there is a more clear-cut fuel cost trend than exists today. Many utility experts are currently projecting fuel cost increases at the rate of 3% per year from now on. If such a projection rate is valid, there is little doubt that wind generators will be cost-effective in areas of good wind potential.

I should also mention to this group that the utility engineer views the current horizontal-axis wind turbine generator designs as complex, expensive, and potential maintenance headaches. There is some justification for this view. If the vertical axis, or more properly cross-axis, machines can be developed which effectively eliminate blade pitch control, yaw control mechanisms, and aircraft type construction, support for wind power systems will be enhanced among technical utility personnel who are utterly devoted to the idea that cost effectiveness is the fundamental precept of engineering. The horizontal axis machine advocates must among other things give greater weight to the major effort that rotor repair, generator replacement, and the like require.

On the optimistic side, the problems of integrating wind generators into a utility system have been largely exaggerated. There are legitimate concerns about the effects of gusting, tower shading, and other input transients on the electrical output of wind generators. Otherwise, there are no special or unusual requirements with which these machines will be faced. Conventional power engineering practice can easily encompass successful and safe installations. Environmental problems, if any, will probably be minimal, at most requiring careful siting. The real need is for low-cost, reliable wind conversion concepts. It is highly gratifying to see that question so ably addressed by this meeting.

In this talk I have presented a dual role for those of us who want wind power to enter the commercial marketplace. We must assume a marketing role as well as our technological responsibilities. To do this we must thoroughly understand our target customer and I hope this talk has helped.

In closing permit me to do a little imagineering. In the future I see many wind power farms, each farm containing a large number of vertical axis wind turbines driving large diameter multi-pole induction generators all connected to a medium voltage distribution bus with simple protective devices. Connection to transmission lines would be accomplished by conventional transformers and switchgear. Your efforts in both marketing and engineering can make this vision a reality and not just a "pipe dream" or mere fantasy.

REFERENCES

1. Federal Funding of Civilian Research and Development, Volume 1: Summary NBS-GCR-ETIP 76-03, by Arthur D. Little, Inc.

2. 19th Steam Station Cost Survey; Electrical World, November 15, 1975.

3. Operational, Cost, and Technical Study of Large Windpower Systems Integrated with an Existing Electrical Utility: Southwest Research Institute Final Report, Executive Summary, for ERDA Contract No. E(11-1)-2621 by R. K. Swanson, R. T. Smith, and C. C. Johnson.

AERODYNAMICS OF THE DARRIEUS ROTOR

Robert E. Wilson

Professor of Mechanical Engineering

Oregon State University

Corvallis, Oregon 97331

INTRODUCTION

Performance models of the Darrieus Rotor have been formulated by Wilson and Lissaman (1), Templin (2), James (3) Muraca (4), Shankar (5) and Strickland (6). The flow models published by Wilson and Lissaman, Shankar and Strickland are identical and have been found to yield the best correlation with experimental results. Figures 1 and 2 illustrate the predicted and measured power and force coefficients for Darrieus Rotors with one, two and three blades.

As can be seen from these figures, there is still ample room for improvement in aerodynamic modeling. The current analysis is in essence a strip theory in which the time-averaged force on a blade element is equated to the mean momentum flux through a streamtube of fixed location and dimensions. The analysis uses quasi-steady aerodynamics neglecting the effects of mutual interference and of more significance, neglects the effects of the rear blades in crossing the vortex sheets of the forward blades (front and rear blade loads are the same). While the analysis correlates well with the available test data, it may be noted that the test data obtained to date has centered on time-averaged quantities such as power and the force in the free stream direction.

CHARACTERISTICS OF THE CURRENT FLOW MODEL

The flow model for the Darrieus Rotor has certain inherent characteristics. These are:

1. The current flow model predicts a maximum power coefficient which is less than that of an actuator disk (0.593). A closed-form solution (1) for a Darrieus Rotor with circular arc blades and $C_D = 0$ yields $C_{p\ max} = 0.536$.
2. The current flow model predicts zero side force if the blades are perpendicular to the radius and the lift is in phase with the angle of attack. Both blade misalignment and a phase angle between the lift and angle of attack result in net side forces.
3. The maximum power coefficient predicted by the current model is extremely sensitive to $C_{L_{max}}$. The maximum lift coefficient has a large effect on the range of operating tip speed ratios. Figure 3 illustrates the dimensionless performance of a family of 3-bladed Darrieus Rotors for which the maximum lift coefficient varies by 0.1.
4. The current flow model predicts a near uniform total torque for a three-bladed rotor at high tip speed ratios. However at lower tip speed ratios, the predicted total torque fluctuates considerably. The torque variation is of particular importance when using synchronous operation. Figure 4 illustrates the total torque as a function of blade position. Note that at a tip speed ratio of 3, there is no longer a near-uniform torque. When using synchronous operation, low tip speed ratios occur at high wind speeds. The character of the stall has a large effect on the torque variation also.

   Figure 5 illustrates the torque history for one blade of the rotor described in Figure 4. Again it may be noted that both the tip speed ratios and the character of the stall have a large effect on the predicted torque history.

5. The starting characteristics of the Darrieus Rotor are a strong function of the high-angle-of-attack aerodynamics.

RECOMMENDATIONS FOR FUTURE WORK

The status of current knowledge concerning the aerodynamics of the Darrieus Rotor suggests further experimental and analytical work.

1. Wind tunnel tests of the Darrieus Rotor should obtain data on the side force and the wake. The side force data is of importance in relation to blade alignment, lead-lag of the lift and to determine whether the wake is being confined by the tunnel walls. Wind tunnel corrections for side force are not currently being used in the process of data reduction. The wake should be traversed to determine if the induced velocities correspond to the predicted wake velocities. The wake measurements are of paramount importance in the establishment of any theory for the Darrieus Rotor.
2. Analytical work on the Darrieus Rotor should develop a better flow model to determine the performance limits and to predict the loads due to wake/blade interaction. The work during 1976 at Oregon State University on the Darrieus Rotor will be directed to this last recommendation. Dr. P.B.S. Lissaman and Dr. W. R. Sears will spearhead the investigation of Darrieus Rotor aerodynamics.

This investigation was supported by NSF Grant AER 74-04014 A03.

REFERENCES

1. Wilson, R. E. and Lissaman, Peter B. S., "Applied Aerodynamics of Wind Powered Machines," Oregon State University, May 1974.

2. Templin, R. J., "Aerodynamic Performance Theory for the NRC Vertical-Axis Wind Turbine," National Research Council of Canada, LTR-LA-160, June 1974.

3. James, E. C., "Unsteady Aerodynamics of Variable Pitch Vertical Axis Windmill," AIAA Paper No. 75-649, AIAA/AAS Solar Energy for Earth Conference, Los Angeles, CA, April 21-24, 1975.

4. Muraca, Ralph J., Stephen, S., Maria, V., and Dagenhart, Ray J., "Theoretical Performance of Vertical Axis Windmills," NASA-Langley Research Center, NASA TM TMX-72662, May 1975.

5. Shankar, P. N., "On the Aerodynamic Performance of a Class of Vertical Axis Windmills," National Aeronautical Laboratory, Bangalore TM AE-TM-13-75, July 1975.

6. Strickland, J. H., "The Darrieus Turbine: A Performance Prediction Model Using Multiple Streamtubes," Advanced Energy Projects Department, Sandia Laboratory, SAND 75-0431, October 1975.

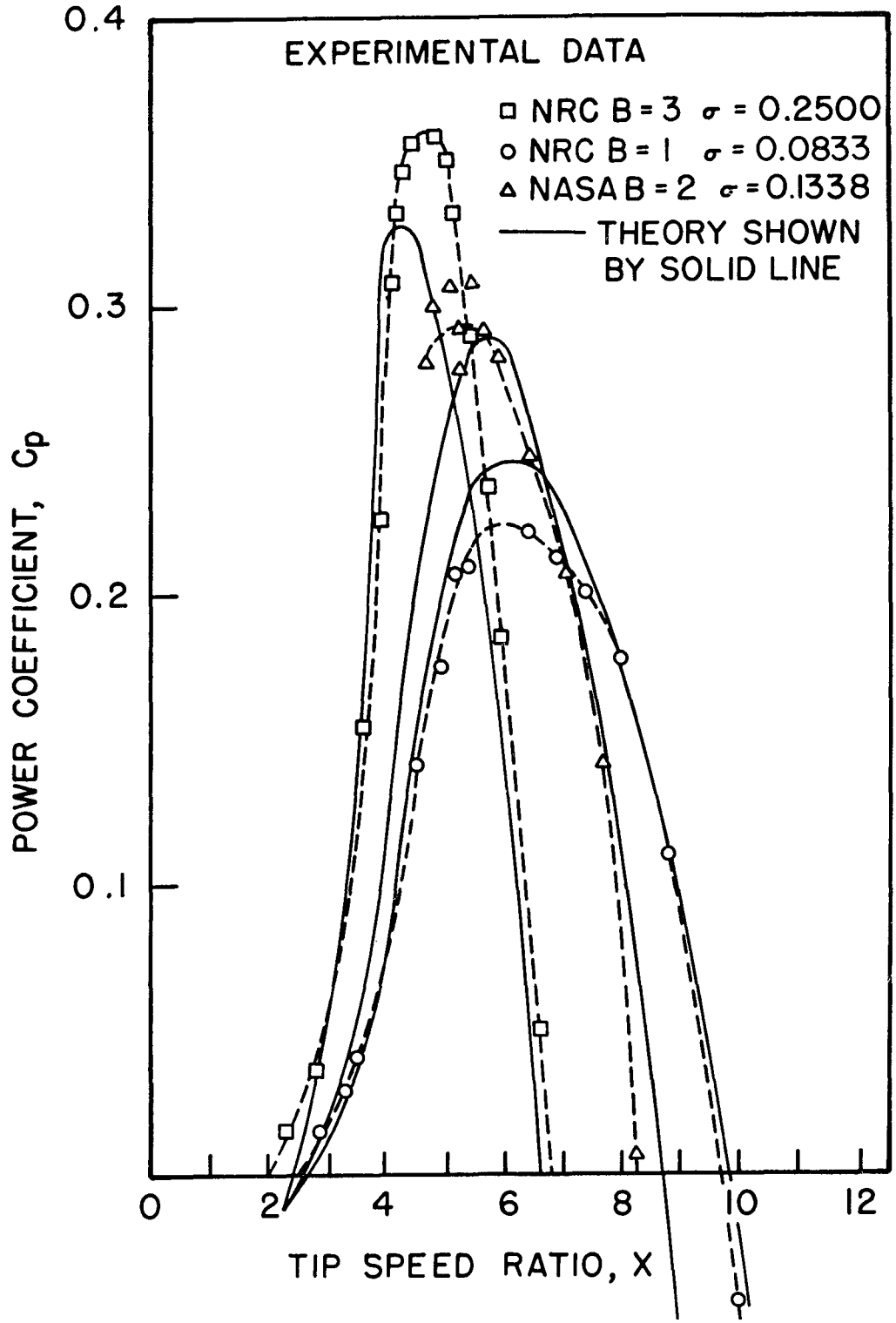

Figure 1. Comparison of Analytical and Measured Power Coefficients for Darrieus Rotors.

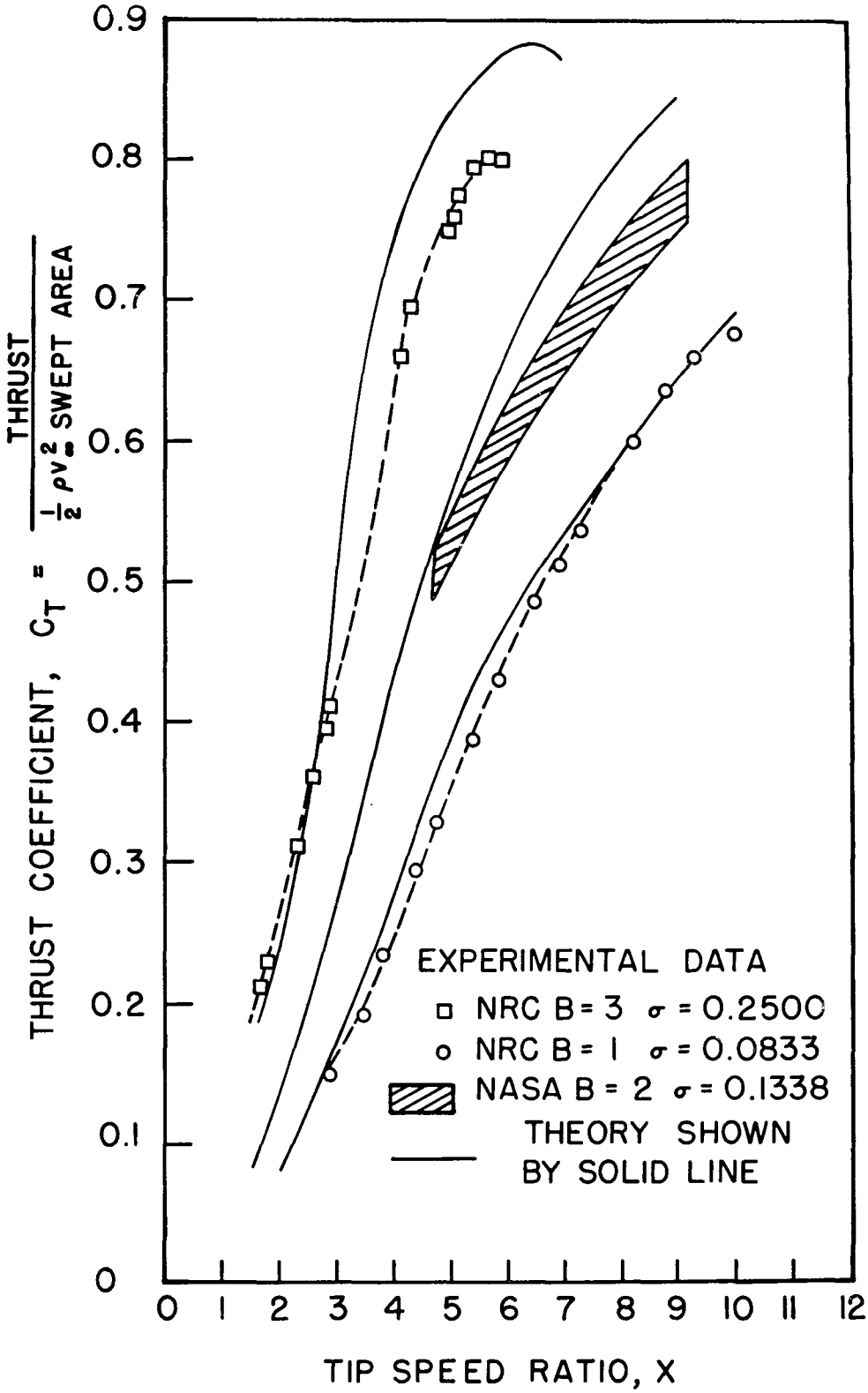

Figure 2. Comparison of Analytical and Measured Force Coefficients for Darrieus Rotors.

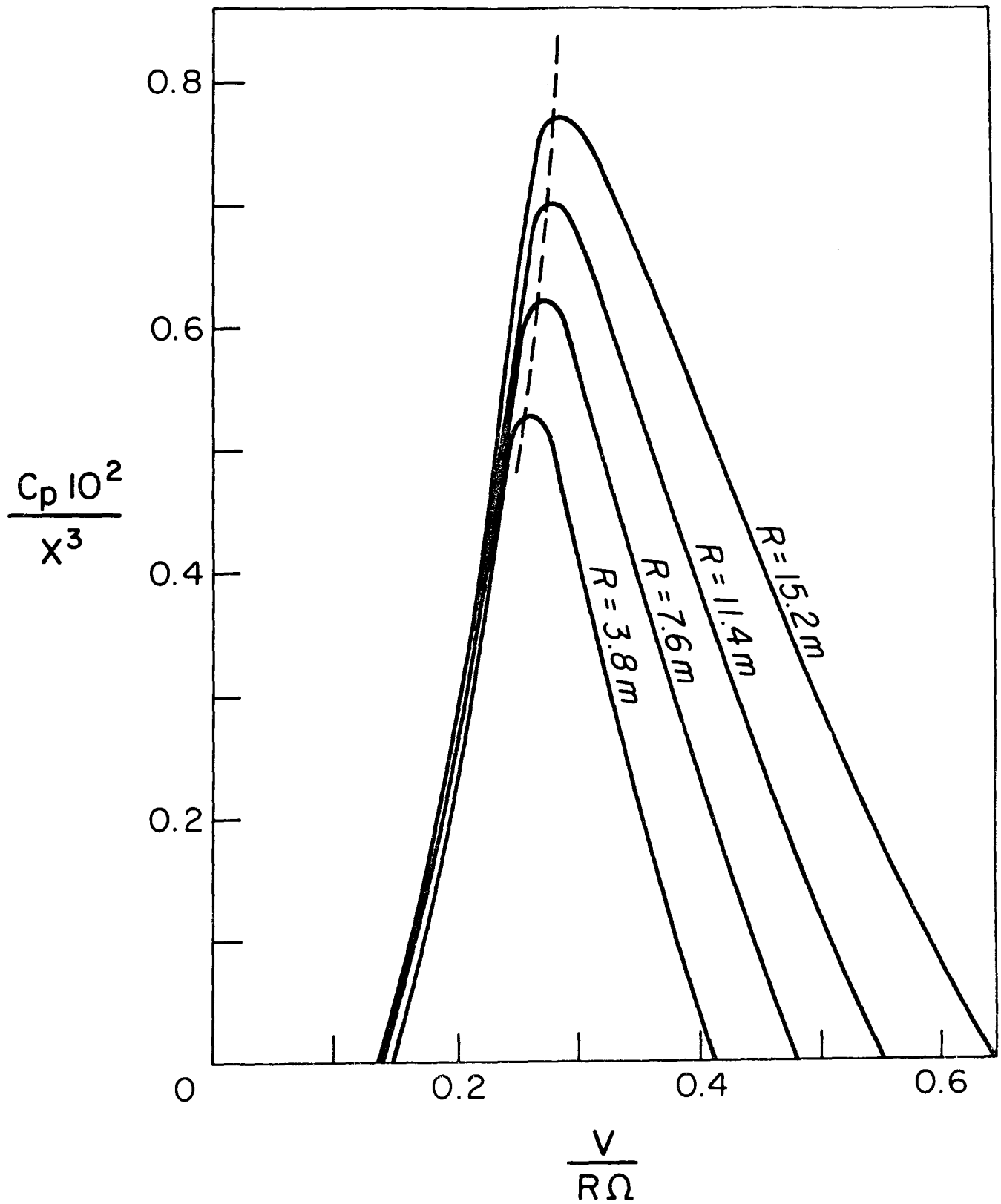

Figure 3. Dimensionless Power Output of a Family of 3-Bladed Darrieus Rotors. $Bc/R_{max} = 0.25$

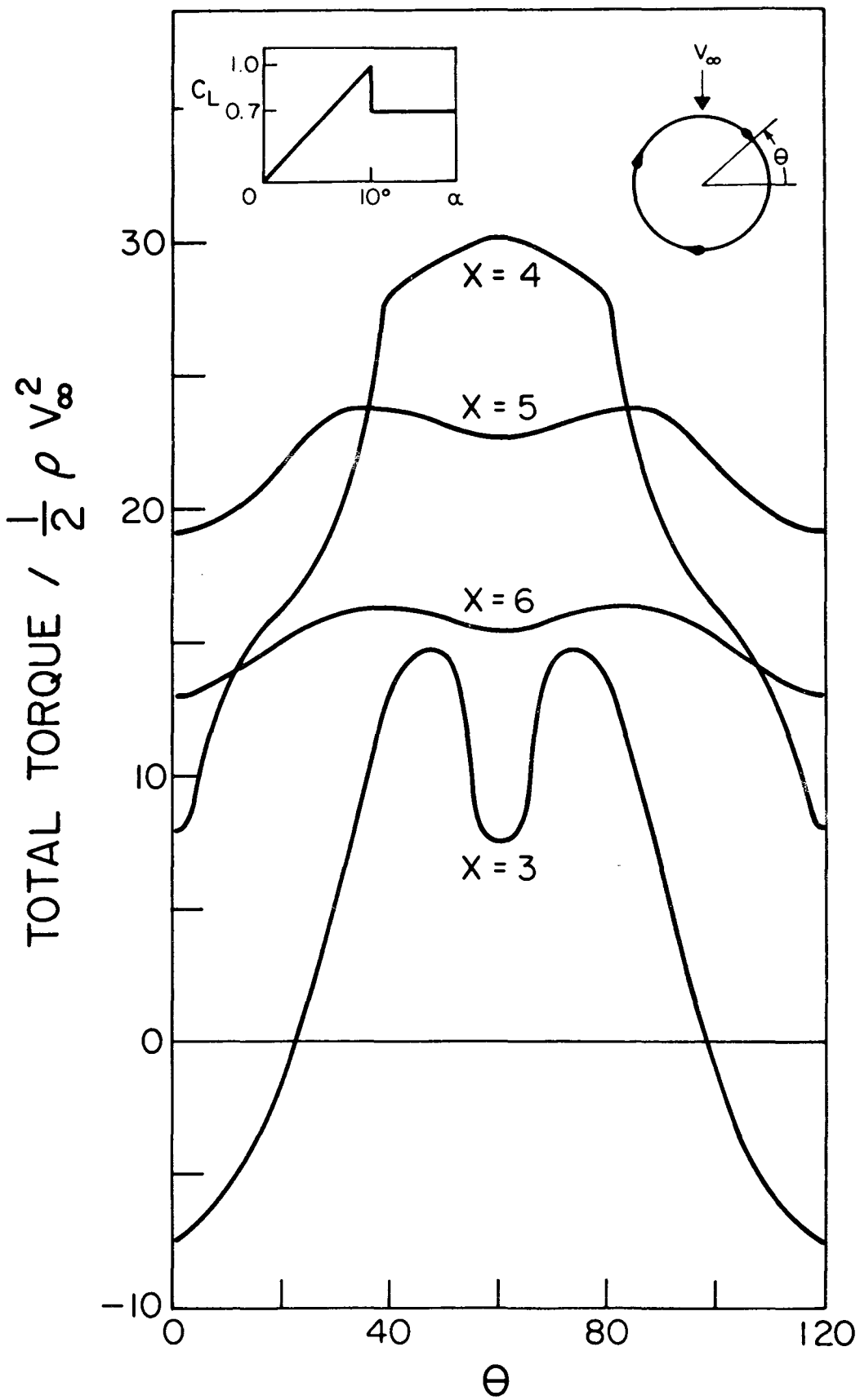

Figure 4. Rotor Torque Vs Blade Position for a 3-Bladed Rotor at Various Tip Speed Ratios. R_{max} = 15 feet, Chord = 1 foot.

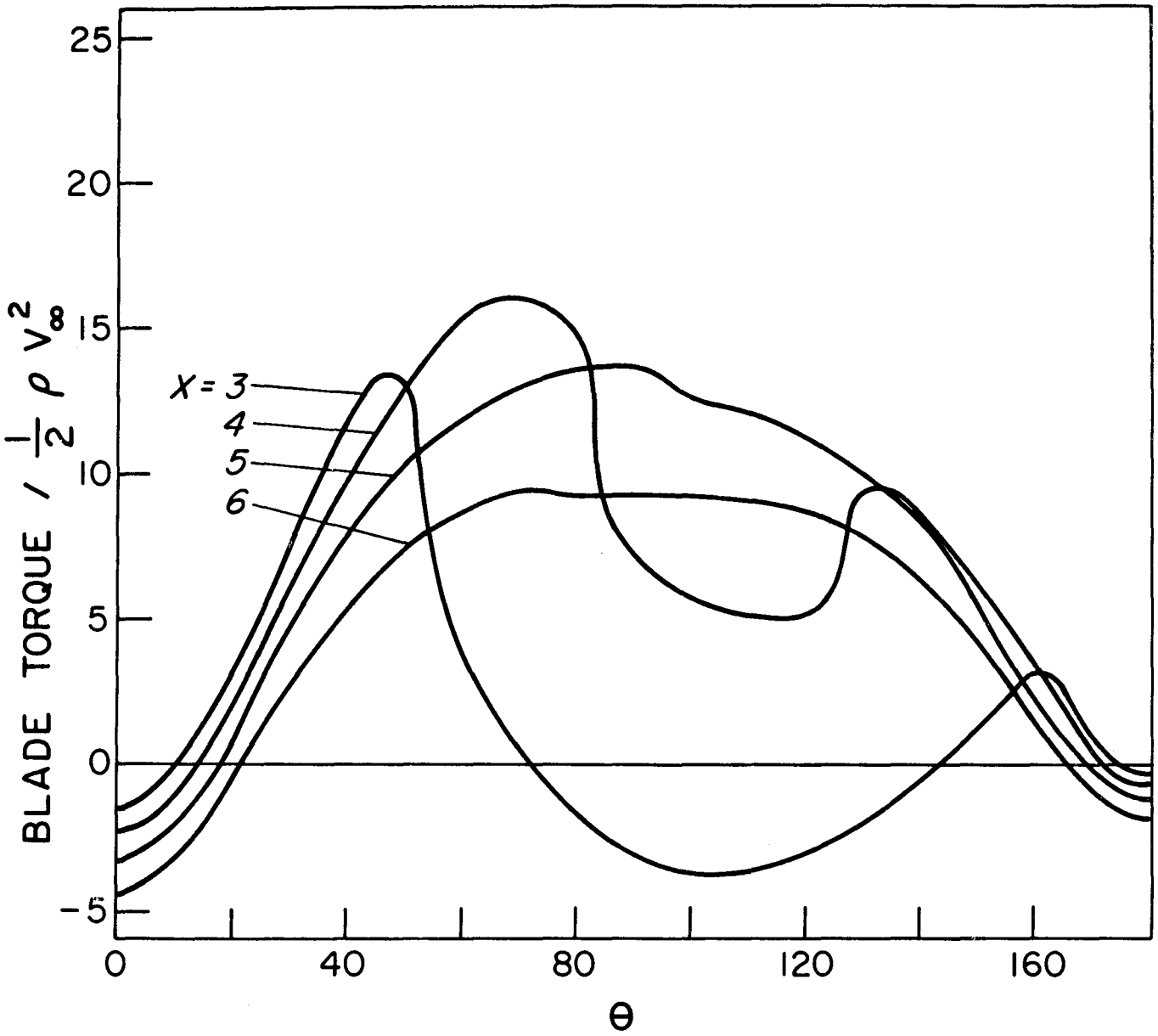

Figure 5. Blade Torque Vs Blade Position for a 3-Bladed Rotor at Various Tip Speed Ratios. R_{max} = 15 feet, Chord = 1 foot.

DARRIEUS STRUCTURAL STUDIES

AT

OREGON STATE UNIVERSITY

Robert W. Thresher
Associate Professor of Mechanical Engineering

and

Edward E. Meyer
National Science Foundation Energy Trainee

PAST STUDIES

The primary objective of the past studies was to examine the performance, operating and structural characteristics of the Darrieus Rotor. This work was a portion of the "Wind Energy Mission Analysis" performed by Lockheed California Company for The Energy Research and Development Administration. Detailed design considerations were not to be undertaken, nor were they feasible in the time allotted for this work. The basic machine configuration considered during these studies was a three-bladed, troposkien-shaped rotor with an NACA 0012 airfoil profile. With this configuration, various elementary structural models were developed to examine the machine behavior under static loading. While these models may not have included all of the physical parameters, it was felt that they did contain the key parameters.

The steady state structural analysis was composed of several individual studies of the various machine components. The studies involved were:

1) Centrifugal blade tension loading.

2) Blade lead-lag bending and torsion stress and deformation.

3) Center column stability.

The following presents a brief description of these various individual studies. A detailed presentation of the work is given in reference [1].

The Blade Structural Properties. Figure 1 gives a summary of the idealized structural properties used for the NACA 0012 airfoil. The skin thickness behind the quarter chord location was selected to be 1/9 the forward skin thickness in order that the center of gravity of the section would be at the quarter chord location. The actual skin thickness could be different if a structural spar is used to carry some of the loading. The aerodynamic studies indicated that an optimum chord, c, which maximized the power coefficient was $c_{opt} = R_{max}/12$; therefore, this was used to define the blade chord. The numerical coefficients for the section inertia properties were determined graphically to arrive at the general relationships shown in Figure 1.

Aerodynamic Forces. The aerodynamic forces are a function of angular position, ϕ, along the length of the blade and a function of angular position, θ , in the blade's circle of revolution. The aerodynamic model developed by Wilson [1] was used to predict these forces and showed fluctuating stall conditions superposed on cyclically varying loads. To compute maximum stresses and deflection, a "worst case" torque producing force was approximated with the function

$$w_t = (\rho_{air} V_w^2 r_{max} \sin\phi) /20 \qquad (1)$$

where w_t is the distributed force along the blade causing rotation; ρ_{air} is the mass density of air and r_{max} is the maximum machine radius.

Deformation Based Design. To obtain a simple deformation model, the following assumptions were made:

1) The blade was assumed to be circular in shape.

2) The direct tension deformation due to the centrifugal loading was assumed to be negligible.

3) The aerodynamic load was that given in equation (1).

4) The allowable blade twist at the center of the rotor was one degree.

5) Centrifugal stiffening effects were neglected.

In essence, the deformation calculated was based only upon the bending and torsion caused by the aerodynamic loads. The twist angle and deflection at the rotor center were computed by a direct application of Castigliano's theorem.

Figure 2 shows the required skin thickness, t, over the forward position of the airfoil section. For the allowable one degree blade twist, the resulting blade tip deflection, about 0.075 m for a machine radius of 10 m, increases linearly with maximum radius.

Other Considerations. A simple stress based design was also developed using simplifying assumptions similar to the above. The results indicate that the skin thickness could be about one half the value required for the deformation based design.

The center column of the Darrieus wind machine is a spinning vertical column which carries the compression load, induced by the rotor blade tension, and a fraction of the output torque. A standard stability analysis shows that the center column presents no unusual design constraints; however, for some situations, the column can amount to a significant proportion of the total machine structural weight.

The direct tension stresses had been considered in detail by Feltz and Blackwell [2] and their results were used directly when required.

An Overview of the Past Studies. These structural studies could be classified as strength of materials design estimates and are best described as "quick and dirty" in the vernacular of the practicing engineer. However, they do provide some insight into potential problem areas for future investigations; these areas are as follows:

1) The cyclic nature of the loading and the fluctuating stall necessitates that future studies include some dynamic effects.
2) The centrifugal forces, which were neglected in portions of the previous studies, should be examined more closely.
3) The aerodynamic force model should be combined, in some fashion, with the structural response in order to predict steady state response.

The most important result of these studies was to show the nature of the coupling between the structural deformations and the aerodynamic forces. A lead-lag deformation changes the blade angle of attack and directly influences the rotor forces, even when the deformations take place quasi-statically.

CURRENT RESEARCH EFFORT

The object of the current research effort is to investigate the static and dynamic response of the Darrieus Rotor using a more realistic model based on a rigorous analytical formulation. Simplifying assumptions are still necessary to achieve a practical solution; however, they will be applied in a more systematic fashion than was possible during the previous study. At this time, the formulation is still being developed, but the following discussion will outline current progress of the work and describe the expected results.

To accomplish the above objective, the following tasks are being accomplished:

1) Formulation of blade kinematics.

2) Formulation of blade strain energy.

3) Formulation of blade potential and kinetic energy .

4) Development of an aerodynamic force model.

5) Development of the blade governing equations.

6) Solution of various problems of practical importance such as: blade deformation under static and quasi-static loading, rotor blade steady state response and blade stability boundaries.

The work has rapidly progressed to tasks 3) and 4), which are the focus of current attention. The following paragraphs will review these accomplishments.

Rotor Blade Kinematics. The development of the blade deformation geometry will be based on the "Bernoulli-Euler" theorem, blade curvature is proportional to bending moment, and Saint-Venant torsion, blade twist per unit length is proportional to applied torque. This is the conventional strength of materials approach and allows the kinematics to be formulated by considering only the deformation of the blade's elastic axis. With these ideas in mind, the blade's elastic axis is defined to be the locus of points described by the position vector

$$\vec{R} = \vec{R}(s) \quad \text{for} \quad 0 \leq s \leq L \tag{2}$$

where L is the blade length. Similarly, the blade's elastic axis undergoing an arbitrary deformation is given by

$$\vec{R}^*(s) = \vec{R}(s) + \vec{V}(s) \tag{3}$$

where the "*" implies vectors in the deformed system and $\vec{V}$ is the blade deformation vector. The deformation, $\vec{V}$, can be written as

$$\vec{V}(s) = u(s)\ \vec{t} + v(s)\vec{n} + w(s)\ \vec{b}$$

where $\vec{t}$, $\vec{n}$ and $\vec{b}$ are three mutually perpendicular unit vectors defining the basis of the deformation. These unit vectors are defined as follows:

$$\begin{aligned} \vec{t} &= \text{the unit tangent} = \frac{\partial \vec{R}}{\partial s} = \vec{R}_s \\ \vec{n} &= \text{the unit normal} = \vec{t}_s/|\vec{t}_s| = \vec{t}_s/k \\ \vec{b} &= \text{the unit binormal} = \vec{t} \times \vec{n} \end{aligned} \tag{4}$$

In addition, it is convenient to define the blade curvature and radius of curvature as

$$\vec{K} = k\vec{n} = (1/\rho)\vec{n} = \text{the blade curvature} \tag{5}$$

where the radius of curvature, ρ, is given by

$$\rho = 1/k = 1/|t_s| \tag{6}$$

For the blade's deformed elastic axis, there is a similar set of unit vectors defined by

$$\begin{aligned} \vec{t}^* &= \vec{R}^*_s = \vec{R}_s + \vec{V}_s = \vec{t} + \vec{V}_s \\ \vec{n}^* &= \vec{R}^*_{ss}/k^* = (k\vec{n} + \vec{V}_{ss})/k^* \\ \vec{b}^* &= \vec{t}^* \times \vec{n}^* \end{aligned} \tag{7}$$

The geometry considered is illustrated in Figure 3.

Bending Deformation and Strain. Figure 4 shows a typical blade element undergoing a bending deformation. Using this figure, it can be seen that a line element of the blade, located by a position vector, $\vec{P}$, undergoes a tangential bending strain given by the expression

$$\varepsilon_t = \frac{\vec{P}\cdot\vec{n} - \vec{P}^*\cdot\vec{n}^* \ (\rho/\rho^*)}{\rho - \vec{P}\cdot\vec{n}} \tag{8}$$

which for small initial curvature, k, can be approximated with

$$\varepsilon_t \approx k\ \vec{P}\cdot\vec{n} - k^*\ \vec{P}^*\cdot\vec{n}^* \tag{9}$$

Now computing the derivatives of the displacement vector, $\vec{V}$, one obtains

$$\vec{V}_{ss} = kf_1\vec{t} + kf_2\vec{n} + kf_3\vec{b} \tag{10}$$

where

$$f_1 = v_{ss}/k + 2u_s + k_s u/k - kv$$
$$f_2 = u_{ss}/k + 2v_s - k_s v/k - ku$$
$$f_3 = w_{ss}/k$$

Computing the curvature in the deformed geometry by taking

$$k^* = (\vec{K}^*\cdot\vec{K}^*)^{1/2} = [\vec{K}\cdot\vec{K} + 2\vec{K}\cdot\vec{V}_{ss} + \vec{V}_{ss}\cdot\vec{V}_{ss}]^{1/2} \tag{11}$$

gives

$$k^* = k(1 + 2f_2 + f_1^{\ 2} + f_2^{\ 2} + f_3^{\ 2})^{1/2} \tag{12}$$

Let the coordinates (ξ_1, ξ_2, ξ_3) be fixed to the blade cross-section and initially coincident with $\vec{t}$, $\vec{n}$ and $\vec{b}$ as shown in Figure 5. Defining β as the angle between ξ_2 and $\vec{P}$, and letting θ be the angle between ξ_2 and $\vec{n}^*$, the tangential strain can be written as

$$\varepsilon_t = k|\vec{P}|\ [\cos\beta - \cos(\beta + \theta)\ k^*/k] \tag{13}$$

Bending Energy. The bending strain energy per unit blade length is computed from

$$U_b = \frac{E}{2} \int_A \varepsilon_t^{\,2}\, dA \tag{14}$$

Substitution of the previous expressions into this equation gives, for a symmetric airfoil

$$\begin{aligned} 2U_b/EI_2k^2 = {} & (1 - 2\cos\theta + \cos^2\theta + I\sin^2\theta) \\ & + 2(\cos^2\theta + I\sin^2\theta - \cos\theta)f_2 \\ & + (\cos^2\theta + I\sin^2\theta - \cos\theta)f_1^{\,2} \\ & + (\cos^2\theta + I\sin^2\theta)f_2^{\,2} \\ & + (\cos^2\theta + I\sin^2\theta - \cos\theta)f_3^{\,2} \end{aligned} \tag{15}$$

where I_2 and I_3 are the blade moments of inertia and $I = I_3/I_2$. In addition, the expression for k^*/k was expanded in a binomial series retaining only quadratic terms.

The Blade Twist Deformation. Referring to Figure 6, the rate of twist of the blade, α, can be seen to be given by

$$\alpha(s) = \theta_s(s) + \tau^*(s) \tag{16}$$

and

$$\tau^*(s) = \vec{n}^*_s \cdot \vec{b}^* \tag{17}$$

Again retaining only up to quadratic terms in the analysis, after considerable algebra, one can obtain

$$\tau^* = kw_s + (w_{ss}/k)_s \tag{18}$$

The torsional strain energy per unit blade length is then found from

$$U_t = \frac{JG}{2} \alpha^2 = \frac{JG}{2} (\theta_s + kw_s + (w_{ss}/k)_s)^2 \tag{19}$$

Displacement Constraint. If it is to be assumed that the elastic axis does not change length during deformation, then the following constraint must be applied in order to obtain consistent deformations: differential length along the elastic axis must be identical in both the undeformed and deformed states; thus

$$(ds)^2 = (ds^*)^2 \tag{20}$$

which leads to the requirement that

$$(1 + u_s - kv)^2 + (v_s + ku)^2 + w_s^2 - 1 = 0$$

A more complete development of these results will be available in reference [3].

Current Status. At this time, the blade kinetic energy is being formulated; this work is proceeding in a manner similar to the results presented here. One of the key problem areas appears to be the formulation of the aerodynamic forces which must be accomplished in a realistic manner, yet not make the solution technique impossibly difficult. The aerodynamic formulations which have been developed, using the multiple stream tube approach, all require iteration techniques and look impractical for coupling with the structural behavior. Several alternate approximate techniques are being considered for further investigation, but it is senseless to speculate on their usefulness at this time. In considering various approaches, it would be useful to have additional data on what is felt to be the problem of highest priority such as:

1) Low tip speed operation.

2) High tip speed operation.

3) Blade stress analysis.

4) Blade dynamic response.

5) Gravitational effects.

6) Blade dynamic stability.

In addition, experimental data from any type of operational system would help to validate the various models which will be developed.

ACKNOWLEDGMENTS

Portions of this work were supported through Lockheed California Company as part of the "Wind Energy Mission Analysis" for The Energy Research and Development Administration under Contract AT(04-3)-1075 and by the Oregon People's Utility Districts Directors' Association with Oregon State University. In addition, Mr. Edward E. Meyer, who is currently developing the formulation, is funded under a National Science Foundation Energy Traineeship.

REFERENCE

1. Thresher, R. W. and Wilson, R. E., "Characteristics of the Vertical Axis Wind Machine," appendix to the Wind Energy Mission Analysis, Lockheed California Company, ERDA Contract AT(04-3)-1075, May 1975.

2. Feltz, L. V. and Blackwell, B. F., An Investigation of Rotation-Induced Stresses of Straight and Curved Vertical-Axis Wind Turbine Blades, SAND74-0379, Sandia Laboratories, Albuquerque, N.M., July 1974.

3. Meyer, Edward E., Dynamics of the Darrieus Vertical Axis Wind Machine, Ph.D. Thesis, Oregon State University, to be completed June 1977.

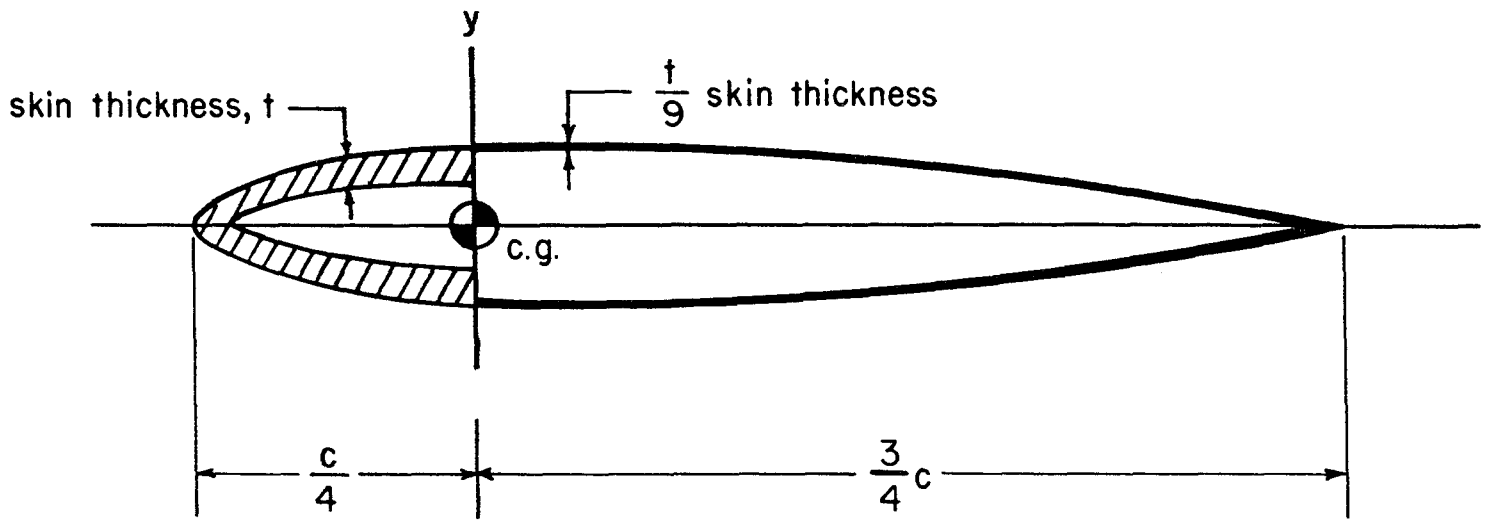

$c_{optimum} \doteq \frac{a}{12} = \frac{r_{max}}{12}$ (Blade Chord)

$I_{xx} \doteq 8.74 \times 10^{-7}\, tr^3$

$I_{yy} \doteq 2.41 \times 10^{-5}\, tr^3$

$C_t \doteq 1.1 \times 10^{-6}\, tr^3$ (Torsional Stiffness)

$A \doteq 0.058\, tr$ (Area)

$A_e \doteq 5.67 \times 10^{-4}\, r^2$ (Enclosed Area)

$W \doteq 1.3 \rho A$ (1.3 factor to cover weight of spars and miscellaneous fasteners)

FIGURE I. BLADE STRUCTURAL PROPERTIES

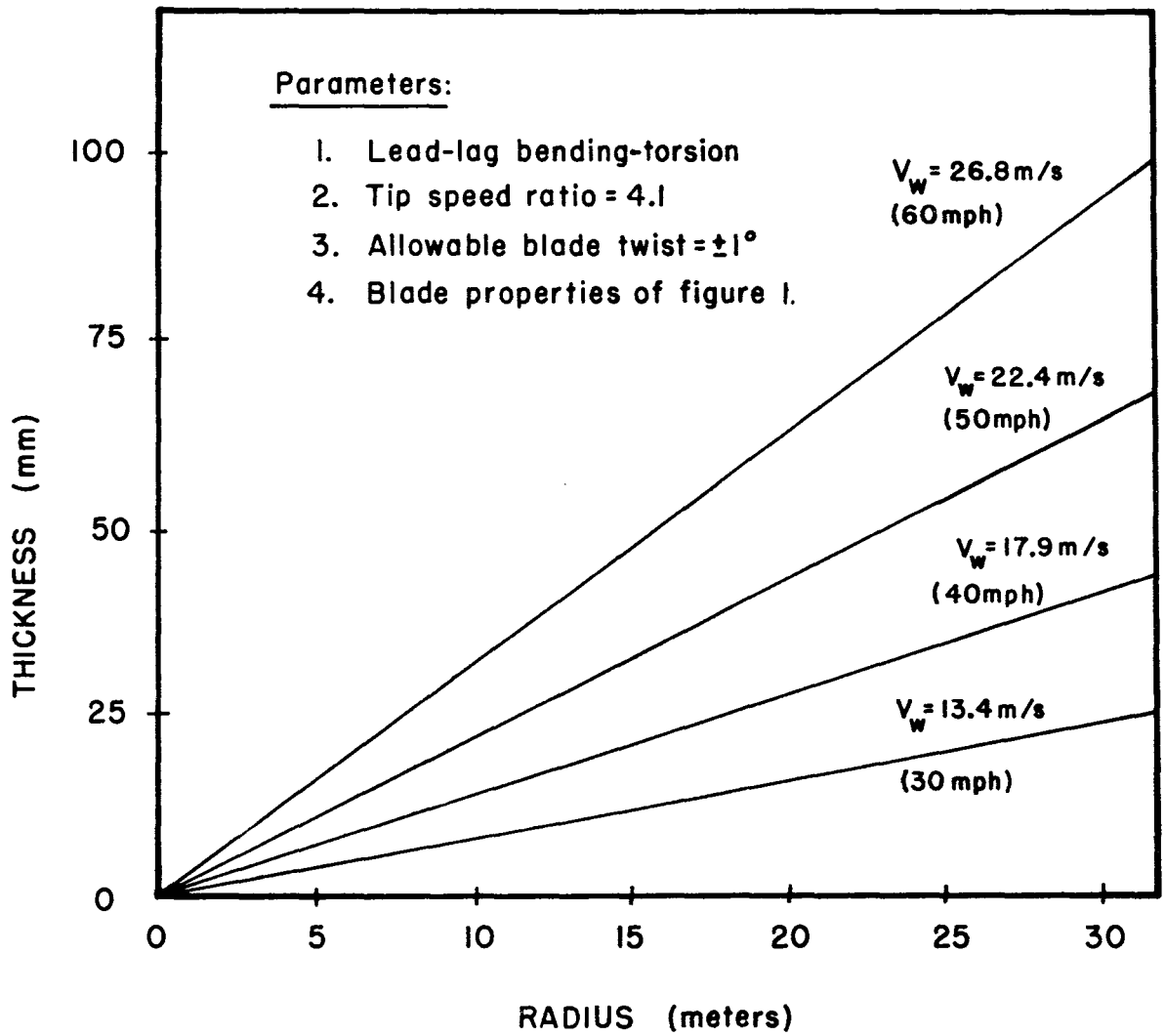

FIGURE 2. REQUIRED SKIN THICKNESS

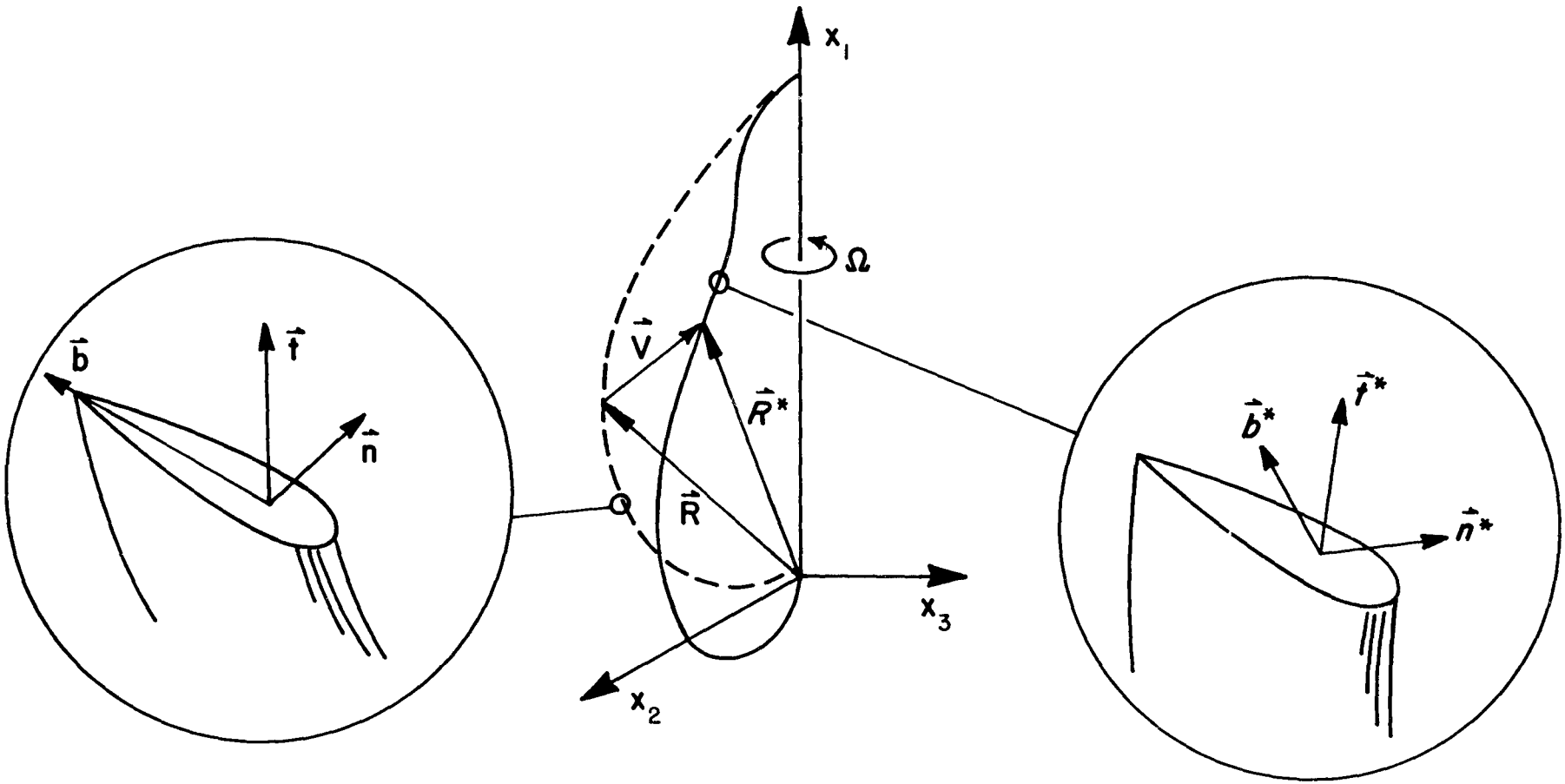

FIGURE 3. ROTOR DEFORMATION GEOMETRY

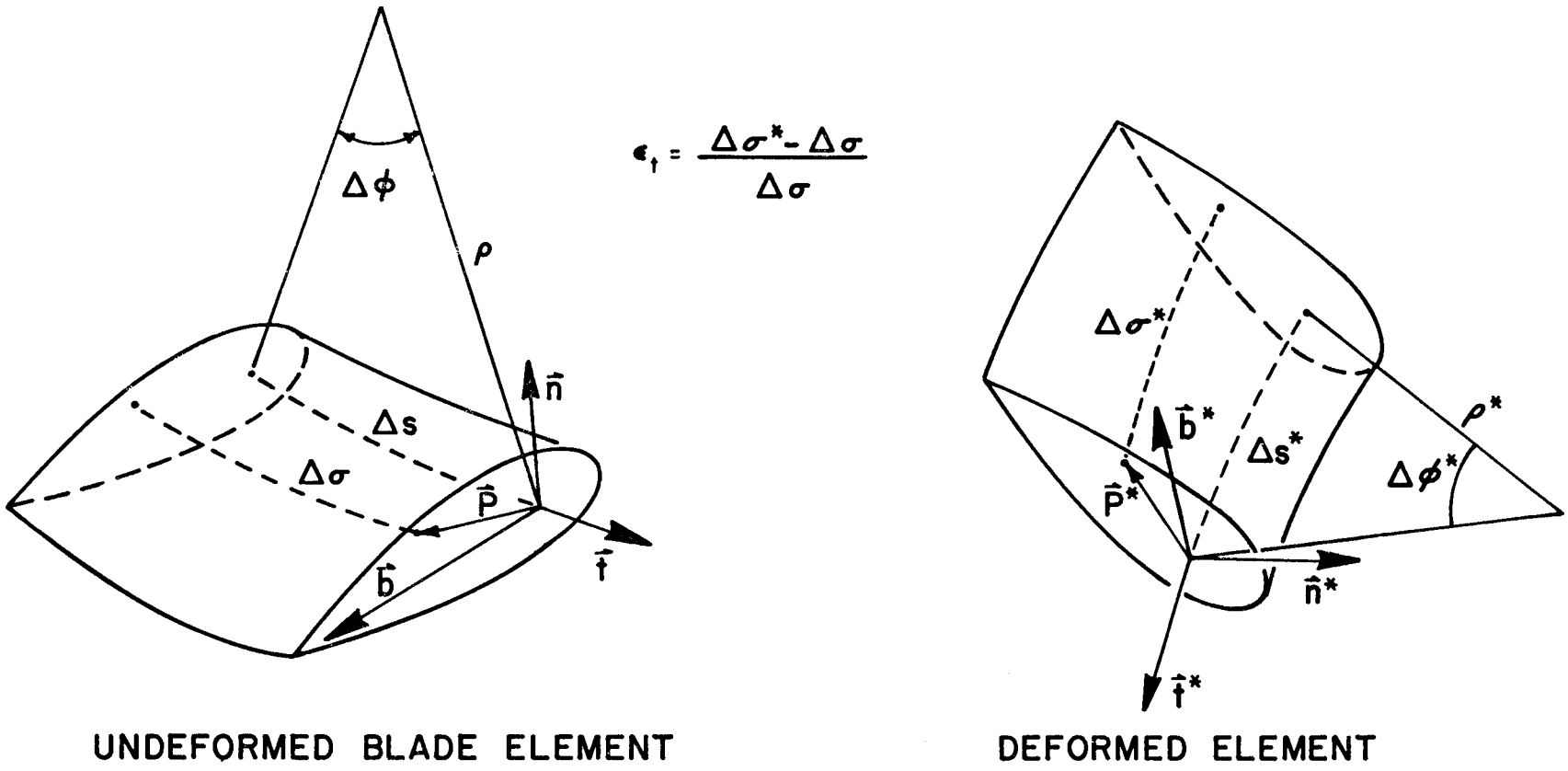

FIGURE 4. BLADE ELEMENT TANGENTIAL STRAIN

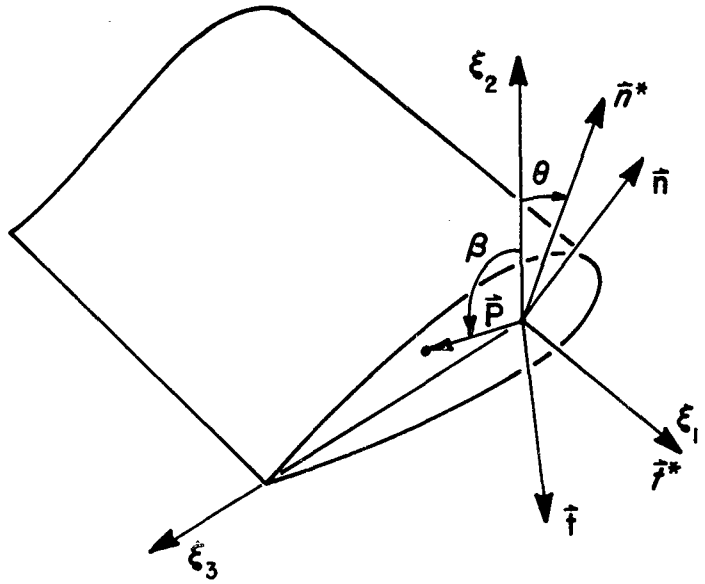

FIGURE 5. THE BLADE-FIXED COORDINATES

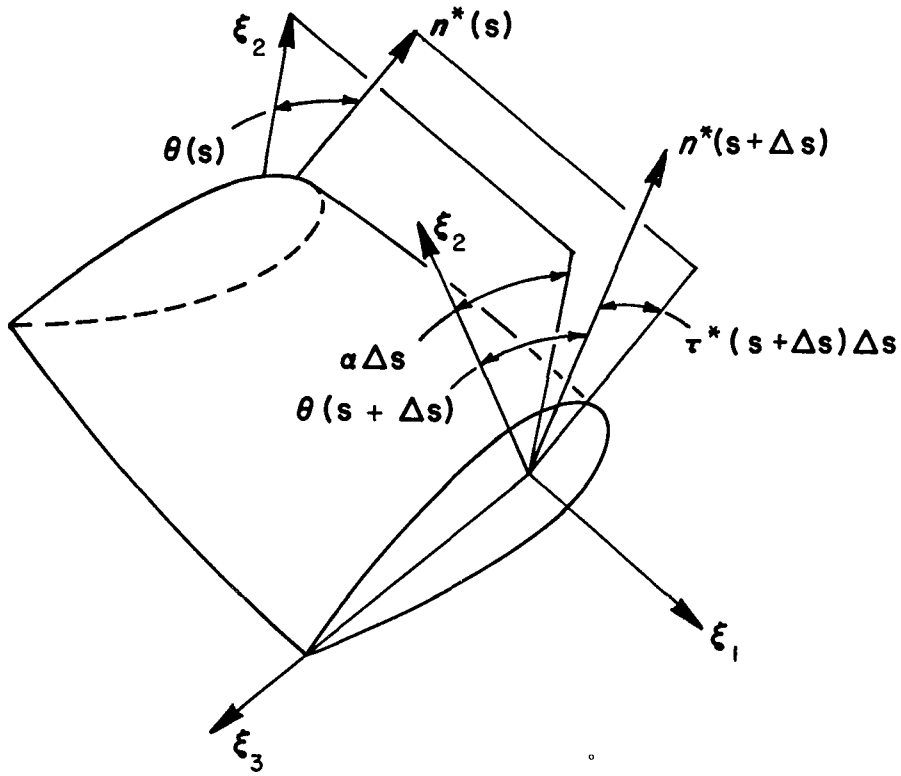

FIGURE 6. BLADE TWIST DEFORMATION

Question: THRESHER

With regard to the blade support tower, you only mentioned stability. What do you feel will control tower design? Also, what are your blade boundary conditons - do you plan to characterize tower compliance (i.e. tower-blade coupling)?

Bob Renter
Sandia

Reply: Our work on the tower design only considered the stability of a flexible spinning column. We found that it was relatively easy to select a column which would carry the loading; however, under certain conditions, it did become relatively heavy. At one point in our studies, we considered examining the column natural frequency as a function of axial loading, but we simply ran out of time and money. I agree with the Sandia conclusion that column stiffness, due to dynamic considerations, will dominate the design.

The current studies could account for tower compliance by introducing springs at the blade attachment points; our model does not include these srpings at this stage of development.

Question: THRESHER

Can you look at the effect of struts in your future analytical studies? If so, could you tell us how you would do it?

Larry Weingarten
Sandia

Reply: The blade model, as currently formulated, does not include struts; however, they could be added to the model as linear springs attached at appropriate locations. More realistic models are also possible, but somewhat more complicated.

COMMERCIAL VERTICAL AXIS WIND TURBINES

L. H. J. Maile

Dominion Aluminum Fabricating Limited
Mississauga, Ontario, Canada

Dominion Aluminum Fabricating is a relatively small engineering and manufacturing company with annual sales in the order of four million dollars. However we are part of a group of about thirty companies with annual sales in excess of $100 million dollars forming Indal Canada Limited. This group is Canada's largest independent producer of aluminum extrusions and a leading secondary manufacturer of aluminum products. The Indal Group was founded in 1964 by Pillar Limited, now RTZ Europe Limited of London, England.

This paper summarizes our activities with vertical axis wind turbines (VAWT) over the past two and a half years, describes our commercially available, "off the shelf" wind turbines and gives a view of some production and design considerations.

Our work on VAWT commenced in January 1974 when we were invited, among others, to submit a proposal to the Canadian Government "To design, manufacture and supply" a quantity of 15ft diameter turbines to a general specification prepared by the National Research Council (NRC) in Ottawa. The D.A.F. proposal was selected from all the submissions received. (We had carried out intensive preliminary work before submitting the proposal). Subsequently six Vertical Axis Wind Turbines were delivered. These turbines have three blades of six inch chord, NACA 0012, with electrical output of one KW at 15 mph wind speed with controls for 24 volt battery charging applications.

It is appropriate to mention that studies by NRC on VAWT had commenced in 1966, eight years prior to our entry into the field.

I wish to acknowledge that brilliant work of Mr. Templin, Mr. South and Mr. Ranji; and also their continuing help and guidance to us, which has in no small way contributed to our understanding of this subject.

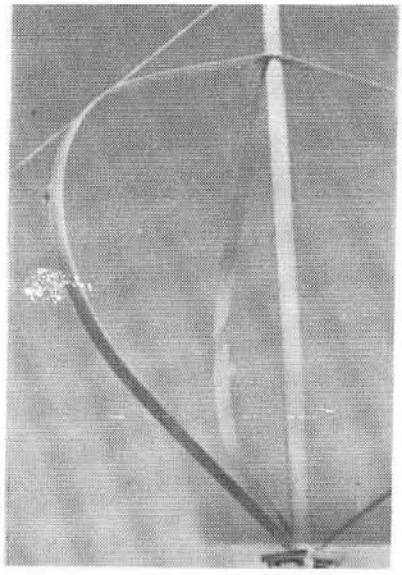

FIGURE 1

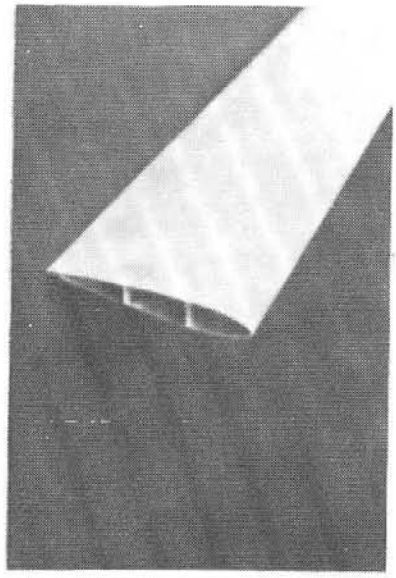

FIGURE 2

Figure 1 shows one of the turbines made for NRC. It was specified to incorporate a savonius rotor for starting purposes, however, DAF decided, with NRC concurrence, to use a permanent magnet motor for starting. This motor runs the turbine up to speed and its operational mode. With adequate wind speed the turbine then delivers power and the motor becomes a generator. With increase of wind speed the generator reaches its maximum output and is switched over to a commercial alternator. Speed limiting is acheived by means of spoiler tabs which can be seen at the equator of each blade. The central column is a single aluminum tube 18 feet high to which the upper end of each blade is attached at a point three feet below the top. The turbine, with bearings top and bottom, rests on an eight foot high tower and is connected via a chain drive to both the alternator and starting motor.

Figure 2 shows the 6 inch chord blade which was bent in our factory and fitted to the central column as a single piece.

After wind tunnel performance tests, the six turbines were sent to various parts of Canada for on-site testing.

One is on Hershel Island in the Arctic. One is in Regina, Saskatchewan for water-pumping evaluation. Another is erected near Ottawa for Defense Research purposes. Two others are in Winnipeg, Manitoba and Kingston Ontario and the final unit was sent to Saskatchewan Power Corporation for their use.

The rotors of these prototypes have stood up well under some extremely adverse conditions and are operating satisfactorily. The biggest problems are the small ones

- in our case the chain drive to the start motor was unsuitable and is being changed. Operating conditions have shown the need for firm foundations. For example a wooden grillage at Hershel Island designed locally, was unsuitable due to its flexibility.

Our view on the wind turbine program was to proceed with further research and development, and not confine ourselves solely to the design and delivery of the six turbines. This work continued in parallel to our design for the NRC contract.

In September 1974 we commenced a study of the feasibility of building a larger turbine in the 200-300 kilowatt size. The results of the study led to our submitting a proposal to the Canadian Government in December 1974, "To develop, design, manufacture and supply a 200 kilowatt Vertical Axis Wind Turbine".

This proposal was accepted when NRC agreed to fund the project. Further discussions with NRC led to an agreed rotor configuration of 120 ft. high by 80 ft. diameter with two 24 inch blades.

Quebec Hydro Commission were included in the project when they agreed to provide a site, erection and the electrical control capability to enable the generator to feed into their 13.2 KV grid system.

Work is well under way for a summer installation this year at the site on the Iles de la Madeleine in the Gulf of St. Lawrence, where wind speed gusts are expected to reach 130 mph.

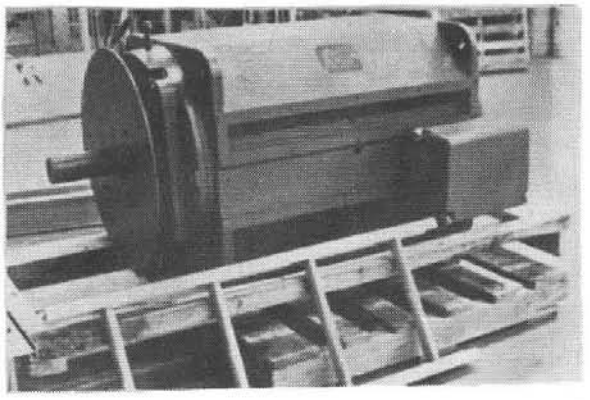

FIGURE 3

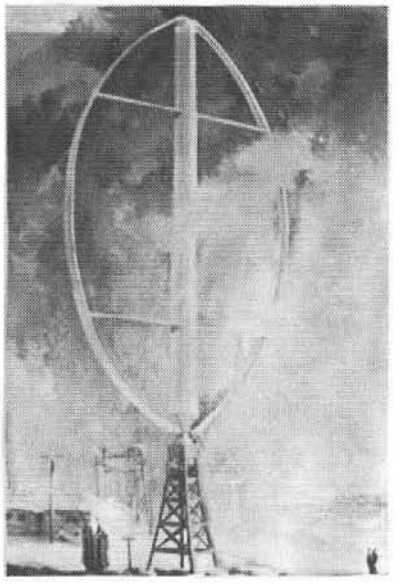

FIGURE 4

Figure 3 shows the squirrel cage induction generator which is a standard commercial item, 300 HP, 3 phase, 60 cycle, 575 volt, 720 rpm with efficiency 92½ percent.

Figure 4 is an artist's view of the turbine at its location on the island. The rotor is aluminum and the 30 ft high supporting tower is structural steel. Two struts support the blades which have overspeed protection spoilers located at their equator.

The turbine drives the generator through a standard gearbox. The electrics are basically simple with the generator delivering power to the grid system through a transformer and circuit breaker. Starting is acheived through an anemometer control, by the induction generator acting as a motor using a reduced voltage starter and capacitors to handle the power factor. The operation is equally simple, in that the power input to the generator will never exceed that required to break out of synchronization. Stopping is acheived by means of a disc brake for routine stops. For emergency conditions such as gearbox or drive shaft failure, where the existance of the power line is not available to limit the turbine speed, speed limiting and stopping is acheived by the operation of the spoilers on the blades. The setting of the spoilers is such that they automatically deploy at a few rpm above the normal operating speed.

Since we are commercially oriented, the turbine has been designed with a view to manufacturing quantities of them. Accordingly we are now prepared to supply similar turbines on a prototype bases with a six month delivery. As soon as we have confirmed expected turbine stress and performance levels at the Iles de la Madeleine site (hopefully by early 1976), we will offer it on the commercial market with the normal guarantees both for performance and life expectancy.

It should not be assumed that the electrical generator size of 200 KW will be the optimum for the 80ft. diameter wind turbine.

Figure 5 made from curves supplied by Mr. Templin of NRC shows the estimated annual yields of the 80ft. turbine at differing average wind speeds, of the type of distribution encountered in Ontario - similar to a Rayleigh distribution. It may be seen for example, that in average wind speeds of 14 mph, it would be advantageous to use a 150 KW generator due to a reduction in cost. Also of interest is the change of rotor speed from 41.5 rpm to about 38 rpm to acheive optimum energy yield. The 200 KW turbine at the Iles de la Madeleine site is expected to produce close to 600 megawatt hours annually.

As the wind turbines become larger they will generally tend to be applied to supplying power to electric grid

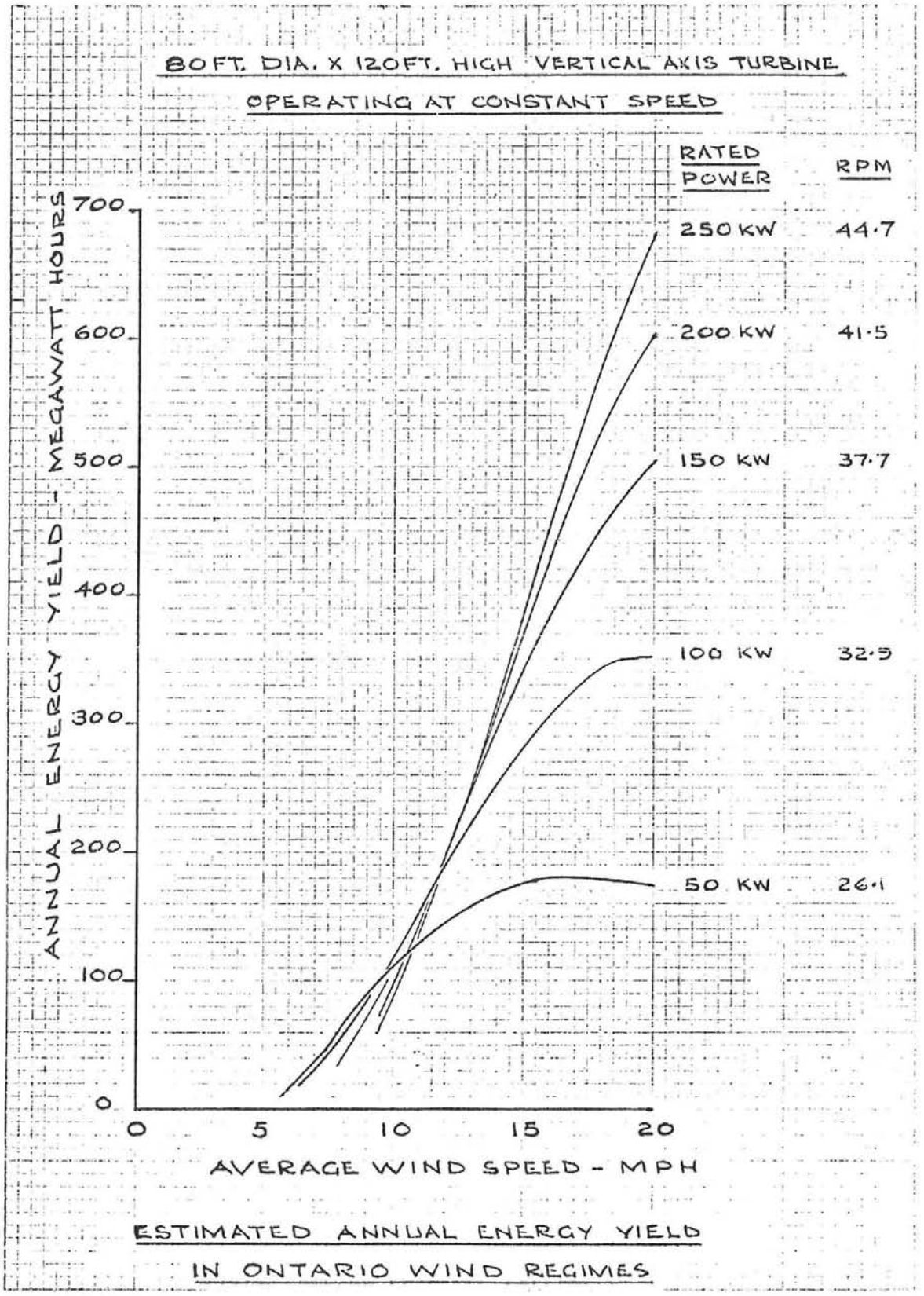
80 FT. DIA. X 120 FT. HIGH VERTICAL AXIS TURBINE
OPERATING AT CONSTANT SPEED
RATED POWER
RPM
250 KW 44·7
200 KW 41·5
150 KW 37·7
100 KW 32·5
50 KW 26·1
ANNUAL ENERGY YIELD - MEGAWATT HOURS
700
600
500
400
300
200
100
0
0
5
10
15
20
AVERAGE WIND SPEED - MPH
ESTIMATED ANNUAL ENERGY YIELD
IN ONTARIO WIND REGIMES

FIGURE 5

systems. But what of smaller wind turbines? Well, since these are likely to serve a variety of applications, and a different market, it is useful to consider them separately.

During the course of the design work for the 200 KW turbine, we designed and built a quarter-scale model 30 feet high and 20 ft. in diameter. This model was erected in the wind tunnel in Ottawa by NRC and monitored for stress levels by Peter South using strain gauges at appropriate points of interest. The stress data collected has been used in the design of the 200 KW turbine.

A computer model was also developed and has been found useful in contributing to our understanding of the rotor vibration modes.

Since the model size seemed to be the logical next incremental size up from the 15ft diameter unit, we took this opportunity to design a commercial turbine 30 ft. high by 20 ft. diameter. This is really a second generation design of the unit tested in the wind tunnel.

We had originally designed the 15 ft. diameter turbine with a view to simple and inexpensive turbine production, however we decided to carryout a complete redesign of the rotor and support tower. Our standard in this size is now 15 ft. diameter, 18 ft. high, with two blades rather than three. This is shown in figure 6.

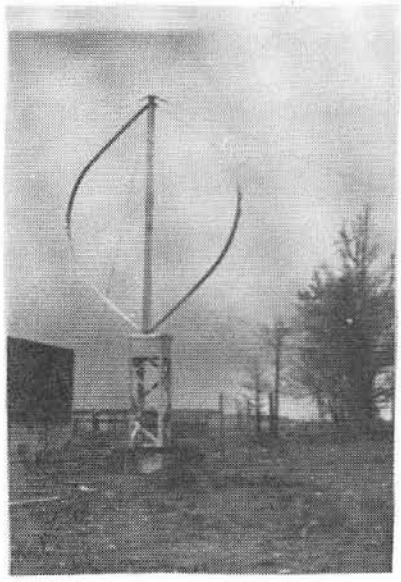

FIGURE 6

FIGURE 7

This 15 ft. turbine has a greater power output than the original design, is also less expensive and has a longer estimated life. Solidity (NC/R) is 0.133, with an electrical output of 4 KVA for resistance loads, and

3.1 KW (3.5 KW later this year) output for battery charging applications at rated wind speeds of 24 mph.

We have made many changes in the evolution of this present design both on the rotor and on the electrics and drive. For example we have used vee belt and timing belt drives, gearboxes and also chain drives at one stage or another. Since there is a serious problem with belt drives in arctic conditions, we had to discard them for these applications.

We have probably spent as much resources on research and development of electrics, as on the rest of the items of the unit put together. As a result we are now able to supply electrical systems for both the 15ft. and 20ft. turbines for three types of user load requirements. These units are now our "off the shelf" turbines.

Figure 7 shows the first commercially produced production turbine to be installed in the U.S.A. It is erected at the U.A.W. site in Onaway, Michigan on top of an existing 85 ft. high steel tower.

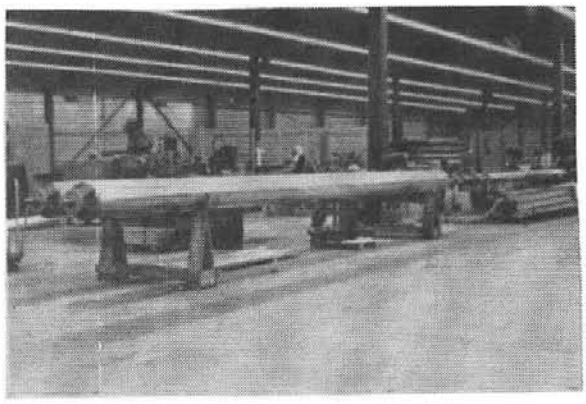

FIGURE 8

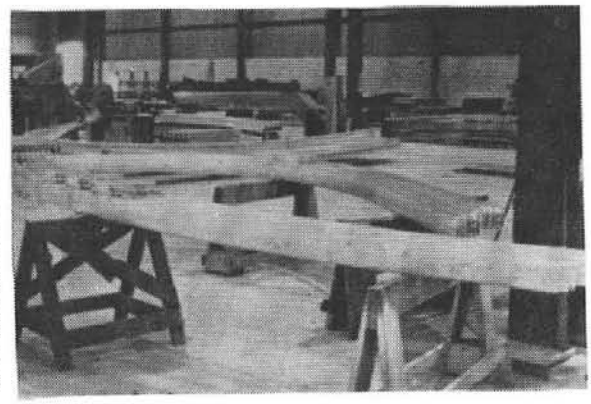

FIGURE 9

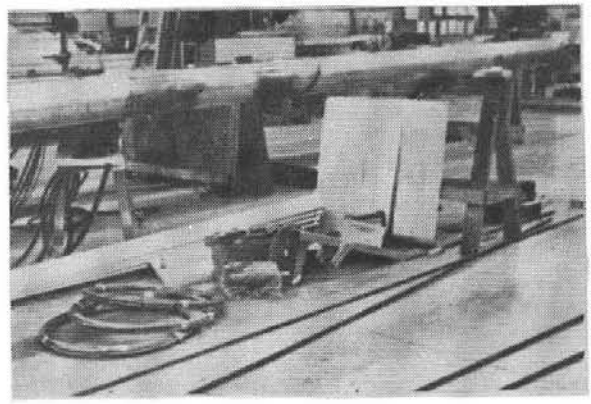

FIGURE 10

Figure 8 shows two of the 30 ft. long rotor columns on the shop floor just prior to shipment. At the rear can be seen a few stock columns for 15 ft. diameter rotors.

Figure 9 shows some rotor blades for both 15 ft. and 20 ft. units.

Figure 10 is a typical turbine in process of parts-assembly prior to packaging and shipment.

We recognize that it is most important to design the system to unit the user requirement and to tailor the unit to the application. The rotor size may not change but its mode of operation will.

Figure 11 illustrates this point, and shows annual energy yields for the 15 ft. diameter turbine. The rotor remains the same except perhaps for spoiler settings in the constant speed case, (60 cycle backfeed), but the electrics are different.

The chart shows typical energy yields for this turbine for windspeeds with a Rayliegh distribution. In actual practice,we would obtain site wind data where possible, and run the data through a computer programed for more exact values of yield.

Figure 12 is similar to figure 11 except that the values shown are for a 20 ft. diameter turbine.

With adequate wind speed data we can readily determine the best generator size, both for optimum energy yield and for overall cost.

The two "backfeed" columns are representative only, since any size up to 14 KVA could be used with this turbine. This case is where the turbine runs at constant speed, and this best operating speed would be determined by the wind regime at the particular site.

I wish to commend ERDA for mading funds available for vertical axis wind turbine research and development, and also the SANDIA personnel for their extensive work to date.

However it would be your remiss of me not to comment on some of the handicaps under which your project is being undertaken, both with horizontal axis as well as vertical axis machines, although I am more familiar with the latter.

In our own operation, I would seriously question any assumption that economic design could be acheived by optimizing parts separately in order to arrive at an optimized whole. This question is particularly significant where design must trade off performance versus cost at every turn. It is vital to be fully aware of not only ones own manufacturing cost and production techniques when making trade-off decisions, but also to closely examine those of others who may be able to supply a similar item more economically.

D.A.F. VERTICAL AXIS WIND TURBINE

PRODUCTION MODEL - 15FT. DIAMETER - 18FT. HIGH ROTOR

NET ANNUAL ENERGY YIELD KILOWATT HOURS			
MEAN ANNUAL WIND SPEED M.P.H.	BATTERY CHARGING	RESISTANCE LOAD	60 CYCLE BACKFEED
	MAXIMUM NET ELECTRICAL OUTPUT 3.5 KW	MAXIMUM NET ELECTRICAL OUTPUT 4.0KVA	MAXIMUM NET ELECTRICAL OUTPUT 4.0KVA
8	2800	3700	2800
9	3800	5000	4100
10	5000	6700	5600
12	7400	10000	9900
14	9500	13200	12000
16	11400	16000	15000
18	13000	18600	17400
20	14200	20500	19500

NOTE:
1. Computed yields are based upon Rayleigh Distribution of Windspeed Frequencies.
2. Yields for any windspeed distribution computed on request.
3. Standard battery voltages are 220V, 110V, 24V. Other voltages can be arranged.
4. Resistance heating 220V normally, 110V available also.
5. Line backfeed may be 60 or 50 cycle, two or three phase, 110V or 220V.

FIGURE 11

D.A.F. VERTICAL AXIS WIND TURBINE

PRODUCTION MODEL - 20FT. DIAMETER - 30FT. HIGH ROTOR

NET ANNUAL ENERGY YIELD KILOWATT HOURS					
MEAN ANNUAL WIND SPEED M.P.H.	BATTERY CHARGING		RESISTANCE LOAD	60 CYCLE BACKFEED	
	MAXIMUM NET ELECTRICAL OUTPUT 6.0 KW	MAXIMUM NET ELECTRICAL OUTPUT 11.0 KW	MAXIMUM NET ELECTRICAL OUTPUT 13 KVA	MAXIMUM NET ELECTRICAL OUTPUT 7.5 KVA	MAXIMUM NET ELECTRICAL OUTPUT 14 KVA
8	6400	5600	7400	7500	6500
9	8600	8300	10800	10500	9500
10	10900	11200	14500	14000	14000
12	15000	17200	23500	20500	23000
14	18800	24000	34000	26500	33500
16	21800	29600	43000	32000	43500
18	24400	34900	51500	36500	53000
20	26200	39400	58500	40300	61000

NOTE: 1. Computed yields are based upon Rayleigh Distribution of Windspeed Frequencies.

2. Yields for any windspeed distribution computed on request.

3. Standard battery voltages are 220V, 110V, 24V. Other voltages can be arranged.

4. Resistance heating 220V normally, 110V available also.

5. Line Backfeed may be 60 or 50 cycle, two or three phase, 110V or 220V.

FIGURE 12

The inability to obtain true cost data is an almost insurmountable handicap for any designer.

Lastly, and perhaps to bring out the point, I would, with deference, suggest to ERDA that forty percent of the funds allocated for the procurement of the next five horizontal axis machines be rerouted. An open tender purchase from industry of Vertical-Axis machines could be initiated with these funds.

I am fairly sure that ERDA by this means would obtain considerably more generating capacity and at the same time arrive at some real world costs.

FEASIBILITY INVESTIGATION OF THE GIROMILL

Robert V. Brulle
McDonnell Aircraft Company
P.O. Box 516
St. Louis, Mo 63166

1. Overview

The Giromill (from cyclogiro windmill) consists of a number of vertical blades rotating around a central tower. The blades rock angles are individually modulated to achieve high wind energy conversion efficiency. This one year ERDA sponsored study concentrated on determining the feasibility of the Giromill for cost effective production of electrical energy.

Figure 1 shows a typical 500 kW Giromill configuration. It has 3 symmetrical constant chord blades, each having a chord (c) of 1.65 meters and a full span (b) of 29.7 meters. The blade modulation actuator is placed at mid span. The blades are attached to the central tower with 3 blade support arms providing a 62.3 meter rotor diameter (D). This results in a rotor aspect ratio (AR_R = b/D) of 0.476, and a rotor solidity (σ = no. of blades x c/D) of 0.079. The blade speed ratio (λ = blade rotational speed/wind speed) is 3.85 when the power coefficient (C_P) is a maximum. This Giromill is sized for placement in a 5.4 mps mean wind ($\bar{V}$) site, and has a rated wind speed (V_R) of 8.1 mps.

The study plan followed is shown in Figure 2. Twenty one different Giromill configurations covering three sizes of Giromill systems were analyzed, varying such parameters as rotor solidity, rotor aspect ratio, rated wind velocity, and number of rotor blades. The performance, design, and cost effectiveness of these 21 configurations were determined. The results of this analysis formed the base for selecting a configuration that was optimized for the least cost of energy. The Giromill configuration depicted in Figure 1 is this optimized system.

2. Giromill Configurations Selected

The pertinent design ground rules employed are shown in Figure 3. To facilitate comparison these ground rules are similar to those used for conventional windmill studies. For expediency of this feasibility study, the generator and RPM speed increaser efficiency was held constant.

Figure 4 summarizes the physical characteristics of the 21 Giromill configurations studied. Note that all 120 and 500 kW configurations studied

had 3 blades. Only the 1500 kW system considered the effect of more blades. A Giromill configuration having two blades was initially investigated but was discarded in favor of a 3 bladed configuration. Three blades produces a positive torque at all points on the rotor orbit, assures starting with the wind from any direction, and has better structural dynamic properties.

3. Performance

The performance characteristics of the Figure 1 Giromill configuration are shown in Figure 5. The effective angle of attack (α_e) referred to in the figure is the nominal commanded value, either positive or negative, around the blade orbit. The actual value varies due to rotor vortex effects and the smoothing of the blade modulation rock angle by the control system. Figure 6 presents the performance results, determined utilizing the Larsen cyclogiro vortex theory.

4. Design Analysis

Various Giromill conceptual designs were investigated as shown in Figure 7. Concept (A) was the original design shown in the June 1975 Wind Energy Workshop Proceedings. The Giromill structural dynamics due to the cable sag and sway, the increased load in the lower bearing due to cable tension, the requirement for the large stiff cable support arms, and the large area of real estate required for the cable tie down were the negative aspects of this type of design. The fixed tower design shown in (B) appeared attractive except for providing a power drive to the generator. There appeared to be no cost effective method of transmitting the rotor torque to a generator drive shaft. Using a single ring and pinion gear at the bottom or middle blade support requires that the entire rotor torque be directed through that gear. This requires a heavy blade support structure. Three ring gears (one at each blade support) could be used, however, the mechanical complexity and the long drive shaft are the negative aspects. Concept (C) was the design selected for this feasibility study, and consists of a simple structural built-up rotating upper tower cantilevered from the lower stationary tower. Two main rotor bearings react the tipping moment. The lower bearing also reacts the rotor weight. A descriptive sketch of this concept is shown in Figure 8.

Blade concepts investigated are shown in Figure 9. Concept (A) had initially shown promise because of its ease of manufacture since it had no ribs. It had, however, a relatively high polar moment of inertia and required

considerable ballast to locate the CG at the pivot point (25% chord). Concept (B) had an extruded leading edge torque box with a sheet trailing edge stabilized by sheet metal ribs fastened to the leading edge extrusion. It was found that a closed "D" type extrusion as shown was expensive and not very practical. Two extrusions, a leading edge and a spar in place of the "D" extrusion was also evaluated, but was still not as attractive as concept (C). Because the blades are symmetrical and have a constant chord they lend themselves to the rolling and brake forming of the leading edge and spar, and constructing as shown in (C). This blade concept was used for the Giromill design analysis.

The generator drive systems looked at are summarized in Figure 10. A ring and pinion gear around the upper tower by the lower main bearing was found to provide an insufficient RPM increase to drive the generator directly and a low ratio speed increaser was still required. The cost for the large ring gear and low ratio speed increaser was greater than for a high ratio speed increaser by itself, hence this concept was discarded. The large diameter of a Giromill's rotor structure could be used to provide a peripheral track for a friction drive wheel attached directly to the generator. Friction drives have been used with obvious success in automobiles and railroad systems, but have not proven suitable in many industrial applications. A friction drive, although attractive for larger high power type Giromills, would require testing and verification before use. For this feasibility analysis this concept was not considered further, and a conventional commercially available RPM speed increaser was used.

Figure 11 shows a sketch of the blade rock angle actuator concept. The rotary actuator is a brushless DC motor driving through an electrical clutch to a speed reducer to the blade. The critical life cycle component was determined to be the bearings. The 120 kW systems required an actuator having a maximum power output of 0.6 HP; the 500 kW required 5 HP, and the 1500 kW 15 HP.

5. Structural Analysis

The structural arrangement of the Giromill was studied as three sub-structures: (1) blades, (2) blade supports, and (3) tower (both upper and lower). Each of these sub-structures were sized using the structural design criteria shown in Figure 12. The loading conditions used in the sizing were: (1) normal operation under rated conditions, (2) operating under wind gust conditions, and (3) non operating (blades declutched) in high winds.

A typical blade limit load cycle used for the blade design is presented in Figure 13. The design of the blades was found to be dictated by the service life requirements. As such, the peak loads associated with normal operation under rated conditions becomes the design loads since the gust wind condition occurs too infrequently to cause fatigue failure. The inertial or centrifugal load component loads the blade sufficiently to prevent a blade load reversal.

An aluminum alloy was selected for the blade material. In addition to the high structural efficiency of aluminum relative to other common materials such as steel, aluminum is easily formed, naturally resistant to galvanic corrosion and the selected alloy, 2024-T6 exhibits good resistance to stress corrosion. The endurance limit of this aluminum, for an assumed stress ratio of zero, and a stress concentration factor of 2.81 which represents a mechanical fastener construction, is 14000 PSI. These blade design characteristics are shown in Figure 14.

The blade supports and upper and lower tower are dictated by both the service life and ultimate load criteria. Commercial steels were selected for these substructures. These substructures are basically compression structures sized to ultimate loads from the storm wind condition; however, members designed to these loads, in general, exhibit limit (expected) operating stresses which exceed fatigue allowables at the member splices. These joints were beefed-up to reduce the operating stresses to an acceptable level. The allowable fatigue of mechanically fastened carbon steel joints is based on 10^9 load cycles and a stress ratio conservatively assumed to be -1.0.

The Giromill system total weight for the 120 and 500 kW systems is shown as a function of rotor aspect ratio in Figure 15. These typical data indicate that low rotor aspect ratio systems have a lower total weight and, more important, that the 500 kW system produces more power per unit weight in the same wind environment (for a weight increase of 223% the power is increased 317%). The structural weight analysis results are tabulated in Figure 16. Note the inclusion of configuration 11-1 which was optimized for lower energy cost.

6. Structural Dynamics

The purpose of the structural dynamics investigation was to determine frequencies and associated mode shapes of the Giromill vibrations, determine

those that are critical, and then identify the problems associated with tuning the critical vibrations to alleviate their criticality.

Figure 17 presents a typical result of a Giromill system structural dynamics analysis. Of all modes identified only the upper tower torsion and bending appeared critical. The blade torsion frequency was not computed since the blade actuator stiffness was not defined. A cursory look using an expected range of blade actuator stiffness values indicated the blade torsion would be satisfactory.

Figure 18 presents a Campbell diagram showing the tower bending and torsion modes, and how they react with the various excitation frequencies. The points of strong forced vibrations are indicated by the circled symbols. The operating rotational speed does not pass through any of the forced vibration points, but is close to several. Note also that starting and stopping the Giromill will require passing through several others. The structural ramifications of these resonant frequencies was not considered in this feasibility analysis. The structural dynamics criteria stipulated was that the natural frequencies and forcing excitations be reasonably separated and that no aeroelastic instabilities exist.

The tower can be tuned to provide acceptable dynamic response characteristics. The corner members of the tower primarily affect the tower bending frequency and the cross members the torsion frequency. Tower diameter also strongly influences the dynamics. The interplay of these three parameters indicated a large range of tower dynamics could be achieved without significantly affecting the tower weight.

7. Control System

The main functional requirement of the control system is to enable the Giromill to generate the maximum rated power output without exceeding the structural and electrical load limitations. The control system performs this function by controlling the blade rock angles so that the desired Giromill power output is maintained in the presence of wind variations. Other control system functions provide for the startup and power interrupt or shutdown situations as they occur to insure that safe operating conditions are met.

An electronic control system was selected for this feasibility study since it appeared easier to implement at this time than a mechanical system. Figure 19 presents a simplified control system functional diagram. The

sensor signals includes such parameters as: the wind velocity and direction, rotor RPM, blade phase angle, vibration level, and electrical power conditions. On the basis of the values of these parameters the control system provides the logic to completely control the Giromill. The blade angle computations block in Figure 19 provides the command (Θ_{R_C}) to the blade rock angle actuators. The actuators respond and provide a rock angle (Θ_R) to the blades. The aerodynamic forces on the blades cause the rotor to turn, generating a power output.

One of the several Giromill system condition and failure detection control loops is shown. This is a comparison between the commanded rock angle and that actually achieved by the blades. A partial failure or binding of one actuator could occur without effecting any other system parameters since the remaining blades could make up the power difference. By comparing the commanded Θ_{R_C} with the actual achieved Θ_R, and assuring they are within a specified tolerance from each other protects against such a failure. If a failure is detected the mode selector will command a shutdown of the Giromill system. Shutdown is accomplished by declutching the blades from their actuator allowing them to weathervane into the wind. Other system condition and failure detection control loops are: excessive vibration level cut off, high and low wind cutoff, electrical power condition cut off, startup sequencing, normal blade declutching and emergency blade declutching.

The Giromill control system functions are, generally speaking, quite similar to the conventional windmill control system. The main difference lies in the blade rock angle control implementation. The rock angle implementation within the control system was incorporated as shown functionally in Figure 20. The implementation consists of computing the blade rock angle for zero angle of attack and no induced effects (Θ_{R_O}), and successively modifying this rock angle to account for the desired effective angle of attack, (α_e), and the induced angle of attack, (α_i). A generator power condition is fed back to make an incremental blade rock angle correction to keep the power output within specification.

The equation that relates the blade rock angle for zero angle of attack assuming no induced effects is:

$$\Theta_{R_O} = \arctan \left[\frac{-\cos\psi}{\frac{\omega R}{V_W} - \sin\psi} \right]$$

ψ - Blade phase angle

ωR - Blade rotational speed

V_W - Wind velocity

This computation is denoted by the Θ_{R_0} function block in the diagram of Figure 20. The Θ_{R_0} thus computed is then modified for the desired α_e which is programmed as a function of wind velocity (shown later). The angle of attack profile box relates the α_e to a positive or negative value depending on the blade phase angle by multiplying by the coefficient C_e. This then provides a rock angle that would provide the desired blade $\pm\alpha_e$ around the rotor but neglects the induced effects.

The induced effects are determined by using as a reference the induced effects α_i computed by the vortex theory program at the α_e for rated power, and then correcting α_i for the actual α_e being commanded. This correction was determined empirically using the vortex theory program, and takes the form of a multiplying constant, C_{α_i}, determined as a function of the actual $\alpha_e/\alpha_{e_{max}}$ being commanded at that time. This was checked out over the range of wind velocities expected, and predicted quite accurately the expected α_i. Since a smooth reference α_i is used, this also smooths the final Θ_R computed. The results of applying this technique are illustrated in Figures 21, 22, and 23.

Figure 21 shows the reference induced angle of attack as computed by the vortex theory and smooth hand faired curve. Figure 22 presents how the magnitude of α_i varies in terms of a multiplying coefficient C_{α_i} plotted against the angle of attack ratio $\alpha_e/\alpha_{e_{max}}$. This curve assumes that the nominal α_e to provide for the desired Giromill operation is being commanded. Figure 23 shows a typical example of how well this technique works. This is for a case where $V_R/V_W = 0.7$, and α_e would nominally be 4.7° to maintain constant power and RPM. $\alpha_{e_{max}}$ for this configuration was 9°. The power output using this technique was about 9% high, and would be reduced using the generator power condition feedback loop to incrementally correct α_e and α_i to get back to the desired power.

This rock angle control technique has been programmed on the computer and functionally checked out. It has also been used to compute the cam profiles for a cam driven blade modulation system proposed for a wind tunnel test model described later.

8. Power Output Evaluation

The Giromill power output was obtained using the performance characteristics integrated over the wind duration curves. The wind duration curves were for a mean wind of 5.4 mps and 8.1 mps. The 120 and 500 kW systems used the 5.4 mps mean wind curve and the 1500 kW systems the 8.1 mps mean wind curve.

It was determined that the maximum yearly power output is obtained when the maximum C_P is located at 0.85 V_R instead of at V_R. This alters the power curve so that rated power is achieved at a wind velocity slightly higher than V_R. This wind velocity is denoted as V_{R_N}. A comparison of the maximum power output curve with that when the max C_P is located at V_R is shown in Figure 24. The optimum curve, when integrated over the wind duration curve, showed a 2% increase in the yearly power output.

Figure 25 presents the resulting α_e variation required to obtain the optimum power output (shown as the dashed curve) plotted in Figure 24. This is the type of α_e profile that is programmed in the control system. Note that there is a velocity range where α_e is kept constant (from 6.9 to 8.7 mps) at 11 deg, and that full power is not obtained until V_W = 8.7 mps. This full power wind velocity is denoted as V_{R_N}, the new rated wind velocity.

9. Cost Analysis

The Giromill cost analysis was conducted using ground rules similar to those used for the conventional windmill studies by GE and Kaman. The ground rules used are summarized in Figure 26.

One of the major cost components of the Giromill turned out to be the main rotor bearings. The upper main bearing size is dictated by the upper tower diameter because of structural dynamic considerations. The lower main bearing size is dictated by the upper tower end cap design and was assumed as 50% of the upper main bearing. The cost estimating relationship used for these bearings is shown in Figure 27.

Figure 28 presents a summary of the subsystem and component costs used in the cost analysis. Note that the blade cost factor is $4.00/lb. This is a consequence of the simple blade design made possible because of the symmetrical untapered and untwisted blade used for the Giromill.

The speed increaser and generator costs were obtained from vendor data, but were increased because of the vertical mounting used with the Giromill. The speed increaser cost was increased 10% and the generator cost 15%.

Other cost elements used are presented in Figure 29. The additional capital costs for final assembly, shipping, land and site development, etc. were based on reference data. The cost of capital was set at 15% of the total installed cost of the Giromill, and covers the following annual charges:

- o Depreciation
- o Cost of indebtedness, interest on bonds and notes
- o Federal income tax
- o State and local taxes
- o Cost of equity, common and preferred stock

This 15% was based on a total financing structure composed of 60% bonds, 10% preferred stock and 30% common stock. The 15% cost of capital agrees well with values used in other current wind power generation programs.

The operations and support costs of 4% considered:

- o Salary for maintenance and supervisory personnel
- o Maintenance and overhaul costs
- o Administrative and general expenses
- o Insurance
- o Miscellaneous expendables

This value of 4% appeared conservative when compared with the values currently used by the electric utilities, but appears warranted at this time for a new system like the Giromill.

Figures 30 and 31 present some typical results of the production costs and cost of energy for the 500 kW system. The top 3 values, configurations 13, 9 and 14, show the cost effect of rated wind speed. The last set of values, configuration 11, was the least cost 500 kW Giromill system. These costs are all based on the initial analyses and did not incorporate any cost optimization in the Giromill design.

The high cost of the main bearings, especially for the large Giromill system having a low rated wind speed (configuration 13) is evident. Note that the energy cost (¢/kWH) exhibits a trend with rated wind similar to that observed with conventional windmills, i.e., having a minimum energy cost at a rated to mean wind ratio near 1.5.

Configuration 11 resulted in the lowest energy cost for a 500 kW system. This sytem was then subjected to a design optimization effort to bring down the cost of energy. The results of this optimization are shown in Figure 32. This figure shows the least energy cost for the 120, 500, and 1500 kW systems

based on the initial design and cost assumptions, and the optimized 500 kW system. Optimization reduced the cost of energy about 28%, from 5.6 to 4.05 ¢/kWH.

10. Wind Tunnel Test Plan

A wind tunnel test to verify the predicted Giromill performance is being implemented under continued ERDA funding and sponsorship. This test will be conducted in the McDonnell Aircraft Co. twenty foot mini-speed wind tunnel. A test of about 50 runs is postulated to acquire sufficient data to verify the theoretically computed Giromill performance. The test is scheduled to be run in October or early November of this year.

A relatively simple test model has been devised. Simplicity has been achieved by using a cam and push rod concept to modulate the blades. Various cam shapes can be used to simulate Giromill performance at different operating points. Their shapes can be determined theoretically using the control system blade modulation method previously explained.

The relationships between the model rotor diameter, RPM, solidity (σ), and blade chord (c) were formulated and are plotted in Figure 33. This figure shows the parameter tradeoffs that were considered in selecting the model design point. A constant tunnel wind speed of 4.5 mps was assumed. A small diameter Giromill rotor operates at a high RPM. A high RPM increases the centrifugal load on the blades and creates greater dynamic problems. Thus, one tends towards selecting a model having a large diameter and high solidity. The diameter of the model is limited by the size of the tunnel. Too large a diameter could create tunnel blockage or flow variations which may invalidate the results of the test. To minimize this effect a small rotor diameter should be selected. Also, the smaller model costs less (usually).

Increasing the solidity of the rotor also has the effect of decreasing the design RPM. There is, however, a limit as to how far the solidity can be increased. This is due to using a cam to modulate the blades. A cam and bellcrank is limited to modulating the blades to approximately ± 45 degrees. As solidity is increased the entire power envelope is shifted towards a lower blade speed ratio (λ) which increases the maximum blade rock angle. The model design point should have a solidity that provides a moderate value of Θ_R, since test points on either side of the design point are required.

Accounting for these relationships resulted in the selection, at this time, of the model design point shown in Figure 33. The rotor diameter is

2.1 meters and has a solidity of 0.314 (based on rotor capture area). This translates to a 3 bladed rotor with a blade chord of 22 cm. The rotor span was chosen to be as large as practical to maximize the various aerodynamic forces to be measured and to avoid tunnel blockage. A span of 1.2 meters was selected. A sketch of the model installed in the wind tunnel is shown in Figure 34.

A tunnel speed of 4.5 mps was used for the above analyses. This value is considered to be about the minimum velocity that will yield consistent measureable data. Increasing the tunnel speed would directly increase the design RPM.

At this time we have chosen to keep the tunnel speed constant, and vary the rotor RPM to obtain test data over a λ region. The RPM range to cover the test points chosen is indicated in Figure 33.

Rotor RPM control will be achieved with an air motor connected to the rotor support pedestal and attached to the rotor shaft through a torque balance and RPM sensor. This air motor can be used to either drive the rotor or absorb the rotor power by changing the air supply back pressure to the motor. The output of a torque balance and RPM sensor will provide the rotor shaft power.

11. Conclusions

A parametric design and cost effectiveness analysis of 120, 150, and 1500 kW Giromill systems has been completed. This preliminary analysis shows that the Giromill appears feasible and cost effective. Energy costs of a 500 kW system placed in a 5.4 mps mean wind site are 4.05 ¢/kWH.

A simplified wind tunnel test model to verify the performance estimates has been devised. Blade modulation is accomplished by use of a cam and push rod concept.

FIGURE 1

GIROMILL CONFIGURATION

500 kW

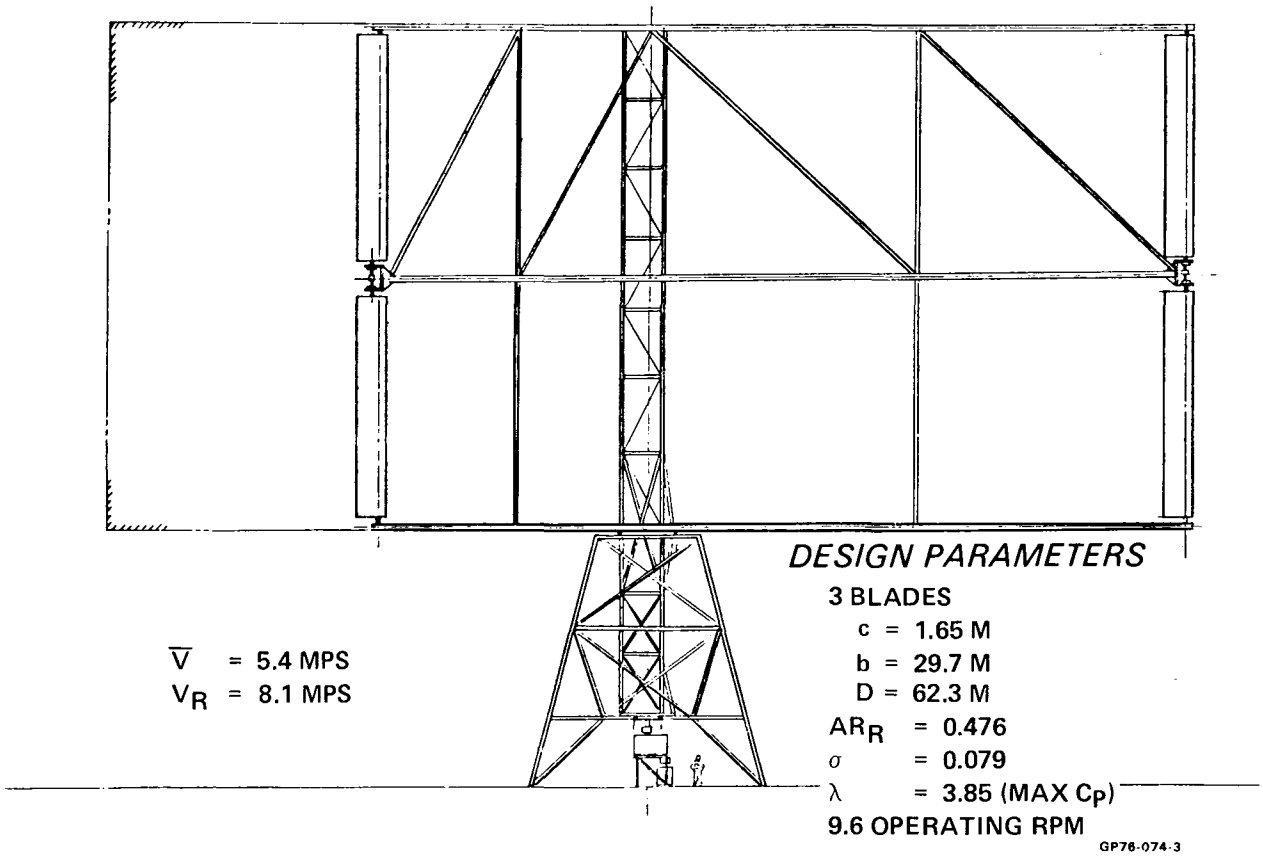

FIGURE 2

STUDY PLAN FOLLOWED

- AERODYNAMIC PERFORMANCE ANALYSIS USING LARSEN CYCLOGIRO VORTEX THEORY COMPUTER PROGRAM
- PRELIMINARY DESIGN OF 21 DIFFERENT GIROMILL CONFIGURATIONS - 120, 500 AND 1500 kW
- COST EFFECTIVE ANALYSIS
- OPTIMIZATION OF MOST COST EFFECTIVE CONFIGURATION
- PREPARATION OF NEXT PHASE WIND TUNNEL TEST PLAN

GP76-374-2

FIGURE 3

DESIGN GROUND RULES

- CONSTANT ROTOR RPM WITH SYNCHRONOUS GENERATOR
- MEAN WIND $\bar{V}$ = 5.4 MPS FOR 120 AND 500 kW SYSTEMS AND 8.1 MPS FOR 1500 kW SYSTEM
- STATIC COMPONENTS DESIGN LIFE OF 50 YEARS
- DYNAMIC COMPONENTS DESIGN LIFE OF 30 YEARS
- WITHSTAND WIND GUSTS TO 27 MPS OPERATING
- WITHSTAND WINDS TO 54 MPS WITH BLADES FREE
- GENERATOR EFFICIENCY 95%
- RPM SPEED INCREASER EFFICIENCY 96%

GP76-0374-4

FIGURE 4

GIROMILL STUDY CONFIGURATIONS

CONFIGURATION		RATED VELOCITY MPS	NUMBER OF BLADES	RPM	ROTOR SOLIDITY	ROTOR ASPECT RATIO	ROTOR DIAMETER METERS	ROTOR SPAN METERS	ROTOR BLADE CHORD METERS
120 kW	1	8.05	3	27.0	0.159	1.073	20.4	21.9	1.08
	2	8.05	3	24.0	0.198	1.073	20.4	21.9	1.35
	3	8.05	3	21.3	0.238	1.073	20.4	21.9	1.62
	4	8.05	3	20.0	0.198	0.746	24.5	18.3	1.62
	5	8.05	3	16.0	0.198	0.477	30.6	14.6	2.02
	6	7.15	3	18.0	0.198	1.073	24.3	26.1	1.61
	7	8.94	3	31.5	0.198	1.073	17.4	18.7	1.15
500 kW	8	8.05	3	17.7	0.079	1.073	43.0	46.2	1.14
	9	8.05	3	15.1	0.119	1.073	43.0	46.2	1.71
	10	8.05	3	12.8	0.159	1.073	43.0	46.2	2.26
	11	8.05	3	11.8	0.079	0.477	64.6	30.8	1.71
	12	8.05	3	11.5	0.119	0.614	56.9	34.9	2.26
	13	7.15	3	11.3	0.119	1.073	51.3	55	2.04
	14	8.94	3	19.7	0.119	1.073	36.7	39.4	1.46
	15	8.05	3	10.1	0.238	1.073	43.0	46.2	3.41
	16	8.05	3	13.5	0.119	0.85	48.3	40.8	1.92
1500 kW	17	11.6	3	18.5	0.159	1.073	43	46.2	2.26
	18	11.6	3	14.6	0.238	1.073	43	46.2	3.41
	19	11.6	3	12.7	0.317	1.073	43	46.2	4.54
	20	11.6	4	14.2	0.238	1.073	43	46.2	2.56
	21	11.6	5	14.6	0.238	1.073	43	46.2	2.04

FIGURE 5

GIROMILL PERFORMANCE CHARACTERISTICS

- 500 kW NOMINAL OUTPUT
- 3 BLADED ROTOR
- SOLIDITY = 0.0793

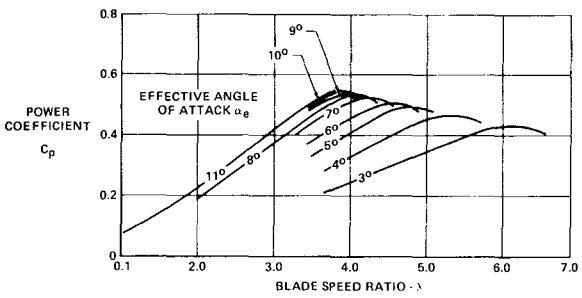

GP76 0374 9

FIGURE 6

PERFORMANCE RESULTS

- POWER OUTPUT INDEPENDENT OF ROTOR ASPECT RATIO (AR_R)
- ROTOR POWER IS PROPORTIONAL TO CAPTURE AREA
- RPM VARIES INVERSELY WITH ROTOR DIAMETER FOR GIVEN POWER
  - HIGH AR_R, HIGH RPM
  - LOW AR_R, LOW RPM
- OPTIMUM RPM VARIES INVERSELY WITH SOLIDITY
  - LOW SOLIDITY, HIGH RPM
  - HIGH SOLIDITY, LOW RPM
- MAXIMUM ROTOR EFFICIENCY IS INDEPENDENT OF NUMBER OF BLADES AND SOLIDITY
- LOW SOLIDITY FLATTENS THE POWER CURVE AT HIGH BLADE SPEED RATIOS
- FOR GIVEN POWER AND SOLIDITY, RPM VARIES DIRECTLY WITH RATED WIND SPEED
  - HIGH RATED WIND, HIGH RPM
  - LOW RATED WIND, LOW RPM

GP76 0374 8

FIGURE 7

CONCEPTUAL DESIGNS INVESTIGATED

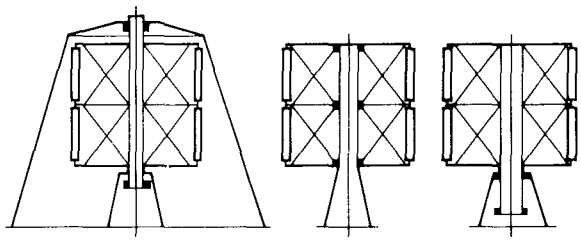

A CABLE SUPPORTED

B FIXED TOWER

C CANTILEVERED ROTOR

GP76 0374 10

FIGURE 8

FINAL CONFIGURATION

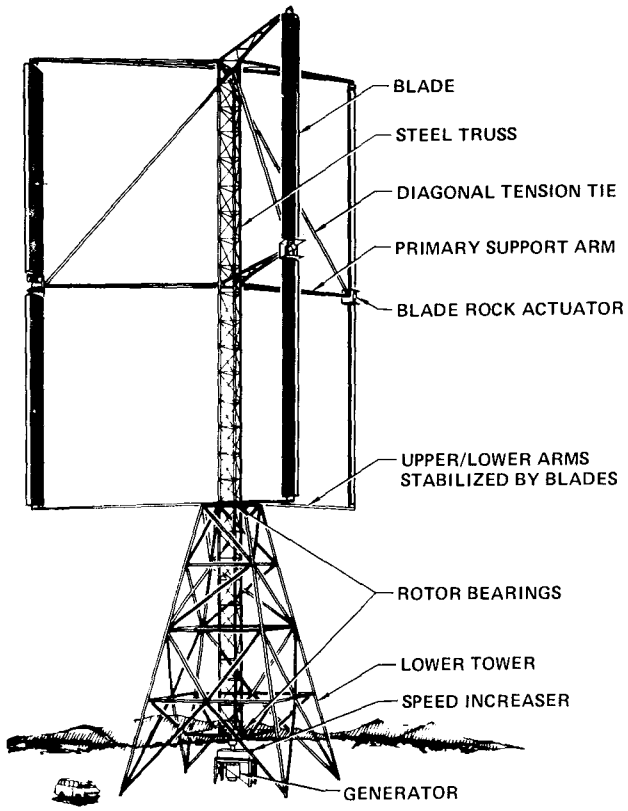

FIGURE 9

BLADE CONCEPTS INVESTIGATED

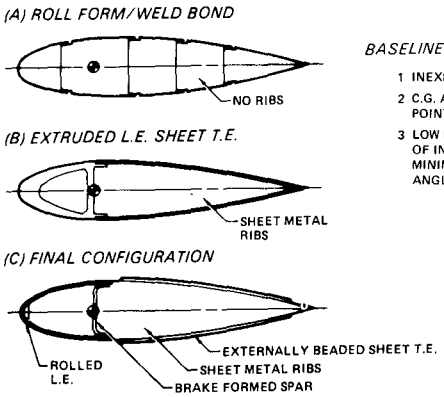

BASELINE REQUIREMENTS

1 INEXPENSIVE
2 C.G. AT PIVOT POINT (25% CHORD)
3 LOW POLAR MOMENT OF INERTIA TO MINIMIZE ROCK ANGLE ACTUATOR

GP76-0374-11

FIGURE 10

GENERATOR DRIVE SYSTEMS INVESTIGATED

- RING/PINION GEAR AROUND MAIN BEARING
  - RPM INCREASE INSUFFICIENT
  - STILL REQUIRED A RPM SPEED INCREASER
- FRICTION DRIVE AROUND A ROTOR-MOUNTED PERIPHERAL TRACK
  - FEASIBLE BUT NEEDS VERIFICATION
  - ESPECIALLY ATTRACTIVE FOR LARGE HIGH POWER GIROMILLS
- CONVENTIONAL RPM SPEED INCREASER

GP76-0374-12

FIGURE 11

BLADE ROCK ANGLE ACTUATOR

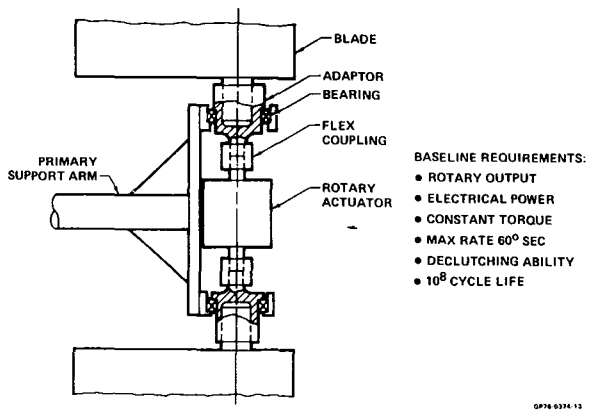

FIGURE 12

STRUCTURAL DESIGN CRITERIA

- NO STRUCTURAL FAILURE UNDER DESIGN ULTIMATE LOADS
- SERVICE LIFE OF DYNAMIC COMPONENTS 30 YEARS, 10^8 CYCLES OF DESIGN LIMIT LOADS
- DESIGN LIMIT LOADS = MAXIMUM EXPECTED LOADS
- ULTIMATE LOADS = FS x LIMIT LOADS
  - BLADES FS = 2.0
  - BLADE SUPPORTS AND TOWER FS = 3.0

FIGURE 13

BLADE LIMIT LOADS

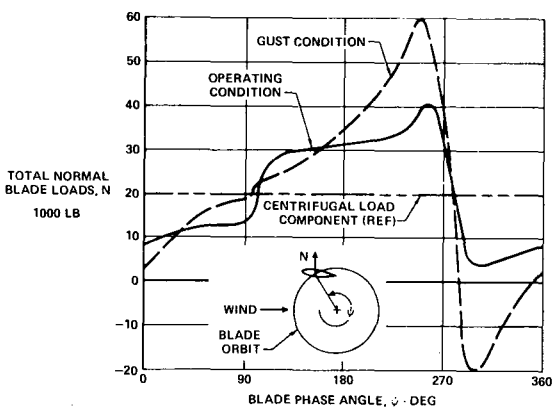

FIGURE 14

BLADE DESIGN CHARACTERISTICS

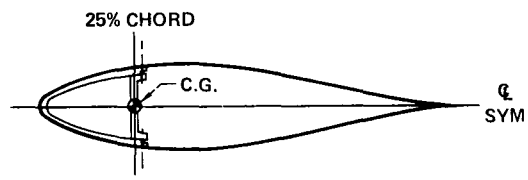

- MATERIAL: ALUMINUM, 2024-T6
- BLADE DESIGN: 30-YEAR SERVICE LIFE
  - LOADS - NORMAL OPERATING CONDITION
  - ALLOWABLE STRESS -

STRESS RATIO	0	(14 KSI)
STRESS CONCENTRATION	2.81	
ENDURANCE LIMIT		

GP76-0374-16

FIGURE 15

LARGER GIROMILLS PRODUCE MORE POWER PER UNIT WEIGHT

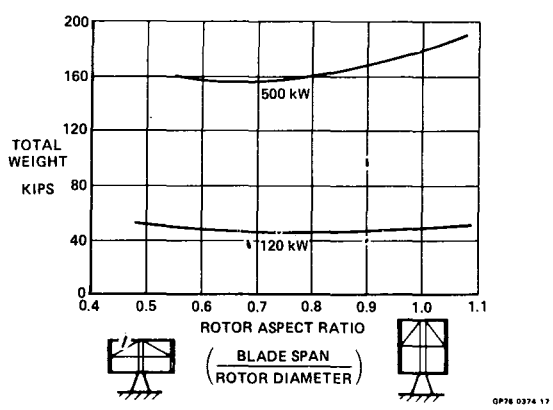

FIGURE 16

GIROMILL WEIGHTS

CONFIGURATION		BLADE WEIGHTS (LB)	BLADE SUPPORT WEIGHTS (LB)	UPPER TOWER WEIGHT (LB)	LOWER TOWER WEIGHT (LB)	TOTAL SYSTEM WEIGHT (LB)
120 kW	1	5,430	8,220	19,280	18,050	50,980
	2	4,230	8,330	19,280	18,050	49,480
	3	4,750	8,390	19,280	18,050	50,470
	4	3,950	12,430	14,220	16,800	47,400
	5	3,950	21,050	10,830	16,450	52,280
	6	5,830	13,190	29,300	21,050	69,370
	7	3,200	5,500	13,390	15,950	38,040
500 kW	8	13,960	38,780	90,790	36,700	180,230
	9	16,960	37,060	98,000	36,800	188,820
	10	14,800	36,970	98,000	36,800	186,570
	11	7,350	79,100	43,180	26,750	156,380
	11-1 (OPTIMIZED)	14,500	57,100	31,200	28,800	131,600
	12	10,930	60,760	54,350	29,200	155,240
	13	19,330	58,750	154,480	46,200	278,760
	14	15,730	24,060	65,540	30,400	135,630
	15	21,280	45,260	117,370	37,950	221,860
	16	NOT COMPLETED				
1500 kW	17	15,460	46,210	91,700	36,990	190,360
	18	24,300	60,350	99,380	37,210	221,240
	19	32,330	65,600	100,280	37,490	235,700
	20	23,830	78,400	101,260	37,780	241,270
	21	28,190	95,930	100,500	37,540	262,160

FIGURE 17

STRUCTURAL DYNAMICS FREQUENCIES

500 kW CONFIGURATION 11-1

MODE	NATURAL FREQUENCY (Hz)
UPPER TOWER TORSION	0.22
UPPER TOWER BENDING	0.34
BLADE TORSION	TORSIONAL SUPPORT UNDEFINED
SUPPORT ARM TANGENTIAL BENDING (IN PHASE, LAG-LEAD ARM BENDING)	1.88
BLADE FLAP BENDING	3.93
SUPPORT ARM VERTICAL BENDING (OUT OF PHASE)	5.12
SUPPORT ARM TANGENTIAL BENDING (OUT OF PHASE)	3.39
SUPPORT ARM TANGENTIAL BENDING (IN PHASE, BLADE MODE)	4.23
SUPPORT ARM VERTICAL BENDING (IN PHASE)	2.96

GP76 0374-1R

FIGURE 18

TOWER DYNAMICS

500 kW CONFIGURATION 11-1

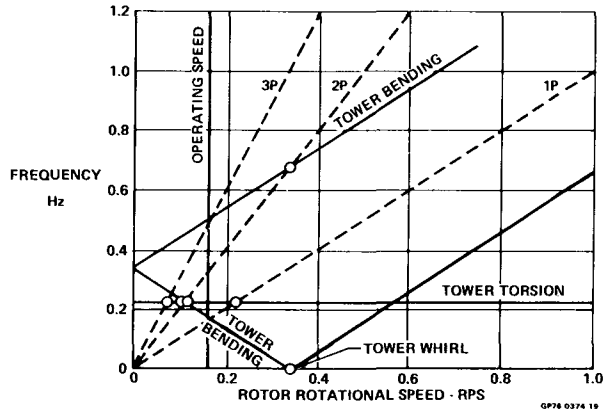

FIGURE 19

GIROMILL CONTROL SYSTEM FUNCTINAL DIAGRAM

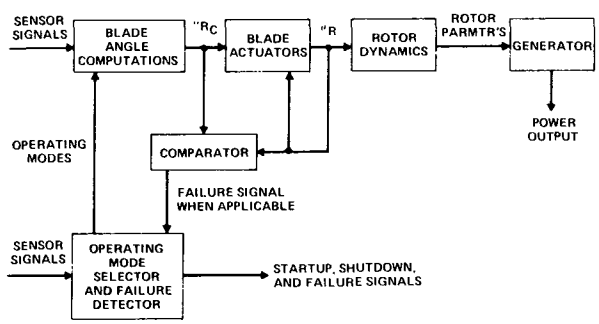

FIGURE 20

BLADE ROCK CONTROL PROCESSOR

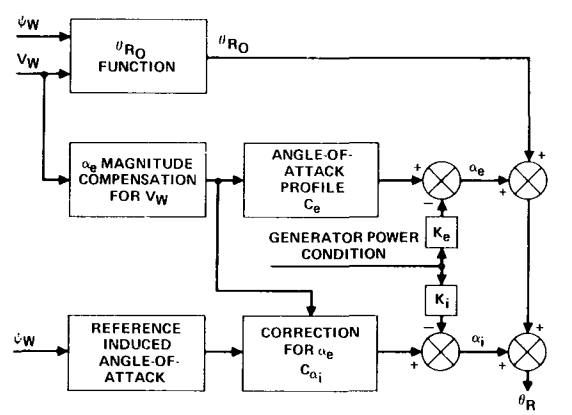

FIGURE 21

INDUCED ANGLE OF ATTACK ALONG THE BLADE ORBT

120 kW CONFIGURATION 2

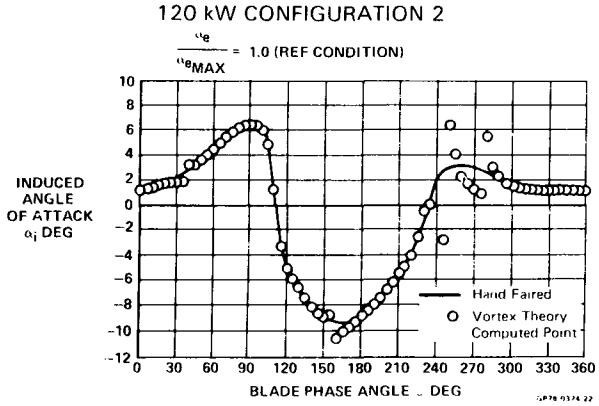

FIGURE 22

INDUCED ANGLE OF ATTACK VARIATION

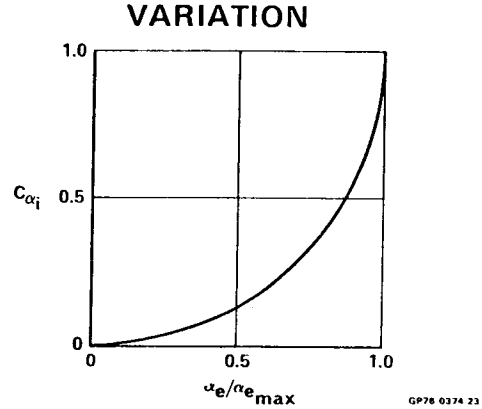

FIGURE 23

ROCK ANGLE COMPUTATION COMPARISON

120 kW CONFIGURATION 2

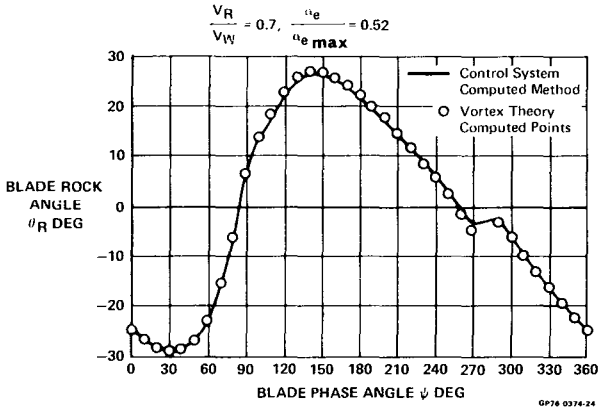

FIGURE 24

GIROMILL POWER CURVES

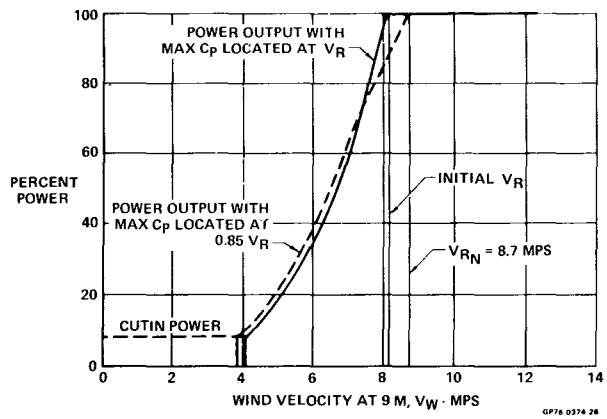

FIGURE 25

OPTIMUM POWER a_e PROFILE

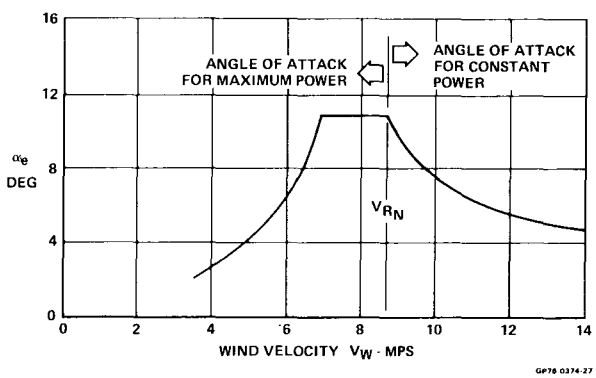

FIGURE 26

GIROMILL SYSTEM COST ANALYSIS GROUND RULES

- 1975 DOLLARS
- PRODUCTION COSTS ONLY FOR 100TH UNIT (NO RDT&E)
- ANNUAL RECURRING COSTS
  - COST OF CAPITAL
  - OPERATION AND SUPPORT (O&S)
- OFF-THE-SHELF EQUIPMENT WHEREVER POSSIBLE
- COST ESTIMATING RELATIONSHIPS (CER) DEVELOPED vs PHYSICAL PARAMETERS (SIZE, POWER OUTPUT, RPM, WEIGHT, ETC.)

GP76-0374-28

FIGURE 27

COST ESTIMATING RELATIONSHIP (CER) FOR LARGE COMBINATION BEARING

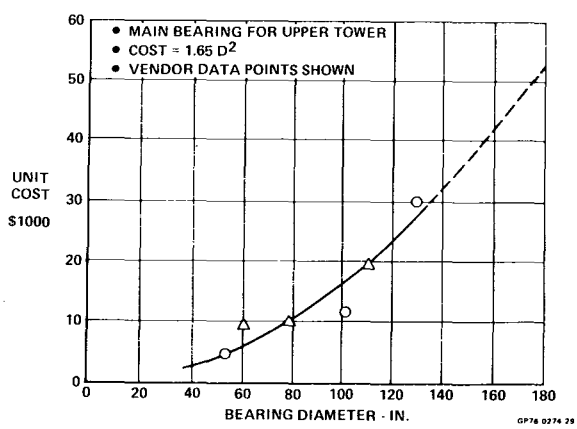

FIGURE 28

SUBSYSTEM AND COMPONENT COSTS

ELEMENT	MATERIAL OR DESCRIPTION	COST FACTORS
TOWER STRUCTURE	CARBON STEEL WELDED OR BOLTED	$0.75/LB
ROTOR BLADE SUPPORTS	TUBULAR CARBON STEEL	$0.75/LB
FOUNDATION	CONCRETE	25% OF TOWER COST
ROTOR BLADES	ALUMINUM	$4.00/LB
DRIVE SYSTEM		
COUPLINGS	SPEED INCREASER, GENERATOR DRIVE SHAFT	$4 TO $5/LB
SPEED INCREASER	120 kW	$15,000 TO $22,000
	500 kW	$26,500 TO $33,000
	1500 kW	$48,000
ELECTRICAL SYSTEM		
GENERATOR	1200 RPM FOR 120 kW	$4,025
	RPM VARIES FOR 500 kW SYSTEM	$23,000 TO $27,000
	450 RPM FOR 1,500 kW	$58,000
	GENERATOR CONTROLS, PANELS, ETC	$4,025
CONTROL SYSTEM		
ACTUATORS	THREE REQUIRED	
	120 kW	$2,400 EACH
	500 kW	$3,400 EACH
	1500 kW	$4,600 EACH
OTHER	CONTROL SYSTEM SENSORS, ETC	$10,000

GP76 0374 30

FIGURE 29
OTHER COST ELEMENTS

COST ELEMENT	DESCRIPTION	COST FACTORS
ADDITIONAL CAPITAL		
INCIDENTAL COSTS	FINAL ASSEMBLY, SHIPPING, ETC	10% OF TOTAL COST
SITE AND PREPARATION	LAND, SITE DEVELOPMENT, SECURITY - 120 kW	$15,000
	500 AND 1500 kW	$30,000
ANNUAL CHARGES		
COST OF CAPITAL	LOAN REPAYMENT, DEPRECIATION, BOND INTEREST, STOCK DIVIDEND, TAXES	15% OF TOTAL CAPITAL
OPERATING AND SUPPORT		4% OF TOTAL CAPITAL
TOTAL		19% OF TOTAL CAPITAL

GP78 0374 31

FIGURE 30
PRODUCTION COST ELEMENTS
500 kW GIROMILL

COSTS IN $1000
CONFIG 13, 9, 14 (AR_R = 1.07, σ = 0.119)
CONFIG 11 (AR_R = 0.48, σ = 0.079)

CONFIG NUMBER / V_R/V_W	TOWER, FOUND. AND BLADE SUPPORT	ROTOR BLADES	ELECTRICAL	DRIVE	MAIN BEARINGS	TOTAL SYSTEM COST*
13/1.33	310	77	31	44	230	723
9/1.50	206	68	29	42	163	538
14/1.67	144	63	27	41	119	424
11/1.50	167	29	31	44	72	373

*Includes $30,400 for Control Systems

GP78 0374 32

FIGURE 31
COST OF ENERGY PRODUCED
500 kW GIROMILL

CONFIG NUMBER / V_R/V_W	INSTALLED COST ($1000)	INSTALLED COST ($/kW)	ANNUAL POWER OUTPUT (kWH)	ENERGY COST (CENTS/kWH)
13/1.33	825	1,651	1,875,000	8.4
9/1.50	622	1,243	1,490,000	7.9
14/1.67	496	993	1,160,000	8.1
11/1.50	441	881	1,490,000	5.6

GP78-0374-33

FIGURE 32
GIROMILL ENERGY COST

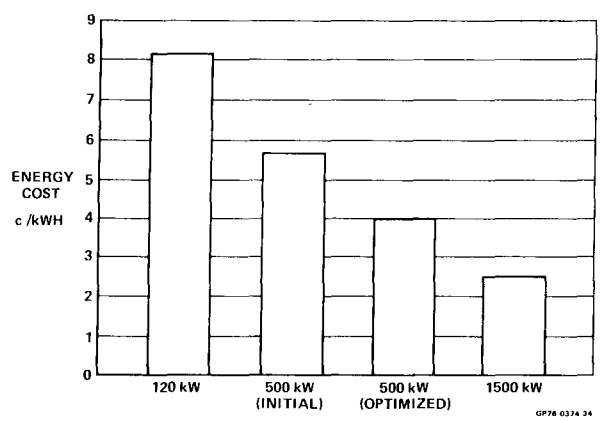

GP78 0374 34

FIGURE 33
MODEL DESIGN PARAMETER RELATIONSHIPS
TUNNEL WIND VELOCITY = 4.5 MPS

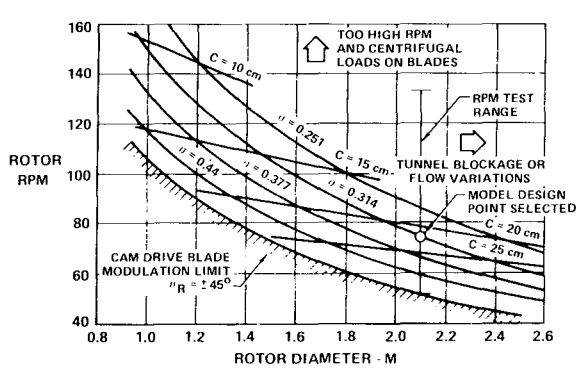

GP78 0374 35

FIGURE 34
GIROMILL TUNNEL INSTALLATION
MINI SPEED FACILITY

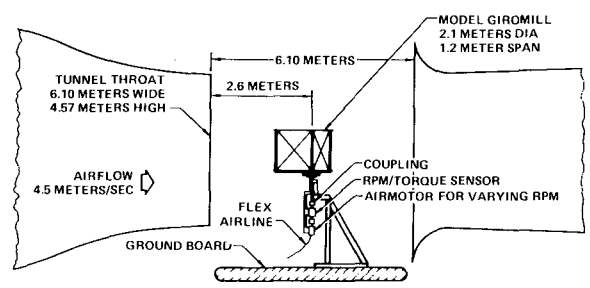

GP78 0374 36

FEASIBILITY INVESTIGATION OF THE GIROMILL

QUESTIONS AND ANSWERS

Mike Bergey - University of Oklahoma

Would you please state the assumptions (V_∞, operational $R\omega/V$) which you used to arrive at your 9 RPM operational speed.

Initial performance calculations assumed that max C_p, located at a λ of 3.85, was achieved at V_R. Later calculations showed that maximum power output was obtained when max C_p is located at 0.85 V_R. For the 500 kW Giromill of Figure 1, max C_p is at 6.9 mps. Recall that these wind velocities are given at a height of 10 meters and should be up rated to the center of the rotor which was assumed at a height of 30 meters.

S. Michlin

How much energy is used up by the blade actuators of the Giromill? What fraction is this of the output?

Maximum blade actuator horsepower calculated for the various systems are:

120 kW Giromill needs 0.6 HP

500 kW Giromill needs 5 HP

1500 kW Giromill needs 15 HP

The amount of power used during a rotor revolution is about 225 watts for the 120 kW system or 0.19% of the output.

Mike Bergey - University of Oklahoma

Is your decision to operate at a constant rotational speed (and therefore varying tip speed ratios and instantaneous power coefficients) primarily a result of generator system considerations?

Our ground rules were to use a synchronous generator tied in to a power grid. Constant rotor RPM is therefore required.

Ben Blackwell - Sandia

Your C_p curve did not show at what tip speed ratio the run away condition occurs. What do you anticipate?

The vortex theory program will not converge to acceptable solutions at blade speed ratios much beyond max C_p. When necessary, for estimating purposes, we fit a parabolic curve to the end points of the C_p curves shown.

Ben Blackwell - Sandia

What airfoil section was used in aerodynamics and structural studies?

The NACA 64_4021 airfoil.

Jim Banas

What effect do the supporting struts and cross-arms have on aero performance?

The blade support arms cause a drag and degrade the performance. The vertical and diagonal struts can perhaps be oriented so that they can act as a Darrieus blade and at least produce enough power to recover their individual drag loss.

Dan Lefever - Sonnewald Service

How soon will McDonnell Douglas make a full scale test machine?

As soon as the feasibility and cost effectiveness have been proven to an acceptable degree and money becomes available.

Lou Divone - ERDA

While you have a higher C_p than other configurations, did you run a test case where you held the rock angle constant at zero, and compare annual energy difference with the marginal cost of the blade rocking and control system?

We (Prof. Larsen and I) looked at running the vortex theory program at $\alpha_e = 0$ but it will not work at that condition. Ben Blackwell is going to try and run some of our conditions on his program for a check. The fact that our results compare favorably with those for the Darrieus rotor is encouraging.

Bob Reuter - Sandia

I didn't understand your comment on why centrifugal loads help the fatigue situation. For a given oscillating stress, an added mean stress reduces life. Look at Goodman diagram. Please comment.

It is correct to say that for a given alternating (oscillating) stress any increase in mean stress results in lower fatigue life. In the presentation, however, the statement regarding centrifugal loads referred to our study of constant power systems and was not intended to be unqualified statement on fatigue analysis.

For Giromill analysis, alternating blade stresses result from airloads on the blade, which reverse once during each revolution of the rotor, and rotor torque is the net effect of the airloads acting on all the blades. Steady state or mean stresses are associated with centrifugal blade loading, thus rpm. Given that power = torque x rpm, higher torques (thus higher alternating

stresses) are required to compensate for lower rpm's in constant power systems. We found that the combination of "high" mean and "low" alternating stresses was less critical than that of the "low" mean and "high" alternating stresses associated with the lower rpm systems which we studied.

Herman M. Drees - Pinson Energy Corp.

Have you analyzed various possible locations of your struts to minimize bending moments in your blade spars?

Yes. For the Giromill system design we evaluated several blade support schemes. Blades were sized, however, to meet the primary design objective of minimum system weight (cost) while also satisfying fatigue and stiffness requirements. This generally led to minimizing the number, thus cost, of blade supports by using non-optimum "heavy" blades of constant cross section.

INNOVATIVE WIND MACHINES; THE THEORETICAL PERFORMANCE OF A VERTICAL AXIS WIND TURBINE

Jerome B. Fanucci and Richard E. Walters
Department of Aerospace Engineering
West Virginia University
Morgantown, WV 26506

Introduction

This project, sponsored by NSF Grant AER 7500367-000, started March 1, 1975. The purpose of the project is to theoretically and experimentally study two wind machine concepts. The first concept is that of a vortex concentrator, i.e., a vertical airfoil is used to form a strong wing tip vortex, and the concentrated energy in the vortex is harnessed by a relatively small, high-speed turbine located downstream of the wing tip. The second machine is a vertical-axis straight-bladed turbine which utilizes high-lift, variable angle-of-incidence circulation-controlled airfoils to form the blades. Some of the results of the first year's research will be presented in this paper, with emphasis on the theoretical results obtained for the vertical axis turbine. An outline of the experimental program for this type of turbine is also discussed. Reference 1 contains more detailed results from the year's work.

The Vortex Concentrator

Approximately 50% of the wind energy research effort at W.V.U. is concerned with the vortex concentrator design. Fig. 1 shows the vertical wing which generates a strong tip vortex. The vortex strength is related to the lift which the wing can produce; Fig. 2 shows the strong influence of the wing tip on the flow immediately downstream of the tip, as visualized by smoke flow around a wind tunnel model. Theoretical calculations have shown that the energy per unit area in the region immediately downstream of the wing tip is increased by a factor of about five. A conceptual model of a wind machine utilizing a high-lift airfoil is shown in Fig. 3.

The Vertical Axis Turbine Experiments

The Vertical Axis Turbine (VAT) experiments will be performed with a free-air outdoor test model. Fig. 4 shows a scale model of the VAT located above an existing small building. The test model will have two blades 3.25 m (10 ft. 8 in.) in length with a rotor radius of 1.52 m (5 ft.). The rotor main shaft is supported by two bearings 1.5 m (5 ft.) apart located in the bearing case which is supported from the building roof by eight struts. For added safety and strength, three guy wires are attached to the top of the shaft, just below the wind direction indicator transmitting selsyn. The VAT will stand approximately 7.6 m (25 ft.) above the building roof, which is about 3.4 m (11 ft.) above ground

level. The rooftop location allows a shaft extension to pass through the building roof and into the building, where the instrumentation and control systems will be located. The VAT test model is designed for an operating tip speed ratio of six at a wind speed of about 6 m/s (19.7 ft/s), with safety margins of from two to four for most components. Power output will be approximately one KW_e.

The major purpose of the machine is to conduct tests of the circulation controlled airfoil concept. This is an airfoil which utilizes high pressure air blown over a rounded trailing edge to obtain high lift coefficients (C_L),[1] e.g., on the order of 3 or more. Preliminary calculations using strip theory show the expected area of operation of a vertical axis wind turbine which utilizes circulation controlled airfoils for the blades (Fig. 5). This theory has several limiting features, so that at the present time an exact operating position on the power coefficient vs. tip speed (C_p vs. $\omega R/V_\infty$) curve cannot be shown. A more exact theory is now being formulated, as described in later sections of this paper.

In order to evaluate fully the validity of theoretical calculations, a test program was devised. For the reasons listed in Fig. 6, it was decided that a test model should be constructed and tested in free air. The advantages of better Reynolds number simulation and having no wind tunnel correction factors to contend with were believed to outweigh the disadvantages of slightly higher costs and a longer time schedule to conduct tests, and the uncertainties introduced by the variable wind velocity which occurs in free air. In order to reduce errors caused by the wind fluctuations, an extensive site survey involving multiple anemometers and wind direction sensors will be conducted.

The VAT test program is outlined in Fig. 7. Initial testing will be performed with blades composed of conventional airfoils having approximately a NACA 0015 cross sectional shape (Fig. 8), and will be followed by tests with blades constructed of circulation controlled airfoils (Fig. 9). The circulation controlled blades will have two plenum chambers near the trailing edge which will be energized alternately, each operating one-half of each rotor revolution. This alternation is necessary to produce the lift forces in the proper direction to obtain maximum rotor torque. The airfoil shape will be a symmetrical (non-cambered) ellipse, with a modified, more-rounded trailing edge which allows better coanda jet formation at the trailing edge. Airfoils of this type have been successfully tested in many wind tunnel experiments,[2] and the principle has also been used to construct a STOL test aircraft at West Virginia University.[3] As seen in Fig. 7, the test program will involve a comparison of results with the 0015 and circulation controlled blades, and tests will be conducted with and without blade cyclic pitch. Blade modifications, such as changes in blade number, blade chord, and rotor solidity, will be considered for later tests.

The VAT instrumentation/control system schematic (Fig. 10) consists of a wind turbine control box and interconnected equipment. Various sensor inputs pass through the control box. The control box outputs consist of a blade flip signal, which allows a signal to be sent to the blade flip actuation mechanism through power slip rings, and data outputs to the Hewlett Packard 9810A calculator-based data acquisition/reduction system. This system also has the ability to provide "control functions" through a calculator-actuated bank of

16 relays. The wind direction indicator (Fig. 11) will be located above the main rotor shaft, and its output signal is provided by a transmitting selsyn. The receiving selsyn is located at the bottom of a power slip ring assembly (Fig. 12), and, in conjunction with a motor, turns the power slip ring assembly for proper alignment with the wind direction as indicated by the transmitting selsyn. The slip rings contain insulated sections around their circumference, so that each ring can be adjusted to pass signals at the proper part of the rotational cycle. This instrumentation package (Fig. 12) is located at the bottom of an extension of the rotating shaft of the VAT, and also contains a tachometer generator to sense rotor rotational velocity and an instrumentation-quality slip ring assembly (not visible in Fig. 12) inside the power slip ring array for the rotor and torque cell strain gage signals. The torque cell (Fig. 13) was manufactured and calibrated at WVU, and contains a strain gage array sensitive to torque and insensitive to axial load and bending moments. The cell will be located below the rotor main shaft and above the belt-driven generator's load takeoff pulley.

The data acquisition/reduction system is shown in Fig. 14, and its schematic in Fig. 15. This portable system, assembled around the Hewlett Packard 9810A computing calculator has various input and output devices, and will be operated "on-line" to provide rapid initial data reduction. The system will also provide certain control signals to the VAT and will contain a turbine stopping capability if certain operating parameters are exceeded.

At this time, construction of the turbine mounting system and the rotor is substantially complete. Fig. 16 shows the rotor in the construction stage mounted horizontally in the shop. The 0015 blades are mounted for the initial fixed attitude operation. Strain gages are being placed at approximately 20 critical locations on the rotor. After mounting and calibration by loading, the VAT will be erected, and testing will be initiated this summer.

The Vertical Axis Turbine Theory

a. Problem Requirements

In order to understand the aerodynamics of a cross-flow wind turbine, which is an unsteady aerodynamic configuration, certain effects should be accounted for in the analysis. First, the analysis should allow for time variations of the blade loadings; this implies that all dependent variables should be functions of time. As a result of the unsteady blade aerodynamics, the resulting shed vorticity should be properly accounted for as well as its interaction with the blades. This vorticity is force-free and therefore should be allowed to convect with its local stream velocity. The interaction of a particular blade with other blades should be noted, and finally the effect of time fluctuations of the free stream wind must be included in the analysis. The effects noted above are vital if a proper evaluation of the aerodynamic performance and the vibrational characteristics of the cross-flow machine are to be accounted for in the design process.

Although the stream tube methods[4] applied to the aerodynamics of cross-flow machines have served a useful purpose, the assumptions used in these analyses cannot account for most of the effects previously mentioned. It is the purpose

of this section to briefly outline a numerical solution for the unsteady lifting characteristics of a variable blade pitch cross-flow wind turbine. Since the blade aspect ratio of these machines is typically high (15 to 20), a two dimensional analysis is used. Because of the complexity of the shed wake, an analytical approach to the problem is prohibitive and it was decided to analyze the problem numerically. The problem will be approached in the spirit of classical potential theory (i.e., viscosity of the fluid is neglected and the fluid is assumed incompressible). In addition, certain symplifying assumptions related to blade thickness and angle of attack, which are well known in classical theory, will be made in order to reduce computer time, but could be accounted for if desired.

b. Analysis

Fig. 17 shows the various coordinate systems used in the analysis. The inertial (ζ, η) coordinate system is located with its origin at the center of rotation with the η axis in the direction of the free stream velocity, Vw. The analysis described here will be restricted to a single blade in a steady free stream. The extension of the method to N-bladed machines with time variable wind will be reported in Ref. 5.

In order to take advantage of the linearization of the boundary condition, which can be applied if the angle of attack is small, a noninertial (x, y) coordinate system is introduced. This system is attached to the reference point on the cambered surface of the blade with the x axis in the direction of the relative inflow velocity, $V_\infty(t)$, as shown in Fig. 17. From the geometry of the system the following expressions result:

$$V_\infty(t) = \omega R\left\{1+\epsilon^2 - 2\epsilon \sin\theta\right\}^{1/2} ,$$

$$\alpha(t) = \alpha_B(t) + \omega t - \beta(t) - \pi/2 , \qquad (1)$$

and $\theta(t) = \omega t$,

where ϵ is the inverse tip speed ratio,

$$\epsilon = V_W/\omega R \quad . \qquad (2)$$

As a consequence of aligning the x-axis with $V_\infty(t)$, the x, y axes rotate with an angular velocity, $\Omega(t)$, with respect to the inertial frame (ζ, η):

$$\Omega(t) = \frac{d\beta}{dt} = \frac{\omega(1-\epsilon\sin\theta)}{(1+\epsilon^2-2\epsilon\sin\theta)} \quad . \qquad (3)$$

The boundary condition on the cambered surface requires that the normal velocity of the blade relative to the (x, y) coordinate system be equal to the normal velocity of the fluid on the surface. Written in the noninertial frame attached to the blade origin, this statement is equivalent to

$$\frac{\partial}{\partial t} f(x,y,t) + (\bar{q} - \bar{V}_B - \bar{\Omega} \times \bar{X}) \cdot \bar{\nabla} f(x,y,t) = 0 \quad , \tag{4}$$

where f(x, y, t) = 0 describes the cambered surface. The vector $\bar{q}$ is the absolute velocity of a fluid particle and is composed of the wind velocity and perturbation velocities (u, v) relative to the inertial frame but resolved into components along the (x, y) axes. Specifically,

$$\bar{q} = -(V_W \sin\beta - u)\hat{x} - (V_W \cos\beta - v)\hat{y} \quad , \tag{5}$$

where $\hat{x}$, $\hat{y}$ are the unit vectors in the x, y directions respectively.

$\bar{V}_B$ is the absolute rectilinear velocity of the blade, i.e., $\bar{V}_B = \bar{\omega} \times \bar{R}$. This results in

$$\bar{V}_B = -\omega R \cos(\theta - \beta)\hat{x} - \omega R \sin(\theta - \beta)\hat{y} \quad , \tag{6}$$

where $\bar{X}$ is the position vector in the noninertial frame.

For uncambered airfoils, for which $y - x \tan\alpha(t) = 0$, the exact boundary condition which results from Eq. 4 is

$$v - x(\sec^2\alpha\,\dot{\alpha} + \Omega) - \tan\alpha\,(V_\infty + u + \Omega y) = 0 \quad . \tag{7}$$

The velocity relative to an observer in the noninertial frame may be found in terms of the absolute velocities using

$$\bar{V} = U\hat{x} + V\hat{y} = \bar{q} - \bar{V}_B - \bar{\Omega} \times \bar{X} \quad . \tag{8}$$

Therefore, the normal velocity V in the (x, y) frame is V = v − Ωx. If the boundary condition (Eq. 7) is linearized for small angles of attack, the resulting boundary condition becomes

$$V = x\dot{\alpha} + V_\infty \alpha \quad . \tag{9}$$

c. Vortex Model

According to potential theory, the loading on a lifting surface may be represented by a distribution of singularities. In this model, a distribution of bound vorticity was employed, and furthermore for numerical convenience, it was assumed that this distributed vorticity could be represented by discrete bound vortices attached to the cambered surface. As shown in Fig. 18, the cambered surface is divided into equal segments of lengths ΔC upon which the vortex is located at the 1/4 point of ΔC. It has been shown by R. M. James[6] that the choice of the 1/4 point of the chord segment for the bound vortex and the 3/4 point for the control point is optimum for the solution of the vorticity distribution in a steady two-dimensional problem. The control points are the locations chosen to satisfy the boundary condition. Finally the Kutta condition is automatically satisfied by this vortex model.

When changes in α(t) and/or $V_\infty(t)$ occur, the flow is unsteady. The consequence of these variations in α or V_∞ with time is a change in the bound

circulation $\Gamma_b(t)$. In an inviscid fluid it can be shown by Kelvin's circulation theorm that

$$\frac{d\Gamma(t)}{dt} = 0 \quad , \tag{10}$$

which implies that any change in the bound circulation must be countered by shed vorticity of appropriate strength and sense. That is if $\Gamma = \Gamma_b + \Gamma_w$, then

$$\frac{d\Gamma_b}{dt} + \frac{d\Gamma_w}{dt} = 0 \quad ,$$

where

$$\Gamma_b = \int_{-c/2}^{c/2} \bar{\gamma}(x)\,dx = \sum_{i=1}^{n} \gamma_i \quad .$$

Once shed, the strength and sense of these vortices remain fixed as they convect with the local stream velocity.

If we consider the blade motion in small Δt time steps, it can be shown that for the mth time interval (for the one bladed case) the equations for the determination of the bound vorticity are of the form

$$\sum_{i=1}^{m} \frac{\gamma_i^{(m)}}{|\bar{\xi}_{b_i} - \bar{\xi}_{c_j}|} - \frac{\sin\mu^{(m)}}{|\bar{\xi}_{\gamma}^{(m)} - \bar{\xi}_{c_j}|}\left\{\sum_{i=1}^{n} \gamma_i^{(m)} - \Gamma^{(m-1)}\right\}$$

$$- \sum_{k=1}^{k=(m-1)} \frac{\sin\mu^{(k)}}{|\bar{\xi}_{\gamma}^{(k)} - \bar{\xi}_{c_j}|}\left\{\Gamma^{(k)} - \Gamma^{(k-1)}\right\} = -2\pi\left\{V_\infty \alpha + x\dot{\alpha}\right\}_{\gamma} \quad , \tag{11}$$

where for convenience, the Eqs. (11) are written in the noninertial (x, y) frame of reference.

The position vectors and the angle μ indicated in Eqs. 11 are defined on Figs. 18 and 19, where $\hat{n}$ is the unit normal to the cambered surface.

Equation 11 is written for the jth control point where $j_{max} = n$ and superscripts designate time steps. The first term in (11) is the contribution of the bound vorticity to the normal velocity at $\bar{\xi}_{cj}$. The second term denotes the contribution of the shed vortex leaving the trailing edge in the current mth time step and the quantity in the brackets is its strength written in terms of the unknown bound vorticity $\sum_{i=1}^{n} \gamma_i^{(m)}$ and the known strength of the previously shed vortex $\Gamma^{(m-1)}$. The third term accounts for the induction at the control point due to the remaining shed vorticity with the understanding that $\Gamma^{(0)} = 0$. In considering multibladed systems, Eq. (11) is modified to account for all the bound and shed vorticity present in the flow. If there are n chord segments per blade and p blades, the number of unknowns will be np. At each time step, Eq. (11) will lead to a matrix formulation of the problem of order np.

d. Computational Procedure

The numerical solution assumes that the continuous blade motion and wake formation can be approximated by considering small discrete time steps. At

time $t = t_o$ there is no circulation on the airfoil or in the wake and at time t_1 (arbitrarily corresponds to $\theta = o$ in this model) the angle of attack and/or velocity changes and a starting vortex is shed whose strength is equal to the strength of the bound vorticity at that time, $\Gamma_v^{(1)} = -\Gamma_b^{(1)} = -\sum_i \gamma_i^{(1)}$. The strengths of the discrete bound vortices are found from (11) where flow conditions are calculated from (1) and the geometry is known. The shed vortex immediately leaves the trailing edge and the blade advances from t_1 to t_2. In the intervening time increment the vortex convects with its own local velocity to some new position in space. Its displacement and velocity have in no way been constrained; it is "force-free".

Since the strength and location of all vortices is known, the velocity at any point in space can be determined using the Biot-Savart law for induced velocities. This is done for the vortex leaving the trailing edge and its displacement during the Δt time increment is added to its previous position vector to find its location at t_2. The process involves resolution of the (u, v) perturbation velocities into components in the inertial frame (ζ, η) and the transformation of its position vector in the (ζ, η) frame to the (x, y) system. For computer programming the complex arithmetic facility of Fortran IV is used. Storing vortex spatial coordinates and velocity components as complex variables simplifies programming considerably. The locations of the shed vortices are computed with

$$\left\{u(x,y),\, v(x,y)\right\}_v^{(1)} \Leftarrow \frac{1}{2\pi}\sum_{i=1}^{n}\frac{\gamma_i^{(1)}}{|\bar{\rho}_v^{(1)} - \bar{\rho}_{b_i}|} \quad , \tag{12}$$

$$\begin{aligned} \left\{u(\zeta,\eta)\right\}_v^{(1)} &= -\left\{u(x,y)\sin\beta + v(x,y)\cos\beta\right\}_v^{(1)} \quad , \\ \left\{v(\zeta,\eta)\right\}_v^{(1)} &= -\left\{u(x,y)\cos\beta + v(x,y)\sin\beta\right\}_v^{(1)} \quad , \end{aligned} \tag{13}$$

$$\bar{q}_v^{(1)} = \left\{V_w + u(\zeta,\eta)\right\}_v^{(1)}\bar{\zeta} + \left\{v(\zeta,\eta)\right\}_v^{(1)}\bar{\eta} \quad , \text{ and} \tag{14}$$

$$\bar{\rho}_v^{(2)}(\zeta,\eta) = \bar{\rho}_v^{(1)}(\zeta,\eta) + \bar{q}_v^{(1)}\Delta t \quad . \tag{15}$$

The transformation between inertial and noninertial coordinate systems is given by the relationships

$$\begin{aligned} x &= -\zeta\sin\beta + \eta\cos\beta + R\sin(\theta-\beta) \quad , \\ y &= -\zeta\cos\beta - \eta\sin\beta - R\cos(\theta-\beta) \quad , \\ \zeta &= -x\sin\beta - y\cos\beta - R\cos\theta \quad , \\ \text{and} \quad \eta &= x\cos\beta - y\sin\beta - R\sin\theta \quad . \end{aligned} \tag{16}$$

*During the Δt increment $\bar{q}_v^{(1)}$ changes constantly since velocity is a function of position and the vortex is in motion. An averaging technique is therefore used for $\bar{q}_v^{(1)}$ and $\bar{\rho}_v^{(2)}$.

At time t_2 the bound vortex strengths are found from (11) and $\Gamma_b^{(2)} = \sum_i^n \gamma_i^{(2)}$. From the conservation of circulation $\Gamma_v^{(2)} = -\left\{\Gamma_b^{(2)} - \Gamma_v^{(1)}\right\}$ and the procedure continues.

It can be seen that at any time t_m the position and strength of all bound and shed vortices is known. Lift and moment coefficients, wake shape, vortex trajectories, and velocity profiles anywhere in the field can then be found.

e. Forces and Moments

The generalized dynamic forces on the blade are composed of a local lift force L normal to the inflow velocity, a local thrust force T parallel to the inflow velocity and a moment M_o about the mid chord. Their derivation, in part follows.

Bernoulli's equation for unsteady, incompressible, inviscid flow written in terms of the inertial frame is

$$\frac{\partial \phi}{\partial t} + \frac{p}{\rho} + \frac{q^2}{2} = F(t) \quad , \tag{17}$$

where ϕ is the velocity potential, p and ρ are the local fluid pressure and density respectively and F(t) is a constant along a streamline. In terms of the nonertial frame and written in $(\bar{s}, n)$ coordinates (parallel and normal to the blade respectively with origin at the mid-chord) it can be shown that neglecting small quantities (17) becomes

$$F(t) = \frac{p}{\rho} + \frac{q^2}{2} + \frac{\partial \phi}{\partial t} - V_{B_s}\frac{\partial \phi}{\partial s} - \left(V_{B_n} + \Omega s\right)\frac{\partial \phi}{\partial n} \quad , \tag{18}$$

where V_{B_s} and V_{B_n} are components of the blade rectilinear velocity in the $\bar{s}$ and $\bar{n}$ directions.

For irrotational flow F(t) is constant everywhere in the field. Considering the flow conditions above and below a point (s, o) on the chord line (upper and lower surfaces of the blade) it is possible to write

$$\frac{p_L - p_u}{\rho} = \left\{\frac{q_u^2 - q_L^2}{2}\right\}_s + \frac{\partial}{\partial t}\left\{\phi_u - \phi_L\right\}_s - V_{B_s}\frac{\partial}{\partial s}\left\{\phi_u - \phi_L\right\}_s - \left\{V_{B_n} + \Omega s\right\}_s \frac{\partial}{\partial n}\left\{\phi_u - \phi_L\right\}_s \quad . \tag{19}$$

Potential theory provides the mechanism for evaluating the right hand side of (19) in terms of vortex strength:

$$\frac{\partial}{\partial s}\left\{\phi_u - \phi_L\right\}_s = -\bar{\gamma}(s) \quad , \quad \frac{\partial}{\partial n}\left\{\phi_u - \phi_L\right\}_s = 0 \quad , \quad \left\{\phi_u - \phi_L\right\}_s = \int_{-c/2}^{s} \bar{\gamma}(s)\, ds \quad ,$$

$$\left\{q_u^2 - q_L^2\right\}_s = -2\bar{\gamma}(s)\, q_s \quad ,$$

and $$\left\{\frac{p_L - p_u}{\rho}\right\}_s = \left\{V_B - q\right\}_s \bar{\gamma}(s) - \frac{\partial}{\partial t}\int_{-c/2}^{s} \bar{\gamma}(s)\, ds \quad , \tag{20}$$

where $\bar{\gamma}$ (s) is the strength of the vortex sheet at any point on the blade chord and relates to a distributed rather than discrete vortex distribution. The usual convention of $\bar{\gamma}$ (s) positive for clockwise circulation is reversed here so that positive circulation (counterclockwise) induces forces yielding torque in the direction of blade rotation. From (20) the expressions for the normal force on the blade per unit span (F_n) and the moment (M_o), the lift and thrust can be found:

$$F_n = \int_{-c/2}^{c/2} (p_L - p_u)_s \, ds = \rho \int_{-c/2}^{c/2} (V_B - q)_s \, \bar{\gamma}(s) \, ds - \rho \int_{-c/2}^{c/2} \frac{\partial}{\partial t} \int_{-c/2}^{s} \bar{\gamma}(s) \, ds \, ds \quad , \tag{21}$$

$$M_o = \int_{-c/2}^{c/2} s (p_L - p_u)_s \, ds = -\rho \int_{-c/2}^{c/2} (V_B - q)_s \, \bar{\gamma}(s) \, s \, ds - \rho \int_{-c/2}^{c/2} s \frac{\partial}{\partial t} \int_{-c/2}^{s} \bar{\gamma}(s) \, ds \, ds \quad , \tag{22}$$

and $L = F_n \cos\alpha = F_n$, $D = -F_n \sin\alpha = -F_n \alpha$ FOR SMALL α . (23)

Details of the numerical integration scheme for equations (21) and (22) will not be shown. They follow from the fact that for the chosen vortex model the strength of a discrete vortex located at the 1/4 point of the ith chord segment is given by $\gamma_i = \bar{\gamma}_i \Delta S_i$ where $\bar{\gamma}_i \Delta S_i = \int_{S_i}^{S_{i+1}} \bar{\gamma}_s \, ds$ expresses the average vortex strength over the segment. It has been assumed that $(V_B - q)_s$ is constant over the segment.

f. Wind Turbine Power

The torque φ (t) developed by the wind turbine is equal to the moment of the blade aerodynamic forces about the (ζ, η) origin. Positive torque is in the direction of rotation, clockwise:

$$\varphi(t) = R\left\{ L \sin(\theta - \beta) - D \cos(\theta - \beta) \right\}^{*} \quad . \tag{24}$$

Since the potential flow analysis ignores viscous effects, the aerodynamic drag term D is supplied from experimental data or by some other method.

A power input to the wind turbine results from applying a moment to the blade's pitching axis which maintains the blade at zero incidence to $V_\infty(t)$. Furthermore, energy must be added to overcome the resulting aerodynamic reaction. Hence, the total power input is

$$P(t) = \left\{ \Omega(t) + \dot{\alpha}(t) \right\} M_o(t) \tag{25}$$

and it must be subtracted from the useful rate of working $W(t) = \omega \varphi$ (t) to arrive at the net rate of energy extraction from the wind,

*The blade normal force calculated from Bernoulli's equation (21) does not account for suction resulting from a sharp leading edge thickness (manifested in the theory by the appearance of a singularity at the leading edge). It is well known, however, that the component of leading edge suction in the lift direction is negligible and in the thrust direction it is cancelled by the component of normal force in the drag direction. For this reason, the term $T = -F_n \cos\alpha$ does not appear in (24).

$$\dot{E}(t) = W(t) - P(t) \tag{26}$$

Theoretical Results for the VAT

a. Computational Procedure

Numerical computations begin at some initial time when no wake is present. As the calculations proceed in small time steps, vorticity is shed from blade trailing edges and the wake is developed. This transient phase corresponds to the starting motion of the wind turbine. When it is determined that a periodic solution results, for the case of periodic or constant wind velocity, the calculation is terminated. Several computational variables affect convergence to this repetitive solution.

The three vortex model closely approximates the correct C_L values, but C_M typically differs by 40% from the proper values. With eight blade segments the situation is corrected.

The number of revolutions $\bar{r}$ necessary to reach C_L convergence depends on the tip speed ratio and the size of the time steps (which may be thought of as $\Delta\Theta$ steps) used in the numerical procedure. For $\Delta\Theta = 8°$ a satisfactory periodic solution results on the 5th revolution and takes approximately 30 minutes of CPU time. For $\Delta\Theta = 4°$ the 4th revolution gives satisfactory results but takes approximately 120 minutes of CPU time. Minimum computer time to achieve the periodic solution is obviously desired. Thus, for purposes of calculating turbine performance, the smaller $\Delta\Theta$ increments are not justified. However, the small $\Delta\Theta$ solution reflects the finer details of the wake structure as well as the transient aerodynamics and may be useful for flutter analysis or other structural design data.

b. Lift Characteristics

Fig. 20 shows the variation of the calculated lift from the steady state value given by classical theory. The difference is obvious but not startling and is explained by recalling that the Darrieus turbine studied here does not exhibit highly unsteady aerodynamics since the blades are fixed. Fig. 21 compares lift coefficient transients with the periodic solution. After 80° of the first revolution the starting transients decay and for all subsequent orbits C_L is well behaved between $\Theta = 0$ and $\Theta = 120°$. For this illustrative one bladed case the dynamics of blade-wake interaction appear in the second revolution and are generally confined to the region between 120° and 240°. Transients diminish in amplitude and frequency until the repetitive solution occurs, typically after four revolutions. The exact relationship between $(\omega R/V_w)$, $\Delta\Theta$, and $\bar{r}$ required for convergence has not yet been determined, though such a relationship almost certainly exists.

c. Wake Details.

Another test for periodicity is the convergence of vortex trajectories (shed at a particular location on the blade orbit) to a predictable path. Generally, wake convergence requires several revolutions more than C_L convergence, but the

last few revolutions produce a negligible effect on performance calculations.

Steps of $\Delta\Theta = 4°$ were used to generate the details of the transient wake shown in Fig. 22. The first few starting vortices, e.g., $\Theta = 8°$, meander downstream into a relatively quiescent flow field and traverse the orbital path at $\Theta = 200°$ when the blade is at $\Theta = 80°$ of its second revolution. As the wake element shed at $\Theta = 24°$ traverses the orbital path, however, it passes very close to the blade (t_2 and t_3). The interaction results in the erratic trajectory shown, inhibits the downstream transition of the vortex, and has an appreciable effect on blade C_L. Transients are exhibited similar to those shown in Fig. 21, but of greater amplitude and frequency. Note also that as the blade passes the vicinity of the $\Theta = 8°$ vortex (t_4) the oscillatory nature of the trajectory increases, indicating the influence of the passing blade. Skepticism of this erratic behavior, or perhaps of the ability to predict it, is not entirely unexpected. The reader is therefore referred to Djojodihardjo and Widnall[7] where it is seen that the calculations of Giesing[8] and Bratt's flow visualization[9] studies agree remarkably for the unsteady potential flow of oscillating airfoils.

The fully developed wake is shown in Fig. 23 for the case of $(\omega R/Vw) = 6$. The solid lines downstream of the turbine represent the locus of the extremities of the shed vortex trajectories. Upstream of the machine these lines represent the path the vortices would have taken had they actually been fluid particles. Definition of the "wake" is somewhat arbitrary, but attempting to illustrate the region of influence of the turbine, the authors have shown the locus of points at which the local velocity is 98%, 99% and 100% of the free stream wind velocity. As shown in Fig. 24, this region extends far beyond the projected frontal area of the turbine, indicating that there may be serious wind tunnel blockage corrections for wind turbines tested in closed tunnels. Since small errors in tunnel speed produce large errors in C_p, this area requires further investigation.

d. Velocity Defect and Blockage Factor

The term "blockage factor" is used to describe the reduction in the windward component of the free stream velocity and blockage, of course, alters turbine performance appreciably. Rather than employing a blockage factor the present method develops aerodynamic characteristics based on calculated local flow conditions. Fig. 25 illustrates calculated cross-wind velocities in the vicinity of the wind turbine for the blade position shown. Note that velocity defect is not symmetrical about the windward axis.

e. Energy Conversion Efficiency (Power Coefficient)

A measure of the efficiency of a wind energy conversion system is given by the power coefficient C_p which is the ratio of power extracted by the turbine to the theoretical maximum available wind energy within the blade swept area. Fig. 26 shows C_p vs $\omega R/Vw$ (tip speed ratio) for two basically different levels of aerodynamic drag. Recall that the present method gives lift characteristics only and drag must be obtained from some other source. Results agree very well with strip theory for maximum C_p and optimum $\omega R/Vw$. Further investigation is required to determine if this agreement extends to other circumstances. The Wilson-Lissaman blockage factor shows significant disparity from either strip theory or the current vortex model numerical solution and its use can not be recommended.

Conclusions

Results presented for the straight bladed Darrieus turbine illustrate the developed capability to model the complex lifting characteristics of cross-flow turbines. Initial research has focused on development of the analysis and the required computer program. Extension of the method to include multi-bladed machines, cyclic blade pitch, and time variant winds is currently in progress. The concept can be modified to accomodate thick airfoils, variable camber, or circulation control blades by changing the vortex model to one with bound vortices distributed on the blade surface rather than the camber line. Since blade aspect ratio is large, typically 15 to 20, the two dimensional analysis should closely approximate the finite blade characteristics. The matter of drag prediction for these devices must be aggressively pursued; it is the remaining obstacle to complete analytical performance prediction. In this regard, the WVU experimental wind turbine will be utilized in conjunction with lift predictions of the current method to deduce drag characteristics.

Continuing Research Efforts

This research and development project is in the process of being continued by ERDA funding. Emphasis in continuing work will be on establishing additional experimental data for the vortex concentrator machine using both wind tunnel and outdoor test models, and performing a preliminary design of the turbine. Theoretical work will consist of a turbulent flow analysis of the wing tip vortex. The experimental effort on the vertical axis turbine will continue with the testing of the various blade configurations on the outdoor test model. The aerodynamic theory for the vertical axis turbine will be extended for N-bladed machines, and will include an evaluation of non-steady (gust) and viscous effects. The aerodynamic strip theory will be reevaluated to determine if it can be modified to produce reasonably valid results at less cost than the more comprehensive vortex theory. In addition, the Allegany Ballistics Laboratory of Hercules, Inc., will perform a study emphasizing the optimum selection of a system configuration for the vertical axis machine, with consideration given to blade design, materials, and fabrication methods as well as a cost study of the system and its components.

Acknowledgements

Many individuals at WVU have contributed to the progress on this project. In particular, J. L. Loth has directed the work on the vortex concentrator and was aided by R. Huq, while G. M. Palmer has aided in the development of the instrumentation and data acquisition/reduction system. S. Yusuff, D. G. Elko, and J. E. Smith have aided in the rotor design and instrumentation, while W. Squire and P. G. Migliore have performed work on the theoretical analysis of the VAT. C. White and L. Metheny have aided on the VAT turbine design and construction. The authors gratefully acknowledge the efforts of these participants.

References

1. Walters, R. E., Fanucci, J. B., Loth, J. L., Migliore, P. G., Ness, N., Palmer, G. M., Squire, W. and Yusuff, S., "Innovative Wind Machines; Final Project Report," TR-50, Department of Aerospace Engineering, West Virginia University, June, 1976.

2. Walters, R. E., Myer, D. P., and Holt, D. J., "Circulation Control by Steady and Pulsed Blowing for a Cambered Elliptical Airfoil," TR-32, Department of Aerospace Engineering, West Virginia University, July, 1972.

3. Loth, J. L., and Fanucci, J. B., and Roberts, S. C., "Flight Performance of a Circulation Controlled STOL Aircraft," AIAA Journal, Vol. 13, No. 3, March, 1976, pp. 169-173.

4. Strickland, J. H., "The Darrieus Turbine: A Performance Prediction Model Using Multiple Streamtubes," Sandia Laboratories Energy Report SAND 75-0431, October, 1975.

5. Migliore, P. G., Fanucci, J. B., and Squire, W., "A Numerical Solution for the Unsteady Lifting Characteristics of Variable Pitch Cross-Flow Wind Turbines," to be presented at the 11th Intersociety Energy Conversion Engineering Conference, September 12-17, 1976, Sahara Tahoe, Nevada.

6. James, R. M. and Schetzer, J. D., "On the Remarkable Accuracy of the Vortex Lattice Discretization in Thin Wing Theory," Douglas Aircraft Company Report No. DAC 67211, February, 1969.

7. Djojodihardjo, R. H. and Widnall, S. E., "A Numerical Method for the Calculation of Nonlinear Lifting Potential Flow Problems," AIAA Journal, Vol. 7, No. 10, p. 2001, October, 1969.

8. Giesing, J. P., "Nonlinear Two-Dimensional Unsteady Potential Flow with Lift," Journal of Aircraft, Vol. 5, No. 2, March-April 1968, pp. 135-143.

9. Bratt, J. B., "Flow Patterns in the Wake of Oscillating Airfoils," R & M 2773, 1953, Royal Aeronautical Establishment, Great Britain.

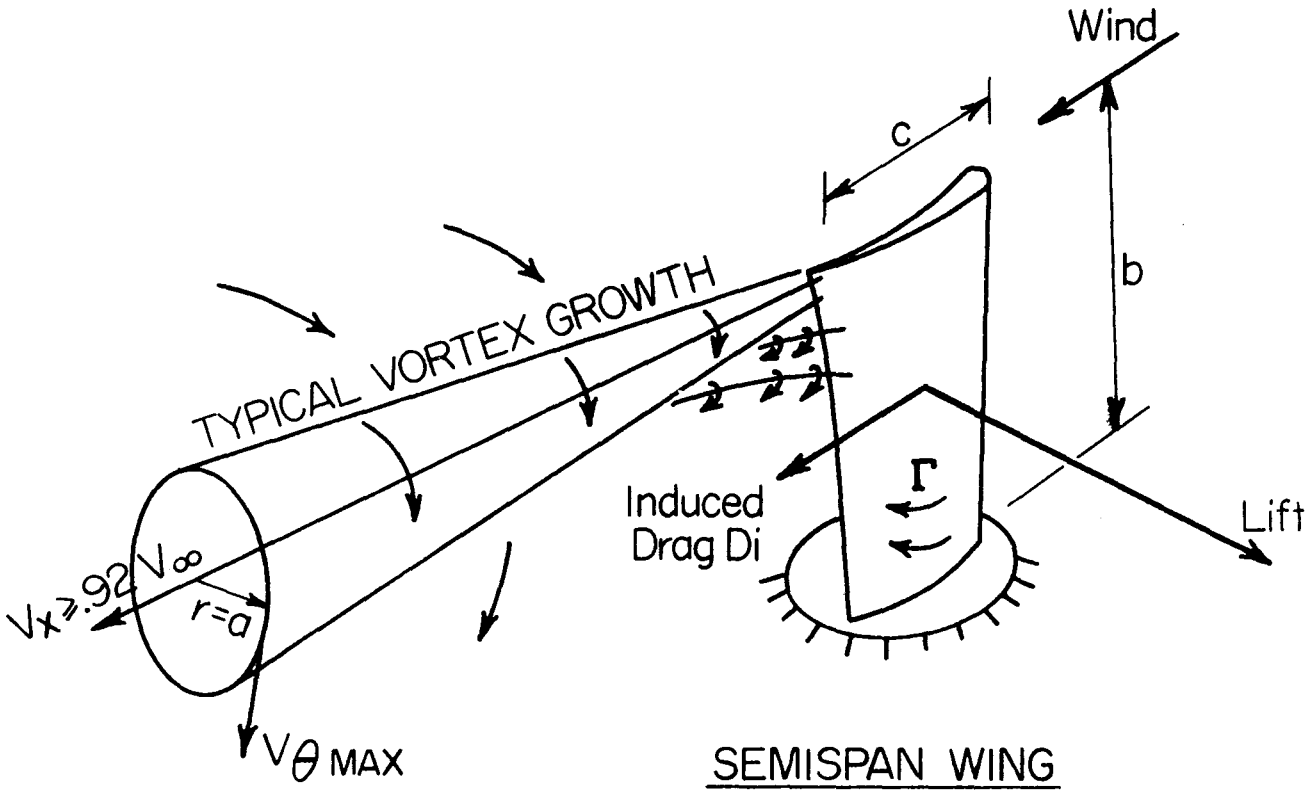

FIGURE 1. VORTEX FORMED BY A SEMISPAN WING.

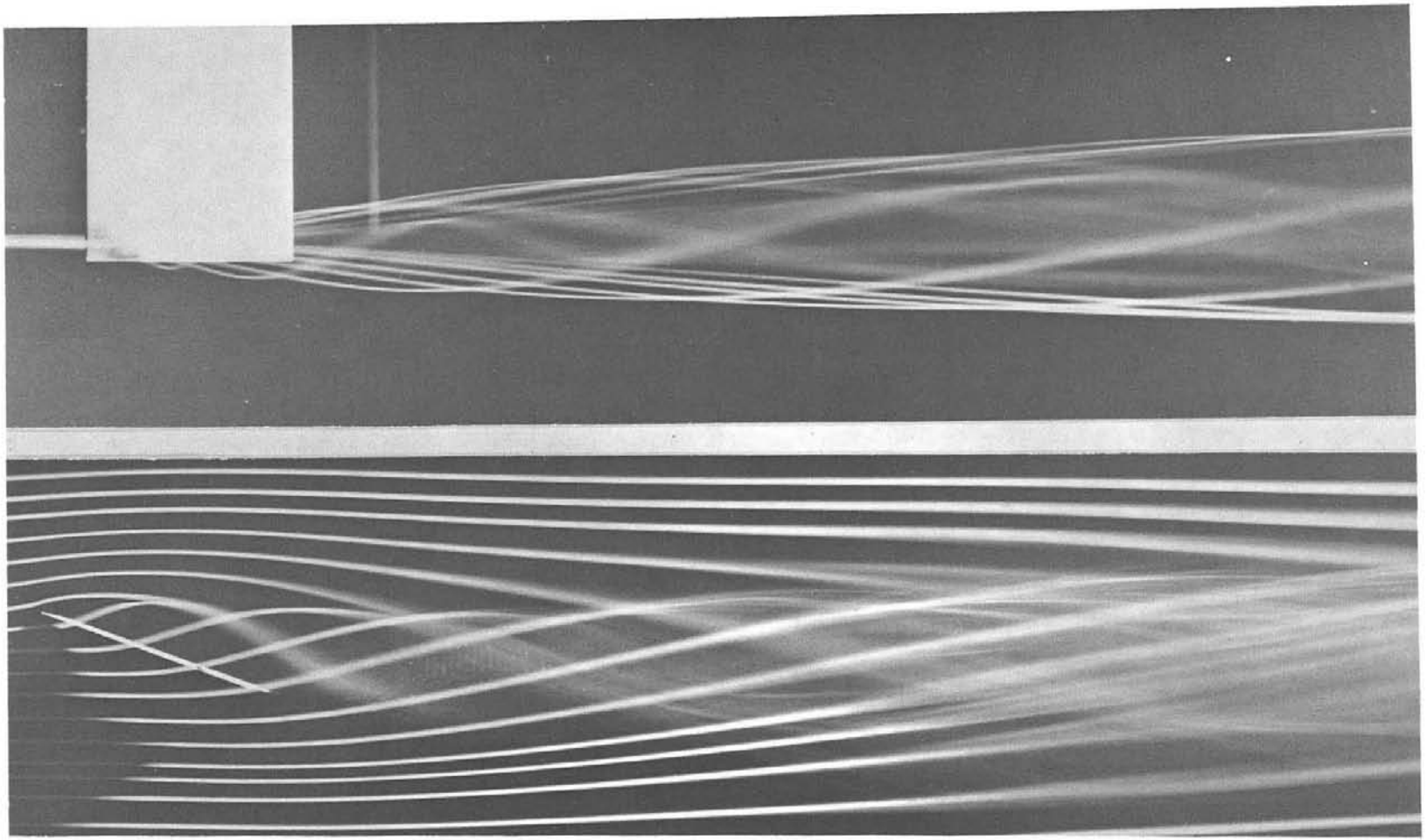

FIGURE 2. SMOKE VISUALIZATION (TOP AND SIDE VIEWS) OF THE VORTEX BEHIND A FLAT PLATE WING.

FIGURE 3. VORTEX MACHINE MODEL.

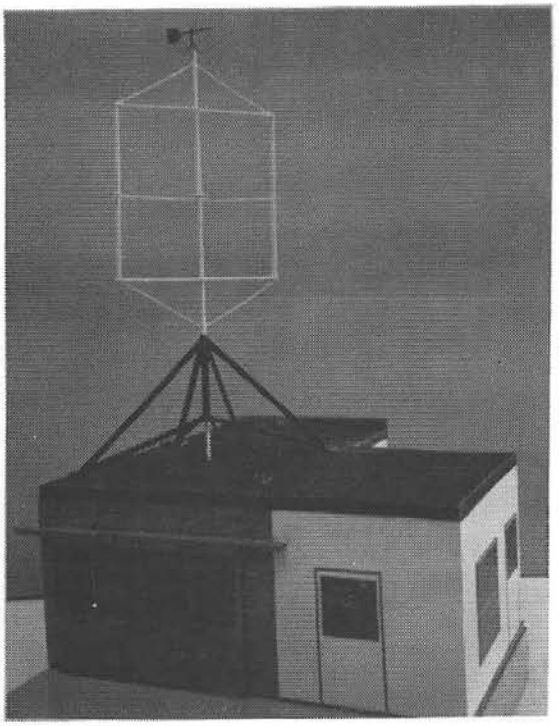

FIGURE 4. VAT TEST MODEL.

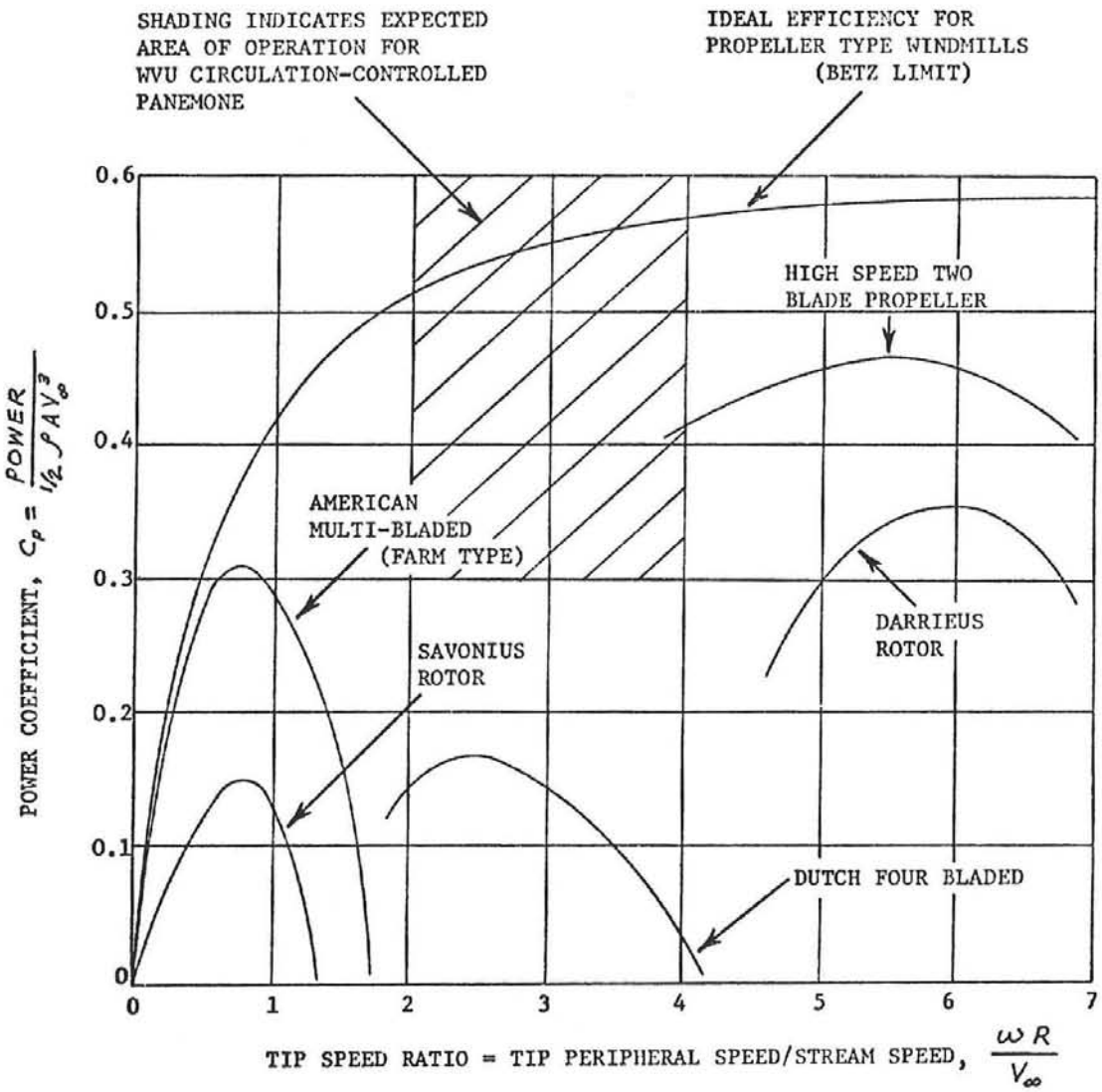

FIGURE 5. TYPICAL PERFORMANCE OF WIND POWER MACHINES.

(FROM WILSON, R. E. AND LISSAMAN, P. B. S., "APPLIED AERODYNAMICS OF WIND POWER MACHINES," OREGON STATE UNIVERSITY, JULY, 1974.)

OUTDOOR TEST MODEL VS. WIND TUNNEL MODEL

ADVANTAGES - OUTDOOR MODEL

- NO TUNNEL BLOCKAGE EFFECTS
- REDUCES REYNOLDS NUMBER EFFECTS
- MORE ACCURATE TORQUE MEASUREMENTS
- OBTAIN MULTI-PURPOSE TEST MODEL
- GAIN OPERATIONAL EXPERIENCE
- ALLOW COMPONENT DEVELOPMENT

DISADVANTAGES - OUTDOOR MODEL

- WIND VARIATIONS
- HIGHER COSTS

FIGURE 6. OUTDOOR TEST MODEL VS. WIND TUNNEL MODEL TEST RATIONALE.

V.A.T. TEST PROGRAM

COMPARISON OF TESTS WITH BLADES OF:

- 0015 AIRFOILS
- CIRCULATION CONTROLLED AIRFOILS

TEST SEQUENCE

- CONSTANT ANGLE OPERATION
- BLADE ARTICULATION ADDED
- BLADE MODIFICATIONS

FIGURE 7. TEST MODEL TEST PROGRAM.

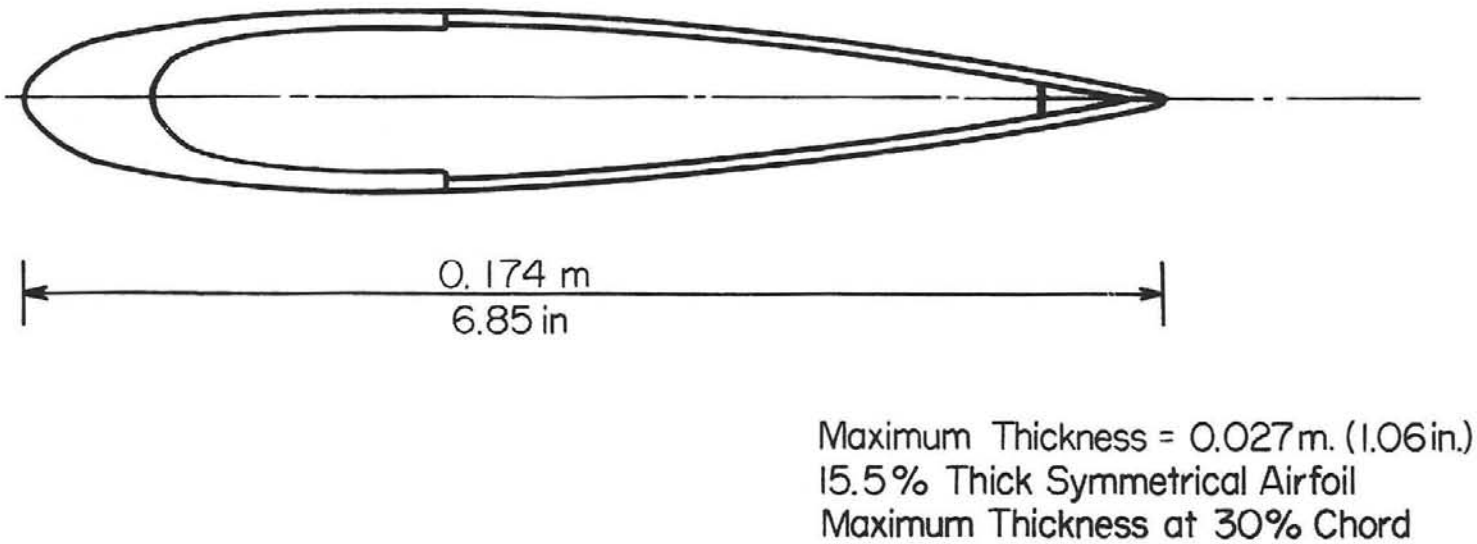

FIGURE 8. SYMMETRICAL TEST MODEL AIRFOIL CROSS SECTION.

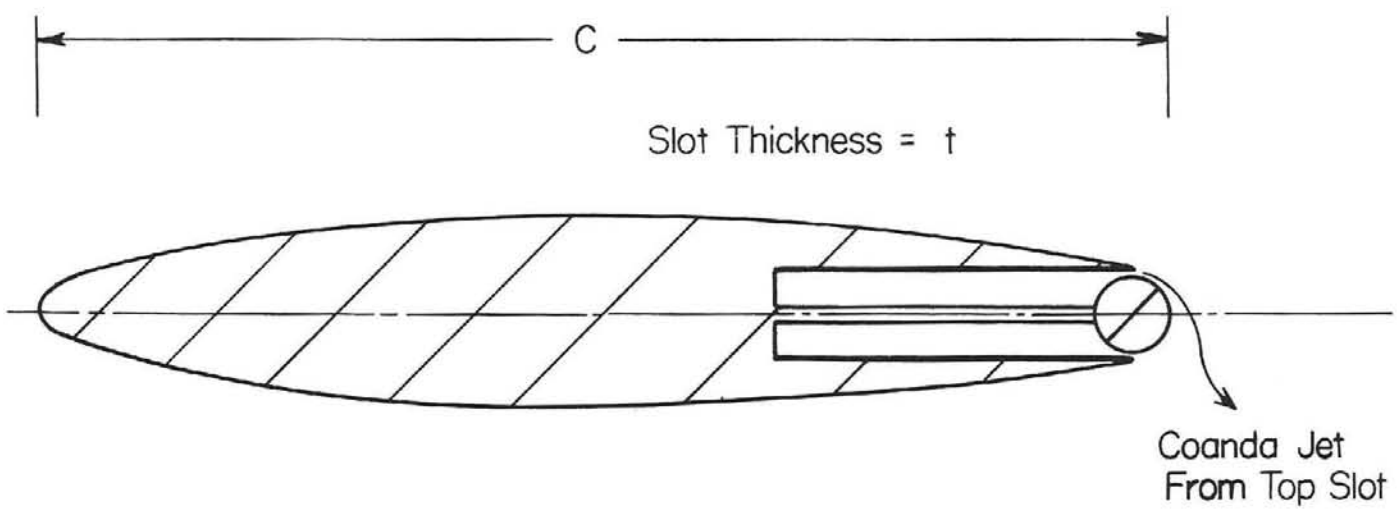

FIGURE 9. CIRCULATION CONTROLLED TEST MODEL AIRFOIL CROSS SECTION.

V.A.T. INSTRUMENTATION/CONTROL SYSTEM

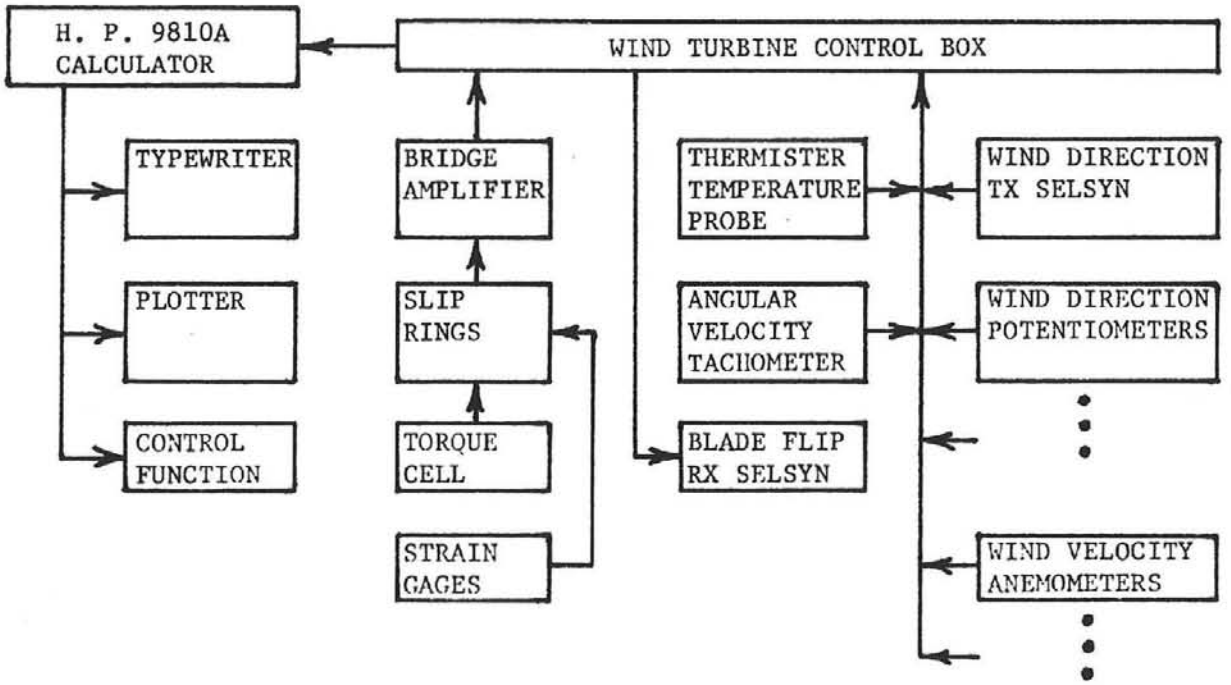

FIGURE 10. TEST MODEL INSTRUMENTATION/CONTROL SYSTEM.

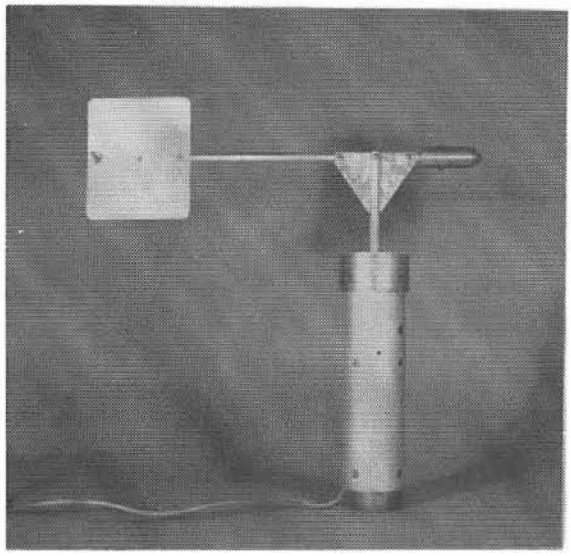

FIGURE 11. WIND DIRECTION TRANSMITTING SELSYN.

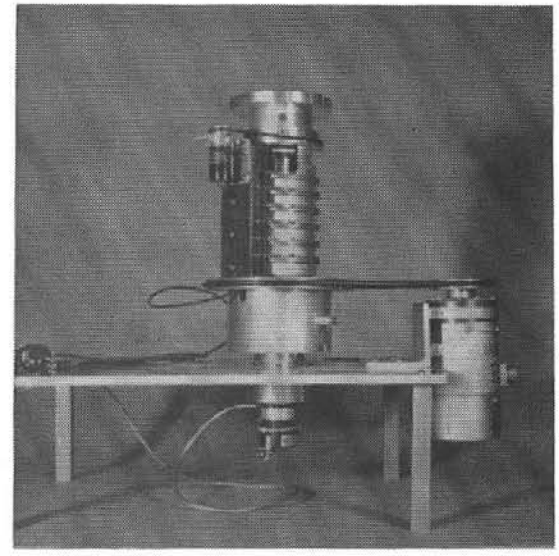

FIGURE 12. SLIP RING ASSEMBLY.

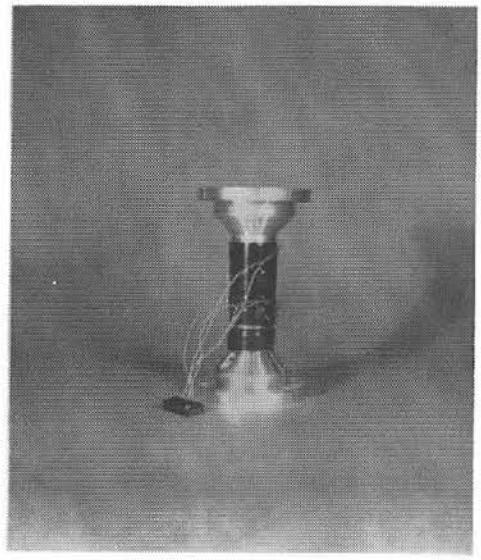

FIGURE 13. TORQUE GAGE.

FIGURE 14. DATA ACQUISITION/REDUCTION SYSTEM.

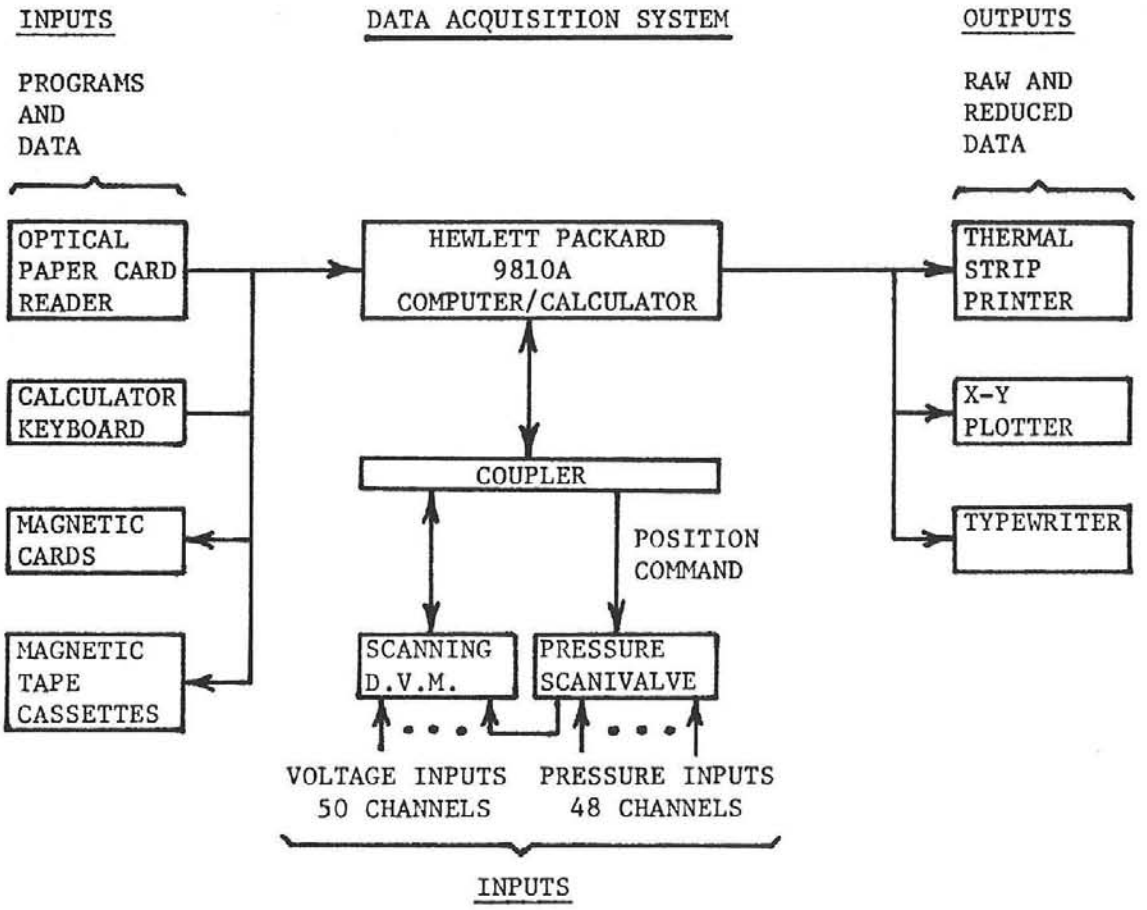

FIGURE 15. DATA ACQUISITION SYSTEM SCHEMATIC .

FIGURE 16. TEST MODEL ROTOR.

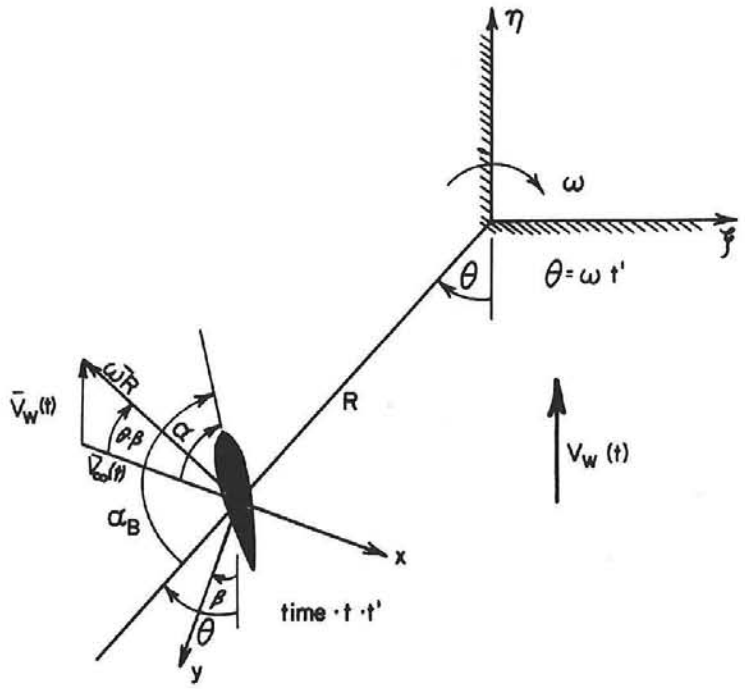

FIGURE 17. COORDINATE SYSTEM.

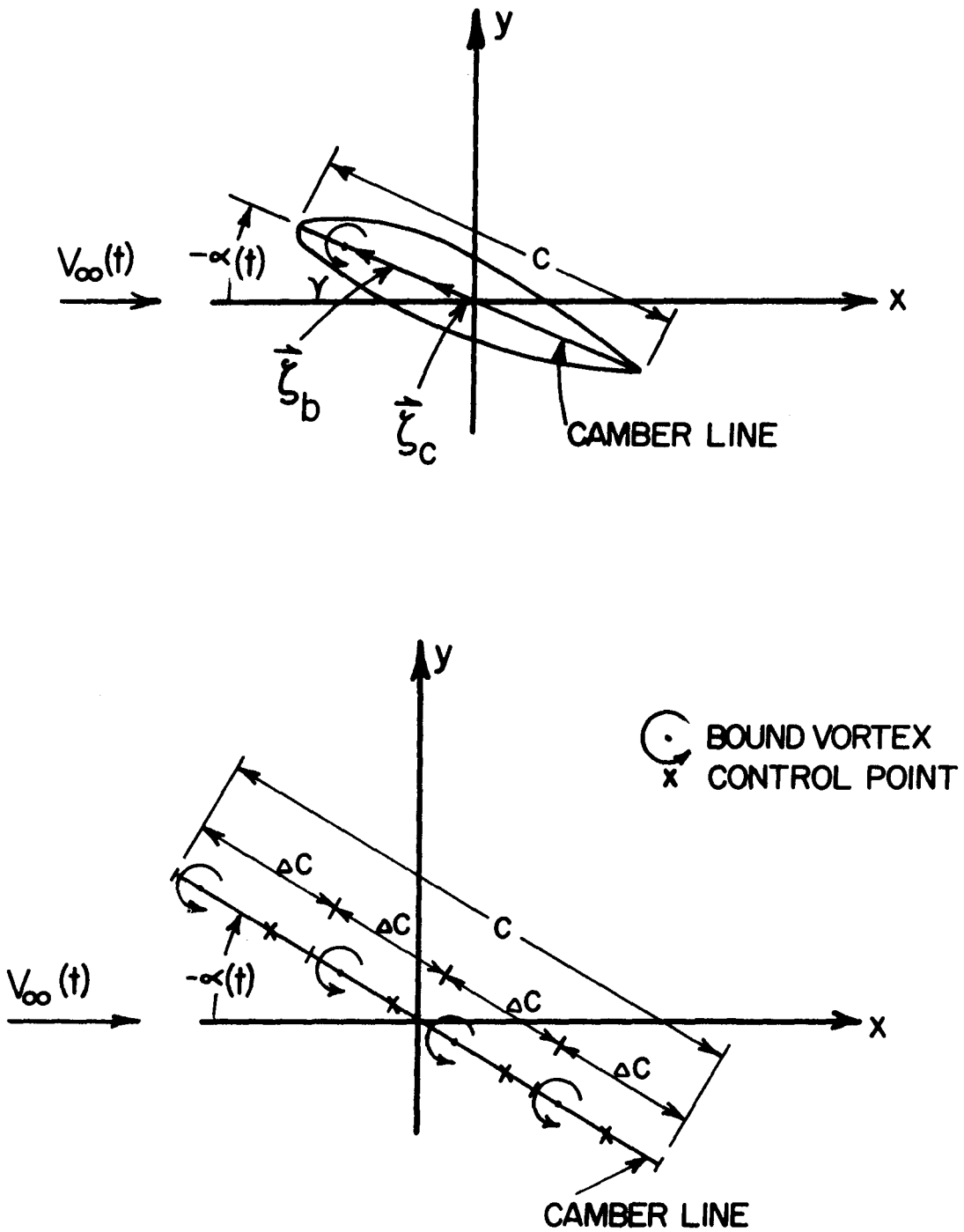

FIGURE 18. POSITION VECTORS OF BOUND VORTEX AND CONTROL POINT (TOP) AND FOUR VORTEX COMPUTATIONAL MODEL (BOTTOM).

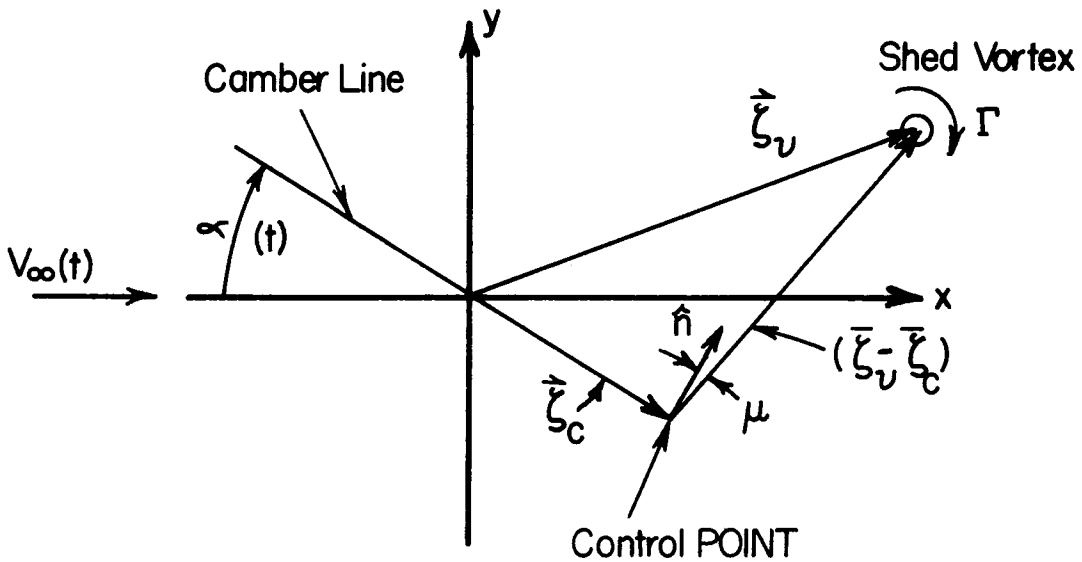

FIGURE 19. POSITION VECTORS OF SHED VORTEX AND CONTROL POINTS.

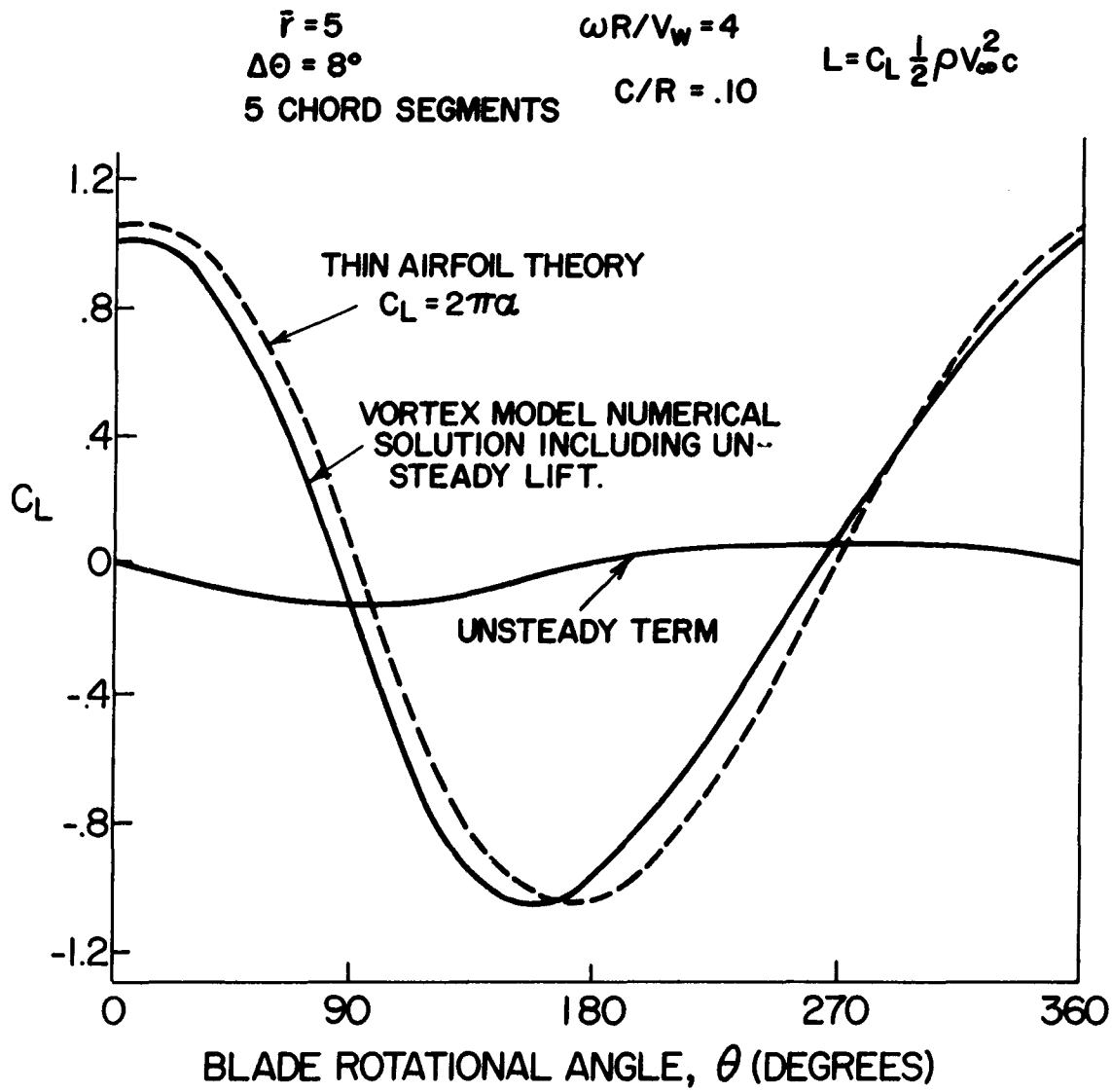

FIGURE 20. CALCULATED LIFT FROM THIN AIRFOIL THEORY AND VORTEX MODEL NUMERICAL SOLUTION.

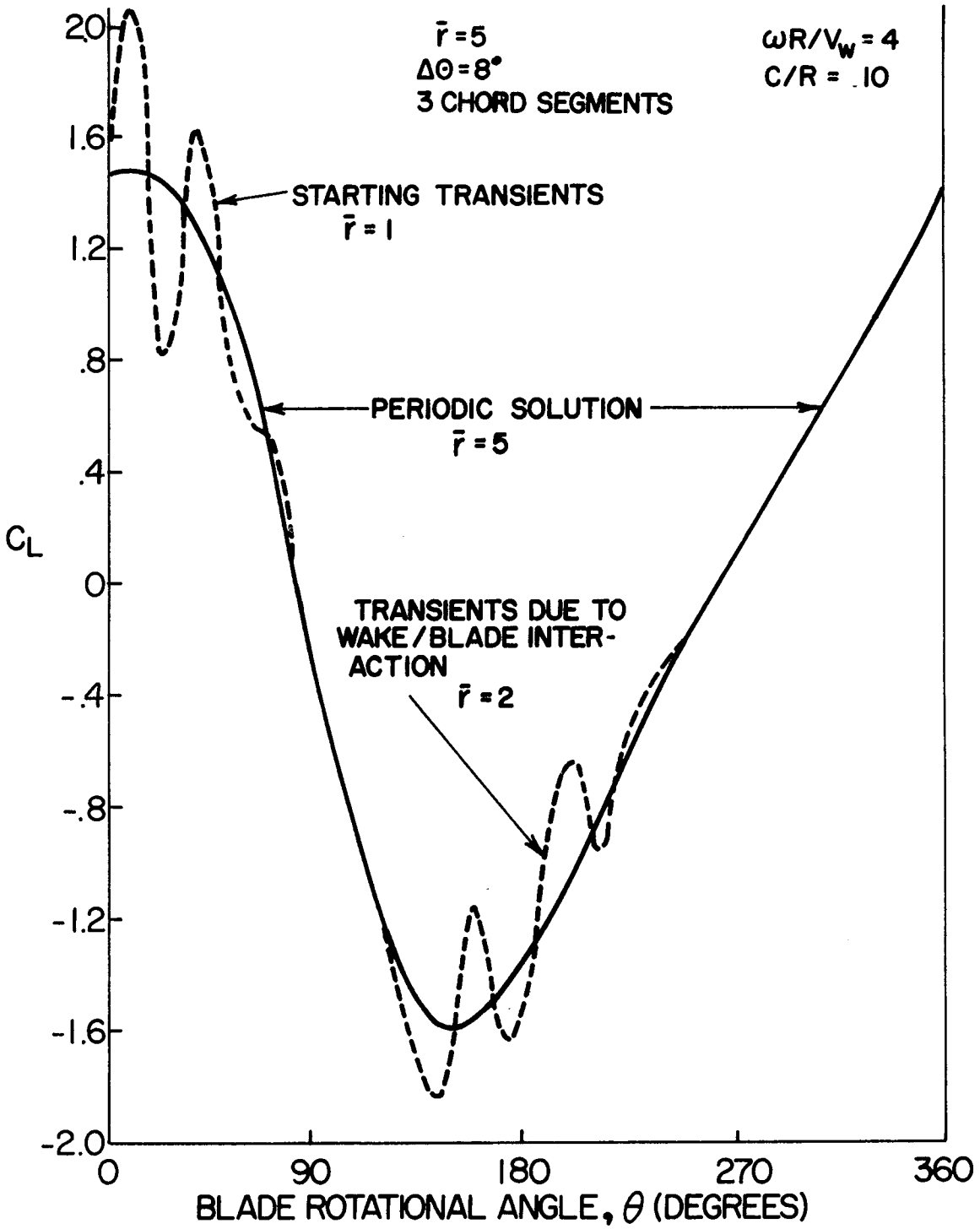

FIGURE 21. C_L TRANSIENTS AND PERIODIC SOLUTION.

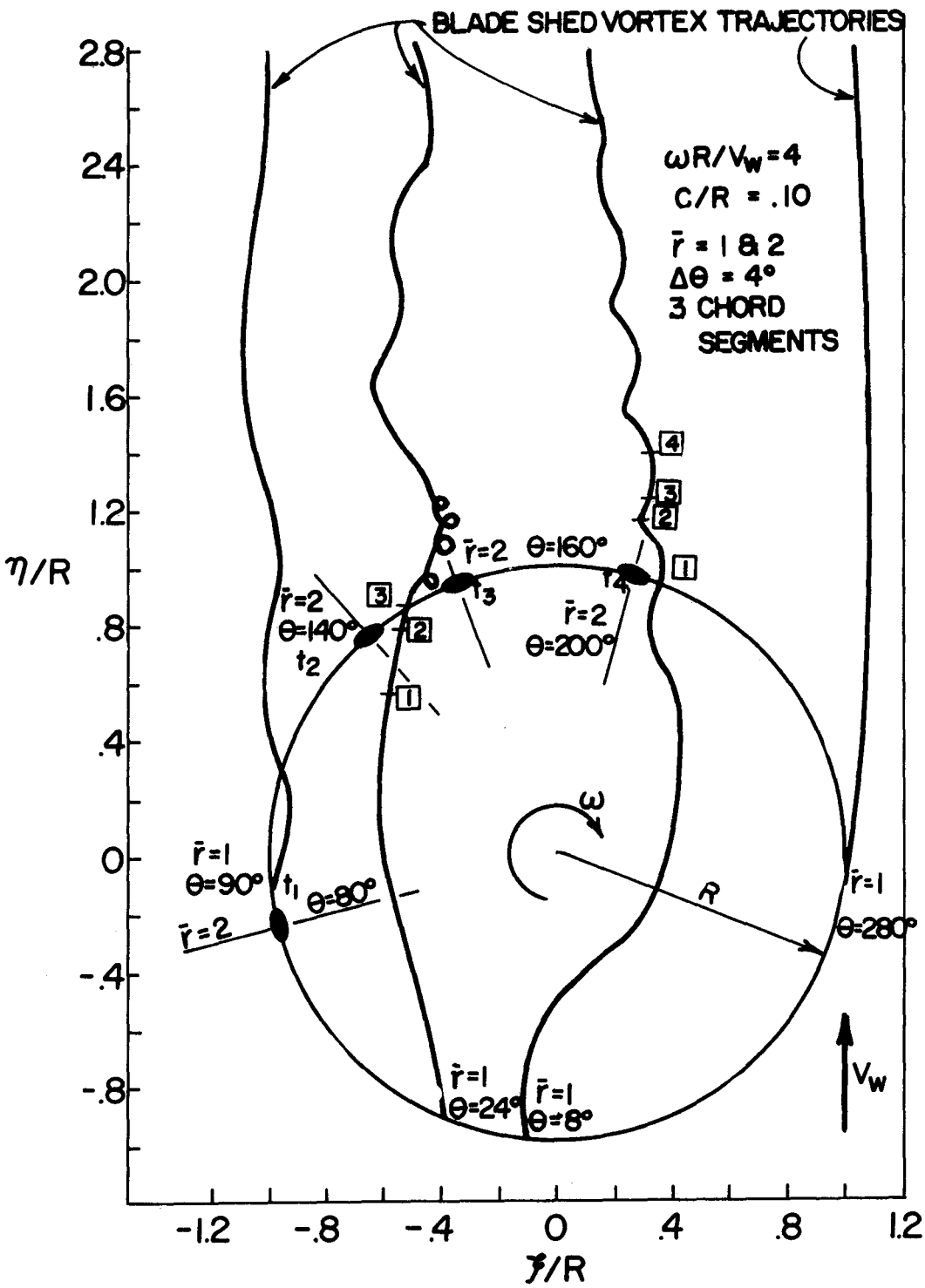

FIGURE 22. THE TRANSIENT WAKE.

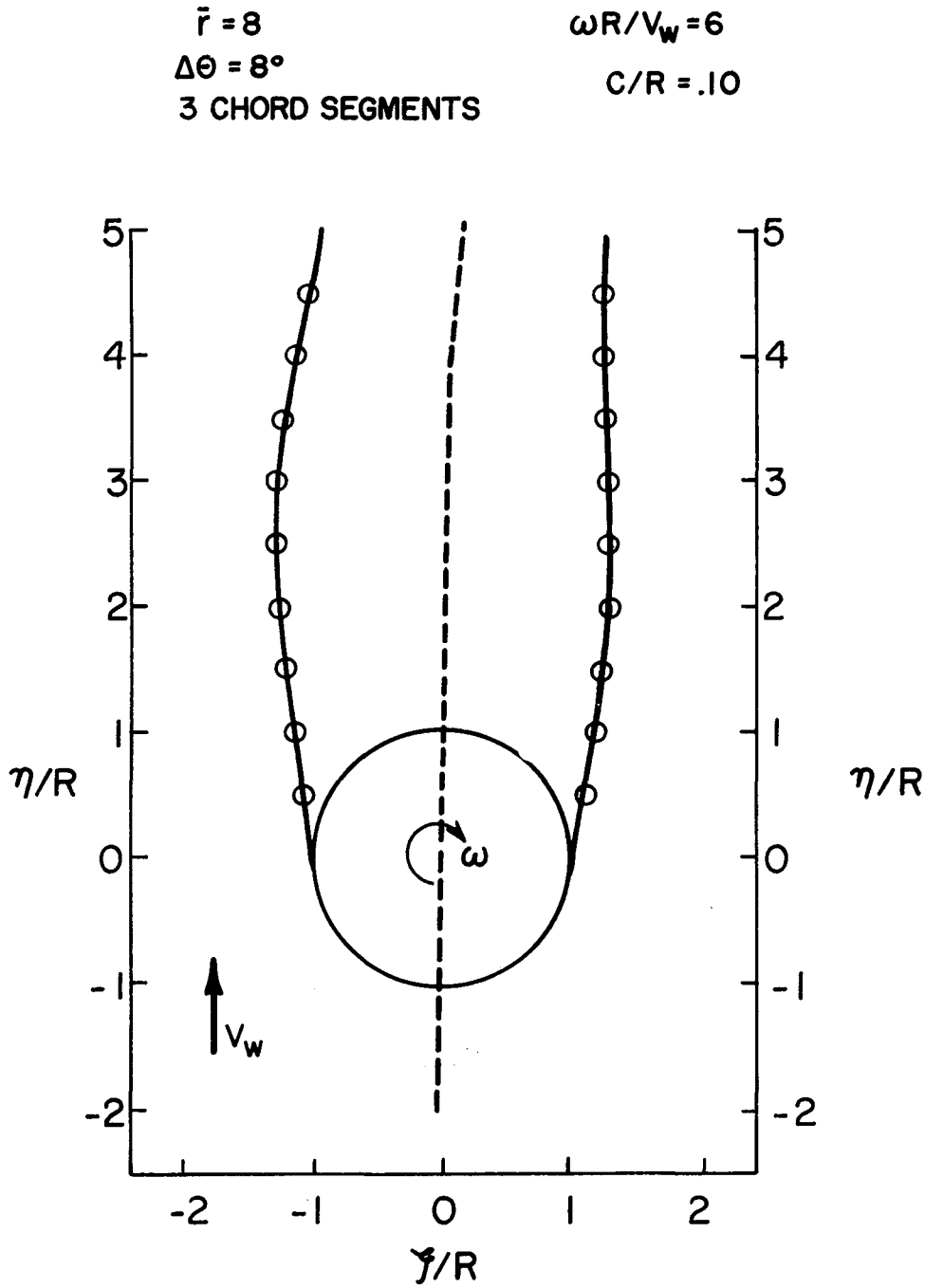

FIGURE 23. VORTEX TRAJECTORIES IN DEVELOPED WAKE.

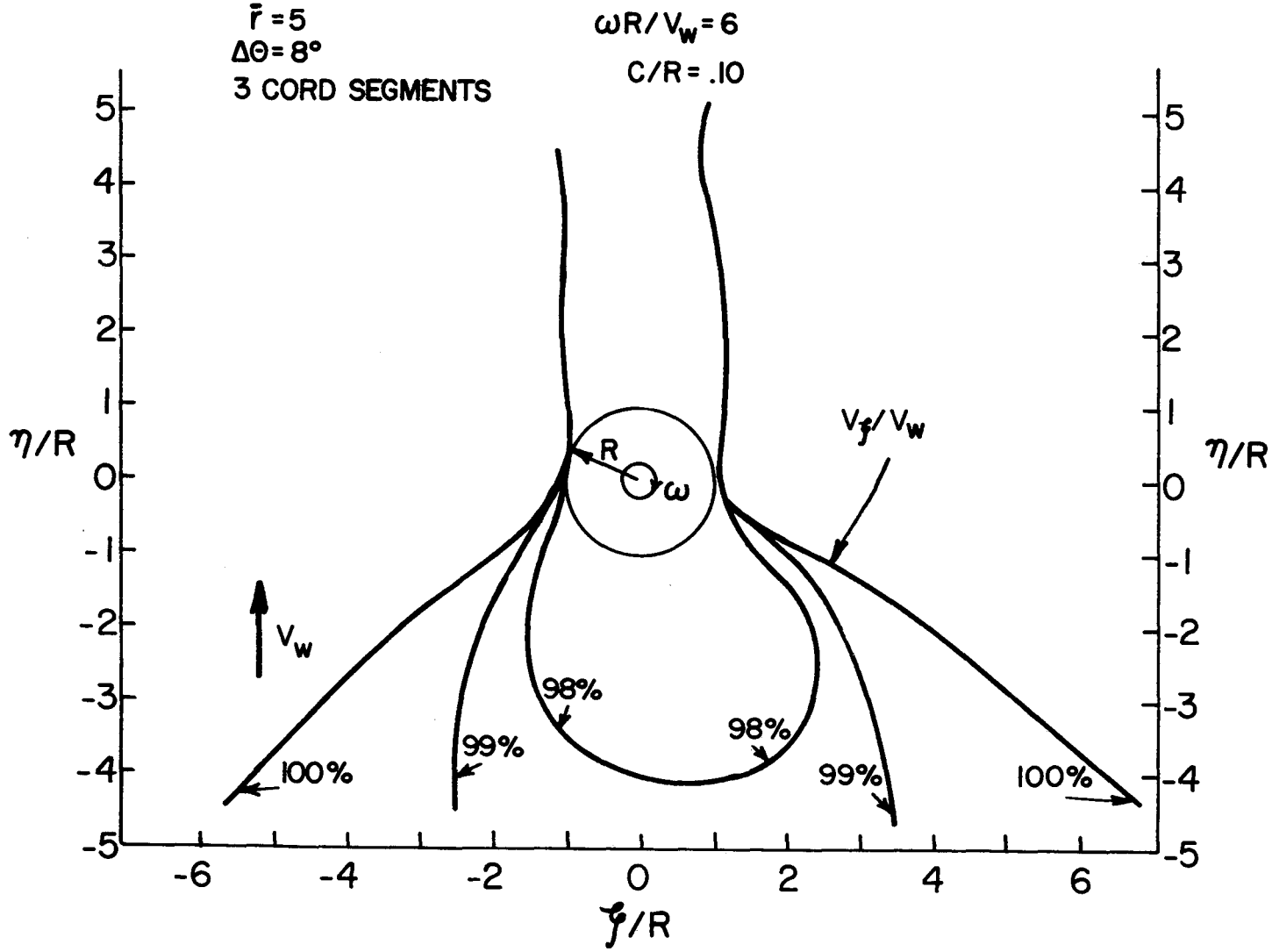

FIGURE 24. LINES OF CONSTANT VELOCITY (WINDWARD COMPONENT) ILLUSTRATING EXPANDED ZONE OF TURBINE INFLUENCE.

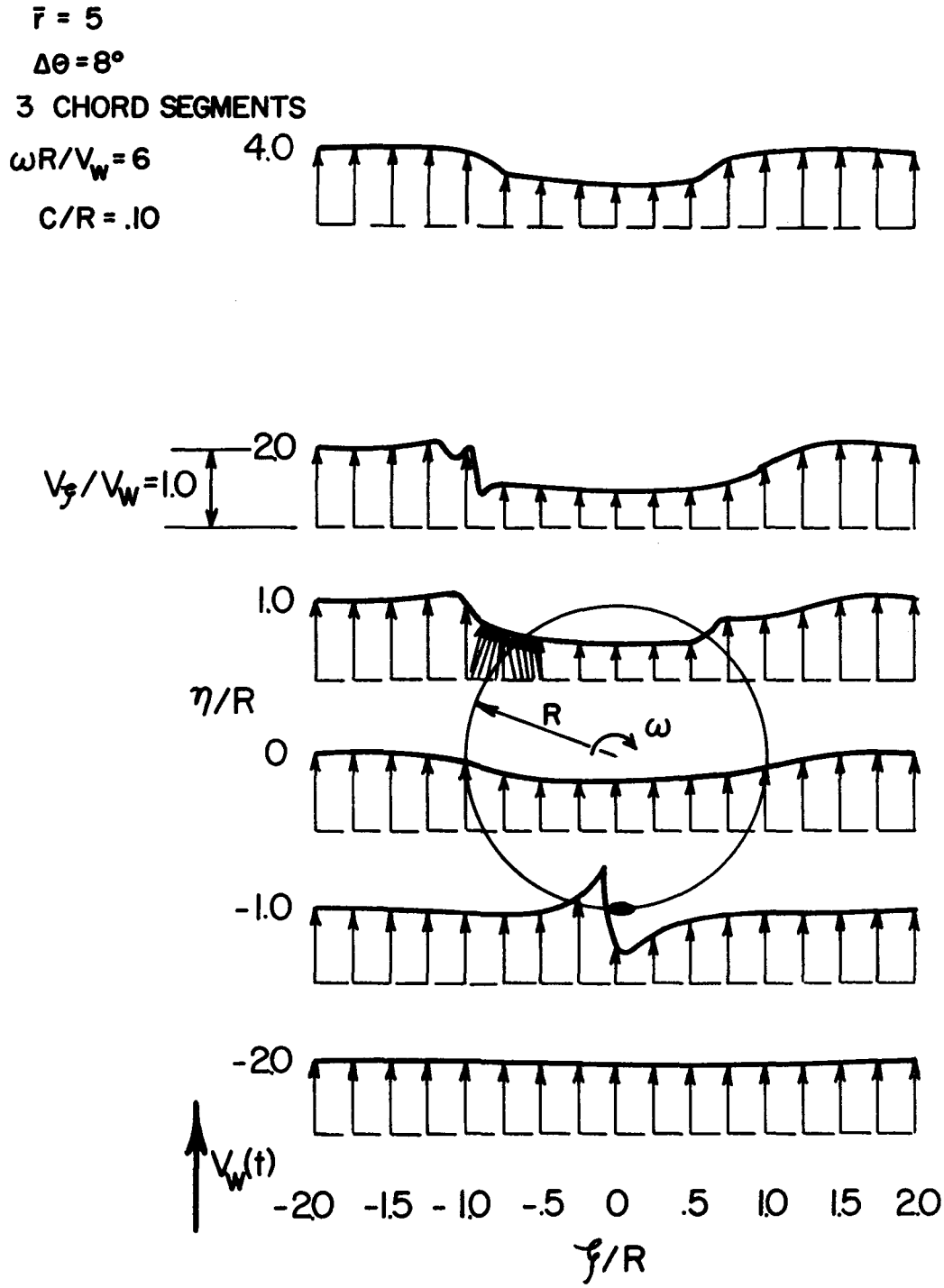

FIGURE 25. VELOCITY DEFECT IN VICINITY OF ROTATING TURBINE.

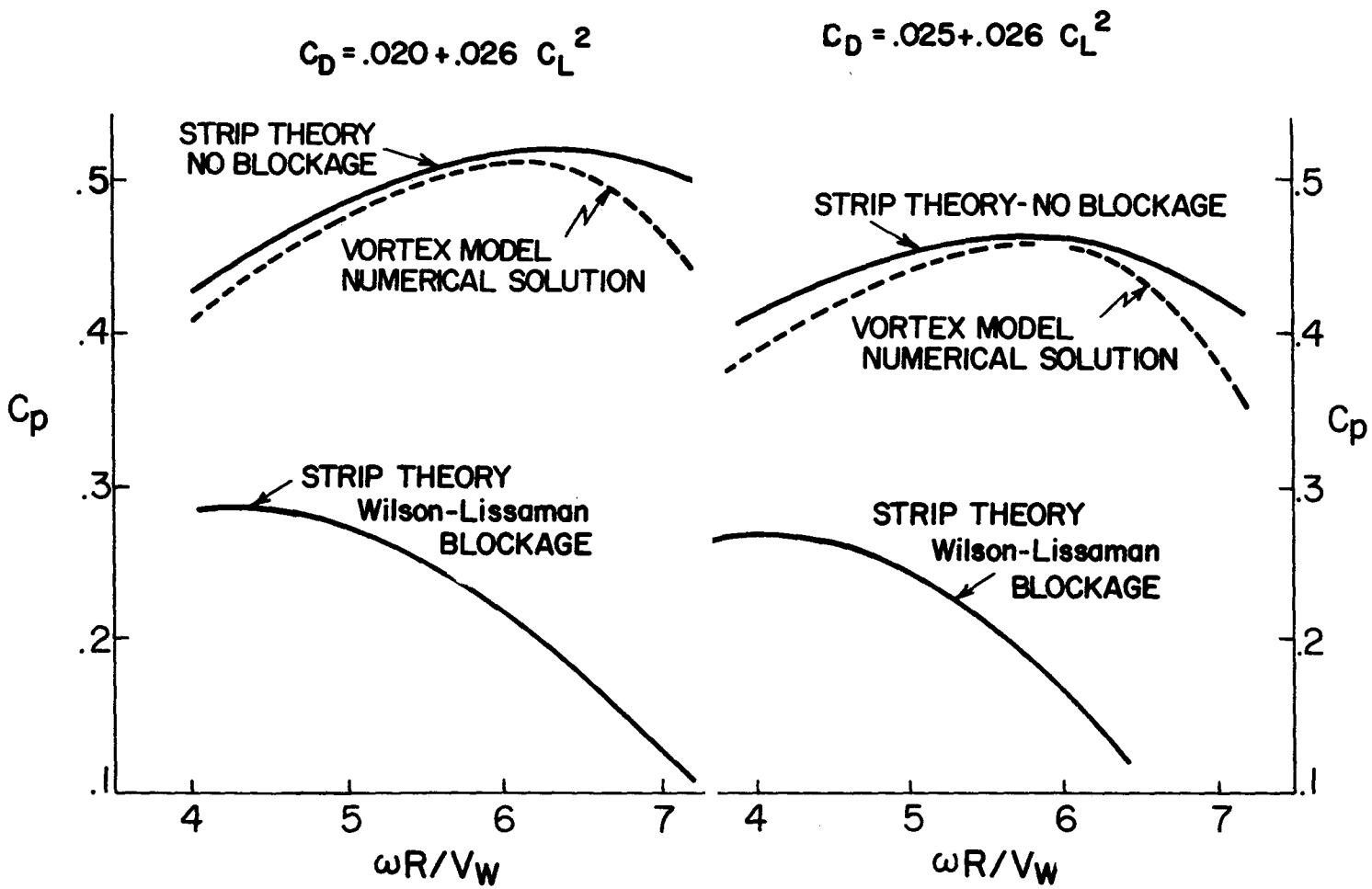

FIGURE 26. POWER COEFFICIENT FOR (ONE) STRAIGHT BLADED DARRIEUS TURBINE.

ANSWERS TO QUESTIONS

J. Strickland (Sandia Laboratories) - Do you include boundary layer or separation effects in your model?

J. Fanucci - As mentioned in the paper this approach follows the classical methods of potential flow, that is, the fluid is inviscid and irrotational. However, it should be pointed out that this analysis is intended to be applied to vertical axis turbines with straight blades which may be articulated. This feature precludes blade stall and thereby increases the efficiency of the turbine.

Bill Sullivan (Sandia Laboratories) - What hope do you see for applying vortex theories to Darrieus rotors where large angles of attack (stall) occur during operation?

J. Fanucci - The phenomenon of blade stall, coupled with nonsteady effects is a problem that challenges the best aerodynamicists. Of course, there is presently ongoing research in related areas, but from what I have seen the advances made require very difficult formulations and are time consuming. I personally would rather consider a configuration which does not stall, and thereby side-step the problem.

Ben Blackwell (Sandia Laboratories) - Do you have a "feel" for what is going to happen to drag on your circulation controlled rotor?

R. Walters - Yes, it's going to be higher than the drag on a regular airfoil. Exact values are dependent on the shape used and the blowing coefficient. The large increase in lift obtainable has been shown in our calculations to date to be the dominant factor (over increased drag). One of the major purposes of the project is to determine if the increased complexity of the system is worthwhile in terms of the performance gained.

R. Hollrock (Kaman) - What is the ratio of the CCR air compressor H. P. required with respect to wind turbine power output?

R. Walters - Computer performance calculations obtained thus far have not been programmed to print out the power required for the circulation control system as a separate item; instead, the calculated power required is subtracted from the turbine power output. In the continuing studies this factor will be considered in evaluating the system costs.

Anonymous - In the field the wind direction can change rapidly; how does that affect your blade articulation?

R. Walters - The blade articulation can be adjusted by the electronics between the wind sensing selsyn and the control system to allow various time delays before the articulation position is changed. Thus, for small wind direction changes, the

controls will not change much. For larger changes, the positions can be changed quite rapidly, since very little mass must be moved to effect the change. Of course, the overall effect, as for any wind turbine which has a directional wind preference, would be to reduce overall efficiency somewhat.

REPORTS OF THE WORKING GROUPS

Chairman: Robert E. Wilson
Oregon State University

REPORTS OF THE WORKING GROUPS

I'd like to open the closing session at this time by expressing my thanks to Sandia for bringing us together and giving us the opportunity to exchange information on the Vertical-Axis or Darrieus or whatever we're going to call it Rotor. I might indicate one side effect of coming down here and that is learning to spell Albuquerque and sometime I'd like to see it.

I'd like to elaborate on the problem of the name, even though it doesn't have a particular answer. We've called it the Darrieus Rotor. Darrieus, of course, did his first work in 1926 and that's a little old and far away. Vertical-Axis Wind Turbine, in fact, appeared in the 1949 Popular Science, as I remember it. We addressed this problem before and called it the Aerodynamic Thresher but at least one person didn't like it--sort of a machine that eats its own vortices. Egg beater, I don't think is very good either. I think maybe some of us could come up with a better name. From my personal viewpoint, I'd like to avoid an acronym but sometimes that is not possible.

At this time we'll hear the reports of the working groups. The first report comes from Emil Kadlec and it concerns the working group associated with System Engineering and Analysis. Emil...

Thank you. The Systems Engineering and Analysis Group was composed of people who were interested in both large and small systems and were representative of industry, both large and small, and government laboratories. The group began by discussing what systems analysis means. No concise definition of systems analysis emerged; however, the general impression was that even though different techniques were used, the basic approaches were similar.

One of the questions regarded the definition of goals in analysis. One of the goals, of course, is to satisfy the market requirements for a wind turbine system. A specific market can't be defined because there are varied uses for small systems, such as pumping, and power for remote locations. There is a completely different potential market for large systems. It, therefore, seems that we will have to identify these markets more accurately before we can begin to see if the particular system we are working on meets the market needs economically.

A recommendation was made by Bob Brulle that a set of guidelines, standards and/or requirements be established. Then comparisons between different systems could be made on a direct basis. That is, we want to make sure that we address the same problems and that we have the same inputs.

There was a discussion that some effort should be initiated to identify a means of obtaining economic credit for capacity displacement. An assessment of this type of credit will be necessary to establish the economic worth of wind turbines.

After adjournment we broke into small groups for discussions of specific subjects and exchange of information.

Are there any questions concerning the systems analysis working group? ...I guess he covered the whole thing.

The next working group report is from Ben Blackwell, Sandia, on the subject of Aerodynamics. Ben...

Thank you, Bob. We had a very lively discussion group last night. At one time I counted at least 22 people that participated in the discussions and I suspect that numerous other people were coming in and out, moving from one group to another.

I'd like to summarize some of the topics that we discussed and really they were technical questions that were raised and I don't think that in the course of the two and one-half hours we were there last night that we managed to solve many of them. But we did manage to raise a number of interesting issues. One of the things that seemed to keep recurring was the aerodynamics data that are used in various computer models to predict performance and loads. We need some additional data, especially with attention to things like the hysteresis loop.

This hysteresis effect is something that increases with increasing Reynolds numbers and Professor Larson indicated that he has seen some data that really indicates substantial hysteresis effects, much more so than any of the lift and drag data that we showed from the Sandia wind tunnel tests.

One of the most difficult parameters to measure experimentally in section testing is the zero lift drag coefficient which has considerable influence on the power coefficient predictions. Effects of unsteady aerodynamics were also brought up numerous times and I think it was the consensus of the group that this was a very important issue, and we were going to have to look at it in the future. It was suggested that tests should actually be run where you cyclically pitch a two-dimensional section in a wind tunnel. Some data like this is available but I think it is quite limited; it indicates that the maximum lift coefficient can be considerably greater than what the quasi-steady value would be at that same angle of track. I suggest this effect will not substantially influence the power coefficient that one might compute but it certainly would have a drastic effect on the maximum loads that a blade would see. Three-dimensional effects are obviously very real effects in something like the curved-bladed Darrieus. It may not be quite as important with the Giromill or straight-bladed Darrieus. With three-dimensional effects on a curved blade, the centrifugal force field that the blade is operating in can have a considerable influence on the stall characteristics of the airfoil. This is an area in which very little information is known at the present time and could certainly stand some investigation in the future.

We touched on wind tunnel testing to determine performance characteristics. The applicability of conventional blockage corrections was questioned and that was again brought up this morning in some of the papers that were presented. We really don't know if they are that applicable and that is something that needs to be investigated because I'm sure there will be more and more wind tunnel-type tests of rotors and if you can't get a good handle on blockage effects you'll never be able to compare very well between free air performance and wind tunnel tests. It was suggested that some theoretical studies in this area might be very fruitful.

In the past it has been general practice to correct Reynolds numbers in wind tunnels based on the so-called turbulence factor, which is determined by measuring the drag on a sphere of particular Reynolds number. I think most people in the group felt that this was completely inadequate and unrelated to anything concerning windmills, and that that type of correction should be completely unrealistic for windmills. In fact, even though wind tunnels have considerable free stream turbulence, so does Mother Nature's wind tunnel. It is probably more realistic taking Reynolds numbers based upon the actual flow conditions and not using the turbulence factor.

Testing in open jet wind tunnels was mentioned as a possible means of reducing the blockage effects.

We touched on field testing and there is not very much we can say about that except we need to know how it should be done and how accurate it is and at this point I don't think we really know that. Certainly we at Sandia had difficulties getting performance data in free air.

Performance models were discussed and in this light what is the appropriate theoretical limit on maximum power coefficient for a Darrieus-type turbine? Is it 16/27 or is it some other magic number? Do we have some additional potential that we should be working for that is not available for horizontal-axis systems? Most people were not venturing their favorite number that should be used instead of 16/27 but I think most people agreed that 16/27 probably is not that valid for a Darrieus-type configuration. Mr. Holme

from Saab indicated that the angle of attack on the up-wind side of the blade can be considerably different from the angle of attack on the down-wind side of the blade because of interference effects. He cited a particular case where this difference in angle of attack might be as high as 5°, I believe he said. This is certainly something that will have to be looked at in the future on some of the more sophisticated performance models.

Last, there were a large number of general questions relating to small systems, some of which had answers and some of which did not. There were a number of people in the group that were interested in small systems. I don't think we were able to answer all those questions because there wasn't that much expertise in the group from people who had actually built small systems and operated them.

That pretty well summarizes the activities. I'd like to thank you people who did participate in the group. I think it was a very worthwhile thing to do and I appreciate the participants taking their time to sit and chew the fat about the subject.

Any questions concerning the Aerodynamic Working Group? Yes...

Norman Ham - I'd like to make a comment. Maybe Ben mentioned it but if so I didn't hear it. With regard to the unsteady airfoil characteristics, of course, the stall is delayed as well as the lift increased. Then when the stall does occur, of course, you get large twisting moments, perhaps of the order of three or four times as much as static twisting moments, when the stall does finally occur dynamically.

Any other questions or comments? Thank you.

The next working group report concerns Structural Design by Bob Reuter, Sandia.

Approximately 20 people attended this working group. We ran a pretty loose session and tried to categorize the comments under the headings of those related to the present program and those related to what we ought to be doing in the future. In addition, there were general comments and comments specifically directed toward the design of the 17-meter system. I'll try to go through some of the highlights of the session and some of the topics that were discussed. I guess we had a typical cross section, about what you'd expect in a group of 20 people, although I think most of the comments came from people in the manufacturing or production side of the house.

One gentleman made the comment that he thought the program was moving too fast and as a result was bypassing a number of important concepts. I'm not sure he would have made that comment had we had the session following the program this morning. I think it's clear enough that there are a number of innovative concepts being funded, even more than what we heard discussed this morning. There were others that felt that the program was just about right.

Another comment was made that certain missions were being ignored. What we're talking about here are possibly the small turbines, the low-rpm applications and maybe some problems associated with the remote site installations, erection and transportation. The suggestion was made that some collapsible blades be designed that could be rolled up and backpacked into remote regions. I don't know off-hand if projects of this nature are being funded at the present time but I do know that there is proposal activity in this area.

Another request was made to the effect that we should begin to think about ways of quantifying the risks that are taken when we begin to remove the conservatism that is built into many of these systems. I guess that is a matter of establishing reliability. That may, in fact, be what happens over the next several years as we satisfy the four areas that are characterized by these four working groups. The structural people have to recognize that the aeronautical engineers are interested in their problems, the systems people are interested in their problems and likewise the electrical with

input/output. I think as all of these systems are operating and results come in and there are many successes beginning to accumulate, some of the conservatism will be more understood and removed in an educated way.

There was some pretty strong feeling about conducting new blade design at a number of locations rather than at just one location. I think we settled that issue by generalizing the requirement that design occur at one place by suggesting that just one place act as a clearing house to assemble all of the design ideas. I don't think we really ever intended to restrict our approach to the blade design to that which would take care of all the design details and go out to industry only for fabrication purposes.

I think we all recognize the possible significance of one of the things that came out of Professor Ham's contribution and that is the apparent unimportance of mass balancing the blades. This opens up a lot of possibilities for blade design, particularly inexpensive blade design, and it may be a fairly exciting prospect. It may also appear on the ledger as another advantage to the curved-bladed Darrieus rotor, compared to the horizontal-axis systems.

I'll cover two other comments that were made that I think are probably worthwhile. The question was raised as to what the material property limits are with regard to blade design. I don't think that's really the way we ought to be looking at it. I think a good counter example is a flywheel. You're trying to store a lot of energy in a flywheel; the faster you spin it the more energy you are going to store, so it becomes a material property limiting system. Eventually it's going to break so you can spin it just so fast before it breaks. A turbine isn't quite the same thing. We have an optimum operating speed, and if we have a blade that can successfully operate at that speed, it's really not a materials problem any more but more of a cost problem.

The other comment that was made is more along the line of a request. Whenever dollar figures are quoted for blades, blade fabrication, design or whatever (not restricted to blades either, it can be for things like towers,

tie-down systems, or any of the components), whoever is doing the figure quoting should be careful to distinguish between recurring costs and those which are not recurring. An example is figures that were thrown out in the last couple of days on blade costs, say $1000 per blade. It is not clear to people that want to get involved in the development of these blades exactly what the significance of that figure is. It was a plea to everyone to be a little more specific about some of the dollar cost figures that are being used.

The other specific comments were related to the design of the 17-m system, and really don't need to be gone into as they were more along the lines of a 1-to-1 question/answer response. They had to do with the tower, blades, and tie-down, essentially.

That about covers it; any questions or comments?

Thank you, Bob.

We next hear from the Electrical Systems Working Group and Tony Veneruso, Sandia.

There were 29 people who participated in this working group. It was very encouraging to see a number of representatives from electrical utilities such as Bonneville, Hydro Quebec, the Bureau of Reclamation, and our own Public Service Company as well as many others who are active in wind turbine technology development and commercialization. Comments from this session fell into four categories: the need for communication and for coordination, critique of Sandia's vertical-axis wind turbine effort and the need for visibility of this turbine development. The remarks made in each of these categories will now be summarized.

There appear to be many alternatives to wind energy conversion systems both in terms of hardware and policy for applications from small farm and rural systems to large utilities. The recommendation was made that some

coordinating body, consisting perhaps of EPRI and ERDA personnel, could provide both technical direction and policy coordination between the utilities and the wind turbine development activities taking place through ERDA.

Concerning communication, the critique was made that many of the individuals involved did not know exactly what was being developed and did not have access to the work previously published.

It was recommended that vertical-axis turbines should be included in a utility demonstration. Further the utility representatives stated that they have offered manpower, some capital, time and facilities to work together with appropriate personnel to install wind energy systems and obtain operational experience. A pumped hydro application was mentioned which would use a vertical axis turbine in a conservative system to obtain the desired confidence and experience. In terms of visibility, I wish to mention that the ERDA demonstration for the vertical-axis turbine has been installed on the Mall in Washington, DC, near the Capitol. It was the first exhibit in operation on the Mall and it gives the vertical-axis wind turbine excellent visibility.

Without exception, the participants found Sandia's effort to be a pragmatic and expedient approach to the electrical power system design. However, a few individuals wished to see more development along the lines of a variable speed approach which uses electronic switching techniques or special generators to increase the kWh output capability of a specific wind turbines. On the other hand, there were comments cautioning that while many electrical techniques may be explored, users, such as utility companies, require a straightforward approach to the electrical system design for them to expediently commercialize wind energy conversion systems. The recommendation was made to utilize the work that ERDA has already funded by making use of appropriate hardware from these programs to explore cost-efficient electrical power conversion for wind turbines. Another comment made by many participants was that electrical engineers need straightforward functional data concerning the vertical-axis wind turbine to permit them to participate in its development and commercialization. The recommendation was made for simple,

functionally descriptive information as to how this machine works, and perhaps preprints of papers presented in the workshop.

Finally, many participants indicated their approval of the workshop but wished the electrical group had more opportunity to meet one another early in the workshop schedule. The recommendation was made to have an early introductory workshop session and perhaps concurrent sessions in which diverse, independent topics are run concurrently; for example, the aerodynamics session concurrent with electrical power. I wish to thank the workshop participants for their critiques and recommendations.

Thank you Tony. We have another speaker before Lou Divone makes the closing remarks. Olle Ljungstrom has been intimately involved with Sweden's wind energy program and would like to say a few words.

Thank you, Mr. Chairman. Before Lou Divone closes this wonderful workshop I would like to say, on behalf of the visitors from abroad, some words of sincere thanks for inviting us to be here and that goes for the Europeans, the Danish, the Dutch and the Swedish; it also goes for the Canadians who are closer by. I just think that this workshop has been great, as most of the previous ones have been, and it has given us a lot of information to use in finding the most cost-effective wind machines. We now have, as most of you certainly know, the IEA, the International Energy Agency, which has set up the WEWP, which is the Wind Energy Working Party. Lou is on that party and I will be on the technical side of it. Dr. Templin and Dr. Pelser of Holland and Maribo Pedersen, who is here, are also on that working party. So we are really getting together. We are really getting going fast, as we saw in the movie, the experiments are going faster all the time and we are working on Concorde over the Atlantic, I would say also in wind energy. That means on Monday you are going to be able to join us even faster after the opening of the across-the-Atlantic supersonic flights. Thank you very much. My thanks go to both the sponsor, ERDA, of course, and the host Sandia. Thank you very much.

Thank you, Olle. The closing remarks will now be given to us by Lou Divone. We all know Lou as our fearless leader.

CHAIRMAN'S CLOSING STATEMENT

Louis V. Divone

I'm an old aeronautical engineer so I think I'll wait about 9 to 18 months before I ride the SST. If you look at the history of aircraft development, the time constant between the birth problems and the fatigue problems keeps getting narrower, so I'm going to study this quite carefully. Seriously... Bob Reuter mentioned that his working group had a one and one-half hour attention span; I don't think that's right. I think it's more like a 56-hour attention span, which is pretty darn good for any collection of human beings. Let me make a couple of brief remarks, although I gather since we're way ahead of schedule I actually have an hour and a half...it will be about three minutes.

I made some comments Tuesday about the fact that the Vertical-Axis Wind Turbine, be it the Darrieus, curved Darrieus, or the articulated system, would have to do a lot better than the conventional systems to really be worth major development programs to end up being viable. I also went through a long list of deterrents to wind energy and all the problems they were going to face. Actually I suppose I was following the old management technique and that is when things are a complete disaster one goes around being very optimistic. Otherwise people get very discouraged and that sort of thing. When things are going quite well, one wants to be a pessimist because otherwise people tend to relax and so forth. I may have been doing a little bit of that. In fact, I want to finish on several up-beat notes.

First, I want to state how really optimistic and how encouraged I am on the vertical-axis systems. I think that the vertical-axis machines represent a very real and a very possible significant advance over the conventional systems. I frankly see a very high potential for these systems and we at ERDA intend to pursue them as rapidly and with whatever support we can. I am also very particularly impressed with the Canadian work, both at NRC and at DAF. They really deserve to be congratulated for the work that is going on there.

I do want to throw in a note of caution though after putting in all of these optimistic words because one always thinks the things one knows less about look better because one hasn't run into the surprising sledgehammer of the unknown problem. I have always felt that no one is really an engineer until he has sat down and stared at the wreckage of his device and seen the light slowly dawn. I think we have to recognize that we are going to run into our own sources of wreckage in the course of this program. But I frankly have a great deal of confidence that we are going to thread our way through and that, in fact, these machines are going to end up being developed, being used, and being successful in a commercial sense.

I would like to make a side comment based on one of the summaries of the working groups regarding knowing what is going on and knowing people. We have as usual been somewhat derelict in getting as much information out as fast as we should. Our Technology Information Center at Oak Ridge and our computer list are slowly beginning to function. I realize some people don't get anything and other people get three copies, one with their set of initials and one with their full name; the computer can't tell that they are the same person. In any event, if there is anyone who is not on our distribution list, we are going to be picking up the list of attendees here and adding that to our distribution list and if the machine works right it will sort things out and you won't get more than one copy. But if you signed your name differently here than at the June workshop, you will be getting two copies of the same things. We will be sending out notifications of workshops, notifications of RFPs, lists of reports that are now available through TIC at Oak Ridge, etc. Hopefully, this will tend to help the situation.

To finish on two other kinds of up-beat notes--being out of the office for a couple of days, kind of an R&R here in Albuquerque, puts me out of touch with the strange world in Washington. For those of you who didn't read the newspaper, I'd like to quote a couple of lines from a news article today. Headline: "House Ups Solar Energy Study Funds...Solar energy got its first big boost of the year Wednesday when the House upped funding authorization for that program by 116 million dollars (that's the delta). The amendment to hike this funding was by Rep. Harold Runnels, Democrat of New Mexico,

who took the floor to urge passage, and he was also backed by Rep. Manuel Lujan, Jr., Republican of New Mexico, who also supported it." It was also supported by congressmen from Oregon and Vermont and some other places. The fact that it was put forth by Congressman Runnels, who comes from not too far from here, is perhaps a result of his having seen the Sandia machine on the way to the airport. This is a significant raise as the budget before that was a little over $2 million. How this gets divided up between the many areas of solar, ocean thermal and wind, of course, I don't know. I think the other thing one has to recognize is, if you understand the Byzantine networks of the way you finally end up with your budget in Washington, that you have to go through about six of these cycles. First OMB, and then authorization bills, and then appropriation bills and congressional committees, etc. We tend to actually just proceed on our own way until the final budget is out, and there are at least three more steps, so this can still cycle quite a bit up and down. I'm not really saying anything about this number. We may or may not end up with our appropriate fraction of it. But it is nice to know that there are a lot of people around the country who feel the same way that we do.

I'll read one last sentence that I thought was really pretty good and this is Congressman Runnels. First, he had reminded his colleagues that he had made his living from the oil industry for the past 35 years but felt that it was time to move quickly on solar energy. "It took us 60 years to deplete our timber supplies, 60 years to go through the coal and 60 years to use up much of our oil and gas. The time has now come to harness the sun to provide for our energy needs." So, as I said, it is nice to know that there are other people who are supporting us.

The last comment I'd like to make is, as I also noted in my little talk Thursday on deterrents, that there are many deterrents that are institutional and not technical in nature. I was pleased to find out from Fred Malver of Honeywell that one of our real concerns in any area that might be a serious deterrent may, in fact, not only <u>not</u> be a deterrent but maybe we're going to get support from that area too. He showed me a bumper sticker that says "Bring Back Windmills" and it's from an Audubon Society

energy message. I'll check with Fred and find out how we can get vast quantities of these things for our, hopefully, small economy cars.

Let me finish up by saying first that I want to thank Sandia for doing an excellent job of going through the million and one details of setting up the conference and then running it. It was nice to be able to sit in the back and watch it all function. I want to thank all of those who presented papers. There were some very excellent papers and I've been sitting in the back scratching my head and taking notes and trying to think about some of the points made. I want to very much thank the foreign visitors who came from quite a long distance to be with us and we wish to invite them back again and hope they can make it to our next workshops.

Lastly, I want to give my personal thanks to all of you for coming here. We will be holding more of these workshops and I hope to see all of you again at some of the others. Thank you.

Are there any questions or comments?

Question

Some of us, in the course of the meeting, have been asked by others for copies of reports and things that we have issued; is there any problem with our sending our reports informally or should they go through the normal distribution channels of ERDA?

Answer

It can be done; however, there is a problem and it is just the magnitude of the task. I think that any professional people who are trying to work on problems that are related can pass drafts and material back and forth. We do have a problem in that we can't get our machinery working and, to be perfectly frank, we are trying to maintain high standards. One of the problems on wind energy, as you are well aware, is that in the past there have been many reports written from all types of sources, some of which didn't necessarily meet the standards that I think we need, from our viewpoint, in federally funded programs. So we are not distributing reports

until we have gone through drafts, had them reviewed by other experts, ourselves, or whatever. Then we get them into TIC and reprint them in quantity and anyone can get them. They cost anywhere from a couple of bucks to five bucks each depending on the page count. That is really the main information dissemination technique. As I said, we have been a bit behind in getting these lists of reports that are now available out to the distribution lists and that has been because of the workload and how things have been flowing and trying to get the machinery set up.

Question (Evan Lefever)

In November I was part of a workshop sponsored by the state government of Pennsylvania and I would like to have a comment from Lou Divone concerning what I heard there. We had an ERDA representative at that state meeting in Harrisburg on Pioneers of Solar Energy. The ERDA representative, I'm sorry I don't know his name, mentioned that they could not efficiently handle any more money than what they were getting. This comment was made last November. Does that sound realistic today for wind or was that only solar?

Answer

All program managers and branch chiefs always could use more money; that's a given, but the way the government functions is that each program lays out its plans and asks for the amount of money it thinks it can use. It goes through a whole series of management reviews regarding everything from the total budget and worries about inflation down to the relative priorities between areas and obviously many programs are planned more optimistically than others, and conversely some would have plans in more depth than some others. Basically then, a set of objectives and funding estimates are achieved which reflect the relative priorities and needs as viewed by the agency and the executive branch. Then if someone asks me if I could use twice as much money, I must say I really can't because one has plans laid out only at that level and to suddenly attempt to do a step function with no plans is very difficult to respond to. You have to remember that the funds for a program for an agency come from Congress. The Congress may elect to appropriate more or less funds than the original agency request. This has been the case many times in the energy field. We would then revise our plans accordingly. I think that is what he was reflecting in his comment.

Any further questions?

Then we will adjourn the meeting and give our closing thanks to Sandia for a good time and to ERDA for supporting it all.

DISTRIBUTION:

TID-4500-R64 UC-60 (249)

Norman D. Ham
Massachusetts Institute of Technology
77 Massachusetts Avenue
Cambridge, MA 02139

L. H. J. Maile
Engineering Manager
Dominion Aluminum Fabricating, Ltd.
3570 Hawkestone Road
Mississauga, Ontario, Canada
L5C 2V8

James H. Strickland
Mechanical Engineering Dept.
Texas Tech University
Lubbock, TX 79409

R. J. Templin
Head, Low Speed Aerodynamics Lab
National Research Council (Canada)
Montreal Road
Ottawa, Canada K1H 6R6

Ai, Daniel K.
Alcoa Tech. Center
(Aluminium Composites of America)
Senior Scientific Assoc.
Alcoa Center, PA 15069

Andrews, Carl
Altruistic Communities
Project Engineer
110 E. Anaheim
Long Beach, CA 90813

Barieau, Dr. Robert
Research Professor
West Texas State Univ.
Box 248, W.T. Station
Canyon, TX 79016

Bea, Karl J.
Enerjair, Ltd.
(American Ultramar, Ltd.)
128 DeWitt Street
Syracuse, NY 13203

Beckman, Ralph
REDE Research Institute
P. O. 212
Providence, RI 02901

Benjamin, John
Pollution Control Research Institute
Assoc. Director
3875 Jackson Station #19
Riverside, CA 92503

Bergey, Mike
Univ. of Oklahoma
Rt #1 Box 151B
Norman, OK 73069

Bill, Donald F.
Org. CDI
1080 N. River Drive
Miami, FL 33136

Bolt, Jan B.D.H.
Fokker-VFW
P. O. Box 7600
Schiphol-cost, The Netherlands
020/731044

Braz, John
TCHUBA
98 Camp Street
Providence, RI 82906

Breed, Robert A.
Wood World
579 Calle Dia
Carpinteria, CA 93013

Carlin, Palmer
Colorado University
Professor Elec. Engineering
2209-4th Street
Boulder, CO 80302

Carlis, Bill
S. W. Energy Options
109 W. California Street
Silver City, NM 88061

Ceiderburg, John W.
Ceiderburg Engineering
Box 259
Aptos, CA 95003

Charron, R.
The American Comm. for Cape Verde
14 Beacon Street
Boston, MA 02108

Clark, John M.
Institute of Arctic Alpine Research
University of Colorado
Boulder, CO 80309

Cole, Alan L.
Northern Illinois University
Dept. of Geography
DeKalb, IL 60115

Craik, Darrell W.
Teledyne Aero-Cal
523 E. Mission Road
San Marcos, CA 92069

Cromack, Dr. Duane E.
Dept. of Mechanical Engineering
University of Mass.
Amherst, MA 01002

Davenport, Steven R.
Oklahoma State University
900 N. Portland
Oklahoma City, OK 73107

Davitian, Harry
Brookhaven Nat'l Lab
Bldg. 475,
Upton, NU 11973

Dennis, Tom L.
Brunswick Corporation
504 Sweetwater Blvd.
Longwood, FL 32750

Dhande, Dr. Sanjay G.
Mechanical Engineering Dept.
University of Florida
Gainesville, FL 32677

Dodge, Robert J.
Automatic Power, Inc.
213 Hutcheson Street
Houston, TX 77003

Dorn, Dr. Dave W.
Lawrence Livermore Laboratory
P. O. Box 808
Livermore, CA 94550

Dougan, David
Hamilton Standard
Area Representative
Box 58096
Houston, TX 77058

Drake, Dr. William E.
Enertech Corporation
P. O. Box 420
Norwich, VT 05055

Drees, Herman M.
Pinson Energy Corporation
76 Ashford Street
Allston, MA 02134

Dunitz, Margie
University of Michigan
1620 Cambridge Rd.
Ann Arbor, MI 48104

Espeset, Nick
Foundation for Rural Technology
903 Pine Street
Boulder, CO 80302

Fanucci, Jerome N.
West Virginia University
Professor and Chairman
Dept. of Aerospace
Morgantown, WV 26506

Fekete, Professor G. I.
McGill Univ.
Asst. Assoc. Professor
Montreal, Canada

Francis, Serre
Rohn Manufacturing Co.
P. O. 23428
San Jose, CA 95153

Frenchman, R. M.
The American Committee for Cape Verde
14 Beacon Street
Boston, MA 02108

Fuller, Gerald
University of Regina
Faculty of Engineering
Regina, Canada

Gillies, Alan
University of Oklahoma
209 Cedar Lane
Moore, OK

Gilmore, Earl H.
WTSU-AC-SIGMA
Rt 1 Box 430
Amarillo, TX 79106

Gordon, Robert
Structural Composites Industries, Inc.
6344 North Irwindale Ave.
Azusa, CA 91702

Gross, William A.
Dean, College of Engineering
University of New Mexico
107 Farris Engr. Center
Albuquerque, NM 87131

Groves, Donald J., Jr.
Public Service Co.
P. O. Box 2267
Albuquerque, NM 87103

Hadlock, R. K.
Battelle Pacific Northwest Laboratory
P. O. Box 999
Richland, WA 93352

Heckman, Ken
Teledyne Aero-Cal
528 E. Mission Rd.
San Marcos, CA 92069

Hill, John M.
University of Wyoming
Assoc. Prof. of Civil Engr.
Laramie, WY 82071

Hill, P. Ward
Hercules, Inc.
P. O. Box 210
Cumberland, MD 21502

Holme, Olof A. M.
SAAB-SCANIA AB Aerospace Div.
Linkoping, Sweden S-58188

Johnson, Steve A.
Wind Energy Association
4594 Creek View Drive
Salt Lake City, UT 84107

Jones, Brian H.
Compositer Engineering Corp.
6960-5 Aragon Circle
Buena Park, CA 90620

Jones, Robert
R&M Ranch, Inc.
570 N. Lillian Way
Los Angeles, CA 90004

Krug, Edwin H.
Lear Siegler, Inc.
Director, Military Planning
4141 Eastern Avenue, SE
Grand Rapids, MI 49508

Langerman, Lowell
Rt 2
Fayette, IA 52142

Larsen, Harold C.
Air Force Institute of Technology
AFIT/END, WPAFB
Dayton, OH 45433

Lechner, T. Michael
Bovay Engineers, Inc.
P. O. Box 30068
Albuquerque, NM 87110

Lefever, Dan
Sonnowald Service
RT #1, Box 457
Spring Grove, PA 17362

Lefever, Evan
Route 2, Box 203
Berkeley Springs WV 25411

Lefever, Tim
Sonnewald Service
Route #1, Box 457
Spring Grove, PA 17362

Lissaman, Peter
Aerovironment
Las Vista
Pasadena, CA 91107

Ljungstroem, Olle
N.E.National Swedish Board for Energy
Source Development
STU, FACK S-(0072)
Stockholm 43, Sweden

Lopez, Gilbert
Bureau of Indian Affairs
P. O. Box 1248
Albuquerque, NM 87103

Malver, Fred
Honeywell, Inc.
2600 Ridgeway Pkwy
Minneapolis, MN 55413

Matakovich, George J.
Store, Matakovich & Wolfberg
715 E. Mission Drive
San Gabriel, CA 91776

McCarthy, John S.
McDonnell Douglas Corp.
345 Gray Avenue
St. Louis, MO 63119

McClure, Paul
University of Texas
Asst. Professor of Aerospace Engr.
Taylor Holl 227
Austin, TX 78712

Marriam, Marshal
Lawrence Berkeley Laboratory
University of Calif.
Dept. of Materials Science
Hearst Mining
Berkeley, CA 94720

Metcalf, Philip
Unarco-Rohn
P. O. Box 2000
Peoria, IL 61601

Meyer, Hans
Windworks
Box 329, Route 3
Mukwonago, WI 53149

McConnell, Robert
Inst. of Research of Hydro-Quebec
1800 Montec Ste Julie
Varrenes, Quebec, Canada JOL 2 PO

Michlin, Steven B.
University of Michigan
1620 Cambridge Rd.
Ann Arbor, MI 48104

Miller, Larry
Oklahoma State Univ.
Technical Institute
900 N. Portland
Oklahoma City, OK 73107

Mims, Forrest M., Jr.
UTSA
234 Five Oaks Drive
San Antonio, TX 78209

Mitcham, Tina
Pollution Control Research Inst.
3875 Jackson Station #19
Riverside, CA 92503

Mortimer, A. J.
Box 72
Oldwick, NJ 08858

Nassar, Dr. Esam
Illinois Institute of Technology
3110 S. State Street
Chicago, IL 60616

Nelson, Dr. Vaughn
West Texas State Univ.
Dept. of Physics
Box 248, W.T. Station
Canyon, TX 79016

Packard, Lyle E.
Packard Marine
505 N. Lake Shore Drive
Chicago, IL 60611

Palmer, Darwin G.
701 Wagon Train, SE
Albuquerque, NM 87123

Park, Jack
Helion
Box 4301
Sylmar, CA 91342

Pedersen, Bjarne Maribo
Tech. Univ. Denmark
Danish Academy of Tech. Sciences
Dept. of Fluid Mech
Bygn 404 DTH, 2800 Lyngby
Denmark

Penrod, Robert
PENROD CO.
P. O. Box 1047
Cape Girardeau, MO 63701

Piepers, G. G.
Reactor Ventrum Nederland
Westerduinweg 3 Petten
(N.H.) The Netherlands

Ramos, A. D.
The American Committee for Cape Verde
14 Beacon Street
Boston, MA 02108

Ramsdell, J. V.
Battelle Pacific Northwest Laboratory
Research Scientist
P. O. Box 999
Richland, WA 99352

Rollins, Charles
Box 737
El Cerrito, CA

Root, David H.
U. S. Geological Survey
Mail Stop 922
Reston, VA 22092

Sandor, Dr. G. N.
M. E. Dept.
University of Florida
Gainesville, FL 32677

Sayler, John P.
American Energy Alternatives, Inc.
P. O. Box 905
Boulder, CO 80302

Scully, Dan
Total Environment Action
Box 47
Harrisville, NH 03450

Seath, Donald D.
Univ. of Texas at Arlington
Aerospace Engr. Dept.
UTA Box 19428
Arlington, TX 76019

Seaverson, Louis A.
Rockwell International
P. O. Box 464
Golden, CO 80401

Sheehan, John L.
Chief Engineer
Sheehan Consultants
5320 Ken Caryl Rd.
Littleton, CO 80123

Shepardson, William P.
Pinson Energy Corp.
76 Ashford Street
Allston, MA 02134

Sholes, John E.
NASA Lewis Research Center
21000 Brook Park Rd.
Cleveland, OH 44135

Skoglund, Victor J.
University of New Mexico
ME 101
Albuquerque, NM 87131

Smith, Brent
ISTARA Research
P. O. Box 735
Boulder, CO 80302

Snyder, Melvin H.
Wichita State University
Wichita, KS 67208

Soderholm, L. H.
USDA-ARS
Room 213 Ag. Engr.
Iowa State University
Ames, IA 50011

South, Peter
National Research Council of Canada
Research Office
Bldg. M-2, Montreal Rd.
Ottawa, Ontario (Canada) KLA ORS

Stein, Bill
Natural Power
Francestown Turnpike
New Boston, NH 03070

Takanashi, Akihiro
University of Florida
Dept. of Mechanical Engineering
Gainesville, FL 32611

Thomann, Gary C.
Wichita State University
Wichita, KS 67208

Thomas, Robert
Wind Harvest Co.
759 Mission
Camarillo, CA 93010

Todd, Clement
U. S. Bureau of Reclamation
Denver FC Bldg. 67 Room 620
Denver, CO 80225

Tsao, Peter
Northern Illinois Univ.
Physics Dept.
DeKalb, IL 60115

Turnquist, Ralph O.
Kansas State Univ.
1100 Pioneer Lane
Manhattan, KS 66502

Van Dalen, Gerritt
FDO-Engineering Consultants
P. O. Box 194
Hengelo, Netherlands

Warchol, Edward J.
Bonneville Power Admin.
P. O. Box 3621
Portland, OR 97208

Weeks, Stanley A.
Agricultural Engr. Dept.
Cornell Univ.
312 Agr. Engr. Dept.
Ithaca, NY 14853

Werner, Charles
Unarco-Rohn
Sales and Engr. Dept.
P. O. Box 2000
Peoria, IL 61601

Wiedenmeier, Mario
Radiology
The University of Texas
Galveston, TX 77550

Wood, Rhande Paul
1180 Alvarado, SE #208
Albuquerque, NM 87108

Worstell, Mark
University of Oklahoma
1319 S. Jenkins - Apt. B
Norman, OK 83069

Zweig, Pete R.
Pollution Control Research Inst.
Associate Director
3875 Jackson Station #19
Riverside, CA 92503

Anthony F. Aimone
c/o Ceasar Aimone
200 Fifth Street
Iron Mountain, MI 49801

Joseph F. Boland
Rockwell International
Rocky Flats Plant
Box 474
Golden, CO 80401

1281 J. H. Biffle
1281 R. Rodeman
1284 W. N. Sullivan
1284 L. I. Weingarten
1324 L. V. Feltz
1330 R. C. Maydew
1333 S. McAlees
1333 B. F. Blackwell
1333 R. E. Sheldahl
5000 A. Narath
5431 D. W. Lobitz
5443 J. W. Reed
5700 J. H. Scott
5710 G. E. Brandvold
5715 R. H. Braasch (100)
5715 R. D. Grover
5715 E. G. Kadlec
5715 R. C. Reuter
5715 A. F. Veneruso
5740 V. L. Dugan
5742 J. F. Banas
8266 E. A. Aas (2)
3141 C. A. Pepmueller (Actg) (5)
3151 W. L. Garner (3)
For: ERDA/TIC (Unlimited Release)

☆ U.S. GOVERNMENT PRINTING OFFICE 1977—777-019/509